Squeezing Blood From A Stone:

Inferences Into The Life and Depositional Environments Of The Early Archaean

Jelte Harnmeijer

A dissertation submitted in partial fulfillment of the requirements for the degree of

Doctor of Philosophy

University of Washington

MMX

Programs Authorized to Offer Degree:
Center for Astrobiology & Early Earth Evolution
and
Department of Earth & Space Sciences

Abstract

A limited, fragmentary and altered sedimentary rock record has allowed few constraints to be placed on a possible Early Archaean biosphere, likewise on attendant environmental conditions. This study reports discoveries from three Early Archaean terrains that, taken together, suggest that a diverse biosphere was already well-established by at least ~3.5 Ga, with autotrophic carbon fixation posing the most likely explanation for slightly older 3.7 - 3.8 Ga graphite.

Chapter 2 aims to give a brief overview of Early Archaean geology, with special reference to the Pilbara's Pilgangoora Belt, and biogeochemical cycling, with special reference to banded-iron formation. Chapter 3 reports on the modelled behaviour of abiotic carbon in geological systems, where it is concluded that fractionations incurred through autotrophic biosynthesis are generally out of the reach of equilibrium processes in the crust. In Chapter 4, geological and geochemical arguments are used to identify a mixed provenance for a recently discovered 3.7 - 3.8 Ga graphite-bearing meta-turbidite succession from the Isua Supracrustal Belt in southwest Greenland. In Chapter 5 and 6, similar tools are used to examine a newly discovered 3.52 Ga kerogenous and variably dolomitized magnetite-calcite meta-sediment from the Coonterunah Subgroup at the base of the Pilbara Supergroup in northwest Australia. Possible implications for the origin of texturally similar banded-iron formation, which may represent a silicified analogue, are discussed. In Chapter 7, structures from ~3.45 Ga kerogenous meta-chert in the Barberton Greenstone Belt, and similarly aged neptunian fissures in the Strelley Pool Chert, are interpreted as likely oncoidal trace-fossils indicative of complex microbial biofilm formation in Early Archaean shallow marine environments. No abiotic analogues to these structures are known.

Carbon isotope analyses of Early Archaean carbonate, graphite and kerogen from different environments are compared in the concluding synthesis. Systematic isotope trends argue against a significant abiotic Fischer-Tropsch origin for syn-sedimentary carbon. The picture that emerges, rather, is consistent with vigorous Early

Archaean pelagic autotrophy, and a benthic biota dominated by fermentation, acetogenesis and methanogenesis. Access to electron acceptors was limited, and seems to have been restricted to sulphate and mineral ferric iron in shallow and deep marine environments, respectively.

TABLE OF CONTENTS

LIST OF FIGURES

LIST OF FIGURES (cont'd)

LIST OF FIGURES (cont'd)

LIST OF FIGURES (cont'd)

LIST OF FIGURES (cont'd)

LIST OF FIGURES (cont'd)

LIST OF FIGURES (cont'd)

LIST OF TABLES

LIST OF TABLES (cont'd)

PREFACE

The Quest for Ancient Life

I am being driven forward
Into an unknown land.
The pass grows steeper,
The air colder and sharper.
A wind from my unknown goal
Stirs the strings
Of expectation.
Still the question:
Shall I ever get there?
There where life resounds,
A clear pure note
In the silence.

- Dag Hammarskjöld

Members of the species *Homo sapiens sapiens* are, to the best of their current knowledge, unique in being able to ponder their own origin. In geological terms, it is only very recently that they have come to discover that sedimentary rocks provide one of the few viable mirrors into their remote past. She is a shattered mirror, however, her vulnerable fragments left exposed to the force of almost four billion years of erosion, weathering, deformation, metamorphism, and contamination. The handful of shards that offer themselves to vigilant field-geologists today offer, at best, a distorted and fragmentary reflection upon our evolutionary beginnings. What reason to expect more than this exists?

Unquestionably, the origin of life on Earth stands as one of the foremost enigmas facing human knowledge. Within the scientists' toolkit, the Earth's rock record provides one of very few gateways to this ancient question. The window of time corresponding to the first preserved evidence of sedimentation abruptly opens about 3.8 billion years ago. The subsequent 600 million or so years of geobiological history, bounded more-or-less *ad hoc* at 3.2 Ga[1], is termed the 'Early Archaean Era'. It forms the focus of this thesis. Only seldom will this study find cause to breach these temporal bounds and infringe on younger territory.

I should have liked to produce a good thesis. This has not come about, but the time is past in which I could improve it.

WALDRON ISLET, SAN JUAN ISLANDS, JULY MMIX

SEATTLE'S CENTRAL DISTRICT, SEPTEMBER MMIX

[1] 1 Ga = 10^9 years ago

ACKNOWLEDGEMENTS

Opportunities for formal expression of gratitude may arise only seldom in my lifetime. Consequently, I should like to treat this particular instance with due reverence. Thanks firstly be to the American tax-paying public for financial support, mediated through a substantial NASA Exobiology grant. For technical support, thanks be to Scott Kuehner (microprobe analysis), Wai Pai Chan (SEM analysis), Diane Cornelius (XRF/ICP analysis), Richard Armstrong (U-Pb zircon dating), Dominc Papineau ($\delta^{15}NH_4^+$ analysis), Julien Foriel ($\delta^{34}S$ analysis) and especially Andrew Schauer (isotope laboratory).

For sample preparation, thanks be to Ryan Lipscomb, Greg Horn, Molly Ravits, Ryan Richardson and especially Kyle Samekk. Thanks be to Allen Devol and Rick Keil for an opportunity to engage in oceanographic research. Thanks be to Mark Ghiorso, Jan Huizenga and James Connolly for assistance in thermodynamic modeling. Thanks be to Jan Veizer for kindly providing ancient carbonate geochemical data. Thanks be to Dick Stewart and Charlotte Schreiber for petrological assistance. Thanks be to Minik Rosing, John Dunlop and Axel Hofmann for field logistics and co-ordination. Thanks be to my committee members Bernard Evans, Olivier Bachmann, John Baross and Vladimir Chaloupka.

For inspiration and friendship, thanks be to Beth Orcutt, **Bonnie Chang**, Carel Haumann, **Cheryl Fitzgerald**, **Cynthia Updegrave**, Daniel Hornal, **Elizabeth Nicholls**, Farah Abdul, Jessica Garvin, **Joshua Strange & family**, Leonard Davis, Lina Aglialoro, the Loyd family, Marwa Maziad, Melanie Lyon, Michelle Koutnik, Michiel Zuidweg, **Nicolás Pinel**, Randy Waugh, Roeland Odijk, Ruby Wells, Silja Talvi, Solmaz Mohadjer, **Tarek Maassarani**, Tom 'Lazer' Finlay, Tony Scruton, William Brazelton and Zach Adam. I further thank Jan-Willem, Joanne, Anna and Elizabeth – distant but ever-present relatives. Friends & family – what is left of a man without them?

Lastly, it befalls me to thank Roger Buick. I was afforded my first glimpse of certain salient features of Roger's personality when he interceded on my behalf, somewhere in Australia's outback, during the opening phases of hand-to-hand combat between myself and his boss[2]. A sincere commitment to justice and truth, not to speak of counterweighing humility, is about as common in tenured professors as it is in mankind. Should my embodiment of these rare traits ever rise above mere aspiration, it will be due to Roger's example.

HOOPA VALLEY INDIAN RESERVATION,
HUMBOLDT COUNTY, JANUARY MMX

[2] My adversary had quite incorrectly inferred the presence of a racist streak in my immediate forebears through appeal to faulty geographical and historical axioms.

1. Epistemic Challenges to Archaean Geobiology

"It may be [...] that all enquiry on our part is set so as to exempt
certain propositions from doubt, if they are ever formulated.
They lie apart from the route travelled by enquiry."
- Ludwig Wittgenstein, *Über Gewißheit* (1969)

1. Introduction

Archaean geobiologists employ a host of different techniques to scrutinize the earliest rock record for clues on early surface conditions and signs of early life. Severe limitations are placed upon any study of ancient rocks, however, careful consideration of which infuses derived conclusions with important caveats. It is the brief purpose of the present chapter to emphasize these caveats.

"[…] I continue to think of the conceptual scheme of science as a tool, ultimately", writes an eminent 20th Century philosopher of science, "for predicting future experience in the light of past experience" (Quine, 1951). This highly general conceptualization of science is highlighted here in order to illustrate the unique epistemic status held by Archaean geology, which is tasked with predicting (as it were) the deep past on the basis of present experience. A method towards this end was proposed by Charles Lyell, who subtitled his *Principles of Geology* (1830-1833) with the words: "An attempt to explain the former changes of the Earth's surface by reference to causes now in operation" (Figure 1). This method, known today as the 'uniformitarian doctrine', was likely inspired by James Hutton, who earlier (1785) stated that, in geology, "[…] no powers are to be employed that are not natural to the globe, no action to be admitted except those of which we know the principle" (cited in Holmes, 1965, p. 44).

The applicability of uniformitarianism to Archaean geology is vehemently defended by adherents today (e.g. Eriksson et al., 1994). But what are we to do when presented, as in the case of enigmatic banded-iron formation, with geological phenomena the 'action' or 'causes' of which are no longer in operation? Would strictly

applied uniformitarianism, to give one further example, not bias our interpretation of early continental differentiation processes towards alignment with the modern, that is, Phanerozoic plate-tectonic paradigm? In this manner, overemphasis of the present may be the key to misunderstanding the past.

2. Over-Representation Through Preservation

Dominant amongst these potential epistemic pitfalls is the *representativeness* of the available data, which is of limited spatial and temporal extent: very old rocks are scarce (Figure 2, 3). As rocks mature, their potential exposure to agents of weathering and erosion increases, as does the probability of structural deformation, with or without accompanying metamorphic and metasomatic overprinting (Figure 4). Consider that, while the age of the Earth is fairly well constrained at 4.56 Ga (Patterson, 1956; Zhang, 2002), the oldest crustal rocks found to-date have an age of 'merely' 3.85 Ga (Allaart, 1976; Cates and Mojzsis, 2007; O'Neill et al., 2007). This leaves a gap of well over half a billion years of Earth history for which the Earth's rock record cannot provide insight.

The Archaean geobiologist, then, has a limited number of outcrops to work with, all of which may represent different depositional environments, ages and locations. But just how representative of early crustal conditions are ancient rocks? Doubtless, the surviving rock record is heavily skewed towards tectonically quiescent environments amenable to preservatory processes. For illustrative purposes, consider briefly the pertinent examples of tectonic, structural and chemical preservation bias.

2.1. Three Pertinent Examples

Firstly, as evidenced by the affiliation of ancient rocks with durable cratons, supra-continental emplacement allows prolonged protection from destructive convergent tectonism and mantle recycling. In consequence, epi- and peri-continental settings enjoy preferential preservation, heavily skewing geological interpretations towards allied diastrophic processes.

Secondly, in the face of the leveling effects of erosion, sedimentary bedding and other planar features approaching vertical orientation will enjoy preferential persistence. The sub-vertical bedding and foliation typifying greenstone belt outcrop (Figure 5) may partly be a preservational artifact. Seismic cross-sections of greenstone belts reveal sheet-like geometries (Figure 6), possibly supporting the interpretation that the diagnostic vertical fabric in fact represents an anomalous and local feature of Archaean granitoid margins.

Thirdly, mineral assemblages that equilibrated under conditions that represent a significant departure from those encountered on or in the modern crust will have faced preferential removal from the geological record: exactly those assemblages that are the most telling of exotic Archaean conditions are most vulnerable. Chemical sediments precipitated on the floor of a more acidic and less oxidizing Archaean ocean, for instance, will be disproportionately affected by exposure to higher pH and fO_2 conditions prevalent today.

Of particular relevance here is the protective role that certain metasomatic and diagenetic phenomena can play. Silicification, in particular, obliterates chemical information but preserves otherwise vulnerable textures to microscopic scale and smaller (Figure 7, consider further silicified oncoids in Chapter 7). Such secondary cryptochrystalline silica is largely impregnable to migrating fluids, invulnerable to redox reactions, insoluble within a wide pH range, and fairly resistant to metamorphism. Consequently, Archaean environments conducive to silicification will be strongly over-represented in the rock record. Such a depositional preservation bias could be expected in marginal regions experiencing high silica influx, such as near-shore environments, and in environments where abrupt decreases in silica solubility cause pervasive silicification, such as at sediment/water interfaces where underlying hot acidic silica-saturated hydrothermal fluids meet overlying cold alkaline marine bottom-waters.

Under some circumstances, the dehydration reactions that accompany progressive low-grade metamorphism also have the paradoxical ability to enhance the preservation potential of rocks relative to less weathering-resistant hydrous protolith.

An example of this effect is seen through contact metamorphism of the Pilbara's lowermost Coonterunah Group, where hitherto undiscovered deep-water metapelites (Chapter 5) have survived only at upper-greenschist facies within the contact aureole of the intrusive Carlindi batholith. Environments conducive to rapid burial, meanwhile, protect rocks from aggressive surface weathering reactions and enhance lithification rates. The eruption of a ~4 km pile of basaltic and lesser gabbroic flows shortly following deposition likely allowed for preservation of the oldest sedimentary carbonate unit yet discovered (Chapter 5).

3. Variability and Secular Change

As contested by a slew of ongoing controversies, some over a century old, the interpretation of a fragmentary – and, as argued above, preservationally-biased - rock record faces considerable challenges. One further issue pertinent to geological evidence for ancient environments merits consideration: how variable were Early Archaean conditions? To what extent is it meaningful, for instance, to speak of '*the* Archaean surface ocean temperature' or '*the* Archaean climate' or '*the* Archaean atmospheric composition'?

Indeed, the case could be made that compared to the Earth System today, a less evolved Archaean prokaryotic ecto-sphere, subject to the vigorous and stochastic behaviour (Nelson, 2004) of a nascent and intermittently bombarded (Anbar et al., 2001; Simonson et al., 2004) planetary crust, would be a *less* efficient dampener of perturbations and consequently experience more frequent and higher amplitude oscillations (cf. Lenton, 2004). Furthermore, a majority of biogeochemically important ions have residence times $< 10^7$ years in modern oceans (Holland, 1978, 1984). The Archaean Era, in comparison, spanned $1.3 \cdot 10^9$ years and its ocean(s) likely experienced enhanced turnover rates of many hydrothermally fluxed ions.

Faced with a scarcity of data, the human mind grasps eagerly for secular trends. Perhaps some consolation can be found in the observation that "[f]alse facts are highly injurious to the progress of science, for they often endure long; but false views, if supported by some evidence, do little harm, for everyone takes a salutary pleasure in

proving their falseness; and when this is done, one path towards error is closed and the road to truth is often at the same time opened." (Darwin, 1871)

4. Candidate Evidence for Life

An obvious approach to early Life would seem to be to examine the rock record for microfossils. However, early biological structures – if preserved - may well have been far simpler and perhaps structurally and functionally different from those encountered today. A second, more subtle approach is to search for chemical fossils, or *biosignatures*. Despite a diverse plethora of putative evidence, no unambiguous proof exists for Early Archaean life (Figure 8 - 10). Purported evidence for life includes: (i) microfossils; (ii) stromatolitic trace fossils; (iii) microstructures housed in volcanic glass; and (iv) isotopically fractionated carbon, sulphur and/or nitrogen.

Early claims of microfossils at Isua (Pflug, 1978, 1979; Pflug and Jaeschke-Boyer, 1979) have been convincingly refuted (Roedder, 1981). More recent purported microfossils elsewhere (Awramik et al., 1983; Walsh and Lowe, 1983, 1985; Schopf and Packer, 1987; Walsh, 1992; Schopf, 1993; Westall et al., 2001; Schopf et al., 2002) are steeped in controversy (Brasier et al., 2002; Brasier et al., 2005). Although compelling, stromatoloids of purported stromatolitic origin (Lowe, 1980; Walter, 1980; Lowe, 1983; Hofmann et al., 1999; van Kranendonk et al., 2003; Allwood et al., 2006) remain susceptible to non-biological interpretations (Buick et al., 1981; Lowe, 1994; Grotzinger and Rothman, 1996; Grotzinger and Knoll, 1999). Endolithic microborings (Furnes et al., 2004; Banerjee et al., 2006) cannot definitively be distinguished from ambient inclusion trails (Knoll and Barghoorn, 1974).

Chemical evidence is, in some ways, more susceptible to ambiguity (e.g. contamination, abiotic non-equilibrium processes – see Chapter 3). Although the conditions facing Early Archaean microbes were very different, the mechanisms of preservation and geological evolution of their decay products was likely similar (Figure 11). Geochemical analysis of some ancient kerogen has yielded surprisingly good biomarker results (Brocks et al., 1999; but see Rasmussen et al., 2008), although it may prove optimistic to expect biomarkers from the older and higher-grade rocks in South

Africa and Australia. Kerogen undergoes thermodynamic re-equilibration to less-informative graphite following diagenesis and metamorphism.

Isotopically light carbon, in the form of graphite, has been reported in Akilia and Isua (Mojzsis et al., 1996; Rosing, 1999; Schidlowski, 2001) but may have arisen through the non-biological decarbonation of siderite (van Zuilen et al., 2002; van Zuilen et al., 2003) or through non-equilibrium thermodynamics (see also Chapter 3). Isotopically depleted kerogen at Barberton and in the Pilbara could be the product ancient Fischer-Tropsch-type ('FTT') synthesis (Fischer, 1935; Ueno et al., 2001; Brasier et al., 2002; Ueno et al., 2003; Ueno et al., 2004; Brasier et al., 2005). Although sulphur isotopic evidence is promising (Shen et al., 2001), little certainty exists regarding ancient sulphur cycling and isotopic fractionation incurred (Philippot et al., 2007; Ueno et al., 2008; Shen et al., 2009). High mobility, the lack of mineralogical sequestration and susceptibility to devolatilization hampers the use of nitrogen isotopes (both as $^{15}N_{org}$ and $^{15}NH_4^+$) as a biosignature, although this has not deterred all workers (Beaumont and Robert, 1998, 1999; Pinti and Hashizume, 2001; van Zuilen et al., 2005; Pinti et al., 2007; Garvin et al., 2009).

4.1. Precautionary Null Hypothesis

In the context of Figure 3, it should be clear that the timing of the transition (slide? step? skip?) from prebiotic to biotic synthesis is of more than cursory interest. The Hadaean Era was ostensibly characterized by more-or-less continuous surface bombardment by comets and meteorites (Kring and Cohen, 2002; Schoenberg et al., 2002), hindering the nascence of Life everywhere – excepting, speculatively, the deep subsurface (Krumholz et al., 1997; Teske, 2005). How long did it take for a biosphere to develop once conditions were suitable? And what are the implications for the existence of life elsewhere?

Because of the great weight which these questions carry, it is proposed that a null-hypothesis be adopted as the point of departure: **any potential evidence of Life that could have formed by non-living processes must be considered as non-evidence.**

5. Structure and Objectives

With the foregoing caveats firmly in mind, the following chapters seek to report on several novel discoveries in old rocks, together with their inferred bearing on early life and environments. Chapter 2 is introductory in nature, introducing key aspects of Early Archaean geobiochemical cycling and generalized and specific aspects of Early Archaean geology. The latter includes consideration of relevant geological and metamorphic aspects of the Pilgangoora Belt in Australia's Pilbara Craton. Through application of the precautionary null hypothesis, outlined above, thermodynamic modelling detailed in Chapter 3 seeks to place quantitative bounds on carbon isotope biosignature studies. Chapters 4 and 5 report new metasediment discoveries in Greenland and Australia, together with accompanying inferences into ancient depositional environments. Chapters 6 and 7 respectively report new isotopic- and trace-fossil- evidence for Early Archaean life from the Pilbara Craton. A brief concluding synthesis is presented in Chapter 8.

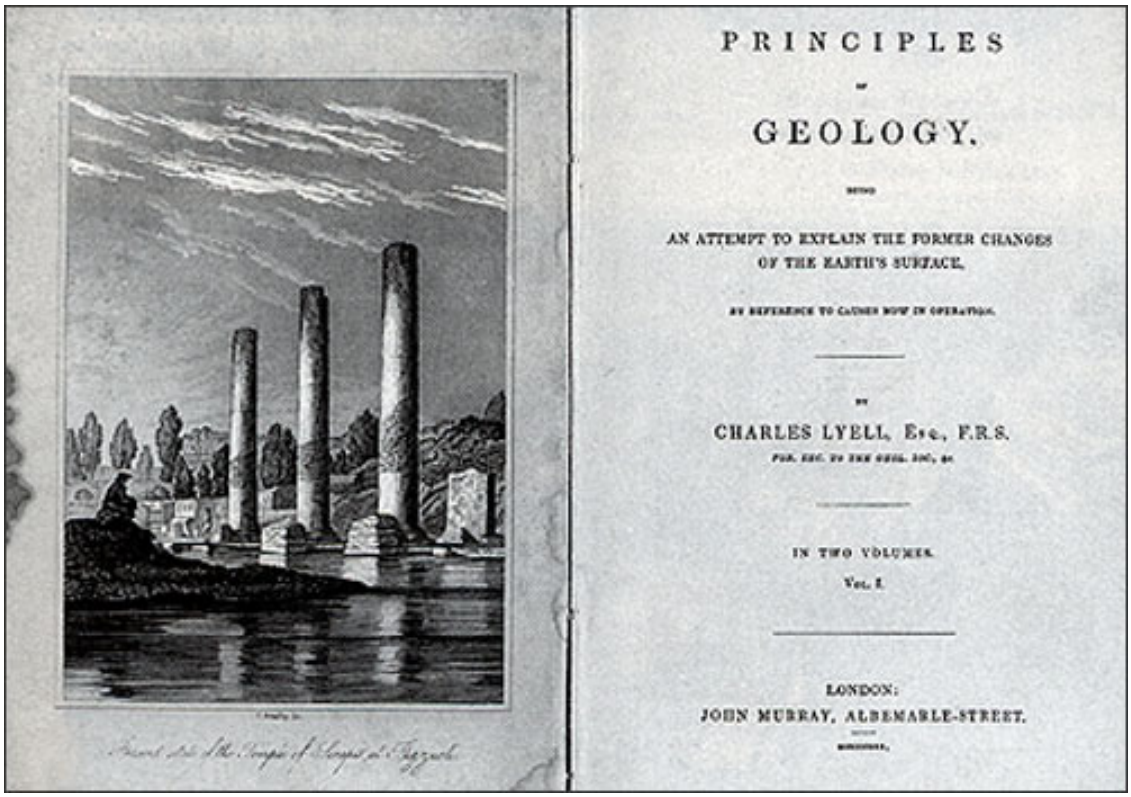

PRINCIPLES

OF

GEOLOGY,

BEING

AN ATTEMPT TO EXPLAIN THE FORMER CHANGES
OF THE EARTH'S SURFACE,

BY REFERENCE TO CAUSES NOW IN OPERATION.

BY

CHARLES LYELL, Esq., F.R.S.

IN TWO VOLUMES.

Vol. I.

LONDON:
JOHN MURRAY, ALBEMARLE-STREET.

Figure 1: Cover of Charles Lyell's *Principles of Geology* (1830-1833), subtitled: "An attempt to explain the former changes of the Earth's surface by reference to causes now in operation".

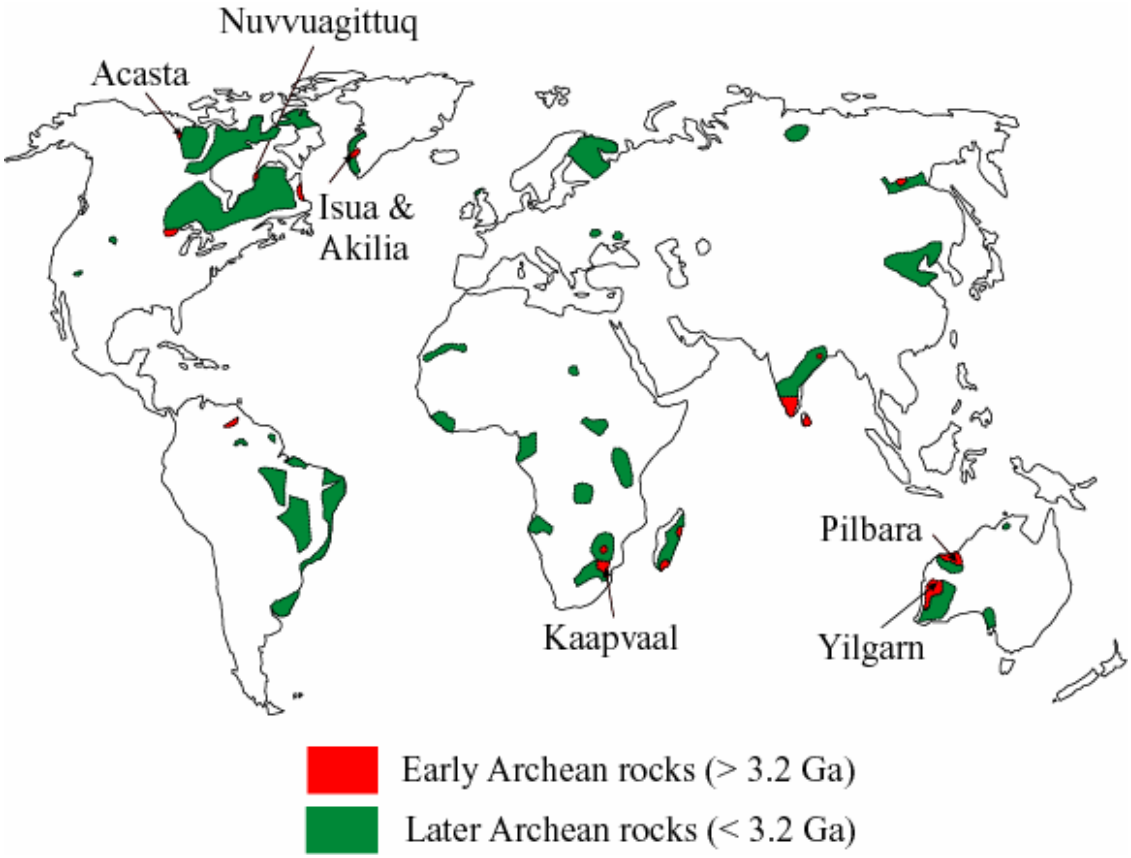

Figure 2: The distribution of Archaean outcrop today.

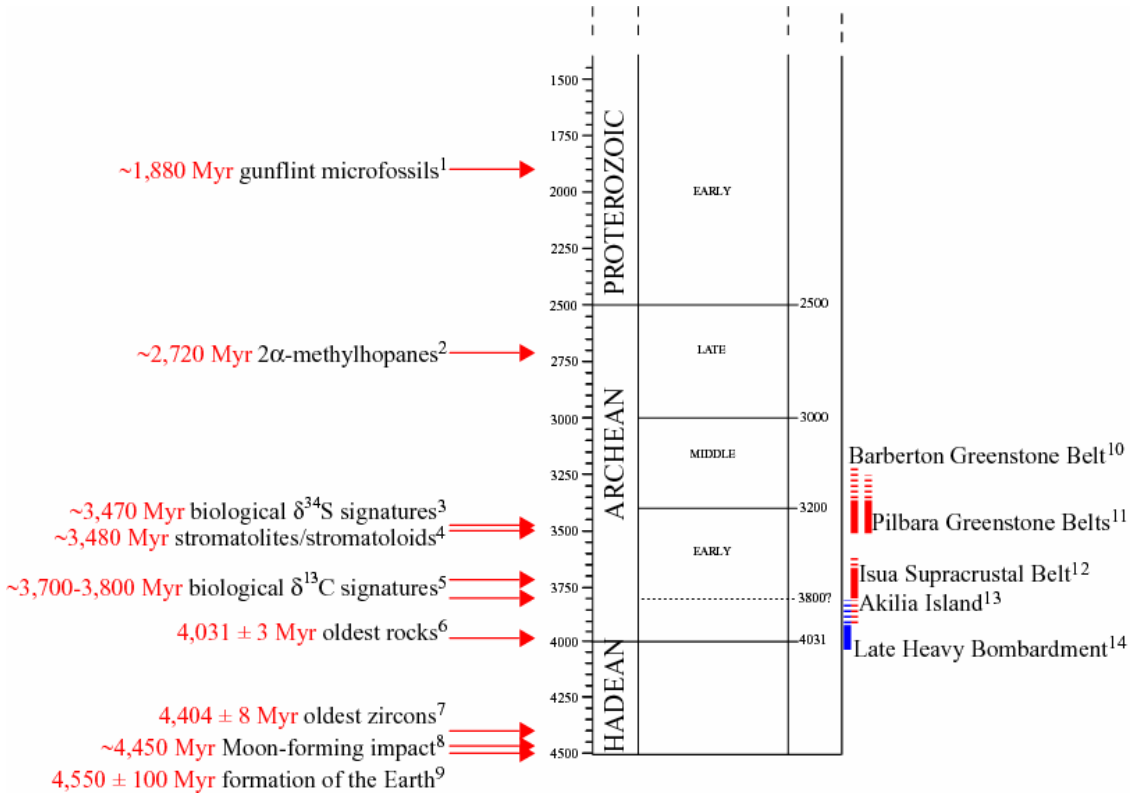

Figure 3: The beginning of geobiological history. Numbered references: 1: Fralick et al. (2002); 2: Brocks et al. (1999); 3: Shen et al. (2001); 4: Walter et al. (1980); 5: Mojzsis et al. (1996) on Akilia Island, Rosing (1999) at Isua; 6: Bowring et al. (1999); 7: Wilde et al. (2001); 8: Zhang (2002); 9: Patterson (1956); 10: Kroner et al. (1996) and Kruner et al. (1991); 11: Buick et al. (1995); 12: Whitehouse et al. (1999), this study (Chapter 3); 13: Nutman et al. (2000), Mojzsis et al. (2002); 14: Kring and Cohen (2002), Schoenberg et al. (2002).

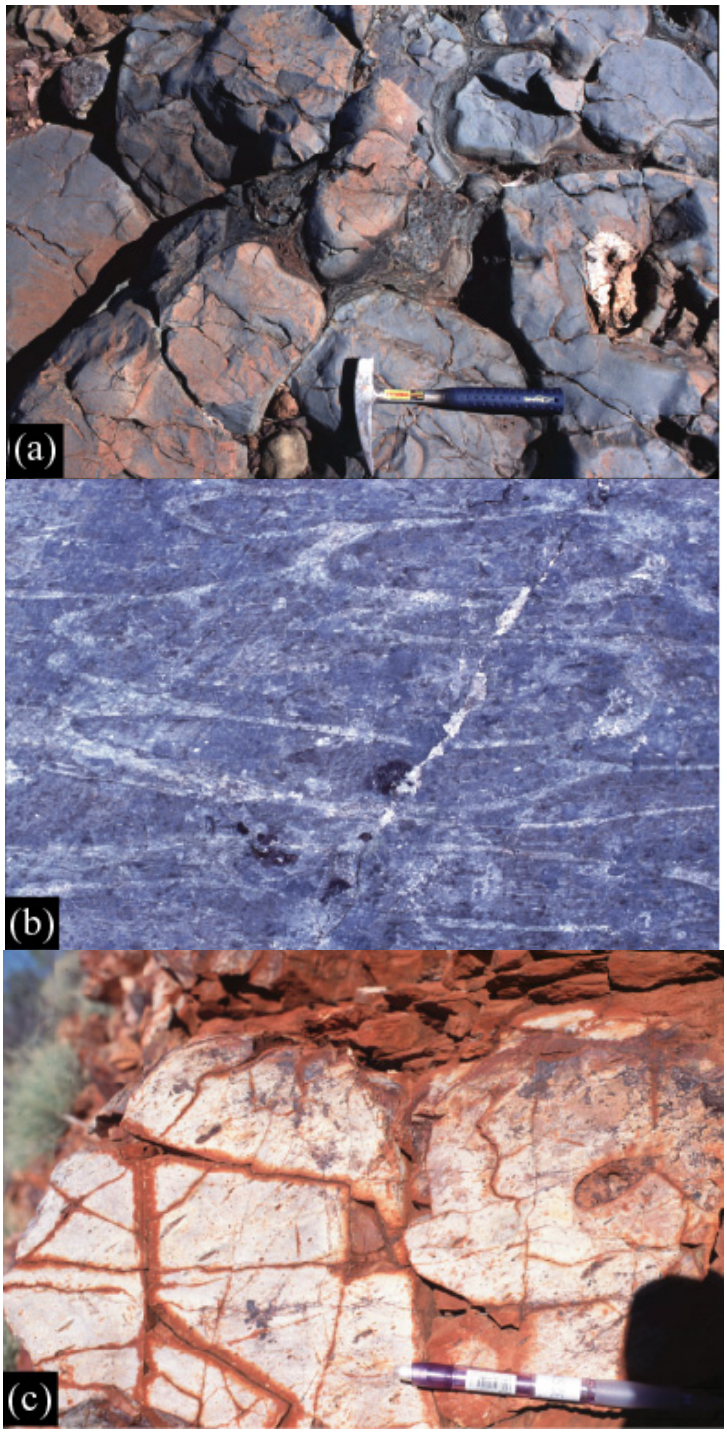

Figure 4: Alteration, deformation and metamorphism of pillow basalt. (a): Magnesian pillow basalt immediately overlying the Strelley Pool Chert, eastern Pilgangoora syncline, Pilbara. (b): Severely flattened, metamorphosed and metasomatized basalt pillows in the central eastern arc of the Isua Supracrustal Belt, scaled to hammer in photograph (a). (c): Severely silicified pillow basalt in the upper Warrawoona Group. This unit was once erroneously mapped as a pillowed rhyolite.

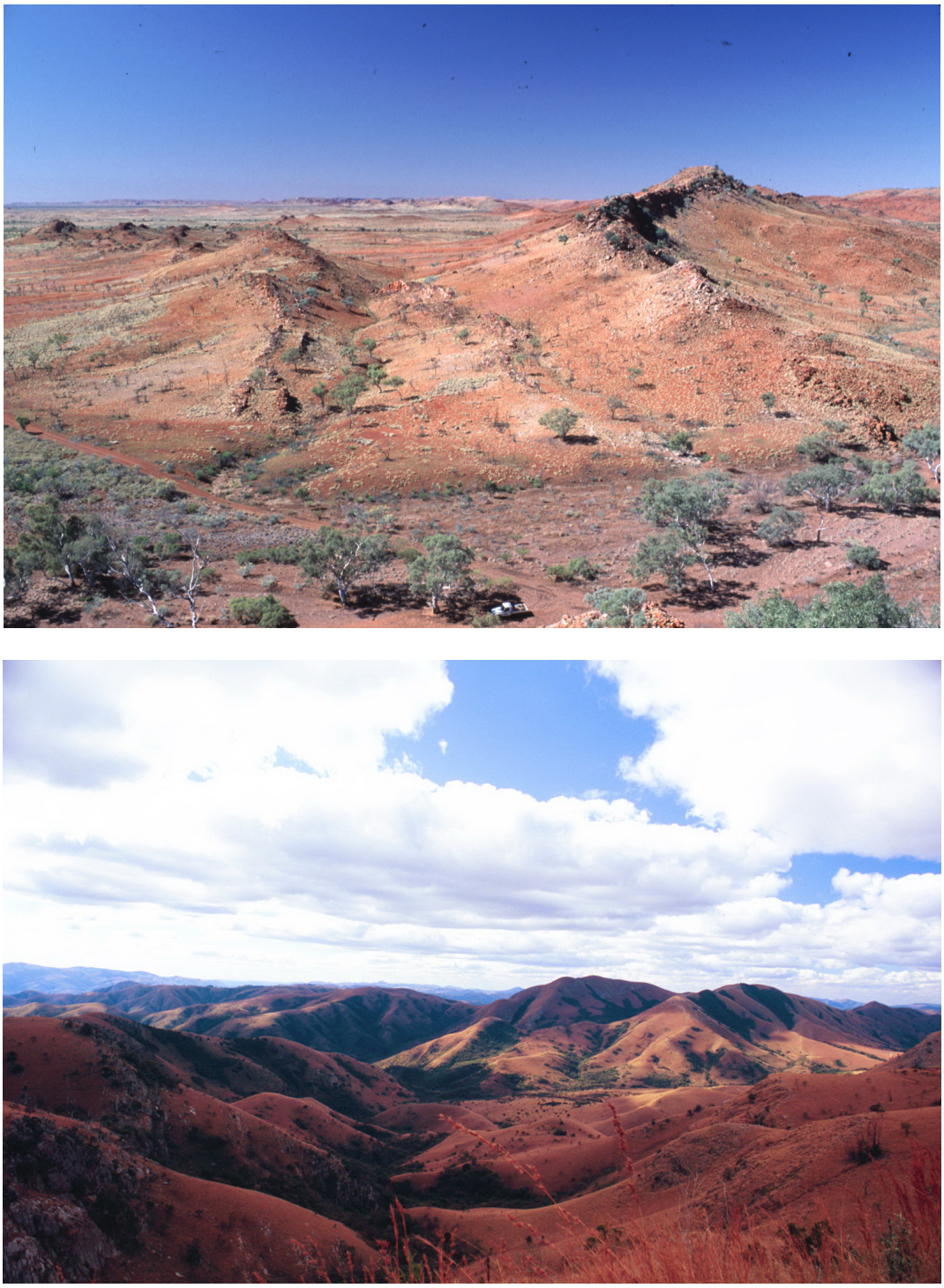

Figure 5: Greenstone belt geomorphology. In typical Early Archaean greenstone belts, such as the Pilbara's Pilgangoora belt (above, note vehicle for scale) and Barberton's Hoogenoeg Formation (below), sub-vertically dipping silicified sedimentary units protrude as prominent ridges above surrounding mafic extrusive and lesser felsic and hyperbyssal volcanics.

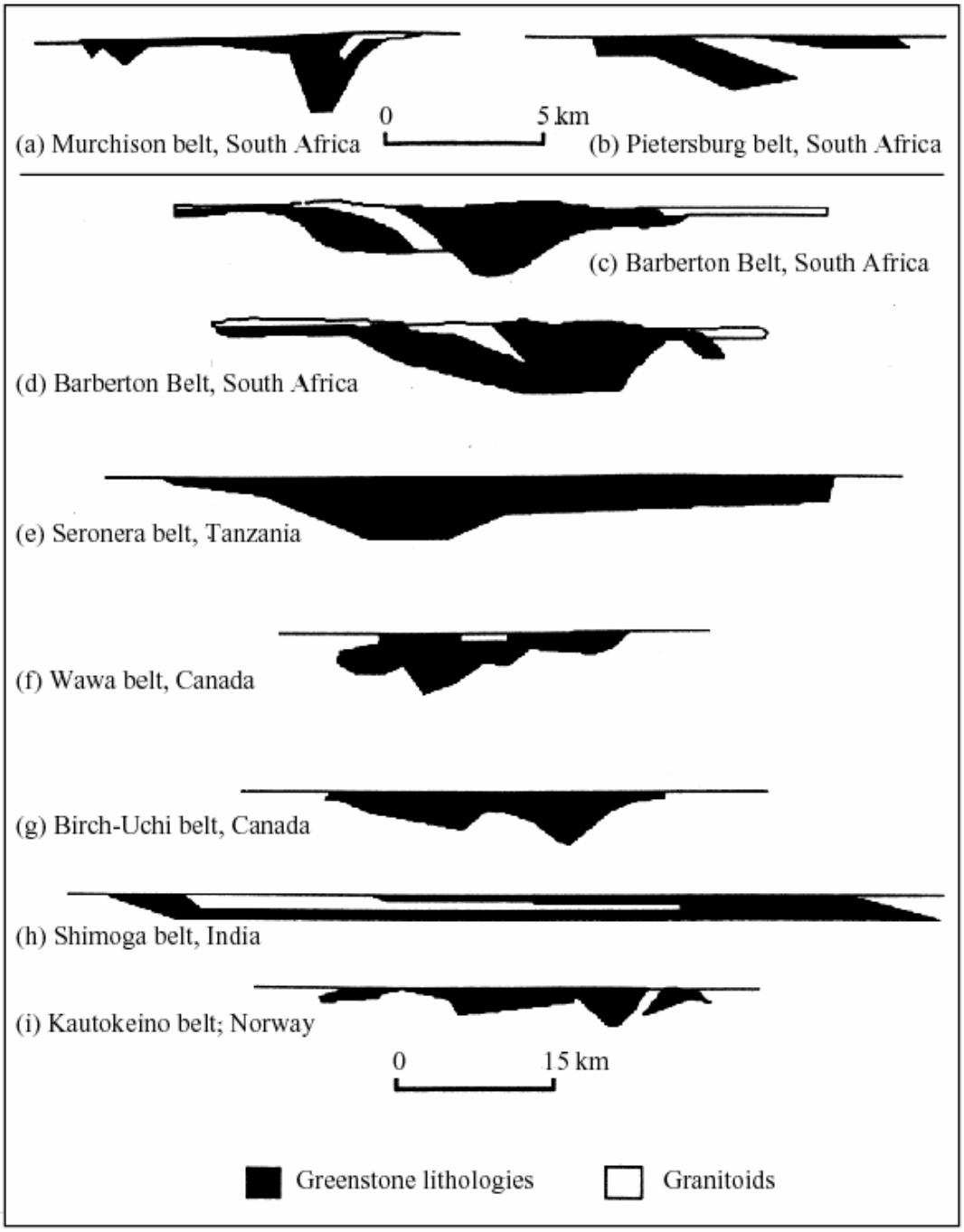

Figure 6: Greenstone belt cross-sections, illustrating sheet-like geometry. Figure after M.C. Dentith (In: de Wit and Ashwal, 1997).

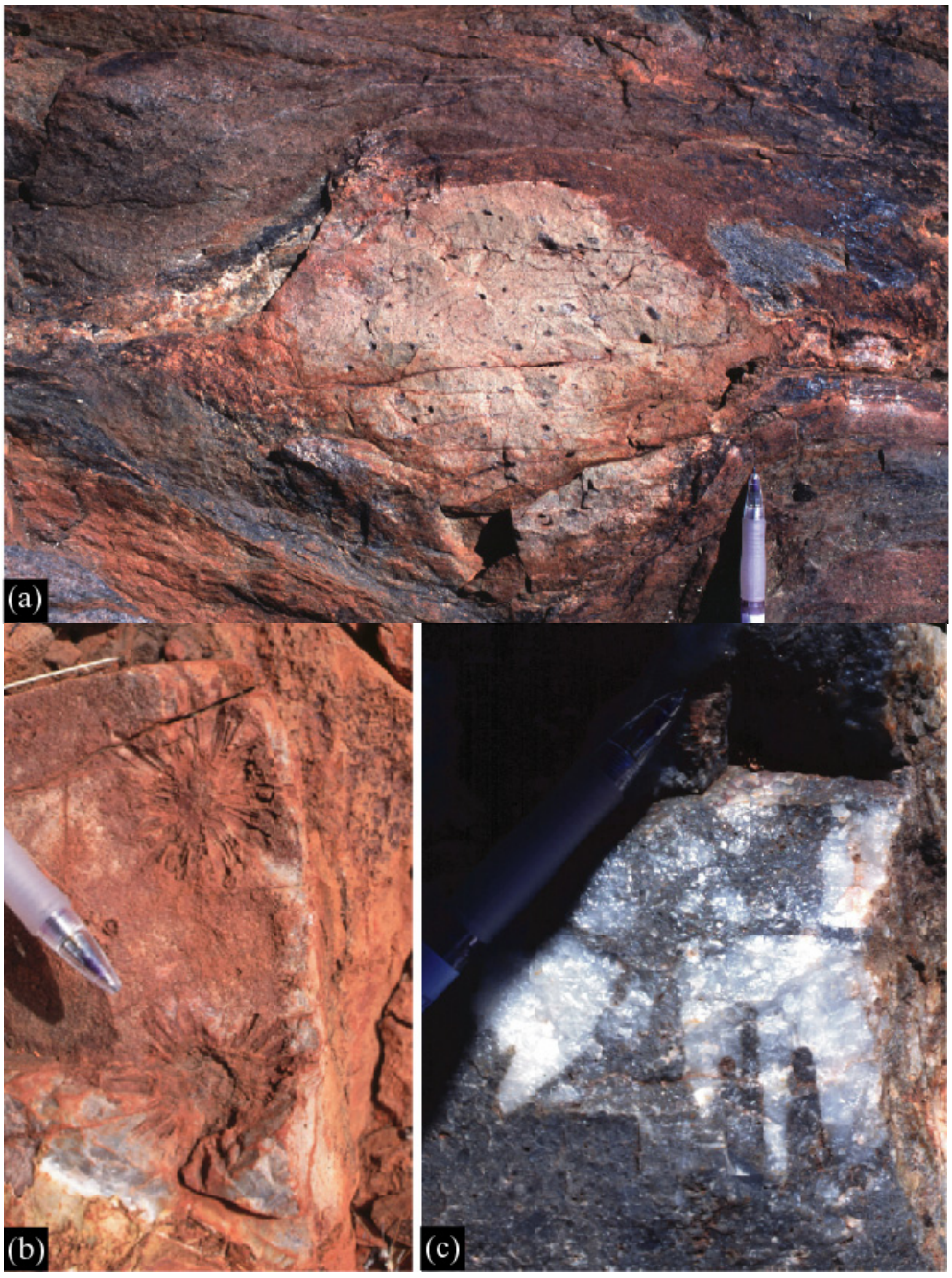

Figure 7: Textural preservation through silicification. (a): Silicified basalt pillow, complete with quartz-filled vesicles, preferentially preserved within a metamafic mylonitic fabric at upper amphibolite facies conditions, northwestern Pilgangoora syncline, Pilbara Craton. (b): Silicified diagenetic gypsum rosettes, North Pole dome, Pilbara Craton. (c): Silicified digitate structures after sulphate, Strelley Pool chert, Pilbara Craton. Although chemical information was pervasively destroyed, textural information was shielded from ~3.5 billion years of alteration, deformation, erosion, metamorphism and weathering through silicification.

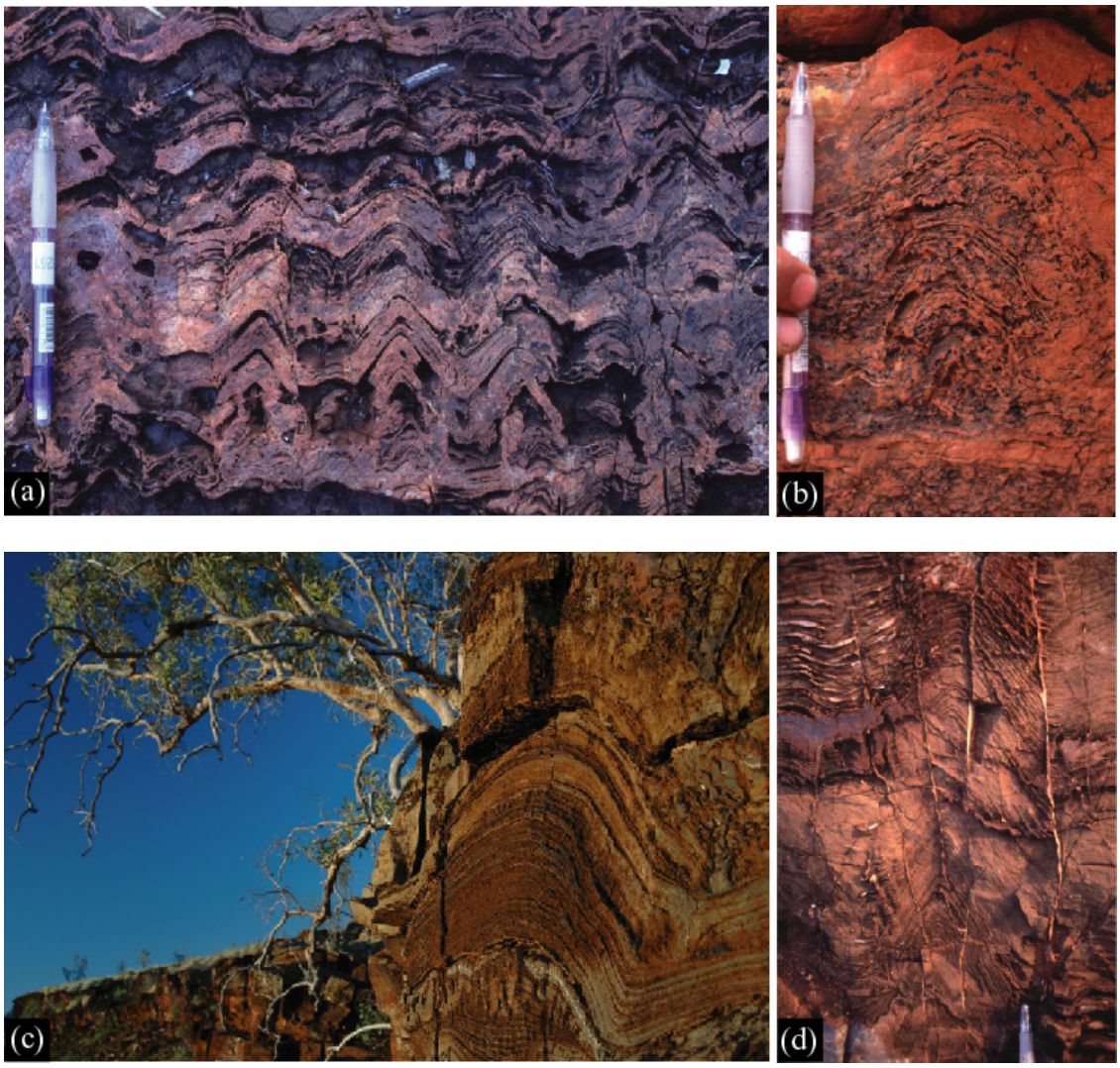

Figure 8: Archaean stromaloids/lites. (a): Silicified dolomitic isoclinal stromatoloids, Strelley Pool chert, central Pilgangoora Syncline, Pilbara. (b): Silicified haematite-stained domal stromatolite, North Pole dome, Pilbara. (c): Late Archaean stromatolite, 2.73 Ga (Blake et al., 2004) Tumbiana Formation, Fortescue Group, western Australia. (d): Mildly silicified dolomitic stromatolite/loid, North Pole dome, Pilbara.

Figure 9: Life or non-life? (a): Cross-section through Late Archaean domal stromatolite, Tumbiana Formation, Fortescue Group, Pilbara. (b): Abiogenic ferruginous ooids in Fortescue Formation, Pilbara. (c): Living stromatolites at Shark Bay, Western Australia. (d): Controversial kerogenous chert bearing spheroidal microfossil-like structures (Schopf and Packer, 1987), Chert VIII, Pilgangoora Syncline, Pilbara. (e): Living lacustrine stromatolites in Thesis Lake, Western Australia.

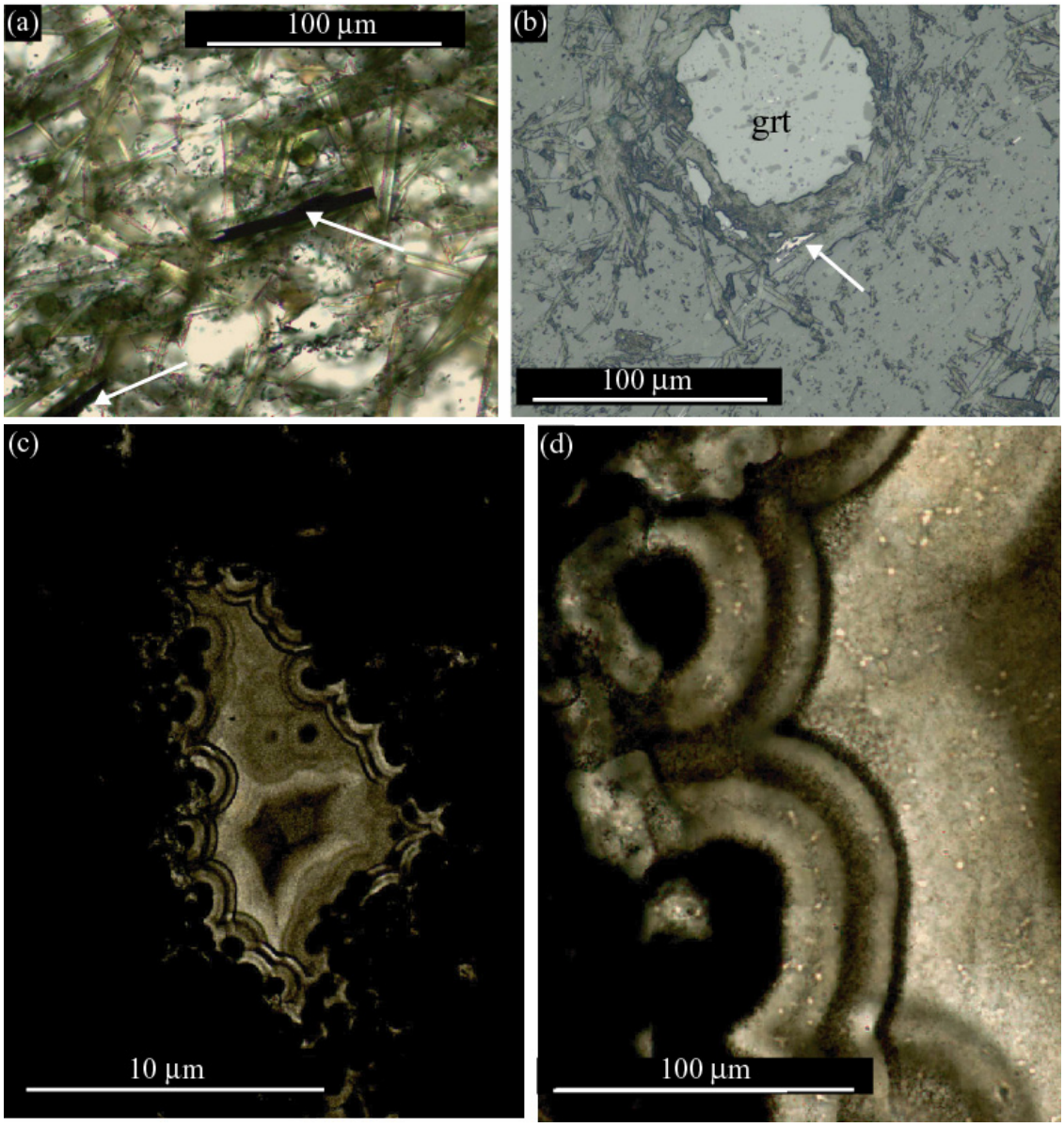

Figure 10: Early Archaean carbonaceous matter. (a, b): Early graphite viewed in (a) plane-polarized light and (b) reflected light in newly discovered metasediments from the Isua Supracrustal Belt. This graphite carries a possibly biogenic carbon isotope signature of $\delta^{13}C_{PDB} \approx -20‰$, compatible with photoautotrophic metabolism. (c, d): granular kerogen remobilized during early growth of chalcedonic quartz in a neptunian fissure of Strelley Pool chert age, Coonterunah Group, Pilbara. This kerogen carries a carbon isotope signature of $\delta^{13}C_{PDB} \approx -35‰$.

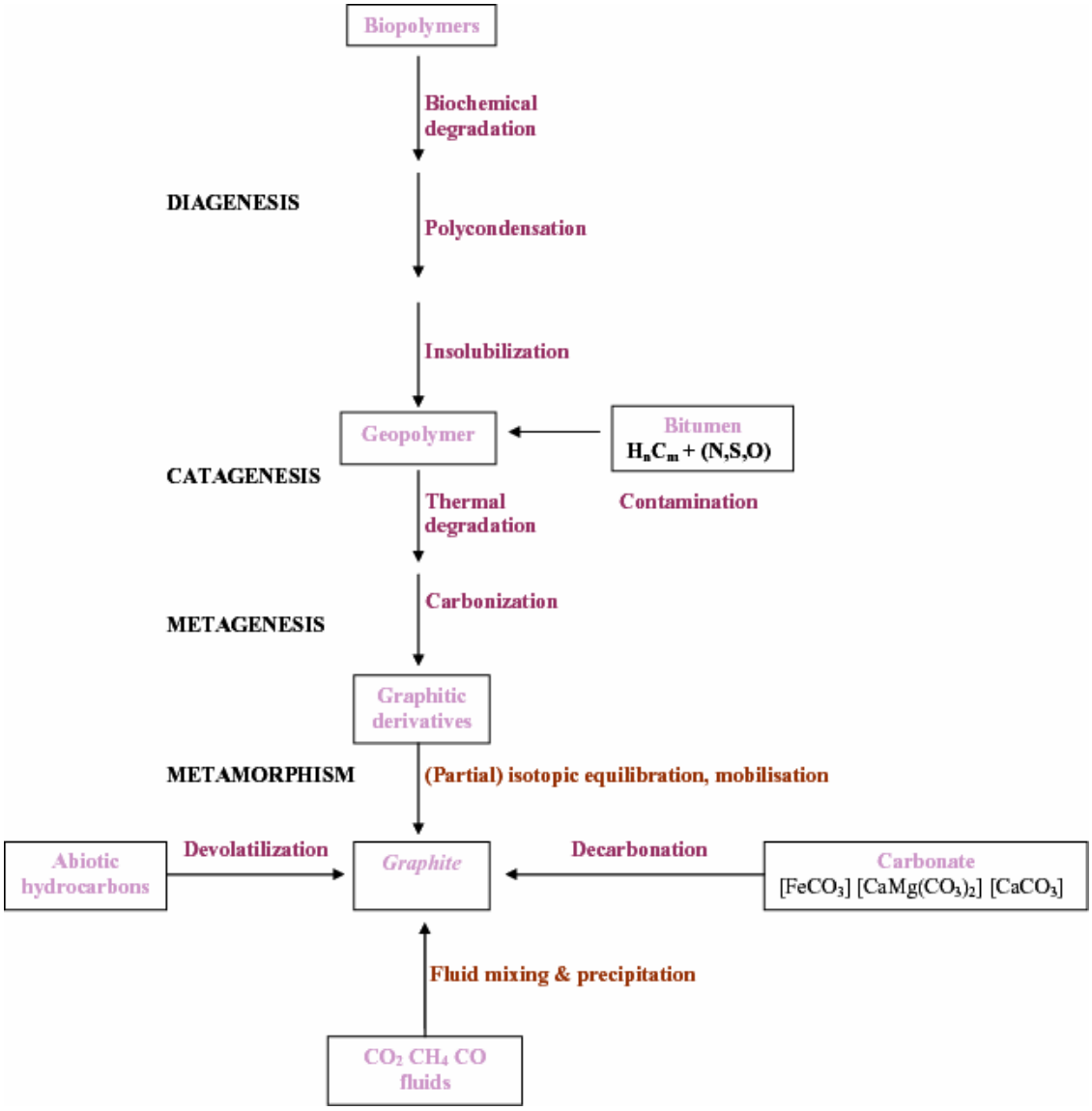

Figure 11: Generalized scheme of the evolution of organic matter (modified after Schopf, 1983).

References

Allaart, J. H., 1976. The pre-3760 m.y. old supracrustal rocks of the Isua area, central West Greenland, and the associated occurrence fo quartz-banded ironstone. In: Windley, B. F. (Ed.), *The Early History of the Earth*. Wiley, London.

Allwood, A. C., Walter, M. R., Kamber, B. S., Marshall, C. P., and Burch, I. W., 2006. Stromatolite reef from the Early Archaean era of Australia. *Nature* **441**, 714-718.

Anbar, A. D., Zahnle, K., Arnold, G. L., and Mojzsis, S. J., 2001. Extraterrestrial iridium, sediment accumulation and the habitability of the early Earth's surface. *J. Geophys. Res.* **102 [E2]**, 3219-3237.

Awramik, S. M., Schopf, J. W., and Walter, M. R., 1983. Filamentous Fossil Bacteria from the Archean of Western Australia. *Precamb. Res.* **20**, 357-374.

Banerjee, N. R., Furnes, H., Muehlenbachs, K., Staudigel, H., and de Wit, M., 2006. Preservation of similar to 3.4-3.5 Ga microbial biomarkers in pillow lavas and hyaloclastites from the Barberton Greenstone Belt, South Africa. *Earth Planet. Sci. Lett.* **241**, 707-722.

Beaumont, V. and Robert, F., 1998. Nitrogen isotopic composition of organic matter from Precambrian cherts: new keys for nitrogen cycle evolution? *Bulletin Societe geologique France* **169**, 211-220.

Beaumont, V. and Robert, F., 1999. Nitrogen isotope ratios of kerogens in Precambrian cherts: a record of the evolution of atmospheric chemistry? *Precamb. Res.* **96**, 63-82.

Blake, T. S., Buick, R., Brown, S. J. A., and Barley, M. E., 2004. Stratigraphic geochronology of a late Archaean flood basalt province in the Pilbara Craton, Australia: constraints on basin evolution, mafic and felsic volcanism and continental drift rates. *Precamb. Res.* **133**.

Bowring, S. A. and Williams, I. S., 1999. Priscoan (4.00-4.03 Ga) orthogneisses from northwestern Canada. *Contrib. Mineral. Petrol.* **134**, 3-16.

Brasier, M. D., Green, O. R., Jephcoat, A. P., Kleppe, A. K., Van Kranendonk, M., Lindsay, J. F., Steele, A., and Grassineau, N. V., 2002. Questioning the evidence for Earth's oldest fossils. *Nature* **416**, 76-81.

Brasier, M. D., Green, O. R., Lindsay, J. F., McLoughlin, N., Steele, A., and Stoakes, C., 2005. Critical testing of earth's oldest putative fossil assemblage from the similar to 3.5 Ga Apex Chert, Chinaman Creek, western Australia. *Precamb. Res.* **140**, 55-102.

Brocks, J. J., Logan, G. A., Buick, R., and Summons, R. E., 1999. Archean molecular fossils and the early rise of eukaryotes. *Science* **285**, 1033-1036.

Buick, R., Dunlop, J. S. R., and Groves, D. I., 1981. Stromatolite Recognition in Ancient Rocks - an Appraisal of Irregularly Laminated Structures in an Early Archean Chert-Barite Unit from North-Pole, Western-Australia. *Alcheringa* **5**, 161-181.

Buick, R., Thornett, J. R., McNaughton, N. J., Smith, J. B., Barley, M. E., and Savage, M., 1995. Record of emergent continental crust ~3.5 billion years ago in the Pilbara Craton of Australia. *Nature* **375**, 574-577.

Cates, N. L. and Mojzsis, S. J., 2007. Pre-3750 Ma supracrustal rocks from the Nuvvuagittuq supracrustal belt, northern Quebec. *Earth Planet. Sci. Lett.* **255**, 9-21.

Darwin, C., 1871. *The descent of man, and selection in relation to sex*. D. Appleton and company, New York.

de Wit, M. J. and Ashwal, L. D., 1997. Convergence towards divergent models of greenstone belts. In: de Wit, M. J. and Ashwal, L. D. Eds.), *Greenstone Belts*. Oxford Science, Oxford.

Eriksson, K. A., Krapez, B., and Fralick, P. W., 1994. Sedimentology of Archean Greenstone Belts - Signatures of Tectonic Evolution. *Earth-Sci Rev* **37**, 1-88.

Fischer, F., 1935. Die Synthese der Treibstoffe (Kogasin) und Schmierole aus Kohlenoxyd und Wasserstoff bei gewohnlichem Druck. *Brennstoff-Chemie* **16**, 1-11.

Fralick, P., Davis, D. W., and Kissin, S. A., 2002. The age of the Gunflint Formation, Ontario, Canada: single zircon U-Pb age determinations from reworked volcanic ash. *Can. J. Earth Sci.* **39**, 1085-1091.

Furnes, H., Banerjee, N. R., Muehlenbachs, K., Staudigel, H., and de Wit, M., 2004. Early life recorded in archean pillow lavas. *Science* **304**, 578-581.

Garvin, J., Buick, R., Anbar, A. D., Arnold, G. L., and Kaufman, A. J., 2009. Isotopic Evidence for an Aerobic Nitrogen Cycle in the Latest Archean. *Science* **323**, 1045-1048.

Grotzinger, J. P. and Knoll, A. H., 1999. Stromatolites in Precambrian carbonates: evolutionary mileposts or environmental dipsticks? *Annual Reviews of Earth and Planetary Science* **27**, 313-358.

Grotzinger, J. P. and Rothman, H. D., 1996. An abiotic model for stromatolite morphogenesis. *Nature* **383**, 423-425.

Hofmann, H. J., Grey, K., Hickman, A. H., and Thorpe, R. I., 1999. Origin of 3.45 Ga coniform stromatolites in Warrawoona Group, Western Australia. *Geol Soc Am Bull* **111**, 1256-1262.

Holland, H. D., 1978. *The chemistry of the atmosphere and oceans*. Wiley, New York.

Holland, H. D., 1984. *The chemical evolution of the atmosphere and oceans*. Princeton University Press, Princeton, N.J.

Holmes, A., 1965. *Principles of Physical Geology*. Ronald Press, New York.

Knoll, A. H. and Barghoorn, E. S., 1974. Ambient pyrite in Precambrian chert: new evidence and a theory. *Proc. Nat. Acad. Sci.* **71**, 2329-2331.

Kring, D. A. and Cohen, B. A., 2002. Cataclysmic bombardment throughout the inner solar system 3.9-4.0 Ga. *J. Geophys. Res.* **107**, 4-1 - 4-6.

Kroner, A., Hegner, E., Wendt, J. I., and Byerly, G. R., 1996. The oldest part of the Barberton granitoid-greenstone terrain, South Africa: evidence for crust formation between 3.5-3.7 Ga. *Precamb. Res.* **78**, 105-124.

Krumholz, L. R., McKinley, J. P., Alrich, G. A., and Suflita, J. M., 1997. Confined subsurface microbial communities in Cretaceous rock. *Nature* **386**, 64-66.

Kruner, A., Bryerly, G. R., and Lowe, D. R., 1991. Chronology of early Archaean granite-greenstone evolution in the Barberton Mountain Land, South Africa, based on precise dating by single zircon evaporation. *Earth Planet. Sci. Lett.* **103**, 41-54.

Lenton, T. M., 2004. Clarifying Gaia: Regulation with or without Natural Selection. In: Schneider, S. H., Miller, J. R., Crist, E., and Boston, P. J. Eds.), *Scientists debate Gaia*. MIT Press.

Lowe, D. R., 1980. Stromatolites 3400-Myr old from the Archean of Western Australia. *Nature* **284**, 441-443.

Lowe, D. R., 1983. Restricted shallow-water sedimentation of early Archean stromatolitic and evaporitic strata of the Strelley Pool Chert, Pilbara Block, Western Australia. *Precambrian Res.* **19**, 239-283.

Lowe, D. R., 1994. Abiological Origin of Described Stromatolites Older Than 3.2 Ga. *Geology* **22**, 387-390.

Mojzsis, S. J., Arrhenius, G., McKeegan, K. D., Harrison, T. M., Nutman, A. P., and Friend, C. R. L., 1996. Evidence for life on earth before 3,800 million years ago. *Nature* **384**, 55-59.

Mojzsis, S. J. and Harrison, T. M., 2002. Origin and significance of Archean quartzose rocks at Akilia, Greenland. *Science* **298**, -.

Nelson, D. R., 2004. Earth's formation and first billion years. In: Eriksson, K. A., Altermann, W., Nelson, D. R., Mueller, P. A., and Catuneanu, O. Eds.), *The Precambrian Earth: Tempos and Events*. Elsevier, Amsterdam.

Nutman, A. P., Bennett, V. C., Friend, C. R. L., and Mcgregor, V. R., 2000. The early Archaean Itsaq Gneiss Complex of southern West Greenland: The importance of field observations in interpreting age and isotopic constraints for early terrestrial evolution. *Geochim. Cosmochim. Acta* **64**, 3035-3060.

O'Neill, J., Maurice, C., Stevenson, R. K., Larocque, J., Cloquet, C., David, J., and Francis, D., 2007. The geology of the 3.8 Ga Nuvvuagittuq (Porpoise Cove) greenstone belt, northeastern Superior Province, Canada. In: van Kranendonk,

M. J., Smithies, R. H., and Bennett, V. C. Eds.), *Developments in Precambrian Geology*.

Patterson, C., 1956. Age of meteorites and the earth. *Geochim. Cosmochim. Acta* **10**, 230-237.

Pflug, H. D., 1978. Yeast-like microfossils detected in oldest sediments of the Earth. *Naturwissenschaften* **65**, 611-615.

Pflug, H. D., 1979. Archean fossil finds resembling yeasts. *Geologica et Palaeotologica* **13**, 1-8.

Pflug, H. D. and Jaeschke-Boyer, H., 1979. Combined structural and chemical analysis of 3,800-Myr-old microfossils. *Nature* **280**, 483-486.

Philippot, P., Van Zuilen, M., Lepot, K., Thomazo, C., Farquhar, J., and Van Kranendonk, M. J., 2007. Early Archaean microorganisms preferred elemental sulfur, not sulfate. *Science* **317**, 1534-1537.

Pinti, D. L. and Hashizume, K., 2001. N-15-depleted nitrogen in Early Archean kerogens: clues on ancient marine chemosynthetic-based ecosystems? A comment to Beaumont,V., Robert,F., 1999. Precambrian Res. 96, 62-82. *Precamb. Res.* **105**, 85-88.

Pinti, D. L., Hashizume, K., Orberger, B., Gallien, J. P., Cloquet, C., and Massault, M., 2007. Biogenic nitrogen and carbon in Fe-Mn-oxyhydroxides from an Archean chert, Marble Bar, Western Australia. *Geochem Geophy Geosy* **8**, -.

Quine, W. v. O., 1951. Two dogmas of empericism, *From a logical point of view*. Harvard University Press, Cambridge, Massachusetts.

Rasmussen, B., Fletcher, I. R., Brocks, J. J., and Kilburn, M. R., 2008. Reassessing the first appearance of eukaryotes and cyanobacteria. *Nature* **455**, 1101-U9.

Roedder, E., 1981. Are the 3.8 *10^9-y-old Isua objects microfossils, limonite-stained fluid inclusions, or neither? *Nature* **293**, 459-462.

Rosing, M. T., 1999. ^{13}C-depleted carbon microparticles in >3700-Ma sea-floor sedimentary rocks from west Greenland. *Science* **283**, 74-76.

Schidlowski, M., 2001. Carbon isotopes as biogeochemical recorders of life over 3.8 Ga of Earth history: evolution of a concept. *Precamb. Res.* **106**, 117-134.

Schoenberg, R., Kamber, B. S., Collerson, K. D., and Moorbath, S., 2002. Tungsten isotope evidence from ~3.8-Gyr metamorphosed sediments for early meteorite bombardment of the Earth. *Nature* **418**, 403-405.

Schopf, J. W., 1983. *Earth's Earliest Biosphere: It's Origin and Evolution.* Princeton University Press, Princeton, New Jersey.

Schopf, J. W., 1993. Microfossils of the early Archean Apex Chert: new evidence of the antiquity of life. *Science* **260**, 640-646.

Schopf, J. W., Kudryavtsev, A. B., Agresti, D. G., Wdowiak, T. J., and Czaja, A. D., 2002. Laser-Raman imagery of Earth's earliest fossils. *Nature* **416**, 73-76.

Schopf, J. W. and Packer, B. M., 1987. Early Archean (3.3-billion to 3.5-billion-year-old) microfossils from Warrawoona Group, Australia. *Science* **237**, 70-73.

Shen, Y., Buick, R., and Canfield, D. E., 2001. Isotopic evidence for microbial sulphate reduction in the early Archaean era. *Nature* **410**, 77-81.

Shen, Y., Farquhar, J., Masterson, A., and Kaufman, A. J., 2009. Evaluating the biogenicity of early Archaean sulphur cycling using quadruple isotope systematics. *Earth Planet. Sci. Lett.* **279**, 383-291.

Simonson, B. M., Byerly, G. R., and Lowe, D. R., 2004. The Early Precambrian Stratigraphic Record of Large Extraterrestrial Impacts. In: Eriksson, K. A., Altermann, W., Nelson, D. R., Mueller, P. A., and Catuneanu, O. Eds.), *The Precambrian Earth: Tempos and Events*. Elsevier, Amsterdam.

Teske, A. P., 2005. The deep subsurface biosphere is alive and well. *Trends Microbiol.* **13**, 402-404.

Ueno, Y., Isozaki, Y., Yurimoto, H., and Maruyama, S., 2001. Carbon isotopic signatures of individual Archean microfossils(?) from Western Australia. *Int Geol Rev* **43**, 196-212.

Ueno, Y., Ono, S., Rumble, D., and Maruyama, S., 2008. Quadruple sulfur isotope analysis of ca. 3.5 Ga Dresser Formation: New evidence for microbial sulfate reduction in the early Archean. *Geochim. Cosmochim. Acta* **72**, 5675-5691.

Ueno, Y., Yoshioka, H., Isozaki, Y., and Maruyama, S., 2003. Origin of 13C-depleted kerogen in ca. 3.5 Ga hydrothermal silica dikes from Western Australia*Goldschmidt*.

Ueno, Y., Yoshioka, H., Maruyama, S., and Isozaki, Y., 2004. Carbon isotopes and petrography of kerogens in similar to 3.5-Ga hydrothermal silica dikes in the North Pole area, Western Australia. *Geochim. Cosmochim. Acta* **68**, 573-589.

van Kranendonk, M. J., Webb, G. E., Kamber, B., and Pirajno, F., 2003. Geological setting and biogenicity of 3.45 Ga stromatolitic cherts, east Pilbara, Australia. *Geochim. Cosmochim. Acta* **67**, A510-A510.

van Zuilen, M., Kattathu, M., Wopenka, B., Lepland, A., Marti, K., and Arrhenius, G., 2005. Nitrogen and argon isotopic signatures in graphite from the 3.8-Ga-old Isua Supracrustal Belt, Southern West Greenland. *Geochem. Cosmochem. Acta* **69**, 1241-1252.

van Zuilen, M. A., Lepland, A., and Arrhenius, G., 2002. Reassessing the evidence for the earliest traces of life. *Nature* **418**, 627-630.

van Zuilen, M. A., Lepland, A., Teranes, J., Finarelli, J., Wahlen, M., and Arrhenius, G., 2003. Graphite and carbonates in the 3.8 Ga old Isua Supracrustal Belt, southern West Greenland. *Precamb. Res.* **126**, 331-348.

Walsh, M. M., 1992. Microfossils and possible microfossils from the Early Archean Onverwacht Group, Barberton Mountain Land, South Africa. *Precamb. Res.* **54**, 271-293.

Walsh, M. M. and Lowe, D. R., 1983. Filamentous microfossils from the 3.1-3.5 billion-year-old Swaziland Supergroup, Barberton Mountain Land, South Africa. *Abstr. XIV Lunar & Planet. Sci. Conf. Houston*, 814-815.

Walsh, M. M. and Lowe, D. R., 1985. Filamentous microfossils from the 3,500-Myr-old Onverwacht Group, Barberton Group, Barberton Mountain Land, South Africa. *Nature* **314**, 530-532.

Walter, M. R., 1980. Palaeobiology of Archaean stromatolites. In: Glover, J. E. and Groves, D. I. Eds.), *Extended Abstracts, Second International Archaean Symposium, Perth, Australia*.

Walter, M. R., Buick, R., and Dunlop, J. S. R., 1980. Stromatolites 3,400-3,500 Myr Old from the North-Pole Area, Western-Australia. *Nature* **284**, 443-445.

Westall, F., de Wit, M. J., Dann, J., van der Gaast, S., de Ronde, C. E. J., and Gerneke, D., 2001. Early Archean fossil bacteria and biofilms in hydrothermally-influenced sediments from Barberton greenstone belt, South Africa. *Precamb. Res*. **106**, 93-116.

Whitehouse, M. J., Kamber, B. S., and Moorbath, S., 1999. Age significance of U-Th-Pb zircon data from early Archaean rocks of west Greenland -a reassessment based on combined ion-microprobe and imaging studies. *Chem. Geol.* **160**, 201-224.

Wilde, S. A., Valley, J. W., Peck, W. H., and Graham, C. M., 2001. Evidence from detrital zircons for the existance of continental crust and oceans on the Earth 4.4 Gyr ago. *Nature* **409**, 175-178.

Wittgenstein, L., 1969. *Über Gewißheit (On Certainty)*. Basil Blackwell, Oxford.

Zhang, Y., 2002. The age and accretion of the Earth. *Earth Science Review* **59**, 235-263.

2A. Carbon Metabolism and Biogeochemical Cycling

This introduction serves to explain core concepts pertinent to Archaean metabolism and biogeochemical cycling.

1. Metabolism: The Basic Framework

1.1. Metabolic Classification

The validity of using carbon isotopes in the search for early life hinges on two simple assumptions, both of which are unconditionally true for all known forms of life:

(i) Early life was carbon-based; and

(ii) Early life employed metabolic processes that exerted a fractionation effect on isotopes of carbon.

The unique properties of carbon which make it a suitable building-block for life are not shared by any other element. In any event, it is safe to assume that carbon-based life today must also have evolved from a carbon-based ancestor. The second assumption is perhaps harder to justify. It is first important to distinguish between *anabolic* and *catabolic* processes, which together form the keystones of metabolism. *Anabolism* is the biological process whereby the functional and structural materials of life, such as cell components, are biosynthesized. *Catabolism*, on the other hand, involves the transformation of energy from outside sources - such as sunlight, heat or chemical bonds in molecules absorbed from the environment – into a compact and transportable form that life-sustaining reactions can use. Organisms can be categorized on the basis of catabolic and anabolic processes, as shown schematically in Figure 1.

An all-encompassing classification scheme is needed as a framework for discussion on microbial diversity. In addition to requiring energy, all known forms of life are carbon-based and require carbon as their primary macronutrient. It is for this reason that life is commonly categorized on the basis of both energy and carbon sources (Figure 1). *Photo*trophs obtain their energy from light and convert this to chemical energy as part of a process called photosynthesis. *Chemo*trophs obtain their energy from chemical compounds. The compounds used by chemotrophs may be either

organic or inorganic. In these two distinct cases the organisms are said to be chemo*organo*trophs or chemo*litho*trophs, respectively.

Carbon is derived from CO_2 in *auto*trophs and from pre-formed reduced organic compounds such as sugars in *hetero*trophs. What would be called 'chemoheterotrophs' are called 'mixotrophs' instead.

1.2. Basic Biochemical Energetics

The release and conservation of metabolic energy in living cells occurs as the result of reduction-oxidation reactions. Biological systems are thus governed by couples of electron acceptors and donors. The amount of energy released during such a redox reaction can be quantified by the 'reduction potential' (E_0') of a couple. Couples with a high (positive) E_0' have a greater tendency to accept electrons, and vice versa. A range of important biological couples, with their corresponding reduction potentials and number of electrons transferred (ne^-) is tabulated in Table 1. By way of example: in the couple $2H^+ / H_2$, which has a potential of –0.42 Volts, H_2 has a relatively large tendency to donate electrons while $2H^+$ does not easily accept them.

The role of electron and proton (H^+) flow is paramount in microbial energetics. In fact, oxidation-reduction reactions may be considered as chains of events resulting in just such a flow: (i) the removal of electrons from an electron donor; (ii) the transfer of electrons through electron carrier(s); and (iii) the addition of electrons to an electron acceptor. Examples of common biological electron carriers are the coenzymes nicotinamide-adenine dinucleotides NAD^+ and $NADP^+$, and the flavin-adenine di- and mono- nucleotides FAD^+ and FMD^+. The type of electron carrier used is not really relevant here – of interest is the nature of the electron donor and acceptor. The major types of catabolism known are summarized on the basis of their electron –donor and –acceptor in Table 2.

Much of the transfer of electrons from donors to acceptors serves the purpose of relaying energy in a compact, transportable form. Energy can then later be released to carry out biological processes. More often than not the function of energy storage itself is performed by high energy phosphate bonds, in molecules such as adenosine

triphosphate (ATP). In some cases, sulfoanhydride (thioester) bonds (found, for example, in derivatives of coenzyme A) serve a similar purpose.

Cellular energy may also be stored in an electrochemical form called the Proton Motive Force (PMF), which results from a potential difference between the intra- and extra-cellular environments. The PMF is perhaps best visualized as analogous to the potential energy present in a charged battery. Conversion between PMF-derived and ATP-derived energy occurs through the action of a membrane-associated enzyme known as ATPase. ATPase functions as a reversible proton channel between the cell exterior and cytoplasm; as protons enter, the dissipation of the PMF drives ATP synthesis from ADP + P_i – and *vice versa*.

The different metabolic strategies employed by living organisms are now compared.

2. Metabolic Diversity

2.1. Chemotrophy

2.1.1. Chemoorganotrophy

Chemotrophs derive their energy from chemical compounds, be they of organic or inorganic origin. The oxidation of organic electron donors for energy generation is known as ‘respiration’. In *aerobic respiration*, oxygen acts as the terminal electron donor. In *anaerobic respiration*, some molecule other than oxygen has to function as the terminal electron acceptor. *Fermentation* is a special type of anaerobic respiration in which an internal substrate acts as the electron acceptor.

The use of pre-formed organic fuels requires complex metabolic machinery whose operation serves the purposes of both catabolism and anabolism. That is, the oxidation of organic electron donors by chemoorganotrophs not only adds to the ATP and PMF pool but also manufactures the building blocks of life. A total of twelve essential precursor building blocks can be identified from which life can make further macromolecules. Figure 2 shows how the central pathways of metabolism responsible for chemoorganotrophy concurrently lead to the manufacture of these twelve precursor molecules. The three pathways shown are (i) the Embden-Meyerhof (‘Parnas’,

'glycolysis') pathway; (ii) the pentose phosphate pathway; and (iii) the tricarboxylic acid (TCA) cycle. All three pathways are operational during aerobic respiration. The TCA cycle in particular has major biosynthetic as well as energetic functions, and for this reason the complete cycle or major portions of it are nearly universal to life. Accordingly, it is not surprising that many organisms are able to use some of the acids produced as electron donors and carbon sources.

In the case of anaerobically respiring organisms the lack of oxygen prevents formation of certain TCA-cycle enzymes, thereby compromising the amount of reducing power generated. Manufacture of the twelve precursor molecules is still made possible through the use of *anapleurotic pathways*: enzymatic reactions or set of chemical reactions that link metabolic pathways, thereby allowing bypass of certain parts of that pathway or allowing the reversal of carbon flow. A noteworthy example of such an anapleurotic pathway is the glyoxylate cycle, which replenishes acids essential to the function of the TCA cycle using the twin enzymes isocitrate lyase and malate synthase.

Aerobic respiration allows for the continued metabolism of glucose through re-oxidation of the reduced forms of NADH and FADH produced by the central metabolic pathways. This occurs along the so-called 'electron transport chain', with oxygen as the terminal electron acceptor. The key intermediates in the electron transport chain differ from species to species, and usually include a variety of flavin enzymes, quinones and cytochrome complexes. The universal net result, however, is the generation of a PMF as protons (H^+) and hydroxyl ions (OH^-) accumulate on opposite sides of the cell membrane.

The major difference between aerobic and anaerobic respiration lies in the terminal electron acceptor used in the electron transport chain, as the electron carriers are similar in the two groups. Terminal electron acceptors used during anaerobic respiration include Fe^{3+}, SO_4^{2-}, CO_2 and NO_3^{2-}, all of which have a less favorable oxidation-reduction potential – and hence produce less ATP - than does O_2.

While it lies outside the scope of this introduction to examine in detail all assimilative and dissimilative mechanisms of anaerobic respiration, it is instructive to

study one example. The use of nitrogen-based substances in metabolism is illustrative of how anabolism and catabolism can rarely be viewed as separate processes. Figure 3 contrasts assimilative and dissimilative respiratory pathways. While both use nitrogen as a terminal electron acceptor in respiration, the former incorporates the end-product into biosynthetic matter while the latter releases the end-products as waste into the atmosphere.

2.1.2. Chemolithotrophy

As an alternative to aerobic and anaerobic respiration, many microorganisms use inorganic electron donors of geological, biological or anthropogenic origin. Examples of such electron donors include hydrogen sulfide (H_2S), hydrogen gas (H_2), ferrous iron (Fe^{2+}) and ammonia (NH_3). Hydrogen bacteria, for example, phosphorylate three molecules of ATP for every molecule of H_2 'respired' using the hydrogenase-mediated reaction:

$$H_2 \rightarrow 2H^+ + 2e^- + NAD^- (+ 3\ ADP + 3\ P_i) \rightarrow NADH^+ (+ 3\ ATP)$$

Other examples are the nitrifying bacteria, which generate ATP through oxidization of ammonia (NH_3) to nitrite (NO_2^-) or nitrite to nitrate (NO_3^-).

These chemolithotrophs rely on aerobic respiratory processes similar to those found in the electron transport chain of most chemoorganotrophs. However, while chemoorganotrophs generally rely on organic compounds such as glucose for both carbon and energy, chemolithotrophs often have to acquire their carbon elsewhere – usually from atmospheric CO_2 or (more rarely) from CH_4.

2.2. Phototrophy

The term 'photosynthesis' refers first and foremost to the conversion of energy in electromagnetic radiation (light) into chemical energy. Additionally, 'photosynthesis' implies an anabolic function; namely, the use of aforementioned chemical energy to 'fix' carbon into structural and functional cell components. The vast majority of photosynthetic organisms use CO_2 as their sole carbon source.

Photoheterotrophs, insignificant on a global scale, use organic compounds as a carbon source. Today, CO_2 is readily available in most environments and was probably never a limiting metabolic agent during the Earth's history.

In addition to carbon and energy, photoautotrophs require input of electrons from a donor (or 'reducing power') in order to fix CO_2. Care should be taken to distinguish this *anabolic* energy-tapping electron flow for the purpose of carbon fixation from that involved in *catabolic* energy generation discussed previously. Commonly, reducing power is generated by the oxidation of water to oxygen in the presence of light. This type of photosynthesis is called **oxygenic** photosynthesis. The production of reducing power in **anoxygenic** photosynthesis, on the other hand, rarely requires light and involves an oxidative reaction (but not oxygen production) such as H_2S -> S^0 and S^0 -> SO_4^{2-}.

Photosynthesis can be categorized into distinct catabolic and anabolic phases. During the 'light reaction' phase ATP and NADPH are synthesized, while fixation of CO_2 into cellular carbon takes place during the 'dark reaction' phase. Two structural types of light-harvesting pigments are commonly used (Allen, 2002):

(i) Isoprenoids, such as the carotenoid β-carotene;

(ii) Tetrapyrroles, which are classed as:

- Bile pigments such as phycobiliproteins used by cyanobacteria and red algal chloroplasts;
- Porphyrins such as chlorophylls and bacteriochlorophylls.

It is important to distinguish between oxygenic and anoxygenic photosynthesis on the level of biochemical processes within the cell. All known oxygenic photosynthesizers make use of a cyclic, anoxygenic pathway called Photosystem I. A similar system is used by anoxygenic photosynthesizers, such as green sulfur bacteria, purple bacteria and *Heliobacterium*. Although the carriers associated with light-induced electron and energy flow in these systems are often species-specific, a general flow summary is instructive:

- Electromagnetic radiation provides the excitation energy needed to activate the *photoreaction center*, turning it into a strong electron donor;
- Subsequent electron flow drives the formation of ATP through phosphorylation of ADP;
- Electron flow through a *quinone* pool leads to charging of NAD(P)H from $NAD(P)^+$;
- Specific *cytochrome* complexes, with the aid of an external electron donor, help energize another photoreaction center;
- Cyclic phosphorylation through electron flow proceeds.

Oxygenic photosynthesizers make use of an additional pathway called Photosystem II, giving rise to the 'Z scheme'. This pathway entails the light-driven breakdown of water into oxygen and hydrogen through *non-cyclic* phosphorylation: the electrons released are used to excite a Photosystem II reaction center before passing into and thus linking the Photosystem I cycle described above. A summary of the main types of photosynthesis is presented in Table 3.

2.3. Auto- and methano- trophy

Having briefly discussed how both phototrophs and chemotrophs make energy and electrons available for carbon fixation, carbon fixation itself can now be examined. Several pathways of biological carbon fixation in which CO_2 or CH_4 are converted into living biomass are known, and tabulated in Table 4.

As implied by the table, the majority of autotrophs make use of the Calvin Benson Cycle, also known as the C_3 pathway or reductive pentose cycle (Allen, 2002), in order to fix CO_2 into cellular carbon. This occurs during the 'dark reaction' phase of photosynthesis. Two other less commonly used mechanisms are the reverse tricarboxylate cycle and the carbon monoxide pathway (Levin et al., 2002).

2.4. Summary of Metabolism

The large array of metabolic types known may, at first, seem overwhelming to the astrobiologist aspiring to understand the range of plausible extraterrestrial biochemistries. However, our preceding discussion reveals several dominant conceptual trends underlying the process of metabolism. These trends prevail irrespective of metabolic type, and may be summarized as shown in Figure 4. The living world shows a rich diversity in metabolic processes. However, perhaps just as remarkable is the ubiquity of key features inherent to metabolism, such as:

- An electron -donor, -carrier and -acceptor responsible for dissimilatory energy conversion using reduction-oxidation reactions. (The electron donor or acceptor may be internal, as is the case in phototrophism and fermentative chemotrophism respectively);
- The use of phosphate bonds for energy storage, transport and release;
- The creation and maintenance of a structural boundary isolating the site of metabolism from the environment;
- The reliance on this boundary for the storage of electrochemical energy, precursor metabolites and carbon-based building blocks.

3. Sources, Sequestration, and Preservation of Organic Matter

Marine, rather than terrestrial, settings dominate both the Early Archaean rock record and contemporary carbon burial alike. Today, only a minor fraction of dead organic matter is preserved in the rock record. Modern oceanic productivity and sediment burial rates of $50 \cdot 10^{15}$ and $0.16 \cdot 10^{15}$ gC yr^{-1} respectively imply average marine preservation efficiencies under 0.5% (Hedges and Keil, 1995). The vast majority (99.0 – 99.9% according to Ronov, 1990) of organic matter that sinks towards the sediment-water interface is recycled back into the biosphere and atmosphere through decomposition. Most (~ 94%) of modern carbon burial occurs in deep-water continental-margin sediments, while only ~ 6% is buried seaward of continental rises (Berner, 1989). Despite their geographical extent, only ~ 4% of burial occurs beneath low-productivity pelagic zones.

Meanwhile, it has long been argued (e.g. Veizer and Hoefs, 1976; Perry and Ahmad, 1977; Schidlowski, 2001) that the lack of long-term variation exhibited by the marine sedimentary organic carbon record, contended by some to hold fast to a steady mean value of 0.5 wt.% organic matter, attests to the persistence of autotrophy since 3.8 Ga (Figure 5). However, several factors control the relative amounts and proportions of organic carbon buried in marine sediments. Today, these include the sedimentation rate (Stein, 1990; Betts and Holland, 1991), overlying primary productivity (Calvert and Pederson, 1992b), organic carbon rain- (or 'irrigation-') rate (Jahnke, 1990), organic carbon degradation rate (Emerson, 1985), bottom-water oxygen concentration (Paropkari et al., 1992; Hartnett and Devol, 2003), and oxygen exposure time (Hartnett et al., 1998).

Now, if widespread Early Archaean-onward autotrophy is assumed (Chapters 4, 5, 6) along with a steady organic carbon preservation rate, continuous complex heterotrophic biology may need to be invoked to account for the persistently low particulate PNC_{org} ('PNC': phosphate – nitrogen – carbon) influx into the lithospheric reservoir. Alternatively, the Archaean may have presented a radically different environment for carbon deposition and preservation. The three major potential differences that may be expected to have affected Archaean carbon cycling are (i) the chemistry of the ocean-atmosphere system; (ii) the ecology and metabolic characteristics of the Archaean biota; and (iii) greater influence of hydrothermal activity on Archaean seawater.

3.1. The pre-eminence of electron acceptors

Relative respiratory contributions of the dominant electron acceptors in contemporary marine sedimentary environments are 17 ± 15%, 18 ± 10% and 62 ± 15% respectively for oxygen, ferric iron and sulphate (Thamdrup and Canfield, 2000). Within the sediment column, bacterial cell densities are highest in the oxic zone (Rusch et al., 2003). These observations may hold little implications for Archaean biogeochemistry, however, as the ultimate oxidizing agent for Fe(III), SO_4^{2-} and other potent anaerobic electron acceptors (Mn(IV), NO_x^-) is photosynthesis-derived O_2, in

which the Archaean ocean was largely deficient (Holland, 2002; Canfield, 2005), with the possible exception of transiently oxygenated surface waters (see discussion in Chapter 5).

The importance of oxygen in organic matter preservation has been a topic of intense debate (Froelich et al., 1979; Reimers and Jr., 1986; Reimers et al., 1986; Archer et al., 1989; Archer and Devol, 1992; Hales et al., 1994). Two schools of thought may be distinguished. One school argues that preservation is largely independent of bottom water oxygen concentration, and depends primarily on the carbon supply, or 'rain rate' (Henrichs and Reeburgh, 1987; Pedersen and Calvert, 1990; Calvert et al., 1992; Calvert and Pederson, 1992a; Ganeshram et al., 1999). The second school recognizes a dominant role for oxygen (Pratt, 1984; Canfield, 1989; Paropkari et al., 1992; Canfield, 1993; Hedges and Keil, 1995; Hartnett, 1998; Hartnett et al., 1998; Hedges et al., 1999; Hoefs et al., 2002; Hartnett and Devol, 2003). More recently, members of the former group have attempted reconciliation by proposing a partial role of oxygen (Cowie et al., 1999), while a threshold O_2 concentration was put forward by adherents of the latter group (Canfield, 1994).

In aerobic environments the concentration of oxygen in sediments drops exponentially from a maximum level at the sediment/water interface, where the value is determined by the overlying O_2 concentration at the base of the water column (Figure 7). In areas that are carbon-limited, such as large parts of the deep ocean, the O_2 concentration levels off to some minimum value at a sediment depth where all metabolizable carbon has been oxidized (Grundmanis and Murray, 1982; Murray and Kuivila, 1990). In slope and shelf environments, which are typically oxygen-limited, the O_2 concentration falls under detection limits below the so-called 'oxygen penetration depth'. Typical penetration depths for O_2 in modern shallow-marine environments are in the range of millimeters.

The following modern suboxic and anoxic environments may provide insight into Archaean processes: (i) extensive stretches of sea floor exposed to permanent and severe oxygen depletion, such as where mid-water oxygen minima intercept continental margins (along much of the eastern Pacific Ocean, off west Africa, and in

the Arabian Sea and Bay of Bengal (Helly and Levin, 2004); (ii) anoxic stratified marine and lacustrine basins such as the Black Sea (Murray et al., 1995; Wakeham et al., 2004; Hiscock and Millero, 2006; Yakushev et al., 2006; Wakeham et al., 2007), the Cariaco Trench (Galimov, 2004; Wakeham et al., 2004) and Kyllaren fjord (van Breugel et al., 2005); and (iii) lakes where chemistry is constrained to an Archaean-like state by local geology. These low-oxygen settings suffer from variably from the effects of bioturbation and irrigation, which are not to be underestimated when seeking Archaean analogies (Martin and Banta, 1992). The major problem with this actualistic uniformitarian approach is that aquatic biogeochemical cycling is strongly coupled to the atmosphere, and there are obviously no terrestrial analogies to high Archaean pCO_2 (and perhaps pCH_4) systems.

3.2. Microbial Ecology

The amount of carbon sequestered within prokaryotic biomass in the open ocean and oceanic subsurface is globally significant, and has been estimated at ~11 and ~310 PgC respectively (Whitman et al., 1998). The bulk of organic matter in aquatic environments is macromolecular in nature and not ready for direct incorporation into bacterial or archaeal cells. Instead, this material has to be 'preconditioned' by extracellular enzymes (i.e. those found outside the cytoplasmic membrane, as defined by Priest (1984) before becoming available for growth and nutrient cycles (Hoppe, 1993). Such enzymes are produced almost exclusively by prokaryotes (Hollibaugh and Azam, 1983).

4. Conclusion

In addition to sourcing both insoluble and soluble electron acceptors, overlying productivity is also the ultimate driving force behind organic carbon production in today's oceans. Although hydrothermal systems may have played an appreciable role in the latter (Baross and Hoffman, 1985), they are thermodynamically precluded from the former. However, no Archaean mid-ocean-ridge hydrothermal vent systems appear to have been preserved. For these reasons, Archaean benthic environments sampling

the surface ocean provide the best available environment to examine geological evidence for ancient biogeochemical cycling. The following chapters present findings from the three oldest preserved benthic environments on Earth: the ~3.7 Ga Isua Supracrustal Belt in southwest Greenland, the ~3.52 Ga Counterunah Subgroup in northwest Australia, and the ~3.45 Hooggenoeg Formation in South Africa. Shallow marine sediments of the ~3.45 Ga Strelley Pool Chert formation, meanwhile, hold crucial insights allowing direct comparison between the Archaean surface and benthic biogeochemical environments.

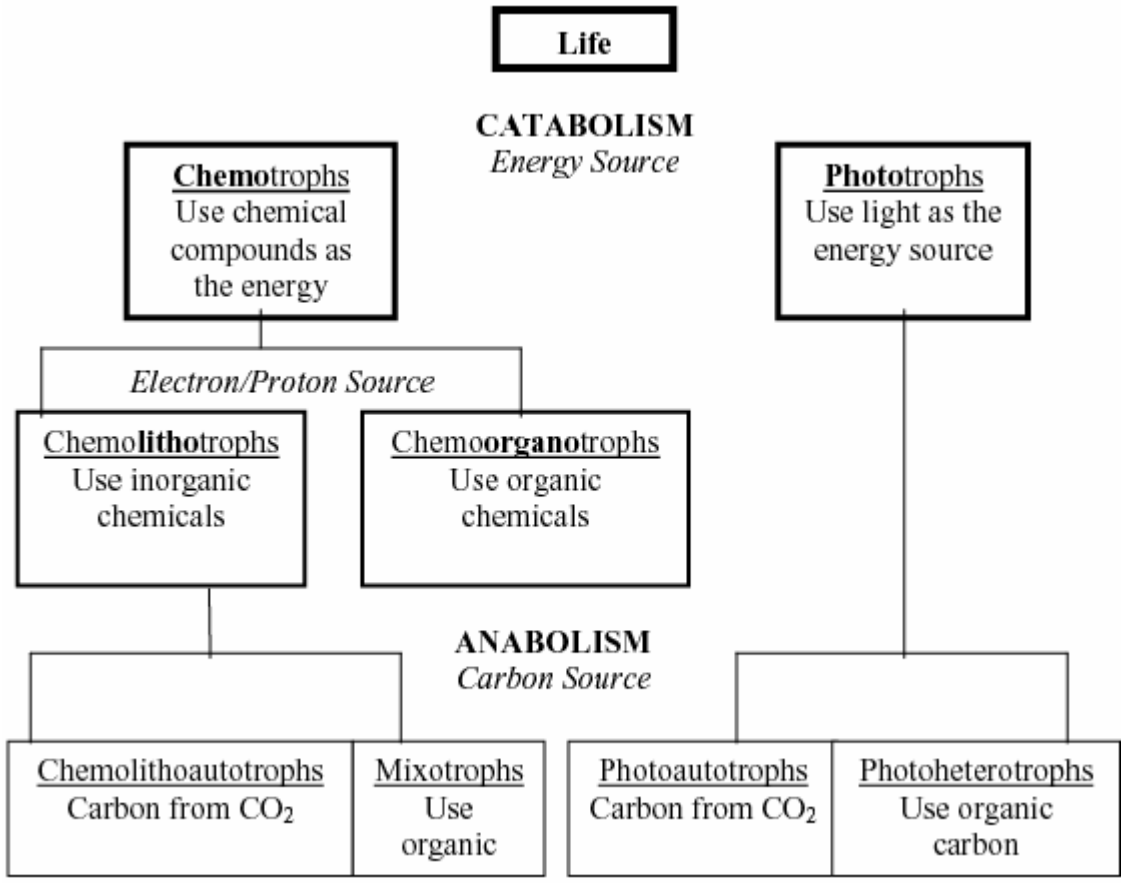

Figure 1: Classification of life in terms of metabolic energy- and carbon sources.

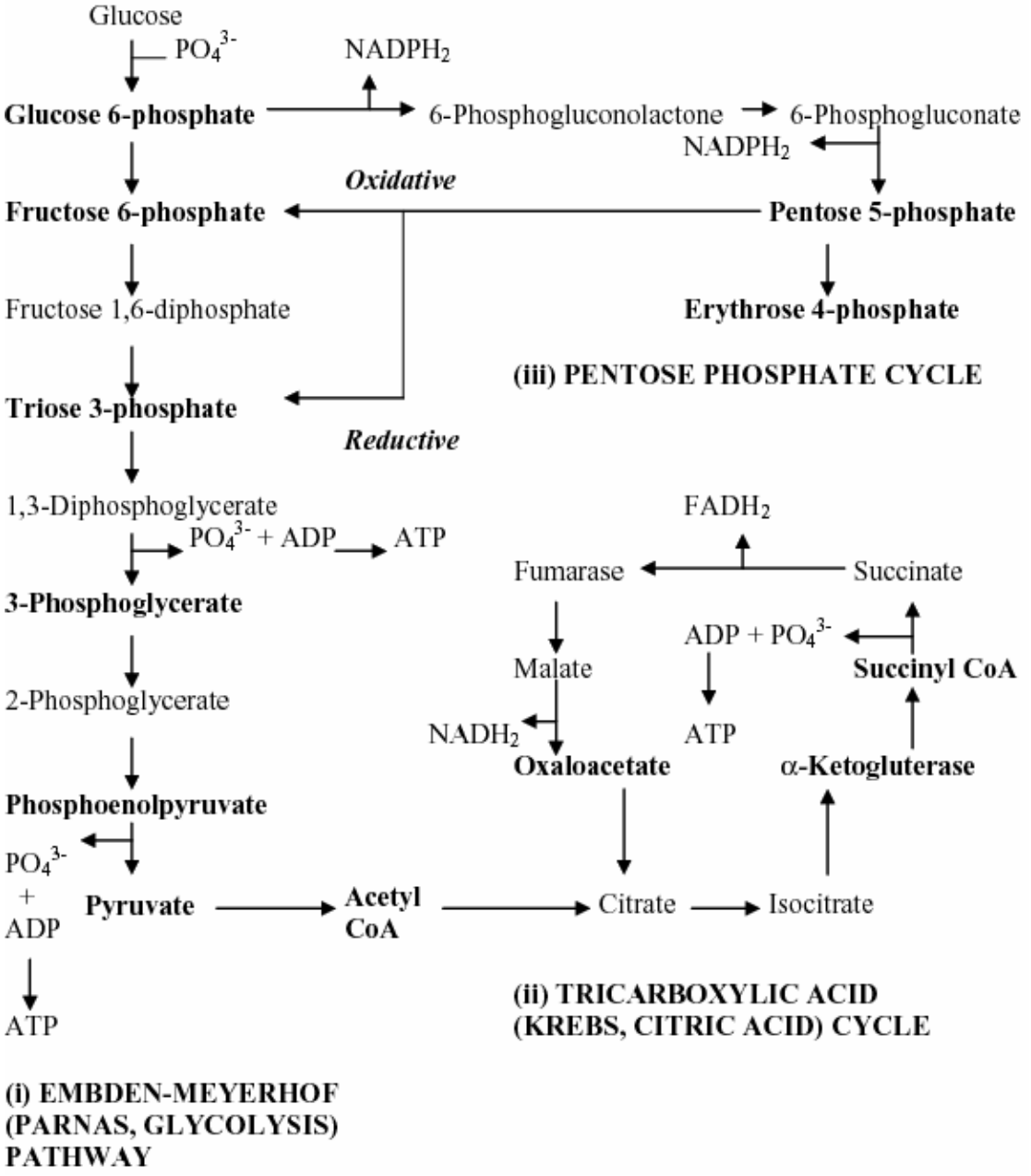

Figure 2: Central fueling and biosynthetic pathways aerobic heterotrophy: (i) The Embden-Meyerhof Pathway; (ii) The tricarboxylic acid cycle; and (iii) The pentose phosphate cycle. The oxidative and reductive branches of the pentose phosphate cycle are shown in ***boldface italics***. Anapleurotic reactions and peripheral pathways (including fermentative and respiratory pathways) are not shown. The 12 precursor metabolites are shown in **boldface**.

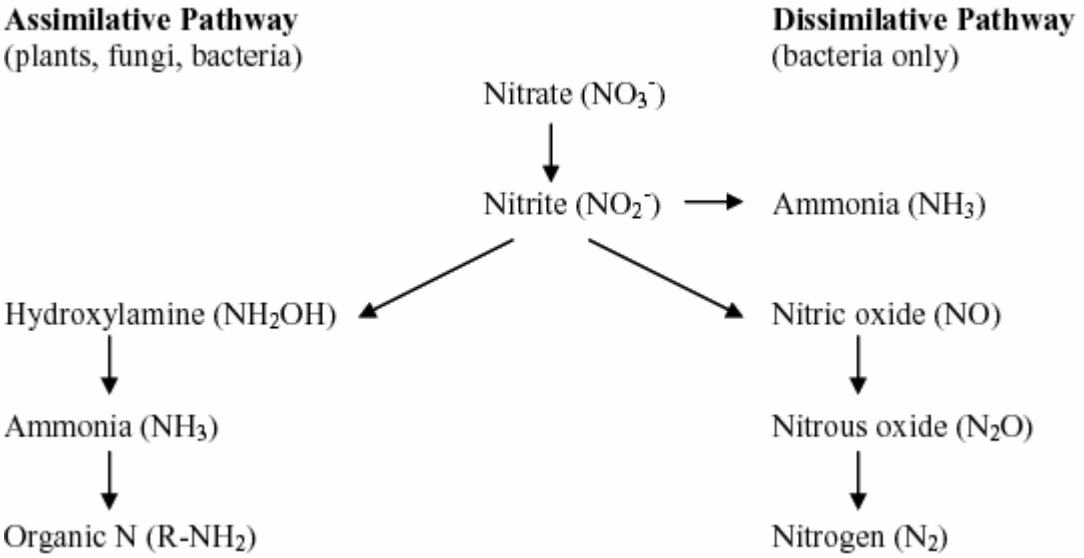

Figure 3: Assimilatory and dissimilatory pathways involving nitrogenous terminal electron acceptors.

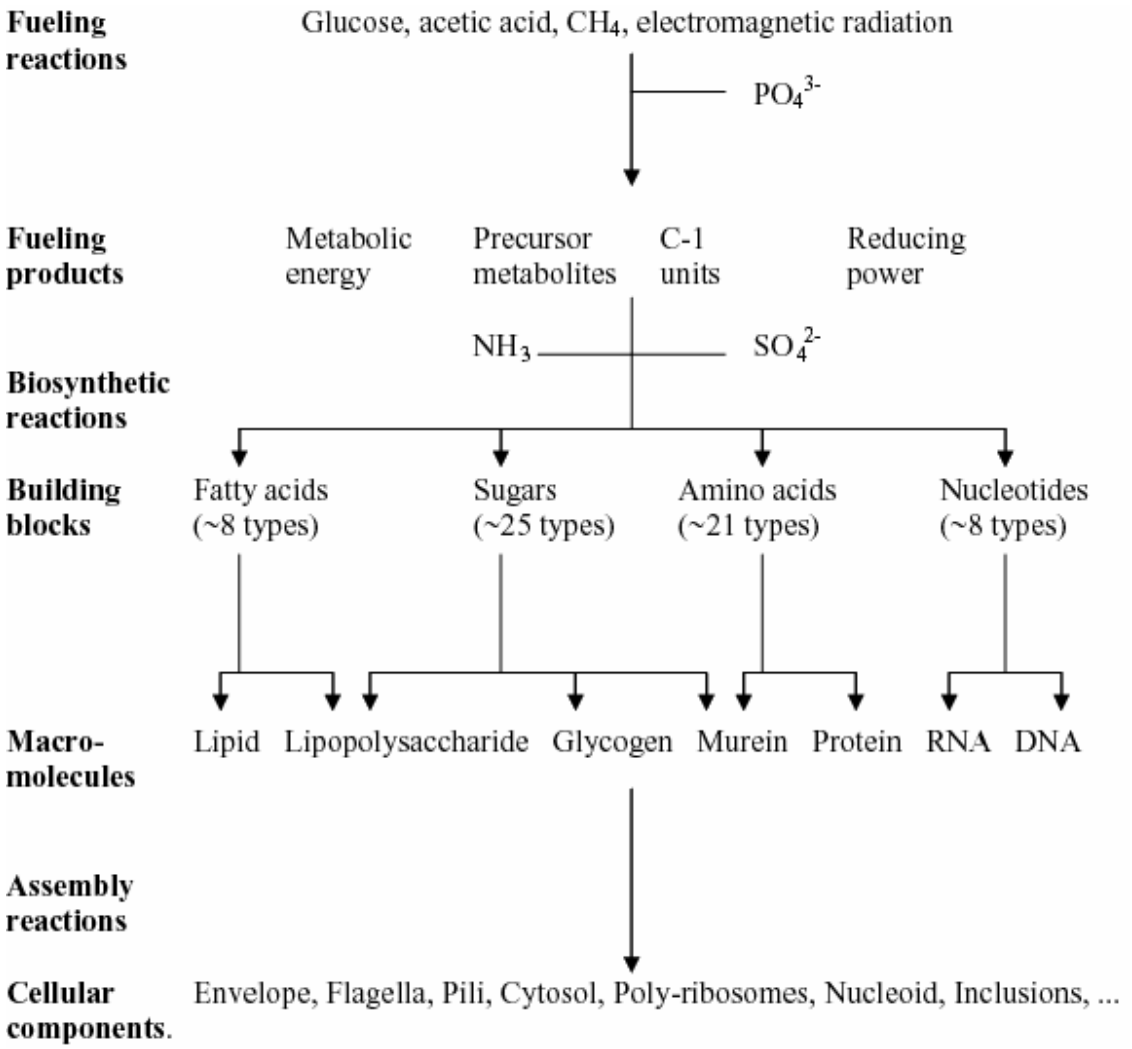

Figure 4: Schematic overview of metabolism.

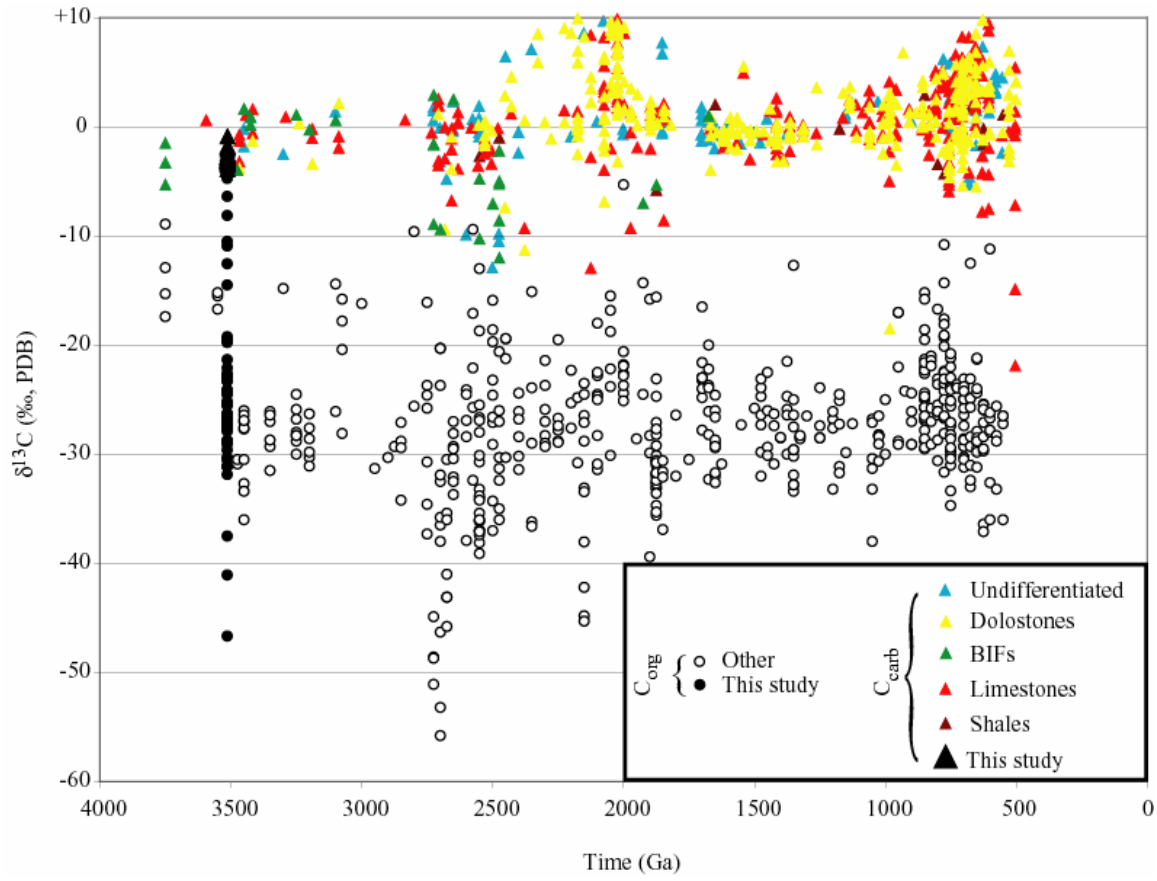

Figure 5: The carbon isotope record over time.

Table 1: Redox couples important to biological systems. Reduction potential given at standard conditions of temperature, pressure, concentration and pH (after Thauer et al., 1977).

e^- acceptor (oxidant)	**e^- donor (reductant)**	**Reduction potential $[E_0']$ (V)**	***n*e^-**
CO_2	Glucose	-0.43	24
$2H^+$	H_2	-0.42	2
CO_2	Methanol	-0.38	6
NAD^+	NADH	-0.32	2
CO_2	Acetate	-0.28	8
S^0	H_2S	-0.28	2
SO_4^{2-}	H_2S	-0.22	8
Pyruvate	Lactate	-0.19	2
$S_4O_6^{2-}$	$S_2O_3^{2-}$	+0.024	2
Fumarate	Succinate	+0.03	2
Cytochrome b_{ox}	Cytochrome b_{red}	+0.035	1
$Ubiquinone_{ox}$	$Ubiquinone_{red}$	+0.11	2
Cytochrome c_{ox}	Cytochrome c_{red}	+0.25	1
Cytochrome a_{ox}	Cytochrome a_{red}	+0.39	1
NO_3^-	NO_2^-	+0.42	2
NO_3^-	N_2	+0.74	5
Fe^{3+}	Fe^{2+}	+0.76	1
$½O_2$	H_2O	+0.82	2

Table 2: Major types of catabolism, with their corresponding electron –donor and –acceptor. Organic e^- donors (carbohydrates) denoted by $(CH_2O)_n$ (after Hardie, 2000).

Process	**Organism**	**Electron Donor(s)**	**Electron Acceptor(s)**
Respiration	Methanogen	H_2, $(CH_2O)_n$	CO_2
	Acetogen	H_2, $(CH_2O)_n$	CO_2
	Sulfate reducer	H_2S, CH_3SH	Sulfate, SO_4^{2-}
	Sulfur reducer	H_2S, CH_3SH	Sulfur, S^0
	Iron reducer	H_2, $(CH_2O)_n$	Ferric Iron, Fe^{3+}
	Denitrifier	N_2, N_2O, NO, NO_2^-	Nitrate, NO_3^-
	Aerobe	$(CH_2O)_n$	Oxygen, O_2
Photosynthesis	Photosynthesizer	Light-driven complexes	Cytochrome, Ubiquinone
Fermentation	Fermenter	$(CH_2O)_n$	Internal: Lactate

Table 3: Major types of photosynthesis.

	Eukaryotes	**Prokaryotes**		
		Cyanobacteria	**Purple bacteria**	**Green bacteria**
Electron donors	H_2O	H_2O, some can use H_2S	H_2S, S^0, H_2, S_2O_3, organic compounds	H_2S, S^0, H_2, S_2O_3, organic compounds
Site of photosynthesis	Thylakoids	Thylakoids	Cell membrane	Cytochromes
Oxygenic	Yes	Yes	No	No
Chlorophyll type	Chlorophyll a	Chlorophyll a	Bacteria-chlorophyll a and b	Bacteria-chlorophyll a and c, d, or e
Photosystem I	Present	Present	Similar	Similar
Photosystem II	Present	Present	Absent	Absent

Table 4: Anabolic pathways used to convert CO_2 and CH_4 into biosynthetic end-products (after Schidlowski, 2001).

(1) CO_2 + ribulose-1,5-biphosphate → phosphoglycerate
- Green plants [Green plants relying on reaction (1) exclusively are termed C3 plants]
- Eukaryotic algae
- Cyanobacteria
- Purple photosynthetic bacteria (Chromatiaceae)
- Purple nonsulfur bacteria (Rhodospirillaceae)
- Chemoautotrophic bacteria

(2) CO_2/HCO_3^- + phosphoenolpyruvate/pyruvate → oxaloacetate
- Green plants [C4 and CAM plants combine reactions (2) and (1)]
- Anaerobic bacteria
- Facultatively aerobic bacteria

(3) $CO_2 + CO_2$ → acetyl coenzyme A/acetate
- Green photosynthetic bacteria (Chlorobiacceae) [via succinyl coenzyme A and α-ketoglutarate]
- Anaerobic bacteria (Acetobacterium woodii, Clostridium acidiurici)
- Methanogenic bacteria [via C1 acceptors]

(4) CO_2 + acetyl coenzyme A → pyruvate/phosphoenolpyruvate
- Green photosynthetic bacteria (Chlorobiacceae) [combine reactions (2), (3) and (4)]
- Clostridium kluyveri
- Autotrophic sulfate reducing bacteria
- Methanogenic bacteria

(5) CH_4 → formaldehyde (HCHO)
HCHO + ribulose monophosphate → hexulose monophosphate
- Type I methanotrophic bacteria

(6) CH_4 → formaldehyde (HCHO)
HCHO + glycine → serine
- Type II methanotrophic bacteria

Table 5: Major reservoirs of inorganic and organic carbon on the modern Earth (modified after a compilation in Hedges and Keil, 1995).

Reservoir		**Size** (x 10^{18} gC)	**Reference**
Sedimentary rocks			
Inorganic	Carbonates	60 000	Berner and Lasaga (1989)
Organic	Kerogen, coal, etc.	15 000	
Active (surficial) pools			
Inorganic	Marine DIC[1]	38	Olsen et al. (1985)
	Soil carbonate	1.1	
	Atmospheric CO_2	0.66	
Organic	Soil humus	1.6	
	Land plant tissue	0.95	
	Marine DOC[2]	0.60	Williams and Druffel (1987)
	Surface marine sediments	0.15	Emerson and Hedges (1988)

[1]DIC (Dissolved Inorganic Carbon) refers to the combined water-soluble components $CO_2 + CO_3^{2-} + HCO_3^- + H_2CO_3$.

[2]DOC (Dissolved Organic Carbon) refers to biologically derived water-soluble carbon-containing molecules.

Table 6: Absolute (x 10^{12} gC yr^{-1}) and relative (% of total burial) organic carbon burial rates in different aquatic environments (modified after Hedges and Keil, 1995).

Sediment type	***Depositional environment***				
	Deltaic	**Shelf**	**Slope**	**Pelagic**	**Total**
Deltaic sediments	70 (44%)	-	-	-	**70 (44%)**
Shelf- and upper slope sediments	-	68 (42%)	-	-	**68 (42%)**
High-productivity, biogenous sediments	-	-	7 (4%)	3 (2%)	**10 (6%)**
Shallow-water carbonates	-	6 (4%)	-	-	**6 (4%)**
Low-productivity, pelagic sediments	-	-	-	5 (3%)	**5 (3%)**
Anoxic basins (e.g. Black Sea)	-	1 (0.5%)	-	-	**1 (0.5%)**
All types	70 (44%)	75 (46.5%)	7 (4%)	8 (5%)	**160 (~100%)**

References

Allen, J. F., 2002. Photosynthesis of ATP - electrons, proton pumps, rotors and poise. *Cell* **110**, 349-360.

Archer, D. and Devol, A., 1992. Benthic Oxygen Fluxes on the Washington Shelf and Slope - a Comparison of Insitu Microelectrode and Chamber Flux Measurements. *Limnol. Oceanogr.* **37**, 614-629.

Archer, D., Emerson, S., and Smith, C. R., 1989. Direct Measurement of the Diffusive Sublayer at the Deep-Sea Floor Using Oxygen Microelectrodes. *Nature* **340**, 623-626.

Baross, J. A. and Hoffman, S. E., 1985. Submarine Hydrothermal Vents and Associated Gradient Environments as Sites for the Origin and Evolution of Life. *Origins Life Evol. Biosph.* **15**, 327-345.

Berner, R. A., 1989. Biogeochemical cycles of carbon and sulfur and their effect on atmospheric oxygen over Phanerozoic time. *Palaeogeography, Palaeoclimatology and Palaeoecology* **73**, 97-122.

Berner, R. A. and Lasaga, A. C., 1989. Modeling the Geochemical Carbon-Cycle. *Sci. Am.* **260**, 74-81.

Betts, J. N. and Holland, H. D., 1991. The oxygen content of ocean bottom waters, the burial efficiency of organic carbon, and the regulation of atmospheric oxygen. *Palaeogeography; Palaeoclimatology; Palaeoecology* **97**, 5-18.

Calvert, S. E., Bustin, R. M., and Pedersen, T. F., 1992. Lack of Evidence for Enhanced Preservation of Sedimentary Organic-Matter in the Oxygen Minimum of the Gulf of California. *Geology* **20**, 757-760.

Calvert, S. E. and Pederson, T. F., 1992a. Organic matter accumulation , remineralization and burial in an anoxic coastal sediment. In: Whelan, J. and Farrington, J. W. Eds.), *Organic carbon accumulation and preservation in marine sediments: How important is Anoxia*. Columbia University Press, New York.

Calvert, S. E. and Pederson, T. F., 1992b. Organic matter accumulation, remineralization and burial in an anoxic coastal sediment. In: Whelan, J. and Farrington, J. W. Eds.), *Organic carbon accumulation and preservation in marine sediments: How important is Anoxia*. Columbia University Press, New York.

Canfield, D., 2005. The early history of atmospheric oxygen. *Annual Review of Earth and Planetary Sciences* **33**, 1-36.

Canfield, D. E., 1989. Sulfate reduction and oxic respiration in marine sediments: implications for organic carbon preservation in euxinic environments. *Deep-Sea Res.* **36**, 121-138.

Canfield, D. E., 1993. Organic matter oxidation in marine sediments. In: Wollast, R., Chou, L., and Mackenzie, F. Eds.), *Interactions of C,N,P, and S biogeochemical cycles*. NATO-ARW.

Canfield, D. E., 1994. Factors influencing organic carbon preservation in marine sediments. *Chem. Geol.* **114**, 315-329.

Cowie, G. L., Calvert, S. E., Pedersen, T. F., Schulz, H., and von Rad, U., 1999. Organic content and preservational controls in surficial shelf and slope sediments from the Arabian Sea (Pakistan margin). *Mar Geol* **161**, 23-38.

Emerson, S. E. and Hedges, J. H., 1988. Processes controlling the organic carbon content of open ocean sediments. *Paleooceanography* **3**, 621-634.

Emerson, S. R., 1985. Organic carbon preservation in marine sediments. In: Sundquist, E. T. and Broecker, W. S. Eds.), *The Carbon Cycle and Atmospheric CO_2: Natural Variations Archean to Present.* Amer. Geophys. Union., Washington, D.C.

Froelich, P. N., Klinkhammer, G. P., Bender, M. L., Luedtke, N. A., Heath, G. R., Cullen, D., Dauphin, P., Hammond, D., Hartman, B., and Maynard, V., 1979. Early Oxidation of Organic-Matter in Pelagic Sediments of the Eastern Equatorial Atlantic - Suboxic Diagenesis. *Geochim. Cosmochim. Acta* **43**, 1075-1090.

Galimov, E. M., 2004. The pattern of delta C-13(org) versus HI/OI relation in recent sediments as an indicator of geochemical regime in marine basins: comparison of the Black Sea, Kara Sea, and Cariaco trench. *Chem. Geol.* **204**, 287-301.

Ganeshram, R. S., Calvert, S. E., Pedersen, T. F., and Cowie, G. L., 1999. Factors controlling the burial of organic carbon in laminated and bioturbated sediments off NW Mexico: Implications for hydrocarbon preservation. *Geochim. Cosmochim. Acta* **63**, 1723-1734.

Grundmanis, V. and Murray, J. W., 1982. Aerobic respiration in pelagic marine sediments. *Geochem. Cosmochim. Acta* **46**, 1101-1120.

Hales, B., Emerson, S. E., and Archer, D., 1994. Respiration and dissolution in the sediments of the western North Atlantic: estimates from models of *in situ* microelectrode measurements of porewater oxygen and pH. *Deep-Sea Res.* **41**, 695-719.

Hardie, D. G., 2000. Metabolic control: a new solution to an old problem. *Curr. Biol.* **10**, 757-759.

Harnmeijer, J., Orcutt, B., Devol, A., and Joye, S., 2005. Quantifying the role of manganese in biotic and abiotic nitrogen cycling. *Geochim. Cosmochim. Acta* **69**, A581-A581.

Hartnett, H. E., 1998. Organic carbon input, degradation and preservation in continental margin sediments: an assesment of the role of a strong oxygen deficient zone. Ph.D., University of Washington.

Hartnett, H. E. and Devol, A. H., 2003. The role of a strong oxygen deficient zone in the preservation and degradation of organic matter: a carbon budget for the continental margins of NW Mexico and Washington. *Geochim. Cosmochim. Acta* **67**, 247-264.

Hartnett, H. E., Keil, R. G., Hedges, J. I., and Devol, A. H., 1998. Influence of oxygen exposure time on organic carbon preservation in continental margin sediments. *Nature* **391**, 572-536.

Hedges, J. I., Hu, F. S., Devol, A. H., Hartnett, H. E., Tsamakis, E., and Keil, R. G., 1999. Sedimentary organic matter preservation: A test for selective degradation under oxic conditions. *Am. J. Sci.* **299**, 529-555.

Hedges, J. I. and Keil, R. G., 1995. Sedimentary organic matter preservation: an assessment and speculative synthesis. *Mar. Chem.* **49**, 81-115.

Helly, J. J. and Levin, L. A., 2004. Global distribution of naturally occurring marine hypoxia on continental margins. *Deep-Sea Res. Part I Oceanogr. Res. Pap.* **51**, 1159-1168.

Henrichs, S. M. and Reeburgh, W., 1987. Anaerobic mineralization of marine sediment organic matter: Rates and the role of anaerobic porcesses in the oceanic carbon economy. *Geomicrobiology J.* **5**, 191-237.

Hiscock, W. T. and Millero, F. J., 2006. Alkalinity of the anoxic waters in the Western Black Sea. *Deep-Sea Res Pt Ii* **53**, 1787-1801.

Hoefs, M. J. L., Rijpstra, W. I. C., and Damste, J. S. S., 2002. The influence of oxic degradation on the sedimentary biomarker record I: Evidence from Madeira Abyssal Plain turbidites. *Geochim. Cosmochim. Acta* **66**, 2719-2735.

Holland, H. D., 2002. Volcanic gases, black smokers, and the Great Oxidation Event. *Geochemica et Cosmochimica Acta* **66**, 3811-3826.

Hollibaugh, J. T. and Azam, F., 1983. Microbial-Degradation of Dissolved Proteins in Seawater. *Limnol. Oceanogr.* **28**, 1104-1116.

Hoppe, H. G., 1993. Use of Fluorogenic Model Substrates for Extracellular Enzyme Activity (EEA) Measurement of Bacteria. In: Kemp, A. E., Shen, Y., Sherr, B., and Cole, D. R. Eds.), *Handbook of Methods in Aquatic Microbial Ecology*. Lewis.

Jahnke, R. A., 1990. Early diagenesis and recycling of biogenic debris at the seafloor, Santa Monica Basin, California. *J. Mar. Res.* **48**, 413-436.

Levin, M., Thorlin, R., Kenneth, R. R., Taisaku, N., and Mercola, M., 2002. Assymmetries i H+/K+-ATPase and cell membrane potentials comprise a very early step in left-right patterning. *Cell* **111**, 77-89.

Martin, W. R. and Banta, G. T., 1992. The measurement of sediment irrigation rates: A comparison of the Br^- tracer and $^{222}Rn/^{226}Ra$ disequilibrium techniques. *Journal of Marine Research* **50**, 125-154.

Murray, J. W., Codispoit, L. A., and Friederich, G. E., 1995. Oxidation-Reduction Environments: The suboxic Zone oin the Black Sea. In: Huang, C. P., O'Melia, C. R., and Morgan, J. J. Eds.), *Aquatic Chemistry: Interfacian and Interspecies Processes*. American Chemical Society, Washington, D.C.

Murray, J. W. and Kuivila, K. M., 1990. Organic matter diagenesis in the Northeast Pacific: Transition from aerobic red clay to sub-oxic hemipelagic sediments. *Deep-Sea Res.* **37**, 59-80.

Olson, D., Garrels, R. M., Berner, R. A., Armentano, T. V., Dyer, M. I., and Taalon, D. H., 1985. The natural carbon cycle. In: Trabalka, J. R. (Ed.), *Atmospheric Carbon Dioxide and the Global Carbon Cycle*. US Dep. Energy, Washington, D.C.

Paropkari, A. L., Babu, C. P., and Mascarenhas, A., 1992. A critical evaluation of depositional parameters controlling variability of organic carbon in Arabian Sea sediments. *Mar. Geol.* **107**, 213-226.

Pedersen, T. F. and Calvert, S. E., 1990. What controls the formation of organic-carbon-rich sediments and sedimentary rocks? *Amer. Assoc. Petrol. Geol. Bull.* **74**, 454-466.

Perry, E. C. and Ahmad, S. N., 1977. Carbon isotope compostion of graphite and carbonate minerals from 3.8-Ga metamorphosed sediments, Isukasia, Greenland. *Earth Planet. Sci. Lett.* **36**, 280-284.

Pratt, L. M., 1984. Influence of Paleoenvironmental Factors on Preservation of Organic-Matter in Middle Cretaceous Greenhorn Formation, Pueblo, Colorado. *Aapg Bulletin-American Association of Petroleum Geologists* **68**, 1146-1159.

Priest, F. G., 1984. Extracellular enzymes. *Aspects of Microbiology* **9**, 1-79.

Reimers, C. E. and Jr., K. L. S., 1986. Reconciling measured and predicted fluxes of oxygen across the deep sea sediment-water interface. *Limnol. Oceanogr* **31**, 305-318.

Reimers, C. E., K.M. Fischer, R. Mereweather, K.L. Smith, J., and Jahnke., R. A., 1986. Oxygen microprofiles measured in situ in deep ocean sediments.

Ronov, A. B., 1990. *Chemical Structure of the Earth's Crust and Chemical Balance of Major Elements*. Izdatel'stvo, Moscow.

Rusch, A., Huettel, M., Reimers, C. E., Taghon, G. L., and Fuller, C. M., 2003. Activity and distribution of bacterial populations in Middle Atlantic Bight shelf sands. *FEMS Microbiol. Ecol.* **44**, 89-100.

Schidlowski, M., 2001. Carbon isotopes as biogeochemical recorders of life over 3.8 Ga of Earth history: evolution of a concept. *Precamb. Res.* **106**, 117-134.

Stein, R., 1990. Organic-Carbon Content Sedimentation-Rate Relationship and Its Paleoenvironmental Significance for Marine-Sediments. *Geo-Marine Letters* **10**, 37-44.

Thamdrup, B. and Canfield, D., 2000. Benthic respiration in aquatic sediments. In: Sala, O. E., Jackson, R. B., Mooney, H. A., and Howarth, R. W. Eds.), *Methods in Ecosystem Science*. Springer, New York.

Thauer, R. K., Jungermann, K., and Decker, K., 1977. Energy conservation in anaerobic chemotrophic bacteria. *Bacteriological Review* **41**, 100-180.

van Breugel, Y., Schouten, S., Paetzel, M., Nordeide, R., and Damste, J. S. S., 2005. The impact of recycling of organic carbon on the stable carbon isotopic composition of dissolved inorganic carbon in a stratified marine system (Kyllaren fjord, Norway). *Org. Geochem.* **36**, 1163-1173.

Veizer, J. and Hoefs, J., 1976. The nature of 18O/16O and 13C/12C secular trends in sedimentary carbonate rocks. *Geochim. Cosmochim. Acta* **40**, 1387-1395.

Wakeham, S. G., Amann, R., Freeman, K. H., Hopmans, E. C., Jorgensen, B. B., Putnam, I. F., Schouten, S., Damste, J. S. S., Talbot, H. M., and Woebken, D., 2007. Microbial ecology of the stratified water column of the Black Sea as revealed by a comprehensive biomarker study. *Org. Geochem.* **38**, 2070-2097.

Wakeham, S. G., Hopmans, E. C., Schouten, S., and Damste, J. S. S., 2004. Archaeal lipids and anaerobic oxidation of methane in euxinic water columns: a

comparative study of the Black Sea and Cariaco Basin. *Chem. Geol.* **205**, 427-442.

Whitman, W. B., Coleman, D. C., and Wiebe, W. J., 1998. Prokaryotes: The unseen majority. *Proc. Natl. Acad. Sci. U. S. A.* **95**, 6578-6583.

Williams, P. M. and Druffel, E. R. M., 1987. Radiocarbon in Dissolved Organic-Matter in the Central North Pacific-Ocean. *Nature* **330**, 246-248.

Yakushev, E. V., Chasovnikov, V. K., Debolskaya, E. I., Egorov, A. V., Makkaveev, P. N., Pakhomova, S. V., Podymov, O. I., and Yakubenko, V. G., 2006. The northeastern Black Sea redox zone: Hydrochemical structure and its temporal variability. *Deep-Sea Res Pt Ii* **53**, 1769-1786.

2B. Banded Iron-Formation: A Continuing Enigma

1. Introduction

iron formation a chemical sedimentary rock, typically thin-bedded and/or finely laminated, containing at least 15% iron of sedimentary origin, and commonly but not necessarily containing layers of chert

- *American Geological Institute Glossary of Geology*

Banded-Iron Formations ('BIFs') are amongst the most controversial of geological deposits. They are characterized by the presence of alternating layers of iron-rich and amorphous silica-rich layers. This dichotomous compositional layering is usually expressed on several scales, from fine sub-millimetre-scale varve-like laminae to metre-scale bands. Even on a microscopic scale, the boundary between the ferruginous and siliceous layers is distinctly abrupt.

This introductory chapter sets out to explore the key aspects of BIFs pertinent to their role in the study of early earth evolution, and outline the major controversies surrounding their interpretation. The focus rests on BIF classification, temporal- and spatial-distribution, constituent behaviour in solution, depositional environment, and origin.

An understanding of the origin of BIFs provides useful insight into conditions existing on, and governing, the early lithosphere, hydrosphere and atmosphere. Iron is used as a metabolic agent by numerous microorganisms. The processes mediated by some of these, including specific species of oxygenic- and anoxygenic-photoautotrophs and chemoferrotrophs, lend credence to the theory of BIF-deposition being, at least in part, a microbially mediated process. Direct evidence for a microbial role in Archaean BIF deposition remains elusive.

All geologists agree that BIFs offer vital insights on the evolution of the early earth. They just can’t agree on what those insights are. A brief description, outlining

the general characteristics of BIFs, is instructive. The following discussion draws upon field data from Australia, southern Africa and Greenland.

1.1. Observations of BIFs in Australia, southern Africa and Greenland

1.1.1. Layering and Composition

The quintessential feature of BIFs is the presence of alternating layers of iron-rich and amorphous silica-rich layers. This dichotomous compositional layering is usually expressed on several scales at any given outcrop, from fine sub-millimetre-scale varve-like laminae to metre-scale bands. Haematite and magnetite dominate the iron-rich layers, sometimes accompanied by lesser -oxides and -sulphides of iron and other metals, such as pyrite, chalcopyrite and ilmenite. Varying amounts of carbonate mineral phases, such as calcite and siderite, may or may not be present in both iron-rich and chert-rich layers. Layers of silica may or may not be jaspilitic, frequently patchily. Even on a microscopic scale, the transition between iron- and silica- bands is, as a rule, abrupt.

Compared to other sedimentary and metasedimentary rocks, BIFs appear to be particularly lacking in phosphate-bearing minerals. Organic matter is also scarce.

1.1.2. Vertical and Horizontal Extent

Both the thickness and lateral extent of BIFs vary greatly. Where closely associated with volcanic successions, such as in the Isua Supracrustal Belt in southwest Greenland and in the Kraaipan Greenstone Belt in South Africa's Northern Province, BIF thickness is on the order of tens of metres.

1.2. Mineralogy

BIF has been classified on the basis of mineralogical composition (James, 1954; James, 1966), proposed tectonic setting (Gross, 1965) and depositional environment (Kimberley, 1978; Simonson, 1985). The large variety of available classification schemes undoubtedly reflects our limited understanding of BIF

formation. James' (1954) original facies concept included oxide-, silicate- and carbonate- facies iron formation thought to correspond to different water depths. A fourth so-called sulphide-facies, containing pyrite [FeS_2] and/or pyrrhotite [Fe_{1-x} S], was once regarded as syngenetic in origin (Fripp, 1976) but has subsequently been suggested to be epigenetic (Phillips *et al.*, 1984; Groves *et al.*, 1987) - with a replacement rather than primary sedimentary origin for sulphide mineralization.

Oxide-rich BIF typically consists of alternating bands of haematite [$Fe^{III}_2O_3$] with or without magnetite [$Fe^{II}Fe^{III}_2O_4$]. Where the iron oxide is dominantly magnetite, siderite [$Fe^{II}CO_3$] and lesser iron silicate are often also present (James, 1966). Silicate-rich BIF is usually dominated by the minerals greenalite, minnesotaite and stilpnomelane. Greenalite [$(Fe^{2+}, Mg)_6$ Si_4 O_{10} $(OH)_8$] and minnesotaite [$(Fe^{2+}, Mg)_3$ Si_4 O_{10} $(OH)_2$] are ferrous analogues of antigorite and talc respectively, while stilpnomelane [$K_{0.6}$ (Mg, Fe^{2+}, Fe^{3+})$_6$ Si_8 Al(O, OH)$_{27}$.2-4H_2O] is a complex phyllosilicate. The varied primary mineralogy of hydrous iron silicates, carbonates and cherts in silicate-facies BIFs is vulnerable to metamorphic recrystallization at low grades.

Carbonate-rich BIF is usually dominated by the minerals ankerite [Ca Fe^{2+} $(CO_3)_2$] and siderite, both of which display highly variable compositions. The overall mineralogy of carbonate-facies BIFs is relatively simple, with roughly equal proportions of chert and ankerite (and/or siderite) expressed as thinly bedded or laminated alternating layers.

Gross (1965) inferred tectonic settings on the basis of BIF size and lithologic associations. *Algoma*-type iron formations are relatively small, and associated with volcanogenic rocks. Total primary iron content rarely exceeds 10^{10} tons (James and Trendall, 1982). Typical lateral extents are under 10 km, with thicknesses in the range 10-100 m (Goodwin, 1973; Appel, 1980; Condie, 1981). Favoured depositional environments for this type of BIF include island arc/back arc basins (Veizer, 1983) and intracratonic rift zones (Gross, 1983).

Superior-type iron formations are larger, and associated with other sedimentary units. Total primary iron content typically exceeds 10^{13} tons (James and Trendall, 1982). Several BIFs classified as Superior-type have been reported to extend over 10^5 km^2 (Trendall and Blockley, 1970; Beukes, 1973). Deposition is thought to have occurred in relatively shallow marine conditions under transgressing seas (Trendall, 1968; Beukes, 1983; Simonson, 1985; Simonson and Hassler, 1996), perhaps on the continental shelves of passive tectonic margins (Gross, 1965).

2. BIF Distribution

2.1. Temporal Distribution

Iron-rich units are not restricted exclusively to the Precambrian geologic record. Younger rocks superficially representing BIFs, commonly termed 'ironstones', are distinctly more Al_2O_3-, P_2O_5- and Fe_2O_3-rich and usually have an oolitic or pisolitic texture (Schopf, 1983) and are conspicuously barren in chert. Unequivocal BIFs appear to be absent from the Phanerozoic record. Table 2 compares characteristics of ironstones and iron formations.

BIFs are found at the very beginning of the rock record, amongst the oldest rocks on Earth. Contrary to earlier belief (Cloud, 1973), there exists a considerable age-spread among Precambrian BIFs. 90% of all iron-formation was deposited between 3.8 Ga and 1.6 Ga, prior to the Paleoproterozoic-Mesoproterozoic boundary (Schopf, 1983; Isley and Abbott, 1999).

Algoma-type tectonic settings are inferred for most older (Early- and Mid-Archaean) BIFs, the vast majority of which are hosted in greenstone-belts. BIFs are generally thicker and of greater lateral extent in the Late Archaean to early Proterozoic basins than in older greenstone belts (Klein and Beukes, 1992), representing a transition to Superior-type BIF deposition. Oxide-facies bands become particularly common during this time, as evidenced by their dominance in some of the largest BIF sites in Western Australia (Groves and Batt, 1984) and Canada (Fyon *et al.*, 1984), both dated at ~ 2.9 – 3.0 Ga. The deposition of the Hamersley Group and Superior region iron-formations marks a prominent volumetric peak in the geological BIF record.

2.2. Spatial Distribution

Apart from the aforementioned early-Archaean BIFs at Isua, large mid-Archaean BIFs occur in the Guyana Shield of Venezuela and Guyana, and the Liberian Shield of Sierra Leone, Guinea, Liberia, and Ivory Coast. Algoma-type sequences are common in Archaean greenstone belts around the world, where they are found associated with (ultra)mafic volcanics. Examples include the Vermilion district of northern Minnesota and the Michipicoten district of north-central Ontario. Other BIFs of late-Archaean age are found in the Yilgarn Block of Western Australia and the Zimbabwe Craton.

Superior-type sequences include the Hamersley Group, the Transvaal Supergroup, the Minas Supergroup, and deposits in the Labrador Trough-Animikie Basin including the Sokoman-, Gunflint- and Biwabik- iron-formations. Superior-type BIFs are rare in other sequences. Because these BIFs are usually devoid of readily-dateable volcanogenic rocks, many of them are of ambiguous age. Some workers (e.g., James, 1982; Chemale *et al.*, 1994; Shchipansky and Bogdanova, 1996) have assumed a synchronous age of ~2.45 Ga for several major Superior-type BIFs.

Other noteworthy BIFs, of more ambiguous classification, include those of Russia's Krivoy Rog district and some from Brazil's Minas Gerais.

3. Chemistry and Metamorphism

Major element concentrations in BIFs of various Proterozoic and Archaean ages were studied by Gole and Klein (1981). Iron formation contains on average 30% total iron ($FeO + Fe_2O_3$). Globally, BIF compositions vary greatly from one to another. However, the bulk-rock major- and trace- element concentrations show remarkable consistency on the unit- and even regional- scale, even for BIFs of different ages and facies (Gole and Klein, 1981). Regional variations do occur in volatile-, S- and Ce-contents (Gnaneshwar and Naqvi, 1994). The regional chemical homogeneity raises the question: how do chemical components in BIFs react to metamorphism? Almost all known BIF exposures are metamorphosed to some degree: was this metamorphism isochemical or did it involve the loss or gain of chemical components? Clearly, an understanding of the behavior of BIFs under changing conditions of pressure and/or temperature is vital to discriminating between primary-/diagenetic- and secondary-minerals and textures. Mineralogical changes incurred during BIF metamorphism lie outside the scope of this paper (see instead Klein, 1983).

3.1. Effects of Metamorphism

Klein (1973) compared the chemistry of late diagenetic to prehnite-pumpellyite facies (low grade) iron-formation samples to those of higher metamorphic grade (up to upper amphibolite facies) from the central and southern parts of the Labrador Trough. It was concluded that the regional metamorphism in the Labrador Trough resulted in loss of volatiles, particularly CO_2 and H_2O. SiO_2 contents also differed significantly between low- and high-grade meta-BIFs, which has been interpreted as reflecting the variable scales of chert- and quartz- banding. Apart from a loss of volatiles, neither the $Fe^{3+}/(Fe^{3+} + Fe^{2+})$ ratio nor major element oxide concentrations appear significantly affected by regional metamorphism.

Kaufman (1996) examined the effects of the intrusion of a ~ 450 ºC diabase sill into the Palaeoproterozoic Kuruman Iron Formation, Transvaal Basin, South Africa. Within 5 m of the intrusive contact, the abundance of iron increases dramatically and

the oxidation state of the sediments fluctuated considerably more than outside the contact aureole. Isotopic and mineralogic systematics within the Kuruman BIF contact aureole resemble those in thermally altered siliceous dolomites and limestones: depletion in carbonate (inorganic) $\delta^{13}C$ and $\delta^{18}O$, and lower total organic carbon (TOC) with enriched $\delta^{13}C_{org}$. Most distinct isotopic and elemental variations occurred within 10 m of the diabase sill, suggesting alteration mainly through volatilization and fluid infiltration.

4. Component Behaviour in Solution

A key question in the enigma of BIFs concerns the genesis of the characteristic alternating iron-rich and silica-rich bands. Given the deep-marine depositional environment inferred for most BIF deposits, some mechanism is required for transporting iron in its' soluble form and subsequently precipitating it, on a regional scale, out of solution. The chemistry of the Archaean lithospheric, oceanic and atmospheric reservoirs - and the operation of biogeochemical cycles linking these - may well have deviated substantially from conditions observed today. A brief look at the behavior of iron and silica in solution is therefore instructive.

4.1. Iron

Ferrous- and ferric- iron (Fe^{2+} and Fe^{3+}) are the prevailing ionic forms for iron migration. High concentrations of Fe^{3+} are stable only under very acidic conditions (pH = 0-2). An increase in pH causes hydrolysis and precipitation of the insoluble $Fe(OH)_3$ hydroxide. The occurrence of such strong acidic solutions in the ocean at any time during the Precambrian - for example due to weathering of an exotic crust – cannot be accounted for by physiochemical processes, even with an extremely CO_2-rich atmosphere (Belevtsev *et al.*, 1982). Furthermore, ferric iron is also unstable in the presence of many electrolytes, particularly SO_4^{2-}.

Acidic thermal solutions *are* (and presumably also *were*) found in regions of volcanic activity. However, such waters are rich in ferrous rather than ferric iron.

Ferrous iron in solution is highly susceptible to oxidation, mainly due to its reaction with rocks, dilution by meteoric waters and the buffering effect of carbonates and silicates. It seems unlikely, therefore, that at any point in Earth's history iron could be transported in solution in the presence of free oxygen.

The ability of iron to migrate increases tremendously in the absence of free oxygen. Appreciable amounts of iron can be dissolved in slightly acidic to neutral anoxic solutions. Under such conditions, changes in parameters such as pCO_2, pressure (≡ water depth), pH and Eh (redox potential) determine whether iron is precipitated as a carbonate, oxide, silicate or other salt.

4.2. Silica

In solution, silica exists as the ionic monomer $Si(OH)_4^0$. In contrast to ferruginous species, the solubility of silica is remarkably independent of the acidity, ranging between 80-100 mg/l across a pH range of 2 - 10. In colloidal form, silica becomes far more soluble, particularly at pH < 4 - 5; thermal waters of present-day volcanic regions contain 200 - 300 mg/l dissolved SiO_2, up to 900 mg/l (Zelenov, 1972). Possible 'triggers' leading to silica precipitation include changes in temperature, pH and electrolyte concentrations – particularly Mg^{2+}, Na^+, and to a far lesser extent Fe^{2+} (Belevtsev *et al.*, 1982).

5. Depositional Environment

Holland (1984) interpreted the four different BIF facies (Section 1) as representing different redox conditions existing at different water depths in a stratified ocean. Oxide-facies BIF precipitated under the most oxidizing conditions, while sulphide-facies BIF was precipitated under the most reducing conditions. Silicate- and carbonate- facies were deposited under intermediate redox conditions.

Several workers have noted the lack of iron-rich sedimentary rocks in shallow-water Archaean successions, which instead may contain other orthochemical units such as local bedded barite, sparse carbonate, and evaporites (in the Barberton: Heinrichs

and Reimer, 1977; Lowe and Knauth, 1977; Reimer, 1990; in the Pilbara: Barley, 1979; Groves *et al.*, 1981; Buick and Dunlop, 1990).

On the basis of such observations and other sedimentological constraints derived from intercalated and associated sediments, the majority of models for BIF deposition involved environments ranging from shelf and upper continental slope to the abyssal plain. The greatest depth of deposition thus-far proposed is 900 m in the Barberton (de Ronde *et al.*, 1997). On the basis of P and Fe^{3+} concentrations, Bjerrum and Canfield (2002) have recently proposed a deep ocean setting for both siderite- and Fe-oxide- enriched BIF and associated shales.

The ages of BIFs and volcanic super-plume events are often statistically indistinguishable (Isley and Abbott, 1999). The petrology of these diverse volcanics ranges from ultramafic through felsic, while chemical affinities to ocean island basalts (OIBs), enriched mid-ocean ridge basalts (MORBs) and normal MORBs (NMORBs) have been reported (Hoffman, 1988). It has been argued that increased hydrothermal activity resulting from these enormous volcanic events promoted BIF deposition (Barley *et al.,* 1997). Units from the Barberton contain massive sulphides and collapsed chimney deposits, indicating proximal high-temperature hydrothermal activity.

The greenstone belt sedimentary successions commonly hosting Algoma-type iron-formations resemble the facies distributed around modern ocean spreading centers and island arcs. Favoured depositional environments for this type of BIF include island arc/back arc basins (Veizer, 1983) and intracratonic rift zones (Gross, 1983).

Mature shelf assemblages, including well-developed carbonate platforms, are found in intimate association with Superior-type iron formations. Thus, BIF deposition occurred in relatively shallow marine conditions under transgressing seas (Trendall, 1968; Beukes, 1983; Simonson, 1985; Simonson and Hassler, 1996), on the continental shelves of passive tectonic margins (Gross, 1965). Limited clastic input suggests that these platform environments were isolated. Schopf (1983) interpreted the coeval development of large continents, continental glaciation and Superior-type BIFs as

representing the transition from local Algoma-type deposition to deposition on extensive oxygenated continental shelves.

To summarize, the majority of Algoma-type BIFs were deposited as parts of volcanosedimentary successions in greenstone belts. For Superior-type BIFs, a depositional environment consisting of a partly isolated, submerged platform on the continental shelf of an Archaean craton is currently in favour with most workers (Konhauser *et al*., 2002).

6. Origin

Despite almost a century of geological studies into the origin of BIFs, a depositional mechanism that adequately explains both their geology (Section 1) and extent (both in space and time - Section 2) remains unclear. The sources of BIF iron and silica, and possible mechanisms of iron precipitation (and, by extension, the phenomenon of alternating iron/silica banding) are discussed next.

6.1. Sources of Iron and Silica

As with other aspects of BIFs, the source(s) of iron have been disputed. Both continental (e.g., Alibert and McCulloch, 1993) and hydrothermal (e.g., Holland, 1973; Simonson, 1985; Dymek and Klein, 1988) settings have been put forward as likely Fe-sources. On the basis of depleted rare earth element (REE) patterns and Nd isotopic signatures, it is now widely accepted that mid-ocean-ridge or hotspot tectonic settings act as a distal hydrothermal source of iron (e.g., Holland, 1973; Morris and Horwitz, 1983; Jacobsen and Pimental-Klose, 1988). This iron output is pulsed, and possibly supplemented by normal continental drainage (e.g., Canfield, 1998). Upwelling currents (Klein and Beukes, 1989) or thermal plumes (Isley, 1995) deliver hydrothermal waters onto the outer continental shelf.

The absence of silica-secreting organisms in Precambrian oceans likely gave rise to conditions at or near the silica saturation point (Siever, 1992). Silica

precipitation can then be achieved through evaporative supersaturation (Garrels, 1987) or coprecipitation with solid-phase iron minerals (Ewers, 1983).

Uniform, regional-scale precipitation of minerals within the depositional basin gave rise to the extensive horizontally continuous mesobands (Trendall and Blockley, 1970; Ewers and Morris, 1981). Until recently, the genesis of the siliceous sequences was attributed either to temporary failure of hydrothermal fluids reaching the depositional site due to changes in ocean circulation (termed 'current reorganization' by Konhauser *et al.*, 2002) or to periods of relative hydrothermal quiescence (Morris, 1993).

In the above scenario, the magnitude and periodicity of hydrothermal activity and influx thus control the relative thicknesses of the iron and chert layers (Morris, 1993). Ge/Si ratios in BIFs suggest that iron and silica fluxes were decoupled, with the latter being predominantly derived from the weathering of continental landmass rather than of hydrothermal origin (Hamade *et al.*, 2003). In such a scenario, alternating chert- and iron- rich layers would reflect competing controls through dominance of continental and hydrothermal sources respectively.

6.2. Iron Oxidation

6.2.1. Clastic Models

The enormous but evenly distributed amounts of iron needed to cover basinal sites of BIF deposition would appear to require the transport of iron its soluble ferrous form. Two exceptions to this requirement exist. The first occurs in recent models of BIF formation that attribute iron deposition to turbiditic flows of hydrothermal muds on the flanks of submarine volcanoes (Krapez *et al.*, 2003; Lascalles, 2007; Pickard *et al.*, 2004; Pecoits *et al.*, 2009). Such models face severe difficulties. For one, they fail to adequately address the mechanism of primary iron oxidation. In contemporary hydrothermal systems, iron exhibits little spontaneous precipitation upon contact with oxygen: on the Eastern Pacific Red Seamount, for instance, ferrous iron in mildly acidic (pH $\approx$ 5) low-temperature fluids that discharge into cold (~ 2 ºC) and

oxygenated (pO_2 = 0.06 atm) bottom-water remains in solution for over 30 years (Alt, 1988). In anoxic Archaean deepwater, such iron oxidation and precipitation would have been even more impeded. Furthermore, a clastic origin fails to account for the paucity of both sedimentary structures and aluminous clastic detritus in canonical BIFs.

A second - and related - hypothesis is that the iron in BIF starts out as a ferrous precipitate, such as siderite, that recrystallizes to magnetite (or haematite, under unusually elevated fO_2) upon metamorphism:

$$Fe^{2+}_{(aq)} + CO_2 + H_2O \rightarrow Fe^{II}(CO_3) + 2\ H^+ \quad (1a)$$

$$3\ Fe^{II}(CO_3) \rightarrow Fe^{III}Fe^{III}Fe^{II}O_4 + CO + 2\ CO_2 \quad (1b)$$

However, siderite decarbonation should precipitate graphite, and commences above ~ 450 ºC under ideal laboratory conditions (French and Rosenberg, 1965; French, 1971). These facts are at odds with the common occurrence of magnetite- and haematite- bearing BIF assemblages barren of carbon at and below upper greenschist facies.

This leaves the controversial question of the mechanism controlling primary oxidation of Fe^{2+} to Fe^{3+}. Four different models have been proposed towards this end, three of which appeal to biology. These are outlined below.

6.2.2. Oxidative Photolysis

Numerous laboratory experiments have shown that the action of sunlight, and particularly ultraviolet (UV) radiation, contributes to Fe^{2+} oxidation (e.g. Cairns-Smith, 1978; Braterman *et al.*, 1983):

$$2\ Fe^{2+}_{(aq)} + 6\ H_2O + h\upsilon \rightarrow 2\ Fe^{III}(OH)_3 + H_2 + 4H^+ \quad (2)$$

Work by Cockell (2002) attempted to constrain the solar UV flux to Earth through time. Due to limited knowledge of key factors such as the partial pressures of CO_2, N_2 and trace gases, an uncertainty of two orders of magnitude exists for Archaean UV fluxes. However, with most workers agreeing on oxygen levels $<10^{-4}$ present

atmospheric levels (PAL), the low ozone column abundance almost certainly allowed for far higher levels and frequencies of UV radiation during Archaean times (Margulis *et al.*, 1976; Kasting and Donahue, 1980; Kasting, 1987). The transition from intense, high-frequency UV-C (λ = 200 - 280 nm) and UV-B (λ = 280 - 320 nm) radiation to lower intensities and frequencies that accompanied the rise of oxygen provides a potential control on the temporal distribution of BIFs.

It has been argued that laboratory experiments attempting to simulate photochemical oxidation are overly simplistic and not representative of the multi-element solutions found in marine environments. For instance, it was mentioned previously that the Precambrian oceans likely had far higher concentrations of amorphous silica (Siever, 1992). Under such conditions, dissolved silica and iron react readily to form an amorphous iron-silicate gel (Hamade *et al.*, 2000), thereby greatly limiting the precipitative effect of UV radiation. Another drawback of the photochemical model is that the site of iron oxidation is restricted to the air/water interface.

6.2.3. Oxygenic Photosynthesis

The demonstrated presence of sulphate in shallow Archaean ocean(s) has led some (e.g., Ohmoto and Felder, 1987) to speculate that oxidizing conditions existed near the surface of a stratified Archaean ocean. Abiotic mechanisms, such as the photolysis of water vapour followed by the escape of hydrogen to space, are inadequate to explain the amount of oxygen incorporated into Precambrian BIFs, however, and so a biotic source must be sought.

Oxygenic photosynthesis entails the light-driven breakdown of water into oxygen. In this scenario, a soluble oxidant such as O_2 would have attained sufficient concentrations in the upper ocean to allow for indirect iron oxidation and precipitation at the oxic/anoxic boundary, inhibiting Fe^{2+} diffusion into overlying waters:

$$4Fe^{2+}_{(aq)} + O_2 + 10H_2O \rightarrow 4Fe^{III}(OH)_3 + 8H^+ \qquad (3)$$

Plankton growth today is strongly dependent on iron supply as a nutrient. Archaean oxygen-producing microorganisms may likewise have flourished during episodic Fe^{2+} (and nutrient) influx events, thereby coupling episodic iron influx with oxygenic photosynthesis-induced precipitation.

6.2.4. Chemolithoautotrophy

In the presence of free oxygen, oxidation of Fe^{2+} can also be performed by chemolithoautotrophic organisms. This mechanism has the obvious advantage of allowing for sub-photic zone oxidation, on par with empirical evidence:

$$12\ Fe^{2+} + O_2 + 2\ CO_2 + 32\ H_2O \rightarrow 2\ [CH_2O] + 12Fe(OH)_3 + 24\ H^+ \quad (4)$$

Laboratory experiments with *Gallionella ferruginea*, which makes use of the above pathway, indicate rates of iron oxidation >60 times faster than abiotic reactions (Søgaard *et al.*, 2000). Given the slow rates of abiotic iron oxide precipitation from oxygenated seawater now, chemolithotrophic mechanisms seem much more likely than passive abiotic oxidation after oxygenic photosynthesis to account for the large amounts and widespread areas of Superior BIFs.

6.2.5. Anoxygenic Phototrophy

Biologically mediated primary oxidation of Fe^{2+} to Fe^{3+} in an otherwise anoxic environment provides an appealing solution to the BIF dilemma. In 1994, Ehrenreich and Widdel announced the discovery of a new type of metabolism, involving the anaerobic oxidation of ferrous iron coupled to CO_2 reduction, by two different strains of purple bacteria. Subcultures were grown in defined mineral media of 10 mmol/liter $FeCO_3$.

Both strains were shown to be capable of both hetero- and auto- phototrophy:

$$4Fe^{2+} + CO_2 + 11H_2O \text{ -> } CH_2O + 4Fe(OH)_3 + 8H^+ \quad (5)$$

In addition to ferrous iron, strain 'SW2' utilizes H_2 + CO_2, monocarboxylic acids, glucose and fructose, while strain 'L7' utilizes H_2 + CO_2, acetate, pyruvate, and glucose as substrates for phototrophic growth. Neither strain utilizes free sulphide, but rather grows on black ferrous sulphide (FeS) to yield sulphate (SO_4^{2-}) and ferric iron. The authors noted that in bicarbonate-rich environments at pH ~7, the redox couple $Fe(OH)_3 + HCO_3^- / FeCO_3$ has a redox potential $E_0' = +0.2$ V, with ferrous iron in this case providing a far more favourable electron donor than in Cloud's (1965, 1973) proposed Fe^{3+}/Fe^{2+} redox couple under acidic conditions ($E_0' = +0.77$ V).

A number of purple and green bacteria are now known to make use of similar pathways (Widdel *et al.*, 1993; Ehrenreich and Widdel, 1994; Heising and Schink, 1998; Heising *et al.*, 1999). The base of the photic zone in today's oceans lies at a depth of ~120 m, but was probably shallower during less luminous Archaean times. However, the absorbance carotenoids used by anoxygenic iron oxidizers exploit the electromagnetic band between 400 and 500 nm, allowing photosynthesis to greater depths than their aerobic competitors (Kappler *et al*., 2006). The existence of iron-oxidizing anoxygenic phototrophs thus forms a tempting explanation for the existence of iron-rich bands in BIFs.

6.2.6. Summary of Biological Processes

As pointed out by Walter and Hofmann (1983), the very existence of fine BIF laminations suggests the absence of burrowing megascopic fauna until after ~1.6 Ga. On the other hand, microbiological mechanisms can potentially account for the precipitation of iron out of solution in a variety of environments, ranging from an anoxygenic photic zone to a (locally?) oxygenated sub-photic zone. However, the production of oxygen at depths anticipated for BIF deposition remains enigmatic, and may require a hithero-unexplored interplay within a complex microbial ecosystem.

Importantly, concentrations of nutrients (P) and trace metals (V, Mn, Co, Zn, and Mo) found in iron-rich BIF bands can easily support microbe populations capable

of precipitating Hamersley-scale BIFs – even during periods of maximum iron precipitation (Konhauser *et al*., 2002).

7. Conclusion

Banded Iron Formations ('BIFs') are highly controversial chemical precipitates characterized by the presence of alternating layers of iron-rich and amorphous silica-rich layers. This dichotomous compositional layering is usually expressed on several scales at any given outcrop, from fine sub-millimetre-scale varve-like laminae to metre-scale bands. Even on a microscopic scale, the boundary between the ferruginous and siliceous layers is distinctly abrupt.

An understanding of the origin of BIFs provides useful insight into conditions existing on the early lithosphere, hydrosphere and atmosphere. Like all sedimentary rocks, BIFs provide the geologist with information regarding the depositional environment, rate of sediment accumulation, and so forth. However, BIFs have proved particularly tantalizing windows on the early earth due to their possible intimate coupling with oxygen concentration and their narrow temporal-, depositional-, and tectonic- niches in the geological record.

In the context of early earth evolution, it is the possible link to an evolving biosphere that makes BIFs particularly interesting. The highly ordered and regionally continuous alternating layering of BIFs, physiochemical constraints aside, should be hard to achieve in a dead environment constantly striving for entropy maximization (Lorenz D., 2002). Apart from being an essential - and sometimes limiting – nutrient, iron is used as a metabolic agent by numerous microorganisms. Some of these, including specific species of oxygenic- and anoxygenic- photoautotrophs and chemoferrotrophs, lend credence to the theory of BIF-deposition being, at least in part, a microbially mediated process. Direct evidence for microbial activity during Archaean BIF deposition remains elusive. Could an interplay of primitive metabolisms, perhaps operating at different redox- and photic- levels within a stratified ocean, have been at work?

The principal enigma remains the BIF banding visible at virtually all scales. That such periodicity can be attributed solely to variations in iron and/or silica influx, be they of hydrothermal or continental origin, is hardly likely. Even in a stratified ocean, both hydrothermal iron production and continental erosion remain highly chaotic phenomena. Perhaps, then, some hithero uncharacterized electrolyte cycle unique to early oceans controlled the regional banding (Chapter 5).

Table 1: Comparison of typical ironstones with iron formations (after James, 1966)

Characteristic	Ironstones	Iron Formations
Age		
Minimum age	Pliocene	Late Precambrian
Major development	Lower Palaeozoic; Jurassic	2.5-3.0 Ga
Maximum age	Palaeo-Proterozoic (~2.0 Ga)	3760 ± 70 Ma
Thickness of major units	1-50 m	50-600 m
Original aerial extent, max. dimension	< 150 km	> 100 km
Physical character	massive to poorly banded; silicate and oxide-facies oolitic	thinly bedded; layers of haematite, magnetite, siderite, or silicate alternating with chert; chert ~50%
Mineralogy		
goethite	dominant	none
haematite	fairly common	common
magnetite	relatively rare	common
chamosite	dominant primary silicate	absent
glauconite	minor	absent
siderite	common	common
calcite	common	rare
dolomite	common	fairly common
pelletal collophane	relatively abundant	absent
greenalite	none	dominant primary silicate
quartz (chert)	rare	major constituent
pyrite	common	common
Chemistry	high iron	low Al, Na, K and minor elements; much lower P

References

Alibert, C., McCulloch, M.T., 1993, 'Rare earth element and neodymium composition of the banded iron formations and associated shales from Hamersley, Western Australia', *Geochicica et Cosmochimica Acta*, **57**, pp. 187-204.

Alt, J.C., 1988, 'Hydrothermal oxide and nontronite deposits on seamounts in the Eastern Pacific', *Marine Geology*, **81**, pp. 227-239.

Appel, P.W.U., 1980, 'On the Early Archaean Isua iron-formation, west Greenland', *Precambrian Research*, **11**, pp. 73-98.

Baglow, N., 1992, 'Bindura', *Geological Survey of Zimbabwe Map, 1:100 000*.

Barley, M. E., Pickard, A. L., and Sylvester, P. J., 1997, 'Emplacement of a large igneous province as a possible cause of banded iron formation 2.45 billion years ago', *Nature*, **385**, pp. 55-58.

Belevtsev, Ya. N., Belevtsev, R. Ya., Siroshtan, R.I., 1982, 'The Krivoy Rog Basin', *In:* Trendall, A.F., Morris, R.C. (eds.), 'Iron-formation: facts and problems', Elsevier, Amsterdam, pp. 211-252.

Beukes, N.J., 1973, 'Precambrian iron-formations of southern Africa', *Economic Geology*, **68**, pp. 960-1024.

Beukes, N.J., 1983, 'Paleoenvironmental setting of iron-formations in the depositional basin of the Transvaal Supergroup, South Africa', *In:* Trendall, A.F., Morris, R.C. (eds.), 'Iron-Formation: Facts and Problems', Elsevier, New York, pp. 131-209.

Beukes, N.J., Klein, C., 1992, 'Models for iron-formation deposition', *In:* Schopf, J.W. and Klein, C. (eds.), 'The Proterozoic Biosphere, a multidisciplinary study', Cambridge University Press, New York, pp. 147-152.

Bjerrum, C.J., Canfield, D.E., 2002, 'Ocean productivity before about 1.9 Gyr ago limited by phosphorus adsorption onto iron oxides', *Nature*, **417**, pp. 159-162.

Braterman, P.S., Cairns-Smith, A.G., Sloper, R.W., 1983, 'Photo-oxidation of hydrated Fe^{2+} - Significance for banded iron-formations', *Nature*, **303**, pp. 163-164.

Buick R., Dunlop, J.S.R., 1990, 'Evaporitic sediments of early Archaean age from the Warrawoona Group, North Pole, Western Australia', *Sedimentology*, **37**, pp. 247-277.

Cairns-Smith, A.G., 1978, 'Precambrian solution photochemistry, inverse segregration, and banded iron-formations', *Nature*, **276**, pp. 807-808.

Cairns-Smith, A.G., 1982, 'Genetic Takeover and the Mineral Origins of Life', Cambridge University Press.

Cloud P., 1965, 'Significance of the Gunflint (Precambrian) flora', *Science*, **148**, pp. 27-35.

Cloud P., 1973, 'Paleoecological significance of the banded iron-formation', *Economic Geology*, **68**, pp. 1135-1143.

Cockell, C.S., 2002, 'Photobiological uncertainties in the Archaean and post-Archaean world', *International Journal of Astrobiology*, **1**, pp. 31-38.

Condie, K.C., 1981, 'Archean Greenstone Belts', Elsevier, Amsterdam, 442 pp.

de Ronde, C.E.I., Channer, D.M., De, R., Faure, K., Bray, C.J., Spooner, E.T.C., 1997, 'Fluid chemistry of Archaean seafloor hydrothermal vents: Implications for the composition of circa 3.2 Ga seawater', *Geochimica et Cosmochimica Acta*, **61**, pp. 4025-4042.

Dymek, R.F., Klein, C., 1988, 'Chemistry, petrology and origin of banded iron-formation lithologies from the 3800 Ma Isua supracrustal belt, west Greenland', *Precambrian Research*, **39**, pp. 247-302.

Ehrenreich, A., Widdel, F., 1994, 'Anaerobic oxidation of ferrous iron by purple bacteria, a new type of phtotrophic metabolism', *Applied and Environmental Microbiology*, **60**, pp. 4517-4526.

Ewers, W.E., Morris, R.C., 1981, 'Studies of the Dales Gorge Member of the Brockman Iron Formation, Western Australia', *Economic Geology*, **76**, pp. 1929-1953.

Ewers, W.E., 1983, 'Chemical factors in the deposition and diagenesis of banded iron-formation', *In:* Trendall, A.F., Morris, R.C. (eds.), 'Banded iron-formation: Facts and problems', Elsevier, Amsterdam, pp. 491-512.

Fedo, C.M., Whitehouse, M.J., 2002, 'Response to: Origin and Significance of Archean Quartzose Rocks at Akilia, Greenland', *Science*, **298**, pp. 917a.

French, B.M., Rosenberg, P.E., 1965, 'Siderite (FeCO3): thermal decomposition in equilibrium with graphite', *Science*, **147**, pp. 1283-1284.

French, B.M., 1971, 'Stability relations of siderite (FeCO3): thermal decomposition in equilibrium with graphite', *American Journal of Science*, **271**, pp. 37-78.

Friend, C.R.L., Nutman, A.P., Bennett, V.C., 'Response to: Origin and Significance of Archean Quartzose Rocks at Akilia, Greenland', *Science*, **298**, pp. 917a.

Fripp, R.E.P., 1976, 'Stratabound gold deposits in Archaean banded iron-formation, Rhodesia', *Economic Geology*, **71**, pp. 58-75.

Garrels, R.M., 1987, 'A model for the deposition of the micro-banded Precambrian iron-formations', *American Journal of Science*, **287**, pp. 81-106.

Gnaneshwar, T., Naqvi, S.M., 1995, 'Geochemistry, depositional environment and tectonic setting of the BIF's of the Late Archaean Chitradurga Schist Belt, India', *Precambrian Research*, **121**, pp. 217-243.

Gole, M.J., Klein, C., 1981, 'Banded iron-formations through much of Precambrian time', *Journal of Geology*, **89**, pp. 169-183.

Goodwin, A.M., 1973, 'Archaean volcanogenic iron-formation of the Canadian shield', *Sci. Terre*, **9**, pp. 23-34.

Gross, G.A., 1965, 'Geology of Iron Deposits in Canada, Volume 1. General Geology and Evaluation of Iron Deposits', *Geological Survey of Canada Economic Report*, **22**.

Gross G.A., 1983, 'Tectonic systems and the deposition of iron-formation', *Precambrian Research*, **20**, pp. 171-187.

Groves, D.I., Batt, W.D., 1984, 'Spatial and temporal variations of Archean metallogenic associations in terms of evolution of granitoid-greenstone terrains

with particular emphasis on Western Australia', *In:* Kroner, A., Hanson, G.M., Goodwin, A.M. (eds.), 'Archaean Geochemistry', Springer-Verlag, Berlin, pp. 73-98.

Groves, D.I., Phillips, N., Ho, S.E., Houstoun, S.M., Standing, C.A., 1987, 'Craton-scale distribution of Archaean greenstone gold deposits: predictive capacity of the metamorphic model', *Economic Geology*, **82**, pp. 2045-2058.

Hamade, T., Phoenix, V.R., Konhauser, K.O., 2000, 'Photochemical and microbiological mediated precipitation of iron and silica', *In:* Proceedings, 10th Annual V.M. Goldschmidt Conference, Oxford, England, pp. 475.

Hamade, T., Konhauser, K.O., Raiswell, R., Goldsmith, S., Morris, R.C., 2003, 'Using Ge/Si ratios to decouple iron and silica fluxes in Precambrian banded iron formations', *Geology*, **31**, pp. 35-38.

Heising, S., Schink, B., 1998, 'Phototrophic oxidation of ferrous iron by a *Rhodomicrobium vannielii* strain', *Microbiology*, **144**, pp. 2263-2269.

Heising, S., Richter, L., Ludwig, W., Schink, B., 1999, '*Chlorobium ferroxidans* sp. noc., a phototrophic green sulfur bacterium that oxidizes ferrous iron in coculture with a "*Geospirillum*" sp. strain', *Archives of Microbiology*, **172**, pp. 116-124.

Hoffman, P.E., 1988, 'United plates of America, the birth of a craton: Early Proterozoic assembly and growth of Laurentia', *Ann. Rev. Earth Planet. Sci.*, **16**, pp. 543-603.

Hofmann, A, Dirks, P.H.G.M., Jelsma, H.A., Matura, N., 2003, 'A tectonic origin for ironstone horizons in the Zimbabwe craton and their significance for greenstone belt geology', *Journal of the Geological Society, London*, **160**, pp. 83-97.

Holland, H.D., 1973, 'The oceans: A possible source of iron in iron formations', *Economic Geology*, **68**, pp. 1169-1172.

Holland H.D., 1984, 'The chemical evolution of the atmosphere and oceans', Princeton University Press, New Jersey, pp. 374-407.

Hunter, M., 1997, 'The tectonic setting of the Belingwe Greenstone Belt, Zimbabwe', *Ph.D. thesis, University of Cambridge*.

Isley, A.E., 1995, 'Hydrothermal plumes and the delivery of iron to banded iron-formation', *Journal of Geology*, **103**, pp. 169-185.

Isley, A.E., Abbott, D.H., 1999, 'Plume-related mafic volcanism and the deposition of banded iron formation', *Journal of Geophysical Research*, **104**, pp. 15461-15477.

Jacobsen, S.B., Pimental-Klose, M.R., 1988, 'A Nd isotope study of the Hamersley and Michipicoten banded iron formations: The source of REE and Fe in Archaean oceans', *Earth and Planetary Science Letters*, **87**, pp. 29-44.

James H.L., 1954, 'Sedimentary facies of iron formation', *Economic Geology*, **49**, pp. 235-293.

James, H.L., 1966, 'Chemistry of the iron-rich sedimentary rocks', *In:* Fleischer, M. (ed.), 'Data of Geochemistry', 6th edition, Paper 440-W, U.S. Govt. Printing Office, Washington D.C.

James, H.L., Trendall, A.F., 1982, 'Banded iron formation: distribution in time and paleoenvironmental significance', *In:* Holland, H.D., Schidlowski, M. (eds.), 'Mineral Deposits and the Evolution of the Biosphere', Springer-Verlag, New York, pp. 199-218.

Kappler, A., Pasquero, C., Konhauser, K.O., Newman, D.K., 2006, 'Deposition of banded iron formations by anoxygenic phototrophic Fe(II)-oxidizing bacteria', *Geology*, **33**(11), pp. 865-868.

Kasting, J.F., 1987, 'Theoretical constraints on oxygen and carbon dioxide concentrations in the Precambrian atmosphere', *Precambrian Research*, **34**, pp. 205-229.

Kasting, J.F., Donahue, T.M., 1980, 'The evolution of atmospheric oxygen', *Journal of Geophysical Research*, **85**, pp. 3255-3263.

Kaufman, A.J., 'Geochemical and mineralogic effects of contact metamorphism on banded iron-formation: an example from the Transvaal Basin, South Africa', *Precambrian Research*, **79**, pp. 171-194.

Kimberley, M.M., 1978, 'Palaeoenvironmental classification of iron formations', *Economic Geology*, **73**, pp. 215-229.

Klein, C., 1973, 'Changes in mineral assemblages with metamorphism of some Precambrian banded iron-formations', *Economic Geology*, **68**, pp. 1075-1088.

Klein, C., 1983, 'Diagenesis and metamorphism of Precambrian banded iron-formation', *In:* Trendall, A.F., Morris, R.C. (eds.), 'Iron-formation: facts and problems', Elsevier, Amsterdam, pp. 417-460.

Klein, C., Beukes, N.J., 1989, 'Geochemistry and sedimentology of a facies transition from limestone to iron-formation deposion in the Early Proterozoic Transvaal Supergroup, South Africa', *Economic Geology*, **84**, pp. 1733-1774.

Klein, C., Beukes, N.J., 1992, 'Proterozoic iron-formations', *In:* Condie, K.C. (ed.), 'Proterozoic Crustal Evolution', Elsevier, Amsterdam, pp. 383-418.

Konhauser, K., Hamada, T., Raiswell, R., Morris, R., Ferris, F., Southam, G., Canfield, D., 2002, 'Could bacteria have formed the Precambrian banded iron formations?', *Geology*, **30**, pp. 1079-1082.

Krapez, B., Barley, M.E., Pickard, A.L., 2003, 'Hydrothermal and resedimented origins of the precursor sediments to banded iron formation: sedimentological evidence from the Early Palaeoproterozoic Brockman Supersequence of Western Australia, *Sedimentology*, **50**(5), pp. 979-1011.

Lepland, A., Arrhenius, G., Cornell, D., 2002, 'Apatite in early Archean Isua supracrustal rocks, southern West Greenland: its origin, association with graphite and potential as a biomarker', *Precambrian Research*, **118**, pp. 221-241.

Lascelles, D. F., 2007, 'Black smokers and density currents: A uniformitarian model for the genesis of banded iron-formations', *Ore Geology Reviews*, **32**, pp. 381-411.

Lorenz, R.D., 2002, 'Planets, life and the production of entropy', *International Journal of Astrobiology*, **1**, pp. 3-13.

Lowe, D.R., Knauth, L.P., 1977, 'Sedimentology of the Onverwacht Group (3.4 billion years), Transvaal, South Africa, and its bearing on the characteristics and evolution of the early earth', *Journal of Geology*, **85**, pp. 699-723.

Margulis, L., Walker, J.C.G., Rambler, M., 1976, 'Reassessment of the roles of oxygen and ultraviolet light in Precambrian evolution', *Nature*, **264**, pp. 620-624.

Martin, A., 1978, 'The geology of the country around Que Que, Gwelo District', *Southern Rhodesia Geological Survey Bulletin*, **83**.

Mojzsis, S.J., Harrison, T.M., 2002, 'Vestiges of a Beginning: Clues to the Emergent Biosphere Recorded in the Oldest Known Sedimentary Rocks', *GSA Today*, **10**, pp. 1-6.

Mojzsis, S.J., Harrison, T.M., 2002, 'Origin and Significance of Archean Quartzose Rocks at Akilia, Greenland', *Science*, **298**, pp. 917a.

Morris, R., Horwitz, R., 1983, 'The origin of the iron-formation-rich Hamersley Group of Western Australia – Deposition on a platform', *Precambrian Research*, **21**, pp. 273-197.

Morris, R., 1993, 'Genetic modelling for banded iron formation of the Hamersley Group, Pilbara craton, western Australia', *Precambrian Research*, **60**, pp. 243-286.

Nisbet, E.G., 1987, 'The Young Earth', Allen & Unwin, Winchester.

Nisbet, E.G., Martin, A., Bickle, M.J., Orpen, J.L., 1993, 'The Ngezi Group: komatiites, basalts and stromatolites on continental crust', *In:* Bickle, M.J., Nisbet, E.G. (eds.), 'The Geology of the Belingwe Greenstone Belt, Zimbabwe', *Geological Society of Zimbabwe Special Publications*, **2**, pp. 121-165.

Ohmoto, H., Felder, R.P., 1987, 'Bacterial activity in the warmer, sulphate-bearing Archaean oceans', *Nature*, **328**, pp. 244-246.

Pecoits, E., Gingras, M.K., Barley, M.E., Kappler, A., Posth, N.R., Konhauser, K., 2009, 'Petrography and geochemistry of the Dales Gorge banded iron formation: Paragenetic sequence, source and implications for palaeo-ocean chemistry', *Precambrian Research*, **172**, pp. 163-187.

Phillips, G.N., Groves, D.I., Martyn, J.E., 1984, 'An epigenetic origin for Archaean banded iron-formation-hosted gold deposits', *Economic Geology*, **79**, pp. 162-171.

Pickard, A.L., Barley, M.E., Krapez, B., 2004, 'Deep-marine depositional setting of banded iron formation: sedimentological evidence from interbedded clastic sedimentary rocks in the early Palaeoproterozoic Dales Gorge Member of Western Australia, *Sedimentary Geology,* **170**(1-2), pp. 37-62.

Russell, M.J., Hall, A.J., 1996, 'The emergence of life from monosulphide bubbles at a submarine hydrothermal redox and pH front', *Journal of the Geological Society, London*, **153**, pp. 1-25.

Siever, R., 1992, 'The silica cycle in the Precambrian', *Geochemica et Cosmochemica Acta*, **56**, pp. 3265-3272.

Simonson, B.M., 1985, 'Sedimentological constraints on the origins of Precambiran iron-formations', *Geological Society of America Bulletin*, **96**, pp. 244-252.

Simonson, B.M., Hassler, S., 1996, 'Was the deposition of large Precambrian iron formations linked to major marine transgressions?', *Journal of Geology*, **104**, pp. 665-676.

Towe, K.M., 1983, 'Precambrian atmospheric oxygen and banded iron formations: a delayed ocean model', *Precambrian Research*, **20**, pp. 161-170.

Trendall A.F., Blockley J.G., 1970, 'The iron formations of the Precambrian Hamersley Group, Western Australia: With special reference to associated crocidolite', *Western Australia Geological Survey Bulletin*, **119**, pp. 336.

Veizer J., 1983, 'Geologic evolution of the Archean-Early Proterozoic Earth', *In:* Schopf, J.W. (ed.), 'Earth's Earliest Biosphere', Princeton University Press, New Jersey, pp. 240-259.

Walter, M.R., Hofmann, H.J., 1983, 'The palaeontology and palaeoecology of Precambrian iron-formations', *In:* Trendall, A.F., Morris, R.C. (eds.), 'Iron-formation: facts and problems', Elsevier, Amsterdam, pp. 373-400.

Widdel, F., Schnell, S., Heising, S., Ehrenreich, A., Assmus, B., Schink, B., 1993, 'Ferrous iron oxidation by anoxygenic phototrophic bacteria', *Nature*, **362**, pp. 834-836.

Wilson, J.F., Nesbitt, R.W., Fanning, C.M., 1995, 'Zircon geochronology of Archaean felsic sequences in the Zimbabwe craton: a revision of greenstone stratigraphy and a model for crustal growth', *In:* Coward, M.P., Ries, A.C. (eds.), 'Early Precambrian Processes', *Geological Society, London, Special Publications*, **95**, pp. 109-126.

2C. Early Archaean Geology & The Pilgangoora Belt

1. Introduction

This project was initially conceived as a quantitative study of the effects of metamorphism on bio-markers and -signatures, with particular emphasis on isotopes of carbon and nitrogen (Figure 1). In this respect, and in some others, the project was a failure. The factors that hampered completion of this objective were: (i) the lack of suitable assemblages allowing quantitative geothermobarometry at all grades; (ii) incomplete equilibration and small grain-sizes in low-grade rocks, hindering petrological and microprobe analysis; (iii) concentrations of organic matter at or below background (contamination) levels, particularly in higher-grade rocks, thwarting $\delta^{13}C_{org}$ and $\delta^{15}N_{org}$ isotope mass-spectrometry, macronutrient (CNPS) microprobe analysis (Figure 2) and NH_4^+ Fourier-Transform Infrared Spectroscopy (FTIR, Figure 3); and (iv) the large non-metamorphic variability of kerogen $\delta^{13}C_{org}$ analyses in individual units.

However, because of several unexpected findings in Early Archaean rocks in Australia, Greenland and South Africa, focus shifted to geological evidence for the nature of ancient sedimentary environments, and biogeochemical processes therein. This introduction serves to give a general overview of Archaean, Pilbara and Pilgangoora Belt geology, in increasing level of detail. Focus rests on particular geological aspects of deep-water carbonates of the Coucal Formation (described further in Chapter 5), and shallow-water carbonates of the Strelley Pool Chert Formation.

2. Generalized Archaean Geology

Judging from the tenacity and diversity of controversies, our understanding of the Earth's crust during Early Archaean times can fairly be described as insecure. A good starting point is to consider how Archaean rocks differ from contemporaneous ones ('inter-era differences'), and what this tells us about the early geosphere. Also worth considering are differences between Archaean terranes ('intra-era differences').

All continents bear Archaean supracrustal exposures (Chapter 1, Figure 2). These Archaean rocks represent about $20 \cdot 10^6$ km^2, or ~ 13%, of approximately $150 \cdot 10^6$ km^2 of continental material exposed today (Burke, 1997). Tradition has seen these divided into 'high-grade' and 'granitoid-greenstone' –sequences.

High-grade Archaean terrains have commonly experienced middle-amphibolite to granulite facies metamorphism, with mineral assemblages equilibrated at ~ 10 ± 1 kbar corresponding to depths of 30 - 40 km (Tarney and Windley, 1977; Martin, 1994). Together with their considerable lateral extent, this has made them viable candidates for pre- and sub-greenstone basement (Kröner, 1981).

Most high-grade Archaean terrains have seen complex polyphase deformation, frequently under sub-horizontal stress regimes. In these and other respects they have often been compared to the batholithic root zones of the main arcs of Mesozoic-Cenozoic Cordilleran fold belts (Kröner, 1981). They are geochemically distinct from gneiss-migmatite complexes in granitoid-greenstone sequences, not least in being distinctly more potassic (Bridgwater and Collerson, 1976). As they have little to tell us about ancient depositional environments and life, they shall not be considered further here.

2.1. Granitoid - Greenstone Terrains

Greenstone belts are deformed volcanic-sedimentary sequences that are typically metamorphosed to greenschist facies, and are commonly intruded by slightly younger 'granitoid' bodies. The resulting association is termed a Granitoid - Greenstone Terrain ('GGT'). Globally, such exposed Archaean shields generally comprise ~ 50% trondjemite-tonalite-granodiorite bodies ('TTG'), ~ 20% granitoid plutons, and ~ 10% tholeiite flows (Condie, 1993), though with much variability.

Volcanic rocks, especially tholeiites, dominate the volcanic-sedimentary sequences, with sediments imparting only minor contributions to most greenstone successions. Komatiites, though frequently absent and not restricted to the Precambrian (Echeverria, 1980; Aitken and Echeverria, 1984), are characteristic. The minerals

chlorite, epidote and/or actinolite are responsible for the distinctive green appearance of greenstone metabasites.

The tectonic style of the granitoids typically takes the form of 30 - 150 km diameter circular to ovoid domal granite-gneiss batholiths[1], with dominant metamorphic foliation and both volcanic and sedimentary bedding all dipping steeply away from the dome centre, giving rise to the characteristic symmetric, synformal greenstone belt cross-sections.

In order to account for shallow (~ 3 – 6 km) crustal depths inferred through geophysical studies, older estimates of stratigraphic thicknesses on the order of ~ 10 – 20 km have come to be revised to ~ 5 km, usually by positing tectonic duplication (see Chapter 1, Figure 6). In comparison to structurally similar Proterozoic orogenic belts, such as the 1.7 - 1.8 Ga Snow Lake-Flin Flon belt in southeast Monitoba (Bell et al., 1975; Moore, 1977), the ~ 2.0 Ga Birimian in West Africa (Burke and Dewey, 1972), and the ~ 1.3 Ga Grenville Province in eastern Canada (Sethuram and Moore, 1973), GGTs exhibit smaller length:width ratios, shorter wavelength folding, and a noteworthy lack of blueschist-facies assemblages.

2.2. Granitoids

On the basis of contact relationships with surrounding volcanosedimentary sequences, GGT-granitoids are divided into three groups (Martin, 1994; Sylvester, 1994): gneissic complexes and batholiths [sic], syntectonic plutons, and late discordant post-tectonic granite plutons.

Gneissic complexes and batholiths, in view of compositional domination by tonalite, trondjemite and granodiorite, are often referred to as ‘TTG’s’. These complexes tend to contain large infolded remnants of supracrustal rocks, commonly including plentiful inclusions of surrounding greenstone belt material. Contacts with greenstone belts proper are usually intrusive, and heavily deformed. Geochemically,

[1] As in greenstone-belt studies elsewhere, the term ‘batholith’ is employed colloquially, and should not be taken to imply intrusive relationships with all surrounding rocks.

they resemble I-type granites, with strong HREE-depletions and a lack of significant Eu anomalies.

Syntectonic plutons display a variety of fabrics, from massive to strongly foliated, concordant to discordant. A gradational fabric, massive in the core and increasingly foliated towards the margins, can be considered characteristic. Geophysical studies have constrained their vertical extent to less than ~ 15 km. Well-developed concordant foliation around the margins of many Archaean syntectonic plutons is suggestive of forceful diapiric injection. Like TTG's, syntectonic plutons also geochemically resemble I-type granites. It is not uncommon for greenstone felsic volcanics to show strong geochemical similarities with contemporaneous granitoids, possibly indicating cogenicity.

Post-tectonic granites, lastly, are often the only *bona fide* granites found in Archaean terrains, and may be anorogenic. They exhibit massive interiors and discordant contacts. Most are of the peraluminous or calc-alkaline variety, resulting from A- or S-type melting of sedimentary or igneous rocks in lower crust.

There is some indication that the duration of orogenic cycles has changed over the Archaean, with Barberton and Pilbara plutonism continuing for ~0.5 Gy after major volcanism, while entire cycles of volcanism, sedimentation, deformation and plutonism occured in less than 50 My in the Late Archaean, frequently followed by 'late' discordant granitoids in the following 50 My.

2.2.1. Archaean Basement

Seismic studies of Granitoid-Greenstone Terranes have consistently revealed crustal thicknesses in the range of 30 to 40 km – much thicker than the volcanosedimentary belts. The nature of the 'basement' underlying Archaean supracrustal sequences has been the subject of intense and prolonged debate, with hypotheses spanning the compositional spectrum from komatiitic through basaltic to sialic. It is an important question, informing our understanding of the onset of continental differentiation and plate tectonics (Blackburn et al., 1985).

The compositional dichotomy of GGTs has led some to draw analogies with continental vis-à-vis oceanic crust, whereby either (1) ancient tonalitic gneisses represent ancient continental-type basement onto which greenstone volcanics were erupted; or (2) greenstones were effectively interpreted as proto-ophiolites, representing primitive oceanic-type crust into which tonalities, granodiorites and granites intruded (Kröner, 1981).

Those who would have a sialic Archaean basement look to the abundant outcrop of ancient granitoid plutons and/or orthogneiss equivalents (Figure 6, 7; see also orthogneiss enclaves at Isua in Chapter 4, Figure 1). It has long been noted that many of these Archaean plutons, however, exhibit clear intrusive relationships with pre-existing volcanic-sedimentary sequences, raising the possibility that they are genetic derivatives thereof (Percival and Card, 1983), and inducing some to posit basement(s) of mafic or even ultramafic affinities (Glikson and Jahn, 1985; Jensen, 1985).

Basal remelting and recycling of a continually basalt-thickened crust has also been considered (Kröner, 1981). Glikson (1995), on the basis of REE and LIL element data, has suggested that early Archaean GGT's were produced through a process of 'sima-to-sial transformation'. In this model, mantle melting produced mafic-ultramafic volcanic units in the first stage, with minor felsic units produced through fractionation. Partial melting of this mafic crust produced tonalite-trondhjemite magma in the second stage. Finally, ensialic anatexis gave rise to LIL-rich granites-adamellites which formed 'hoods' above tonalite-migmatite batholiths, together with the characteristic discrete intrusions.

Little is known about the tectonic processes operating on the early Earth, and explanations for the stress, strain and metamorphic regimes in Granite-Greenstone Terrains span the kinematic spectrum from extensional through vertical to compressional. Without exception, Archaean greenstone terranes have undergone multiple episodes of (both ductile and brittle) deformation. There is no general agreement as to the role and veracity of vertical forces accompanying pluton intrusion. Canonically, metamorphic grade ranges from greenschist (or locally prehnite-

pumpellyite) to amphibolite facies, with higher grades occurring around margins of belts in pluton aureoles. Assemblages equilibrated at low pressures.

Early Archaean deformation, as found in the Barberton and the Pilbara, was classically attributed either to vertical tectonics through gravity-driven diapiric uprise of granitoids (Schwerdner and Lumbers, 1980), or to plate-tectonic induced far-field horizontal stresses effected on a layered granite-greenstone crust. Appeal has also been made to crustal thickening.

2.3. Greenstones

Several authors have commented on the progressive development of volcanism within greenstone belts, with initial komatiitic flows progressing through more widespread tholeiitic basaltic units, and finally coming to be overlain by intermediate and/or felsic calc-alkaline units (Allard et al., 1985; Blackburn et al., 1985; Glikson and Jahn, 1985; Jensen, 1985; Padgham, 1985; Thurston et al., 1985). Accompanying this alleged trend of ultrabasic-to-acid volcanism are increases in the relative amount of volcaniclastics to lave flows, and in (still highly subordinate) layered chert. These parallel trends are thought to indicate the evolution from voluminous oceanic eruption of a mafic lava plain or plateau to the formation of more localized arc-like calc-alkaline and tholeiitic stratovolcanoes and intervening sedimentary basins. However, close inspection of greenstone belt stratigraphy shows that exceptions to this canonical trend are the rule.

Early Archaean sedimentation can be divided into detrital and (bio)chemical, with biology playing an uncertain role in the formation of the latter. Detrital sediments are dominated by volcanoclastics, with rare evidence for a terrigenous component (e.g. Isua Supracrustal Belt meta-turbidites, Chapter 4; Coonterunah Subgroup meta-pelites, Chapter 5). Mid- and Late- Archaean greenstone belts often contain significant thicknesses of clsatic turbidites and, in some instances, terrestrial fluvial to deltaic terrigenous sediments.

Chemical sediments comprise cherts, carbonates, evaporites and banded-iron formation.Silicification is widespread in Archaean volcano-sedimentary sequences.

2.3.1. Kerogen

Insoluble hydrocarbon material ('kerogen') is a common component in Early Archaean greenstone-belt cherts, and is found in three different geological contexts: (i) Within bedded sedimentary units; (ii) Within cement-like pre-diagenetic chert; and (iii) Within cross-cutting post-diagenetic dykes.

Bedded sediment-hosted kerogen is found in a wide variety of sediments, but is most abundant in laminated carbonates (see thin-section photomicrographs of carbonate-hosted kerogen, Chapter 5) and cherts (Figure 5 (c)). It can occur in a wide variety of textural associations, including as coatings on grains (Figure 4 (a – c)), as matrix material, and in variably reworked detrital and breccia clasts. Kerogenous cement-like pre-diagenetic chert is common in neptunian fissures underlying unconformity surfaces (Figure 5 (d)). It is typically less abundant within bedded cherts, where it can be recognized by its production of soft-sediment deformation structures in associated sedimentary lithofacies prior to lithification (Figure 4 (f)).

Cross-cutting relationships show that much of the kerogenous chert in Early Archaean terrains likely post-dates sedimentation and fills cross-cutting chert dykes (Figure 4 (d, e, g)). Great care is needed in discriminating between these kerogen sources when drawing biological inferences from the kerogen (Buick, 1984).

3. Regional Geological Setting: The Pilbara

The ~193000 km^2 Pilbara Craton comprises a ~ 3.655 – 2.85 Ga Archaean granitoid-greenstone terrane ('GGT') together with unconformably overlying volcano-sedimentary sequences of the Late Archaean to Early Proterozoic 2.77 – 2.40 Ga Mount Bruce Supergroup of the Hamersley Province (Trendall, 1990). The craton is bounded at its eastern margin by the Proterozoic Paterson Orogen, at its southern and southeastern margin by the Proterozoic Capricorn Orogen and Proterozoic Ashburton, Bresnahan and Bangemall Basins, at its western margin by the Permian Carnarvon Basin and at its northeastern and northern margins by the Silurian-Devonian Canning Basin and the Indian Ocean (Figure 6).

Hamersley rocks once overlying the northern third of the craton have been largely eroded to expose the underlying GGT lithologies. Archaean units of the craton lie in a belt stretching roughly 500 km east-west and 200 km north-south (Figure 6, 7). North- to northeast-trending crustal-scale strike-slip faults dissect the craton, some of which are used to define the West-, Central- and East- Pilbara structural domains, with rocks older than 3300 Ma found only in the latter (Barley and Bickle, 1982).

Domical, ovoid, multi-component gneissic-to-granitic suites ~ 3655 - 2850 Ma in age comprise the 'granitoid' component of the terrane, visible on Figure 7 as paler areas. The term 'granitoid' is applied colloquially to designate this heterogeneous component, which comprises gneissic units of dominantly granodioritic composition, foliated supracrustal relics, and foliated-to-massive syn- to post-tectonic plutons exhibiting intrusive relationships with both surrounding gneisses and greenstones. Seismic and gravity studies reveal that these granitoids extend to nearly 15 km beneath the surface (Drummond, 1988).

The earliest granitoid phases are dominated by tonalite, trondhjemite and granodiorite, with granite *sensu strictu* gaining prominence over time. Granitoids record a polyphase and prolonged history of intrusion and deformation, with region-wide events at 3470 - 3400 Ma, 3325 - 3290 Ma, 3270 - 3235 Ma and 2940 - 2920 Ma (Nelson et al., 1999). Two older xenolithic phases, a ~ 3655 Ma gneissic xenolith in the Warrawagine Complex (Nelson et al., 1999) and a ~ 3578 Ma gabbroic anorthosite enclave in the Shaw Complex (McNaughton et al., 1988), have also been discovered.

3.1. The Pilbara Supergroup

Granitoid-gneiss domes are separated by narrow, steeply dipping almost contemporaneous ~ 3515 – 2950 Ma volcanosedimentary greenstone belts of the Pilbara Supergroup, which are confined to the upper ~ 5 km of crust (Drummond, 1988). The relationship between granitoids and interspersed greenstones is complex. Intrusive granitoid contacts and broadly coincident felsic volcanism in greenstones are emphasized by workers favoring a role for vertical diapiric granitoid emplacement (Collins, 1989; van Kranendonk and Collins, 1998), while faulted or sheared contacts

are put forward by others in support of a dominant role for horizontal tectonics in the juxtaposition of granitoids and greenstones (Bickle et al., 1980; Bettenay et al., 1981; Bickle et al., 1985).

The greenstone belts characteristically form tight, upright, shallowly plunging synclines with vertical to subvertical limbs oriented parallel to regionally trending belts. The McPhee and North Pole Domes, where sedimentary bedding steepens gradually and radially away from domal centers, provide important structural exceptions (Hickman, 1983, 1984). Some workers argue that greenstone dips gradually decrease with stratigraphic height, which in their view suggests deposition in thickening wedge-shaped carapaces adjacent to growing granitoid diapirs (Hickman, 1975; Hickman, 1983, 1984; van Kranendonk, 2000; van Kranendonk et al., 2002). Greenstone metamorphism ranges from prehnite-pumpellyite to mid-amphibolite facies conditions, with the majority of rocks bearing assemblages indicative of peak metamorphism at greenschist facies (Terabayashi et al., 2003).

Greenstones comprise a restricted range of lithologies, overwhelmingly (~75 – 90%) dominated by mafic volcanic rocks of an extrusive origin, many of which were lithified in a sub-aqueous environment. In the eastern Pilbara, is has been proposed that extensive sheets of mafic lavas gave rise to basins and shallow water platforms, in which partly sub-aerial calc-alkaline volcanic centres controlled major topographic relief (Barley et al., 1979; Barley, 1980). Pyroclastic and epiclastic volcanic sediments of calc-alkaline affinity formed sheets around these elevated volcanic centres and are interleaved with the mafic lavas.

Very low-grade magnesian basalts commonly exhibit relict igneous clinopyroxene, which is replaced by tremolite at higher grades. Komatiites (MgO > 18%) exhibiting extrusive spinifex textures are relatively scarce in Pilbara greenstone sequences, and where they occur are closely associated with magnesian basalt. Pilbara komatiites are characterized by the assemblage antigorite-tremolite-chlorite ± olivine, and commonly also contain carbonate. Intermediate to felsic volcanic flows and gabbroic-to-doleritic sills comprise most of the remaining igneous outcrop.

Emphatically subordinate to these extrusive and hyperbyssal igneous units are a diverse array of relatively thin but laterally extensive and continuous rocks of (for the most part) uncontroversially sedimentary origin. These sedimentary lithofacies, which occur together in distinct packages within much thicker volcanic piles, have commonly undergone extensive chemical alteration but locally exhibit good textural preservation.

The stratigraphical nomenclature of the Pilbara Supergroup has changed appreciably over time, and has been complicated by the challenge of correlation across both structural domains and greenstone belts (Figure 8). Four stacked unconformity-bound stratigraphic intervals are presently recognized by the Geological Survey of Western Australia, consisting of (i) the ~ 3.515 – 3.427 Ga Warrawoona (formerly Coonterunah) Group; (ii) the ~ 3.40 - 3.315 Ga Kelly (formerly Warrawoona) Group; (iii) the ~ 3.24 Ga Sulphur Springs Group; and (iv) the ~ 3.2 – 2.0 Ga Gorge Creek Group (van Kranendonk, 2006).

Exposures reveal up to 10 km of autochtonous stratigraphy, although thickness varies considerably from belt to belt. Stratigraphic correlation between Warrawoona units is fraught with difficulty and the possibility that the Warrawoona Group may represent a regional amalgamation of broadly coeval but distinct greenstone successions cannot currently be ruled out (Krapez, 1993).

The oldest greenstones are found in the Coonterunah Subgroup, the lowermost subgroup of the Warrawoona Group. Lithologically, it is dominated by extrusive mafic rocks consisting mostly of tholeiitic to magnesian basalt, with lesser felsic volcanic units and but volumetrically minor cherts. Rare volcanoclastic and carbonate sedimentary units are locally preserved (Chapter 5). It has been recognized only in the Pilgangoora Belt, where it attains a maximum stratigraphic thickness of ~6500 m and a lateral extent of ~50 km, and is unconformably overlain by the Strelley Pool Chert and Euro Basalt formations described below. The lower contact of the Coonterunah Subgroup, where exposed, is intruded by granitoids of the Carlindi Suite (outcrop photos of tectonized and intrusive contacts, Figure 20).

Elsewhere in the East Pilbara structural domain, the upper Warrawoona Group represents the lowermost expression of the Pilbara Supergroup. It is dominantly

composed of tholeiitic and magnesian basalt and gabbro with significant felsic volcanic and volcanoclastic units, minor localized ultramafic units, and minor but widespread cherty sedimentary units.

The 3238 - 3235 Ma Sulphur Springs Group unconformably overlies the Kelly Group. It is confined to the supracrustal belts immediately adjacent to the Strelley Granite, and finds most prominent expression in the Soanesville and Pincunah Belts. An eruption age of ~3235 Ma, coeval with the adjoining Strelley Granite, has been obtained for the Kangaroo Caves Formation at the stratigraphic top of the Sulphur Springs Group (Buick et al., 2002). Magnesian to tholeiitic basalt, dacite, andesite, volcanic and volcaniclastic rhyolitic units, epiclastic sediments, and cherts predominate.

Ages intermediate between that of the Kelly Group and overlying Sulphur Springs Group have been obtained for the Golden Cockatoo Formation in the northeastern Yule Granitoid Complex, adjacent to the Pincunah Belt (van Kranendonk, 2000), for which the stratigraphical position remains unclear.

Overlying the Sulphur Springs Group is the dominantly sedimentary Gorge Creek Group. It is composed of fine- to medium-grained clastic sediments (Figure 12 (a, b)) and banded-iron formation (Figure 12 (c)), in addition to magnesian and tholeiitic basalt, commonly pillowed. It has been described as a sequence of platform to trough sediments (Eriksson, 1982). Alluvial platform deposits have been described in the eastern and western Pilbara (though these rocks are probably from the overlying De Grey Group), and turbidite troughs are found in the south-eastern and central Pilbara (Barley, 1980). Although the Gorge Creek Group is widespread throughout the Pilbara, its age and regional correlatives are poorly constrained.

Locally and unconformably overlying the Gorge Creek Group is the 2.99 Ga volcano-sedimentary Whim Creek Group and the ~2.95 Ga (Wingate, 1999) DeGrey Group, whose constituents are also of poorly constrained age. In the East Pilbara structural domain, the Whim Creek Group consists of mafic and felsic volcanics and fine- to coarse-grained epiclastic sediments, and can be distinguished from underlying units by the relative paucity of rocks of volcanic derivation. The DeGrey Group

includes the conspicuous Lalla Rookh Sandstone, a thick package of fluvial and lacustrine sediments structurally emplaced between the Pilgangoora Belt and North Pole Dome. Deposition of both Gorge Creek- and DeGrey Group sediments in small restricted strike-slip basins (Krapez and Barley, 1987; Krapez, 1993) may account for the lack of Pilbara-wide correlations.

Deposition of the Pilbara Supergroup ceased by 2.85 Ga. Unconformably overlying the granitoids and greenstones of the Pilbara Craton are the generally flat-lying to shallowly-dipping supracrustal rocks of the Fortescue Group that form the stratigraphic base of the Mount Bruce Supergroup, deposition of which commenced at ~2757 Ma (Arndt et al., 1991; Blake et al., 2004). The Mount Bruce Supergroup is divided into the Fortescue, Hamersley and Turee Creek Groups, only the first of which is represented in the north Pilbara. The Fortescue Group is predominantly composed of subaerially erupted tholeiitic flood basalts and epiclastic sediments (Blake, 1984; Nelson et al., 1992; Blake, 1993).

Regional metamorphism in the Pilbara is largely strain-controlled (Barley et al., 1979). The overall range of metamorphism varies from prehnite-pumpellyite or sub-greenschist facies in low-strain domains to amphibolite facies in zones exhibiting intense deformation. It has long been recognized that both the metamorphic grade and the intensity of deformation within the greenstones increase towards the contact with granitoid or gneiss bodies (Hickman, 1972b; Bickle et al., 1980).

4. Pilgangoora Belt Lithology

The Pilgangoora Greenstone Belt (‘PGB’) comprises the northern part of the irregularly-shaped Pilgangoora Syncline, which is bounded by Carlindi Granitoid Complex to the north and west, the Yule Granitoid Complex to the south, and the truncating Lalla Rookh-Western Shaw Fault to the east. Greenstones of the Pilgangoora Syncline have been divided into the geologically distinct northern Pilgangoora Belt and southern Pincunah Belt along the Mount York Deformation Zone.

Within the Pilgangoora Belt, emphasis here is placed on the oldest exposures, consisting of the Warrawoona and Kelly Groups, together with the basal contact with intrusive Carlindi granitoids. The ensemble forms a continuous ~50 km long belt in which ~6500 m of Warrawoona and up to ~3500 m of Kelly successions are exposed (Figure 9).

The Carlindi Granitoid is the largest of the Pilbara granitoid-gneiss suites and complexes. Carlindi granitoid exposure has gentle relief and is most prevalent within 1 – 2 km of the greenstone contact, where it is encountered in and near creek-beds or as isolated domes protruding above surrounding Quaternary cover. Isolated Carlindi granitoid outcrop has been reported as far as 30 km from greenstones (Green, 2001). Strong weathering has frequently given rise to friable and poorly preserved outcrop. Distinctly light-coloured soil conceals granitoid subcrop.

Warrawoona and Kelly Group exposure is under strong lithological control and more variably preserved than acidic plutonic rocks. In both, silicified sedimentary packages tilted to near vertical jut out as prominent ridges above the flat Carlindi landscape. Exposure of mafic extrusives and intrusives, markedly less silicified than chert units, occupy flatter valleys between chert ridges. With the exception of regional and local manifestations of several ductile and brittle deformation events, described below, sedimentary and volcanic bedding dips steeply (70 - 85º) away from the underlying contact with Carlindi granitoid, which is roughly parallel to bedding.

Bearing thin (< 5 m) chert ridges, Warrawoona Group outcrop is exposed as low, undulating hills. This gentler geomorphology terminates abruptly at the unconformable contact (Figure 11 (a)) with the overlying pervasively silicified sub-aqueous and sub-aerial sediments of the 8 – 30 m Strelley Pool Chert (‘SPC’) of the Kelly Group, which crop out as a prominent and near-continuous ridge for most of the ~50 km strike-length of the belt. Units underlying this unconformity together represent the lowermost known exposure of the Pilbara Supergroup, and collectively comprise the Coonterunah Subgroup of the Warrawoona Group, which has been further subdivided into the magnesian basalts, tholeiites and mafic intrusives of the lowermost Table Top Formation, mafic and felsic volcanic units and lesser but well-exposed

cherts of the intermediate Coucal Formation, and tholeiites and mafic intrusives of the upper Double Bar Formation.

Possible correlates of the SPC have been reported from the Coongan, North Shaw and Kelly Belts and the North Pole Dome. The SPC bears several distinct sedimentary lithofacies assemblages (Barley and Bickle, 1982; Lowe, 1983; Rasmussen and Buick, 1999), including siliciclastic sediments, epiclastic volcanic sediments, carbonates, evaporites and carbonaceous muds. Evidence of local and intermittent sub-aerial exposure and erosion is provided by the interlayering of some sedimentary structures with mafic lavas (Barley et al., 1979).

Some of the oldest putative evidence of life comes from the SPC (Lowe, 1980, 1983; Buick and Barnes, 1984; Dimarco and Lowe, 1989b, a). Stromatoloidal cones of 2 – 15 cm diameter are common in the laminated SPC lithofacies in the Pilgangoora Belt, and have also been observed in other belts (Dunlop et al., 1978; Lowe, 1980; Walter, 1980; Lowe, 1983; Buick and Barnes, 1984; Dimarco and Lowe, 1989a; van Kranendonk, 2000). They are frequently interpreted as ‘stromatolites’ (e.g. Allwood et al., 2006; Allwood et al., 2008) i.e. laminated benthic microbial deposits (Kalkowsky, 1908; Riding, 1999).

Two volcanosedimentary meta-chert units (‘Chert VII’ and ‘Chert VIII’) and up to ~3500 m of mafic volcanics, hyperbyssals and intrusives of the Euro Basalt Formation overlie the SPC and represent the remainder of Kelly Group outcrop in the Pilgangoora Belt. Spherical μm-scale structures in black chert from Chert VIII (Figure 4 (g)) have been interpreted to be of cyanobacterial origin (Schopf and Packer, 1987), although cross-cutting relationships suggest that this chert may not be of sedimentary origin. An unambiguous sub-horizontal to angular unconformity with the overlying siliciclastic units of the Gorge Creek Group (Figure 12 (b)) marks the upper termination of the Kelly Group.

Several episodes of silicification have affected the Pilgangoora Belt. As in bedded meta-cherts, high quartz abundances and granular rather than cryptocrystalline quartz textures in mafic rocks are indicative of pre-peak-metamorphic silicification

This has preferentially affected more permeable and porous units in mesoscopic alteration zones, commonly in the top ~ 5 m of volcanic flows (see further Chapter 5).

All Pilgangoora Belt protoliths have been metamorphosed to at least lower greenschist facies, and the 'meta' prefix to lithologic names will therefore be taken as implied. Chert formed during Cenozoic silicification forms an important exception, and metamorphosed and non-metamorphosed chert will be therefore be designated with the traditional 'meta-chert' and 'chert'. Like Pilbara rocks elsewhere, Pilgangoora Belt outcrop has also undergone variable and generally pronounced post-metamorphic alteration and weathering. Ferruginous surface outcrop bears thin oxidised mantles, and gossanous boxwork after pyrite and probably carbonate is common in the evaporite lithofacies of the SPC. Silcrete and ferricrete commonly alter metachert on elevated plateaux and rises, and in depressions. Depressions bear evidence of calcretization, probably altering calcic basalts.

4.1. Coonterunah Subgroup

4.1.1. Table Top Formation

The Table Top Formation is dominated by up to ~2000 m of variably silicified and metamorphosed mafic extrusive- and intrusive- units. Extrusive units consist almost entirely of fine-grained basalt, with grain sizes of ~0.5 mm in outcrop that has undergone the least metamorphic recrystallization. In zones of greater recrystallization in which volcanic textures are absent or have been obliterated, it is not always possible to distinguish between massive basalts and dolerite protoliths. The base of the Table Top Formation bears the only magnesian basalt in the Coonterunah Group, characterized by < 250 m of variolitic flows with well-developed ocelli (Figure 13 (a, b)). Up to 20 m of pyroxene-phyric komatiitic basalt overlie this, with elongate needles completely altered to amphibole. This unit marks the only known occurrence of komatiite (*sensu lato*) in the Pilgangoora Belt.

The remainder of the mafic volcanic rocks in the Table Top Formation, and in the Coonterunah Group as a whole, are tholeiitic and generally massive in character. Pillows are uncommon, and vesicles and amygdales are rare to absent. Where present,

pillows are well-preserved with distinct cores, margins and rinds, with long axes in the range of 50 - 150 cm. Ripple cross-laminated volcanogenic sediment occurs on some flow-tops of amygdaloidal basalt (Figure 13 (c, d)).

Intrusive rocks exhibit a textural continuum (up to ~15 mm range in groundmass grain-sizes) from hyperbyssal (sub-volcanic) doleritic to gabbroic. Mafic intrusives occur as tabular conformable to semi-conformable bodies, commonly capped by extrusive flows. Intrusive intrusions occur as cumulate xenoliths in the lower Table Top Formation (Figure 13 (e, f)).

Mafic intrusion pre-dated Carlindi plutonism and associated metamorphism. In coarser rocks at lower metamorphic grades, exsolution lamellae betray rare relict igneous assemblages of clinopyroxene and (even more rarely) green-pink pleochroic orthopyroxene, together with plagioclase and hornblende. However, both intrusive and extrusive mafic rocks are dominated by metamorphic assemblages of amphibole (25 - 50% ferro-actinolite, with alumino-ferrotschermakite at amphibolite facies), albite (25 - 50%), epidote (~ 10 %), chlorite (0 - 20%), and quartz (5 - 20%), together with trace amounts of leucoxene and opaque oxides (magnetite and ilmenite). Margarite (up to ~ 10%) is sometimes present. Minor localized coarse ankeritic alteration is also present, particularly in more vesicular and amygaloidal outcrops.

4.1.2. Coucal Formation

The Coucal Formation immediately overlies the Table Top Formation. Coucal Formation metasediments are described in detail in Chapter 5. For much of its lateral extent, two or three prominent metachert-BIFs near the base of the Coucal Formation represent the full complement of preserved Coonterunah sedimentation. Metachert units are up to ~ 8 meters thick at their eastern-most occurrence, and gradually thin to ~ 0.5 meters or less towards the west-north-westerly fold closure of the the Pilgangoora Syncline. They exhibit mm- to cm- scale alternating, planar to gently undulating and anastomosing, dark and light banding. Black bands comprise either magnetite or black, variably kerogenous, chert. Overlying the intermediate metachert unit is a rarely preserved ~35 m section of interleaved bimodal tephra and planar laminated, variably

silicified micritic-carbonate. Red, haematite-rich layers alternating with white bands of clear to milky white pure cryptocrystalline quartz occur towards the westward and eastward terminations of outcrop, and appear to represent alterations of the planar laminated carbonate.

The presence of Ca-Mg silicates within metachert bands, Fe-Ca-Mg silicates along the planar interfaces with ferruginous bands, and widespread metachert after laminated carbonate is highly suggestive of diagenetic silicification of an aragonite, calcite and/or dolomite precursor to at least some planar Coonterunah metachert bands.

Rocks overlying Coucal cherts are dominated by ~1000 m of fine-grained, occasionally pillowed, tholeiitic basalt and lesser hyperbyssals and intrusives texturally similar to tholeiites of the underlying Table Top Formation described above.

A laterally extensive unit consisting of various facies of felsic volcanic affinity occurs at the top of the Coucal Formation. This unit shows a distinctive brecciated appearance in outcrop, weathering into rounded blocks. Facies include highly vesicular and amygdaloidal hyaloclastic breccias of dacitic to rhyolitic affinity and flow-banded dacite. Where terminated by the Warrawoona-Kelly unconformity, one unit is over >200 m thick. These felsic volcanics are dominantly composed of 1 - 5 mm quartz and heavily pyrophyllite-altered rectangular feldspar phenocrysts and stretched ~ 1.5 cm spheroidal amygales set in a highly silicified and sericitized beige to light-green groundmass assemblage of fine (< 0.1 mm) quartz and albite-altering muscovite with variable amounts of chlorite and trace quantities of opaque oxides.

U-Pb chronology of a brecciated hyaloclastic rhyolite sample from this unit has constrained of the age of the Coucal Formation to 3515 ± 3 Ma (Buick et al., 1995). The style of blocky pumiceous autobrecciation exhibited by this unit is typical of felsic volcanic deposition in deep aqueous environments (Fisher and Schmincke, 1984).

4.1.3. Double Bar Formation

The Double Bar Formation, overlying the Coucal Formation, is dominated by ~3500 m of fine-grained, occasionally pillowed, tholeiitic basalt and lesser

hyperbyssals and intrusives texturally similar to that those of the lower Table Top Formation. Thin interbeds of volcanoclastic fine-grained mafic tuff are occasionally preserved.

4.2. Carlindi Granitoids

The base of the Table Top Formation is intruded by the Carlindi Granitoid (Figure 20 (a – c)). Where exposed, this contact is variably tectonized, ranging from highly kinematic with contact-parallel foliation in greenstone country rock and gneissic granitoid (Figure 20 (a)), to cross-cutting with massive igneous textures and plentiful tabular angular greenstone xenoliths in granitoid (Figure 20 (b, c)).

Quartz-feldspar ratios are compatible with a granodioritic or monzograntic composition for Carlindi Granitoids, although normative calculations instead indicate trondjemitic or granitic classification (Green, 2001). Massive outcrops with igneous textures consists of euhedral plagioclase (40 – 50%), quartz (30 – 40%) and microcline (10 – 20%) with lesser dark green prismatic hornblende (5 - 10%) and biotite phenocrysts (0 – 5%). Grain-sizes of these dominant minerals commonly fall in the range of 5 - 10 mm, with some phenocrysts measuring up to ~40 mm. Accessory minerals, generally subhedral to euhedral, include epidote, clinozoisite, opaque oxides, muscovite, zircon, rutile and apatite. Hornblende and epidote have commonly undergone variable chloritization. On the basis of greater (~5 %) muscovite abundances and poikilitic microcline with plagioclase and quartz inclusions, Green (2001) distinguished a separate monzogranite member of the Carlindi granitoid suite.

A quartz-phyric microgranite bearing well-rounded spherical 1 – 2 mm beta-quartz and subhedral to euhedral 1 – 3 mm orthoclase phenocrysts intrudes the coarser Carlindi granitoid near the center of the Belt at Neptunian fissure locale (2) (see below). This has been dated by U-Pb zircon geochronology at 3464 ±x Ma (Buick et al., 1995), younger than other dated Carlindi granitoids by ~ 20 Ma.

4.3. Kelly Group

Like the underlying Coonterunah Subgroup exposure, the Kelly Group consists in large part of volcanic rocks. Outcrop is dominated by pillowed tholeiitic lavas, interlayered with varied cherty sediments and volcanics of more calc-alkaline affinity.

4.3.1. Strelley Pool Chert

The basal unit of the Kelly Group in the Pilgangoora Belt, which concordantly overlies the basal unconformity with the Coonterunah Subgroup, is the the Strelley Pool Chert. This unit gradually thins from a maximum thickness of ~ 30 m in the eastern segment, through ~ 20 m to ~ 8 m in the central segment and disappears altogether in the highly strained western segment. Lateral continuity suggests that a gradually thinning ~ 150 - 30 cm fuchsitic chert unit in the region of the Pilgangoora Syncline closure is correlative with the Strelley Pool Chert.

Up to five differentiable lithofacies assemblages make up the SPC. The basal assemblage, immediately and unconformably overlying Coonterunah Subgroup volcanics, consists of well-sorted and well-rounded 0 – 6 m thick orthoquartzitic sandstone with minor chert-pebble conglomerate. This assemblage is sometimes absent, and cannot be recognized in the western, higher grade quarter of strike. Clast diameters range from 1.5 – 2.0 mm, and are thoroughly cemented in a sericitized quartzitic matrix. In addition to well-rounded spherical quartz (~75 – 90%), clasts include sub- to well-rounded pyrite, chloritized mafic volcanics, magnetite, anhedral to euhedral ilmenite, rounded completely sericitizied felsic volcanics, and sub-hedral zircon, in decreasing order of abundance (Figure 14 (a, b)). Sedimentary textures include normal grading and both planar and trough cross-bedding.

The most prominent SPC assemblage is the overlying planar- to wavy-laminated meta-chert unit, locally stromatoloidal, that overlies the quartzitic sandstone or Coonterunah rocks where no basal sandstone underlies (Figure 15 (c)). This unit is locally brecciated. Lamination consists of incompletely silicified dolomite in isolated low-grade outcrops, but is more typically completely replaced by either or both pre- and post-metamorphic (meta-)chert (Figure 22 - 24). Dolomite is variably ferruginous

but sub-ankeritic (< 20 % $FeCO_3$). Stromatoloidal cones occur on some bedding surfaces and have typical diameters of ~ 2 cm, with similar heights.

A crystal-fan lithofacies is occasionally found near the top of, but always within, the laminated lithofacies assemblage. Crystals occur as elongate 2 – 8 cm long and 0.5 – 1.0 cm wide digitate shapes, showing six-sided cross-sections and square terminations suggestive of an aragonite precursor (Chapter 1, Figure 7 (c)). Dark-brown dolomitic mud fills intercrystalline spaces where incompletely silicified.

Two distinctive volcanoclastic meta-cherts mark the upper SPC lithofacies assemblage, and are characterized by varying degrees of apple-green fuchsitic alteration. Such chromium alteration appears to be a typical feature of the upper lithofacies of Early Archaean sedimentary cherts where they are overlain by magnesian volcanics. It is also seen at the top of meta-cherts in the lower Barberton stratigraphy (Figure 5 (e)), and is not obviously associated with ultramafic units at either locale.

The lower unit consists of a silicified greenish grain-supported anatase-rich sandstone, massive to normally graded (Figure 15 (e, f)). Unit thickness varies from ~270 cm to absent, but where encountered is typically ~ 20 - 40 cm thick. Clast diameters are also highly variable, from as large as ~15 mm to as small as ~0.5 mm, but medium to fine sand is typical. The majority of clasts are variably chloritized, highly angular and distinctly arcuate, representing silicified pseudomorphs after unwelded shards of mafic glass.

The upper unit consists of silicified greenish-grey to grey siltstone-to-lutite (Figure 16 (c)). This unit is plane-laminated at lower grades, with sedimentary bedding becoming increasingly massive with metamorphic recrystallization. Laminar thicknesses are on the order of ~ 0.1 – 0.5 mm. A zebraic texture resulting from pressure dissolution is common, as are flame structures and intra-clast brecciation. Also locally present are thorougly silicified 2 - 8 mm euhedral crystals with ~ 0.5 – 1.0 mm pseudo-hexagonal cross-sections and oblique pyramidal terminations (outcrop photographs, Figure 14 (c)), that have been interpreted elsewhere as pseudomorphs of gypsum (Buick and Dunlop, 1990) (Figure 14 (d, e)).

Alternating planar-banded (1 – 10 mm) black and white kerogenous cherts are found throughout the Strelley Pool Chert. Kerogen is also present in massive black chert, which commonly occurs in a variety of textural associations, including as tabular fragments in megabreccia, as cross-cutting dyke-like structures with thicknesses on the order of 10 – 40 cm, and less commonly as an early cement-like matrix to metachert mega-breccia (Figure 4 (f), Figure 5 (c)).

4.3.2. Euro Basalt Volcanics and Cherts

The Euro Basalt Formation comprises up to 3500 m of pillowed (and more rarely massive) tholeiitic and magnesian basalt flows, with intrusive gabbro and lesser localized doleritic flows. The mafic stratigraphy of the Euro Basalt is interrupted by two conformable ridge-forming 0 – 5 m chertified volcanoclastic units, colloquially named ‘Chert VII’ and ‘Chert VIII’.

Kelly Group mafic volcanism is distinguished from that of the underlying Warrawoona Group by the greater prevalence of pillow structures and amygdales, and greater abundance of variolitic magnesian basalt. Vesicles are larger, more abundant, and more densely concentrated, indicative of shallower eruption under lower confining pressures. Doleritic flows can be distinguished by sudden decreases in grain-size at upper contacts. Igneous assemblages of both magnesian and tholeiitic basalts of the Euro Basalt member are compositionally similar to that described for the underlying Coonterunah Subgroup, as also born out by geochemical similarities (Green et al., 2000).

Chert VII is dominated by a very fine-grained plane to cross-laminated silicified bluish-grey mafic lutite, variable in thickness. A massive mafic mudstone immediately overlies this unit. It contains abundant ~ 0.5 mm euhedral diagenetic gypsum pseudomorphs, hexagonal in cross-section and unambiguously monoclinic in transection, with thin white alteration haloes and occasional lithic cores. Gypsum orientations are not quite random, tending towards the bedding-parallel. This unit is more pyritic than the lutite unit at the top of the Strelley Pool Chert, with pyrite of varying roundness and grainsize, but generally fairly cubic. Black kerogenous veins

cross-cut both meta-chert lithofacies. Chert VIII is similar in many respects to Chert VII, and was also highly gypsiferous. It contains a graded silicified mafic sandstone-conglomerate unit at the top. Clasts are highly varied, with a high proportion of black and white banded chert clasts.

4.3.3. Neptunian fissures

Dyke-like structures are associated with Kelly Group sedimentary meta-cherts at 3 localities in the Pilgangoora Belt (see map inset, Chapter 7, Figure 1). Structures at sites (1) and (2) occur in the eastern and central belt segments, respectively, and are associated with the Strelley Pool Chert (Figure 15 (a – c)). They are interpreted to be neptunian fissures that formed through crustal rupture at the time of Strelley Pool Chert deposition, and were filled by material derived from above whilst opening. A final dyke-like structure occurs at site (3) in the western segment of the belt, and is associated with Chert VII. However, because metamorphism has obliterated sedimentary structures and textural relationships, this particular structure cannot confidently be interpreted as a neptunian fissure.

At fissure site 1, a single ~ 220 m deep fissure passes from the Strelley Pool Chert downwards through the Warrawoona-Kelly unconformity into underlying Coonterunah rhyolite (geological map, Chapter 7, Figure 1). This fissure is 270 cm wide at its top within the Strelley Pool Chert, and gradually thins to 20 cm at its tail. At fissure site 2 in the central segment of the belt, five fissures (designated (a) through (e), from east to west, hereafter) also pass from the Strelley Pool Chert downwards through the Warrawoona/Kelly unconformity into underlying Carlindi granitoid (geological map, Chapter 7, Figure 4). Fissures (a) through (d) are 400, 300, 400, 700 and 400 meters deep, respectively. At ~700 m, fissure 2(d) is the deepest observed in the Pilgangoora Belt, and has previously been interpreted as a feeder dyke to the SPC (Lindsay et al., 2005).

All fissures have near-vertical (80º – 90º) dips, and are sub-perpendicular to their associated chert units and the dominant regional orientation of the underlying greenstone-granitoid contact. Below bedded chert units, their proximal host rock has

undergone variable silicification within 1 - 5 m of fissure walls, with alteration increasing towards the fissure contact (Figure 15 (b)).

Contact relations between fissures and the Strelley Pool Chert are occasionally preserved. Where the top of the fissure can be identified within SPC, it is accompanied by slump structures and intense brecciation directed towards the fissure opening. Soft-sediment deformation structures are absent in underlying sediment, which instead shows terminated contacts with fissure walls (Figure 18, 19).

Fissure material is dominated by a diversity of silicified clastic lithologies, angular mega-breccia of varied composition, cement-like matrix chert, mm- to cm-scale banded chert, and chalcedonic quartz. Neptunian volcanoclastic sediment is dominated by silicified mafic siltstone and sandstone, which at site (1) can be traced directly to its source in stratigraphically overlying clastic meta-chert lithofacies in the SPC. Contacts between neptunian clastic material and bracciated clasts of silicified laminated carbonate often show impinging structures (Figure 20 (a, b)). As these structures occur on some surfaces but not on others, they are likely flame structures rather than corrosion pits.

Mega-breccia fragments range from pebble- to meter- size, and include cohesive blocky angular clasts of Carlindi granitoid (Figure 16 (a, b)), variably silicified planar- and wavy- laminated dolomite (Figure 16 (c, d), silicified mafic sandstone (Figure 16 (e, f), Figure 17 (a, b)), and silicified mafic lutite (Figure 17 (c, d)). The combined ensemble of fissure breccia clasts represent all lithofacies identified in the Strelley Pool Chert. Despite the presence of silicified lutite texturally indistinguishable from that of the SPC, gypsum crystallites are absent, suggesting that their formation occurred during diagenesis after fissure filling.

Where present, chalcedonic quartz has grown along the outer fissure edges, parallel to fissure walls, and clearly post-dates neptunian sedimentation and breccia in-fill (Figure 17 (d, e)). Chalcedony formed during final phases of neptunian opening, perhaps during periods of restricted sedimentary input during low-stand(s) when the fissure mouths emerged above sealevel.

Observations suggest that at least some of the fissures opened during deposition of the laminated carbonate lithofacies, the lower section of which remained cohesive during fissure formation. Structural features are compatible with early syn-SPC fissure opening. None of the fissures pass into Euro Basalt volcanics immediately overlying the SPC, and all record Pilgangoora deformation events. For example, fissure (1) has undergone folding during Pilgangoora Syncline-related deformation (D_7), while sinistral fissure-parallel shear-zones in host granitoid at sire (2) post-date prominent fissure cleavage fabric, and probably represent exploitation of the fissure/granitoid lithological discontinuity during regional N- to NNE- faulting (D_5), rather than reactivation of an earlier fault-related fabric.

Structural relationships with underlying granitoid-greenstone contacts and the lack of fissure-related shearing suggest that fissures opened in response to flexural crustal tension, likely in response to diapiric uprise of underlying granitoid(s). It is noteworthy that felsic rocks are rare in the Pilgangoora Belt, and underlie the Warrawoona-Kelly unconformity in only two areas, both of which contain fissures. In contrast, fissures are never encountered within vastly more common (> 95 % of the Warrawoona-Kelly unconformity strike-length) mafic Coonterunah units, suggesting that fissure formation was under strong lithological control. Perhaps granitoid and rhyolite locales represented erosion-resistant topographic highs, atop a surrounding mafic plane or plateau, in which sequential alternation of sub-aerial exposure and drowning allowed for the episodic entrapment of sedimentation.

Superficially similar dyke-like structures at North Pole Dome bear kerogenous chert of similar (low) isotopic composition to Pilgangoora Belt neptunian fissures (Chapter 7, see also Concluding Chapter). Although they have received varied geological interpretations (Hickman, 1972a; Dunlop, 1976; Nijman et al., 1998a; Ueno et al., 2004), a neptunian origin has thus far been recognized only by Buick (1985).

5. Structural Geology

Regional deformation histories were proposed by Hickman (1983) and more recently by Blewett (2002), and a comprehensive sequence-stratigraphic model was proposed by Krapez (1993). The majority of structural studies, however, have focused specifically either on the West Pilbara (Kiyokawa, 1983) or the East Pilbara (Bickle et al., 1985; Collins, 1989; Zegers et al., 1996; van Kranendonk, 1997; Collins et al., 1998; Nijman et al., 1998b; van Haaften and White, 1998; van Kranendonk and Collins, 1998; Zegers et al., 1998; Kloppenburg et al., 2001). A five-fold deformation history was recently proposed to address the structural history and timing of gold mineralization in the northern part of the field area (Baker et al., 2002). These are compared with results from the present study in Table 1.

The Pilgangoora Belt, taken as a whole, records a complex deformation history. However, in rocks of the Warrawoona and Kelly Group in the eastern and central segments of the Pilgangoora Belt, most of the deformation events find expression only in localized shear-zones, if at all. This situation changes rapidly within the region of the Pilgangoora Syncline closure, where all but three of D_1 through D_{tect} deformation are recorded (Table 1).

In the lower-grade segment of the belt, D_1, D_2, D_5 and D_7 fabrics are dominant, with isoclinal F_3 folding, associated with M_3 talc in Kelly Group meta-cherts and M_3 cummingtonite-grunerite in Warrawoona Group magnetite meta-cherts, of local importance. All fabrics are overprinted by low-amplitude (~ 5 km-scale wavelength) gentle N-S directed folding, associated with on-going tectonism associated with subduction of the Australian plate under Indonesia (D_{tect}).

The first recognizable fabric in the field-area, D_1, overprints primary bedding in the Coonterunah Group, and is developed as bedding-parallel slaty cleavage or schistosity. Localized upright folds, associated with dextral kinematics in Coonterunah meta-cherts, record pre-Kelly Group deformation. Because this fabric is highly variable and so cannot be easily interpreted, it is not treated seperately here.

D_1 fabric pre-dates the unconformably overlying Warrawoona Group lithologies. The earliest recognizable non-primary fabric in the Warrawoona Group,

D_2, overprints S_1 schistosity and slaty cleavage in the Coonterunah Subgroup. S_2 foliation is bedding-parallel in Kelly-Group volcanosediments, while giving rise to a composite fabric in obliquely striking Coonterunah Subgroup rocks.

Regional N- to NNE- trending D_5 faults cut through volcanosedimentary horizons, and across the contact with the Carlindi granitoid. Many of these faults show evidence of more recent reactivation.

Post-D_5 fabric is dominated by D_7 deformation, characterized by shallowly south-plunging lineations and (~500 – 3000 m) macroscale folds (F_7) that refold ductile and brittle fabrics of older events. The most prominent regional structures resulting from D_7 deformation are the Pilgangoora Syncline, two smaller folds immediately southwest of it, and open folds refolding earlier NE-plunging isoclinal F_3 folds immediate south-east of the Iron Stirrup mine.

6. Diagenesis, Metamorphism and Alteration

An understanding of the diagenetic, metamorphic and alteration history of the field area is imperative to the interpretation of depositional environments and biosignatures.

6.1. Early Dolomitization and Silicification

Diagenetic dolomitization and both diagenetic and hydrothermal silification are described for Coonterunah Subgroup rocks in Chapter 5. Sedimentary chert samples of the Strelley Pool Chert also bear evidence of early (pre-metamorphic) dolomite formation and concurrent or closely antecedent silicification that is similar to the localized ‘selective’ type described in deeper marine meta-sediments from the Coonterunah Subgroup.

Abundant isolated sparry dolomite rhombs are preserved within SPC meta-chert (Figure 22), commonly in association with kerogen. Diagenetic dolomite is readily distinguished from unbedded sugary metasomatic carbonate, typically void-filling, that grows perpendicular to surfaces and has a granular texture (Figure 23 (a)). SPC dolomite is euhedral, and saddle dolomite is absent. Isolated rhombs in a meta-chert

matrix are remarkably invariable in size across the entire lateral extent of the Strelley Pool Chert metamorphic facies that bears pre-metamorphic carbonate, with 100 – 120 μm planar crystal faces (Figure 22). This is highly suggestive of early silicification by fluids whose chemical composition is seawater-controlled. In less silicified samples, variably sized dolomite crystals occurs along distinct lamellae, with near-pure dolostone in sites that have escaped silicification. Similar dolomite spar textures have been interpreted elsewhere to indicate the preferential silicification of calcite (or aragonite) subsequent to the inception of dolomitization, but before dolomitization was sufficiently advanced beyond formation of individual crystals (Laschet, 1984; Knauth, 1994).

SPC dolomite is variably silicified to meta-chert and chert (Figure 23 (b - h), Figure 24). Early silicification of isolated spar is identified by grains with skeletal textures and rounded amoeboid quartz blebs of ~ 10 - 20 μm diameter containing remobilized kerogen. In carbonate-rich meta-cherts and some samples bearing carbonate cut by quartz veins, distinct dissolution-silicification fronts occur parallel to carbonate-metachert contacts (Figure 24), similar to those observed in localized metachert replacement of precursor carbonate in the Coonterunah Subgroup (compare dissolution-silicification front in Chapter 5, Figure 10 (k, l)).

6.2. Metamorphism

In the absence of assemblages allowing quantitative geothermobarometry, metamorphism had to be studied through calculation of P-T diagrams and pseudosections. Pseudosections were constructed for meta-mafics in the Al-Fe-Mg-Na-Si-CO_2-H_2O system (Chapter 5, Figure 14) using bulk analyses for meta-basalts (Figure 28, 29) reported in Green (2001). P-T diagrams were constructed for meta-cherts in the Ca-Fe-Mg-Si-CO_2-H_2O system and Ca-Mg-Si-CO_2-H_2O sub-system (Figure 30; see also Chapter 5, Figure 16, 17). Although useful, the low grades of metamorphism restrict the applicability of these tools to qualitative assessment only. The resulting metamorphic zonation is summarized in Figure 31.

6.2.1. Early Metamorphism

In addition to post-depositional hydrothermal alteration and burial, Kelly and Warrawoona Group rocks have been metamorphosed to at least sub-greenschist and lower-greenschist facies, respectively. In both units, initial metamorphism undoubtedly accompanied early tilting to sub-vertical. Surviving early metamorphic textures in Kelly and Warrawoona mafic rocks that pre-date regional metamorphism include the widespread presence of chlorite after both olivine and augitic clinopyroxene, and the replacement of plagioclase by albite. The presence of early prehnite-pumpellyite in Kelly Group meta-basalt pillow rims and prehnite in meta-chert (Figure 26 (a - c)) in the eastern segment of the Pilgangoora Belt marks the lowest metamorphic grade encountered, and may date back to this nascent phase of metamorphism. No prehnite is encountered in any underlying Warrawoona rocks of any kind, suggesting that they experienced higher grades of pre-regional metamorphism. Any related planar fabric associated with early tiliting would have been obliterated by similarly oriented oriented foliation associated with later metamorphic events, and no evidence of an accompanying early lineation fabric survives.

6.2.2. Carlindi-Granitoid Thermal Metamorphism

Two prominent later metamorphic gradients can be distinguished on the basis of structural, textural and mineralogical evidence. The older (M_1) is a ~ 100 - 350 m thermal metamorphic gradient increasing towards the intrusive contact with the ~3.48 Ga (Buick et al., 1995) Carlindi Granitoid complex to the north. The fabric associated with contact metamorphism varies from hornfels to a strong contact-parallel foliation, now with sub-vertical dip. Characteristic M_1 assemblages are defined by chlorite-actinolite-epidote in meta-basalts, -dolerites and -gabbros, tremolite- or actinolite-quartz in metachert-carbonates, and grunerite- or cummingtonite-quartz in ferruginous meta-cherts. Frustratingly, these peak assemblages do not allow for a quantitative assessment of the depth of intrusion. However, on the basis of P-T pseudosections calculated for metamafic rocks with Coonterunah bulk compositions, M_1 metamorphism occurred at low but poorly constrainable pressures. In particular, the

absence of almandine-garnet, the absence of metamorphic calcic clinopyroxene (diopside-hedenbergite series) or pargasite in favour of tremolite, and presence of highly sodic plagioclase, together suggest contact metamorphism at somewhat unusually low pressures, well below 3500 bars and probably closer to ~ 2000 bars. This low metamorphic pressure, taken together with the observation that the M_1 hornfels assemblage remains consistent for ~30 km of strike, suggest plutonism occurred from below.

M_1 fabric is restricted to Coonterunah Subgroup rocks, and does not penetrate the Warrawoona-Kelly unconformity, even where the unconformity itself coincides with the upper stratigraphic termination of Carlindi granitoid. Similarly, thermal metamorphism has not affected neptunian fissures penetrating into Coonterunah rhyolite or Carlindi granitoid.

6.2.3. Pilgangoora Syncline Metamorphism

Overprinting M_1 and earlier metamorphic fabrics is a pronounced regional fabric (M_7) associated with metamorphic grades increasing westward, under strain control. M_7 fabric is sub-parallel to bedding for most of Coonterunah strike, until culminating abruptly in lower amphibolite facies assemblages associated with the ~ 2.88 Ga (Baker et al., 2002) Pilgangoora Syncline fold (D_7) closure that marks the west-northwestward extent of both Warrawoona and Kelly Group volcano-sedimentary outcrop. Highest grade assemblages are defined by sillimanite in Gorge Creek Group meta-psammites, and one single local occurrence of almandine-andesine-ferrotschermakite amphibole, with post-M_7 retrogressive chlorite, in silicified meta-volcanics (Figure 27 (a – d)). Widespread renewed plutonism accompanies M_7, including intrusion of a garnet pegmatite dyke swarm intruded along D_7 fold cleavage planes.

Within Warrawoona and Kelly Group lithologies, variations in the conditions of peak metamorphism associated with more localized individual deformation events (M_4 – M_6, M_8 – M_{10}) are, at best, limited to talc formation in carbonate-metacherts and chlorite in meta-mafics, and nowhere exceed those of associated with M_1 or M_7.

6.3. Carbonate-Chert Assemblages

The bulk geochemistry of most outcropping meta-chert is overwhelmingly dominated by silica, with variable amounts of Ca, Mg and Fe rarely exceeding 1 wt.% in higher-grade meta-cherts and resilicified cherts. Significant occurrences of calcite and dolomite are largely restricted to localized zones of low silicification. Other than trace quantities of opaque oxides, and with the exception of localized occurrences of banded post-metamorphic jasperitic chert or clasts thereof and detrital magnetite grains in the basal clastic unit, Fe-bearing phases are absent from the Strelley Pool Chert. Ferruginous minerals do occur in Coonterunah Subgroup assemblages in localized horizons that bear magnetite at low grade. In view of these low Ca, Mg and Fe abundances, Pilgangoora SiO_2-dominated chert units offer little potential for constraining metamorphic conditions. In theory, the presence of even small amounts of dolomite with or without calcite in chert allows for qualitative geothermometry, although steeply sloping univariant P-T curves prevent constraint of metamorphic pressures.

Through talc- and tremolite-forming reactions, dolomite ceases to coexist with quartz. In more hydrous assemblages (Figure 26 (e)):

$$3Dol + 4Qtz + H_2O \rightarrow Tc + 3Cc + 3CO_2 \quad (1)$$

At higher xCO_2, tremolite is formed (Figure 26 (d)):

$$5Dol + 8Qtz + H_2O \rightarrow Tr + 3Cc + 7CO_2 \quad (2)$$

Assuming that calcite does not get removed, the upper limit of tremolite is set by the appearance of diopside in quartz-rich rocks:

$$Tr + 3Cc + 2Qtz \rightarrow 5Di + 3CO_2 + H_2O \quad (3)$$

While in dolomite-rich rocks, co-existing dolomite and tremolite react to give calcite and forsterite:

$$Tr + 11Dol \rightarrow 8Fo + 13Cc + 9CO_2 + H_2O \quad (4)$$

Forsterite and diopside are nowhere observed in Strelley Pool Chert or Coonterunah Subgroup metacherts. On the basis of the forgoing, the following assemblages can be expected with progressive metamorphism in the Ca-Mg-bearing cherts (tabulated graphically in Figure 31):

(i) Protolith assemblage: qtz + dol

(ii) Lower greenschist facies assemblage:

Lower xCO_2: qtz + tlc ± dol ± cc

Higer xCO_2: qtz + trem ± dol ± cc

(iii) Upper greenschist facies assemblage: qtz + trem ± cc

(iv) Lower amphibolite facies assemblage:

qtz > dol: qtz + di ± cc

qtz < dol: qtz + trem ± cc

In siliceous assemblages, the thermal stability limit of calcite is set by the formation of wollastonite (at ~640 ºC and 680 ºC at 1000 and 2000 bars, respectively):

$$Cc + Qz \rightarrow Wo + CO_2 \quad (5)$$

The near-absence of carbonate in quartz-tremolite assemblages after carbonate-chert protoliths suggests calcite-poor bulk compositions close to the quartz-dolomite join (consider stability fields in Ca-Mg-Si space in Chapter 5, Figure 17), compatible with the calcite-barren dolomitic-metachert assemblages encountered locally at lower grades. However, these inferences rely on system closure with respect to Ca, Mg and Si, which is an assumption that is far from secure. Siliceous fluids frequently accompanied deformation and metamorphic events, and dissolution textures at carbonate-quartz contacts preserved at low grade in cherts from both the Coonterunah Subgroup and Strelley Pool Chert (Figure 24, see also in Warrawoona Group, Chapter 5, Figure 10 (k – n)) attest to the efficient removal of Ca and Mg from carbonate-bearing systems during Pilbara metamorphism.

Honey-coloured grunerite-amphibole is present in fibrous habit in higher-grade Coonterunah ferruginous cherts, sometimes in co-existence with lath-like amphiboles

of the tremolite-actinolite series. The latter display systematic variation in optical properties, varying from apleochroic with low second-order blue birifringence, to mild greenish-yellowing pleochroism and upper first-order birifringence. In the system Ca-Mg-Fe-Si-fluid, grunerite can form through one or more of the following candidate reactions (Gole, 1980):

$$7Ca(Fe,Mg)(CO_3)_2 + 8SiO_2 + H_2O \rightarrow (Fe,Mg)_7Si_8O_{22}(OH)_2 + CaCO_3 + 7CO_2$$

$$\text{Fe-dol} + \text{qtz} \rightarrow \text{grun} + \text{cc} + CO_2 \quad (6)$$

$$8\,(Fe,Mg)CO3 + 8SiO2 + H2O \rightarrow (Fe,Mg)_7Si_8O_{22}(OH)_2 + 7CO_2$$

$$\text{sid} + \text{qtz} + H_2O \rightarrow \text{grun} + CO_2 \quad (7)$$

$$7Fe_3Si_4O_{10}(OH)_2 \rightarrow 3Fe_7SiO_{22}(OH)_2 + 4SiO_2 + 4H_2O$$

$$\text{minnesotaite} \rightarrow \text{grun} + \text{qtz} + H_2O \quad (8)$$

$$7Fe_3O_4 + 24SiO_2 + 3H_2O \rightarrow 3Fe_7Si_8O_{22}(OH)_2 + 5O_2$$

$$7\text{ mt} + 24\text{ qtz} + 3\ H_2O \rightarrow 3\text{ grun} + 5O_2 \quad (9)$$

Textural evidence was found only for reactions (6) and (9) (thin-section photographs of grunerite-forming reactions, Chapter 5, Figure 10 (j)). Silicates associated with high-grade banded-iron formations, such as pyroxene group minerals, riebeckite, and fayalite, are absent from the ferruginous cherts examined, as are the ferroan carbonates ankerite and siderite, and the low-grade ferruginous silicates greenalite and minnesotaite.

6.4. Post-metamorphic Alteration

6.4.1. Silicification

Pilgangoora Belt rocks have undergone extensive post-metamorphic silicification (discussed further in Chapter 5). In a high-precision isotopic examination of cherts from a 330 meter-long drillcore through the Warrawoona-Kelly unconformity, measurable quantities (> 0.05 wt.% CO_2) of Archaean carbonate were

only encountered below ~ 142 m (Table 2). The occurrence of carbonate in drillcore is restricted to more silicification-resistant dolomite spar.

6.4.2. Haematization

The presence of ferric iron in primary minerals, such as magnetite and haematite, constitutes an important proxy for oxidation fugacities of palaeoenvironments. Ferric oxides in deep-marine sediments of the Coonterunah Subgroup are of post-metamorphic origin, as shown in Chapter 5. The shallow-marine sediments of the Strelley Pool Chert also contain occasional ferric oxide minerals, most particularly in the form of fine haematite granules, and a drillcore study was undertaken to determine their origin.

SPC haematite of demonstrably secondary origin is shown in Figure 32. Secondary haematite occurs in close association with cross-cutting quartz or chlorite veins (Figure 32 (a - e)), diffusing outwards from penetrative structures, or as finely dispersed granules lining mineral faces (Figure 32 (f, g)). SPC haematite of a different textural association occurs in bedding-parallel lenses, also observed locally in SPC laminated carbonate lithofacies and breccia (drillcore and outcrop photographs, Figure 32 (a – g)). Frequently, this bedding-parallel haematite does not cross-cut any earlier fabric, and pre-dates multiple episodes of chlorite, quartz and pyrite veining. If primary, its presence would point to the existence of localized oxygenated conditions in shallow waters of Early Archaean near-shore environments. However, its very fine grain-size, its red colouration and the rather nebulous boundaries to the lenses suggests instead a secondary peak-metamorphic origin, because fine red haematite recrystallizes to coarser grey haematite well below sub-greenschist facies temperatures (Catling and Moore, 2003). As all rocks in the SPC examined here have experienced at least prehnite-pumpellyite facies metamorphism, with minimum temperatures of over 250 ºC, pre-metamorphic fine red haematite would not survive.

7. Geological Synthesis

The geological history of the older sequences of the Pilgangoora Belt is depicted in Figure 33 and 34. During deposition of the Coonterunah Subgroup, deep-water subaqueous eruption of low-viscosity basalts of increasingly tholeiitic character took place upon an unknown, possibly sialic, basement. Eruptive hiatuses were marked by silicified tops to volcanic piles and chert caps, which stand testimony to high seawater silica concentrations. Localized rhyolitic flows, flanked by silicified breccia, represented local topographic highs in a mafic plane.

An eruptive event gave rise to deposition of ~35 m of felsic tephra, temporarily changing the nature of hydrothermal seafloor alteration and diagenesis, and shifting the chemistry of the benthic environment, thereby allowing for the preservation of unsilicified micritic carbonates. Carbonate sedimentation and organic irrigation continued, but the return to a hot mafic substrate following renewed mafic seafloor volcanism re-initiated pervasive silification (or dissolution) of any carbonates.

Shallow intrusion and diapiric uprise of the Carlindi granitoids resulted in a large-scale domal topography and general uplift. Erosion levelling this topography resulted in the loss of at least 3000 m of volcanosedimentary Coonterunah and sialic Carlindi material (perhaps along with other younger units of the Warrawoona Group), some of which came to be deposited and preserved in the basal sandstone of the Strelley Pool Chert. Silicified peri-tidal sediments of the Kelly Group record a different environment from that of the deep-marine Coonterunah Subgroup, and provide evidence for stratified ocean hydrochemistry in the Early Archaean (Chapter 5).

Further doming caused flexural crustal rupture of sections of the Strelley Pool Chert during reef-like carbonate precipitation, resulting in the opening of neptunian fissures. Cohesive lithified rocks descended into the fissures as megabreccia in a soft carbonate and organic-matter matrix. Sequential shoaling and drowning ensured entrapment of unconsolidated mafic volcanoclastic silt and sand and provided a favorable environment for prokaryotic consortia (Chapter 7).

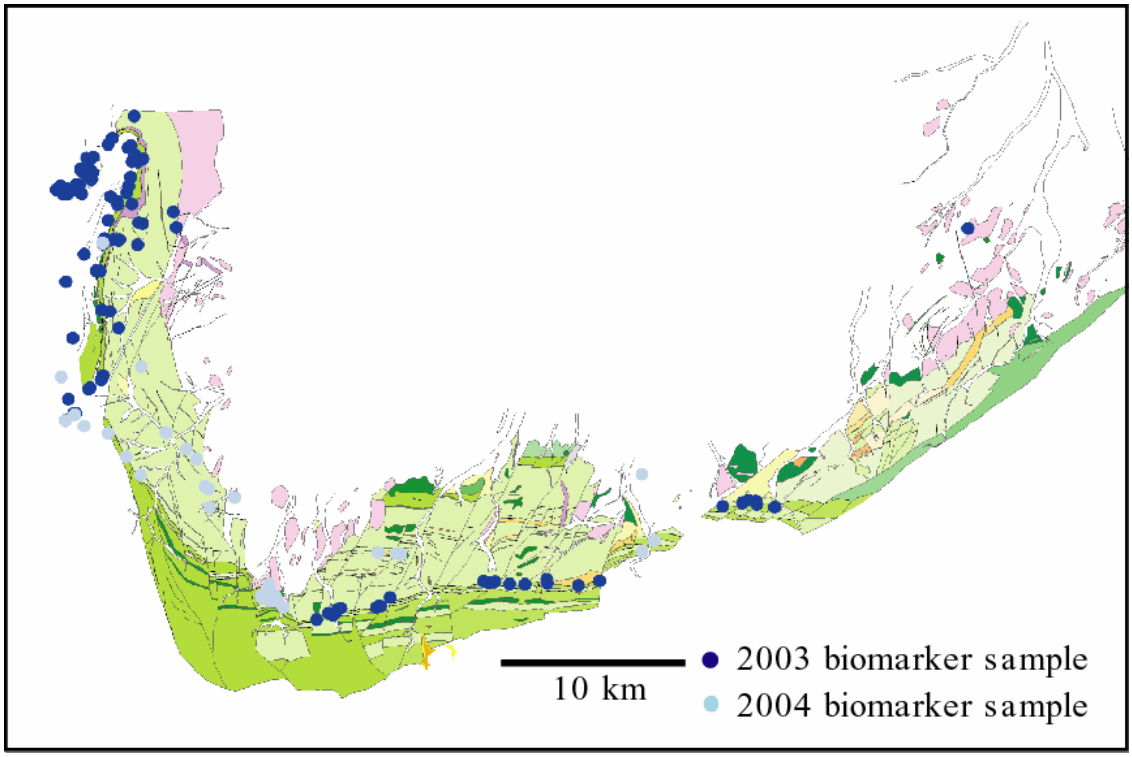

Figure 1: Biomarker sampling localities in the Pilgangoora Belt.

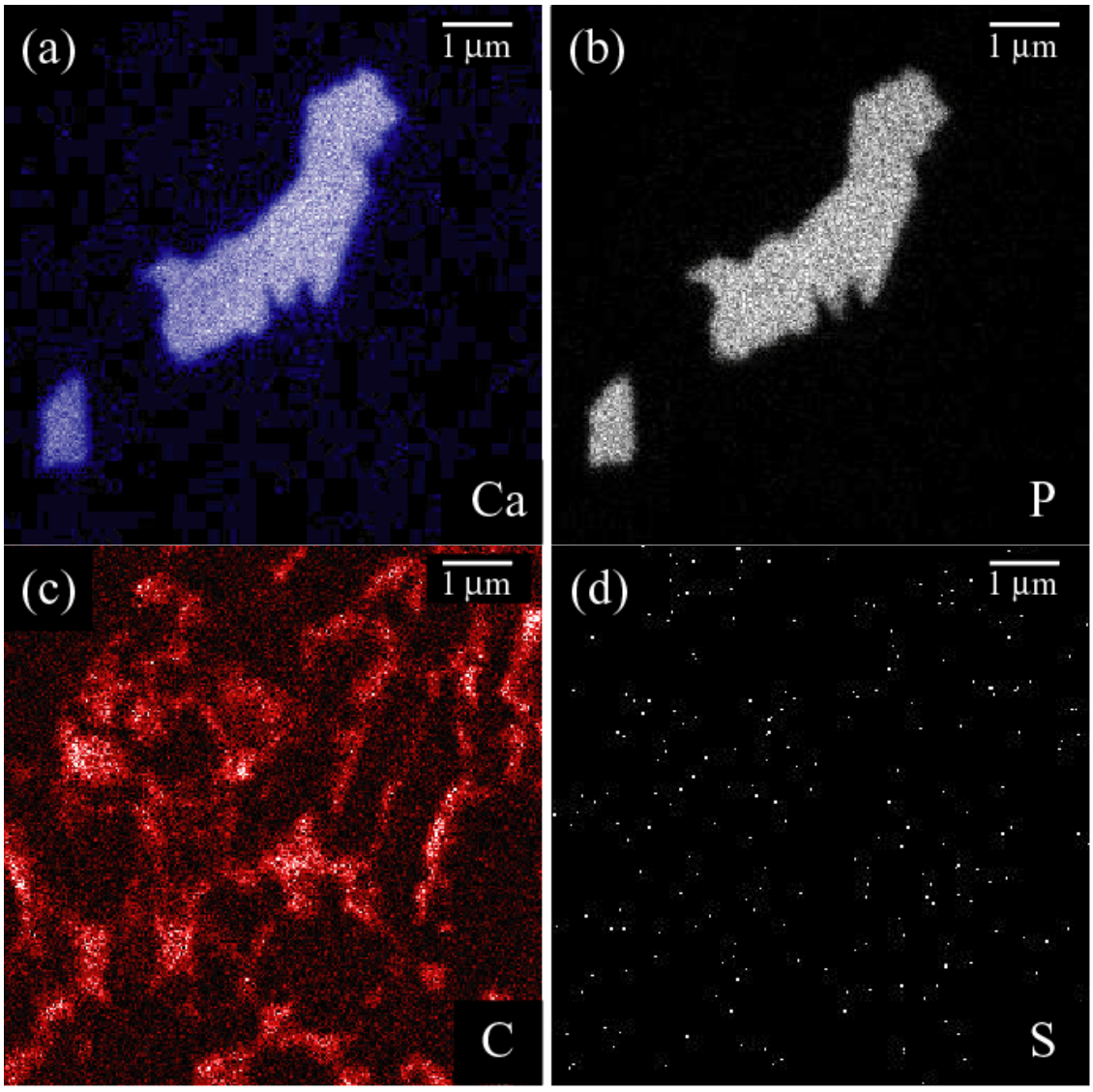

Figure 2: Macronutrient calcium-, phosphorus-, carbon- and sulphur- element maps of BIF-hosted graphitic apatite from the Isua Supracrustal Belt in southwest Greenland. Sulphur occurs below detection levels, while the graphitic coating on apatite cannot readily be distinguished from interference effects on crystal faces. No nitrogen was detected.

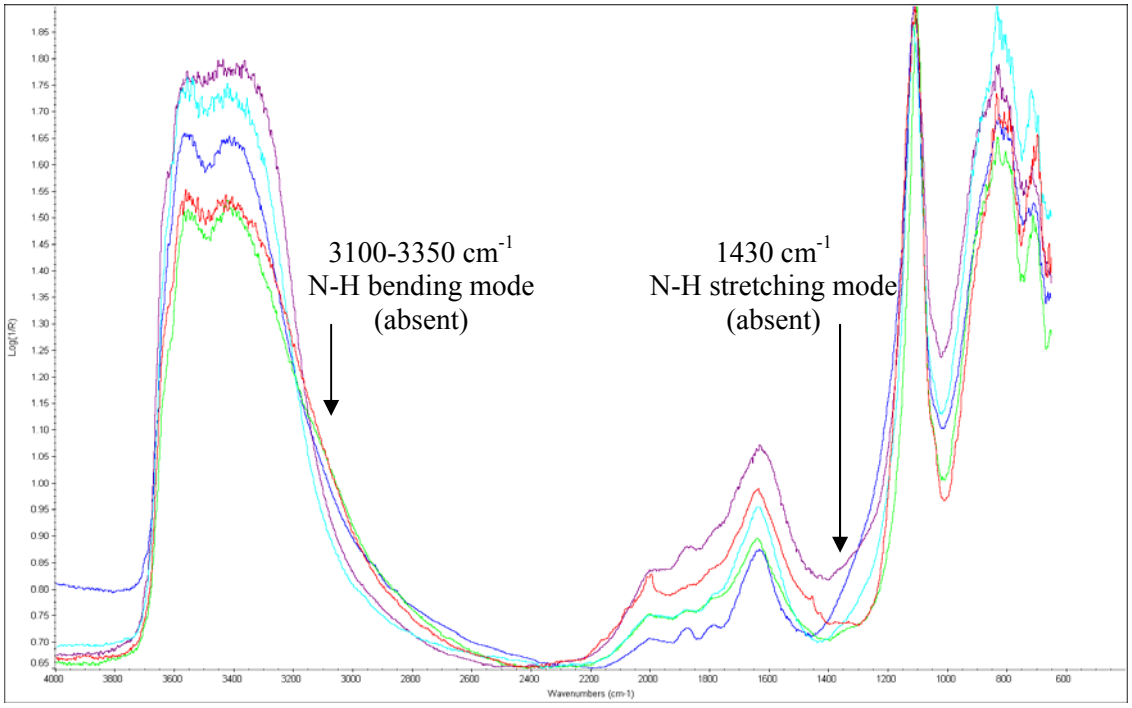

Figure 3: Waveform output from Fourier-Transform Infrared Spectroscopy study of sheet-silicate hosted biogenic ammonia in Pilbara metapelites. NH_4^+ was also not found in Isua Supracrustal Belt metaturbidites.

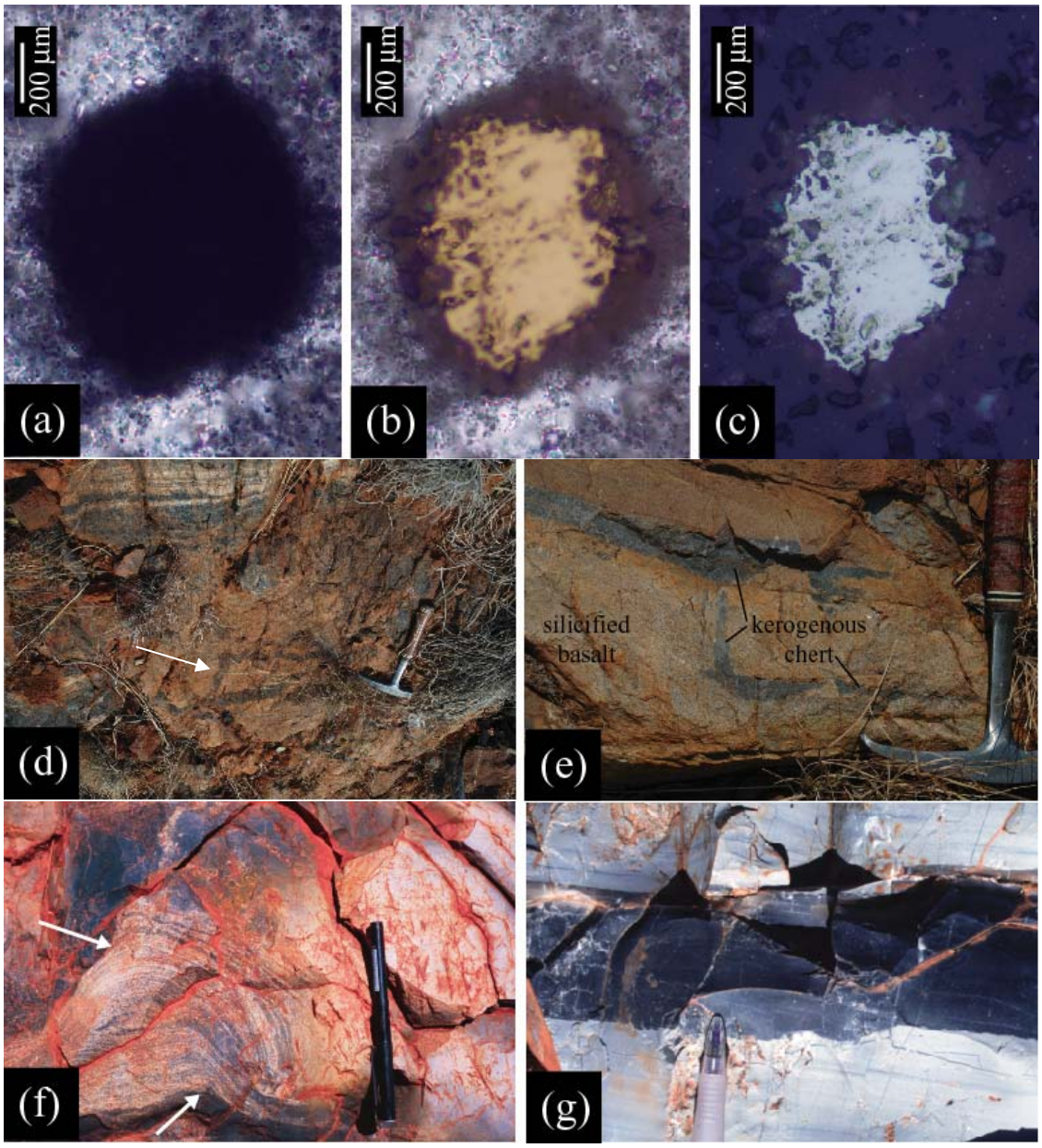

Figure 4: Textural associations of Early Archaean kerogen. (a – c): Plane-polarized (a), cross-polarized (b) and reflected-light (c) photomicrograph of kerogen-coated pyrite from the Pilbara's Strelley Pool Chert, Kelly Group. (d, e): Outcrop photographs of kerogenous chert cross-cutting silicified basalt immediately below the black-white banded H_2C chert in the Hooggenoeg Formation, Onverwacht Group, Barberton. (f): Cement-like black kerogenous chert deforming silicified laminated carbonate in the Strelley Pool Chert, Kelly Group, Pilbara. Top arrow shows black chert-filled scour surface, lower arrow shows silicified laminated lithofacies draping black chert. (g): Black kerogenous chert sub-parallel to and cross-cutting sedimentary bedding in Chert VII, Kelly Group, Pilbara.

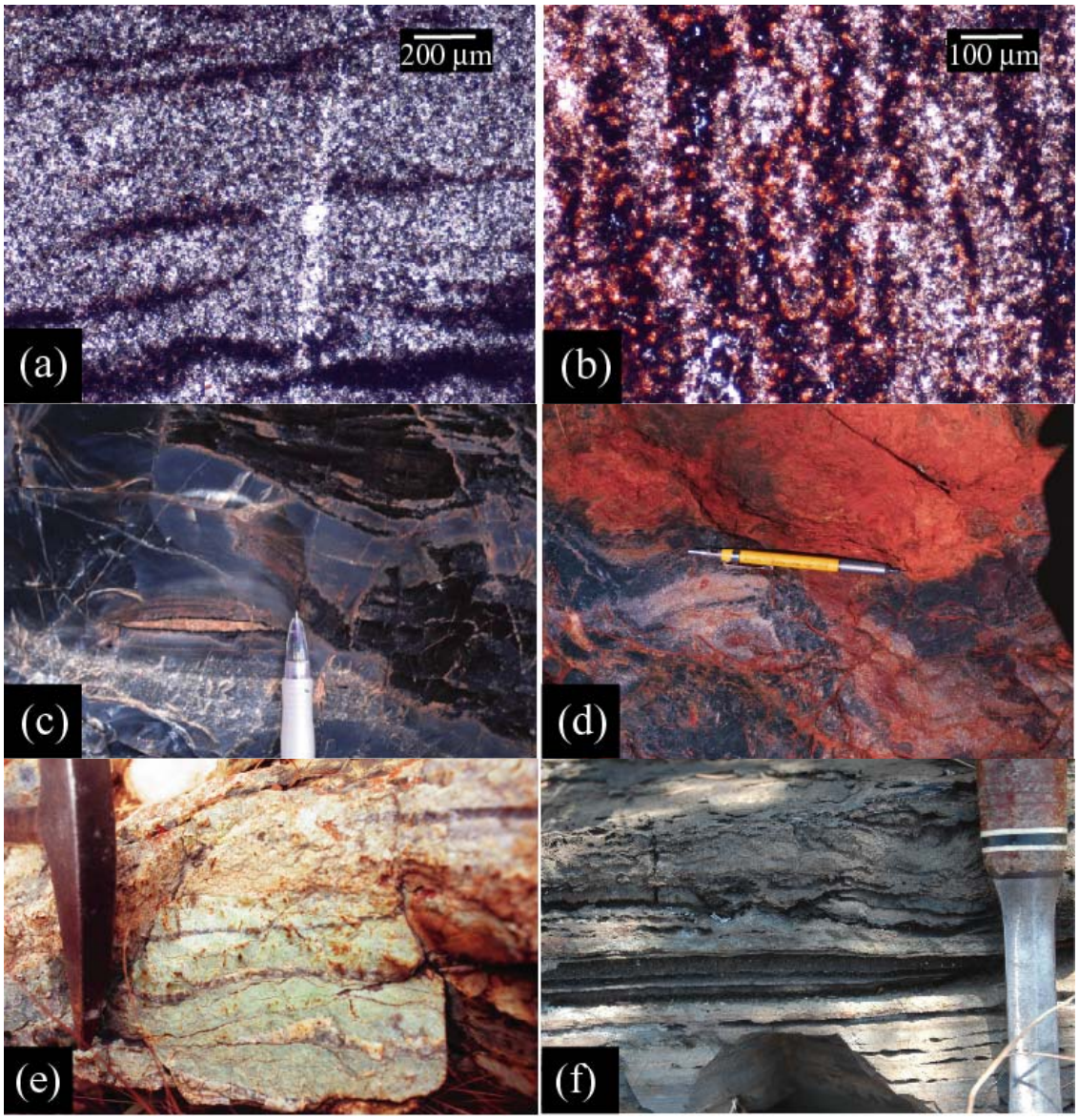

Figure 5: Chert alteration. (a, b): Reddish oxidation stains on kerogen granules in Coonterunah ferruginous meta-chert at high metamorphic grade. (c): Laminated black kerogenous chert and carbonate in the Strelley Pool Chert. (d): Silicified laminated carbonate breccia and cement-like kerogenous black chert matrix in neptunian fissure under the Strelley Pool Chert. (e): Fuchsitic alteration in silicified laminated meta-chert of the Komati Formation, Barberton Greenstone Belt. (f): Carbonate alteration on accretionary lapilli horizons in 'K2v' Member, Kromberg Formation, western limb of Onverwacht anticline, Barberton Greenstone Belt.

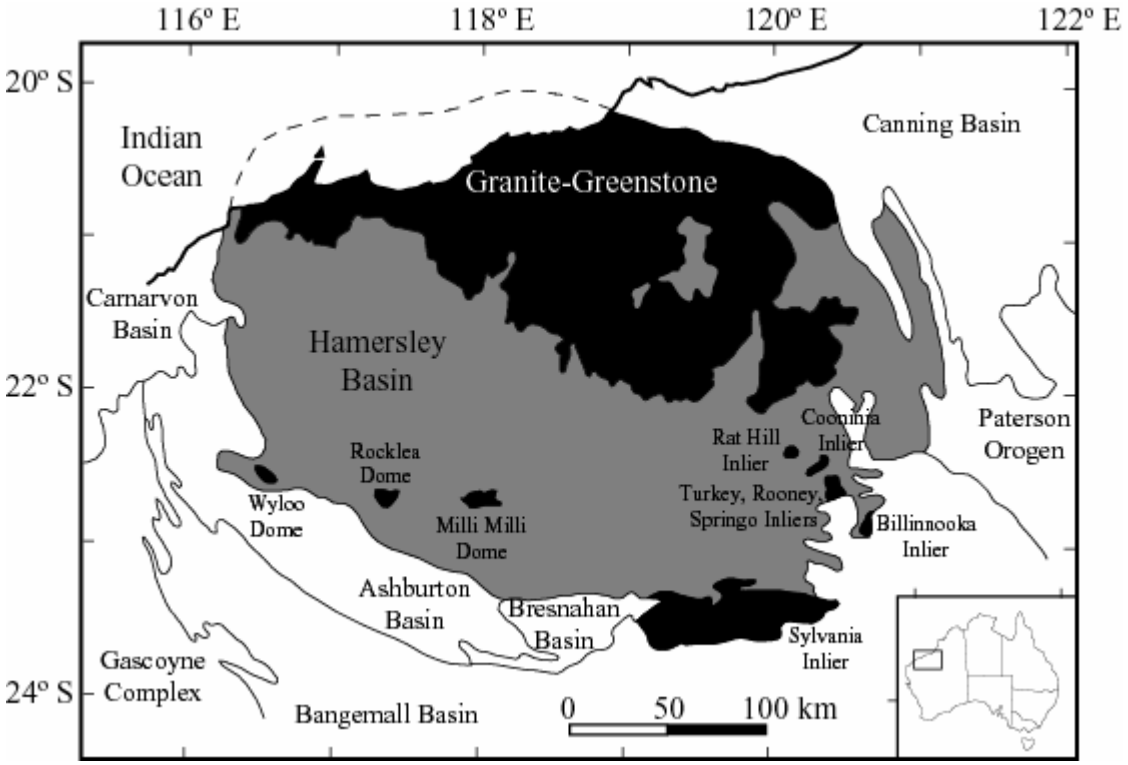

Figure 6: Distribution of Archaean granite-greenstone and unconformably overlying lithologies of the Late Archaean-Early Proterozoic Hamersley Basin in the Pilbara Craton, along with bounding terrains (adapted after Green, 2001; Tyler, 1990).

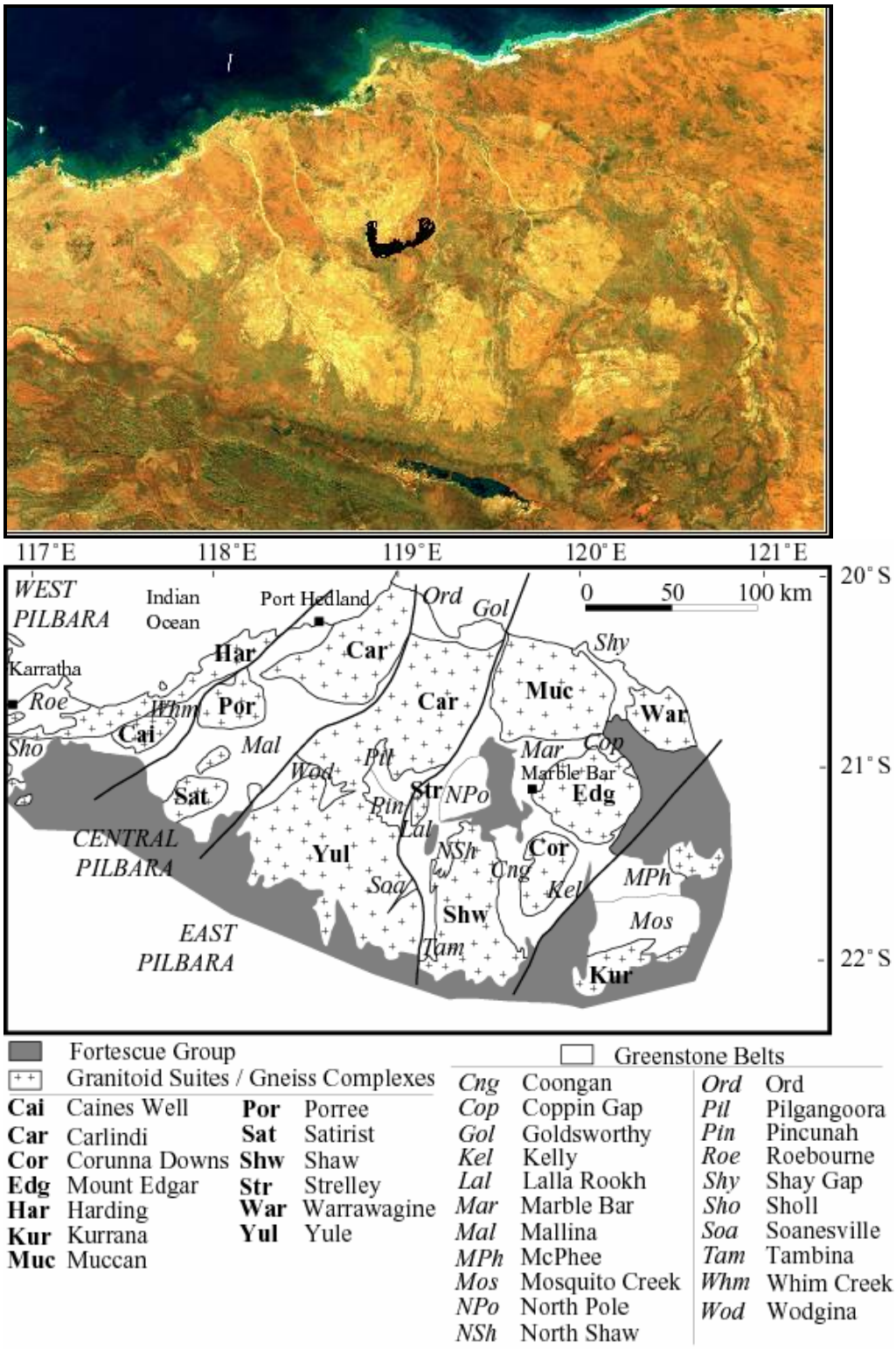

Fortescue Group

Granitoid Suites / Gneiss Complexes

Cai	Caines Well	**Por**	Porree
Car	Carlindi	**Sat**	Satirist
Cor	Corunna Downs	**Shw**	Shaw
Edg	Mount Edgar	**Str**	Strelley
Har	Harding	**War**	Warrawagine
Kur	Kurrana	**Yul**	Yule
Muc	Muccan		

Greenstone Belts

Cng	Coongan	*Ord*	Ord
Cop	Coppin Gap	*Pil*	Pilgangoora
Gol	Goldsworthy	*Pin*	Pincunah
Kel	Kelly	*Roe*	Roebourne
Lal	Lalla Rookh	*Shy*	Shay Gap
Mar	Marble Bar	*Sho*	Sholl
Mal	Mallina	*Soa*	Soanesville
MPh	McPhee	*Tam*	Tambina
Mos	Mosquito Creek	*Whm*	Whim Creek
NPo	North Pole	*Wod*	Wodgina
NSh	North Shaw		

Figure 7: Satellite image (above, study area superimposed) and structural domain map (below) of granitoid suites/gneiss complexes and greenstone belts in the northern Pilbara (adapted after Blewett, 2002; Green, 2001).

Group	Subgroup	Formation	Dominant Lithology	Thickness (m)
Whim Creek				900
DeGrey		Mosquito Creek & relatives		5000
		Lalla Rookh & relatives	Epiclastics, carbonate, felsic volcanics	3000
Gorge Creek		Paddy Market	Fine-grained sediments, banded-iron formation	?
		Corboy		1500
		Pincunah Hill		?
		Nimingarra	Banded-iron formation	?
		Tank Pool	Quartzite	?
Sulphur Springs		Kangaroo Caves	Dacite to rhyolite volcanics & volcanoclastics, chert	?
		Kunagunarrina	Magnesian basalt to komatiite, chert, shale	?
		Leilira	Sandstone, shale, quartzite	?
		Six Mile Creek	Tholeiitic to magnesian basalt	?
		Wyman (Golden Cockatoo)	Porphyritic rhyolite	1000
Kelly	Salgash	Euro Basalt	Magnesian to tholeiitic basalt	2000
(Warrawoona)		Strelley Pool Chert	Sandstone, silicified carbonate, mafic volcanoclastics	20
Warrawoona		Panorama	Rhyolite, volcanoclastics	1000
		Apex Basalt	Magnesian to tholeiitic basalt, gabbro	2000
		Duffer	Dacite to rhyolite, volcanoclastics	5000
	Talga Talga	Dresser	Magnesian basalt, clastic sediments, evaporites; pillows	3000
		Mt. Ada	Tholeiitic to magnesian basalt, gabbro; pillows	2000
		McPhee	Theleiitic to magnesian basalt, gabbro, ultramafic intrusives	100
(Coonterunah)	Coonterunah	Double Bar	Tholeiitic basalt, gabbro; pillows	2500
		Coucal	Tholeiitic basalt, dacite to rhyolite, volcanoclastics, chert, carbonate	1500
		Tabletop	Tholeiitic to magnesian basalt, gabbro; pillows	2500

Figure 8: Stratigraphic divisions of the East Pilbara structural domain of Pilbara Supergroup in the Pilgangoora Belt.

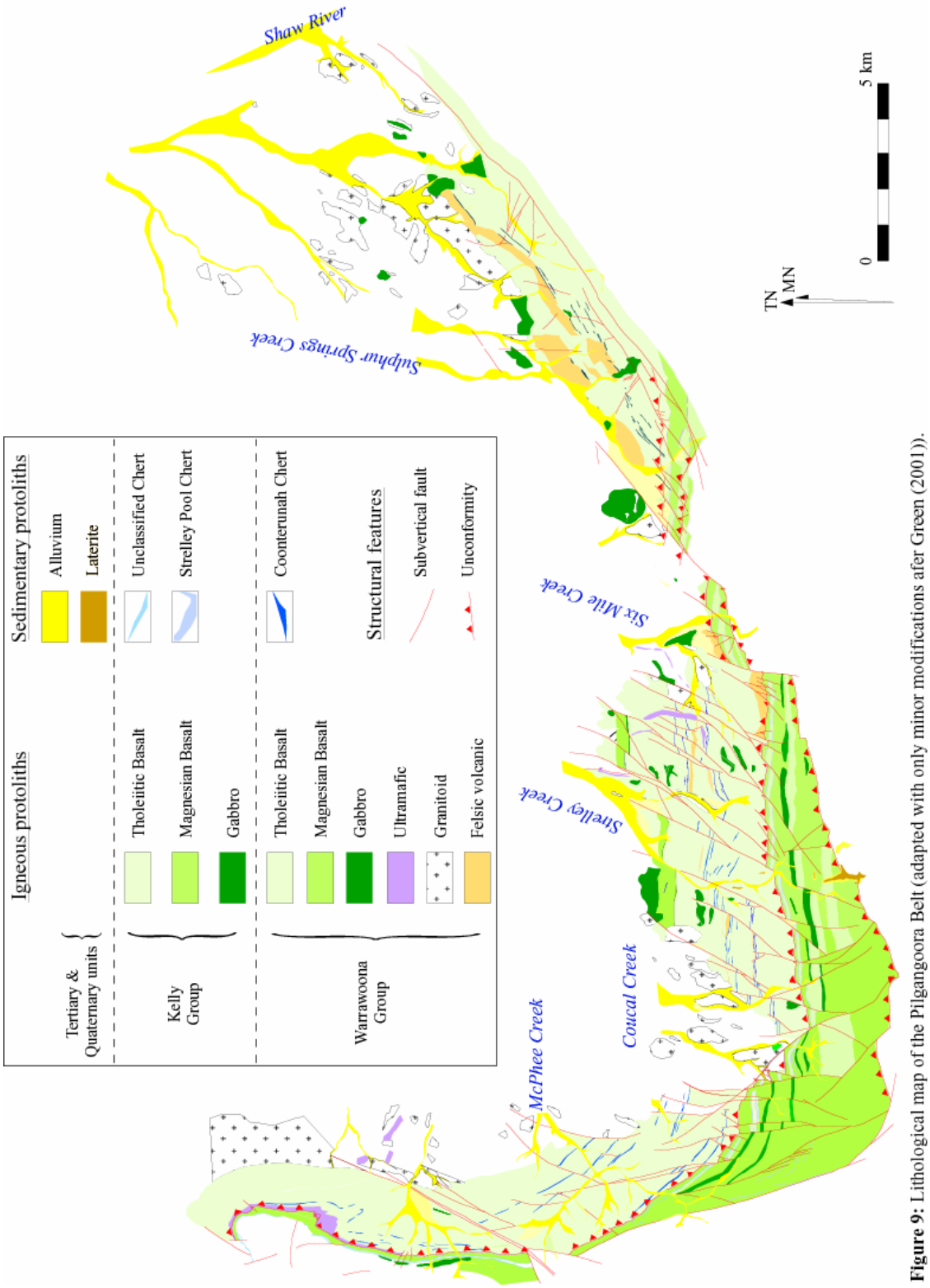

Figure 9: Lithological map of the Pilgangoora Belt (adapted with only minor modifications afer Green (2001)).

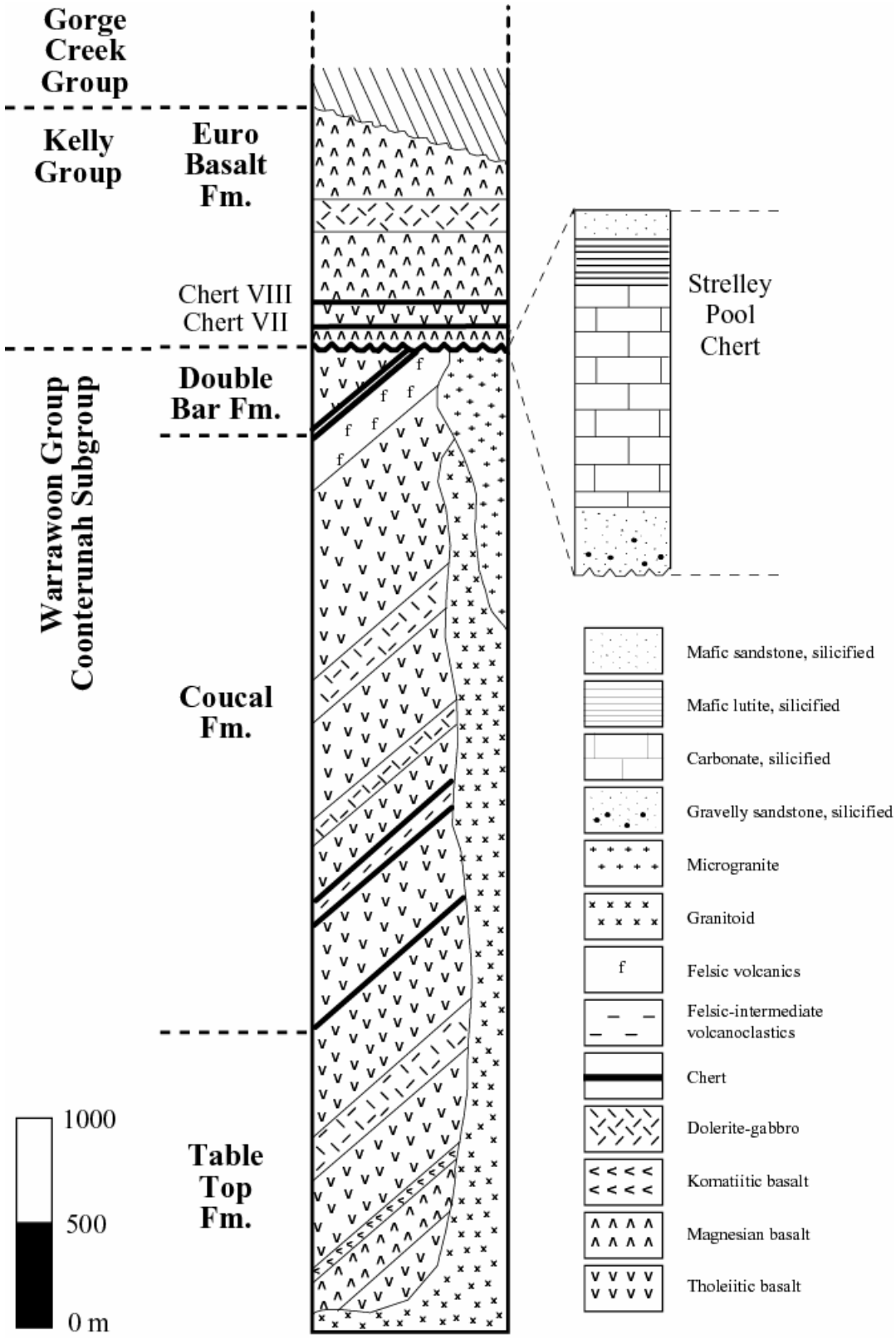

Figure 10: Stratigraphic section of the Pilgangoora Belt (after Green (2001)).

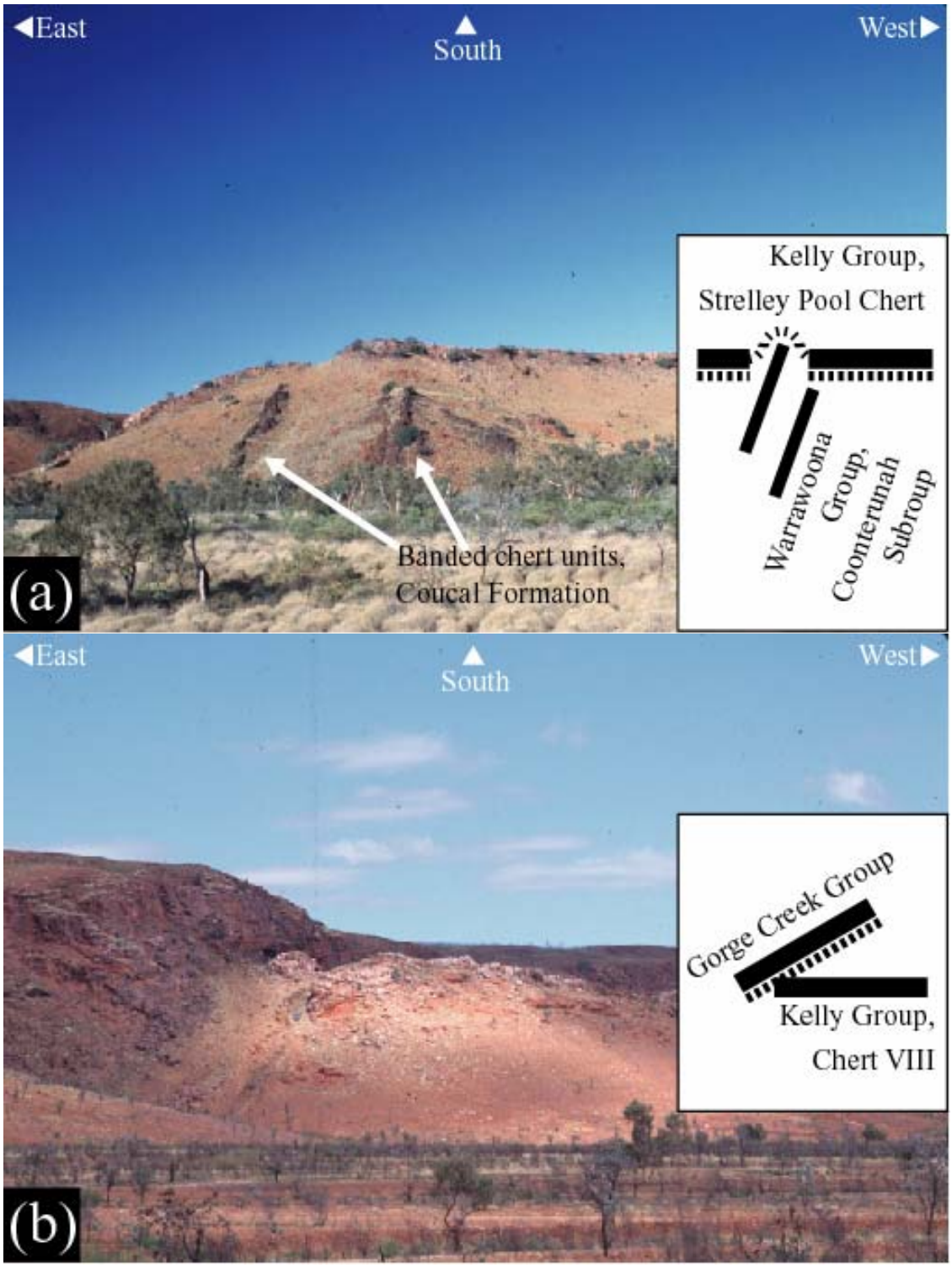

Figure 11: Field photographs showing regional-scale angular unconformity between (a): Warrawoona Group and Strelley Pool Chert of Kelly Group and (b): Chert VIII of Kelly Group and clastic sediments of the Gorge Creek Group (b).

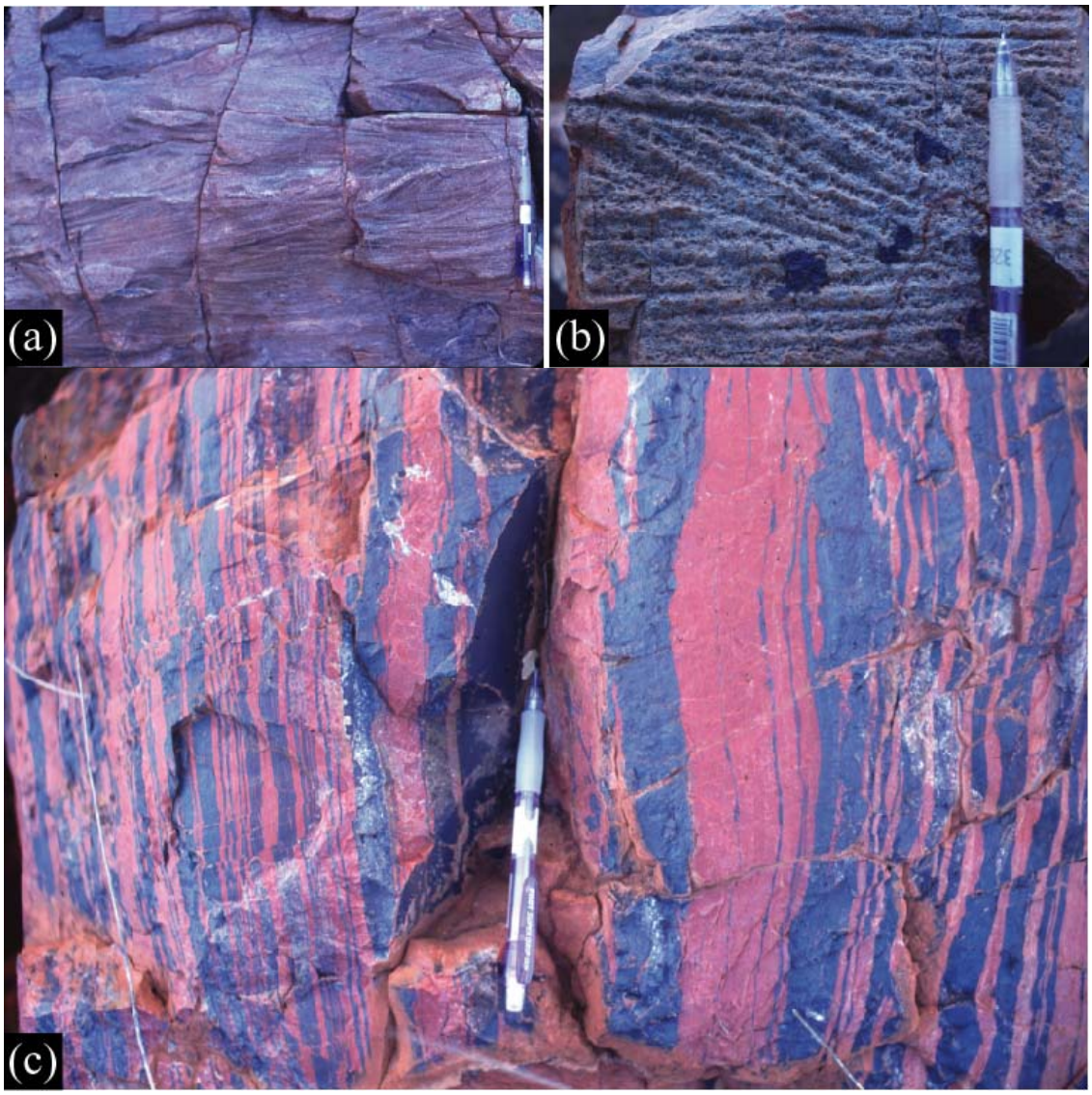

Figure 12: Gorge Creek Group sediments. (a, b): Trough cross-bedding in fluvial arenite, Lalla Rookh Formation, Gorge Creek Group. (c): Haematite-jasper banded-iron formation, Cleaverville Formation, Gorge Creek Group.

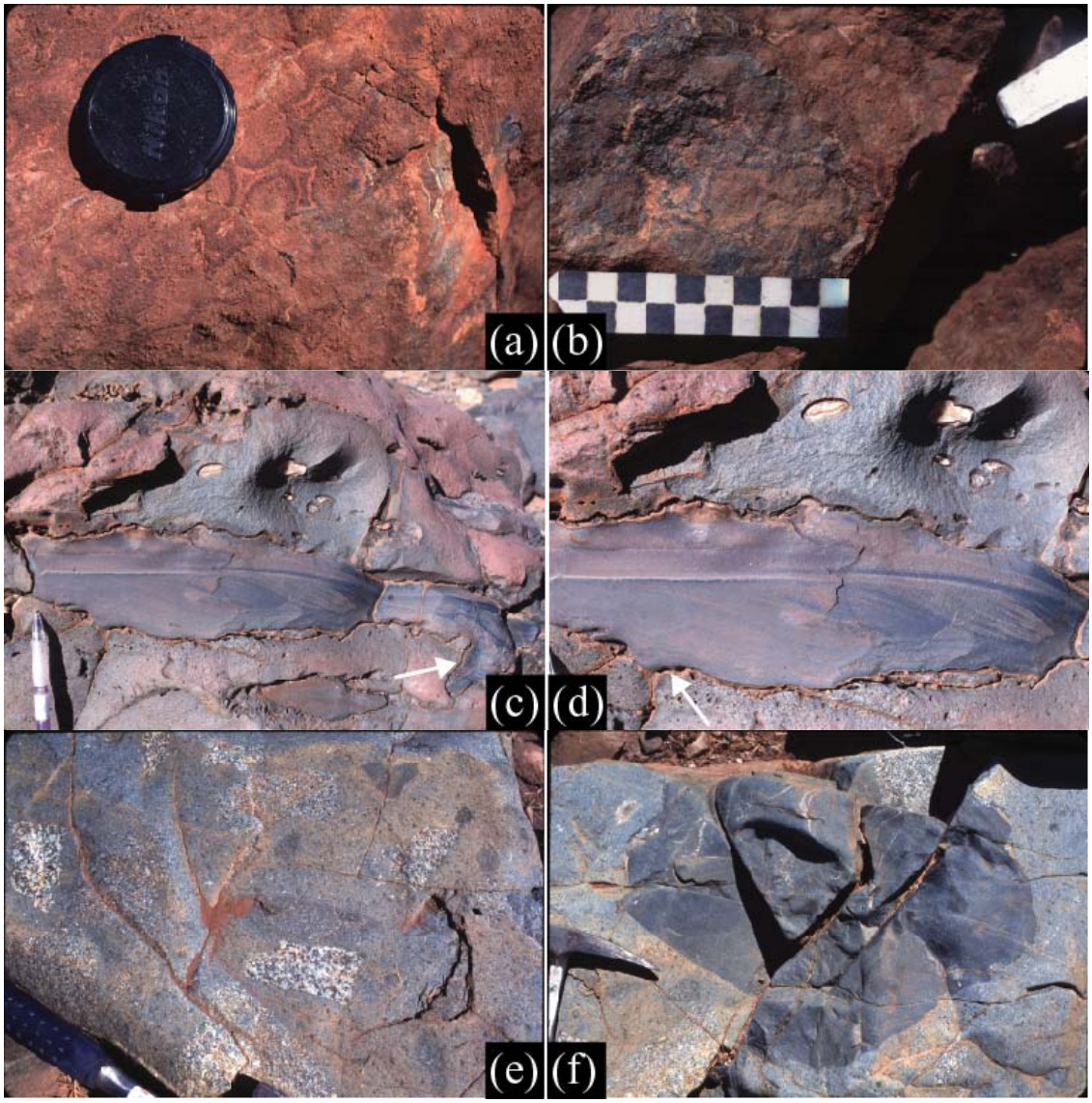

Figure 13: Basalt features in the Pilgangoora Belt. (a, b): Occelli in magnesian basalt, showing interlocking ridge-forming clinopyroxene rims with light-greenish pale albite-chlorite centers. (c, d): Ripple-laminated tuffaceous sediment atop scoriaceous flow tops in tholeiitic Coonterunah basalt, arrows point to sediment infill (left) and flow-top (right). (e, d) Gabbro and dolerite cumulate xenoliths in Coonterunah Subgroup basalt.

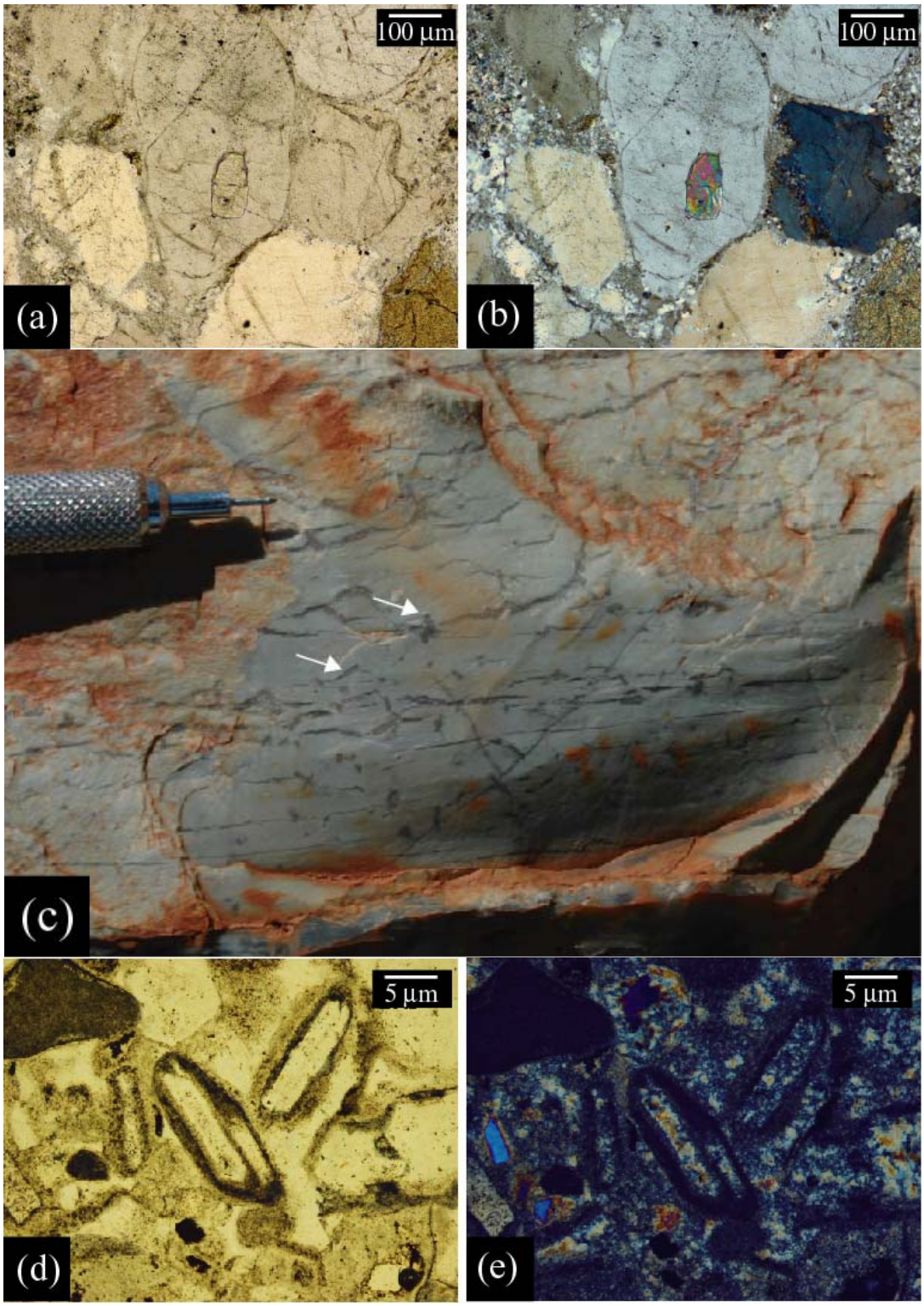

Figure 14: Selected Strelley Pool Chert lithofacies. (a, b): Embayed zircon in basal rounded orthoquartzite. (c): Silified diagenetic gypsum crystallites in outcrop. (d, e): Thin-section photomicrographs of silicified gypsum from the North Pole barite deposit.

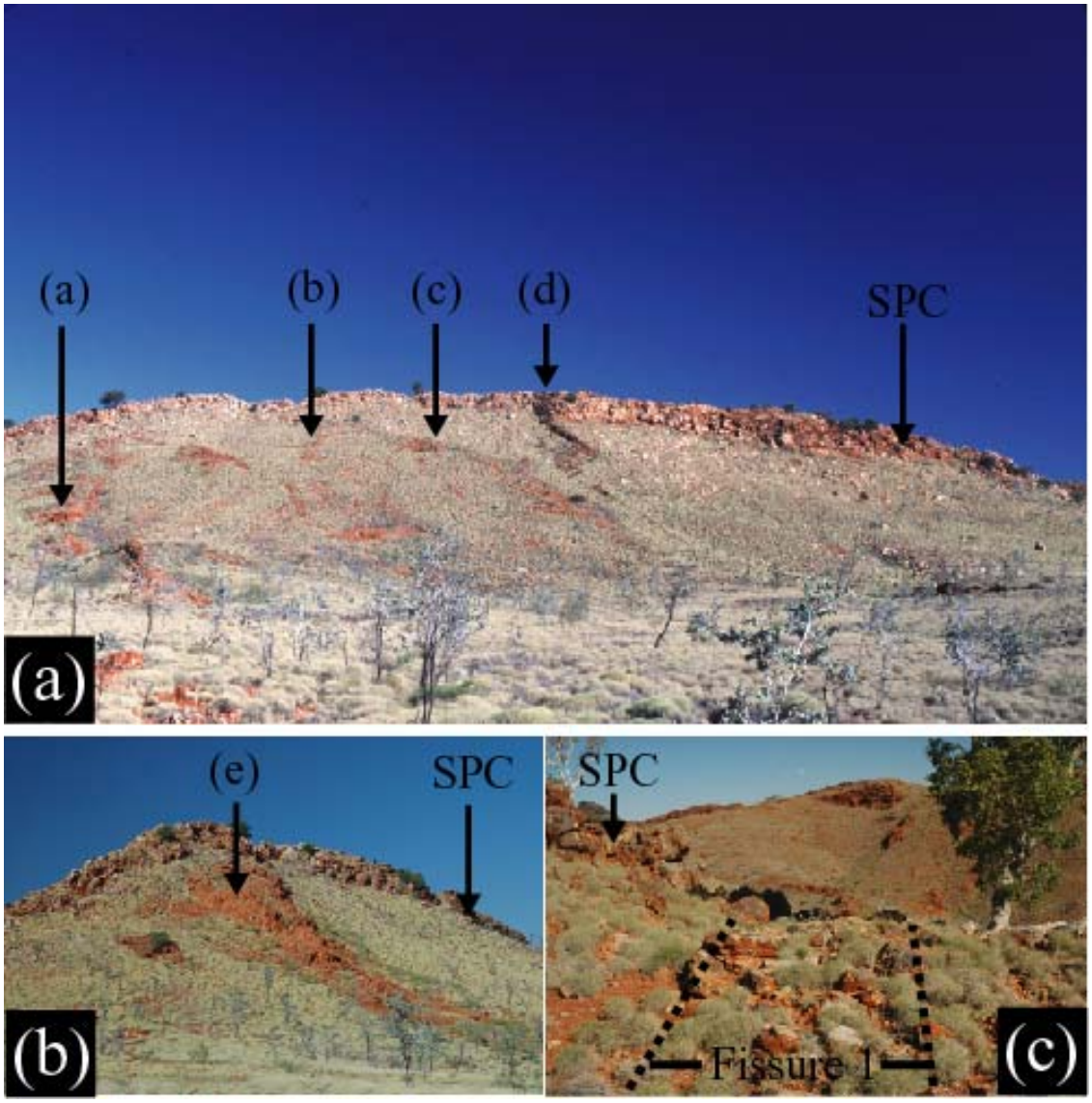

Figure 15: Field photographs of neptunian fissures, looking southwards along younging stratigraphy. (a, b): Fissure site 2. (c): Fissure site 1.

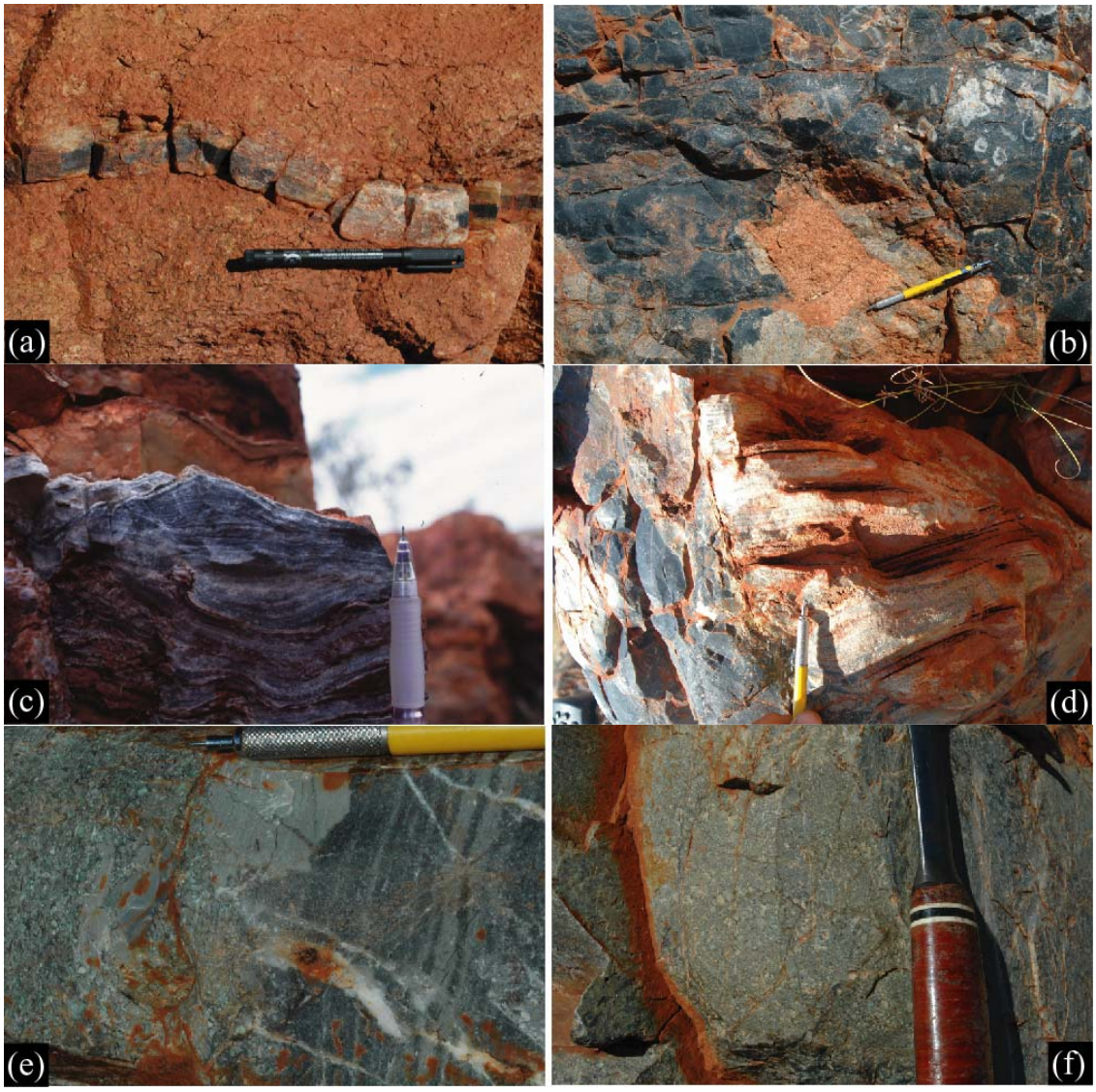

Figure 16: Carlindi granitoid and SPC units compared with allochtonous fissure breccia, pencil points stratigraphically upwards. (a): Saprolitic Carlindi granitoid with black chert vein. (b): Tabular granitoid clast in neptunian fissure. (c): Silicified wavy-laminated carbonate lithofacies of SPC. (d): Silicified wavy-laminated carbonate megabreccia in neptunian fissure. (e, f): Silicified mafic arenite in bedded SPC, compare with Figure 17.

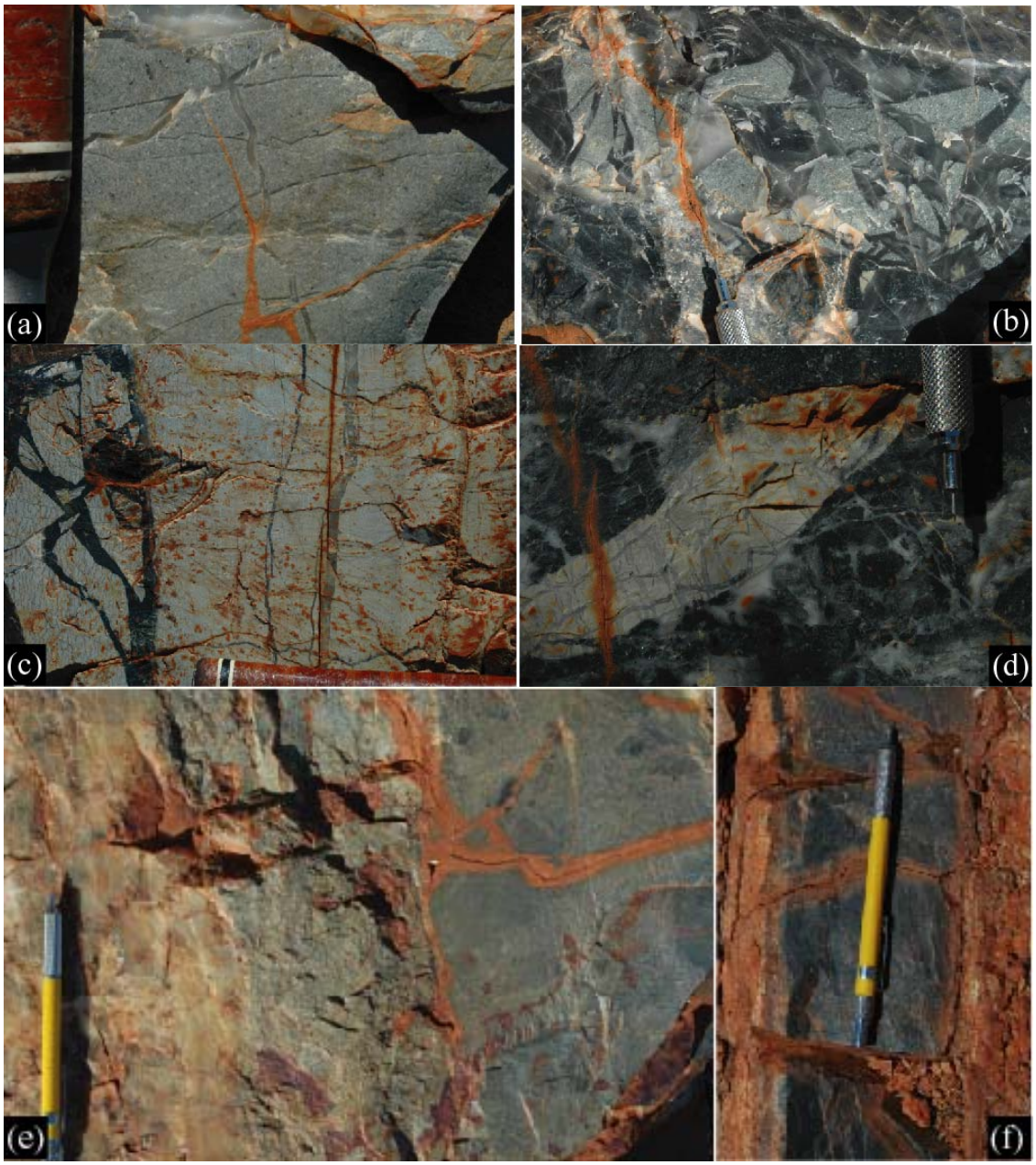

Figure 17: Autochtonous SPC units compared with allochtonous fissure breccia, pencil and hammer points stratigraphically upwards. (a): Bedded silicified mafic arenite with hydraulic fractures. (b): Angular breccia of silicified arenite in neptunian fissure. (c): Bedded silicified mafic lutite. (d): Angular breccia of silicified magic lutite in neptunian fissure. (e): Silicified mafic sand- and siltstone and chalcedonic quartz in neptunian fissure. (f): Silicified mafic siltstone in contact with granitoid.

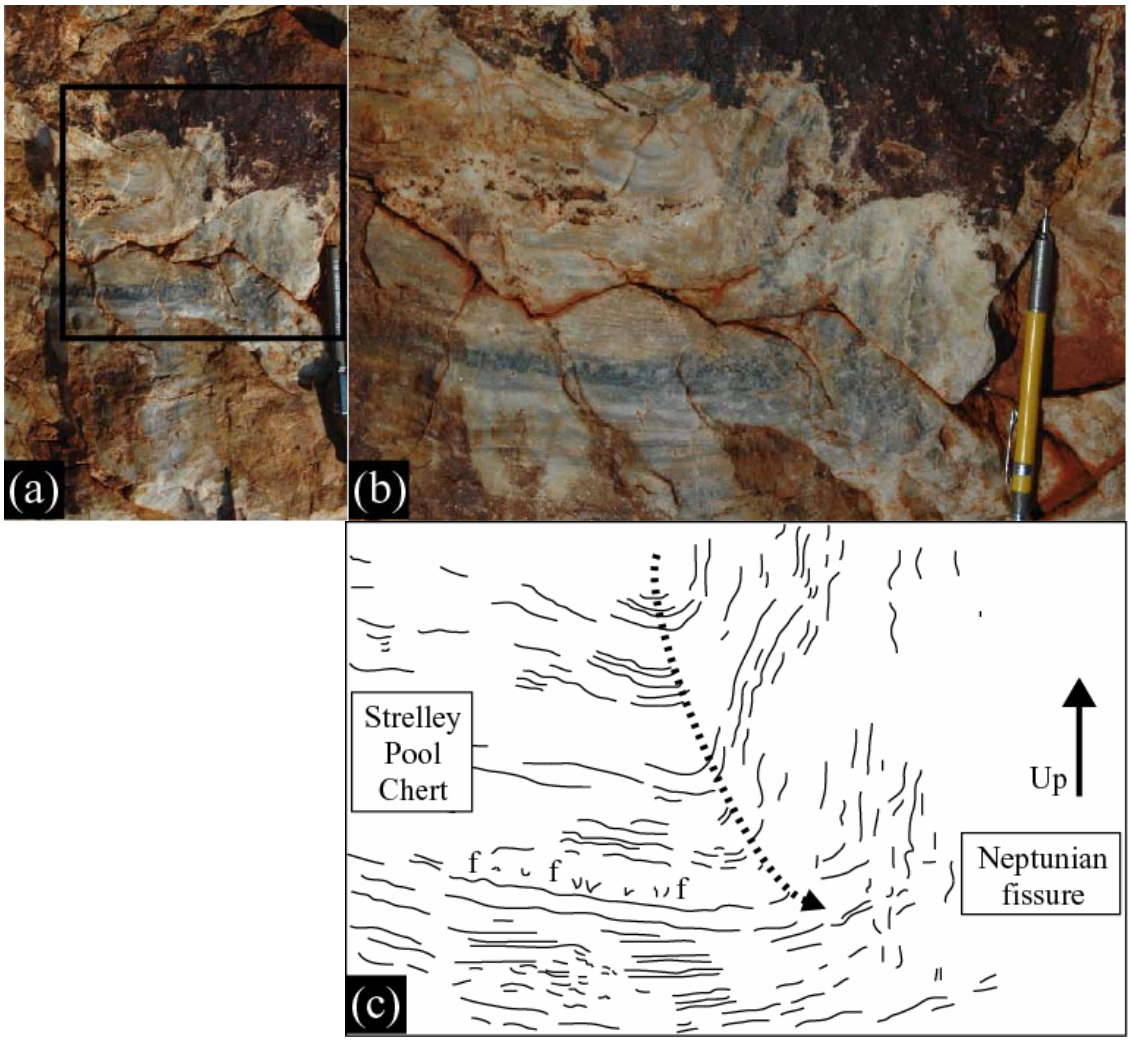

Figure 18: Outcrop photographs (a, detail: b) and interpretative sketch (c) of slump structure at contact between SPC and neptuninan fissure. Flame structures labelled with 'f' in (c).

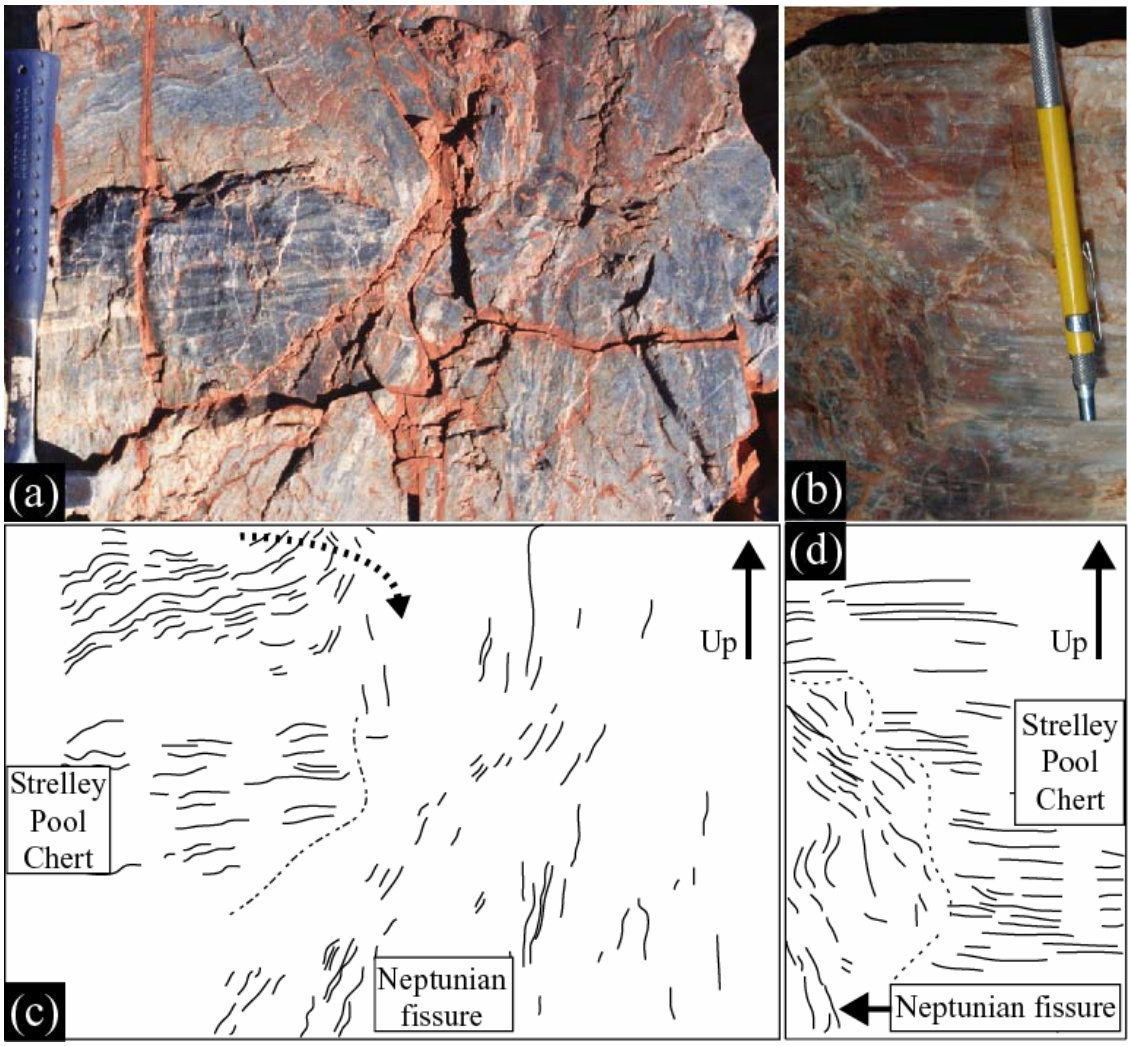

Figure 19: Outcrop photographs (a, b) and interpretative sketches (c, d) of slump structures at contact between SPC and neptuninan fissure.

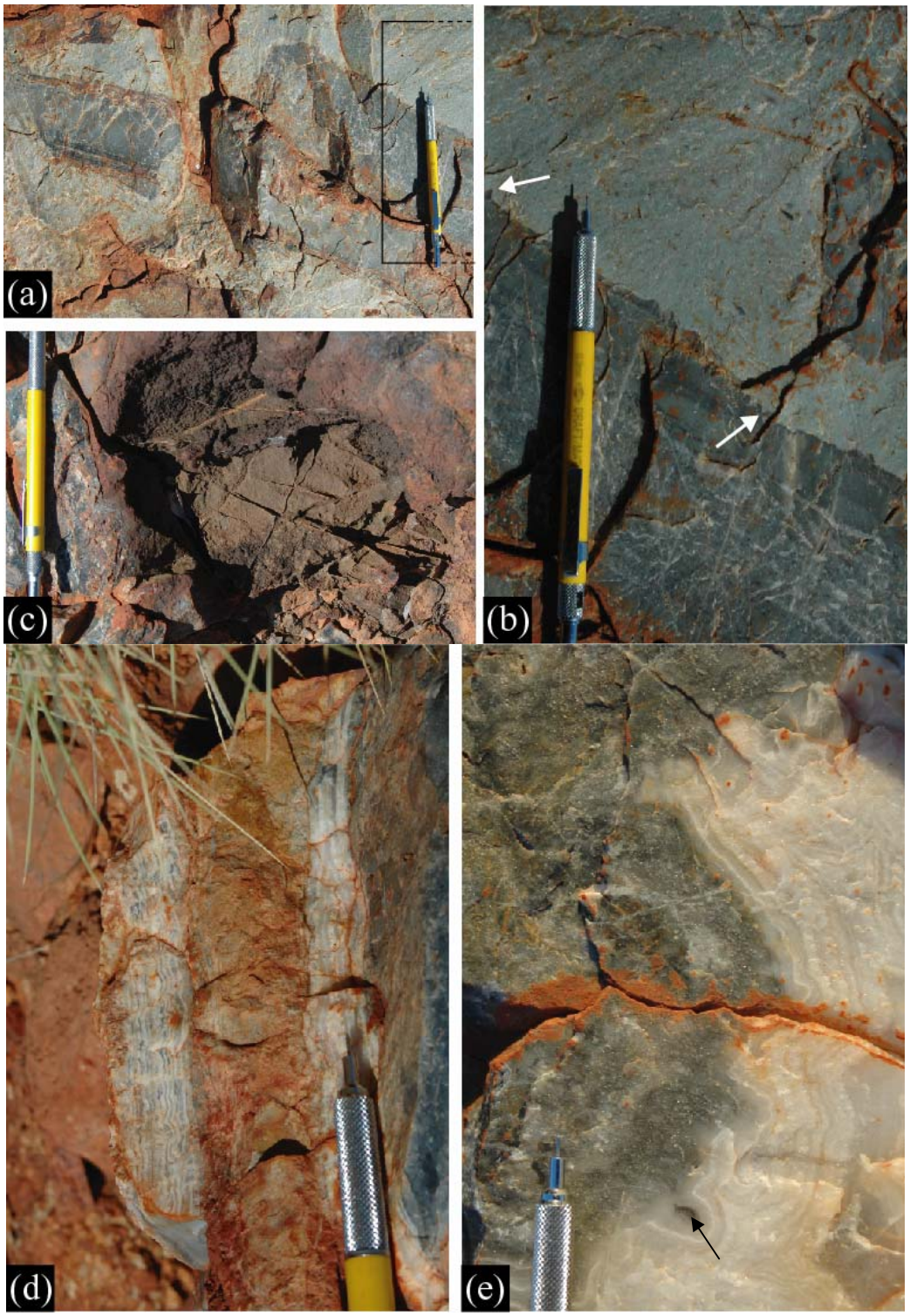

Figure 20: Textural relationships within neptunian fissures. (a, b): Silicified laminated megabreccia showing impingement structures which occur on the upper contact surface only. (c): Dolomite megabreccia, isotopically indistinguishable from SPC dolomite from which it is likely sourced. (d, e): Late wall-parallel chalcedonic quartz.

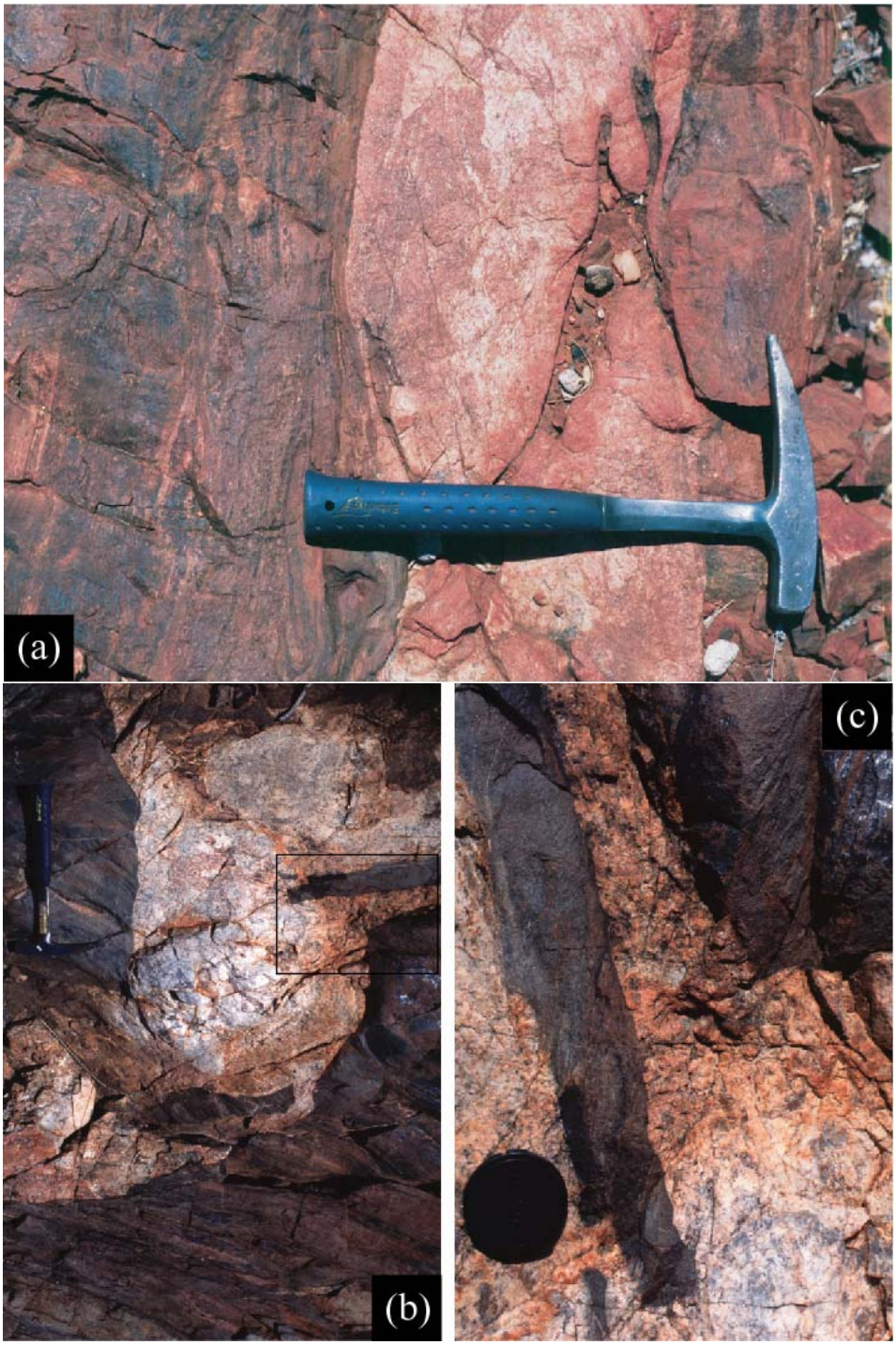

Figure 21: Outcrop photographs of contact relationships between Carlindi granitoid and amphibolite-facies Table Top metamafics. (a) Kinematic contact parallel to dominant foliation in both rock types, gneissic fabric in Carlindi granitoid. (b) Intrusive contact cross-cutting dominant foliation in metamafics, plutonic fabric in Carlindi granitioid. Box shows area of rotated photograph (c), which shows angular and tabular brecciation of countryrock.

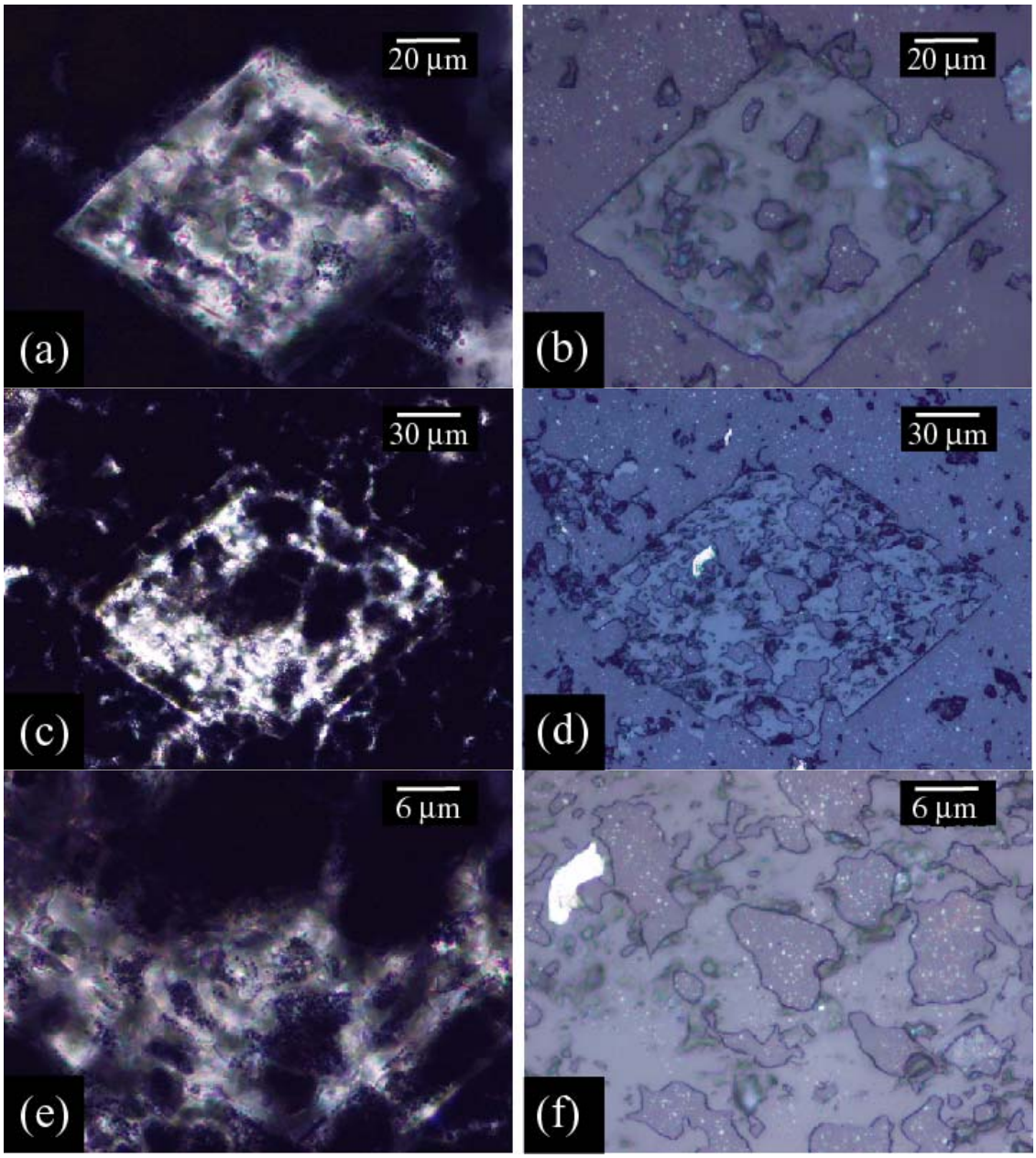

Figure 22: Thin-section photomicrographs of partially silicified early sparry dolomite in Strelley Pool Chert silicified laminated carbonate lithofacies obtained from drillcore. (a - f): Dolomite spar with kerogenous inclusions and concentrated kerogenous outer rim. (e, f): Detail of dolomite in (c, d), showing rim (e) and core (f). (g, h) Thoroughly silicified dolomite spar in drusy quartz. Note kerogen displacement towards top-right of dolomite pseudomorph.

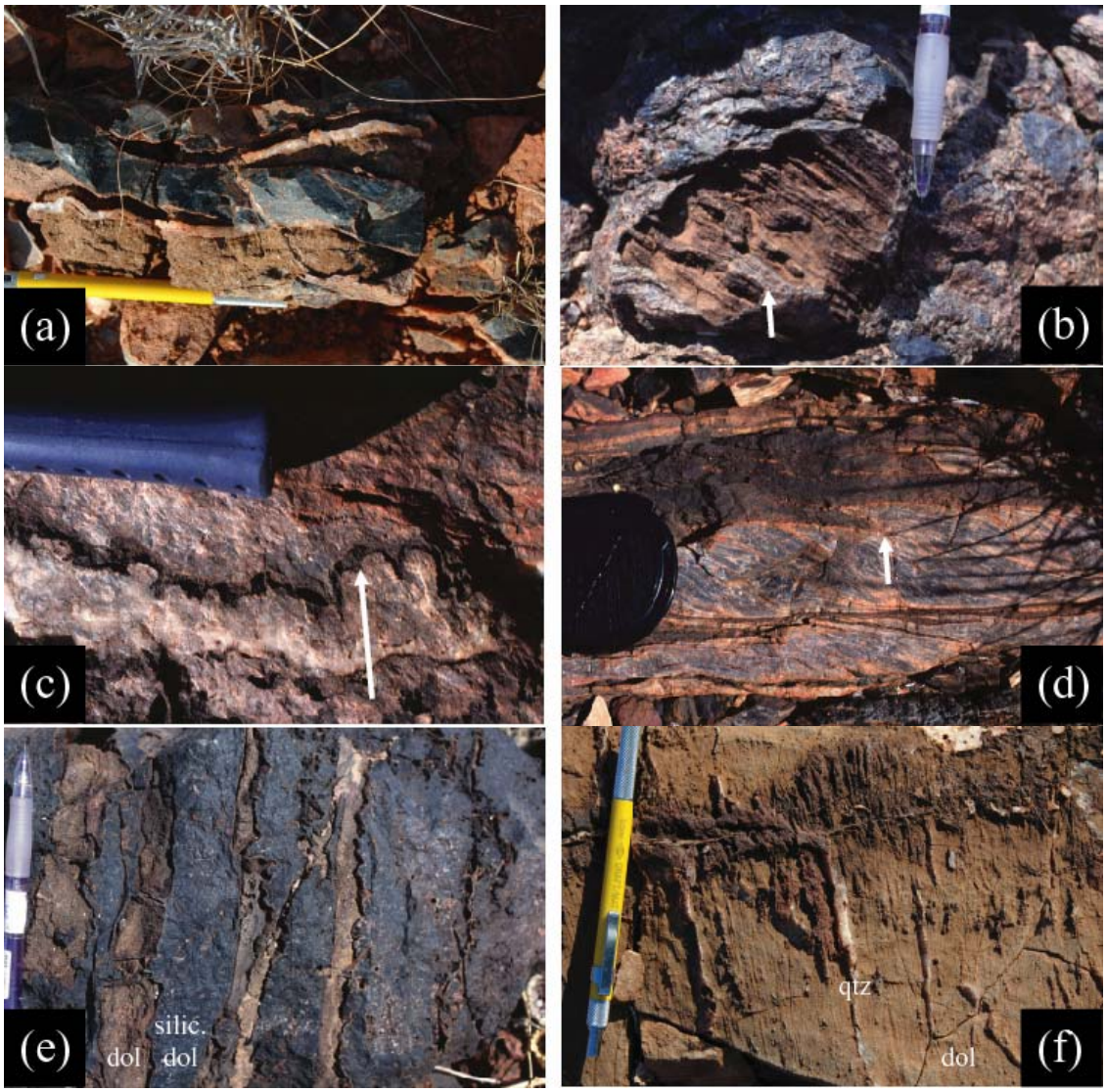

Figure 23: Outcrop photos of SPC carbonate type occurences and contact relations (see also basaltic carbonate metasomatism, Chapter 5, Figure 25). (a): Late, post-peak-metamorphic ankerite alteration enveloping chert in neptunian fissure. (b - h): Early Archaean shallow-marine dolomitization and silicification. (b): Laminated Strelley Pool Chert dolomite boulder in silicified neptunian fissure breccia. The selective silicification of boulder lamellae appears to be associated with silicification in the fissure matrix. (c): Dolomite stylolitization, evincing remobilization of pre-existing dolomite upon silicification. Chert now metamorphosed to sugary metachert. (d): Tectonized sinistral S_7 fabric in metachert-dolomite: dolomitization and silicification precede Pilgangoora synclinaization. The sinistral fabric, which clearly post-dates dolomite silicification, is associated with Pilgangoora Synline closure at ~2.8 Ga. Note talc formation on dolomite-metachert contacts, absent elsewhere. (e): Patchily silicified dolomite enclosing unsilicified stylolitic dolomite domains. (f): Selective lamellar silicification associated with perpendicularly cross-cutting quartz veins.

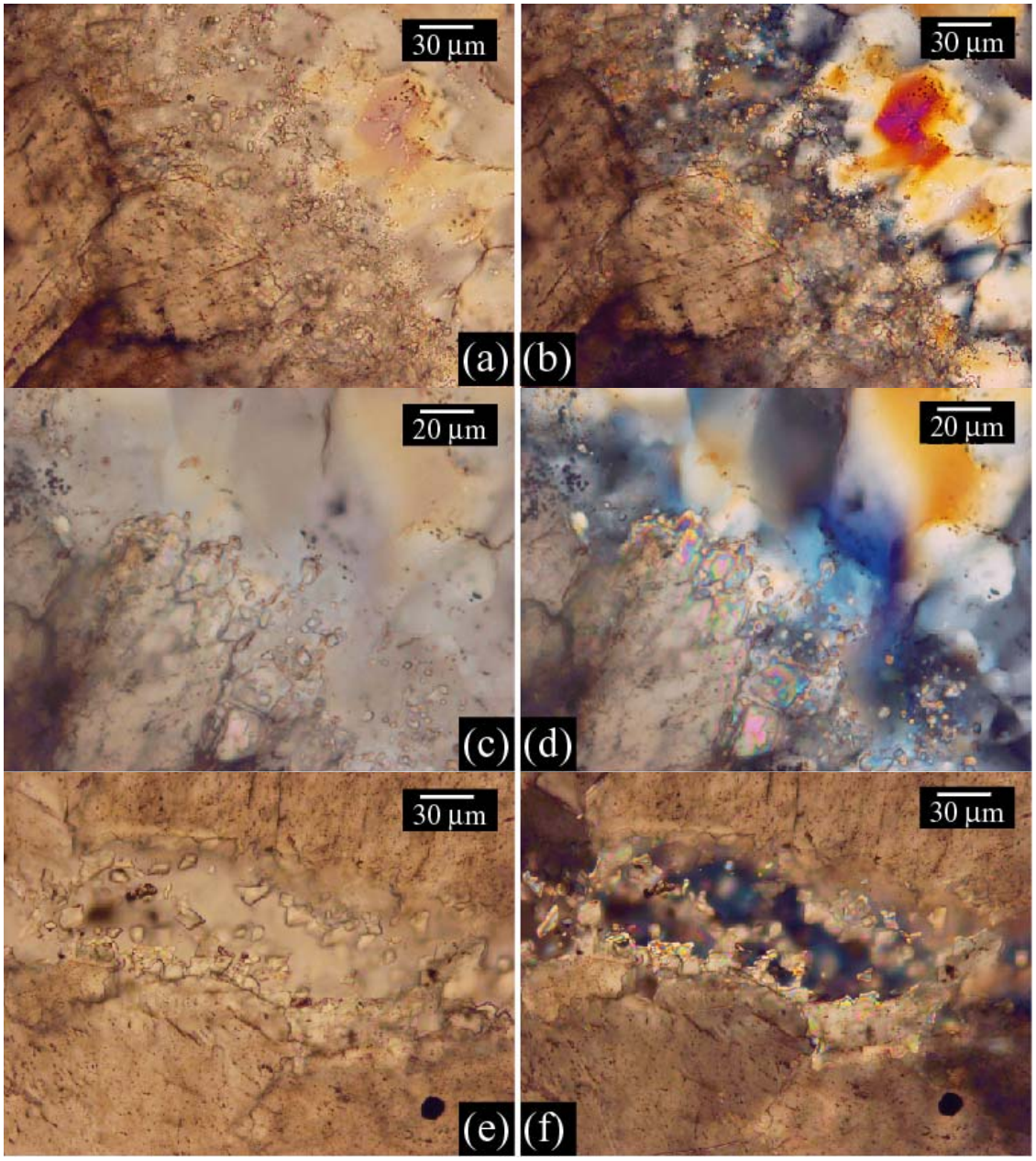

Figure 24: Thin-section photomicrographs of carbonate dissolution-silicification textures in low-grade SPC. (a – d): Silicification front in dolomite. (e, f): Quartz-vein. Note oval fluid-inclusions in reaction zone.

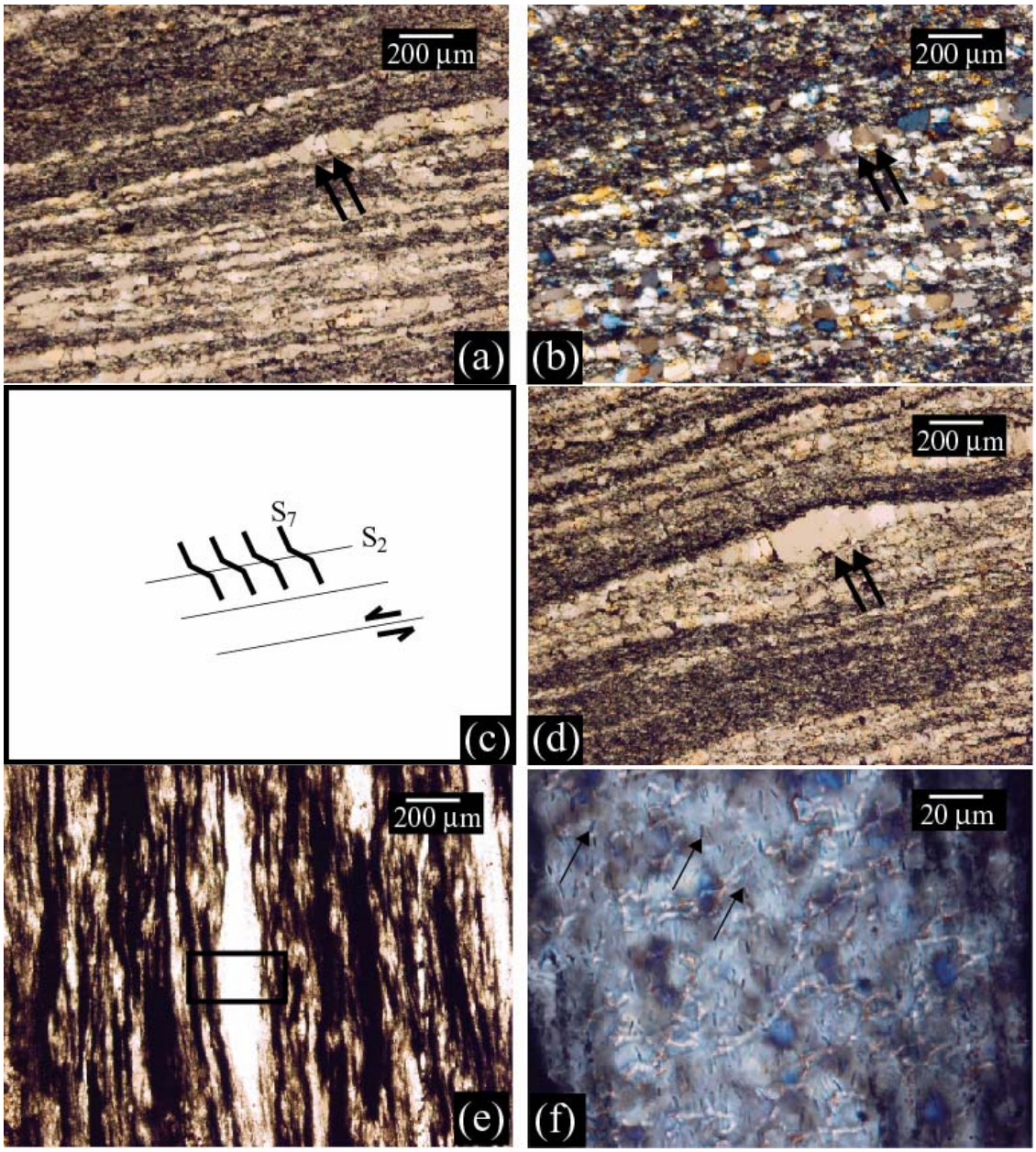

Figure 25: Petrological evidence for early silicification in foliated Strelley Pool Chert. (a, b): S_7 crenulation cleavage cross-curring quartz bands. (c, d): S_7 crenulation and sinistral quartz boudinage. (e, f): Evidence for precursor carbonate in foliated alternating quartz/kerogen Strelley Pool Chert. Box in (e) shows area of photomicrograph of small tremolite crystals alligned parallel to S_7 in quartz band (f).

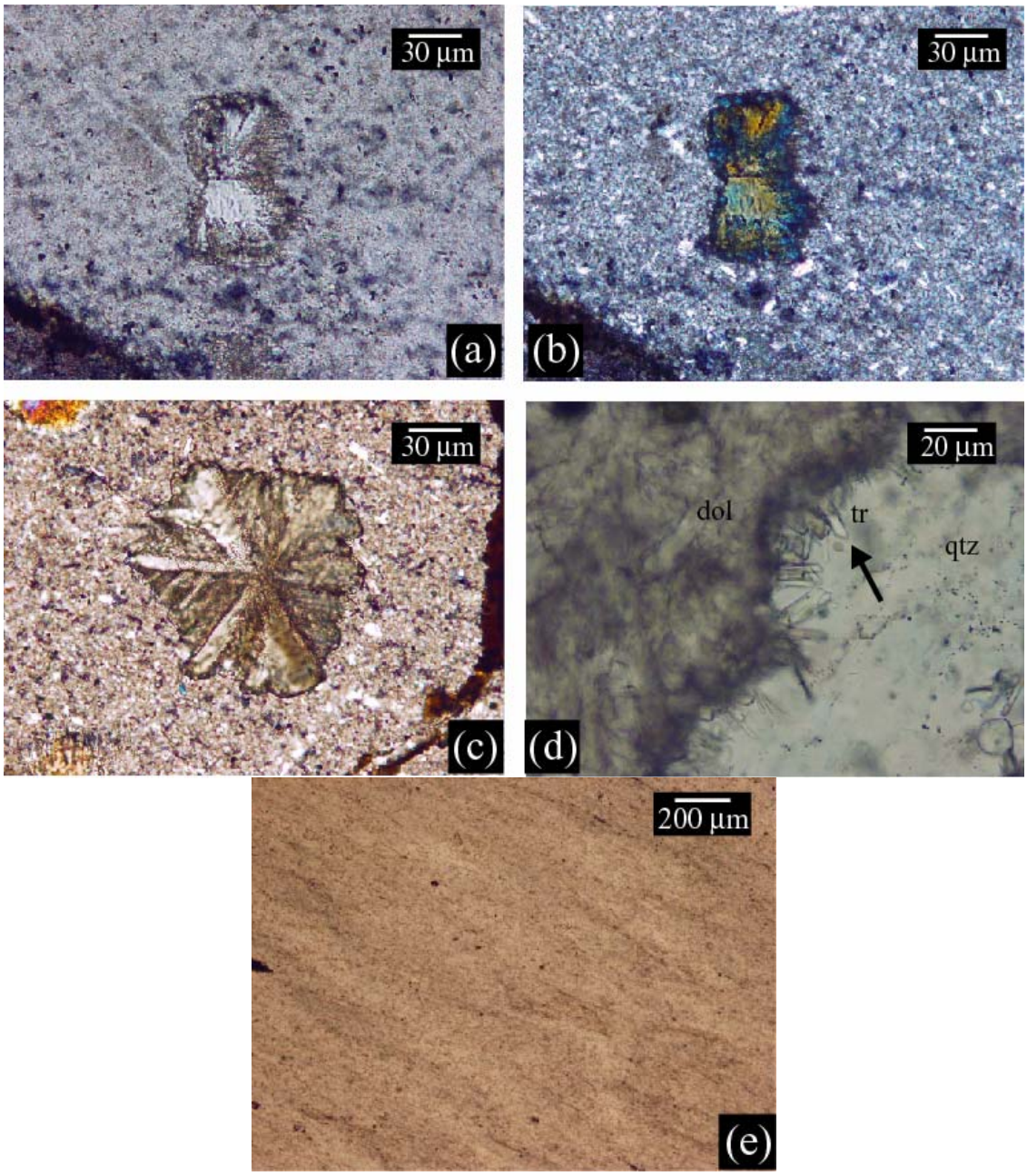

Figure 26: Thin-section photomicrographs of assemblages delineating lower-grade metamorphic facies in SPC. (a – c): Classic 'bow-tie' texture in prehnite in Strelley Pool Chert. (d): Incomplete reaction of dolomite and quartz to form tremolite on grain contacts in M_1 contact aureole. (e): Typical schistose metachert-talc texture.

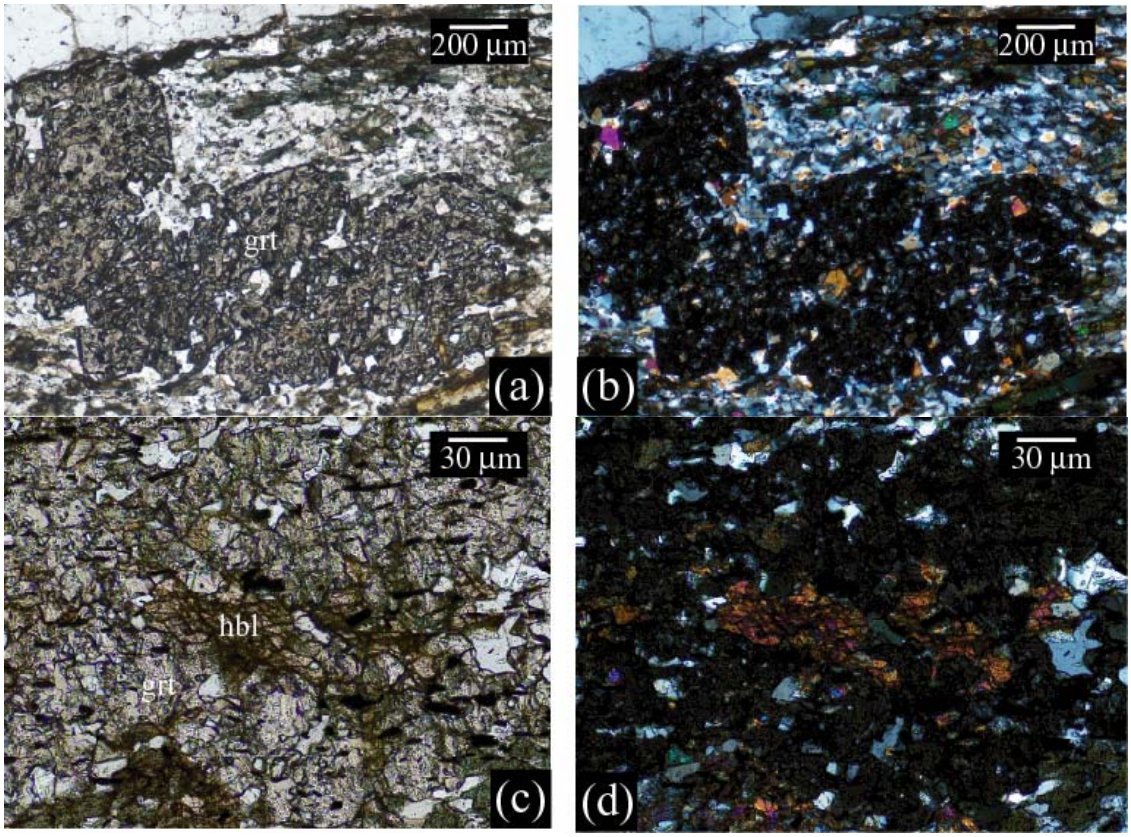

Figure 27: Thin-section photomicrographs of assemblages delineating highest-grade metamorphic facies in SPC. (a, b): Almandine-oligoclase-quartz in Coonterunah Subgroup silicified metamafic. (c, d): Alumino-ferrotschermakite amphibole in equilibrium with almandine in lower amphibolite-facies Coonterunah Subgroup metamafics.

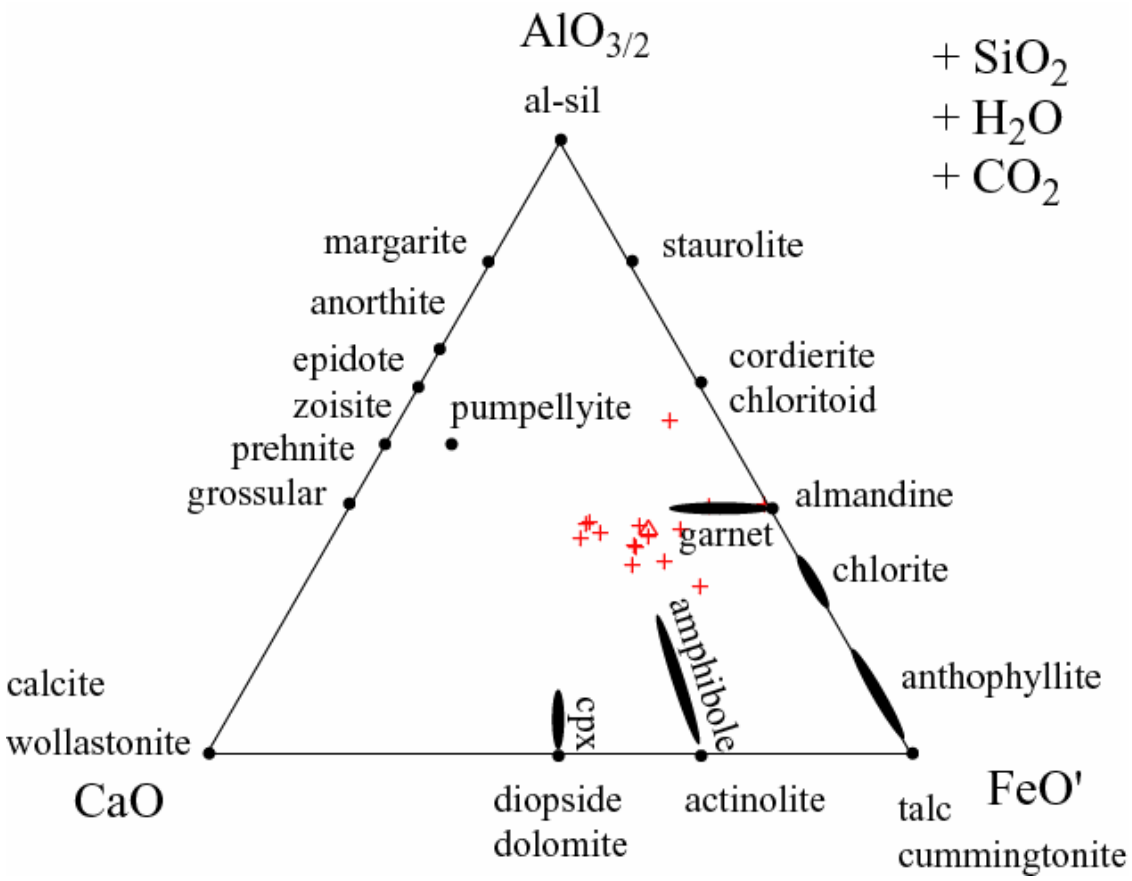

Figure 28: Ternary ACF phase diagram (Spear, 1995) with Pilgangoora Belt basalt compositions (red crosses). Triangle shows average composition. FeO' = FeO + MgO.

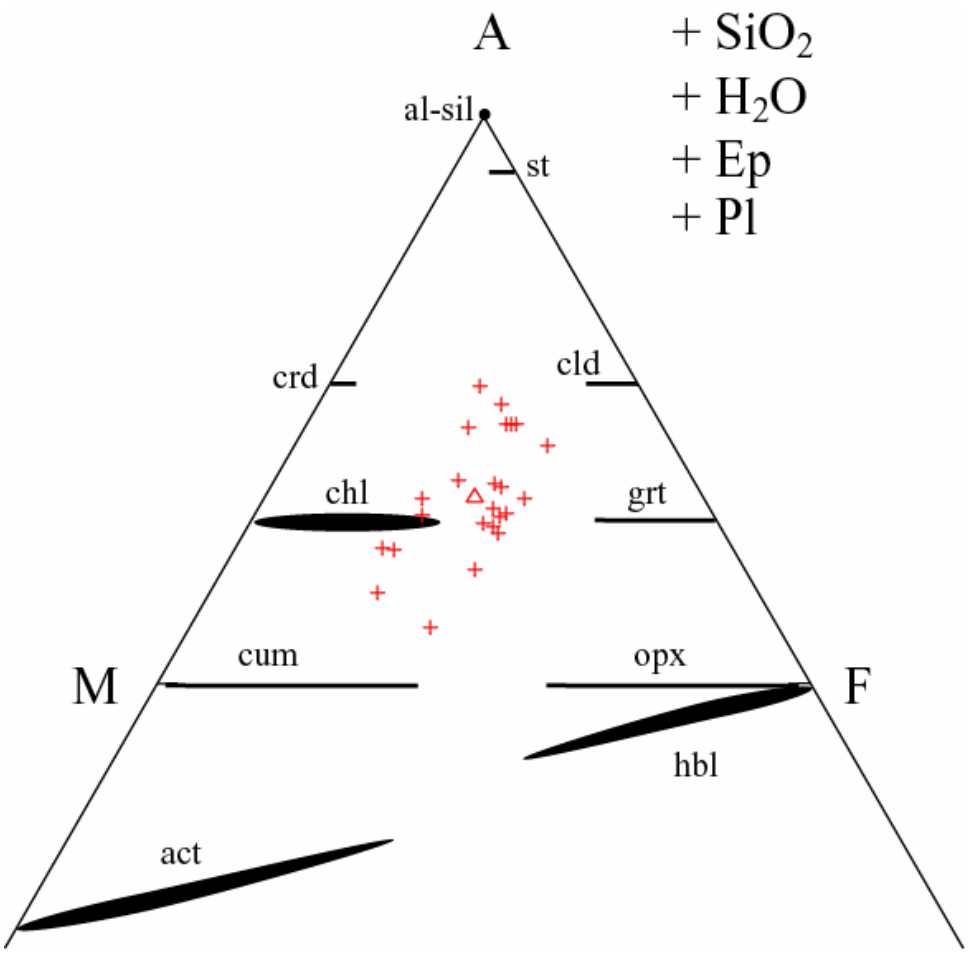

Figure 29: Ternary AFM phase diagram projected from epidote and plagioclase (Spear, 1995) showing Pilgangoora Belt basalt compositions (red crosses) and selected mineral fields. A = $0.5AlO_{1.5}$ - 0.75CaO; F = FeO; M = MgO.

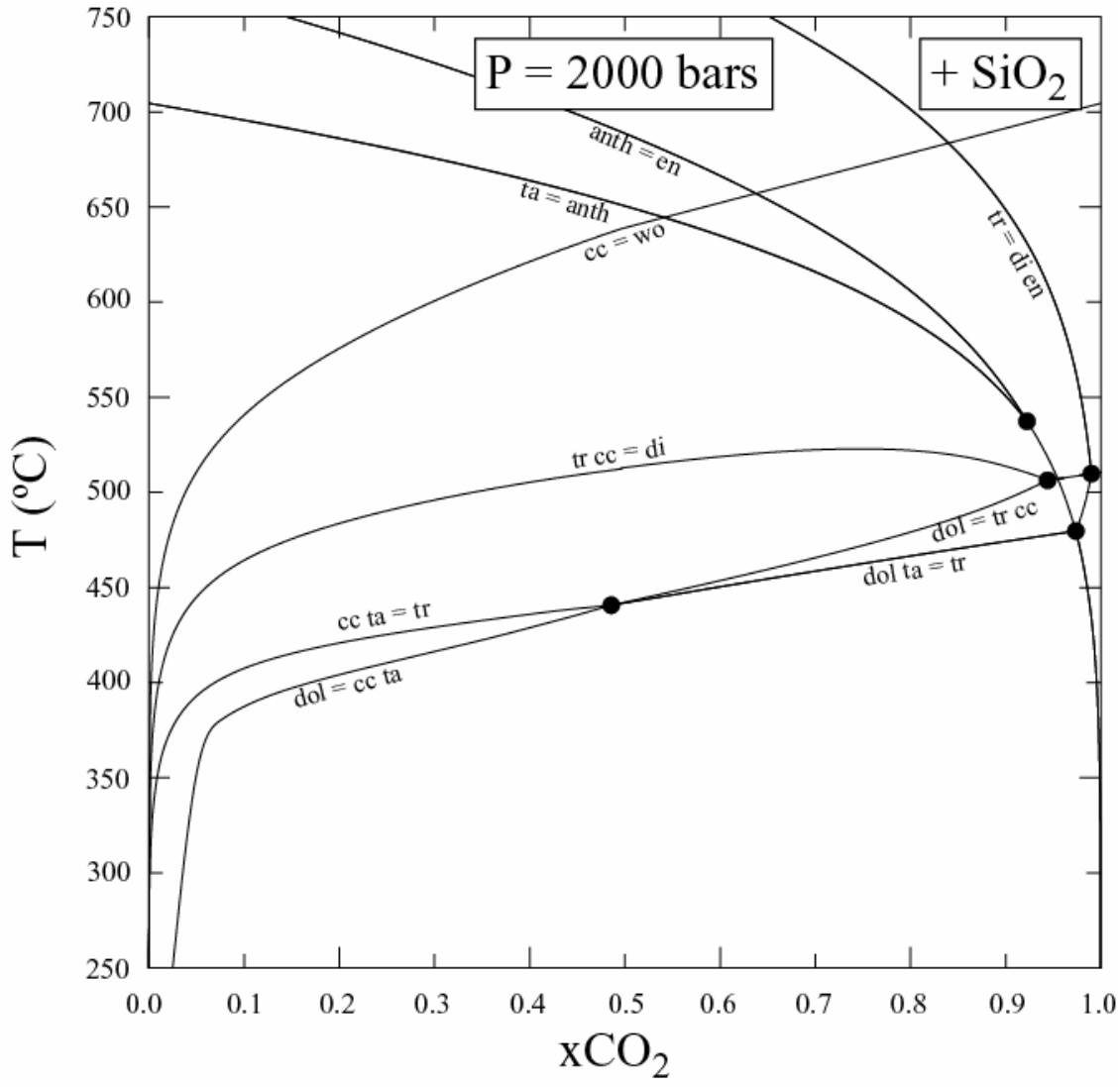

Figure 30: T-xCO_2 diagram in the Ca-Mg+Si+fluid system calculated at P = 2000 bars.

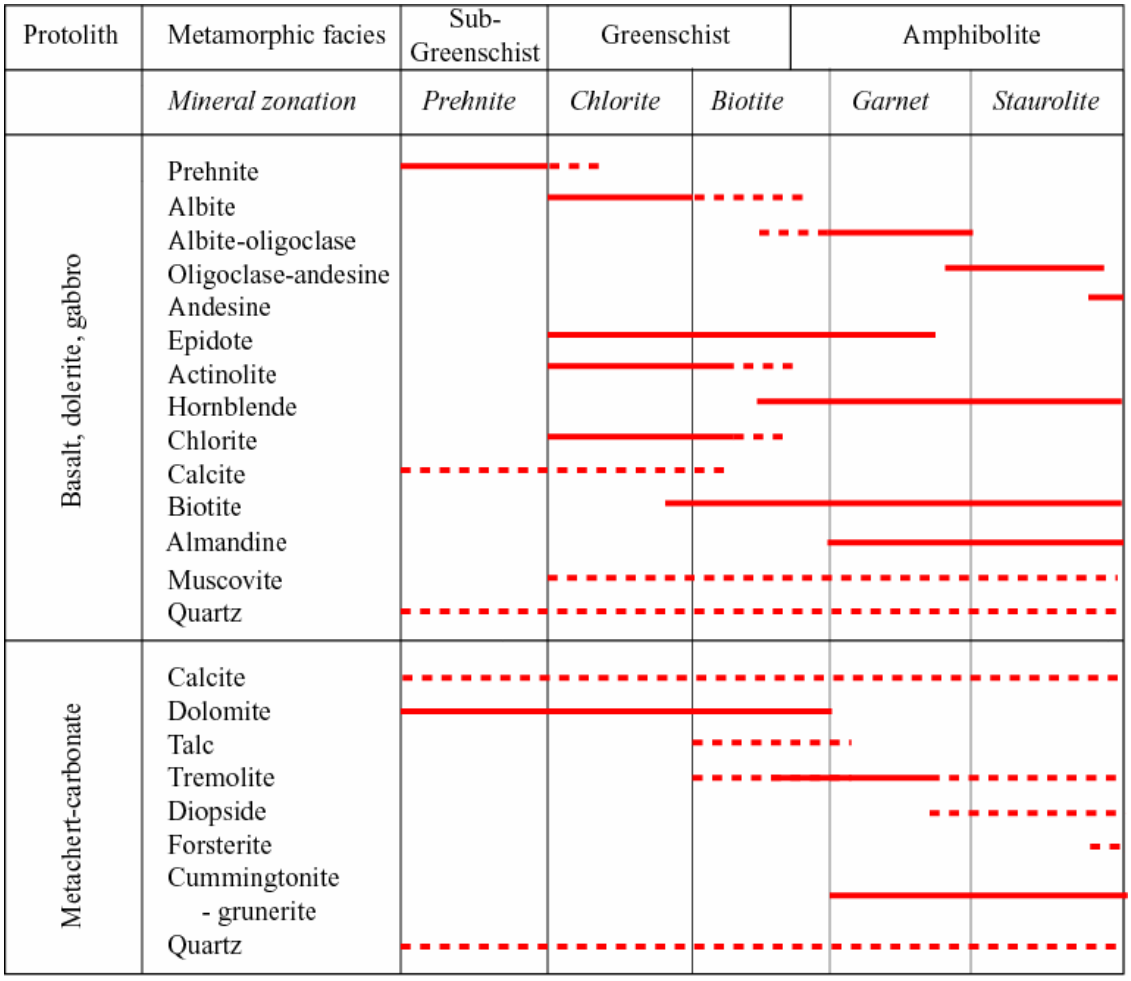

Figure 31: Pilgangoora Belt metamorphic zonation diagram.

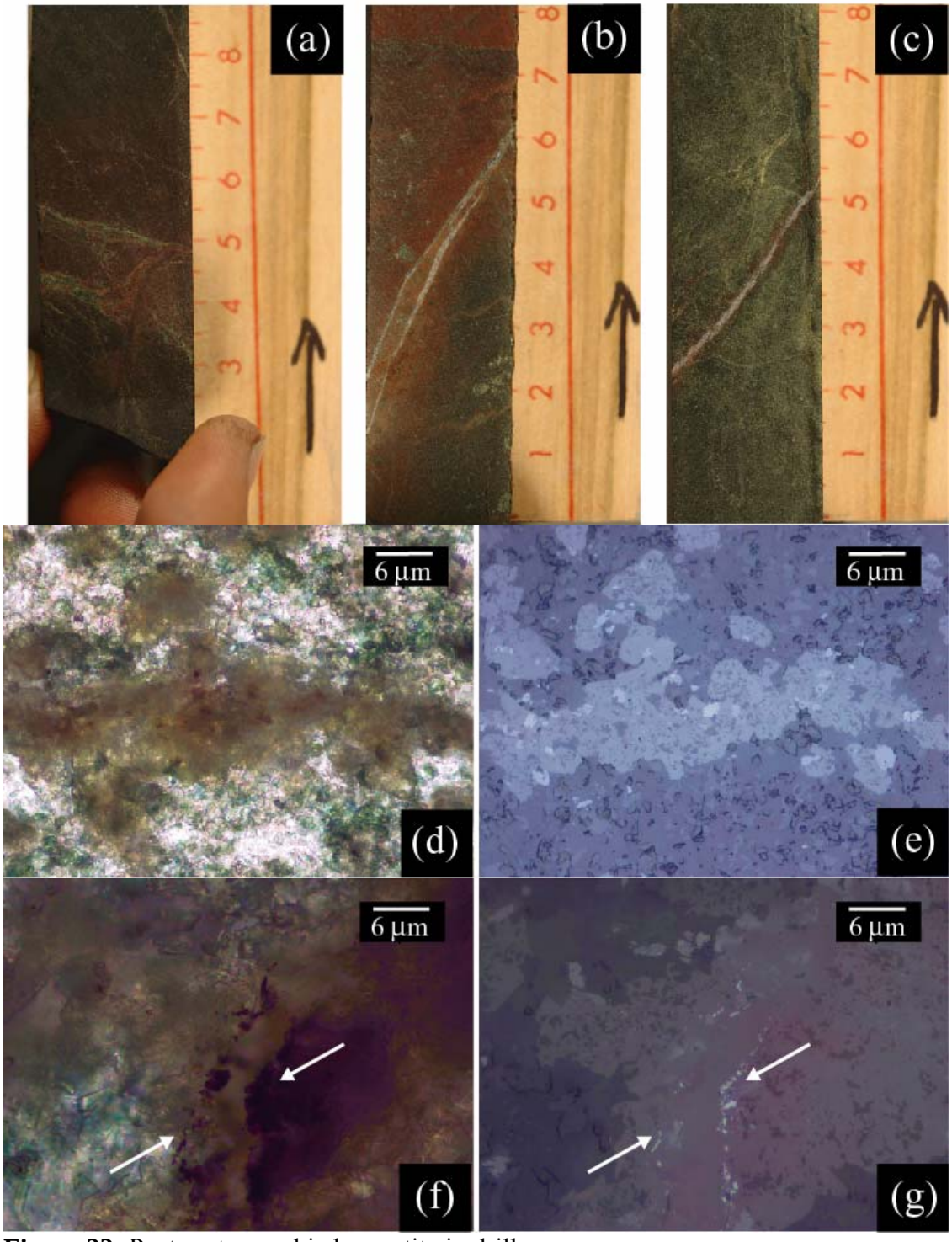

Figure 32: Post-metamorphic haematite in drillcore.

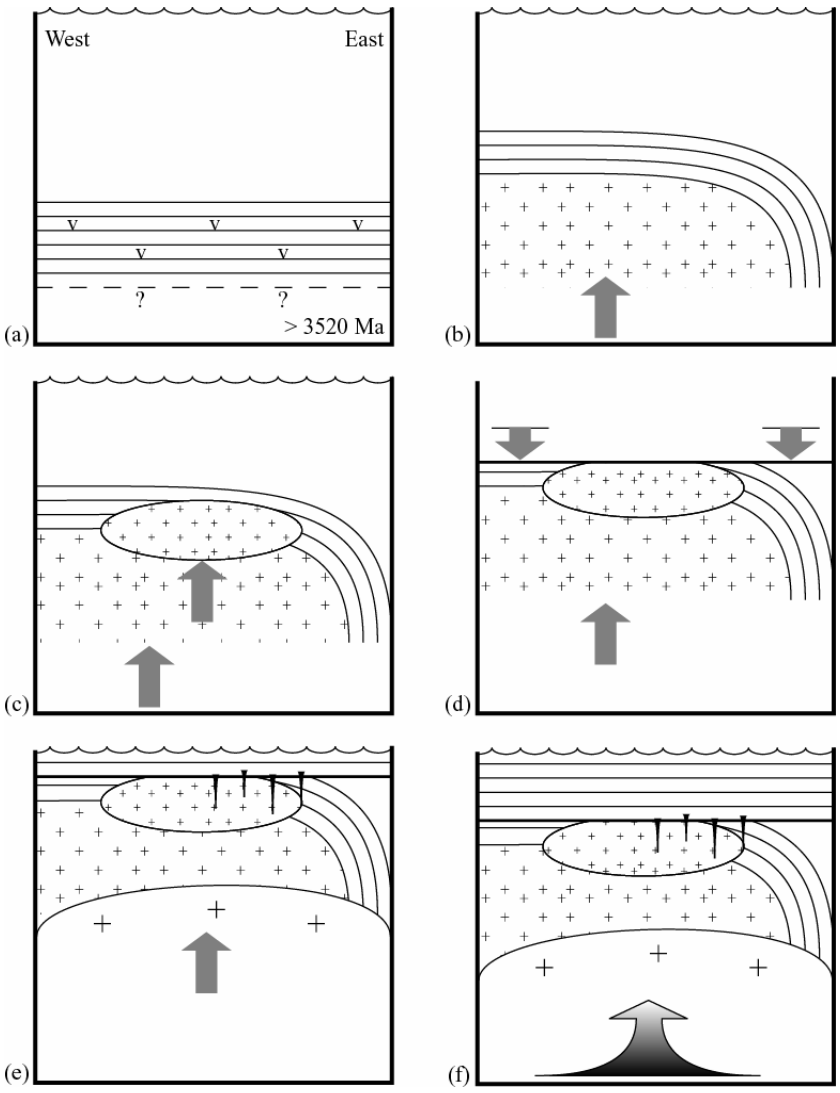

Figure 33: Major structural and tectonothermal events in the Pilgangoora Belt up until Kelly Group tilting. (a): Deposition and extrusion of >6.5 km Coonterunah deep-marine sediments and lavas at ~3517 Ma onto an unknown, possible sialic basement. (b): Intrusion of Carlindi granitoid suite at 3468-3484 Ma. Contact metamorphism to upper greenschist and local lower amphibolite facies in a ~500 m wide aureole. Doming-related steepening of eastern Coonterunah units. (c): Shallow crustal emplacement of Carlindi-related microgranite at 3468-3484 Ma. (d): Exhumation, leveling and erosion prior to deposition of unconformably overlying Kelly Group. (e): Crustal flexure resulting from continued uplift and doming give rise to the development of 250-750 meter deep neptunian fissures, which sample deposition of the shallow marine and subaerial sediments of the ≤ 3458 Ma Strelley Pool Chert, Warrawoona Group. (f): Upright tight synclinal tilting at < 3235 Ma results in the present sub-vertical bedding of Coonterunah, Warrawoona and Gorge Creek group, characteristic of greenstone belts in the Pilbara and elsewhere. Tilting likely occurred in response to large-scale diapiric uplift.

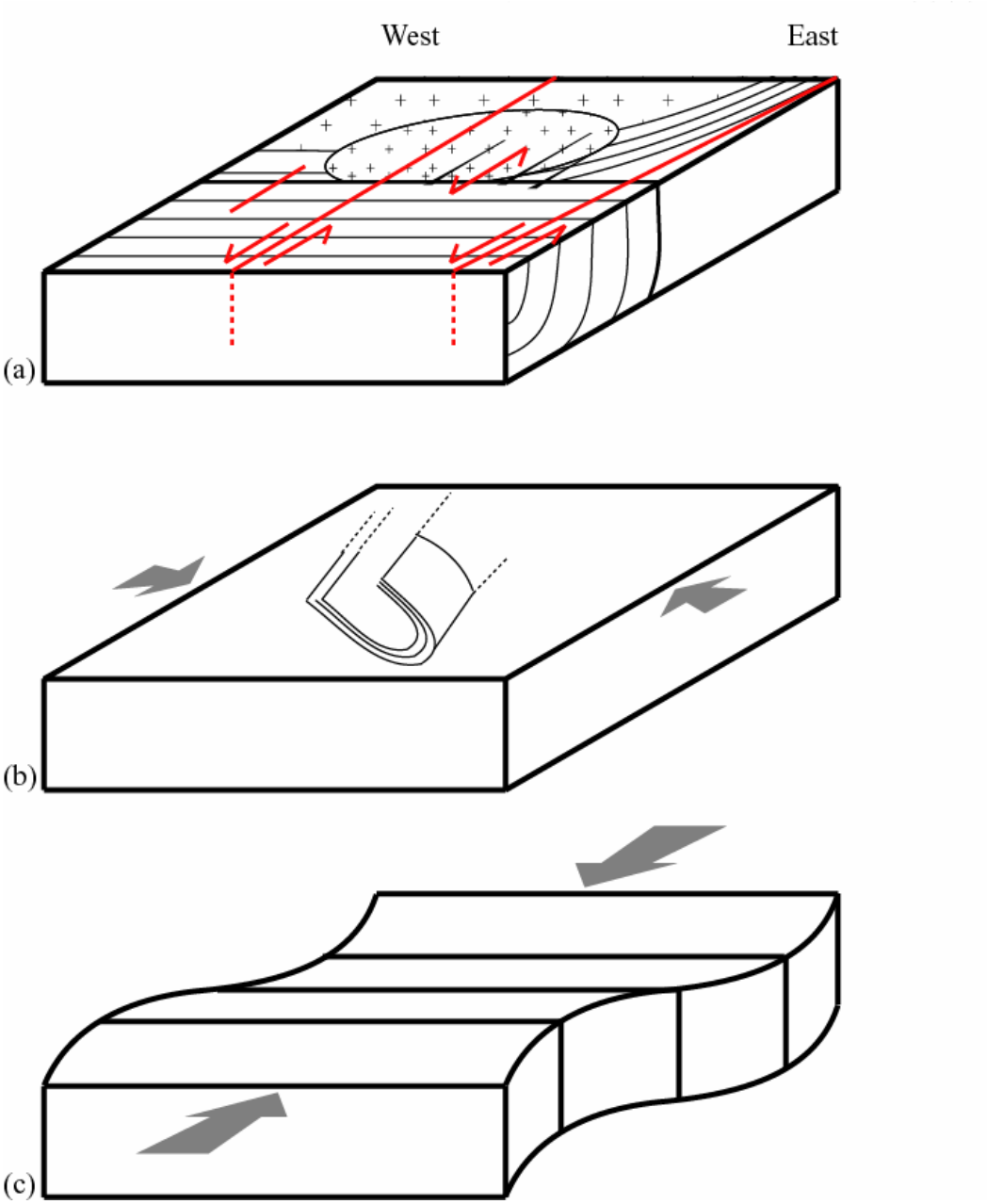

Figure 34: Major structural and tectonothermal events in the Pilgangoora Belt after Kelly Group tilting. (a): Regional N- to NNE- directed dominantly sinistral strike-slip faulting. Re-activation along rheologically vulnerable planes, such as Neptunian fissures (b): Development of shallowly south plunging Pilgangoora syncline at ~2890 Ma (Neumayr et al., 1998), associated with strain-controlled lower amphibolite-facies metamorphism, Au-mineralization and garnet-bearing pegmatite dykes along fold cleavage planes. (c): Long-wavelength broad gentle north-south directed folding associated with continuing subduction of Indonesia slab under Australia.

Table 1: Structural geology of the Pilgangoora Belt compared with other studies.

This study	*Baker et al. (2002)*	*Blewett (2002)*	*Brief description*
D_1	D_1	D_1	Pre-Kelly foliation fabric, found in Coonterunah only
D_2	D_2	D_2	Early Kelly and Warrawoona foliation fabric
D_{n-f}	Not reported	Not reported	Seafloor rupturing and formation of Neptunian fissures
D_3		D_3	NE-plunging isoclinal folding
D_4		D_4	NW-plunging closed folding
D_5		D_5	N- to NNE- striking sinistral shearzones
D_6		D_6	S-plunging upright tight folding
	D_3		Broad, open folding
		D_7	ENE-WSW folding
D_7	D_4		Regional open folding, sinistral shearing, granitic pegmatite dyke emplacement
D_8		D_8	Minor N-S shortening, chevron-like moderate to steep E-plunging fold hinges
D_9		D_9	NW-SE striking crenulations
Not recognized as a separate event	D_5		Brittle faulting
D_{tect}	Not reported	Not reported	Ongoing N-S directed gentle km-scale folding

Table 2: Down-core silicification trends revealed by carbonate analyses of Warrawoona-Kelly drillcore.

Sample	Analysis	Mass	CO_2	CO_2	± 1σ	$\delta^{13}C_{carb}$	± 1σ	$\delta^{18}O_{carb}$	± 1σ
		(mg)	(µg)	(wt.%)		(‰, PDB)		(‰, PDB)	
143.27m	rep1	6.276	2.9	0.05		-3.90	0.22	-20.70	0.23
163.40m	rep1	2.344	57.6	2.46		1.67	0.03	-17.77	0.04
	rep2	2.221	52.9	2.38		1.64	0.02	-17.84	0.02
	rep3	4.720	56.9	1.21		1.63	0.04	-18.31	0.05
	rep4	1.896	50.9	2.68		1.65	0.01	-18.07	0.04
	mean			*2.18*	*0.66*	*1.65*	*0.02*	*-18.00*	*0.25*
163.70m	rep1	3.568	58.0	1.62		1.66	0.02	-18.49	0.03
	rep2	1.535	49.0	3.19		1.68	0.02	-18.42	0.04
	rep3	1.488	49.0	3.29		1.66	0.03	-18.40	0.03
	rep4	3.473	57.2	1.65		1.62	0.03	-18.64	0.04
	mean			*2.44*	*0.93*	*1.65*	*0.03*	*-18.48*	*0.13*
310.53m	rep1	14.394	51.1	0.36		-0.68	0.03	-17.21	0.03
	rep2	11.136	44.3	0.40		-0.57	0.03	-16.79	0.06
	rep3	7.825	31.6	0.40		-0.62	0.04	-17.03	0.05
	mean			*0.39*	*0.03*	*-0.06*	*0.06*	*-17.38*	*0.21*
311.64m	rep1	10.747	57.6	0.54		-0.10	0.03	-16.62	0.04
	rep2	11.430	57.6	0.50		-0.10	0.02	-16.64	0.06
	rep3	5.878	37.4	0.64		-0.16	0.04	-16.98	0.03
	mean			*0.56*	*0.07*	*-0.12*	*0.04*	*-16.75*	*0.20*
312.32m	rep1	11.361	38.7	0.34		-0.72	0.02	-16.01	0.03
	rep2	14.750	48.0	0.33		-0.73	0.03	-15.96	0.13
	rep3	5.239	17.2	0.33		-0.81	0.03	-16.25	0.07
	mean			*0.33*	*0.01*	*-0.75*	*0.05*	*-16.07*	*0.15*
313.37m	rep1	14.971	52.4	0.35		0.15	0.04	-16.48	0.05
	rep2	14.822	54.4	0.37		0.16	0.02	-16.28	0.02
	rep3	6.488	28.2	0.43		0.07	0.02	-16.64	0.02
	mean			*0.38*	*0.04*	*0.12*	*0.05*	*-16.47*	*0.18*

References

Aitken, B. G. and Echeverria, L. M., 1984. Petrology and Geochemistry of Komatiites and Tholeiites from Gorgona-Island, Colombia. *Contrib. Mineral. Petrol.* **86**, 94-105.

Allard, G. O., Caty, J.-L., and Gobeil, C., 1985. *The Archean supracrustal rocks of the Chibougamau area*. Geological Association of Canada.

Allwood, A. C., Walter, M. R., Burch, I. A., and Kamber, B. S., 2008. 3.43 billion-year-old stromatolite reef from the Pilbara Craton of Western Australia: ecosystem-scale insights to early life on Earth. *Precamb. Res.* **158**, 198-227.

Allwood, A. C., Walter, M. R., Kamber, B. S., Marshall, C. P., and Burch, I. W., 2006. Stromatolite reef from the Early Archaean era of Australia. *Nature* **441**, 714-718.

Arndt, N. T., Nelson, D. R., Compston, W., Trendall, A. F., and Thorne, A. M., 1991. The age of the Fortescue Group, Hamersley Basin, Western Australia, from ion microprobe zircon U-Pb results. *Australian Journal of Earth Sciences* **38**, 261-281.

Baker, D. E. L., Seccombe, P. K., and Collins, W. J., 2002. Structural history and timing of gold mineralization in the northern East Strelley Belt, Pilbara Craton, Western Australia. *Economic Geology* **97**, 775-785.

Barley, M. E., 1980. Evolution of Archaean calc-alkaline volcanics: a study of the Kelly Greenstone Belt and McPhee Dome, eastern Pilbara Block, Western Australia. Ph.D. thesis, University of Western Australia.

Barley, M. E. and Bickle, M. J., 1982. Komatiites in the Pilbara Block, Western Australia. In: Arndt, N. T. and Nisbet, E. G. Eds.), *Komatiites*. George Allen and Unwin, London, United Kingdom.

Barley, M. E., Dunlop, J. S. R., Glover, J. E., and Groves, D. I., 1979. Sedimentary evidence for an Archaean shallow-water volcanic-sedimentary facies, eastern Pilbara Block, Western Australia. *Earth Planet. Sci. Lett.* **43**, 74-84.

Bell, K., Blenkinsop, J., and Moore, J. M., 1975. Evidence for a Proterozoic Greenstone Belt from Snow Lake, Manitoba. *Nature* **258**, 698-701.

Bettenay, L. F., Bickle, M. J., Boulter, C. A., Groves, D. I., Morant, P., Blake, T. S., and James, B. A., 1981. Evolution of the Shaw Batholith - an Archaean granitoid-gneiss dome in the eastern Pilbara, Western Australia. *Geological Society of Australia Special Publication* **7**, 361-372.

Bickle, M. J., Bettenay, L. F., Boulter, C. A., Groves, D. I., and Morant, P., 1980. Horizontal tectonic interaction of an Archean gneiss belt and greenstones, Pilbara Block, Western Australia. *Geology* **8**, 525-529.

Bickle, M. J., Morant, P., Bettenay, L. F., Boulter, C. A., Blake, J. A., and Groves, D. I., 1985. Archean tectonics of the Shaw batholith, Pilbara Block, Western Australia: Structural and Metamorphic tests of the batholith concept. In: Ayres, L. D. (Ed.), *Evolution of Archean Supracrustal Sequences*.

Blackburn, C. E., Bond, W. D., Breaks, F. W., Davis, D. W., Edwards, G. R., Poulson, K. H., Trowell, N. F., and Wood, J., 1985. Evolution of Archean volcanic-sedimentary sequences of the western Wabigoon subprovince and its margins: a review, *Geological Association of Canada special paper ;*. Geological Association of Canada, St. Johns, Nfld.

Blake, T. S., 1984. Evidence for stabilization of the Pilbara Block, Australia. *Nature* **307**, 721-723.

Blake, T. S., 1993. Late Archaean crustal extension, sedimentary basin formation, flood basalt volcanism and continental rifting: the Nullagine and Mount Jope Supersequences, Western Australia. *Precamb. Res.* **60**, 185-241.

Blake, T. S., Buick, R., Brown, S. J. A., and Barley, M. E., 2004. Stratigraphic geochronology of a late Archaean flood basalt province in the Pilbara Craton, Australia: constraints on basin evolution, mafic and felsic volcanism and continental drift rates. *Precamb. Res.* **133**.

Blewett, R. S., 2002. Archaean tectonic processes: a case for horizontal shortening in the North Pilbara Granite-Greenstone Terrane, Western Australia. *Precamb. Res.* **113**, 87-120.

Bridgwater, D. and Collerson, K. D., 1976. Major Petrological and Geochemical Characters of 3,600 My Uivak Gneisses from Labrador. *Contrib. Mineral. Petrol.* **54**, 43-59.

Buick, R., 1984. Carbonaceous filaments from North Pole, Western Australia - are they fossil bacteria in Archean stromatolites? *Precamb. Res.* **24**, 157-172.

Buick, R., 1985. Life and conditions in the Early Archaean: Evidence from 3500 m.y. old shallow-water sediments in the Warrawoona Group, North Pole, Western Australia. Ph.D. thesis, University of Western Australia.

Buick, R. and Barnes, K. R., 1984. Cherts in the Warrawoona Group: Early Archaean silicified sediments deposited in shallow-water environments. In: Muhling, J. R., Groves, D. I., and Blake, T. S. Eds.), *Archaean and Proterozoic basins of the the Pilbara, Western Australia: evolution and mineralization potential*. University of Western Austrlia, Perth.

Buick, R., Brauhart, C. W., Morant, P., Thornett, J. R., Maniw, J. G., Archibald, N. J., Doepel, M. G., Fletcher, I. R., Pickard, A. L., Smith, J. B., Barley, M. E., McNaughton, N. J., and Groves, D. I., 2002. Geochronology and stratigraphic relationships of the Sulphur Springs Group and Strelley Granite: a temporally distinct igneous province in the Archaean Pilbara Craton, Australia. *Precamb. Res.* **114**, 87-120.

Buick, R. and Dunlop, J. S. R., 1990. Evaporitic sediments of early Archaean age from the Warrawoona Group, North Pole, Western Australia. *Sedimentology* **37**, 247-277.

Buick, R., Thornett, J. R., McNaughton, N. J., Smith, J. B., Barley, M. E., and Savage, M., 1995. Record of emergent continental crust ~3.5 billion years ago in the Pilbara Craton of Australia. *Nature* **375**, 574-577.

Burke, K., 1997. Foreword, *Greenstone Belts*. Clarendon Press.

Burke, K. C. and Dewey, J. F., 1972. Orogeny in Africa. In: Dessauvagie, T. F. J. and Whiteman, A. J. Eds.), *African Geology*.

Catling, D. C. and Moore, J. A., 2003. The nature of coarse-grained crystalline hematite and its implications for the early environment of Mars. *Icarus* **165**, 277-300.

Collins, W. J., 1989. Polydiapirism of the Archean Mount Edgar Batholith, Pilbara Block, Western Australia. *Precamb. Res.* **43**, 41-62.

Collins, W. J., Van Kranendonk, M. J., and Teyssier, C., 1998. Partial convective overturn of Archaean crust in the east Pilbara Craton, Western Australia: driving mechanisms and tectonic implications. *Journal of Structural Geology* **20**, 1405-1424.

Condie, K. C., 1993. Chemical-Composition and Evolution of the Upper Continental-Crust - Contrasting Results from Surface Samples and Shales. *Chem. Geol.* **104**, 1-37.

Dimarco, M. J. and Lowe, D. R., 1989a. Petrography and provenance of silicified early Archaean volcaniclastic sandstones, eastern Pilbara Block, Western Australia. *Sedimentology* **36**, 821-836.

Dimarco, M. J. and Lowe, D. R., 1989b. Shallow-water volcaniclastic deposition in the early Archean Panorama Formation, Warrawoona Group, eastern Pilbara Block, Western Australia. *Sediment Geol* **64**, 43-63.

Drummond, B. J., 1988. A review of crust/upper mantle structure in the Precambrian areas of Australia and implications for Precambrian crustal evolution. *Precamb. Res.* **40/41**, 101-116.

Dunlop, J. S. R., 1976. The geology and mineralization of part of the North Pole barite deposits, Pilbara region, Western Australia. B.Sc (hons), University of Western Australia.

Dunlop, J. S. R., Muir, M. D., Milne, V. A., and Groves, D. I., 1978. A new microfossil assemblage from the Archaean of Western Australia. *Nature* **274**, 676-678.

Echeverria, L. M., 1980. Tertiary or Mesozoic Komatiites from Gorgona Island, Colombia - Field Relations and Geochemistry. *Contrib. Mineral. Petrol.* **73**, 253-266.

Eriksson, K. A., 1982. Geometry and internal characteristics of Archaean submarine channel deposits, Pilbara Block, Western Australia. *J Sediment Petrol* **52**, 383-393.

Fisher, R. V. and Schmincke, H.-U., 1984. *Pyroclastic rocks*. Springer-Verlag, Berlin ; New York.

Glikson, A. Y., 1995. Asteroid/comet mega-impacts may have triggered major episodes of crustal evolution. *Eos, Transactions, American Geophysical Union* **76**, 49, 54-55.

Glikson, A. Y. and Jahn, B.-M., 1985. REE and LIL elements, eastern Kaapvaal Shield, South Africa : evidence of crustal evolution by 3-stage melting. In: Ayers, L. D., Thurston, P. C., Card, K. D., and Weber, W. Eds.), *Evolution of Archean Supracrustal Sequences*. Geological Association of Canada.

Gole, M. J., 1980. Mineralogy and Petrology of Very-Low-Metamorphic Grade Archean Banded Iron-Formations, Weld Range, Western-Australia. *Am. Mineral.* **65**, 8-25.

Green, M. G., 2001. Early Archaean crustal evolution: evidence from ~3.5 billion year old greenstone successions in the Pilgangoora Belt, Pilbara Craton, Australia. Ph.D., University of Sydney.

Green, M. G., Sylvester, P. J., and Buick, R., 2000. Growth and recycling of early Archaean continental crust: geochemical evidence from the Coonterunah and Warrawoona Groups, Pilbara Craton, Australia. *Tectonophysics* **322**, 69-88.

Hickman, A. H., 1972a. The North Pole barite deposits, Pilbara Goldfield. *Geological Survey of Western Australia, Annual Report* **1972**, 57-60.

Hickman, A. H., 1972b. Precambrian structural geology of part of the Pilbara region. *Geological Survey of Western Australia, Annual Report* **1972**, 68-73.

Hickman, A. H., 1975. Precambrian structural geology of part of the Pilbara region, *Western Australia Geological Survey Annual Report*. Geological Survey of Western Australia, Perth.

Hickman, A. H., 1983. Geology of the Pilbara Block and the environs. *Australian Geological Survey*.

Hickman, A. H., 1984. Archaean diapirism in the Pilbara Block, Western Australia. In: Kroner, A. and Greiling, R. Eds.), *Precambrian Tectonics Illustrated*. E. Schweizerbart'sche Verlagsbuchhandlung, Stuttgart, Germany.

Jensen, L. S., 1985. Stratigraphy and petrogenesis of Archean metavolcanic sequences, southwestern Abitibi Subprovince, Ontario. In: Ayres, L. D., Thurston, P. C., Card, K. D., and Webber, W. Eds.), *Evolution of Archean supracrustal sequences*. Geological Association of Canada.

Kalkowsky, E., 1908. Oolith und Stromatolith im norddeutschen Buntsandstein. *Zeitschrift der Deutschen geologischen Gesellschaft* **60**, 68-125.

Kiyokawa, S., 1983. Stratigraphy and structural evolution of a Middle Archaean greenstone belt, northwestern Pilbara Craton, Australia. Ph.D., University of Tokyo.

Kloppenburg, A., White, S. H., and Zegers, T. E., 2001. Structural evolution of the Warrawoona Greenstone Belt and adjoining granitoid complexes, Pilbara Craton, Australia: implications for Archaean tectonic processes. *Precamb. Res.* **112**, 107-147.

Knauth, L. P., 1994. Petrogenesis of Chert. *Rev Mineral* **29**, 233-258.

Krapez, B., 1993. Sequence stratigraphy of the Archaean supracrustal belts of the Pilbara Block, Western Australia. *Precamb. Res.* **60**, 1-45.

Krapez, B. and Barley, M. E., 1987. Archaean strike-slip faulting and related ensialic basins: evidence from the Pilbara Block, Australia. *Geol. Mag.* **124**, 555-567.

Kröner, A., 1981. *Precambrian plate tectonics*. Elsevier, Amsterdam.

Laschet, C., 1984. On the origin of cherts. *Facies* **10**, 257-290, 19 Figs.

Lindsay, J. F., Brasier, M. D., McLoughlin, N., Green, O. R., Fogel, M., Steele, A., and Mertzman, S. A., 2005. The problem of deep carbon - An Archean paradox. *Precamb. Res.* **143**, 1-22.

Lowe, D. R., 1980. Stromatolites 3400-Myr old from the Archean of Western Australia. *Nature* **284**, 441-443.

Lowe, D. R., 1983. Restricted shallow-water sedimentation of early Archean stromatolitic and evaporitic strata of the Strelley Pool Chert, Pilbara Block, Western Australia. *Precambrian Res.* **19**, 239-283.

Martin, H., 1994. Archean grey gneisses and the genesis of continental crust. In: Condie, K. C. (Ed.), *Archean Crustal Evolution*. Elsevier, Amsterdam ; New York.

McNaughton, N. J., Green, M. D., Compston, W., and Williams, I. S., 1988. Are anorthositic rocks basement to the Pilbara Craton? *Geological Society of Australia Abstract* **21**, 272-273.

Moore, J., J.M., 1977. Orogenic volcanism in the Proterozoic of Canada. Geological Association of Canada.

Nelson, D. R., Trendall, A. F., and Altermann, W., 1999. Chronological correlations between the Pilbara and Kaapvaal cratons. *Precamb. Res.* **97**, 165-189.

Nelson, D. R., Trendall, A. F., de Laeter, J. R., Grobler, N. J., and Fletcher, I. R., 1992. A comparative study of the geochemical and isotopic systematics of late Archaean flood basalts from the Pilbara and Kaapvaal Cratons. *Precamb. Res.* **54**, 231-256.

Neumayr, P., Ridley, J. R., McNaughton, N. J., Kinny, P. D., Barley, M. E., and Groves, D. I., 1998. Timing of gold mineralization in the Mt York district, Pilgangoora greenstone belt, and implications for the tectonic and metamorphic evolution of an area linking the western and eastern Pilbara craton. *Precamb. Res.* **88**, 249-265.

Nijman, W., de Bruijne, K. C. H., and Valkering, M. E., 1998a. Growth fault control of early Archaean cherts, barite mounds and chert-barite veins, North Pole Dome, eastern Pilbara, Western Australia. *Precamb. Res.* **88**, 25-52.

Nijman, W., Willigers, B. J. A., and Krikke, A., 1998b. Tensile and compressive growth structures: relationships between sedimentation, deformation and granite intrusion in the Archaean Coppin Gap greenstone belt, Eastern Pilbara, Western Australia. *Precamb. Res.* **88**, 83-108.

Padgham, W. A., 1985. *Observations and speculations on supracrustal successions in the Slave structural province*. Geological Association of Canada.

Percival, J. A. and Card, K. D., 1983. Archean Crust as Revealed in the Kapuskasing Uplift, Superior Province, Canada. *Geology* **11**, 323-326.

Rasmussen, B. and Buick, R., 1999. Redox state of the Archean atmosphere: evidence from detrital heavy minerals in ca. 3250-2750 Ma sandstones from the PIlbara Craton, Australia. *Geology* **27**, 115-118.

Riding, R., 1999. The term stromatolite: towards an essential definition. *Lethaia* **32**, 321-330.

Schopf, J. W. and Packer, B. M., 1987. Early Archean (3.3-billion to 3.5-billion-year-old) microfossils from Warrawoona Group, Australia. *Science* **237**, 70-73.

Schwerdner, W. M. and Lumbers, S., 1980. The Continental crust and its mineral deposits : the proceedings of a symposium held in honour of J. Tuzo Wilson held at Toronto, May, 1979, *Geological Association of Canada special paper ;*, [Waterloo, Ontario] Geological Association of Canada,.

Sethuram, K. and Moore, J. M., 1973. Petrology of Metavolcanic Rocks in Bishop-Corners-Donaldson-Area, Grenville-Province, Ontario. *Can. J. Earth Sci.* **10**, 589-614.

Spear, F. S., 1995. *Metamorphic phase equilibria and pressure-temperature-time paths*. Mineralogical Society of America, Washington, D.C.

Sylvester, P. J., 1994. Archean Granite Plutons. In: Condie, K. C. (Ed.), *Archean Crustal Evolution*. Elsevier, Amsterdam.

Tarney, J. and Windley, B. F., 1977. Chemistry, thermal gradients and evolution of the lower continental crust. *Journal of the Geological Society of London* **134**, 153-172.

Terabayashi, M., Masada, Y., and Ozawa, H., 2003. Archean ocean-floor metamorphism in the North Pole area, Pilbara Craton, Western Australia. *Precamb. Res.* **127**, 167-180.

Thurston, P. C., Ayres, L. D., Edwards, G. R., Gelinas, L., Ludden, J. N., and Verpaelst, P., 1985. Archean bimodal volcanism. In: Ayres, L. D., Thurston, P.

C., Card, K. D., and Weber, W. Eds.), *Evolution of Archean Supracrustal Sequences*. Geological Association of Canada.

Trendall, A. F., 1990. Pilbara Craton - Introduction, *Geology and mineral resources of Western Australia*. Western Australia Geological Survey, Perth.

Tyler, I. M., 1990. Inliers of granite-greenstone terrane., *Geology and Mineral Resources of Western Australia*. .Western Australia Geological Survey.

Ueno, Y., Yoshioka, H., Maruyama, S., and Isozaki, Y., 2004. Carbon isotopes and petrography of kerogens in similar to 3.5-Ga hydrothermal silica dikes in the North Pole area, Western Australia. *Geochim. Cosmochim. Acta* **68**, 573-589.

van Haaften, W. M. and White, S. H., 1998. Evidence for multiphase deformation in the Archean basal Warrawoona Group in the Marble Bar area, east Pilbara, Western Australia. *Precamb. Res.* **88**, 53-66.

van Kranendonk, M., 2006. Volcanic degassing, hydrothermal circulation and the flourishing of life on Earth: A review of the evidence from c. 3490-3240 Ma rocks of the Pilbara Supergroup, Pilbara Craton, Western Australia. *Earth Science Review* **74**, 197-240.

van Kranendonk, M. J., 1997. Results of field mapping, 1994-1996, in the North Shaw and Tambourah 1:100000 sheet areas, eastern Pilbara Craton, northwestern Australia. University of Newcastle/AGSO.

van Kranendonk, M. J., 2000. *Geology of the North Shaw 1:100 000 sheet: Western Australia Geological Survey*. Western Australia Geological Survey, Perth.

van Kranendonk, M. J. and Collins, W. J., 1998. Timing and tectonic significance of Late Archaean, sinistral strike-slip deformation in the Central Pilbara Structural Corridor, Pilbara Craton, Western Australia. *Precamb. Res.* **88**, 207-232.

van Kranendonk, M. J., Hickman, A. H., Smithies, R. H., and Nelson, D. R., 2002. Geology and tectonic evolution of the Archean North Pilbara Terrain, Pilbara Craton, Western Australia. *Economic Geology* **97**, 695-732.

Walter, M. R., 1980. Palaeobiology of Archaean stromatolites. In: Glover, J. E. and Groves, D. I. Eds.), *Extended Abstracts, Second International Archaean Symposium, Perth, Australia*.

Wingate, M. T. D., 1999. Ion microprobe dabbeleyite and zircon ages for late Archaean mafic dykes of the Pilbara Craton, Western Australia. *Aus. J. of Earth Sci.* **46**, 493-500.

Zegers, T. E., de Keijzer, M., Passchier, C. W., and White, S. H., 1998. The Mulgandinnah Shear Zone: an Archean crustal scale strike-slip zone, eastern Pilbara, Western Australia. *Precamb. Res.* **88**, 233-247.

Zegers, T. E., White, S. H., de Keijzer, M., and Dirks, P., 1996. Extensional structures during deposition of the 3460 Ma Warrawoona Group in the eastern Pilbara Craton, Western Australia. *Precamb. Res.* **80**, 89-105.

3. Mimicking Biological Carbon Isotope Signatures in Fe-C-O-H Systems

1. Introduction

The assumption of chemical equilibrium bounds much of our present theoretical understanding of natural processes. One area of research where the imposition of this assumption has particularly profound consequences, and towards which attention is drawn here, is that of carbon isotope systematics in ancient- and extraterrestrial- biosignature studies.

Of the stable isotope systems, fractionations of carbon are amongst the best understood. Despite this, the ability to differentiate between carbon of non-biological and biological origin is far from secure, as amply evidenced by ongoing controversies such as the ambiguous biogenicity of 3.8 Ga graphite in Isua, southwest Greenland (e.g. Mojzsis et al., 1996; Mojzsis and Harrison, 2000; Rosing, 1999; Schidlowski, 1988; Schidlowski, 1993; Schidlowski, 2001; van Zuilen et al., 2002; van Zuilen et al., 2003), the purported Fischer-Tropsch-type synthesis of 3.5 Ga kerogen in the Pilbara, northwest Australia (e.g. Brasier et al., 2002; Brasier et al., 2005; Schopf et al., 2002; Schopf and Packer, 1987; Ueno et al., 2004), and the origin of carbonaceous phases in meteorites (e.g. McKay et al., 1996; McSween, 1997; McSween and Harvey, 1998). Progress towards resolving these important problems affects our understanding of how, when, where and why life began.

At and above greenschist facies metamorphic conditions, carbonaceous material becomes increasingly graphitic in nature. Kerogen, loosely defined as ‘insoluble non-crystalline organic material’, is a common constituent of low-grade sedimentary rocks spanning the rock-record as far back as 3.5 Ga. Although disagreement exists in the application of the term ‘graphitic kerogen’ (e.g. Marshall et al., 2007), kerogen exhibits similar petrological behaviour (colour, reflectivity, etc.) to graphite. At temperatures considered in this study (T > 400 °C), kerogen transforms to graphite. Kerogen is therefore assumed to share the same isotopic and thermodynamic properties as

graphite. To avoid confusion, the term 'reduced carbon' is used to denote both kerogen and graphite.

This paper sets out to examine the limits on the derived isotopic signature of reduced carbon that can possibly result through both closed- and open- system equilibrium processes under geologically relevant conditions of P, T and fO_2. Calculations are performed within the thermodynamic space $1000 > P > 10000$ bar, $400 < T < 1200$ °C and $\log(fO_2^{QFM})-6 < \log(fO_2) < \log(fO_2^{QFM}) + 8$.

Because the simple molecules H_2O, O_2, H_2, CO, CO_2 and CH_4 represent the most abundant and geochemically reactive components of geological fluids (Horita, 2001), fluid thermodynamic behaviour can appropriately be described within the C-O-H system. Relevant geological processes are those that impart an isotopic fractionation on the order of that mediated by enzymatic metabolism, here considered as $\Delta\delta^{13}C \leq -15‰$ (Figure 1). Processes explicitly considered are isotopic re-equilibration with carbon in metasomatic C-O-H fluids and/or carbonate, precipitation of remobilized carbon, devolatilization of organic matter, and *de novo* carbon production resulting from decarbonation reactions of carbonates.

Under the assumption of equilibrium, the isotopic behaviour and evolution of carbon under the sway of these processes is largely quantifiable. To this end, a Modified Redlich-Kwong (MRK) equation of state built on recent thermodynamic fluid species data is coupled with recent advances in our understanding of equilibrium isotope fractionation to arrive at a versatile model for the isotopic behavior and evolution of reduced carbon interacting with C-O-H fluids in the system Fe-C-O-H. The component Fe is added to extend consideration to isotopic interaction with carbonate minerals. Because the potential for isotopic fractionation is limited at the higher decarbonation temperatures required for carbonates outside the Fe-C-O-H system (calcite, dolomite, ankerite, magnesite, rhodochrosite, etc.), restricting treatment to siderite alone is justified.

This approach uncovers the conditions under which geological equilibrium processes are capable of mimicking biological $\delta^{13}C$ fractionation. Based on these

results, the validity of the equilibrium assumption, with particular reference to Origin of Life studies, is discussed.

2. Model

2.1. The Modified Redlich-Kwong Equation of State

The modeling of fluids consisting of sub- or super- critical fluid mixtures of multiple components requires an understanding of how their chemical potentials respond to changes in state variables such as δP, δT and changes in composition, δx_i. Equations of state are equations that attempt to capture the relationship between these state variables, and thereby allow for the calculation of chemical potentials. The Redlich-Kwong equation of state (Redlich and Kwong, 1949), which incorporates parameters relevant to molecular dynamics of C-O-H fluids of interest here, takes the form:

$$P = \frac{RT}{V-b} - \frac{a}{(V^2+bV)(T)^{0.5}} \qquad (1)$$

Here, constant b accounts for repulsive forces by parameterizing molecular size and constant a accounts for intermolecular attraction. For fluids bearing molecules exhibiting a large dipole moment, such as H_2O and CO_2, a modified Redlich-Kwong ('MRK') equation was proposed (de Santis et al., 1974; Flowers, 1979; Holloway, 1984). The mixing parameters and thermodynamic constants used (after a compilation in Frost and Wood, 1995), are tabulated in Table 1 below. The MRK equation offers excellent correlation with experimental data, except at extreme metamorphic grades (P > 15000 bars, T > 1100 °C) not germane to the crustal environment (Belonoshko and Saxena, 1991; Frost and Wood, 1995; Kerrick and Jacobs, 1981).

Using this MRK equation of state, an expression for the fugacity co-efficient, ϕ_i, can be derived (Prausnitz, 1969):

$$\ln\phi_i = \ln\left(\frac{V}{V-b}\right) +$$

$$\frac{b_i}{V-b} - \frac{2\sum_{j=1}^{\hat{i}} a_{i,j}X_j}{bRT^{\frac{3}{2}}}\ln\left(\frac{V+b}{V}\right) + \frac{ab_i}{b^2RT^{\frac{3}{2}}}\left(\ln\left(\frac{V+b}{V}\right)\right) - \frac{b}{V+b}) - \ln\left(\frac{PV}{RT}\right) \qquad (2)$$

Here, $a = \sum_i \sum_j x_i x_j a_{i,j}$ and $b = \sum_i x_i b_i$. Values adopted are tabulated in Table 2.

2.2. The Reduced Carbon Saturation Surface

Phase-equilibrium experiments and other thermodynamic studies involving graphite have proven to be difficult to interpret, and have led to somewhat conflicting results. These problems stem largely from variability in the crystalline nature, ordering and thermodynamic properties of graphite (Koziol, 2004). Within the C-O-H system, the presence of reduced carbon is assumed to imply fluid saturation, with the activity of reduced carbon fixed at unity. On this reduced carbon saturation surface, pairs of C-O-H species' fugacities can now be related to one another through *P*- and *T*- dependent equilibrium constants, $k_{(i,,j)}$. In the case of reduced carbon equilibrating with the fluid components CO and CO_2, for instance:

$C + 0.5\ O_2 = CO$: $k(O_2,CO) = fCO/(fO_2)^{0.5}$

$$= \frac{\gamma CO \cdot pCO}{(\gamma O_2 \cdot pO_2)^{0.5}} = \frac{\gamma CO \cdot xCO \cdot P}{(\gamma O_2 \cdot xO_2 \cdot P)^{0.5}} \qquad (3a)$$

$C + O_2 = CO_2$: $k(O_2,CO_2) = fCO_2/fO_2$

$$= \frac{\gamma CO_2 \cdot pCO_2}{\gamma O_2 \cdot pO_2} = \frac{\gamma CO_2 \cdot xCO_2 \cdot P}{\gamma O_2 \cdot xO_2 \cdot P} \qquad (3b)$$

Similar expressions can be constructed for the other C-O-H species. The assumption of fluid ideality ($\gamma_i = x_i$), together with the condition $\sum x_i = 1$, now allows for the capture of x_i from the roots of quadratic equations (e.g. Ohmoto and Kerrick, 1977) or thermodynamic data tables (e.g. Chase, 1998). This approximate fluid composition is

used to seed an iterative re-calculation of the fugacity coefficients (Eqn. 2) and equilibria (such as Eqn. 3a,b), which converges upon the final, non-ideal fluid composition (e.g. Hall and Bodnar, 1990). The stability field of reduced carbon, together with the composition of the equilibrating fluid, is hereby laid bare in $P - T$ space by fixing any single compositional variable x_j.

2.3. Oxygen Fugacity and Reduced Carbon Stability

In addition to pressure and temperature, the geological environment often lends further constraints on the composition of C-O-H fluids by virtue of the mineral assemblage with which the fluid equilibrates. To this end, the oxygen fugacity, fO_2, provides a useful proxy. Oxygen fugacities in geological systems typically lie within +6 log units and -8 log units of the FMQ buffer, which inhabits a median position (Figure 2) amongst the commonly used buffers in $fO_2 - T$ space (Frost, 1991). The range $[\log(fO_2^{QFM}) - 6] < \log(fO_2) < [\log(fO_2^{QFM}) + 8]$ spans the buffering capabilities of a broad range of geological environments, and is adopted in this study.

Fluids outside the compositional stability field of reduced carbon (Figure 2) are prohibitively oxidizing or reducing. Here, reduced carbon is unstable with respect to CO/CO_2 or CH_4, respectively. In practice, because of equilibria with H_2, reduced carbon remains stable with respect to CH_4 under geologically relevant fO_2 conditions. The degree of dissociation into CO and CO_2 is likewise small under a broad range of conditions. This is because the conversion of all available reduced carbon to $CO\text{-}CO_2$ commonly requires prohibitively high activities of O_2 at sub-solidus temperatures. From a thermodynamic perspective, the abundance of reduced carbon - in diverse rock types – is hence unsurprising.

The graphite stability field expands with pressure. With increasing temperature, reduced carbon-fluid equilibria are increasingly in favour of the fluid phase (‘degassing’), causing amounts of reduced carbon to decrease and the stability field to shrink with respect to solid-state oxygen buffers. The continued ability to provide reduced carbon buffering capacity depends on the amount of carbon, $\sum C$, present in the

system. Evidently, reduced carbon is unstable under highly oxidized conditions, such as provided by assemblages in some haematitic (≈ 'MH' buffer) banded iron-formations ('BIFs'). This may account for the paucity of organic matter in these and other oxidized sediments of controversial biogenicity.

3. Thermodynamic Behaviour of C-O-H Fluids

An overview of the behaviour of C-O-H fluids and the stability of reduced carbon, which are well understood (Connolly, 1995; Holloway, 1984; Huizenga, 2001), is called for. The ternary C-O-H diagram (Figure 3) lends itself well to this purpose.

3.1. Binary and Subcritical Behaviour

As pointed out by Holloway (1984), in the presence of reduced carbon at pressures above $P \approx 300$ bars and temperatures around $T \approx 400$ °C, supercritical C-O-H fluids will consist of either CH_4-H_2-H_2O mixtures or CO_2-CO-H_2O mixtures. Schematically, this situation arises when the reduced carbon saturation isotherm intersects with the CH_4-H_2O or CO_2-H_2O binary, respectively (see T = 400 °C isotherm, Figure 3). At these lower temperatures, fluid equilibria dictate that either H_2/CH_4 or CO/CO_2 ratios are exceedingly low. Any isotopes of carbon in the fluid phase interacting with reduced carbon thus effectively become restricted to a single species, either CH_4 or CO_2. Further consideration of C-O-H fluid behaviour below the binary intersection temperature is relevant here only in so far as it affects the relative amount of reduced carbon precipitating in the system.

Below $T \approx$ 400 °C, CH_4-H_2O fluids gradually undergo unmixing into two separate subcritical CH_4-rich and H_2O-rich phases (Price, 1979). Below ~275 °C, CO_2-H_2O fluids similarly undergo unmixing, into CO_2-rich- and H_2O-rich- phases (Takenouchi and Kennedy, 1964). Unmixed phases become increasingly pure with lower temperatures. Reduced carbon precipitation will still be largely controlled through reduced carbon-CH_4-H_2O-O_2 or reduced carbon-CO_2-H_2O-O_2 equilibria, or an externally imposed oxygen buffer, as the case may be.

Although fluid unmixing may exert some effect on the isotopic equilibrium fractionation with reduced carbon, such considerations become secondary in light of the increasing tendency towards isotopic disequilibrium at these lower temperatures.

3.2. General Supercritical Behaviour

The coincidence of the C-O-H fluid composition with the reduced carbon saturation isotherm described above is a special case. More generally, the molar fractions of CO_2, H_2O, O_2, CO, H_2 and CH_4 are variably fixed in the fluid, depending on constraints placed on the system due to the geological environment. In the case of a single supercritical fluid, three different scenarios can be envisaged under specified *P*, *T* conditions: (i) a fluid whose composition falls outside the stability field of reduced carbon, and is not externally buffered – in which case the relative proportions of species are set by the fluid equilibria themselves; (ii) a fluid whose composition falls outside the stability field of reduced carbon, but is externally buffered; and (iii) a buffered fluid whose composition falls within the stability field of reduced carbon.

3.2.1. Unbuffered Supercritical Fluids

In a system consisting of a single unbuffered supercritical C-O-H fluid, only one phase is present and the system consequently enjoys four degrees of freedom. Hence, in addition to *P* and *T*, the molar proportions of any two of the fluid species must be specified to fix all the others. Consequently, constraints on the isotopic behaviour exhibited by carbon within these fluids can only be sought in their source (e.g. ultramafic versus acidic volcanism). This scenario, though rare, may arise during the passage of a hydrothermal fluid through 'oxidatively-unreactive' lithologies, such as cherts (cryptocrystalline SiO_2). In practice, the presence of small amounts of metal oxides and/or sulfides (particularly combinations of pyrrhotite, pyrite, magnetite and haematite) sets constraints on fO_2 in all but the purest of cases.

In accordance with the controls on reduced carbon stability described above, reduced carbon precipitation may ensue through increased pressures, decreased temperatures, or the external imposition of more reducing conditions.

3.2.2. Buffered Supercritical Fluids, Reduced Carbon Unstable

fO_2-buffers fix fO_2 at a specified P, T. The imposition of such a buffer, expressed in terms of the fugacity of any fluid component in the C-O-H system, restricts the system's degrees of freedom to three. At a specified P, T and fO_2 the system can now be completely described through specification of any remaining compositional variable, such as xH_2O or xCO_2.

3.2.3. Buffered Supercritical Fluids, Reduced Carbon Stable

The behaviour of supercritical fluids within the stability field of reduced carbon naturally merits special consideration. The presence of reduced carbon in the presence of an external buffer adds a strong constraint to the system, reducing its degrees of freedom to two. At a specified P, T and fO_2, the system is invariant, allowing exact determination of the isotopic behaviour of reduced carbon. Figure 4 illustrates calculated 'carbon-saturated' fluid behaviour as a function of temperature at P = 10000 bar.

4. Behaviour of Carbon in Fe-C-O-H System

4.1. Decarbonation of Carbonate

Carbonate minerals whose composition falls within the solid solution space defined by the end-members calcite ($CaCO_3$), dolomite ($CaMg(CO_3)_2$), and siderite ($FeCO_3$) have been common rock-forming minerals throughout geological time. Less common carbonates include magnesite ($MgCO_3$), rhodochrosite ($MnCO_3$) and smithsonite ($ZnCO_3$). The thermal decomposition –or 'decarbonation'– of carbonates can purportedly lead to the precipitation of reduced carbon (Sharp et al., 2003; van Zuilen et al., 2003).

Using a continuous-flow technique within a 3 bar He pressure environment, Sharp et al. (2003) reported the commencement of decarbonation at 720, 600 and 450 ºC for calcite, dolomite and siderite respectively. Higher pressures can be expected to require higher decomposition temperatures, as univariant decarbonation curves have a positive slope in *P-, T-* space (e.g. Kerrick, 1974). Because the potential for isotopic fractionation is limited at the higher decarbonation temperatures required for carbonates outside the Fe-C-O-H system, only the decarbonation of siderite need be considered here.

The decarbonation of siderite has been studied by numerous workers (French, 1971; French and Eugster, 1965; French and Rosenberg, 1965; Frost, 1979; Goldsmith et al., 1962; McCollom, 2003; McCollom, 2004; Mel'nik, 1982; Rosenberg, 1967; Sharp et al., 2003; Weidner, 1968; Weidner, 1972; Yui, 1966). Within the stability field of reduced carbon, the reaction proceeds to form iron oxide:

$$6\ FeCO_3 = 2\ Fe_3O_4 + 2\ x\ CO + 4\ y\ CO_2 + (6 - 2\ x - 4\ y)\ C + (5 - x - 4\ y)\ O_2 \qquad (4)$$

Here, the molar coefficients x and y are determined through reduced carbon-vapor equilibration in the C-O system, $C + O_2 = CO_2$ and $C + 0.5\ O_2 = CO$.

In the system reduced carbon-C-O, all compositional fluid variables (xCO_2, xCO and xO_2) are fixed at a specified *P, T*. We can exploit this fact to determine the amount of reduced carbon precipitated as a function of *P, T* by solving for *x, y* in reaction (04). Above the decarbonation temperature, ~1 mole of reduced carbon and ~5 moles of CO_2 are generated for every 6 moles of siderite decarbonated (Figure 5). With increasing temperature, the CO/CO_2 ratio of the evolved fluid increases, while the amount of reduced carbon precipitated decreases up to the limit of its stability.

The foregoing assumes that fO_2 is not externally buffered above the stability of graphite. If this were the case, the relative amounts of CO_2, CO and O_2 produced would now be determined by the equilibrium $CO + 0.5\ O_2 = CO_2$. The assemblage siderite – magnetite - C-O-fluid (or, at $fO_2 > fO_2^{MH}$, the assemblage siderite - haematite - C-O-fluid) is divariant.

5. Isotopic Behaviour of Carbon in Fe-C-O-H Systems

5.1. Parameterizing the Isotopic Behavior of Individual Compounds

The β-factor, or 'reduced isotopic partition function ratio', is a useful parameter when studying the effect of metamorphism or metasomatism on isotopic exchange. β-factors parameterize the isotopic behavior of individual substances, allowing for the calculation of the overall equilibrium fractionation effect α in reactions involving isotopic interaction between two or more substances. Explicitly, the isotope fractionation factor $\alpha_{A\text{-}B}$ between two substances A and B undergoing equilibrium exchange is equal to the ratio of their individual β-factors β_A and β_B:

$$\alpha_{A-B} = \frac{\beta_A}{\beta_B} \qquad \text{or} \qquad \ln \alpha_{A-B} = \ln \beta_A - \ln \beta_B \tag{5}$$

The alpha factor α allows determination of the isotopic ratio of two species. The isotopic ratio for a species A, R_A, can also be expressed in the customary δ_A notation:

$$\alpha_{A-B} = \frac{R_A}{R_B} \qquad R_A = \frac{(\frac{^{13}C}{^{12}C})_A}{(\frac{^{13}C}{^{12}C})_{std}} \qquad \delta^{13}C_A = (R_A - 1) \cdot 1000 \tag{6}$$

Here, subscript 'std' refers to the known isotopic ratio in a laboratory standard, such Peedee Belemnite ('PDB'). Equations (05) and (06) are applicable to all carbon species in the system Fe-C-O-H under consideration. The β-factors for reduced carbon, CO_2, CO, CH_4 and siderite are compared in Figure 6. The distinctly higher β-factors exhibited by CO_2 result in its isotopic enrichment relative to CH_4 and CO.

The effect of pressure on isotopic fractionation is usually taken to be negligible (Chacko et al., 2001), as studies at geologically relevant pressures have consistently revealed negligible (<0.1‰) pressure-induced corrections (e.g. Clayton et al., 1975; Hamann et al., 1984; Joy and Libby, 1960). In the case of graphite, however, Kharlashina and Polyakov (1992) noted that β-values exhibit an anomalously large pressure-dependence, on the order of 1‰ over 10 kbar. From a kinetic perspective, it is well known that elevated pressures lead to enhanced isotopic exchange rates (Clayton

et al., 1975; Matsuhisa et al., 1979; Matthews et al., 1983a; Matthews et al., 1983b; Matthews et al., 1983c).

5.2. Isotopic Equilibration of Reduced Carbon with C-O-H fluids

In the presence of C-O-H fluids, reduced carbon isotopically interacts with fluid-phase CO_2, CO and CH_4. Under the assumptions specified above, coupling of the thermodynamic- (xCO_2, xCO and xCH_4) and isotopic- (βCO_2, βCO, βCH_4 and $\beta redC$) behaviour allows calculation of $\delta^{13}C_C$ as a function of P, T and fO_2:

$$\alpha_{C\text{-}fluid} = (\beta CO_2/\beta redC)\cdot xCO_2 + (\beta CO/\beta redC)\cdot xCO + (\beta CH_4/\beta redC)\cdot xCH_4 \quad (7)$$

$$R_{redCs} = \alpha_{C\text{-}fluid} \cdot R_{fluid}$$

$$\delta^{13}C_{redC} = (R_{redC} - 1)\cdot 1000 \quad (8)$$

Here, R_{fluid} and R_C refer to the isotopic ratios in the bulk fluid and reduced carbon, respectively. Figure 7(a-c) shows the isotopic fractionation of reduced carbon equilibrating with C-O-H fluids in fO_2 - T space at three different pressures.

5.3. Isotopic Equilibration in Carbonate-Reduced Carbon Systems

The carbonate-reduced carbon system has received considerable attention because of its potential use as a geothermometer. Theoretical (Bottinga, 1969; Chacko et al., 1991; Golyshev et al., 1981; Polyakov and Kharlashina, 1995a), empirical (Dunn and Valley, 1992; Kitchen and Valley, 1995; Morikiyo, 1984; Valley and Oneil, 1981; Wada and Suzuki, 1983) and laboratory (Scheele and Hoefs, 1992) methods have been employed to study the temperature-dependence of isotope equilibrium fractionation within the calcite-graphite system (Figure 8a, b). The temperature-dependence of the dolomite β-factor (Golyshev et al., 1981; Wada and Suzuki, 1983) and siderite β-factor (Carothers et al., 1988; Golyshev et al., 1981; Jimenez-Lopez and Romanek, 2004; Zhang et al., 2001) have also been investigated. Carbonate β-factors roughly increase with decreasing cation radius.

Significant divergence exists between studies focusing on lower temperatures ($270 < T < 650$ °C) and those addressing higher temperatures ($T > 650$ °C). Theoretical calculations are consistent with the data at high temperatures, suggesting that the deviation of low-temperature natural sample data from theory results from incomplete equilibration and kinetic effects at depressed temperatures.

Isotopic carbonate-reduced carbon equilibria are also important to geobiologists studying metamorphosed rocks (Figure 9). Isotope re-equilibration between reduced carbon and carbonate during metamorphism is commonly invoked, for example, to explain the $\delta^{13}C$ distribution in the 3.8 Ga Isua Supracrustal Belt and Akilia Gneiss of southwest Greenland (Mojzsis et al., 1996; Mojzsis and Harrison, 2000; Schidlowski, 1988; Schidlowski, 2001; Schidlowski et al., 1979).

In a simple closed system, the bulk $\delta^{13}C$ is time-invariant, and carbon isotope systematics can easily be constrained using the mass balance equations:

$$\delta^{13}C_{bulk} = \delta^{13}C^{i}_{redC}\, X_{redC} + \delta^{13}C^{i}_{carb}\, X_{carb}$$
$$= \delta^{13}C_{bulk} = \delta^{13}C^{f}_{redC}\, X_{redC} + \delta^{13}C^{f}_{carb}\, X_{carb} \qquad (9)$$

Here, the superscripts *i* and *f* refer to the initial and final, or pre- and post- metamorphic states respectively; the subscripts '*bulk'*, *'C'* and '*carb'* refer to the combined, reduced carbon and carbonate components, respectively; X is the molar fraction of a given component (capitalized to distinguish it from fluid compositions discussed previously) such that $X_{redC} + X_{carb} = 1$. It should be noted that for realistic geological systems, the molar fractions X_{redC} and X_{carb} are unlikely to be time-invariant due to processes such as the interaction with graphitic fluids and CO_2 degassing of carbonates. These complications are considered in Section 5.5 below.

Equations (09) can be recast into a form incorporating $\Delta_{carb\text{-}C}\,(T)$, the isotopic fractionation factor between carbonate and organic carbon:

$$\delta^{13}C_{bulk} = \delta^{13}C^{f}_{redC} + \Delta_{carb\text{-}C}\, R_x\, (1 + R_x)^{-1} \qquad (10)$$

Here, the important variable R_x is the molar ratio X_{carb} / X_{redC}. The isotopic behaviour in a system governed by equation (10) is illustrated in Figure 10.

5.5. Carbon Isotopic Fractionation During Decarbonation

The process of decarbonation can ostensibly produce graphite *de novo* at temperatures as low as $T \approx 450$ ºC. Good experimental data on the isotopic fractionation during the decarbonation of different carbonate minerals is scarce. In one study, the measured carbon isotope fractionation between calcite or dolomite and evolved CO_2 (from which the isotopic evolution of reduced carbon may be calculated) was negligible, whereas the $\delta^{13}C$ of evolved CO_2 during laboratory decarbonation of siderite increased as a function of reaction process from an initial + 1 ‰ to a maximum of +5 ‰ (Sharp et al., 2003). These findings agree with calculations of carbonate-reduced carbon-CO_2 equilibration (Figure 11). In the absence of more or contradictory experimental data, therefore, equilibration calculations will be used to examine the isotopic evolution of reduced carbon in systems undergoing carbonate decarbonation.

5.5.1. Closed System Decarbonation

During complete closed system decarbonation, the isotopic evolution of reduced carbon will equilibrate with evolved CO_2 and CO:

$$\delta^{13}C_{FeCO_3} = \delta^{13}C_{CO_2} \cdot xCO_2 + \delta^{13}C_{CO} \cdot xCO + \delta^{13}C_{redC} \cdot xredC \tag{11}$$

$$\alpha_{C\text{-}fluid} = (\beta CO_2/\beta redC) \cdot xCO_2 + (\beta CO/\beta redC) \cdot xCO$$

$$\delta^{13}C_{fluid} = \frac{\delta^{13}C_{CO_2} \cdot xCO_2 + \delta^{13}C_{CO} \cdot xCO}{xCO_2 + xCO} \tag{12}$$

$$R_{CO_2} = R_{redC} \frac{\beta_{CO_2}}{\beta_{redC}} \quad \text{and} \quad R_{CO} = R_{redC} \frac{\beta_{CO}}{\beta_{redC}} \tag{13}$$

$$R_{redC} = \frac{R_{FeCO_3} \cdot \beta_{redC} \cdot x_{redC}}{\beta_{redC} \cdot x_{redC} + \beta_{CO_2} \cdot x_{CO_2} + \beta_{CO} \cdot x_{CO}} \tag{14}$$

Reduced carbon produced through this mechanism will be isotopically depleted relative to precursor carbonate by between 2 and ~8 ‰, depending mostly on the

temperature of peak metamorphism (Figure 12). Severely depleted (< -15 ‰ relative to precursor carbonate) reduced carbon cannot be produced through this mechanism.

5.5.2. Open System Decarbonation

Both organic matter and carbonate may undergo open-system devolatilization. Unlike closed-system isotopic equilibration, the isotopic signature of the remnant carbon reservoir will evolve over time. Open-system devolatilization reactions follow a Rayleigh distillation curve:

$$\delta^{13}C^{final} = (\delta^{13}C^{initial} + 1000) \cdot f^{(\alpha - 1)} - 1000 \quad (15)$$

Here, f refers to the fraction of carbon remaining following devolatilization, $0 \leq f \leq 1$; and α refers to the fractionation factor between the released volatiles and the devolatilizing carbon pool.

For the open-system devolatilization of carbonate, the isotopic signature of carbonate itself evolves with time:

$$\delta^{13}C_{carb} = (\delta^{13}C^{i}_{carb} + 1000) \cdot f^{(\alpha - 1)} - 1000 \quad (16)$$

It is assumed that the precipitated reduced carbon equilibrates isotopically with remnant carbonate, such that $R_{redC} = R_{carb} \frac{\beta_{redC}}{\beta_{carb}}$. This seems a reasonable assumption, given that thermodynamics constrain decarbonation temperatures above ~450 °C where solid-solid isotope exchange is unlikely to suffer from severe disequilibrium effects. The real difficulty, rather, lies in determining the fractionation factor α that governs the isotopic composition of the released volatiles.

In the laboratory, graphite is produced even if a constant He atmosphere is maintained. The devolved fluid is oversaturated in CO with respect to CO_2 and reduced carbon, causing precipitation of the latter. This suggests that, even under these extremely dynamic artificial open-system conditions, thermodynamic equilibration is partly occurring. Figure 13(a-c) shows the results of calculations on the final isotopic

signature of *de novo* graphite assuming perfect isotopic and thermodynamic equilibrium with devolved CO-CO_2 fluid.

As under closed-system conditions, the production of non-biological reduced carbon with a severely depleted isotopic signature is predicted to occur only at low pressures ($P < 1000$ bar).

In the case of the devolatilization of abiotic hydrocarbon, $C_nH_mO_l$, both the geological environment and the hydrocarbon composition affect the relative amounts of CO_2, CO and CH_4 in the evolved gas. Unfortunately, little is known about the individual isotopic behaviour of more complex hydrocarbons (e.g. Chung et al., 1988). In consequence, we assume that the isotopic properties of graphite hold for kerogen. The isotopic evolution of a devolatilizing organic carbon reservoir governed by the form of equation (18) is illustrated in Figure 14.

At high CO_2/CH_4 ratios, and in the absence of carbonate, this mechanism can theoretically lead to reduced carbon as fractionated as $\Delta\delta^{13}C_{redC}$ = -40 ‰ relative to its pre-devolatilization signature.

6. Discussion

6.1. Summary

Under the explicit assumption of complete isotopic equilibrium and C-O-H fluid behaviour dictated by Modified-Redlich-Kwong (MRK) equation of state, a detailed investigation of the non-biological production of isotopically depleted reduced carbon from an isotopically heavy precursor reservoir of magmatic carbon and/or carbonate carbon in the system Fe-C-O-H was conducted. Starting with a C-O-H fluid reservoir isotopically representative of a magmatic origin ($\delta^{13}C_{fluid} \approx$ -5 ‰), the production of reduced carbon bearing a signature within the range of biological processes ($\delta^{13}C_{final} <$ -15 ‰) is restricted to very reducing conditions: over 8 log units below fO_2^{QFM} at geologically relevant pressures. With increasing temperature, the amount of carbon precipitated decreases but endures little isotopic shift.

The production of reduced carbon that accompanies the decarbonation of common rock-forming carbonates (dolomite, calcite and siderite) is frequently put forward as a source for isotopically reduced carbon. The nature of the carbonate cation has a significant effect on its isotopic behaviour, particularly at low temperatures. However, with the exception of siderite, decarbonation occurs at temperatures prohibitively high for significant isotopic fractionation. The decarbonation of an isotopically heavy carbon reservoir representative of marine siderite ($\delta^{13}C_{carb} \approx 0$ ‰) within a closed equilibrating system is not conducive to the production of isotopically light reduced carbon ($\delta^{13}C_{final} < -15$ ‰). It is worth noting that the geological literature is suspiciously barren of petrological evidence for this mechanism happening outside the laboratory. This author has never encountered evidence for carbonate-derived graphite in metacarbonates.

Replacing the constraint of closed-system equilibrium for one of open-system Rayleigh-style degassing, but conserving the assumption of equilibrium isotopic exchange between carbonate and reduced carbon, does little to improve the potential for isotopically light reduced carbon production under geologically relevant conditions of P, T and fO_2. In fact, equilibrium considerations require that the continued decarbonation of carbonate isotopically enriches, rather than depletes, the reduced carbon produced.

In the absence of carbonate, and at temperatures below 500 °C, open-system Rayleigh-style degassing of graphite-like hydrocarbon material can theoretically give rise to carbon with 'life-like' isotope signatures if high CO_2/CH_4 ratios ($R > 1$) predominate in the devolved gas. However, large fractions ($f > 0.5$ at $T = 300$ °C and $f > 0.9$ at $T = 500$ °C) of precursor hydrocarbon material must be devolatilized for this to occur. Thus, large quantities of pre-existing concentrated non-biological hydrocarbon would be required.

6.2. Conclusion

The production of severely isotopically depleted ($\Delta\delta^{13}C \leq$ -15‰) reduced carbon from an unfractionated carbon pool at isotopic and thermodynamic equilibrium is challenging under conditions relevant to geological systems. Only under exceptional circumstances can commonly invoked processes, such as graphite precipitation from C-O-H fluids and the decarbonation of carbonates, give rise to carbon fractionation incurred during enzymatically-mediated metabolic processes.

The non-biological production of isotopically depleted carbon capable of mimicking a biological isotopic fingerprint, therefore, necessitates conditions of severe disequilibrium - reminiscent of biological systems themselves (e.g. Shock, 1992). For carbon isotopes to acquire their intended utility in biosignature studies, therefore, requires that the operation of disequilibrium processes involving carbonic fluids be incontrovertibly refuted. Unless this precondition is met, isotopically depleted reduced carbon remains, by itself, an unsuitable indicator of primitive biology in highly metamorphosed rocks.

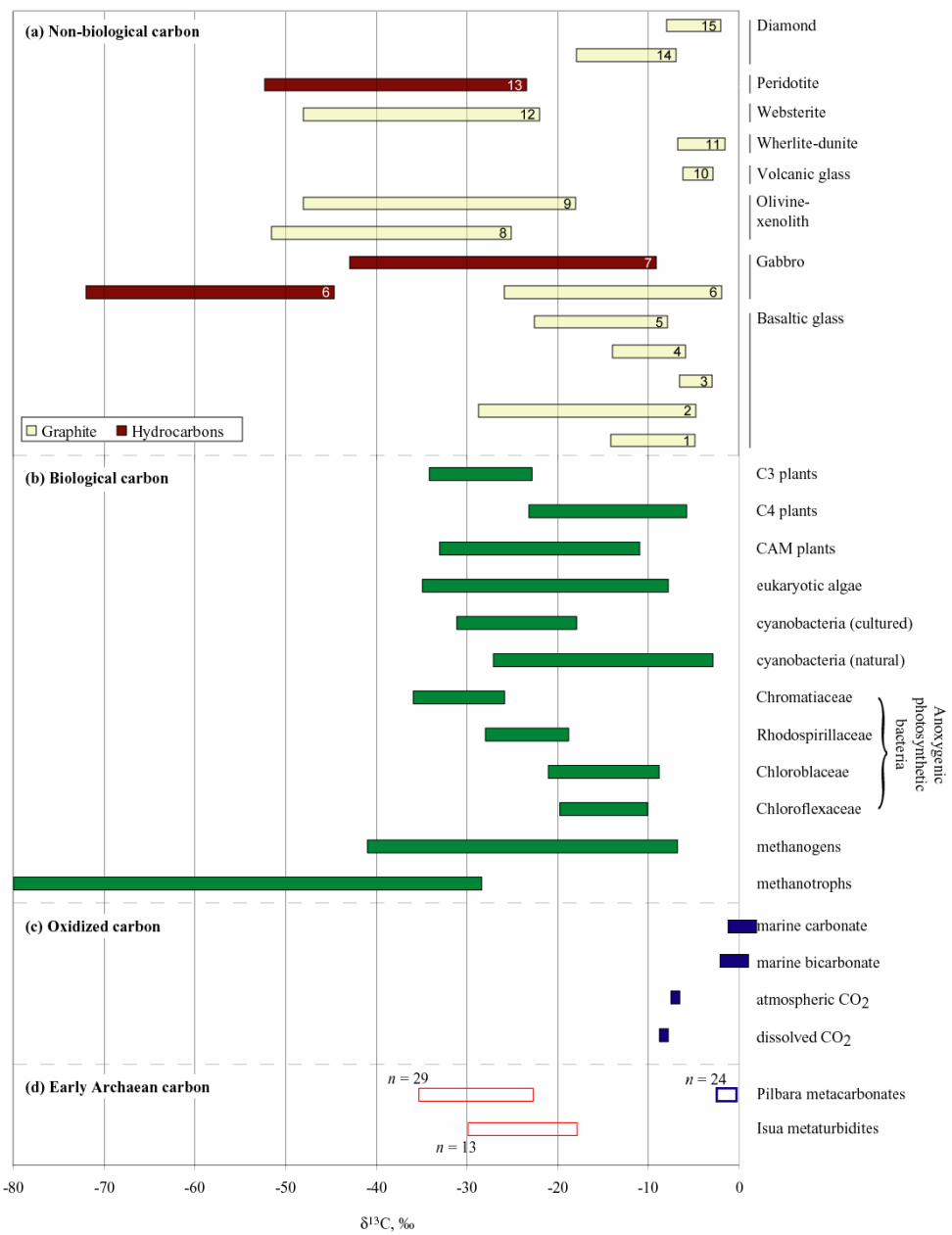

Figure 1: Isotopic fractionation of carbon. (a): Graphite and hydrocarbons hosted in a variety of igenous rocks. Reference numbers in bars: 1. Blank et al. (1993); 2 & 4. Des Marais and Moore (1984); 3. Javoy and Pineau (1991); 5. Mattey et al. (1984); 6 & 7. Kelley and Fruh-Green (1999); 8 & 9. Hoefs (1975); 10. Gerlach and Taylor (1990); 11 & 12. Pineau and Mathez (1990); 13. Sugisaki and Mimura (1994); 14. Swart et al. (1983); 15. Deines (1980). (b): Biological carbon (after Schidlowski, 2001). (c): Atmospheric and marine dissolved carbon. (d): Reduced and carbonate carbon from >3.7 Ga lower-amphibolite-facies metaturbidites from the Isua Supracrustal Belt, Greenland and >3.52 Ga upper-greenschist-facies metasedimentary carbonate from the Pilbara Craton, Australia (Chapter 5, 6, 8).

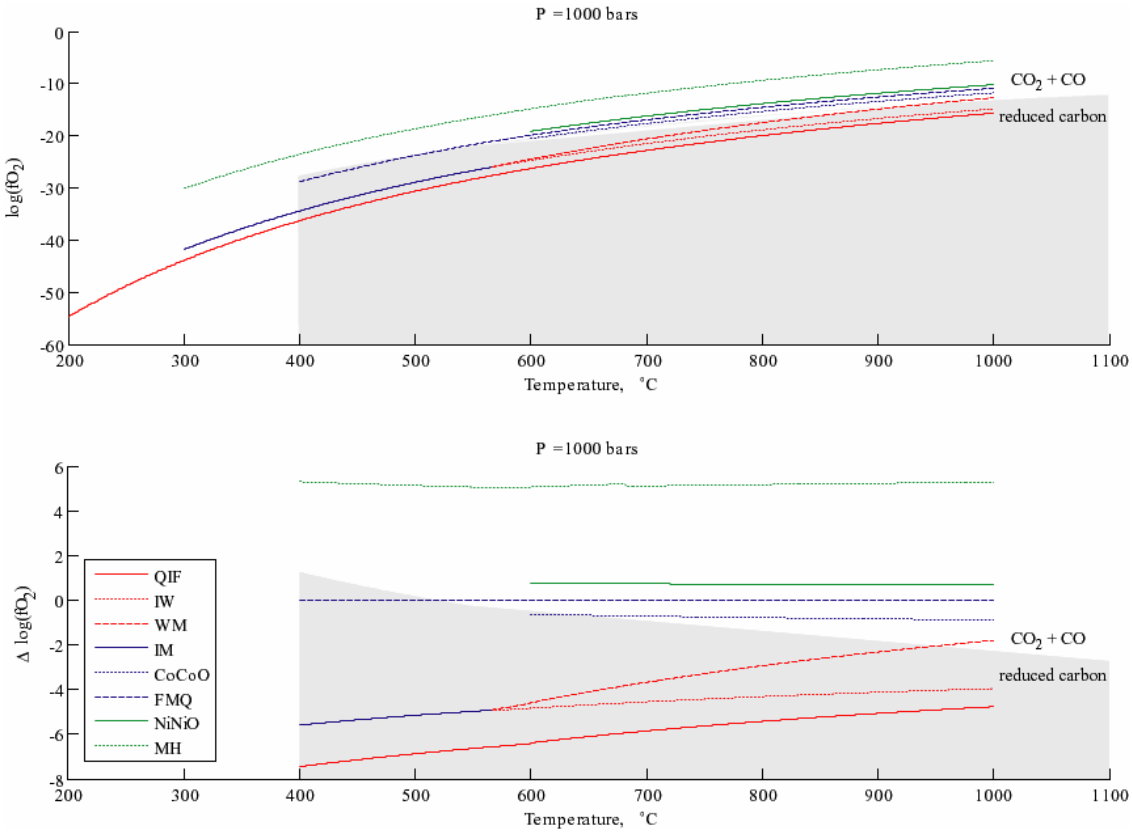

Figure 2: Oxygen buffers and graphite stability plotted in $fO_2 - T$ space. The graphite stability field is shown in grey. (a) A range of common oxygen buffers at P= 1000 bars. (b) Oxygen buffers, at P= 1000 bars, plotted in $\Delta fO_2 - T$ space relative to the FMQ buffer: $\Delta\ log(fO_2) = log(fO_2) - log(fO_2^{FMQ})$. All buffers lie within 6 log units above and 8 log units below the FMQ buffer, corresponding to the oxygen fugacity range considered in this study. Buffer abbreviations used: QIF: Fe2SiO4 = 2Fe + SiO2 + O_2; IW: 2 FexO = 2x Fe + O_2; WM: 2x/(4x-3) Fe3O4 = 6/(4x-3) FexO + O_2; CoCoO: 2 CoO = 2 Co + O_2; FMQ: 2 Fe3O4 + 3 SiO2 = 3Fe2SiO4 + O_2; NiNiO: 2 NiO = 2 Ni + O_2; MH: 6 Fe2O3 = 4 Fe3O4 + O_2. For the QIF and FMQ buffers, the alpha-beta quartz phase transition at T (°C) $\approx 573 + 0.025\ P$ (bar) was taken into account.

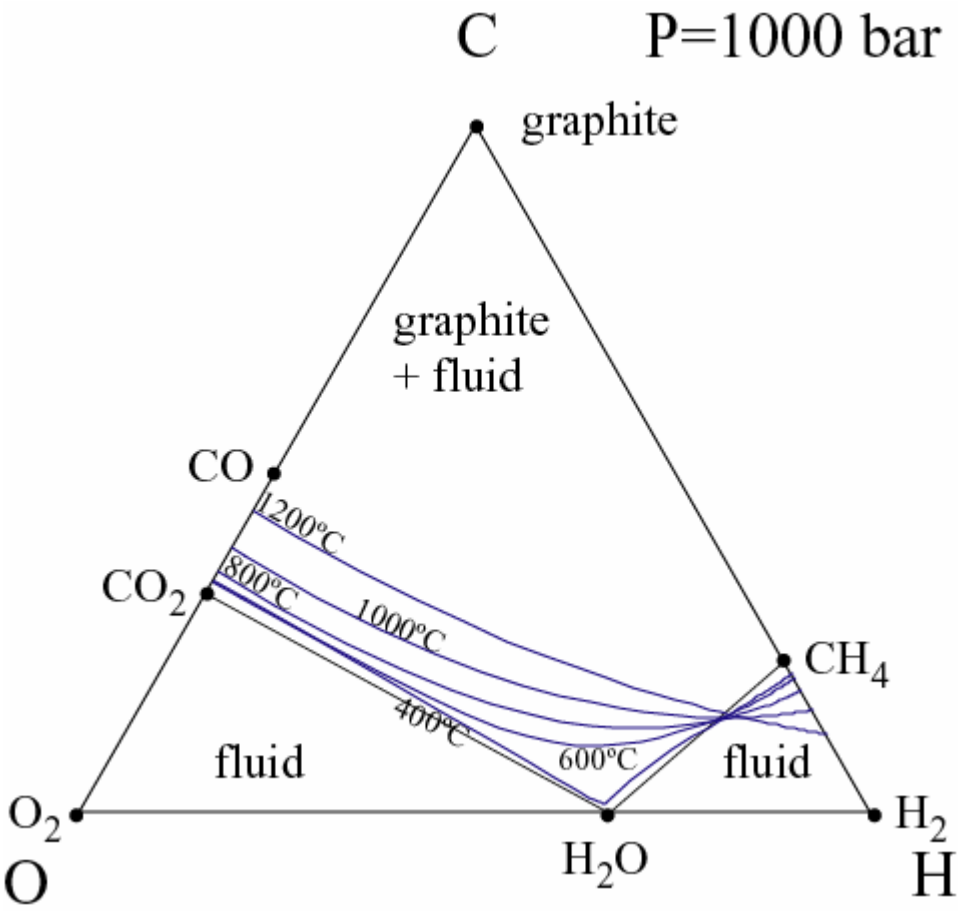

Figure 3: The ternary C-O-H diagram, showing calculated graphite saturation isotherms at T = 400, 600, 800, 1000 and 1200 °C. Note the near-overlap of the isotherms with the CO_2-H_2O and H_2O-CH_4 binary joins at T = 400 °C, and the continued dominance of CO_2 and CH_4 over CO and H_2, respectively, even at elevated temperatures.

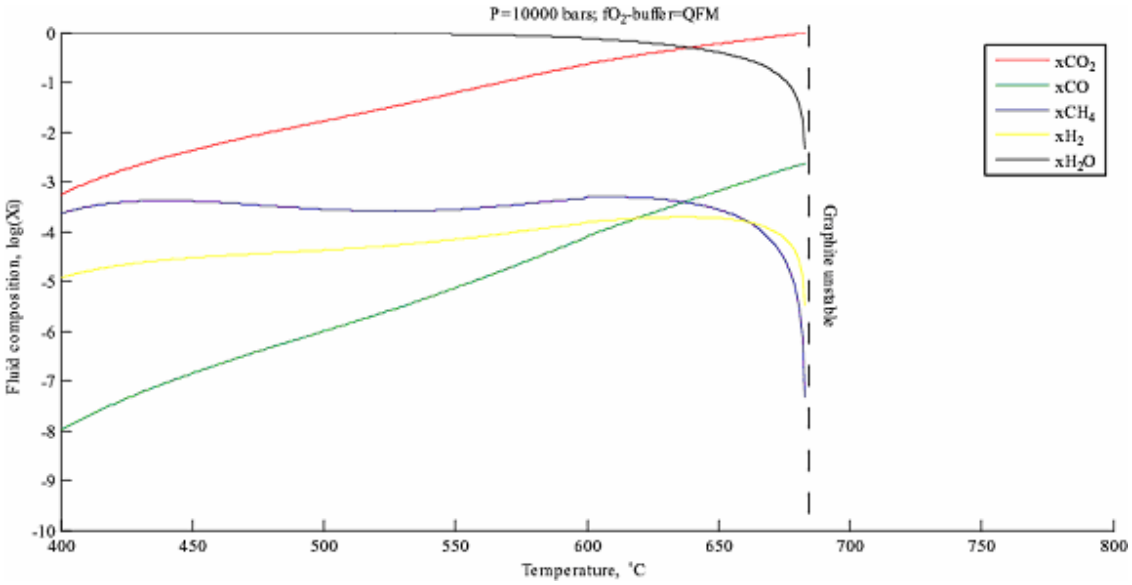

Figure 4: Fugacities of CO_2, H_2O, O_2, CO, H_2 and CH_4 as a function of *P*, *T* and fO_2 in a supercritical graphite-saturated C-O-H fluid.

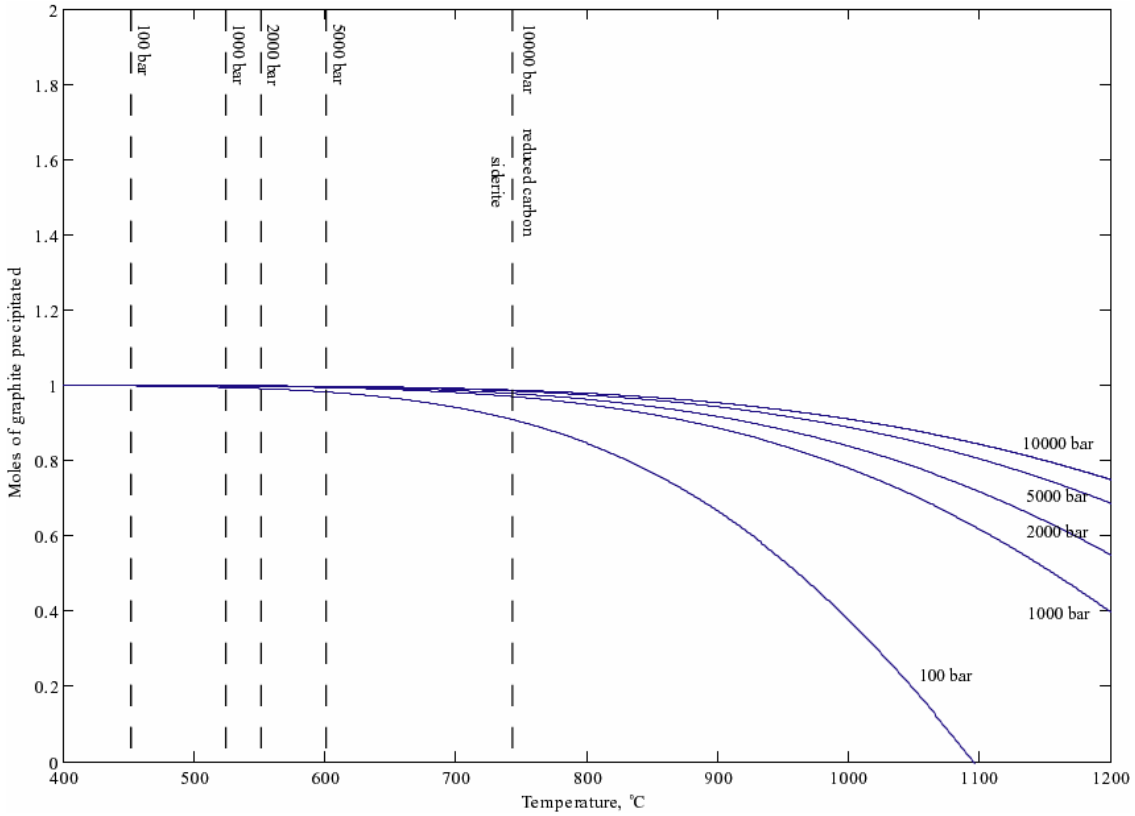

Figure 5: Number of moles of graphite precipitated for every 6 moles of siderite decarbonated as a function of temperature at different pressures, as per reaction (4). Dashed lines indicate stability of siderite at specified pressures. Closed-system equilibrium conditions are assumed.

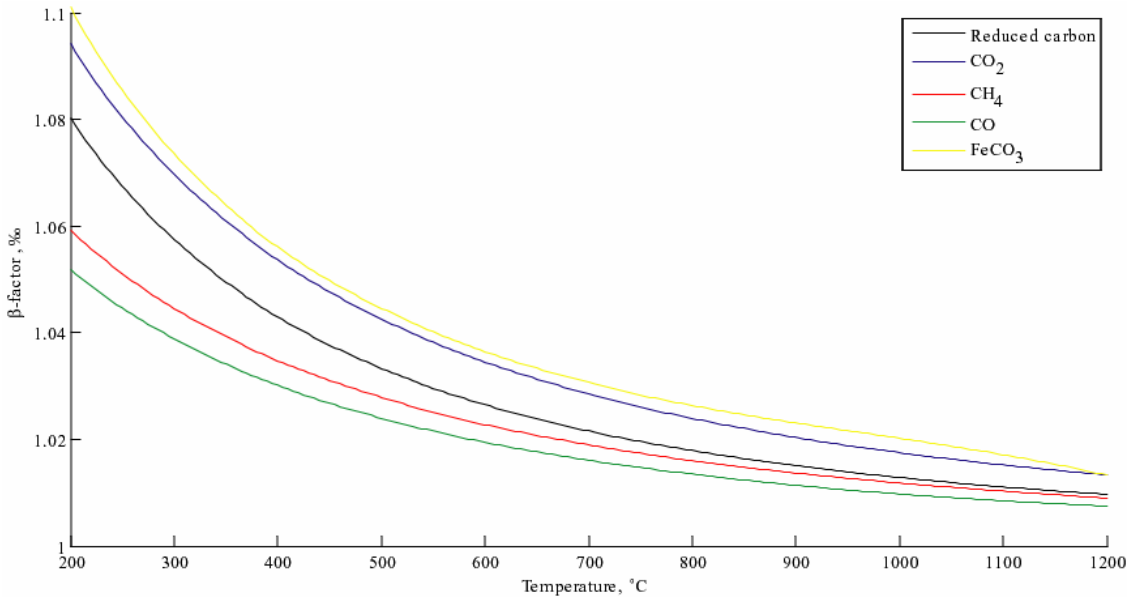

Figure 6: Theoretical β-factors of CO_2, CO and CH_4 as a function of temperature, calculated using thermodynamic and quantum mechanical data for gaseous molecules compiled in (Richet and Bottinga, 1977) with minor amendments proposed by (Horita, 2001). Note the deviating behaviour exhibited by 'heavier' CO_2 relative to the more reduced species CH_4 and CO.

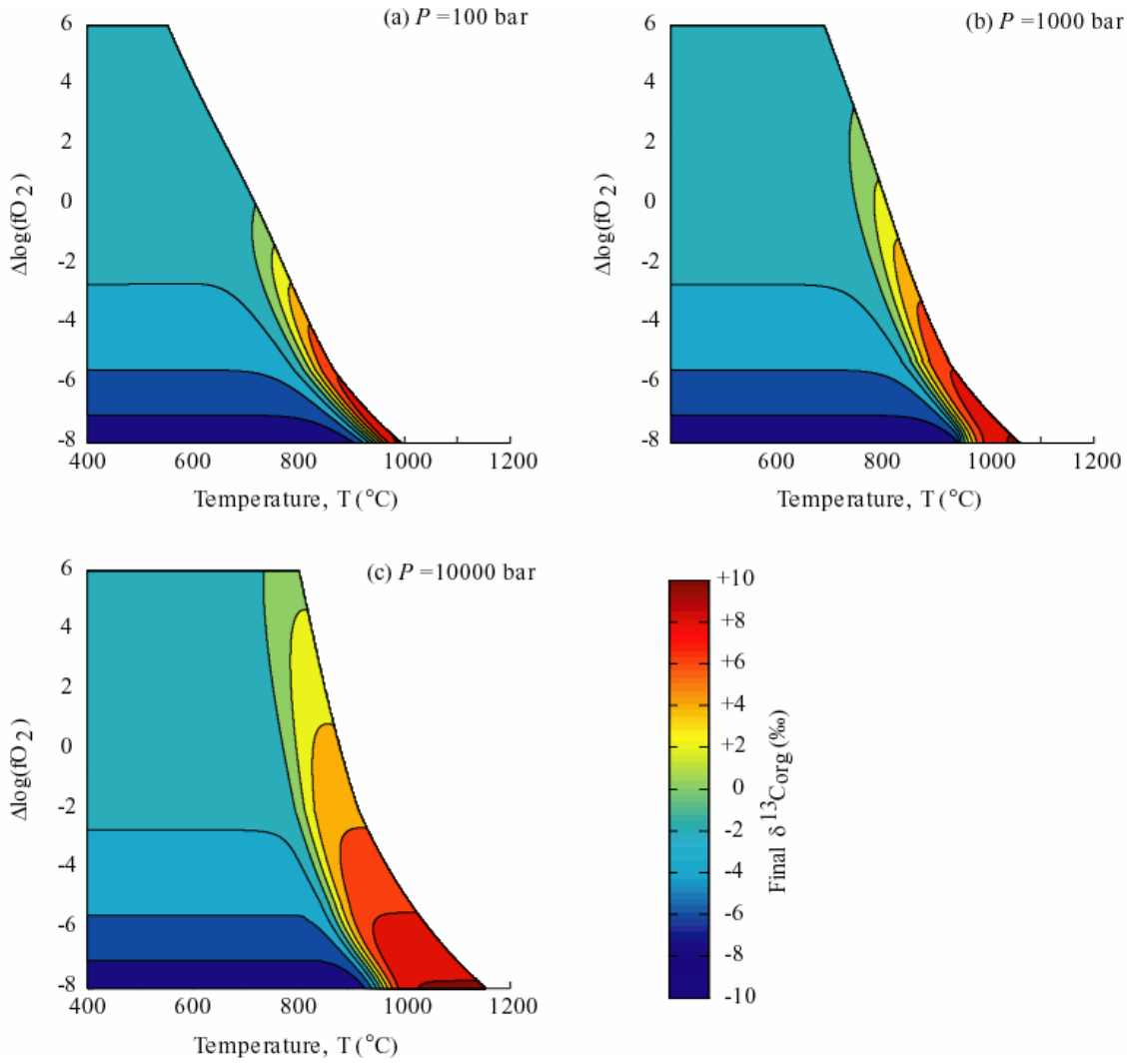

Figure 7: Contour plots showing the isotopic fractionation of reduced carbon equilibrating with C-O-H fluid (with $\delta^{13}C_{fluid}$ = -5 ‰) in fO_2 - T space at P = (a) 100, (b) 1000 and (c) 10000 bars.

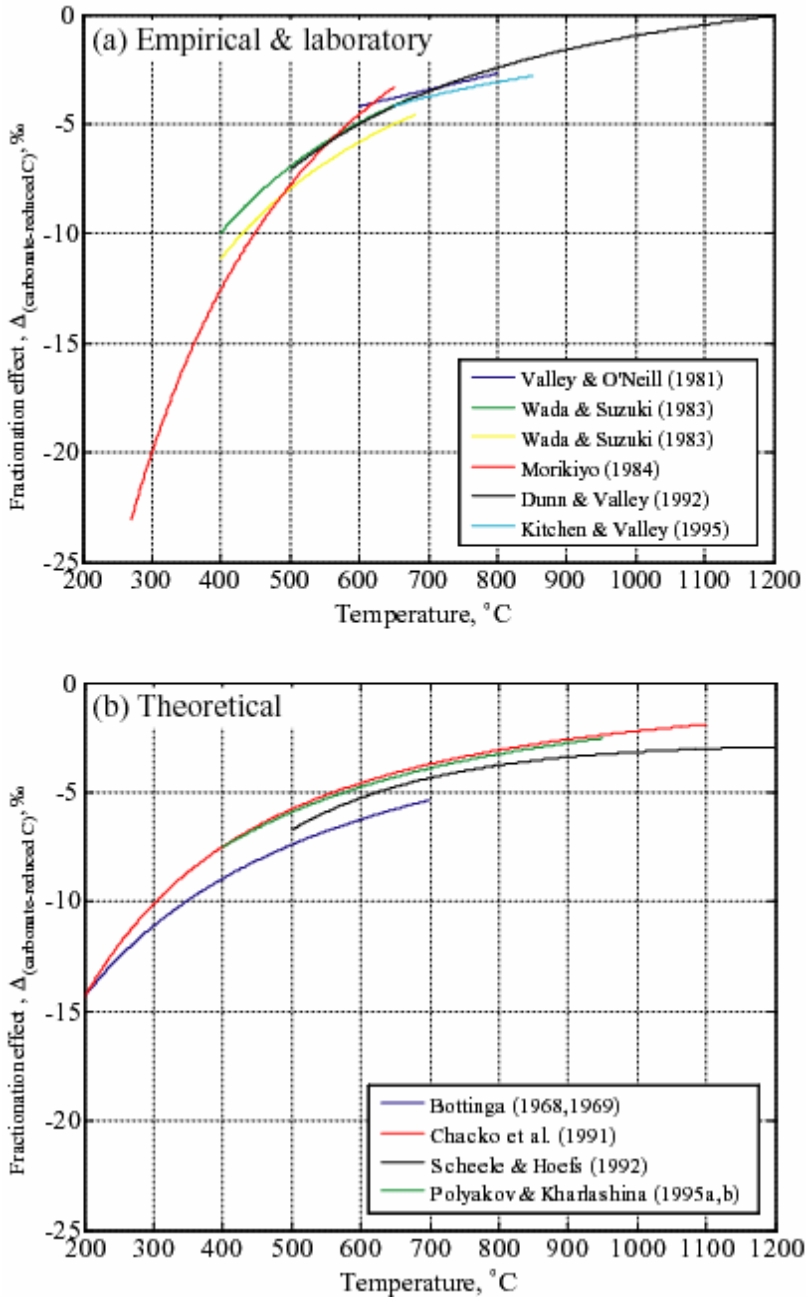

Figure 8: (a): Theoretical (**blue** curve – Bottinga (1968; 1969); **green** curve – Chacko et al. (1991); **red** curve – Polyakov and Kharlashina (1995a; 1995b)) and laboratory (**black** curve – Scheele and Hoefs (1992)) results for carbon isotope fractionation within the calcite-graphite system. (b): Emperical results for carbon isotope fractionation within the calcite-graphite system. **Blue** curve – Valley and O'Neil (1981); **green** curve – Wada and Suzuki (1983); **yellow** curve – dolomite, Wada and Suzuki (1983); **red** curve – Morikiyo (1984); **black** curve – Dunn and Valley (1992); **cyan** curve – Kitchen and Valley (1995). All curves calculated using cubic spline fitting.

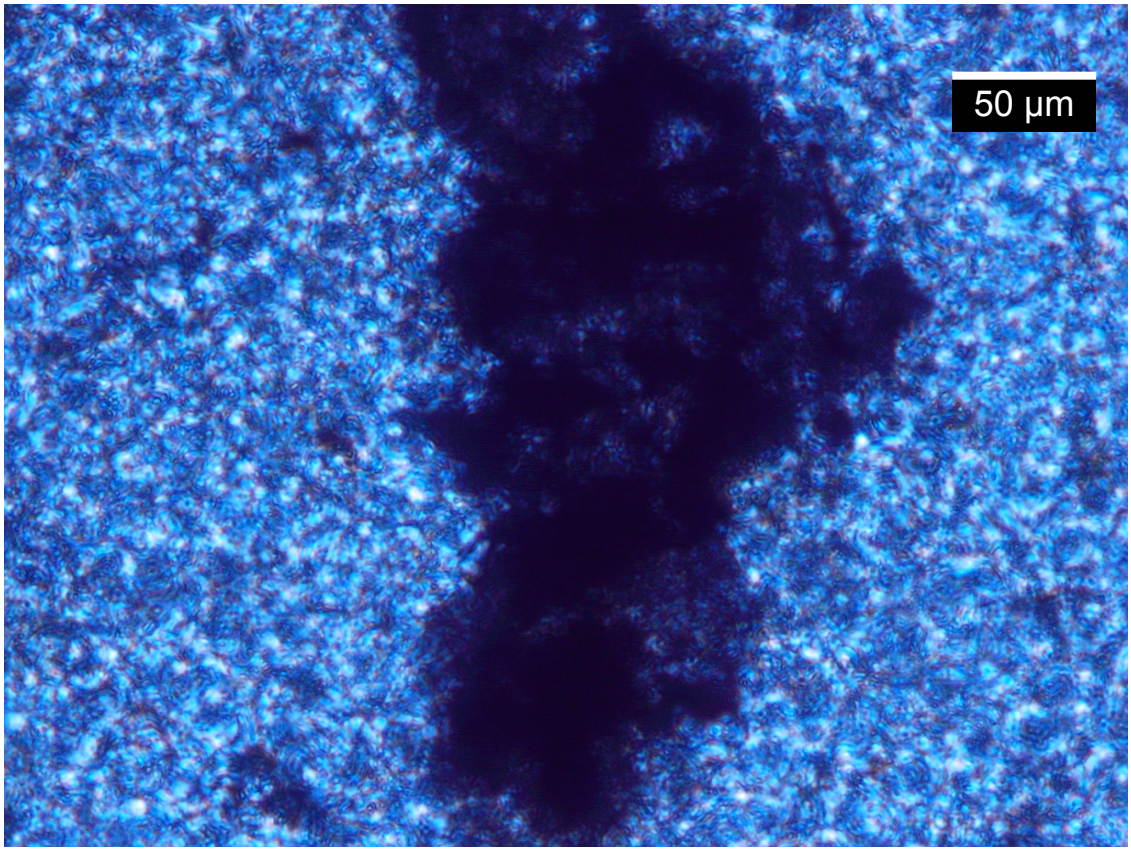

Figure 9: Thin-section photographs of reduced carbon in thermodynamic equilibrium with carbonate. Amoebal graphitic kerogen enclosed in ferruginous dolomite in the greenschist-facies ~3.5 Ga Strelley Pool Chert, Warrawoona Group, Pilbara Craton, Western Australia.

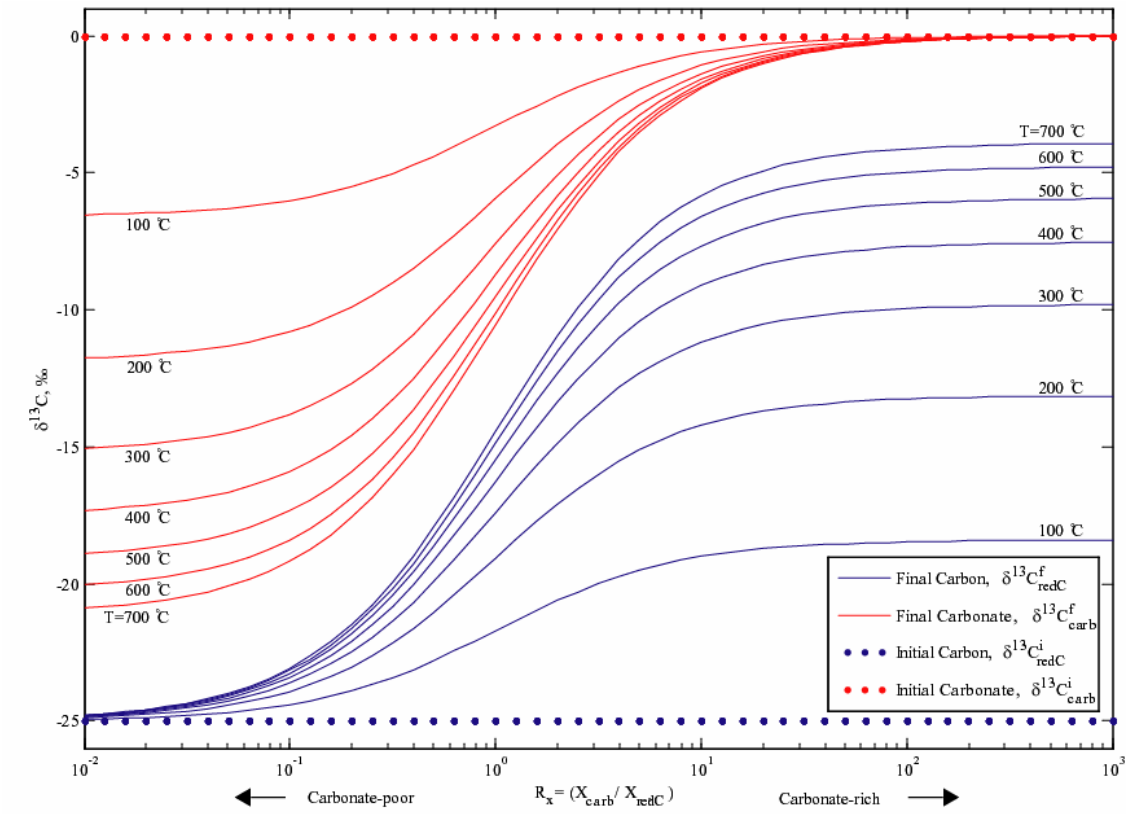

Figure 10: Modelled carbon isotope ratios resulting from equilibrium closed-system interaction between reduced carbon (blue curves) and carbonate (red curves) at different temperatures (100 < T < 700 °C). Non-equilibrium invalidates the lower-temperature calculations. Dotted lines indicate initial isotope ratios, set at $\delta^{13}C^{i}_{C}$ = -25 ‰ and $\delta^{13}C^{i}_{carb}$ = 0 ‰. Higher temperatures tend to drive the isotope ratios of the two distinct carbon reservoirs together. Note the importance of the R, the ratio of carbonate, X_{carb}, to organic carbon, X_C, in determining the final observed $\delta^{13}C^{f}_{C}$.

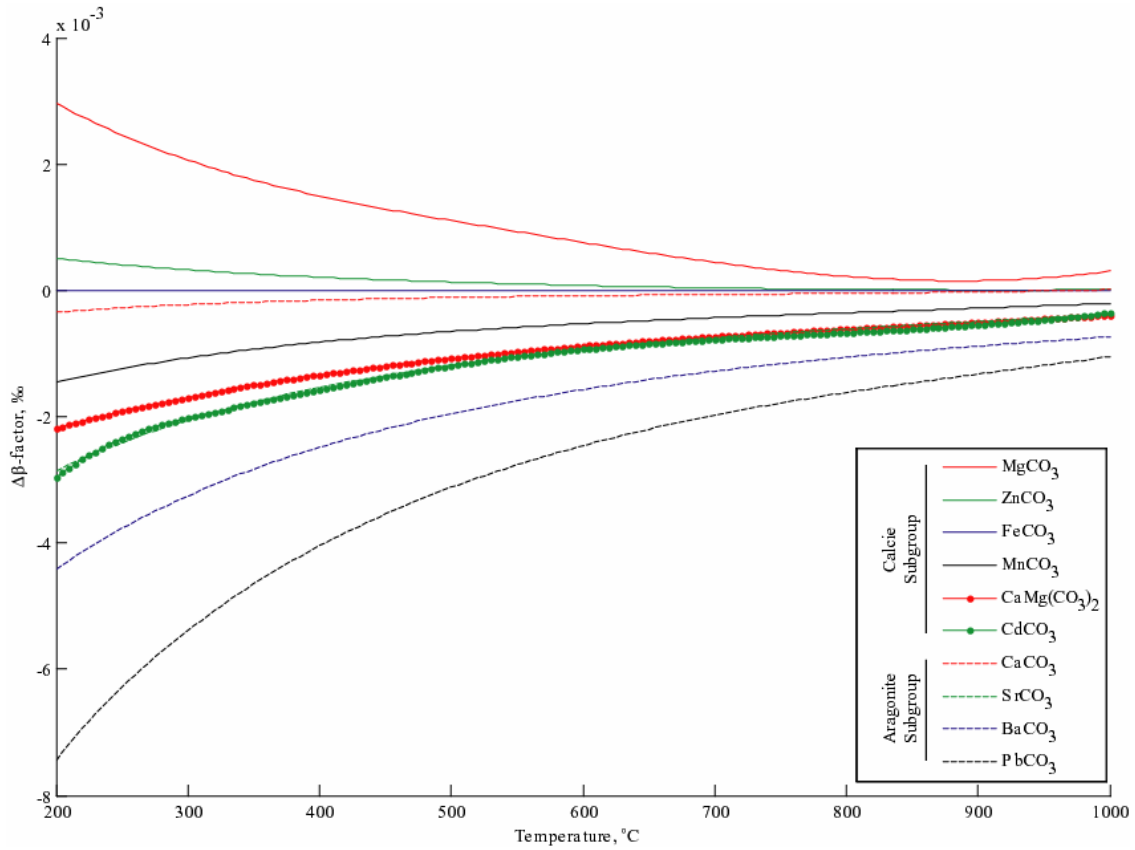

Figure 11: β-factors for a variety of carbonates in the calcite and aragonite subgroups plotted relative to siderite ($FeCO_3$) as a function of temperature. β-factors decrease with increasing metal^{++} cation radius. Plot based on cubic spline fitting of data in Golyshev et al. (1981).

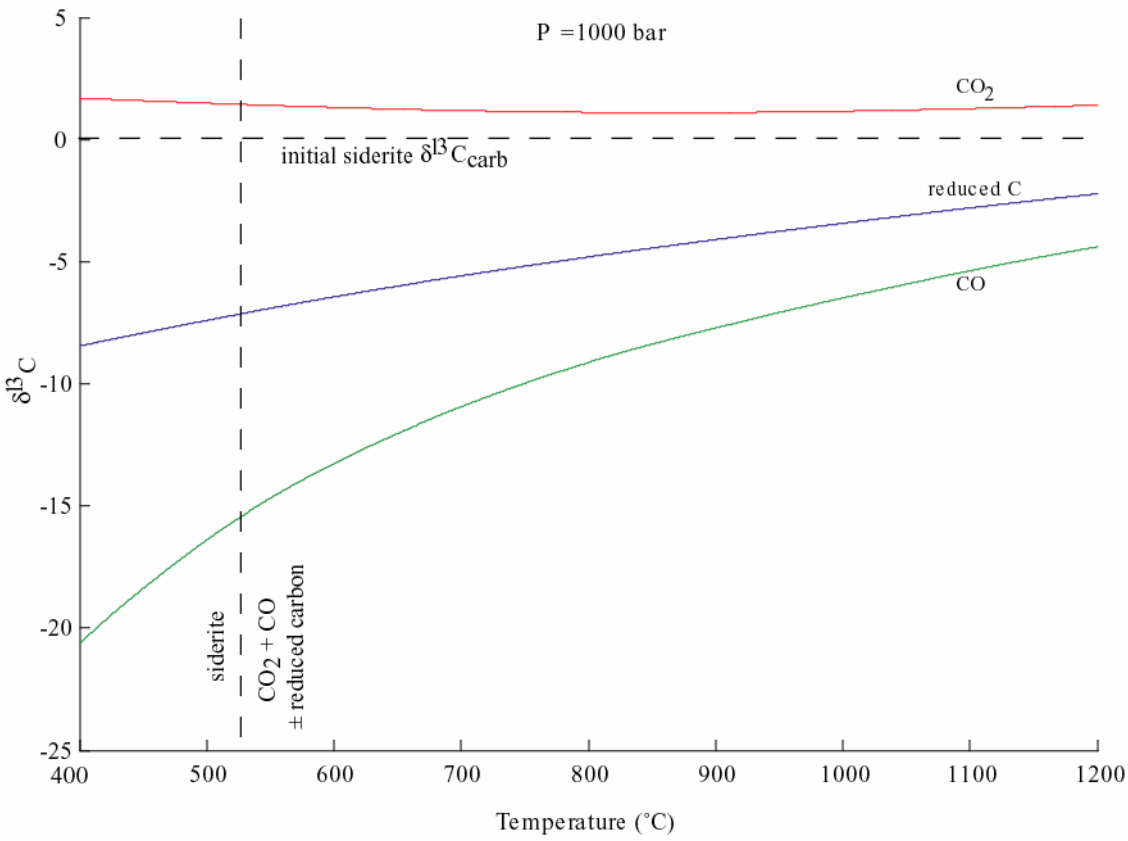

Figure 12: Modelled carbon isotope ratios in the reaction products of closed-system equilibrium decarbonation of siderite (initial $\delta^{13}C^{i}_{carb}$ = 0 ‰, horizontal dashed line) as a function of temperature at P = 1000 bar. Vertical dashed line indicates maximum temperature of siderite stability at the specified pressure.

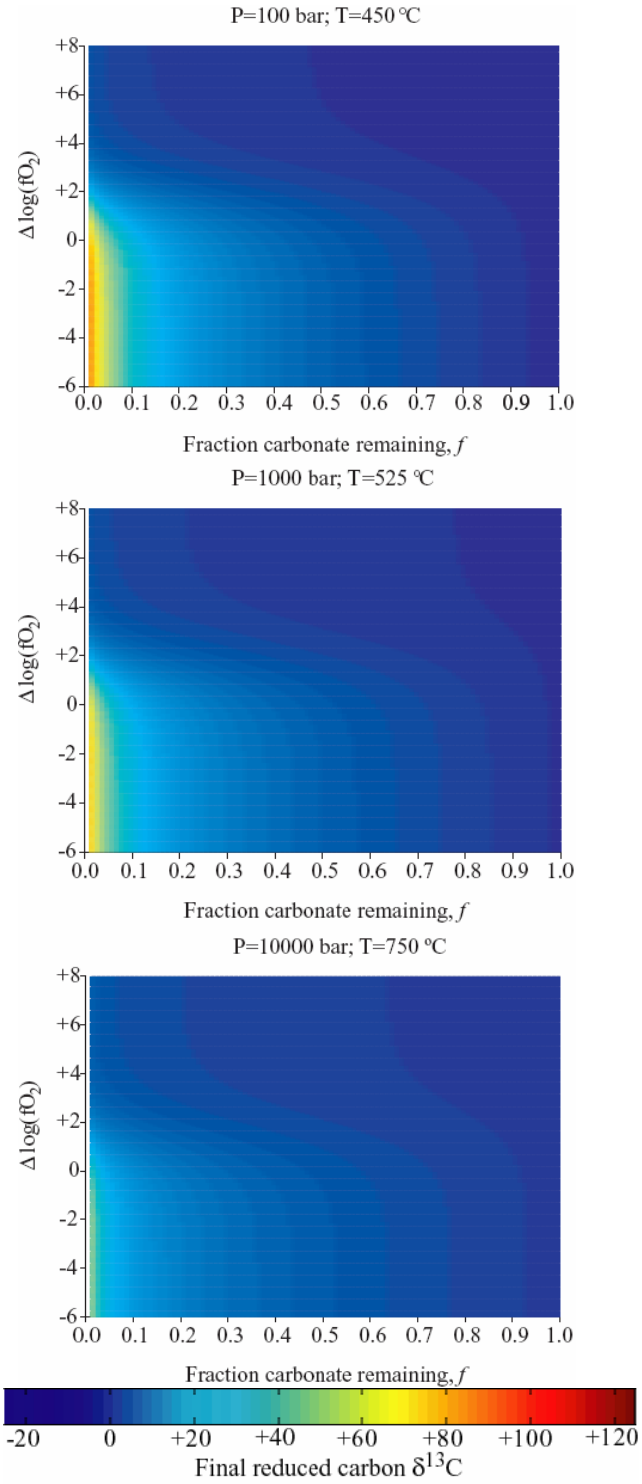

Figure 13: Contour plots of isotopic composition of carbon produced through open-system equilibrium decarbonation of siderite (initial $\delta^{13}C^{i}_{carb}$ = 0 ‰) as a function of the ratio CO_2 to CO in the emitted gas (R_c), and the fraction of carbonate remaining (f). Calculations performed along the univariant decarbonation curve of siderite.

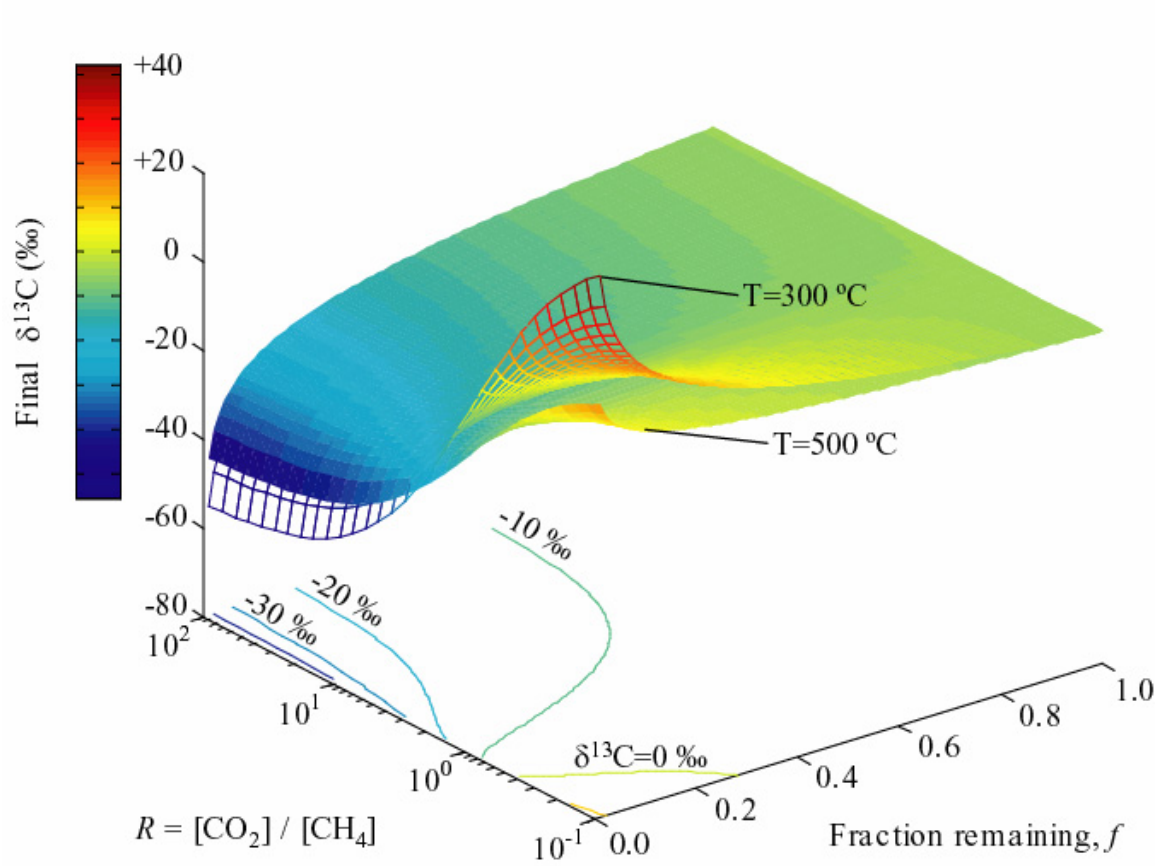

Figure 14: Isotopic fractionation incurred from open-system devolatilization (Rayleigh-type distillation) of graphite-like organic hydrocarbons with an initial isotope signature $\delta^{13}C$ = -5 ‰. The final isotope signature of remaining reduced carbon is plotted as both a function of R_c, the ratio CO_2 to CH_4 in the emitted gas, and f, the fraction of hydrocarbon remaining following devolatilization. The transparent and filled surfaces represent devolatilization at temperatures T = 300 and 500 ºC respectively. Labeled projected 10‰ contours show values in R-f space giving rise to remnant reduced carbon with $\delta^{13}C$ = -40 to + 10‰ for T = 500 ºC.

Table 1: Mixing parameters and thermodynamic constants used in Modified Redlich-Kwong (MRK) equation of state, as proposed by Frost and Wood (1995).

Molecule	**Moment (Debyes)**	***a*** **(at T=1000 K)**	***b*** **(cm^3 $mole^{-1}$)**
H_2	0.00	3.6	15.2
O_2	0.00	17.2	22.1
CH_4	0.02	31.6	29.7
CO_2	0.18	83.0	29.7
CO	1.38	17.0	27.3
H_2O	1.85	88.0	14.6

Table 2: Values taken on by $a_{i,j}$ ($i \neq j$) in the expansion of the MRK equation of state (de Santis et al., 1974). *K* is the equilibrium constant for the reaction $H_2O + CO_2 = H_2O$-CO_2 complex.

i	***j***	$a_{i,j}$
Non-polar	Non-polar	$[a_i a_j]^{0.5}$
Non-polar	H_2O or CO_2	$[a_i a_j^{(0)}]^{0.5}$
H_2O	CO_2	$[a_i^{(0)} a_j^{(0)}]^{0.5} + 0.5\, R^2 T^{2.5} K$

Table 3: Commonly-used oxygen buffers, expressed in the form $\log (fO_2) = A/T + B + C(P-1)/T$, with *T* in Kelvin and *P* in bars. See also Figure 4(a,b). Buffer equilibria compiled in Frost (1991).

Buffer	**Equilibrium constants**			**Temperature range (°C)**		**Equilibrium reaction**
	A	**B**	**C**	**Min**	**Max**	
αQIF	-29435.7	7.391	0.044	423	~573*	Fe2SiO4 = 2Fe + SiO2 + O_2
βQIF	-29520.8	7.492	0.050	~573*	900	Fe2SiO4 = 2Fe + SiO2 + O_2
IW	-27489.0	6.702	0.055	565	1200	2 FexO = 2x Fe + O_2
WM	-32807.0	13.012	0.083	565	1200	2x/(4x-3) Fe3O4 = 6/(4x-3) FexO + O_2
IM	-28690.6	8.130	0.056	300	565	0.5 Fe3O4 = 1.5 Fe + O_2
CoCoO	-24332.6	7.295	0.052	600	1200	2 CoO = 2 Co + O_2
FMαQ	-26445.3	10.344	0.092	400	~573*	2 Fe3O4 + 3 SiO2 = 3Fe2SiO4 + O_2
FMβQ	-25096.3	8.735	0.110	~573*	1200	2 Fe3O4 + 3 SiO2 = 3Fe2SiO4 + O_2
NiNiO	-24930.0	9.360	0.046	600	1200	2 NiO = 2 Ni + O_2
MH	-25497.5	14.330	0.019	300	573	6 Fe2O3 = 4 Fe3O4 + O_2
MH	-26452.6	15.455	0.019	846	955	6 Fe2O3 = 4 Fe3O4 + O_2
MH	-25700.6	14.558	0.019	955	1373	6 Fe2O3 = 4 Fe3O4 + O_2

* Alpha-beta quartz transition at T [°C] = 573 + 0.025 P [bar].

References

Belonoshko, A. and Saxena, S.K., 1991. A Molecular-Dynamics Study of the Pressure-Volume-Temperature Properties of Supercritical Fluids .2. Co2, Ch4, Co, O2, and H-2. Geochimica Et Cosmochimica Acta, 55(11): 3191-3208.

Blank, J.G., Delaney, J.R. and Desmarais, D.J., 1993. The Concentration and Isotopic Composition of Carbon in Basaltic Glasses from the Juan-De-Fuca Ridge, Pacific-Ocean. Geochimica Et Cosmochimica Acta, 57(4): 875-887.

Bottinga, Y., 1968. Calculation of Fractionation Factors for Carbon and Oxygen Isotopic Exchange in the System Calcite-Carbon Dioxide-Water. Journal of Physical Chemistry, 72: 800.

Bottinga, Y., 1969. Carbon isotope fractionation between graphite, diamond and carbon dioxide. Earth and Planetary Science Letters, 5(5): 301-307.

Brasier, M.D. et al., 2002. Questioning the evidence for Earth's oldest fossils. Nature, 416: 76-81.

Brasier, M.D. et al., 2005. Critical testing of earth's oldest putative fossil assemblage from the similar to 3.5 Ga Apex Chert, Chinaman Creek, western Australia. Precambrian Research, 140(1-2): 55-102.

Carothers, W.W., Adami, L.H. and Rosenbauer, R.J., 1988. Experimental Oxygen Isotope Fractionation between Siderite-Water and Phosphoric-Acid Liberated Co2-Siderite. Geochimica Et Cosmochimica Acta, 52(10): 2445-2450.

Chacko, T., Cole, D.R. and Horita, J., 2001. Equilibrium oxygen, hydrogen and carbon isotope fractionation factors applicable to geologic systems. Stable Isotope Geochemistry, 43: 1-81.

Chacko, T., Mayeda, T.K., Clayton, R.N. and Goldsmith, J.R., 1991. Oxygen and Carbon Isotope Fractionations between Co2 and Calcite. Geochimica Et Cosmochimica Acta, 55(10): 2867-2882.

Chase, M.W., 1998. NIST-JANAF Thermochemical Tables, Fourth edition. Journal of Physical and Chemical Reference Data, Monograph 9.

Chung, H.M., Gormlya, J.R. and Squiresa, R.M., 1988. Origin of gaseous hydrocarbons in subsurface environments: Theoretical considerations of carbon isotope distribution. Chemical Geology, 71(1-3): 97-104.

Clayton, R.N., Goldsmith, J.R., Karel, K.J., Mayeda, T.K. and Newton, R.C., 1975. Limits on Effect of Pressure on Isotopic Fractionation. Geochimica Et Cosmochimica Acta, 39(8): 1197-1201.

Connolly, J.A.D., 1995. Phase-Diagram Methods for Graphitic Rocks and Application to the System C-O-H-Feo-Tio2sio2. Contributions to Mineralogy and Petrology, 119(1): 94-116.

de Santis, R.D., Breedvelde, G.F.J. and J.M., P., 1974. Thermodynamic Properties of Aqueous Gas-Mixtures at Advanced Pressures. Industrial & Engineering Chemistry, Process Design and Development, 13(4): 374-377.

Deines, P., 1980. The Carbon Isotopic Composition of Diamonds - Relationship to Diamond Shape, Color, Occurrence and Vapor Composition. Geochimica Et Cosmochimica Acta, 44(7): 943-961.

Des Marais, D.J. and Moore, J.G., 1984. Carbon and Its Isotopes in Mid-Oceanic Basaltic Glasses. Earth and Planetary Science Letters, 69(1): 43-57.

Dunn, S.R. and Valley, J.W., 1992. Calcite Graphite Isotope Thermometry - a Test for Polymetamorphism in Marble, Tudor Gabbro Aureole, Ontario, Canada. Journal of Metamorphic Geology, 10(4): 487-501.

Flowers, G.C., 1979. Correction of Holloways (1977) Adaptation of the Modified Redlich-Kwong Equation of State for Calculation of the Fugacities of Molecular-Species in Supercritical Fluids of Geologic Interest. Contributions to Mineralogy and Petrology, 69(3): 315-318.

French, B.M., 1971. Stability relations of siderite (FeCO3): thermal decomposition in equilibrium with graphite. American Journal of Science, 271: 37-78.

French, B.M. and Eugster, H.P., 1965. Experimental control of oxygen fugacities by graphite-gas equilibriums. Journal of Geophysical Research, 70: 1529-1539.

French, B.M. and Rosenberg, P.E., 1965. Siderite (FeCO3): thermal decomposition in equilibrium with graphite. Science, 147: 1283-1284.

Frost, B.R., 1979. Mineral Equilibria Involving Mixed-Volatiles in a C-O-H Fluid Phase - Stabilities of Graphite and Siderite. American Journal of Science, 279(9): 1033-1059.

Frost, B.R., 1991. In: D.H. Lindsley (Editor), Oxide Minerals: petrologic and magnetic significance.

Frost, D.J. and Wood, B.J., 1995. Experimental Measurements of the Graphite C-O Equilibrium and Co2 Fugacities at High-Temperature and Pressure. Contributions to Mineralogy and Petrology, 121(3): 303-308.

Gerlach, T.M. and Taylor, B.E., 1990. Carbon Isotope Constraints on Degassing of Carbon-Dioxide from Kilauea Volcano. Geochimica Et Cosmochimica Acta, 54(7): 2051-2058.

Goldsmith, J.R., Graf, D.I., Witters, J. and Northrop, D.A., 1962. Studies in the system CaCO3-MgCO3-FeCO3: 1. Phase relations; 2. A method for major element spectrochemical analysis; 3. Compositions of some ferroan dolomites. Journal of Geology, 70: 659-688.

Golyshev, S.I., Padalko, N.L. and Pechenkin, S.A., 1981. Fractionation of Stable Isotopes of Carbon and Oxygen in Carbonate Systems. Geokhimiya(10): 1427-1441.

Hall, D.L. and Bodnar, R.J., 1990. Methane in Fluid Inclusions from Granulites - a Product of Hydrogen Diffusion. Geochimica Et Cosmochimica Acta, 54(3): 641-651.

Hamann, S.D., Shaw, R.M., Lusk, J. and Batts, B.D., 1984. Isotopic Volume Differences - the Possible Influence of Pressure on the Distribution of Sulfur Isotopes between Sulfide Minerals. Australian Journal of Chemistry, 37(10): 1979-1989.

Hoefs, J., 1975. Ein Beitrag zur Isotopengeochemie das Kohlenstoffs in mamatischen Gesteinen. Fortschrift Mineralogie, 52: 475-478.

Holloway, J.R., 1984. Graphite-Ch4-H2o-Co2 Equilibria at Low-Grade Metamorphic Conditions. Geology, 12(8): 455-458.

Horita, J., 2001. Carbon isotope exchange in the system CO2-CH4 at elevated temperatures. Geochimica Et Cosmochimica Acta, 65(12): 1907-1919.

Huizenga, J.M., 2001. Thermodynamic modelling of C-O-H fluids. Lithos, 55(1-4): 101-114.

Javoy, M. and Pineau, F., 1991. The volatile record of a "popping" rock from the Mid-Atlantic Ridge at 14 degrees N: Chemical and isotopic composition of gas trapped in the vesicles. Earth and Planet. Sci. Lett., 107: 598-611.

Jimenez-Lopez, C. and Romanek, C.S., 2004. Precipitation kinetics and carbon isotope partitioning of inorganic siderite at 25 degrees C and 1 atm. Geochimica Et Cosmochimica Acta, 68(3): 557-571.

Joy, H.W. and Libby, W.F., 1960. Size effects among isotopic molecules. Journal of Chemical Physics, 33(4): 1276.

Kelley, D.S. and Fruh-Green, G.L., 1999. Abiogenic methane in deep-seated mid-ocean ridge environments: Insights from stable isotope analyses. Journal of Geophysical Research-Solid Earth, 104(B5): 10439-10460.

Kerrick, D.M., 1974. Review of Metamorphic Mixed-Volatile (H2o-Co2) Equilibria. American Mineralogist, 59(7-8): 729-762.

Kerrick, D.M. and Jacobs, G.K., 1981. A Modified Redlich-Kwong Equation for H2o, Co2, and H2o-Co2 Mixtures at Elevated Pressures and Temperatures. American Journal of Science, 281(6): 735-767.

Kharlashina, N.N. and Polyakov, V.B., 1992. The Effect of Pressure on the Equilibrium Isotope Fractionation in Minerals - Silicates, Calcite, Rutile. Geokhimiya, 2: 189-200.

Kitchen, N.E. and Valley, J.W., 1995. Carbon-Isotope Thermometry in Marbles of the Adirondack Mountains, New-York. Journal of Metamorphic Geology, 13(5): 577-594.

Koziol, A.M., 2004. Experimental determination of siderite stability and application to Martian Meteorite ALH84001. American Mineralogist, 89(2-3): 294-300.

Marshall, C.P. et al., 2007. Structural characterization of kerogen in 3.4 Ga Archaean cherts from the Pilbara Craton, Western Australia. Precambrian Reasearch, 155: 1-23.

Matsuhisa, Y., Goldsmith, J.R. and Clayton, R.N., 1979. Oxygen Isotopic Fractionation in the System Quartz-Albite-Anorthite-Water. Geochimica Et Cosmochimica Acta, 43(7): 1131-1140.

Mattey, D.P., Carr, R.H., Wright, I.P. and Pillinger, C.T., 1984. Carbon Isotopes in Submarine Basalts. Earth and Planetary Science Letters, 70(2): 196-206.

Matthews, A., Goldsmith, J.R. and Clayton, R.N., 1983a. On the mechanisms and kinetics of oxygen isotope exchange in quartz and feldspars at elevated temperatures and pressures. Geological Society of America Bulletin, 94(3): 396-412.

Matthews, A., Goldsmith, J.R. and Clayton, R.N., 1983b. Oxygen isotope fractionation between zoisite and water. Geochemica et Cosmochimica Acta, 47(3): 645-654.

Matthews, A., Goldsmith, J.R. and Clayton, R.N., 1983c. Oxygen isotope fractionations involving pyroxenes; the calibration of mineral-pair geothermometers. Geochemica et Cosmochimica Acta, 47(3): 631-644.

McCollom, T.M., 2003. Formation of meteorite hydrocarbons from thermal decomposition of siderite (FeCO3). Geochemica et Cosmochimica Acta, 67(2): 311-317.

McCollom, T.M., 2004. Experimental study of potential sources of organic carbon in rocks from the Early Earth, Astrobiology Science Conference. Cambridge, NASA/AIMS, pp. 99.

McKay, D.S. et al., 1996. Search for past life on Mars: possible relic biogenic activity in martian meteorite ALH84001. Science, 273: 924-930.

McSween, H.Y.J., 1997. Evidence for life in a martian meteorite? GSA Today, 7(7): 1-7.

McSween, H.Y.J. and Harvey, R.P., 1998. An evaporation model for formation of carbonates in the ALH84001 martian meteorite. International Geology Review, 40: 774-783.

Mel'nik, Y.P., 1982. Precambrian banded iron-formations, physicochemical conditions of formation. Developments in Precambrian Geology, 5. Elsevier, Amsterdam.

Mojzsis, S.J. et al., 1996. Evidence for life on earth before 3,800 million years ago. Nature, 384(7 November): 55-59.

Mojzsis, S.J. and Harrison, T.M., 2000. Vestiges of a beginning: clues to the emergant biosphere recorded in the oldest known sedimentary rocks. GSA Today, 10(4): 1-6.

Morikiyo, T., 1984. Carbon Isotopic Study on Coexisting Calcite and Graphite in the Ryoke Metamorphic Rocks, Northern Kiso District, Central Japan. Contributions to Mineralogy and Petrology, 87(3): 251-259.

Ohmoto, H. and Kerrick, D., 1977. Devolatilization Equilibria in Graphitic Systems. American Journal of Science, 277(8): 1013-1044.

Pineau, F. and Mathez, E.A., 1990. Carbon Isotopes in Xenoliths from the Hualalai Volcano, Hawaii, and the Generation of Isotopic Variability. Geochimica Et Cosmochimica Acta, 54(1): 217-227.

Polyakov, V.B. and Kharlashina, N.N., 1995a. The Use of Heat-Capacity Data to Calculate Carbon-Isotope Fractionation between Graphite, Diamond, and Carbon-Dioxide - a New Approach. Geochimica Et Cosmochimica Acta, 59(12): 2561-2572.

Polyakov, V.B. and Kharlashina, N.N., 1995b. Direct Calculation of Graphite and Diamond Beta-Factor Values by Use of Heat-Capacity Experimental-Data. Geokhimiya, 8: 1213-1227.

Prausnitz, 1969. Molecular Thermodynamics of Fluid-Phase Equilbria. Prentice-Hall, Englewood Cliffs, N.J., 156 pp.

Price, L.C., 1979. Aqueous Solubility of Methane at Elevated Pressures and Temperatures. American Association of Petroleum Geologists Bulletin, 63(9): 1527-1533.

Redlich, O. and Kwong, J.N.S., 1949. On the Thermodynamics of Solutions. V: An Equation of State. Fugacities of Gaseous Solutions. Chemical Review, 44: 233-244.

Richet and Bottinga, Y., 1977. A review of hydrogen, carbon, nitrogen, oxygen, sulphur, and chlorine stable isotope fractionation among gaseous molecules. Annual Review of Earth and Planetary Science, 5: 65-110.

Rosenberg, P.E., 1967. Subsolidus relations in the system CaCO3-MgCO3-FeCO3 between 350 C and 550 C. American Mineralogist, 52: 787-796.

Rosing, M.T., 1999. ^{13}C-depleted carbon microparticles in >3700-Ma sea-floor sedimentary rocks from west Greenland. Science, 283(29 January): 74-76.

Scheele, N. and Hoefs, J., 1992. Carbon Isotope Fractionation between Calcite, Graphite and Co2 - an Experimental-Study. Contributions to Mineralogy and Petrology, 112(1): 35-45.

Schidlowski, M., 1988. A 3800-million-year isotopic record of life from carbon in sedimentary rocks. Nature, 333(26 May): 313-318.

Schidlowski, M., 1993. The beginnings of life on Earth: evidence from the geological record. In: J.M. Greenberg, C.X. Mendoza-Gomez and V. Pirronello (Editors), The Chemistry of Life's Origins. Kluwer Academic Publishers, Netherlands, pp. 389-414.

Schidlowski, M., 2001. Carbon isotopes as biogeochemical recorders of life over 3.8 Ga of Earth history: evolution of a concept. Precambrian Research, 106(1-2): 117-134.

Schidlowski, M., Appel, P.W.U., Eichmann, R. and Junge, E., 1979. Carbon isotope geochemistry of the 3.7 x 10^9-yr-old Isua sediments, west Greenland: implications for the Archaean carbon and oxygen cycles. Geochimica et Cosmochimica Acta, 43: 189-199.

Schopf, J.W., Kudryavtsev, A.B., Agresti, D.G., Wdowiak, T.J. and Czaja, A.D., 2002. Laser-Raman imagery of Earth's earliest fossils. Nature, 416: 73-76.

Schopf, J.W. and Packer, B.M., 1987. Early Archean (3.3-billion to 3.5-billion-year-old) microfossils from Warrawoona Group, Australia. Science, 237: 70-73.

Sharp, Z.D., Papike, J.J. and Durakiewicz, T., 2003. The effect of thermal decarbonation on stable isotope compositions of carbonates. American Mineralogist, 88(1): 87-92.

Shock, E.L., 1992. Chemical Environments of Submarine Hydrothermal Systems. Origins of Life and Evolution of the Biosphere, 22(1-4): 67-107.

Sugisaki, R. and Mimura, K., 1994. Mantle Hydrocarbons - Abiotic or Biotic. Geochimica Et Cosmochimica Acta, 58(11): 2527-2542.

Swart, P.K., Pillinger, C.T., Milledge, H.J. and Seal, M., 1983. Carbon Isotopic Variation within Individual Diamonds. Nature, 303(5920): 793-795.

Takenouchi, S. and Kennedy, G.C., 1964. The binary system H2O-CO2 at high temperatures and pressures. American Journal of Science, 262: 1055-1074.

Ueno, Y., Yoshioka, H., Maruyama, S. and Isozaki, Y., 2004. Carbon isotopes and petrography of kerogens in similar to 3.5-Ga hydrothermal silica dikes in the North Pole area, Western Australia. Geochimica Et Cosmochimica Acta, 68(3): 573-589.

Valley, J.W. and Oneil, J.R., 1981. C-13-C-12 Exchange between Calcite and Graphite - a Possible Thermometer in Grenville Marbles. Geochimica Et Cosmochimica Acta, 45(3): 411-419.

van Zuilen, M.A., Lepland, A. and Arrhenius, G., 2002. Reassessing the evidence for the earliest traces of life. Nature, 418: 627-630.

van Zuilen, M.A. et al., 2003. Graphite and carbonates in the 3.8 Ga old Isua Supracrustal Belt, southern West Greenland. Precambrian Research, 126(3-4): 331-348.

Wada, H. and Suzuki, K., 1983. Carbon Isotopic Thermometry Calibrated by Dolomite-Calcite Solvus Temperatures. Geochimica Et Cosmochimica Acta, 47(4): 697-706.

Weidner, J.R., 1968. Phase equilibria in a portion of the system Fe-C-O from 250. to 10000 bars and 400 °C to 1200 °C and its petrologic significance, Pennsylvania State University, 162 pp.

Weidner, J.R., 1972. Equilibria in the system Fe-C-O part I: siderite-magnetite-carbon-vapor equilibrium from 500 to 10,000 bars. American Journal of Science, 272: 735-751.

Yui, S., 1966. Decomposition of siderite to magnetite at lower oxygen fugacities: a thermodynamical interpretation and geological implications. Economic Geology, 61: 768-776.

Zhang, C.L. et al., 2001. Temperature-dependent oxygen and carbon isotope fractionations of biogenic siderite. Geochimica Et Cosmochimica Acta, 65(14): 2257-2271.

4. A Metasedimentary Succession From the Isua Supracrustal Belt

1. Introduction

The provenance of Earth's oldest sedimentary rocks is controversial. Highly metamorphosed (granulite-facies) banded iron formation >3.85 Ga old has been reported from Akilia Island in Greenland (Mojzsis et al., 1996), but its age (Myers and Crowley, 2000) and origin (e.g. Fedo and Whitehouse, 2002a, 2002c, 2002b) have been disputed. The recently discovered ~3.75 Ga Nuvvuagittuq supracrustal belt in Quebec, Canada, contains highly metamorphosed banded quartz-magnetite-amphibole/pyroxene rocks interpreted as chemical sediments, highly deformed quartz-biotite schists possibly of a conglomeratic origin and laminated psammopelitic schists perhaps representing altered amphibolites or sediments (Cates and Mojzsis, 2007; Dauphas et al., 2007), but detailed sedimentological studies have not yet proven their provenance. Purported ~3.8 Ga sedimentary carbonates from Isua, Greenland (e.g. Schidlowski et al., 1979) have been reinterpreted as metasomatic derivatives of ultramafic volcanics (Rose et al., 1996). The sedimentary identity of meta-conglomerates (Fedo, 2000) from the same locality has been queried, with a tectonic origin proposed instead (Nutman et al., 1984; Nutman and Bridgwater, 1986). Isua "meta-pelites" comprising garnet-biotite-plagioclase schists (Boak and Dymek, 1982) have recently been re-interpreted as metamorphosed and metasomatized mafic igneous rocks (Rosing et al., 1996). Perhaps the only ~3.8 Ga rocks that are generally accepted as having a certain sedimentary origin are some Isua banded iron formations (e.g. Dauphas et al., 2004) and a small outcrop of meta-turbidite, also at Isua (Rosing, 1999).

Thus far, no convincing evidence exists for sialic crust contributing to any >3.7 Ga sedimentary pile. However, the issue of provenance is important. It can potentially inform us about ancient tectonic processes, the composition of the primordial upper crust, and the style of depositional environments at a time when the Earth was first capable of hosting a biosphere. But caution is warranted, as outcrops >3.7 Ga are rare and may over-represent environments conducive to preservation rather than those

typifying Earth's ancient surface. Moreover, reading through post-depositional deformational and metamorphic overprints is difficult. Clearly, more occurrences of less disrupted earliest Archean sedimentary rocks would help resolve these problems.

Here we describe a newly discovered, more extensive and better preserved outcrop of turbiditic metasediments from the Isua supracrustal belt that displays more compelling evidence of a sedimentary origin. These rocks also provide possible mineralogical evidence for continental erosion, providing new information about the nature and processing of the Earth's oldest crust.

2. General Geology

The newly discovered outcrop occurs on the edge of the retreating inland ice sheet in the Isua region of western Greenland (Fig. 1). It lies at the northeastern end of the arcuate Isua supracrustal belt, a 3-4 km wide succession of supracrustal rocks ~35km in strike length surrounded by the Amîtsoq and Ikkattoq gneisses in the Akulleq terrane. The age of the Isua rocks is fairly tightly constrained, with all evidence indicating deposition between 3.7 and 3.8 Ga (Boyet et al., 2003; Nutman et al., 1997). The rocks have undergone multiple episodes of deformation, causing a pervasive schistosity and stretching lineation with localized sheath folds. However, some areas have experienced relatively low strain, with broad open folding predominating and primary structures such as pillows (Appel et al., 1998) and syn-volcanic dykes (Furnes et al., 2007) surviving.

3. Low-strain metasediments

The low-strain domain hosting the newly-discovered metasediments covers an area of ~200 x 250 meters (Fig. 1). Dips of bedding and the major foliation, which is sub-parallel to bedding, are sub-vertical and the general strike is northeast, though deformed around moderately open to moderately tight folds. Bedding has been disrupted by irregular intrusions of post-peak-metamorphic dolerite, which can be distinguished from older Ameralik dykes by their lack of plagioclase megacrysts. However, metasedimentary units and their contacts still show considerable lateral

continuity. The metamorphic grade, usually at or above upper amphibolite facies at Isua (Rollinson, 2003), is relatively low, with peak metamorphic foliation defined by chlorite- and biotite-dominated assemblages that equilibrated at upper greenschist conditions. Locally, garnet-bearing assemblages representing lower amphibolite facies conditions developed under strain control. The scarcity of retrogressive hydrous minerals and/or carbonate suggests that the metasediments remained remarkably closed to subsequent fluid alteration. Mineral assemblages are dominated by varying amounts of quartz, biotite, chlorite and magnetite with frequent occurrences of garnet, stilpnomelane, amphibole or cordierite. Important accessory minerals include graphite, zircon, pyrite, ilmenite and epidote. Carbonate, mostly ferroan -calcite and -dolomite, is a minor and local secondary constituent adjacent to veins.

The limited strain, low metamorphic grade and slight retrogression have allowed preservation of primary textures and compositions, permitting a degree of sedimentological reconstruction. Amongst the most striking features of the sedimentary package are the diversity of original clast sizes and the repetition of meter-scale graded units. Despite stretching and recrystallization, the preservation of reworked laminated clasts shows that protolith grainsize ranged from cobbles (Fig. 3a) to silt, with pure biotite schists that cap graded packages evidently representing recrystallized mudstones. Sedimentary structures other than coarse bedding have been poorly preserved, with some quartzites exhibiting vague lenticular layering suggestive of cross-bedding and several metagreywacke units showing undulose bedding surfaces reminiscent of ripple-marking.

Texturally, the sedimentary protoliths ranged from conglomerate to mudstone. The conglomerates consist of well-rounded cobbles and pebbles that are grain-supported in the lower parts (Fig. 3a) of beds but float in a biotite-chlorite matrix above, becoming diamictites. They are polymictic, consisting of at least three distinct clast lithologies. The dominant clast type is now composed of clear sugary quartzite and presumably represents recrystallized massive white chert (c.f. Fedo, 2000). Other sugary quartzite clasts show relict grey and white planar compositional layering on a 2-5mm scale, possibly originally banded chert or silicified lutite. Less commonly, tabular

clasts are composed of fine magnetite-quartz crystals, probably derived from banded iron formation, or chlorite/biotite-quartz, possibly pelitic intraclasts. Large clasts at the base of some beds protrude below others, though whether this is due to scour infilling during deposition or gravitational loading during diagenesis is unclear given subsequent deformation.

Conglomeratic diamictite beds grade up into gravelly or gritty micaceous quartzite predominantly consisting of angular, 0.5-2mm, single-crystal (if smaller than 1mm) or polycrystalline quartz grains with a finer biotite-chlorite-quartz matrix. The rock is plane-laminated at a 0.5-1mm scale with quartz-rich (~90%) or phyllosilicate-rich layering, the latter containing scattered 1-2mm garnet porphyroblasts. Such beds can also form the base of graded units. This lithology in turn grades up into massive grain-supported quartzite with 0.1-0.5mm well-sorted quartz crystals with <15% biotite-chlorite matrix. Though the former have been recrystallized, grading is visible and discrete laminae contain quartz of different grain-size, suggesting that a facsimile of depositional grain-size is still preserved. In places, undulose to lenticular pelitic partings that are too discontinuous and too irregular to be crenulation cleavages hint at an original cross-bedded structure. 0.05-0.15mm sub-rounded to angular, euhedral to sub-euhedral zircons (Fig. 5) and similarly sized but distinctly more rounded (sub-rounded to rounded) pyrite grains are scattered between and within quartz grains.

Zircon and pyrite abundances and size distributions vary systematically with sedimentary composition and texture, and are strictly associated with quartzose rather than metapelite layers. Grains co-vary in the range 10-150μm, with a median size of 20-25μm. Grain diameters also roughly correlate with the grain sizes of associated quartz. Further, pyrites with high rounding and sphericity are frequently concentrated together with zircons within ‘heavy-mineral’ lamellae housing hydraulically equivalent grains of similar size and density. All of these features point to a detrital origin for these mineral grains.

The quartzites are best interpreted as metamorphosed muddy quartz arenites. By decreasing the relatively proportions of quartz grains and increasing those of matrix while also decreasing clast grain size to <0.2mm, these quartzites usually pass up into

meta-siltstone in which the proportion of matrix rises to 70%. The uppermost component of graded packages is well-foliated biotite-chlorite±cordierite schist with <5% 0.1mm quartz grains. These rocks lack compositional layering, suggesting an argillaceous mudstone protolith.

The other principal rock type in the metasedimentary succession is massive to compositionally-layered quartz-biotite-chlorite-garnet schist. Massive beds are up to 2 meters thick, with no apparent grading or compositional change upwards. Compositional layers are 1-5cm thick, often with undulose contacts resembling load structures or ripple marks, and defined by varying contents of quartz relative to phyllosilicates. Quartz grain size varies between laminae, with grains <0.5mm in quartzose laminae but 0.1-0.15mm in phyllosilicate-rich layers. Garnets are concentrated in the phyllosilicate layers and along lamina contacts, as are submicron-sized black opaque grains of uncertain affinities. Well-rounded, subspheroidal grains of pyrite ~0.05mm in diameter form diffuse heavy-mineral laminae and graphite flakes 0.1mm long are scattered through phyllosilicate-rich layers. Quartzose laminae contain up to 2% rounded apatite grains, appreciably more than is observed in BIF-hosted quartz. Small (~0.01mm) rounded to elliptical blebs of carbonate occur as inclusions within quartz grains. The protolith, whether massive or layered, was probably greywacke.

Distinctive units of massive quartzite also occur. Recrystallized quartz grains with well-developed 120º triple junctions make up ~80% of the rock, exhibiting a homogeneous size distribution with diameters consistently 0.3-0.7mm. Euhedral crystals of carbonate occupy intergranular space. Smaller round to elliptical carbonate inclusions occur within quartz grains, often exhibiting linear distributions probably marking previous quartz crystal faces. Both peak-metamorphic and retrogressive chlorite occurs, the latter locally replacing biotite. These rocks are best interpreted as metamorphosed clean, well-sorted quartz arenites.

A different rock type occurs in the upper part of the stratigraphic succession, resembling amphibolite in composition but evidently sedimentary in origin because of its thin concordant bedding, weak planar compositional layering on a 5-10cm scale and

unusual mineralogy. Unlike amphibolites derived from igneous protoliths, these rocks consist of up to 15% dark green-black amphibole and 10-30% chlorite but also with 40-50% quartz and up to 10% pale pink garnet. They may have been derived from basaltic pyroclastic or epiclastic sediments, such as tuffs or basaltic sandstones.

The entire section of clastic metasediments is ~175 metres thick, overlain by quartz-magnetite-grunerite±cummingtonite metamorphosed banded iron formation. The contact between the clastic metasediments and BIF is nowhere exposed, being covered by moraine or intruded by dolerite. Though deformation of the BIF is markedly more intense than in the clastic sediments, showing sheath folds compared with open folding in the clastic metasediments, the similarity in metamorphic grade and the known propensity of BIF to take up regional stress through ductile deformation suggests that the clastic and chemical sedimentary packages are conformable. However, due to the poor exposure, we cannot rule out the possibility that the BIF overlies an unconformity or has been emplaced by a fault.

4. Geochemistry

Geochemical analysis was performed by Washington State University GeoAnalytical Lab using in-house procedures for XRF (Johnson et al., 1999) and ICP (http://www.sees.wsu.edu/Geolab/note/icpms.html) analyses. Chondrite normalizations (subscripted 'CN' hereafter) were calculated using data in Sun and McDonough (1989), shale normalizations (Post-Archaean Average Shale, 'PAAS', subscripted 'SN' hereafter) were calculated using data in Nance and Taylor (1976).

Major element compositions (Table 1) are homogeneous and largely controlled by the relative amounts of quartz, magnetite, annite (Fe-biotite) and chamosite (Fe-chlorite) with or without amphibole, garnet or cordierite. As a result, the metasediments are characterized by a variably aluminous, iron- and silica-rich geochemistry, which varies systematically with original clay mineral content, as proxied by Al_2O_3 wt.%. Immobile trace- and rare-earth-element abundances describe linear mixing arrays between a variably reworked BIF-like chemical precipitate and an aluminous, possibly mixed, clastic metasediment.

4.1. Major Elements

In terms of major element abundances, Archaean shales and greywackes have been found to be generally enriched in Na, Ca, Mg and Fe and depleted in Si and K compared to post-Archaean counterparts (McLennan, 1982; McLennan and Taylor, 1984). With the exception of high iron concentrations, these features are not observed in the Isua metasediments.

Na_2O is generally lacking, and occurs mostly in association with amphiboles of probable metamafic origin. CaO concentrations vary between 0.5 wt.% and 4.5 wt.% and are controlled by the presence of carbonate (typically ferroan-calcite and -dolomite) rather than silicate minerals, usually associated with veins. Extensive carbonate metasomatism, as found in some parts of Isua (Rose et al., 1996), is confined to the lowermost ~10 meters of stratigraphy only.

Total Fe concentrations vary between ~3 wt.% in quartzitic aluminosiliclastic metasediments to almost 40 wt.% in samples with discontinuous magnetite lamellae. The absence of micro- or meso-scale Si/Fe banding suggests that magnetite is not a primary precipitate. Metasedimentary chlorite Fe-Mg chemistry resembles in its variability that of marine chloritic schists from Barberton (Toulkeridis et al., 1996).

High K/(Na + silicate Ca) ratios, if primary, point to advanced stages of chemical weathering (McLennan et al., 2004; Nesbitt, 2004). Unfortuantely, no petrological means exist to discount early K-metasomatism, for instance through K addition or substitution for Na and/or Ca (Fedo et al., 1995). Geochemical and other considerations point to a dominantly primary origin for potassium, however. Firstly, potassium metasomatism is not pervasive at Isua, even in basalts that have experienced significant Fe enrichment (Polat and Frei, 2005). Isua BIFs are also lacking in potassium (Dymek and Klein, 1988). Secondly, K/Rb ratios are remarkably invariant (Fig. 11), and distinctly lower than magmatic values (Shaw, 1968). This stands in contrast to fractionation trends expected from metasomatism, which tends to raise K/Rb ratios (Field and Clough, 1976). Magmatic or supermagmatic K/Rb ratios are associated with Early Archaean potassic metasomatism, as in Barberton K-enriched silicification zones (data in Hofmann and Harris, 2008), Pilbara cherts (Minami et al.,

1995; Sugitani et al., 2002), Barberton cherts (data in Hofmann and Harris, 2008; Rouchon and Orberger, 2008) and the majority of more variable Isua schists (data in Bolhar et al., 2005a). Thirdly, K/Rb ratios similar to those of the Isua metasediments are observed in contemporary marine sediments known to be unmetasomatized (Ingram and Lin, 2002; Pache et al., 2008). Witwatersrand shales with primary potassium, although more variable, likewise show similar K/Rb ratios to those reported here (Wronkiewicz and Condie, 1987).

4.2. Trace Elements

Normalization to Al_2O_3 allows comparison to trace element endowment relative to PAAS ('enrichment factors', Ross and Bustin, 2009) (Fig. 6). The metasediments have shale-like concentrations of the redox-insensitive immobile elements Hf, La, Sc, Yb and Zr. Ga is shale-like to mildly enriched (< 2.6x $PAAS_{Al}$). Pb concentrations are more variable, varying from highly depleted to shale-like to quite enriched. The redox-sensitive elements Cr and Ni are highly enriched, on the other hand. Ni enrichment varies between 1.6x and 10x $PAAS_{Al}$, with Cr showing lower enrichment factors between 2.0x to 5.1x. Y concentrations are variable but, on average, shale-like. Nb, Th, and U concentrations, meanwhile, are rather narrowly confined between 0.3x and 0.6x $PAAS_{Al}$. Ce occurs in shale-like to mildly depleted concentrations.

Mobile elements show highly variable enrichments, often in excess of $PAAS_{Al}$ averages. Ba, Cs, and Rb are enriched up to 10x, 5x and 3.6x $PAAS_{Al}$ respectively. About a third of samples are $Cs_{SN\text{-}Al}$ depleted, however, while Ba and Rb concentrations only rarely fall below shale-like values. Sr endowments are also highly variable. In low-calcium samples, Sr is depleted (0.5x $PAAS_{Al}$) to very depleted (0.02x $PAAS_{Al}$).

The redox-sensitive mobile elements Mn and Zn are highly enriched, respectively up to ~12x and ~5x $PAAS_{Al}$. V concentrations are shale-like, while Cu endowments are highly variable, ranging from 0.1x – 10x $PAAS_{Al}$.

4.3. Rare Earth Elements

On the whole, REE concentrations and characteristics vary systematically between BIF-like and aluminosilicate endmembers (Fig. 7). BIF-dominated metasedimentary REE concentrations are as low as 20 - 30 ppm, with ∑REE increasing roughly linearly to ~100 ppm in aluminosilicate-rich metasediments (Fig. 8(a)), exceeding the maximum REE concentrations reported from pure chemical sediments elsewhere at Isua (Bolhar et al., 2004). Nevertheless, some general observations apply to all metasediments: REE profiles differ from PAAS in that they exhibit upward sloping LREEs, mildly downward sloping HREEs, and anomalous La, Eu and Y concentrations. Ce is non-anomalous (Fig. 9), with Pr/Pr* ≈ 1 ($Pr/Pr^* = [Pr/(Ce/2 + Nd/2)]_{SN}$).

Both BIF- and aluminous clastic-dominated metasediments exhibit flat to gently downward sloping $HREE_{SN}$ distributions, with $(Tb/Lu)_{SN} = 0.90 – 1.30$. $LREE_{SN}$ depletion is correlated with the relative dominance of a BIF-like component, with $(Gd/Pr)_{SN} = 1.6 – 2.2$ in magnetite-rich samples and $(Gd/Pr)_{SN} < 1.6$ in magnetite-poor aluminous metasediments.

La anomalies are ubiquitous, but decay systematically with increasing aluminous clastic content (Fig. 8(b)). La anomalies are very high in BIF-rich metasediments, with La/La* = 1.3 – 1.5 ($La/La^* = [La/(3Pr - 2Ce)]_{SN}$), decaying to (still dominantly superchondritic) values of La/La* = 1.0 – 1.2 where aluminous clastics are dominant.

Al-poor metasediments are endowed with markedly superchondritic Y/Ho ratios, with maximum values of 45 – 46 for BIF-dominated samples. This Y anomaly decreases systematically and sharply with increasing Al_2O_3 (Fig. 8(c)). Al-rich (>6 wt.% Al_2O_3) metasediments have narrow chondritic- and PAAS-like Y/Ho ratios of ~ 26 - 30.

Metasediment Eu concentrations are noticeably more erratic than other REE characteristics. However, if the subset of samples lacking magnetite laminae is considered seperately, Eu anomalies increase systematically with increasing Al_2O_3 (compare filled and unfilled circles, Fig. 10). Overall, Eu anomalies are slightly

subchondritic to strongly superchondritic, with Eu/Eu* varying between 0.93 and 1.45. (Eu/Eu* = $[Eu/(Sm * Gd)^{0.5}]_{CN}$). The magnetite fraction in pure magnetite-BIF collected adjacent to the study area carries an extreme Eu-enrichment of Eu/Eu* = 2.3.

4.4. REE Closure

As born out by geochemical studies elsewhere at Isua (e.g. Blichert-Toft et al., 1999; Gruau et al., 1996; Rose et al., 1996), the possibility of hydrothermal and metasomatic alteration and metamorphic remobilization merits careful consideration. Several lines of evidence suggest, however, that REE concentrations in the metasediments have remained closed to post-diagenetic alteration. An intercalated metamafic unit exhibits a slightly negative (Eu/Eu* = 0.84) anomaly, in agreement with analyses of relatively unmetasomatized analogues from elsewhere at Isua (e.g. Polat et al., 2002). Metasediment REE trends, meanwhile, are highly uniform throughout the sequence. Low-REE BIF-dominated metasediments preserve positive La anomalies and Y/Ho ratios, which furthermore decay systematically with increasing aluminosilicate content. These features cannot be reconciled with a proleptic hydrothermal overprint, and argue strongly in favor of a primary origin for the REE distributions.

5. Interpretation

The compositions of the metasediments are best explained by mixing between a BIF-like chemical precipitate and an aluminous siliciclastic endmember. That a BIF component was present is revealed by BIF clasts in the rudites, by the unusually ferruginous major-element chemistry of all metasediments and by their rare-earth element patterns. The aluminous silicate component is manifested by the high pelite content of the finer-grained facies, by REE distributions in the most aluminous metasediments and by other trace-element ratios. As we argue below, trace element ratios and other considerations suggest that the aluminous endmember itself represents a shale-like component derived from thorough mixing of both mafic and felsic (possibly continental) sources.

5.1. Chemical Precipitate Component

Other than iron and silica, elemental concentrations in the chemical precipitate endmembers were low. Geochemical signatures in those samples most enriched in this component (e.g. ISB02/058B and ISB02/056) resemble other ferruginous chemical sediments precipitated from Archaean seawater, including BIFs at Isua and elsewhere in southern West Greenland (Bolhar et al., 2004; Frei and Polat, 2007; Friend et al., 2008).

REE profiles also suggest the presence of a BIF-like component, with LREE highly depleted relative to MREE and HREE, and positive La, Eu and Y anomalies and no Ce anomalies (compare brown field, Fig. 7). The absence of a Ce anomaly, as found in Phanerozoic seawater and precipitates (Shields and Webb, 2004), is indicative of sedimentation and diagenesis under low-oxygen conditions (Alibo and Nozaki, 1999). No evidence was found for the negative Ce-anomaly reported from some Isua BIFs (Dymek and Klein, 1988) and altered Archaean metasediments (Hayashi et al., 2004). Strongly positive La_{SN} anomalies, meanwhile, are characteristic of marine waters of all ages (Bau and Dulski, 1996; de Baar et al., 1991), as is the relative LREE depletion (Elderfield, 1988; Sholkovitz et al., 1994). Relatively flat $HREE_{SN}$ distributions suggest a negligible role for desorption control on REE concentrations.

The positive Y anomaly encountered in contemporary marine waters is thought to result from Y/Ho fractionation associated with enhanced scavenging of Ho during removal by sinking particulate matter from the surface to deep -ocean (Nozaki et al., 1997). Hydrothermal fluids, likely to have been important controls on Archaean ocean chemistry, may also exhibit Y/Ho enrichment. Although modern high-temperature discrete-flow hydrothermal fluids exhibit chondritic Y/Ho ratios (Bau and Dulski, 1999; Douville et al., 1999), two mechanisms by which such fluids may undergo post-conduit Y/Ho fractionation can be envisaged: (i) diffuse flow in short and shallow convective cells where seawater-rock equilibrium has not yet been established, producing fluids which have conserved a seawater-like Y-enriched signature; and (ii) preferential REE scavenging during localized Fe-Mn oxy-hydroxide precipitation,

initiated through mixing of hot hydrothermal fluids with cold seawater. The latter process leaves Y-depleted hydrogenetic Fe-Mn crusts and Y-enriched hydrothermal fluids (Bau, 1996).

The strongly positive Eu anomaly is a well-known feature of Archaean chemical precipitates (Bau and Moller, 1993; Bolhar et al., 2005b; Danielson et al., 1992; Derry and Jacobsen, 1990; Fryer, 1977). This anomaly is thought to result from the preferential weathering of highly Eu-enriched feldspars, especially plagioclase (McDonough and Frei, 1989), in hydrothermal systems. It is often taken as evidence for both greater hydrothermal input, and lower fO_2 (and perhaps pH) conditions prohibiting Fe-precipitation at hydrothermal conduits, during Archaean times (Michard and Albarede, 1986).

5.2. Aluminous Clastic Component

With the important exception of the Eu anomaly, the geochemical features of a chemical precipitative origin diminish with increasing aluminous contribution. Y/Ho ratios converge to chondritic values typical of both Precambrian and Phanerozoic pelites and metagreywackes, and are well-explained by a mixing curve constructed between BIF- (Y/Ho = 46, no Al_2O_3) and pelite- (Y/Ho = 27, Al_2O_3 = 15 wt.%) endmembers (Fig. 7(c)). Gd/Yb ratios (Fig. 12) are typical of Archaean turbidites (McDonough and Frei, 1989; McLennan, 1993).

Eu anomalies are important for Archaean provenance studies. Although high, Eu anomalies do not correlate with BIF-derived magnetite and fall well below those of pure BIFs sampled here or elsewhere at Isua (Frei and Polat, 2007; Polat and Frei, 2005). It has been argued that a secular trend of decreasing Eu/Eu* ratios can be recognized in the Archaean sedimentary record, ascribed to an increasing cratonic contribution with time (Gao and Wedepohl, 1995). Next oldest to the Isua metasediments described here, chlorites in the 3.25 Ga Fig Tree Bien Venue Formation carry similar Eu anomalies (1.18 – 1.53) (Kohler and Anhaeusser, 2002), with other Fig Tree pelites carrying chondritic to slightly superchondritic ratios (0.96 - 1.02) (McLennan et al., 1983; Wildeman and Condie, 1973). Progressing to younger rocks,

Eu anomalies in the 3.2 Ga Moodies Group metasediments are slightly negative (0.88 – 0.90) (Hessler and Lowe, 2006; McLennan et al., 1983), while pronounced negative anomalies in the ~3.0 Ga Pongola (McLennan et al., 1983; Wronkiewicz and Condie, 1989) and ~2.8 Ga upper Witwatersrand (Wronkiewicz and Condie, 1987) Supergroups are ascribed to the weathering of intracratonic granites. In other respects, Isua aluminosiliciclastic REE distributions reported here are similar to those of Archaean shales from the Fig Tree, Moodies, Pongola and Witwatersrand Groups (compare dark-grey field, Fig. 7).

The absence of negative Eu anomalies, in quartzitic samples or elsewhere, implies little or no cratonization and active intracrustal differentiation in the hinterland provenance, thereby discounting appreciable contributions from intracratonic granites and/or rhyolites (McLennan, 1993). Common mantle-derived rocks such as MORB and island arc basalts generally lack Eu-anomalies, and therefore also cannot account for the observed anomalies.

The range of Eu-enriched candidate source rocks is restricted. Eu fractionation can be achieved, however, through plagioclase accumulation during differentiation or partial melting of plagioclase-rich fractions, and is held responsible for the variably positive anomalies (Eu*/Eu = 1.3 – 2.0) observed in several Isua and other Greenlandic granodiorites and tonalites (Nutman et al., 1999; Wedepohl et al., 1991). These values correspond well with those observed in our metasediments.

Positive Eu anomalies in Isua aluminous metasediments stand in marked contrast to felsic quartzo-feldspathic schists and garnet-mica schists from Isua, which exhibit pronounced negative Eu_{CN} anomalies (Bolhar et al., 2005a; Polat and Frei, 2005). Some workers have interpreted these schists as being of felsic volcanic origin (e.g. Allaart, 1976), although recent interpretations view them as deformed recrystallized pillow lavas and/or tectonically disrupted tonalitic sheets (Myers, 2001). Boulder- and matrix- like material from a purported conglomerate unit, controversially interpreted as derived from the erosion of acid volcanogenic sediment or of tuffaceous origin (Bridgwater and McGregor, 1974), also shows subchondritic Eu anomalies (Moorbath et al., 1975). Textural considerations, such as the notable scarcity of

feldspar, further suggest that the aluminous metasedimentary component was unrelated to Isua felsic rocks of ambiguous origin.

6. Provenance

Bulk conservative trace metal ratios, such as La-Th-Sc and Th-Sc-Zr/10 ternary discrimination diagrams (Fig. 13) (Bhatia and Crook, 1986), Zr/Ti-Nb/Y plots (Fig. 14) (Pearce and Cann, 1973) and La/Th-Hf plots (Fig. 15) (Floyd and Leveridge, 1987) are suggestive of an overall continental island arc provenance, with an intermediate (andesitic-dacitic) affinity.

Several lines of evidence argue against a single uniform intermediate extrusive volcanic source, however. Firstly, geochemical features which are said to typify early Archaean andesites, such as HREE- and Y- depletions, are conspicuously lacking, while relationships between Th, La, La/Yb, Zr/Y, Ti/V, Hf/Yb and Ti/Zr ratios are incompatible with all major recognized types of Precambrian andesites (Condie, 1989). Also absent are the slight negative Eu anomalies diagnostic of andesites of all ages. Secondly, the abundance and grain-size of zircons, and the well-graded laminae of coarse quartz grains in which they are enclosed, are characteristic features of many metasedimentary units that call for a felsic origin. The presence of primary positive Eu anomalies rule out the possibility of bimodal basaltic-rhyolitic volcanism, leaving a plutonic source as the most viable candidate source for a significant part of the aluminous fraction.

In an attempt to better constrain the aluminous metasediment source composition, element ratios built from permutations of Ce, Cr, Nb, Ni, Th, Ti and Yb concentrations, normalized to Upper Continental Crust ('UCC', Taylor and McLennan, 1985) were examined (Fig. 16). Elements were selected on the basis of (i) immobility during transport and post-depositional alteration; (ii) lack of susceptibility to marine chemical fractionation (La and Y) and sedimentary hydraulic sorting (Zr in zircon); (iii) reasonable agreement on their concentrations in the upper continental crust (e.g. Condie, 1993; Taylor and McLennan, 1985). Ni, despite its concentration in density-

sorted sulphides, was included because of its important role in previous Archaean provenance studies.

Metasediment trace-element ratios have quite limited variation and are minimally affected by BIF-derived signatures. The lack of systematic mineralogical or stratigraphical correlations suggests either a single homogeneous source or effective mixing of heterogeneous sources. With few exceptions, provenance ratios fall well outside the range exhibited by Isua boninites (light-grey field, Fig. 16), which dominate mafic outcrop in the surrounding terrain (Polat et al., 2002). Ratios show a more UCC-like signature, requiring a more sialic provenance to explain the aluminous fraction, as further testified by close correspondences to signatures from epi-continental Archaean shales elsewhere (for instance, compare with Witwatersrand shales, dark-grey field, Fig. 16). Although selected trace-element ratios in nearby TTGs (Nutman et al., 1999; Nutman et al., 1996) are variable, a 35%-65% averaged diorite-boninite or tonalite-boninite mixture fits our geochemical data well.

Cr and Ni concentrations and Cr/Ni ratios (~1.1) are low by Archaean standards, which can be ascribed to a paucity of komattiitic source material, in agreement with field evidence from Isua indicating few ultramafic rocks in the region. Thus, the more mafic contribution to the aluminous component is more likely to be derived from the boninitic basalts that make up a large part of the Isua stratigraphy.

Textural evidence (e.g. BIF and metachert clasts, coarse quartz, detrital zircons), trace element ratios (e.g. Th enrichment, Nb and Ti depletion) and REE systematics (e.g. persistent chondritic to slightly superchondritic Eu ratios throughout the succession) are most compatible with a well-mixed and well-weathered boninite-tonalite source supplemented with variably reworked Fe-Si chemical sediments. It is probable that bimodal mixing of a boninitic oceanic island arc component with a more evolved sialic, and possibly continental, chemically weathered plutonic source gave rise to the new Isua meta-sediments.

Grain-sizes and a correlation with sheet-silicate content indicate a distal source for detrital pyrites. The stability of pyrite in the Early Archaean detrital sediments

lends further credence to arguments favoring low fO_2 conditions early in Earth history (e.g. Rasmussen and Buick, 1999).

7. Discussion

A turbiditic depositional setting is indicated by the abundant grading in coarser-grained units, the cyclicity from coarse to fine grain-sizes within depositional packages, the argillaceous matrix present in most rudaceous and arenaceous facies, the possible presence of cross-lamination in some meta-greywackes, and the thick meta-pelite units probably representing hemi-pelagites capping graded depositional packages. This supports similar deep-water depositional environments inferred for metasediments elsewhere at Isua (Rosing, 1999).

The metasediments apparently reflect a well-weathered mixed source containing both mafic (boninitic) and felsic (tonalitic) igneous rocks and precipitated ferruginous-siliceous sediments (BIF). The abundance of coarse mono-crystalline quartz suggests that the felsic igneous component may be attributable to a plutonic source. Collectively this provenance resembles younger Archean granite-greenstone terrains, which would imply the pre-existence of continental crust, as the voluminous emplacement of granitoids into greenstone successions renders the crust cool, buoyant and rigid, the functional definition of continental crust (Buick et al., 1995). In contrast, the occurrence of boninitic rocks amongst the Isua volcanics has previously been used to deduce a intra-oceanic subduction zone setting (Polat et al., 2003). This interpretation was strengthened by the recent discovery of a fragmented ophiolite-like succession (Furnes et al., 2007). However, the lithologies (e.g. coarse quartz arenites) and derived detrital components (e.g. abundant zircons) described herein are atypical of such settings. Determining the crystallization ages of these zircons could be very informative, as a broad spectrum of dates significantly older than the depositional age of their host sediment would also imply a continental origin. If so, the Isua supracrustal belt may record distinct tectonic environments for its meta-igneous and meta-sedimentary components and so may represent a structural aggregation of terrains or an unconformity-bounded juxtaposition of stratigraphic successions of differing age and

origin, like some younger Archean supracrustal belts. In either case, the presence of a continental provenance for part of the sedimentary detritus would have profound implications for Earth's tectonic evolution, as previous evidence for >3.5 billion year old continental crust comes only from the survival of a wide age spectrum of >4.0 Ga zircons in detrital metasediments from Jack Hills, Mt. Narryer and Diemals in western Australia (e.g. Harrison et al., 2005; Hopkins et al., 2008; Maas et al., 1992; Wyche et al., 2004). If continental crust was also extant in another part of the world very early in Earth's history, then it is quite likely that its volume was not vanishingly small, as postulated in some crustal evolutionary models (e.g. Collerson and Kamber, 1999; Taylor and McLennan, 1995), and was perhaps closer to modern levels, as proposed in others (e.g. Armstrong, 1991; Bowring and Housh, 1995; Green et al., 2000).

Preliminary U-Pb dating on three samples has revealed individual zircon ages of 3704 ± 3 Ma, 3713 ± 2 Ma and 3817 ± 4 Ma (Harnmeijer et al., in prep.), compatible with the conclusions based on geological and geochemical evidence reported here.

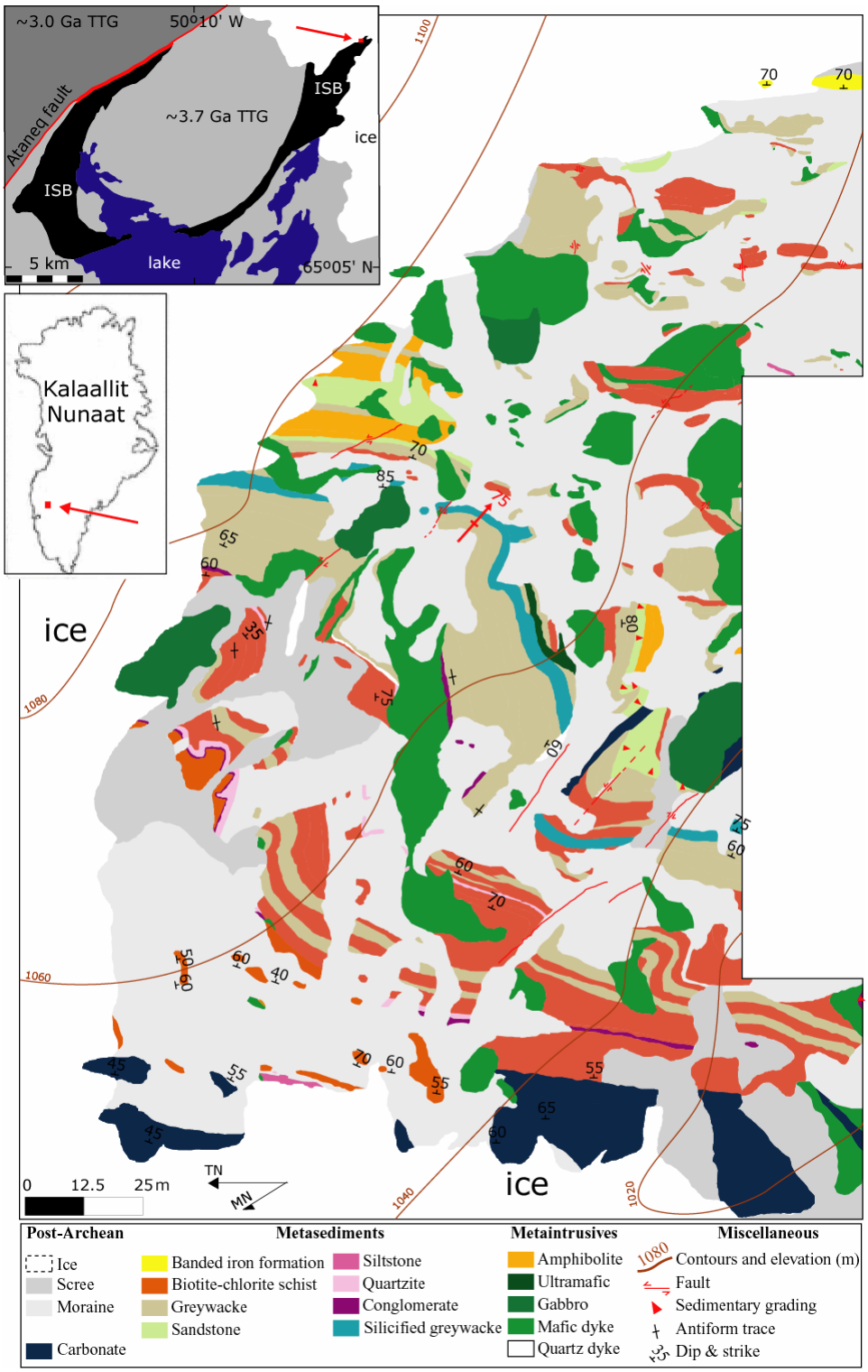

Figure 1: Geological map of meta-turbidite outcrop, with insets showing location and regional geology, with meta-turbidite locality marked by red arrows and squares; TTG=Tonalite Trondjemite Gneiss complex (After Frei et al., 2002; Myers, 2001).

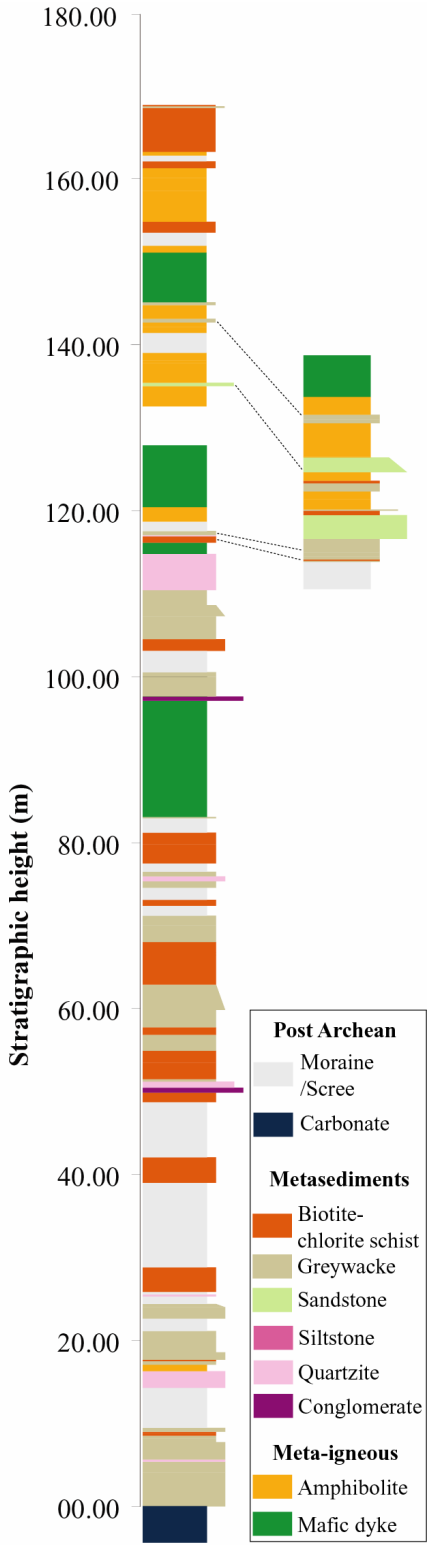

Figure 2: Stratigraphic section. A section obliterated by a cross-cutting dyke was mapped in parallel: marker beds are joined by tie-lines in figure.

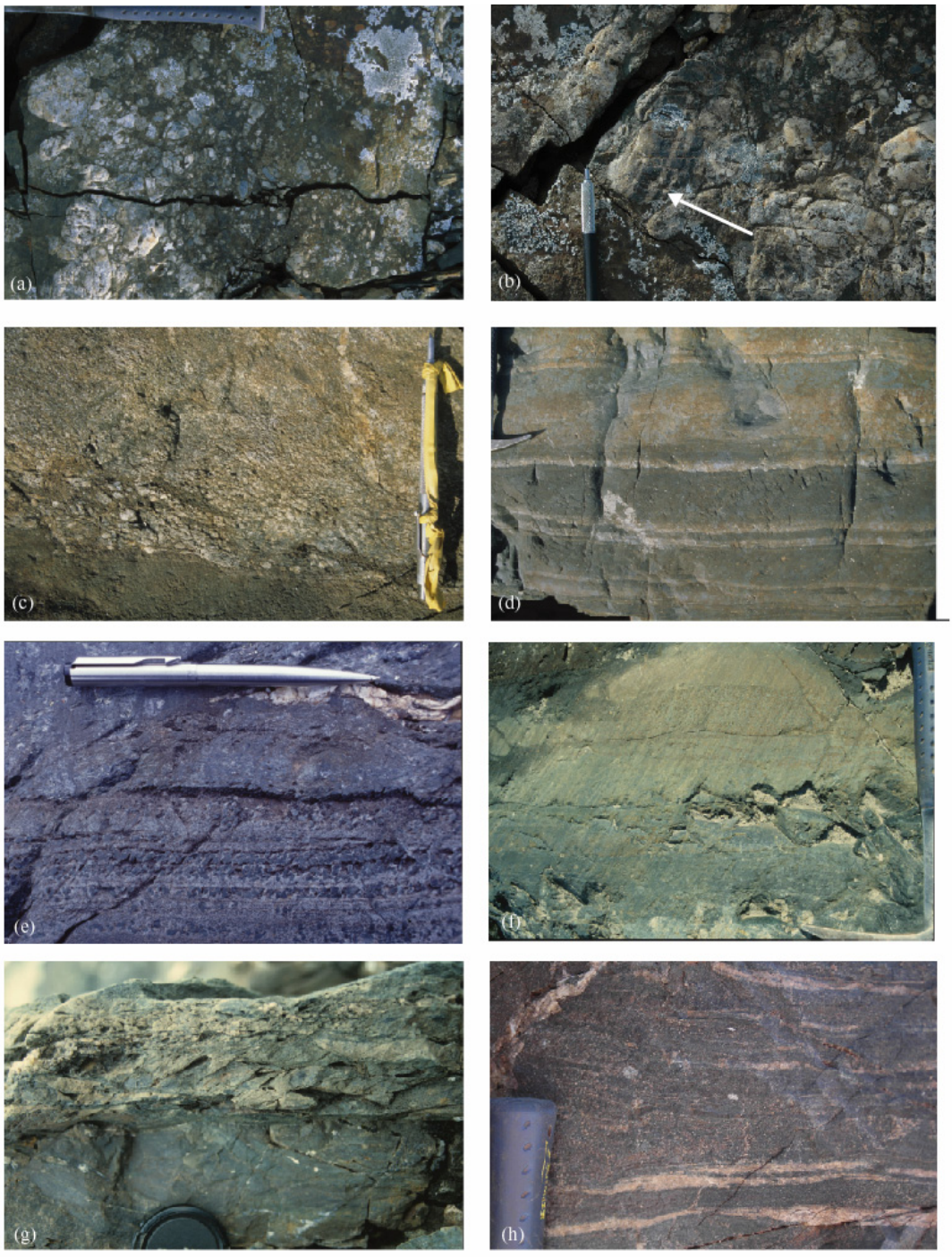

Figure 3: Meta-sediment outcrop photos. (a, b): Polymictic metaconglomerate with layered magnetite/quartz clasts. (c): Graded gravelly metaquartzite. (d): Undulose laminated meta-greywacke, (e): Pinnitized cordierite porphyroblasts define layers plane-parallel to sedimentary bedding - note steep overprinting fabric. (f): Coarse- and fine- grained beds in pelitic meta-sandstone. (g): Possible ripple cross-lamination in meta-siltstone. (h): Truncated bedding in gritty sandstone.

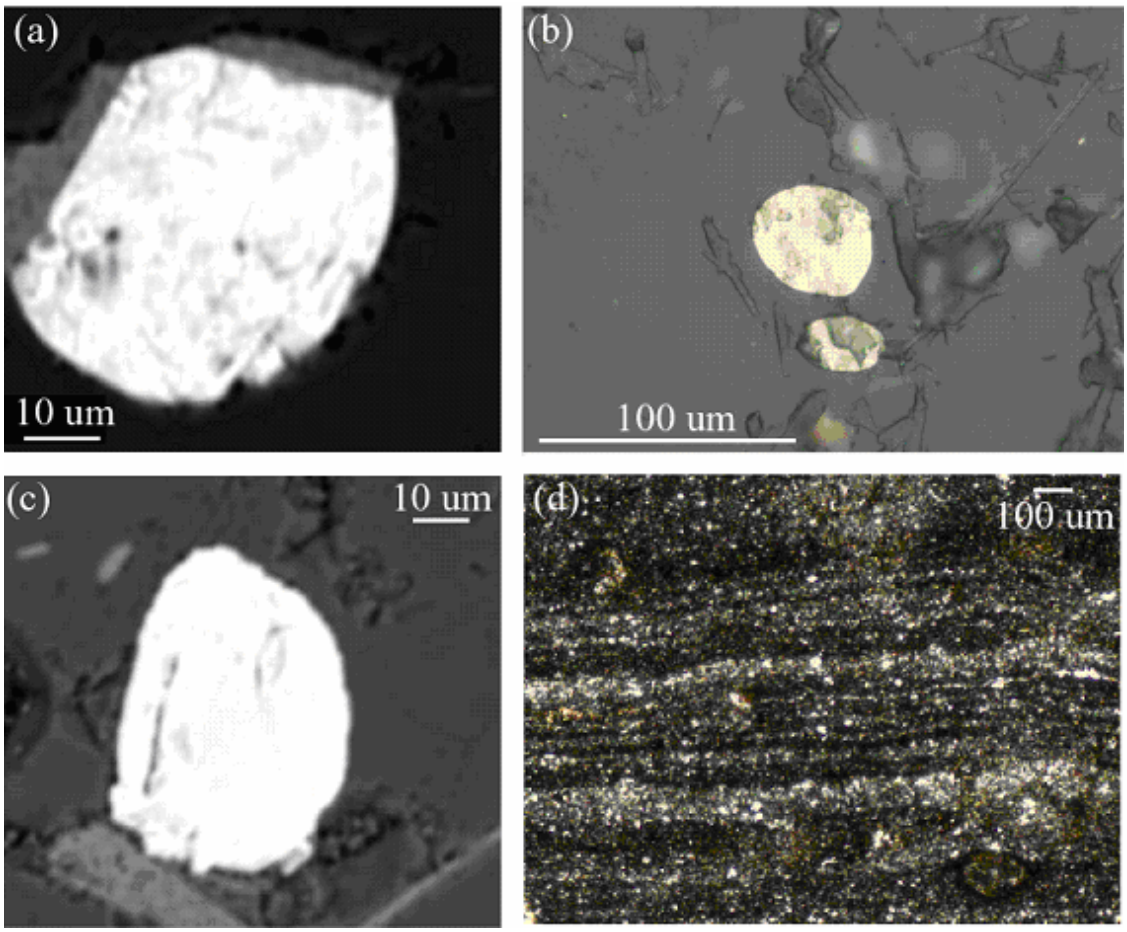

Figure 4: Photomicrographs. (a): Back-scattered electron photograph of a detrital pyrite with chlorite rim. (b): Reflected light photomicrograph of detrital pyrite grains. (c): Back-scattered electron image of a detrital zircon. (d): Plane-polarized photomicrograph showing undulose fine quartz/biotite-chlorite lamination.

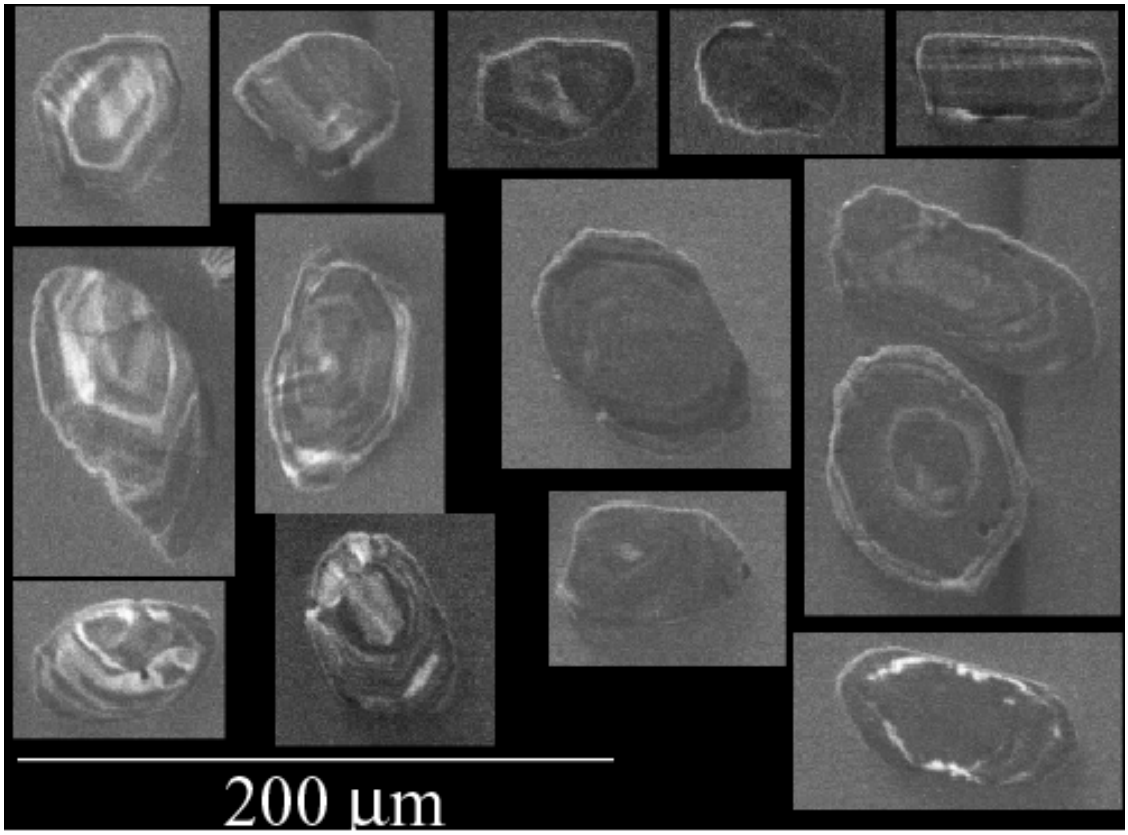

Figure 5: Cathode luminescence photographs of selected fine zircon size-fraction separates.

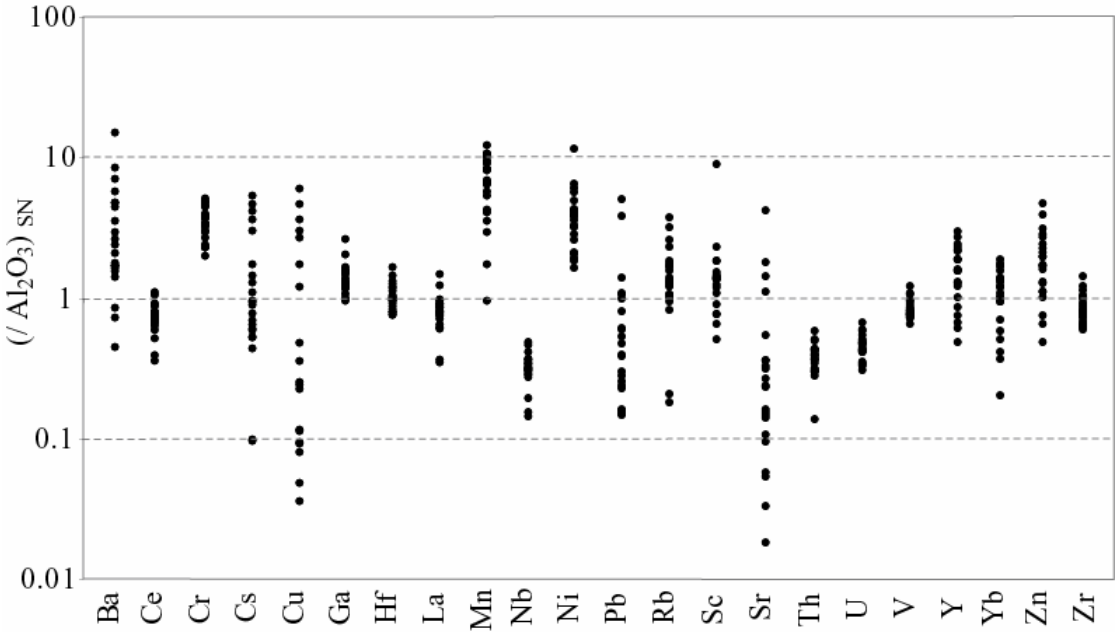

Figure 6: Shale- and Al_2O_3- normalized trace-element concentrations.

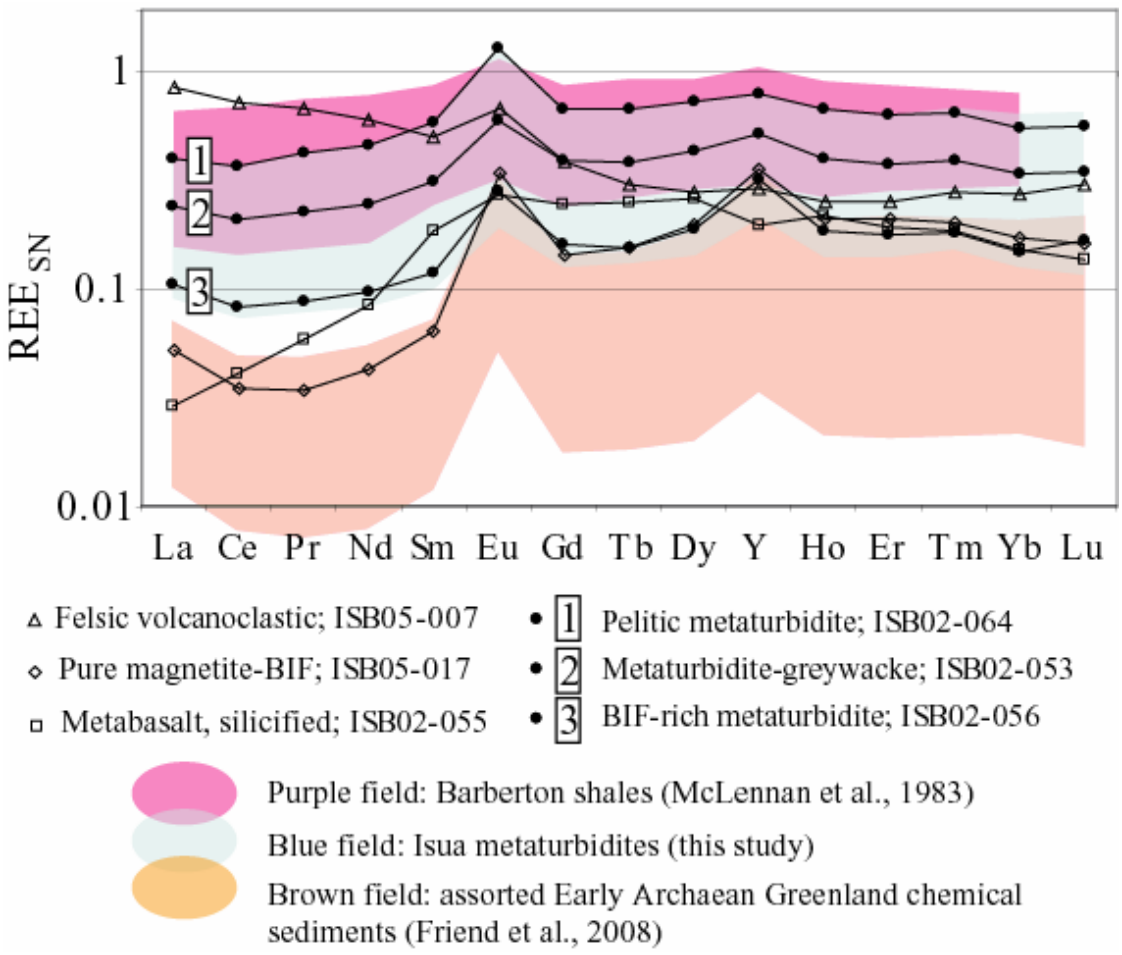

Figure 7: Shale-normalized REE concentrations.

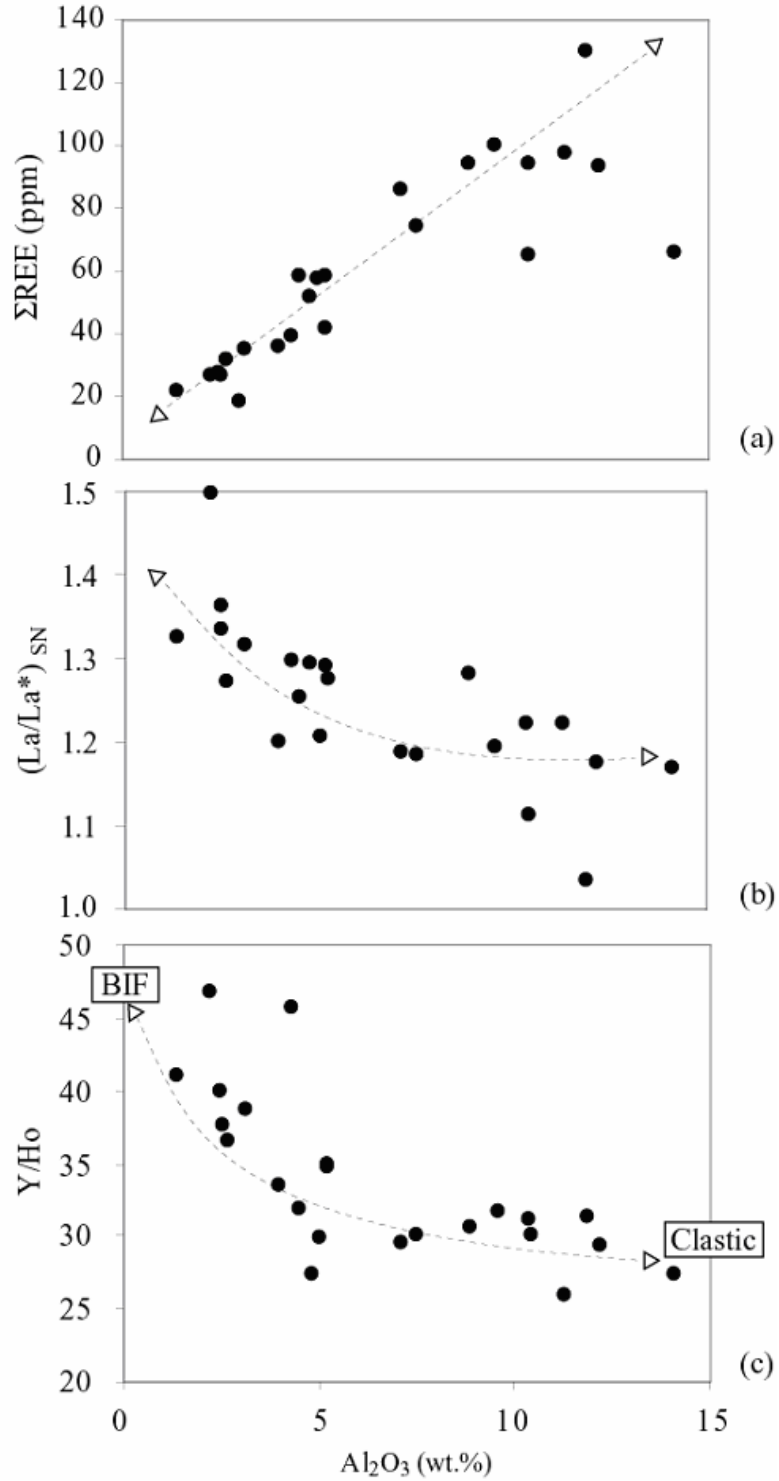

Figure 8: (a): Total REE, (b): La/La*, and (c): Y/Ho ratios plotted versus Al_2O_3. Also shown is a hypothetical mixing curve constructed between BIF-like (Y/Ho = 46, Y = 6 ppm, no Al_2O_3) and pelitic (Y/Ho = 27, Y = 25 ppm, Al_2O_3 = 15 wt.%) endmembers. The curve does not account for silica dilution effects.

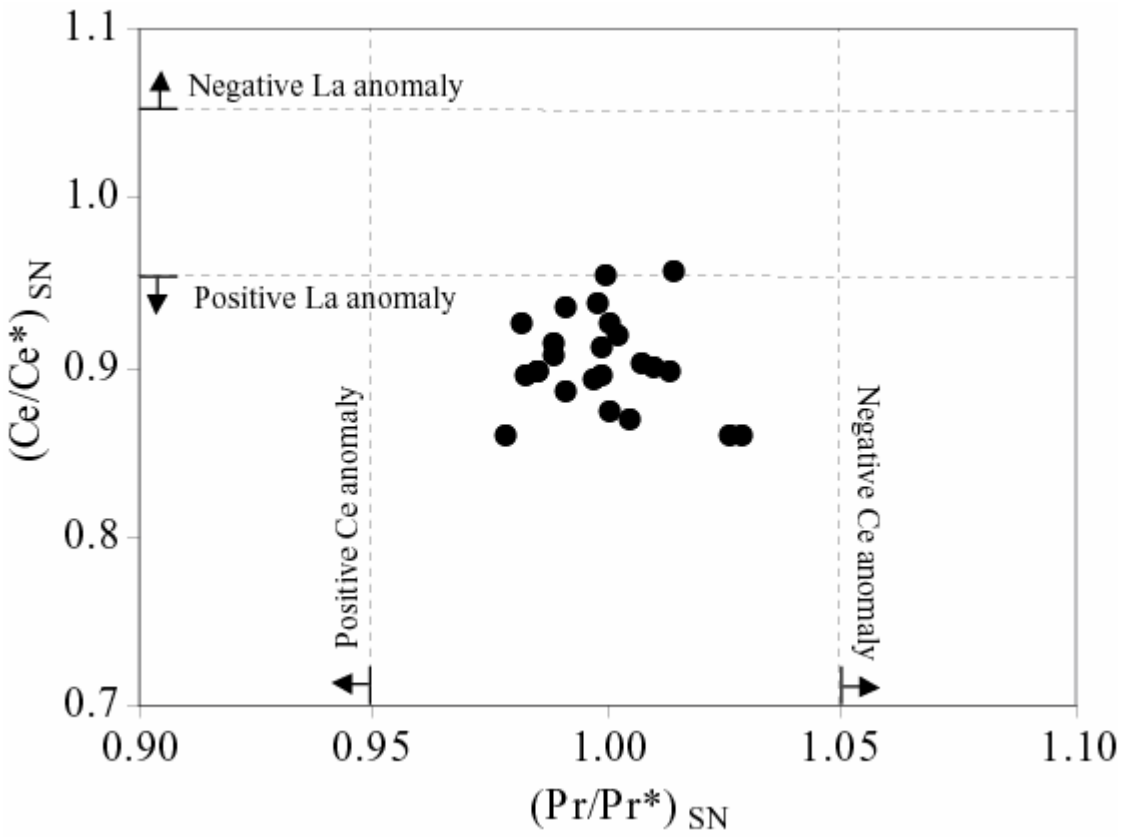

Figure 9: Ce/Ce* versus Pr/Pr* diagram (after Bau and Dulski, 1996).

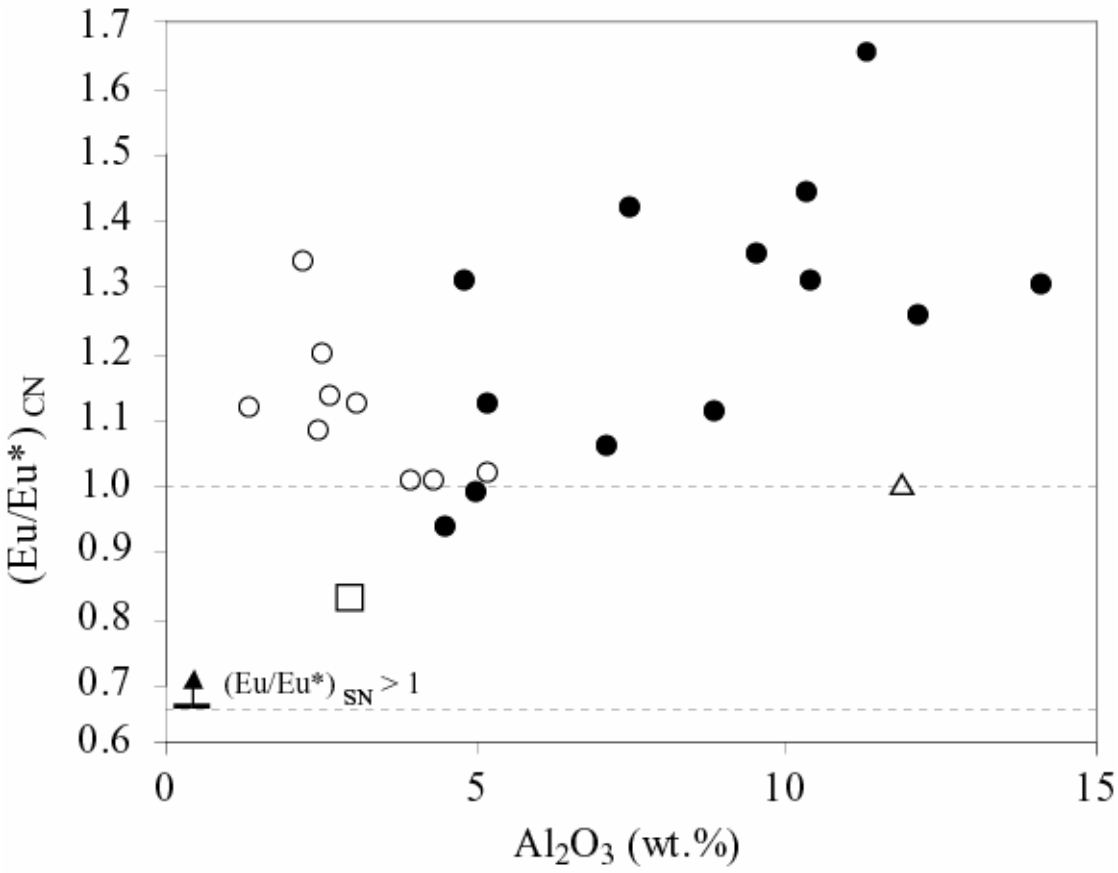

Figure 10: Eu/Eu* versus Al_2O_3. Open/closed circles denote sample with/out magnetite laminae. Other symbols as in Figure 7.

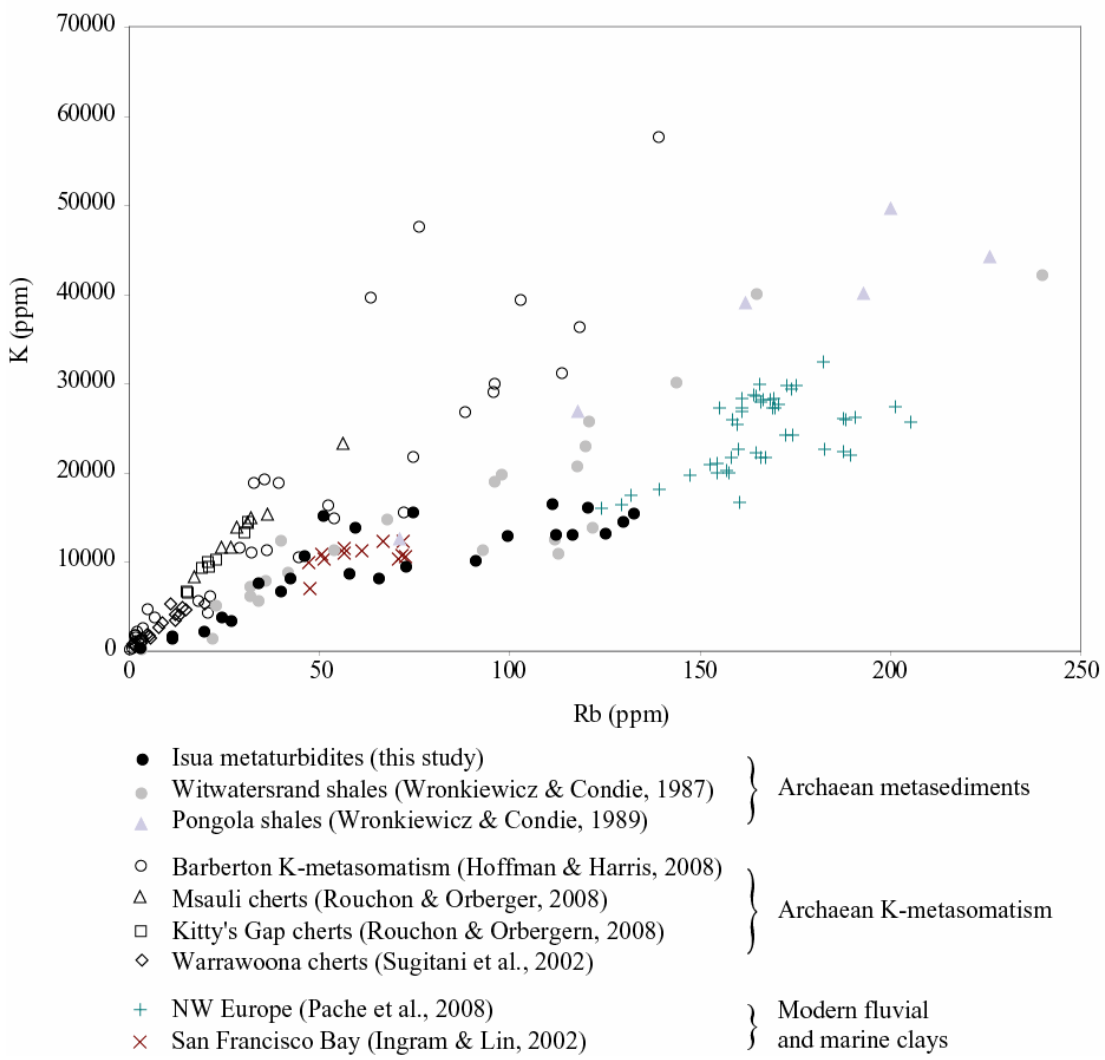

Figure 11: K versus Rb concentrations compared for selected clays, Archaean metasediments, and Archaean metasomatized rocks.

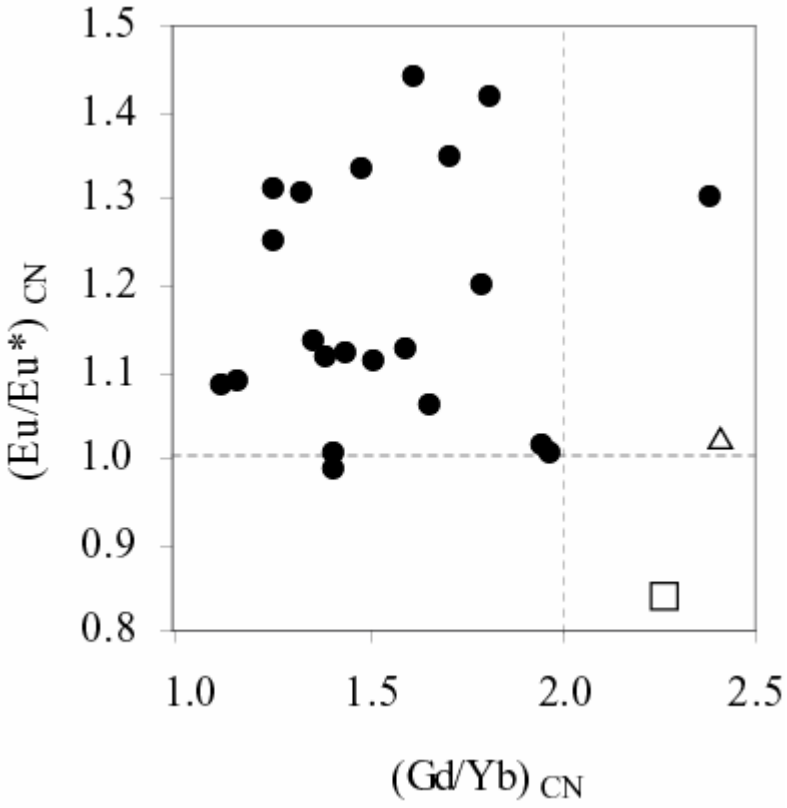

Figure 12: Chondrite-normalized Eu/Eu* versus Gd/Yb diagram.

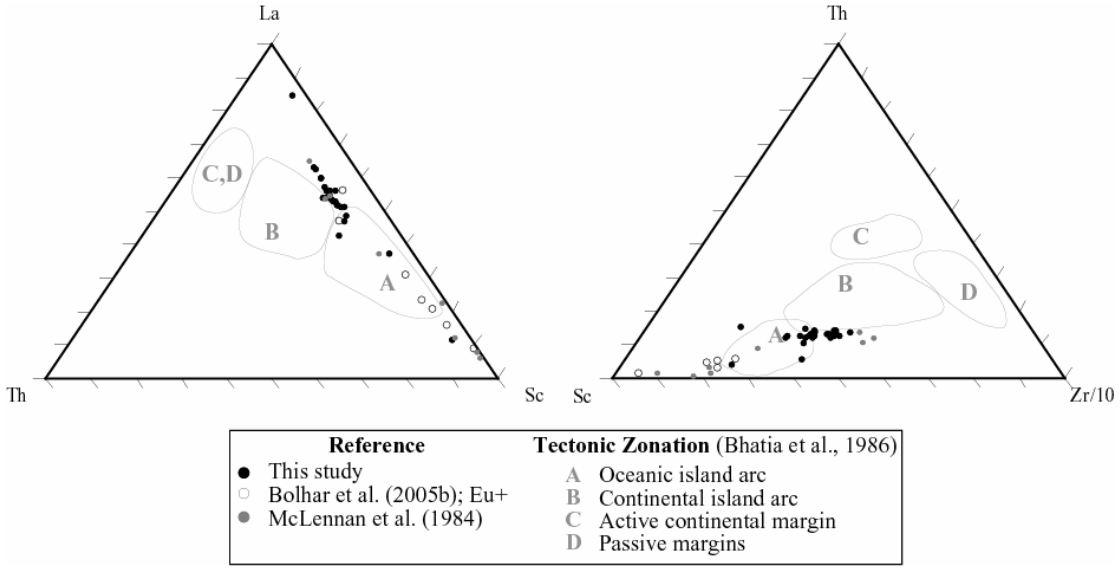

Figure 13: Ternary La-Sc-Th and Th-Zr/10-Sc discrimination diagrams (Bhatia and Crook, 1986) comparing new Isua metasediments with previous studies (Bolhar et al., 2005; McLennan et al., 1984).

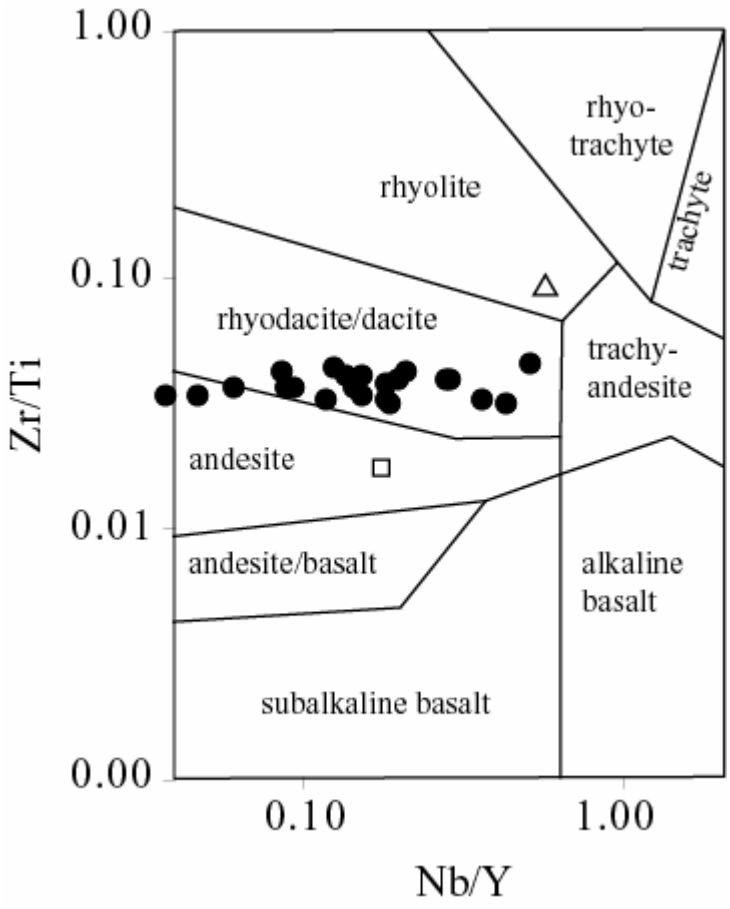

Figure 14: Zr/Ti – Nb/Y tectonic discrimination diagram. Symbols as in Figure 7.

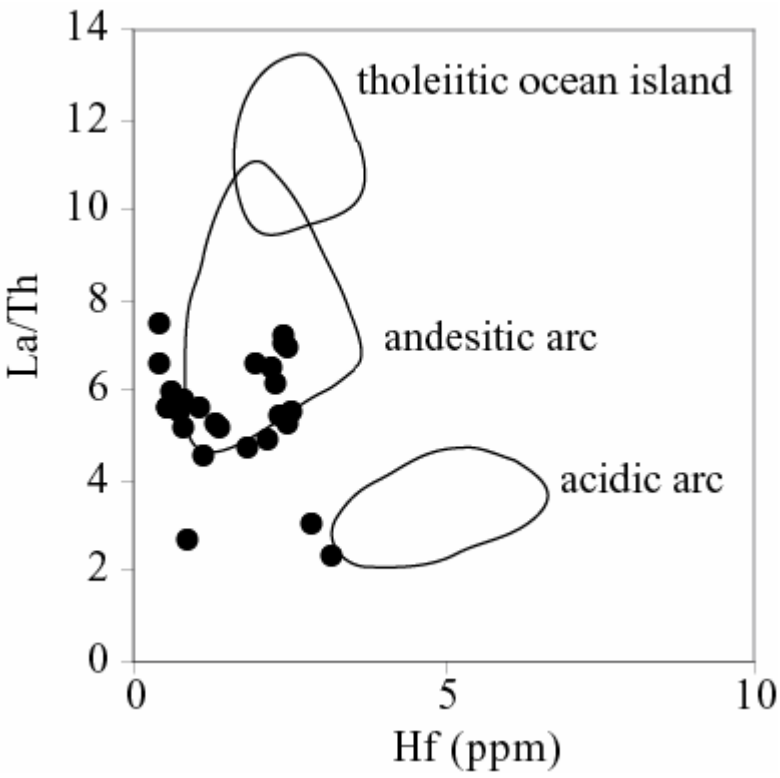

Figure 15: La/Th – Hf igneous provenance diagram.

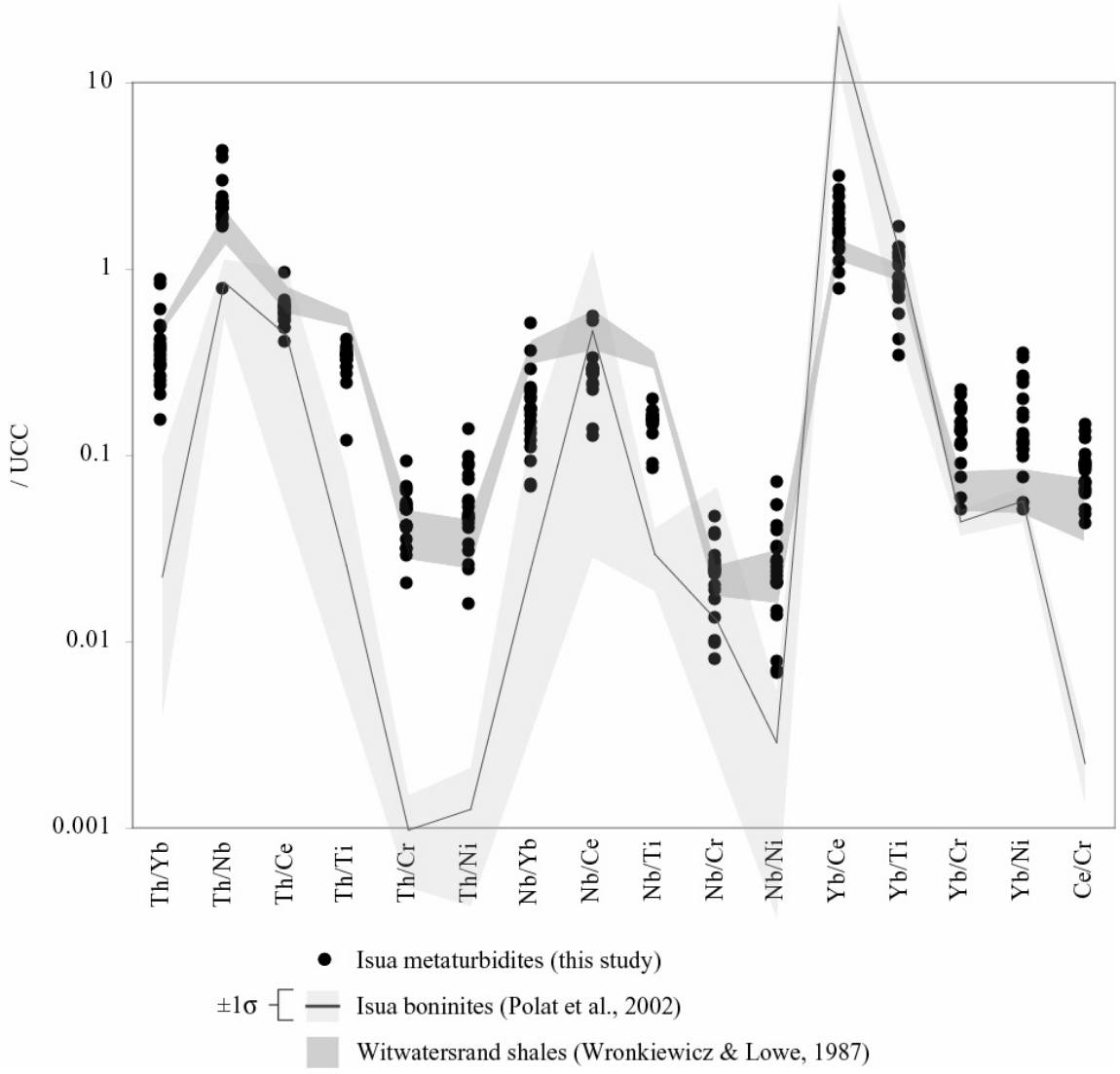

Figure 16: PAAS-normalized trace-element ratios (Barbera et al., 2009) comparing new metasediments to Isua boninites (light grey, Polat et al., 2002) and Witwatersrand shales (dark grey, Wronkiewicz and Condie, 1987). The latter is constructed from combined averages from the Parktown-Brixton, Promise Roodepoort, Booysens and K8 groups.

Table 1: Geochemical data.

	GROUP:	Sericitize wavy qtzite	Amph.	Meta-ma (tuff?)	Meta-turbidites								
	ID:	05-007	02-054	02-055	02-053	02-058A	02-058C	02-060	02-061	02-062	02-064	05-003	05-009A	05-010
Major Element Oxides	**SiO2**	72.64	72.80	78.77	60.14	70.08	84.05	77.96	64.28	67.61	68.98	73.28	75.44	63.70
	TiO2	0.177	0.259	0.284	0.192	0.209	0.113	0.118	0.387	0.398	0.392	0.098	0.328	0.516
	Al2O3	11.90	4.52	2.97	5.19	5.22	2.51	2.66	8.86	10.37	9.57	2.46	7.51	14.11
	FeO*	5.69	14.23	7.68	21.77	15.22	5.31	6.67	18.42	13.88	14.07	12.60	10.85	11.37
	MnO	0.036	0.111	0.257	0.314	0.106	0.059	0.099	0.418	0.340	0.497	0.149	0.293	0.078
	MgO	1.84	1.11	2.04	1.34	1.75	0.72	0.85	1.38	1.22	1.35	0.99	1.05	1.38
	CaO	0.35	0.48	2.08	0.70	0.40	2.49	4.31	0.62	0.28	0.37	3.46	0.33	0.15
	Na2O	3.43	0.01	0.11	0.10	0.02	-0.01	-0.01	-0.01	1.74	1.14	0.08	0.84	4.49
	K2O	1.28	1.93	1.57	1.97	1.03	0.26	0.40	1.56	1.21	0.97	0.90	0.19	0.45
	P2O5	0.056	0.053	0.031	0.045	0.041	0.023	0.024	0.085	0.061	0.055	0.023	0.053	0.063
	L.O.I.	1.58										4.15	1.63	1.97
Rare Earth Elements	**La**	31.45	13.18	1.09	9.01	7.98	4.51	5.05	13.07	14.63	15.09	3.72	11.82	9.78
	Ce	57.07	20.37	3.29	16.71	14.40	8.08	9.47	24.96	28.24	29.22	6.74	23.41	20.42
	Pr	5.93	2.90	0.52	2.00	1.72	0.95	1.13	3.15	3.47	3.70	0.8	2.9	2.56
	Nd	19.19	11.23	2.67	7.82	6.65	3.75	4.40	12.71	13.67	14.64	3.14	11.44	10.28
	Sm	2.77	2.21	1.03	1.75	1.33	0.76	0.91	2.83	2.95	3.20	0.71	2.42	2.25
	Eu	0.74	0.62	0.30	0.65	0.41	0.30	0.33	1.11	1.41	1.40	0.26	1.09	0.95
	Gd	1.79	1.84	1.15	1.80	1.13	0.75	0.88	3.28	3.02	3.15	0.76	2.28	2.22
	Tb	0.23	0.22	0.19	0.29	0.15	0.11	0.14	0.55	0.49	0.51	0.13	0.36	0.39
	Dy	1.22	0.91	1.14	1.87	0.82	0.72	0.84	3.50	2.95	3.15	0.9	2.23	2.38
	Y	7.82	4.24	5.31	13.69	5.58	5.58	7.10	23.62	19.21	21.10	8.39	13.54	12.06
	Ho	0.25	0.13	0.22	0.39	0.16	0.15	0.19	0.77	0.62	0.67	0.21	0.45	0.44
	Er	0.73	0.27	0.55	1.07	0.42	0.40	0.58	2.11	1.72	1.80	0.62	1.23	1.04
	Tm	0.11	0.04	0.07	0.15	0.06	0.06	0.08	0.29	0.25	0.25	0.09	0.17	0.13
	Yb	0.76	0.28	0.42	0.93	0.39	0.35	0.53	1.79	1.54	1.52	0.56	1.04	0.77
	Lu	0.13	0.05	0.06	0.15	0.06	0.05	0.09	0.28	0.25	0.24	0.09	0.16	0.13
Transition Metal Elements	**Sc**	3.2	6.9	8.4	5.9	5.4	3.0	3.1	10.4	10.3	10.8	2.8	7.8	10.2
	V	12.3	33.2	66.3	34.9	32.7	15.0	16.0	56.1	61.6	62.7	13.8	47.6	72.2
	Cr	26.5	117.3	70.7	112.0	120.3	49.1	56.2	163.1	177.9	179.7	52.4	145.9	163.4
	Ni	13.5	33.9	28.4	73.9	63.4	29.5	29.3	83.1	106.9	117.2	14.5	82.4	67.0
	Cu	0.0	0.1	18.0	16.4	1.1	0.6	0.0	5.6	1.3	0.9	17.2	4.4	3.5
	Ga	17.6	7.3	6.1	6.5	7.2	3.6	5.6	11.7	13.2	12.6	3.0	9.9	14.7
	Zn	27.8	39.9	23.3	52.3	45.2	19.2	20.1	43.9	34.3	42.6	29.8	37.4	40.7
	As		9.2	0.0	9.7	6.2	6.7	8.0	3.0	6.4	13.0			
	Bi		3.5	3.8	5.0	6.6	3.8	4.0	5.4	6.3	5.5			
Strongly Lithophile High Field Streng	**Cs**	1.39	6.09	8.65	14.79	5.21	1.18	2.31	6.17	4.28	3.29	5.83	0.58	1.07
	Pb	14.07	1.31	2.02	1.61	0.82	13.17	2.92	12.99	2.79	4.74	2.77	1.87	2.16
	Zr	97	71	29	46	49	27	30	75	79	85	21	76	98
	Hf	3.23	1.97	0.91	1.37	1.40	0.77	0.84	2.25	2.36	2.52	0.61	2.18	2.92
	Nb	4.46	2.18	0.96	1.88	1.60	0.86	0.90	2.79	2.99	3.07	0.75	2.69	4.45
	Ta	0.41	0.17	0.07	0.16	0.12	0.07	0.06	0.22	0.24	0.25	0.06	0.22	0.31
	Th	14	1.99	0.41	1.71	1.54	0.83	0.88	2.02	2.71	2.87	0.67	2.42	3.23
	U	7.32	0.43	0.08	0.40	0.36	0.20	0.20	0.49	0.55	0.68	0.19	0.66	0.78
	Rb	46.3	120.6	125.4	111.4	58.0	19.8	27.1	116.5	91.0	65.8	34.2	11.4	24.4
	Sr	88	5.1	11	13	8	29	50	3.1	35.6	14.7	37	21	46
	Ba	802	726	6505	1020	795	72	321	540	494	547	396	114	349

Table 1: Geochemical data (cont'd).

	GROUP:									Magnetite-rich samples				BIF	BIF
	ID:	05-012A	05-013	05-019	05-020	05-025	05-027	05/003 ®	05/19 ®	02-056	02-058B	02-065	05-005	05-017	05-017QD
Major Element Oxides	**SiO2**	81.98	79.18	57.01	68.92	72.17	60.07			50.56	58.16	55.23	48.25	34.36	34.36
	TiO2	0.067	0.269	0.433	0.451	0.361	0.430			0.077	0.131	0.165	0.108	0.013	0.013
	Al2O3	1.38	5.02	11.30	12.17	7.14	10.42			2.24	4.32	3.98	3.10	0.22	0.22
	FeO*	3.20	9.72	20.17	7.67	13.65	18.95			36.33	26.69	29.96	39.60	57.54	57.54
	MnO	0.081	0.155	0.113	0.207	0.436	0.394			0.123	0.206	0.277	0.123	0.049	0.049
	MgO	0.43	1.11	2.15	1.18	1.29	1.94			1.35	1.23	1.65	1.48	1.32	1.32
	CaO	6.69	0.55	0.14	0.30	0.56	0.24			0.58	0.24	0.13	0.24	0.81	0.81
	Na2O	0.00	0.01	0.36	4.40	0.01	0.00			0.13	0.00	0.02	0.26	0.02	0.02
	K2O	0.16	1.14	1.85	1.74	1.54	1.56			0.80	1.66	1.82	0.97	0.03	0.03
	P2O5	0.012	0.057	0.078	0.077	0.074	0.077			0.044	0.045	0.055	0.047	0.055	0.055
	L.O.I.	5.84	1.34	2.61	1.21	1.39	2.97						2.21	-1.38	
Rare Earth Elements	**La**	3.4	9.1	18.43	14.52	14.02	7.61	3.68	18.49	3.98	5.33	6.73	5.21	1.99	
	Ce	5.91	18.18	34.33	29.03	26.58	16.46	6.66	34.31	6.62	9.14	12.59	9.06	2.8	
	Pr	0.69	2.20	4.59	3.58	3.32	2.06	0.79	4.57	0.78	1.09	1.53	1.09	0.31	
	Nd	2.64	8.69	18.4	14.1	12.9	8.2	3.1	18.2	3.09	4.16	5.90	4.21	1.39	
	Sm	0.56	1.83	3.97	3	2.69	2.00	0.69	3.94	0.66	0.93	1.21	0.94	0.36	
	Eu	0.21	0.56	2.07	1.17	0.9	0.93	0.26	2.04	0.31	0.34	0.36	0.37	0.37	
	Gd	0.59	1.64	3.64	2.72	2.51	2.37	0.77	3.67	0.75	1.14	0.98	1.08	0.67	
	Tb	0.1	0.27	0.48	0	0.41	0.44	0.13	0.49	0.12	0.20	0.14	0.18	0.12	
	Dy	0.62	1.7	2.15	2.68	2.55	2.82	0.91	2.11	0.83	1.32	0.75	1.18	0.87	
	Y	5.75	11.05	7.8	17	15.96	17.7	8.39	7.89	8.57	13.38	4.80	10.07	9.58	
	Ho	0.14	0.37	0.3	0.59	0.54	0.59	0.21	0.29	0.18	0.29	0.14	0.26	0.21	
	Er	0.40	1.03	0.55	1.76	1.45	1.64	0.62	0.57	0.52	0.83	0.39	0.73	0.61	
	Tm	0.06	0.16	0.06	0.27	0.2	0.23	0.09	0.06	0.07	0.12	0.06	0.1	0.08	
	Yb	0.35	0.96	0.34	1.79	1.25	1.48	0.55	0.37	0.42	0.67	0.41	0.62	0.48	
	Lu	0.05	0.16	0.06	0.28	0.20	0.23	0.09	0.06	0.07	0.11	0.08	0.1	0.07	
Transition Metal Elements	**Sc**	1.8	5.9	8.5	11	8.8	11.8	2.9	8.4	2.6	4.7	4.9	3.1	0.3	
	V	7.9	30.4	68.4	69.3	43.0	68.0	2.9	3.4	17.1	35.5	33.9	29.4	3.4	
	Cr	26.6	69.3	148.6	159.4	110.8	176.4	1.7	1.5	56.8	117.6	112.9	69.8	1.54	
	Ni	12.6	26.4	106.6	67.7	43.4	85.7	26.2	17.1	39.0	48.7	73.5	50.1	17.1	
	Cu	0.0	1.5	3.3	8.1	9.0	9.6	13.3	14.3	10.2	33.7	48.9	29.1	14.3	
	Ga	2.3	5.6	15.4	12.2	8.8	13.5	0.6	3.4	6.1	6.7	6.9	4.9	3.4	
	Zn	10.2	36.0	63.9	26.5	41.2	98.1	68.1	61.6	28.2	46.4	70.0	42.4	61.6	
	As									16.3	14.3	11.4			
	Bi									4.4	4.9	5.1			
Strongly Lithophile High Field Streng	**Cs**	0.57	3.70	6.88	5.62	5.30	5.63	5.80	6.87	8.17	4.89	2.01	10.21	0.54	
	Pb	5.57	1.19	1.87	2.07	2.86	8.83	2.77	1.86	2.32	1.80	2.24	1.94	1.65	
	Zr	17	67	82	85	82	84	21	82	15	28	39	22	1	
	Hf	0.47	1.89	2.47	2.55	2.34	2.51	0.61	2.46	0.44	0.85	1.08	0.65	0.04	
	Nb	0.51	2.33	3.39	3.29	2.92	3.3	0.75	3.42	0.32	0.84	1.34	0.48	0.04	
	Ta	0.04	0.19	0.27	0.26	0.23	0.25	0.06	0.27	0.04	0.08	0.10	0.06	0	
	Th	0.52	1.94	2.57	2.62	2.28	1.10	0.66	2.65	0.53	1.04	1.20	0.88	0.07	
	U	0.15	0.49	0.64	0.82	0.59	0.71	0.18	0.64	0.11	0.32	0.28	0.21	0.02	
	Rb	11.6	73	132.9	130.1	99.7	112.4	34.4	133.8	40.1	59.5	51.2	42.4	3	
	Sr	61	5	28	70	4	2	38	28	8.4	7.3	2.4	5	4	
	Ba	98	498	624	696	586	550	391	623	1142	387	228	901	8	

References

Alibo, D.S., Nozaki, Y., 1999. Rare earth elements in seawater: Particle association, shale-normalization, and Ce oxidation. Geochim. Cosmochim. Acta 63(3-4), 363-372.

Allaart, J.H., 1976. The pre-3760 m.y. old supracrustal rocks of the Isua area, central West Greenland, and the associated occurrence fo quartz-banded ironstone, in: The Early History of the Earth, B.F. Windley, ed., Wiley, London, pp. 177-189.

Appel, P.W.U., Fedo, C.M., Moorbath, S., Myers, J.S., 1998. Recognizable primary volcanic and sedimentary features in a low-strain domain of the highly deformed, oldest known (~3.7-3.8 Gyr) greenstone belt, Isua, Greenland. Terra Nova 10(2), 57-62.

Armstrong, R.L., 1991. The persistent myth of crustal growth. Aus. J. of Earth Sci. 38, 613-630.

Barbera, G., Lo Giudice, A., Mazzoleni, P., Pappalardo, A., 2009. Combined statistical and petrological analysis of provenance and diagenetic history of mudrocks: Application to Alpine Tethydes shales (Sicily, Italy). Sediment Geol 213, 27-40.

Bau, M., Moller, P., 1993. Rare-Earth Element Systematics of the Chemically Precipitated Component in Early Precambrian Iron Formations and the Evolution of the Terrestrial Atmosphere-Hydrosphere-Lithosphere System. Geochim. Cosmochim. Acta 57(10), 2239-2249.

Bau, M., 1996. Controls on the fractionation of isovalent trace elements in magmatic and aqueous systems: Evidence from Y/Ho, Zr/Hf, and lanthanide tetrad effect. Contrib. Mineral. Petrol. 123(3), 323-333.

Bau, M., Dulski, P., 1996. Distribution of yttrium and rare-earth elements in the Penge and Kuruman iron-formations, Transvaal Supergroup, South Africa. Precamb. Res. 79(1-2), 37-55.

Bau, M., Dulski, P., 1999. Comparing yttrium and rare earths in hydrothermal fluids from the Mid-Atlantic Ridge: implications for Y and REE behaviour during

near-vent mixing and for the Y/Ho ratio of Proterozoic seawater. Chem. Geol. 155(1-2), 77-90.

Bhatia, M.R., Crook, K.A.W., 1986. Trace-Element Characteristics of Graywackes and Tectonic Setting Discrimination of Sedimentary Basins. Contrib. Mineral. Petrol. 92(2), 181-193.

Blichert-Toft, J., Albarede, F., Rosing, M., Frei, R., Bridgwater, D., 1999. The Nd and Hf isotopic evolution of the mantle through the Archean. Results from the Isua supracrustals, West Greenland, and from the Birimian terranes of West Africa. Geochim. Cosmochim. Acta 63(22), 3901-3914.

Boak, J.L., Dymek, R.F., 1982. Metamorphism of the Ca-3800 Ma Supracrustal Rocks at Isua, West Greenland - Implications for Early Archean Crustal Evolution. Earth Planet. Sci. Lett. 59(1), 155-176.

Bolhar, R., Kamber, B.S., Moorbath, S., Fedo, C.M., Whitehouse, M.J., 2004. Characterisation of early Archaean chemical sediments by trace element signatures. Earth Planet. Sci. Lett. 222(1), 43-60.

Bolhar, R., Kamber, B.S., Moorbath, S., Whitehouse, M.J., Collerson, K.D., 2005a. Chemical characterization of earth's most ancient clastic metasediments from the Isua Greenstone Belt, southern West Greenland. Geochim. Cosmochim. Acta 69(6), 1555-1573.

Bolhar, R., Van Kranendonk, M.J., Kamber, B.S., 2005b. A trace element study of siderite-jasper banded iron formation in the 3.45 Ga Warrawoona Group, Pilbara Craton - Formation from hydrothermal fluids and shallow seawater. Precamb. Res. 137(1-2), 93-114.

Bowring, S.A., Housh, T., 1995. The Earth's early evolution. Science 269(15 September), 1535-1540.

Boyet, M., Blichert-Toft, J., Rosing, M., Storey, M., Telouk, P., Albarede, F., 2003. 142Nd evidence for early Earth differentiation. Earth Planet. Sci. Lett. 214, 427-442.

Bridgwater, D., McGregor, V.R., 1974. Field work on the very early Precambrian rocks of the Isua area, southern West Greenland. Rapp. Grønlands Geol. Unders 65., 49–53.

Buick, R., Thornett, J.R., McNaughton, N.J., Smith, J.B., Barley, M.E., Savage, M., 1995. Record of emergent continental crust ~3.5 billion years ago in the Pilbara Craton of Australia. Nature 375(15 June), 574-577.

Cates, N.L., Mojzsis, S.J., 2007. Pre-3750 Ma supracrustal rocks from the Nuvvuagittuq supracrustal belt, northern Quebec. Earth Planet. Sci. Lett. 255(1-2), 9-21.

Collerson, K.D., Kamber, B.S., 1999. Evolution of the continents and the atmosphere inferred from Th-U-Nb systematics of the depleted mantle. Science 283, 1519-1522.

Condie, K.C., 1989. Geochemical Changes in Basalts and Andesites across the Archean-Proterozoic Boundary - Identification and Significance. Lithos 23(1-2), 1-18.

Condie, K.C., 1993. Chemical-Composition and Evolution of the Upper Continental-Crust - Contrasting Results from Surface Samples and Shales. Chem. Geol. 104(1-4), 1-37.

Danielson, A., Moller, P., Dulski, P., 1992. The Europium Anomalies in Banded Iron Formations and the Thermal History of the Oceanic-Crust. Chem. Geol. 97(1-2), 89-100.

Dauphas, N., van Zuilen, M., Wadhwa, M., Davis, A.M., Marty, B., Janney, P.E., 2004. Clues from Fe isotope variations on the origin of early Archean BIFs from Greenland. Science 306(5704), 2077-2080.

Dauphas, N., Cates, N.L., Mojzsis, S., Busigny, V., 2007. Identification of chemical sedimentary protoliths using iron isotopes in the 3750 Ma Nuvvuagittuq supracrustal belt, Canada. Earth and Planet. Sci. Lett. 254(3-4), 358-376.

de Baar, H.J.W., Schijf, J., Byrne, R.H., 1991. Solution Chemistry of the Rare-Earth Elements in Seawater. European Journal of Solid State and Inorganic Chemistry 28, 357-373.

Derry, L.A., Jacobsen, S.B., 1990. The Chemical Evolution of Precambrian Seawater - Evidence from Rees in Banded Iron Formations. Geochim. Cosmochim. Acta 54(11), 2965-2977.

Douville, E., Bienvenu, P., Charlou, J.L., Donval, J.P., Fouquet, Y., Appriou, P., Gamo, T., 1999. Yttrium and rare earth elements in fluids from various deep-sea hydrothermal systems. Geochim. Cosmochim. Acta 63(5), 627-643.

Dymek, R.F., Klein, C., 1988. Chemistry, Petrology and Origin of Banded Iron-Formation Lithologies from the 3800-Ma Isua Supracrustal Belt, West Greenland. Precamb. Res. 39(4), 247-302.

Elderfield, H., 1988. The Oceanic Chemistry of the Rare-Earth Elements. Philosophical Transactions of the Royal Society of London Series a-Mathematical Physical and Engineering Sciences 325(1583), 105-126.

Fedo, C.M., Nesbitt, H.W., Young, G.M., 1995. Unraveling the Effects of Potassium Metasomatism in Sedimentary-Rocks and Paleosols, with Implications for Paleoweathering Conditions and Provenance. Geology 23(10), 921-924.

Fedo, C.M., 2000. Setting and origin for problematic rocks from the >3.7 Ga Isua Greenstone Belt, southern west Greenland: Earth's oldest coarse clastic sediments. Precamb. Res. 101, 69-78.

Fedo, C.M., Whitehouse, M.J., 2002a. Metasomatic origin of quartz-pyroxene rock, Akilia, Greenland, and implications for Earth's earliest life. Science 296, 1448-1452.

Fedo, C.M., Whitehouse, M.J., 2002b. The origin of a most contentious rock - Response. Science 298(5595), 961-962.

Fedo, C.M., Whitehouse, M.J., 2002c. Origin and significance of Archean quartzose rocks at Akilia, Greenland - Response. Science 298(5595), -.

Field, D., Clough, P.W.L., 1976. K/Rb ratios and metasomatism in metabasites from a Precambrian amphibolite–granulite transition zone. Journal of the Geological Society 132(3), 277-288.

Floyd, P.A., Leveridge, B.E., 1987. Tectonic Environment of the Devonian Gramscatho Basin, South Cornwall - Framework Mode and Geochemical

Evidence from Turbiditic Sandstones. Journal of the Geological Society 144, 531-542.

Frei, R., Rosing, M., Waight, T.E., Ulfbeck, D.G., 2002. Hydrothermal-metasomatic and tectono-metamorphic processes in the Isua supracrustal belt (west Greenland): a multi-isotopic investigation of their effects on the Earth's oldest oceanic crustal sequence. Geochim. Cosmochim. Acta 66, 467-486.

Frei, R., Polat, A., 2007. Source heterogeneity for the major components of similar to 3.7 Ga Banded Iron Formations (Isua Greenstone Belt, Western Greenland): Tracing the nature of interacting water masses in BIF formation. Earth Planet. Sci. Lett. 253(1-2), 266-281.

Friend, C.R.L., Nutman, A.P., Bennett, V.C., Norman, M.D., 2008. Seawater-like trace element signatures (REE+Y) of Eoarchaean chemical sedimentary rocks from southern West Greenland, and their corruption during high-grade metamorphism. Contrib. Mineral. Petrol. 155(2), 229-246.

Fryer, B.J., 1977. Rare-Earth Evidence in Iron-Formations for Changing Precambrian Oxidation-States. Geochim. Cosmochim. Acta 41(3), 361-367.

Furnes, H., de Wit, M., Staudigel, H., Rosing, M., Muehlenbachs, K., 2007. A vestige of Earth's oldest ophiolite. Science 315(5819), 1704-1707.

Gao, S., Wedepohl, K.H., 1995. The Negative Eu Anomaly in Archean Sedimentary-Rocks - Implications for Decomposition, Age and Importance of Their Granitic Sources. Earth Planet. Sci. Lett. 133(1-2), 81-94.

Green, M.G., Sylvester, P.J., Buick, R., 2000. Growth and recycling of early Archaean continental crust: geochemical evidence from the Coonterunah and Warrawoona Groups, Pilbara Craton, Australia. Tectonophysics 322(1-2), 69-88.

Gruau, G., Rosing, M., Bridgwater, D., Gill, R.C.O., 1996. Resetting of Sm-Nd systematics during metamorphism of >3.7 Ga rocks: implications for isotopic models of early earth differentiation. Chem. Geol. 133, 225-240.

Harrison, T.M., Blichert-Toft, J., Muller, W., Albarede, F., Holden, P., Mojzsis, S.J., 2005. Heterogeneous Hadean hafnium: Evidence of continental crust at 4.4 to 4.5 Ga. Science 310, 1947-1950.

Hayashi, T., Tanimizu, M., Tanaka, T., 2004. Origin of negative Ce anomalies in Barberton sedimentary rocks, deduced from La-Ce and Sm-Nd isotope systematics. Precamb. Res. 135(4), 345-357.

Hessler, A.M., Lowe, D.R., 2006. Weathering and sediment generation in the Archean: An integrated study of the evolution of siliciclastic sedimentary rocks of the 3.2 Ga Moodies Group, Barberton greenstone belt, South Africa. Precamb. Res. 151(3-4), 185-210.

Hofmann, A., Harris, C., 2008. Silica alteration zones in the Barberton greenstone belt: A window into the subseafloor processes 3.5-3.3 Ga ago. Chem. Geol. 257, 224-242.

Hopkins, M., Harrison, T.M., Manning, C.E., 2008. Low heat flow inferred from >4 Gyr zircons suggests Hadean plate boundary interactions. Nature 456, 493-496.

Ingram, B.L., Lin, J.C., 2002. Geochemical tracers of sediment sources to San Francisco Bay. Geology 30(6), 575-578.

Johnson, D.M., Hooper, P.R., Conrey, R.M., 1999. XRF Analysis of Rocks and Minerals for Major and Trace Elements on a Single Low Dilution Li-tetraborate Fused Bead. Adv. X-Ray Anal. 41, 843-867.

Kohler, E.A., Anhaeusser, C.R., 2002. Geology and geodynamic setting of Archaean silicic metavolcaniclastic rocks of the Bien Venue Formation, Fig Tree Group, northeast Barberton greenstone belt, South Africa. Precamb. Res. 116(3-4), 199-235.

Maas, R., Kinny, P.D., Williams, I.S., Froude, D.O., Compston, W., 1992. The Earths Oldest Known Crust - a Geochronological and Geochemical Study of 3900-4200 Ma Old Detrital Zircons from Mt Narryer and Jack Hills, Western-Australia. Geochim. Cosmochim. Acta 56(3), 1281-1300.

McDonough, W.F., Frei, F.A., 1989. Rare Earth Elements in Upper Mantle Rocks, in: Reviews in Mineralogy, volume 21100-145.

McLennan, S.M., 1982. On the Geochemical Evolution of Sedimentary-Rocks. Chemical Geology 37(3-4), 335-350.

McLennan, S.M., Taylor, S.R., Kroner, A., 1983. Geochemical Evolution of Archean Shales from South-Africa .1. The Swaziland and Pongola Supergroups. Precamb. Res. 22(1-2), 93-124.

McLennan, S.M., Taylor, B.E., 1984. Archaean Sedimentary Rocks and Their Relation to the Composition of the Archaean Continental Crust, in: Archaean Geochemistry, A. Kroner, G.N. Hanson and A.M. Goodwin, eds., Springer, Berlin, pp. 47-72.

McLennan, S.M., Taylor, S.R., Mcgregor, V.R., 1984. Geochemistry of Archean Meta-Sedimentary Rocks from West Greenland. Geochim. Cosmochim. Acta 48(1), 1-13.

McLennan, S.M., 1993. Geochemical approaches to sedimentation, provenance, and tectonics, in: Processes Controlling the Composition of Clastic Sediments, M.J. Johnson and A.R. Basu, eds., Special Paper 284, Geological Society of America, Boulder, Colorado, pp. 21-39.

McLennan, S.M., Bock, B., Hemming, N.G., Hurowitz, J.A., Lev, S.M., McDaniel, D.K., 2004. The roles of provenance and sedimentary processes in the geochemistry of sedimentary rocks, in: Geochemistry of Sediments and Sedimentary Rocks: Evolutionary Considerations to Mineral Deposit-Forming Environments7-37.

Michard, A., Albarede, F., 1986. The Ree Content of Some Hydrothermal Fluids. Chemical Geology 55(1-2), 51-60.

Minami, M., Shimizu, H., Masuda, A., Adachi, M., 1995. Two Archean Sm-Nd ages of 3.2 and 2.5 Ga for the Marble Bar Chert, Warrawoona Group, Pilbara Block, Western Australia. Geochem J 29(6), 347-362.

Mojzsis, S.J., Arrhenius, G., McKeegan, K.D., Harrison, T.M., Nutman, A.P., Friend, C.R.L., 1996. Evidence for life on earth before 3,800 million years ago. Nature 384(7 November), 55-59.

Moorbath, S., Onions, R.K., Pankhurst, R.J., 1975. Evolution of Early Precambrian Crustal Rocks at Isua, West Greenland - Geochemical and Isotopic Evidence. Earth Planet. Sci. Lett. 27(2), 229-239.

Myers, J.S., Crowley, J.L., 2000. Vestiges of life in the oldest Greenland rocks? a review of early Archean geology in the Godthaabsfjord region, and reappraisal of field evidence for 3850 Ma life on Akilia. Precamb. Res. 103, 101-124.

Myers, J.S., 2001. Protoliths of the 3.8-3.7 Ga Isua greenstone belt, West Greenland. Precamb. Res. 105(2-4), 129-141.

Nance, W.B., Taylor, S.R., 1976. Rare-Earth Element Patterns and Crustal Evolution .1. Australian Post-Archean Sedimentary-Rocks. Geochim. Cosmochim. Acta 40(12), 1539-1551.

Nesbitt, H.W., 2004. Petrogenesis of siliciclastic sediments and sedimentary rocks, in: Geochemistry of Sediments and Sedimentary Rocks: Evolutionary Considerations to Mineral Deposit-Forming Environments39-51.

Nozaki, Y., Zhang, J., Amakawa, H., 1997. The fractionation between Y and Ho in the marine environment. Earth Planet. Sci. Lett. 148(1-2), 329-340.

Nutman, A.P., Allaart, J.H., Bridgwater, D., Dimroth, E., Rosing, M., 1984. Stratigraphic and geochemical evidence for the depositional environment of the early Archaean Isua Supracrustal Belt, Southern West Greenland. Precamb. Res. 25, 365-396.

Nutman, A.P., Bridgwater, D., 1986. Early Archean Amitsoq Tonalites and Granites of the Isukasia Area, Southern West Greenland - Development of the Oldest-Known Sial. Contrib. Mineral. Petrol. 94(2), 137-148.

Nutman, A.P., McGregor, V.R., Friend, C.R.L., Bennett, V.C., Kinny, P.D., 1996. The Itsaq Gneiss Complex of southern west Greenland; The world's most extensive record of early crustal evolution (3900-3600 Ma). Precamb. Res. 78(1-3), 1-39.

Nutman, A.P., Mojzsis, S.J., Friend, C.R.L., 1997. Recognition of >=3850 Ma water-lain sediments in West Greenland and their significance for the early Archaean Earth. Geochim. Cosmochim. Acta 61(12), 2475-2484.

Nutman, A.P., Bennett, V.C., Friend, C.R.L., Norman, M.D., 1999. Meta-igneous (non-gneissic) tonalites and quartz-diorites from an extensive ca. 3800 Ma terrain south of the Isua supracrustal belt, southern West Greenland: constraints on early crust formation. Contrib. Mineral. Petrol. 137(4), 364-388.

Pache, T., Brockamp, O., Clauer, N., 2008. Varied pathways of river-borne clay minerals in a near-shore marine region: A case study of sediments from the Elbe- and Weser rivers, and the SE North Sea. Estuar. Coast. Shelf Sci. 78(3), 563-575.

Pearce, J.A., Cann, J.R., 1973. Tectonic Setting of Basic Volcanic-Rocks Determined Using Trace-Element Analyses. Earth Planet. Sci. Lett. 19(2), 290-300.

Polat, A., Hofmann, A.W., Rosing, M.T., 2002. Boninite-like volcanic rocks in the 3.7-3.8 Ga Isua greenstone belt, West Greenland: geochemical evidence for intra-oceanic subduction zone processes in the early Earth. Chem. Geol. 184(3-4), 231-254.

Polat, A., Hofmann, A.W., Munker, C., Regelous, M., Appel, P.W.U., 2003. Contrasting geochemical patterns in the 3.7-3.8 Ga pillow basalt cores and rims, Isua greenstone belt, Southwest Greenland: implications for post magmatic alteration processes. Geochemica et Cosmochimica Acta 67(3), 441-457.

Polat, A., Frei, R., 2005. The origin of early Archean banded iron formations and of continental crust, Isua, southern West Greenland. Precamb. Res. 138(1-2), 151-175.

Rasmussen, B., Buick, R., 1999. Redox state of the Archean atmosphere: evidence from detrital heavy minerals in ca. 3250-2750 Ma sandstones from the PIlbara Craton, Australia. Geology 27(2), 115-118.

Rollinson, H., 2003. Metamorphic history suggested by garnet-growth chronologies in the Isua Greenstone Belt, West Greenland. Precamb. Res. 126(3-4), 181-196.

Rose, N.M., Rosing, M.T., Bridgwater, D., 1996. The origin of metacarbonate rocks in the Archaean Isua supracrustal belt, West Greenland. Am. J. Sci. 296(9), 1004-1044.

Rosing, M.T., Rose, N.M., Bridgwater, D., Thomsen, H.S., 1996. Earliest part of Earth's stratigraphic record: A reappraisal of the >3.7 Ga Isua (Greenland) supracrustal sequence. Geology 24(1), 43-46.

Rosing, M.T., 1999. ^{13}C-depleted carbon microparticles in >3700-Ma sea-floor sedimentary rocks from west Greenland. Science 283(29 January), 74-76.

Ross, D.J.K., Bustin, R.M., 2009. Investigating the use of sedimentary geochemical proxies for paleoenvironment interpretation of thermally mature organic-rich strata: Examples from the Devonian-Mississippian shales, Western Canadian Sedimentary Basin. Chem. Geol. 260, 1-19.

Rouchon, V., Orberger, B., 2008. Origin and mechanisms of K-Si-metasomatism of ca. 3.4-3.3 Ga volcaniclastic deposits and implications for Archean seawater evolution: Examples from cherts of Kittys Gap (Pilbara craton, Australia) and Msauli (Barberton Greenstone Belt, South Africa). Precamb. Res. 165(3-4), 169-189.

Schidlowski, M., Appel, P.W.U., Eichmann, R., Junge, E., 1979. Carbon isotope geochemistry of the 3.7 x 10^9-yr-old Isua sediments, west Greenland: implications for the Archaean carbon and oxygen cycles. Geochim. Cosmochim. Acta 43, 189-199.

Shaw, D.M., 1968. A review of K-Rb fractionation trends by covariance analysis. Geochim. Cosmochim. Acta 32, 573-601.

Shields, G.A., Webb, G.E., 2004. Has the REE composition of seawater changed over geological time? Chem. Geol. 204(1-2), 103-107.

Sholkovitz, E.R., Landing, W.M., Lewis, B.L., 1994. Ocean Particle Chemistry - the Fractionation of Rare-Earth Elements between Suspended Particles and Seawater. Geochimica Et Cosmochimica Acta 58(6), 1567-1579.

Sugitani, K., Yamamoto, K., Wada, H., Binu-Lal, S.S., Yoneshige, M., 2002. Geochemistry of Archean carbonaceous cherts deposited at immature island-arc setting in the Pilbara Block, Western Australia. Sediment Geol 151(1-2), 45-66.

Sun, S.S., McDonough, W.F., 1989. Chemical and isotopic systematics of oceanic basalts: implications for mantle composition and processes, in: Magmatism in

the Ocean Basins, A.D. Saunders and M.J. Norry, eds., Geological Society Special Publication 42313-345.

Taylor, S.R., McLennan, S.M., 1985, The Continental Crust: its Composition and Evolution, 312 pp., Blackwell Scientific, Oxford.

Taylor, S.R., McLennan, S.M., 1995. The Geochemical Evolution of the Continental-Crust. Reviews of Geophysics 33(2), 241-265.

Toulkeridis, T., Clauer, N., Kroner, A., 1996. Chemical variations in clay minerals of the Archaean Barberton Greenstone Belt (South Africa). Precamb. Res. 79(3-4), 195-207.

Wedepohl, K.H., Heinrichs, H., Bridgwater, D., 1991. Chemical Characteristics and Genesis of the Quartz-Feldspathic Rocks in the Archean Crust of Greenland. Contrib. Mineral. Petrol. 107(2), 163-179.

Wildeman, T.R., Condie, K.C., 1973. Rare-Earths in Archean Graywackes from Wyoming and from Fig Tree Group, South-Africa. Geochim. Cosmochim. Acta 37(3), 439-453.

Wronkiewicz, D.J., Condie, K.C., 1987. Geochemistry of Archean Shales from the Witwatersrand Supergroup, South Africa - Source-Area Weathering and Provenance. Geochim. Cosmochim. Acta 51(9), 2401-2416.

Wronkiewicz, D.J., Condie, K.C., 1989. Geochemistry and Provenance of Sediments from the Pongola Supergroup, South Africa - Evidence for a 3.0-Ga-Old Continental Craton. Geochim. Cosmochim. Acta 53(7), 1537-1549.

Wyche, S., Nelson, D.R., Riganti, A., 2004. 4350-3130 Ma detrital zircons in the Southern Cross Granite-Greenstone Terrane, Western Australia: Implications for the early evolution of the Yilgarn Craton. Australian Journal of Earth Sciences 51(1), 31-45.

5. An Early Archaean Deep-Marine Micritic Banded-Iron Formation

1. Introduction: Carbonates in the Early Archaean

The lack of evidence for Early Archaean carbonate sedimentation is oft remarked upon (Grotzinger, 1994; 1997; Nakamura and Kato, 2002, 2004). The first carbonate platforms were not deposited until ~ 2.95 Ga (Kusky and Hudleston, 1999), and only came to be well-established by ~ 2.5 Ga (Eriksson et al., 1998). Peritidal Early Archaean sedimentary carbonates or their metamorphosed equivalents have been found in granite-greenstone associations in the Kromberg Formation, upper Onverwacht Group (Viljoen and Viljoen, 1969) and Mapepe Formation, Fig Tree Group (Heinrichs and Reimer, 1977; Lowe and Knauth, 1977; Lowe and Nocita, 1996) of South Africa's Swaziland Supergroup, the Strelley Pool Chert, Kelly Group (Lowe, 1983) and Dresser Formation, Warrawoona Group (Groves et al., 1981; Buick and Dunlop, 1990)(see also Chapter 2C) of Australia's Pilbara Supergroup, and the Sargur Marbles of India (Radhakrishna and Naqvi, 1986). These rocks have all seen partial to complete early silicification (Buick and Barnes, 1984; Toulkeridis et al., 1998)(see also Chapter 2C). Structural, textural and mineralogical similarities between these (and other Precambrian) carbonates with modern analogues have led many to invoke analogous microbiological calcification processes (e.g. Kazmierczak and Kempe, 2004).

In contrast, evidence for carbonate deposited below the Archaean wavebase (> 200m; (Mueller et al., 1994)) is exceedingly rare (Milliman, 1974; Garcia-Ruiz, 2000), being restricted to siderite or ankerite of still relatively shallow 'carbonate facies' banded-iron formation (James, 1954), or rocks of metasomatic origin, such as the re-interpreted Isua carbonate (Rose et al., 1996) and some other Archaean instances (Veizer et al., 1989b). The paucity of ancient deep-water sedimentary carbonate is particularly puzzling in light of speculation that Earth's earliest oceans were (i) deep (Condie, 1997), emerging from abyssal-like Hadaean depths (Eriksson et al., 2005); and (ii) highly supersaturated with respect to calcium carbonate (Grotzinger and

Kasting, 1993; Grotzinger, 1994), and probably to dolomite, ankerite and siderite as well (Holland, 1984).

Part of the explanation undoubtedly has to do with a lack of preserved basinal settings relative to shallow marine settings (Eriksson et al., 1997; Eriksson et al., 2005), but this leaves their absence in the few preserved Archaean deep basins unexplained. Additional explanations can and have been put forward, including: (i) Prohibitively acidic oceans, perhaps due to high pCO_2 or ferrous iron control on ocean chemistry; (ii) Prohibitively low dissolved inorganic carbon ('DIC') concentrations, perhaps due to low pCO_2; (iii) Prohibitively low alkaline earth cation concentrations (Kazmierczak and Kempe, 2004), perhaps due to low weathering and/or fluvial fluxes and/or high ocean floor weathering sinks; (iv) Kinetic inhibition of carbonate formation, perhaps through high Fe^{2+} concentrations (Sumner and Grotzinger, 1996); (v) The lack of microbiological mitigation, perhaps due to primitive microbial metabolism and/or nutrient limitations; and (vi) Prohibitively deep marine environments, lying below the carbonate compensation depth ('CCD').

An alternate hypothesis put forward here is that Early Archaean deep-sea carbonate, though precipitated in copious amounts, came to be pervasively and rapidly replaced, with the extant record failing to do justice to its geobiochemical importance. We describe geological, sedimentological and geochemical aspects of the earliest recorded instance of preserved deep-water carbonate from the Coonterunah Subgroup at the base of the Pilbara Supergroup, and discuss implications for Precambrian biogeochemical cycling and the origin of the enigmatic banded-iron formations.

2. Geological Description

2.1. Coonterunah Subgroup Geology

The ~ 6500 m thick 3.518 Ga Coonterunah Subgroup, which contains the oldest known units of the Pilbara Supergroup, has only been recognized in the Pilgangoora Syncline (Figure 1 - 3). The stratigraphic sequence described here lies in the middle of the Coucal Formation, which conformably overlies up to 2000 meters of sporadically pillowed mafic extrusives, hyperbyssals and rare komatiites of the Table Top

Formation. The Double Bar Formation, overlying the Coucal Formation, is also dominated by mafic extrusives, in the form of occasionally pillowed, tholeiitic basalt and lesser gabbros. The Counterunah Subgroup was intruded by the ~3.48 Ga (Buick et al., 1995) Carlindi Granitoid complex, with the Table Top Formation occupying the base of preserved Pilbara volcanism and sedimentation.

A regional unconformity bounds the Coonterunah Subroup from the overlying silicified shallow marine and intermittently subaerial sediments of the Strelley Pool Chert, which represents the lowest member of the Kelly Group in the Pilgangoora Belt. The unconformity varies laterally from concordant to angular in style.

All Coonterunah rocks have been metamorphosed to at least lower greenschist facies, and the lithologic 'meta' prefix will be taken as implied. Chert formed during Cenozoic silicification forms an important exception, and metamorphosed and non-metamorphosed chert will be therefore be designated with the traditional 'meta-chert' and 'chert'. Metamorphic grades increase westward under regional strain control, culminating in lower amphibolite facies assemblages associated with the ~ 2.88 Ga (Baker et al., 2002) Pilgangoora Syncline fold closure that marks the westward extent of volcano-sedimentary outcrop. The regional metamorphic fabric overprints an earlier ~ 100 – 350m hornfels gradient towards the intrusive contact with the Carlindi Granitoid complex to the north.

For much of their lateral extent, two or three prominent metachert-BIFs near the base of the Coucal Formation represent the full complement of preserved Coonterunah sedimentation. These units are up to ~ 8 meters thick at their eastern-most occurrence, and gradually thin to ~ 0.5 meters or less towards the west-north-westerly fold closure of the the Pilgangoora Syncline. They exhibit mm- to cm- scale alternating planar to gently undulating dark and light banding.

Dark banding is commonly due to magnetite, which occurs in variable modal amounts in cherts from trace quantities to >90% in magnetite laminae. Magnetite is increasingly crystalline with increasing grade, and ultimately reacts with quartz to yield grunerite. Where magnetite bands are distinct at higher grade, Fe-Mg amphibole has grown in thin sheets on the planar contact with quartzitic bands (e.g. Figure 4(e)). Both

magnetite and later amphibole crystals have suffered variable oxidation, with late staining by maghemite, limonite, goethite and haematite absent to pervasive.

Some dark bands are dominated by > 90% meta-chert rather than magnetite. Although some of this meta-chert bears trace quantities of kerogen, the black colour is predominantly attributable to small quantities of opaque oxides, mostly magnetite. Light banding is due to pure metachert that has a pronounced sugary texture (e.g. Figure 4 (d)).

Locally, a further style of banding is observed as post-metamorphic cryptocrystalline chert rather than sugary meta-chert, sometimes alternating with haematite (Figures 4(f, g)). Haematite occurs as a microcrystalline jasperitic coating on chert in earthy dark-red bands that alternate with pure white chert bands. Prominent patches of this late haematization occur towards the western- and eastern- most outcrop of Coucal cherty-BIF.

2.2. Carbonate and Tephra Section

A third style of banding is more rarely encountered in the form of alternating 1 - 5 mm thick laminae of magnetite and carbonate (Figure 4, 5), in which carbonate bands are variably silicified to meta-chert. The most prominent such lithofacies found is 32 cm thick, with several similar but thinner 1-3 cm-scale units stratigraphically above and below. This prominent unit is also the best preserved, and exhibits a lateral extension of at least ~5 km with outcrop bounded by sinistral N-S strike-slip faults of ~ 0.5 km throw towards the east and west. Outcrop is fairly continuous, interrupted only by ~ 10 – 20 m displacements along NNE trending faults.

Laminae are prone to thickening and thinning, frequently pinching out laterally altogether on scales of 1 – 10 cm. Compared to magnetite, carbonate minerals have a distinctively more granular, almost sugary appearance, reflecting a greater tendency towards recrystallisation. Magnetite laminae and individual crystals are finer, forming solid cohesive bands in which individual grains are not visible to the naked eye. Domal ~1.5 – 4.0 mm diameter flame structures intrude downward into both carbonate and magnetite laminae (Figure 6 (a, b)). Stromatolitic features are absent.

The prominent carbonate-magnetite lithofacies stratigraphically and conformably overlies a ~35 m thick package of graded tuffaceous wackes to siltstones and chlorite- biotite-quartz pelites (Figure 7, 8). Tephra units exhibit alternating dark and light banding due to alternating chloritized and sericitized glass, bearing bimodal lithic constituents. Where present, grading is normal.

The base of the volcanoclastic package is marked by a thoroughly silicified hyaloclasite (sample PC06-037) with coarse (200 – 300 μm) blocky altered K-feldspar phenocrysts and fibrous crystals of metamorphic (late) actinolite. An overlying pebbly tuffaceous wacke (sample PC06-039) exhibits alternating bimodal layers bearing well-rounded coarse (200 – 500 μm) 'beta-quartz' morphology and angular lath-like crystal vitric tuff phenocrysts and sub-ellipsoidal sub-spherical amygdales and vesicles in a eutaxitic groundmass of squashed chloritized basaltic glass. Abundant recrystallized beta-quartz crystals and albite phenocrysts suggest a mixed bimodal rhyolitic-dacitic progeny for the crystal/vitric component, with a bimodal ash source bearing a basaltic component. Metapelites are dominated by alternating layers of quartz and Fe-chlorite with lesser Fe-biotite.

Immediately underlying the mixed volcanoclastic-carbonate sequence is a ~18 m-thick tholeiitic basalt pile, capped by a basaltic hyaloclastite. The top ~ 2 m of this volcanic pile has seen pervasive silification, which has also affected the lowermost ~2 m of tuffaceous units, likely accounting for their superior preservation relative to immediately overlying tuffaceous units that crop out poorly.

~ 60 m of doleritic gabbro immediately overly the mixed volcanoclastic-carbonate sequence, terminated by a prominent ~ 8 m thick magnetite-metachert, with minor patchily silicified carbonate, marking the top of the middle sedimentary horizon of the Coucal Formation. Several overlying kilometers of largely tholeittic basalts, variably pillowed, make up the Double Bar Formation and the remainder of the Coonterunah Subroup.

Basalts bear only rare vesicles and amygdales, while basalt hydrovolcanic tuff, coarse pumice and accretionary lapilli are absent from volcanoclastic units. No coarse (> clay size) terrigenous clastic sediments are present. No large-scale cross-bedding

was observed, while cross-lamination is rare. These igneous and sedimentary textures together indicate a low-energy depositional setting and water-depths well below wave base, with tephra evidently derived from sub-aerially erupted submarine fallout (Fisher and Schmincke, 1984; Einsele, 2000). Interlayering with metapelites suggests modest rates of carbonate and magnetite lamina formation, not incompatible with seasonal deposition.

2.3. Carbonate-Magnetite Mineralogy

Samples from both the prominent 32cm thick layer and lesser carbonate layers were examined with the aid of a transmitted and reflected-light polarizing microscope, and the former further analyzed with a JEOL-520 electron microprobe with wavelength and energy dispersive capabilities.

Mineralogically, the carbonate unit is dominated by magnetite, calcite and dolomite, with some rhodochrosite and trace amounts of apatite and kerogen. Magnetite and both dominant carbonate minerals, which are commonly in contact with one another, are moderately equigranular, and have grain-sizes mostly in the 25 – 50 μm range (Figures 5(a - d)), although weathered magnetite grains can be as small as 5 μm or less.

Boundaries between magnetite and carbonate laminae are distinct (Figure 5 (a - c)). For descriptive purposes, carbonate laminaee can be bundled (Figure 4) into four magnetite-rich (m_1 – m_4) and three carbonate-rich (c_1 – c_3) alternating cm-scale mesobands. Both mesoband and entire unit thickness exhibit minimal lateral variation. Volumetrically, carbonate laminae comprise about 20% of the lower, more magnetite-rich 16cm ($m_1 – c_1 – m_2$) portion and 50% of the upper, more carbonate-rich 16cm ($c_2 – m_3 – c_3 – m_4$) portion of the unit.

Magnetite laminae consist of pure (Ni-poor) magnetite, which have undergone variable weathering to maghaemite. In patches of more extensive weathering, limonite with or without fine-grained hematite oxidation rinds and lesser goethite are also observed. Rare apatite, present as small (1 - 5 μm) anhedral crystals, is most commonly observed in association with magnetite. No kerogen is observed within magnetite

laminae, although the densely packed interlocking opaque mineral mass would be expected to obscure its presence.

Carbonate laminae consist of equidimensional granular dolomite and calcite, with the relative proportions and chemical composition of carbonate phases exhibiting little inter-laminar variation within individual samples. Calcite is pure, with a dominant stoichiometry of $Ca_{0.95\text{-}1.00}Mg_{0.05\text{-}0.00}(CO_3)$, and only very rarely as magnesian as $Ca_{0.90}Mg_{0.10}(CO_3)$. Dolomite exhibits dolomite-ankerite solid solution, varying from pure dolomite $CaMg(CO_3)_2$ to $Ca_{1.0}Mg_{0.8}Fe_{0.2}(CO_3)_2$. More ferroan dolomite tends to be associated with magnetite, but this relationship is far from exclusive. Where present, rhodochrosite is texturally associated with dolomite, occurring as narrow elongate rims. No Mn-bearing minerals are found in pure magnetite laminae. Siderite, absent in most samples, is rarely observed as subhedral crystals along magnetite-carbonate interfaces.

Unlike the whole-rock carbonate homogeneity, lateral mineralogical variation is pronounced, with molar Ca/Mg ratios varying from 2.88 in the most calcite-rich outcrop to 1.27 in the most dolomite-rich outcrop, corresponding to a range between 49 and 85 wt.% dolomite. Rhodochrosite constitutes between 1.2 and 2.4 wt.% of carbonate lamellae in most calcitic and more dolomitic samples, respectively.

Kerogen occurs as small < 5 μm greenish-black amoeboid blebs (Figure 5 (d)), mostly at triple junctions of adjoining calcite, and less commonly in association with dolomite. Pyrite and ilmenite, otherwise common Archaean accessory minerals, are conspicuously absent from both magnetite and carbonate laminae, as are aluminous silicates and chert. What little silica can be detected is uniquely confined to limonitic alteration of magnetite, where it constitutes up to ~3 wt.% of limonite.

3. Alteration & Metamorphism

3.1. Early Silicification

'Early silicification' designates both pore-precipitation of and mineral replacement by silica prior to peak metamorphism (M_2 or M_7, see below; also Chapter 2), and is not to be confused with post-metamorphic 'late silification' discussed below.

Early silicification was widespread in the Pilgangoora rocks, including the Coonterunah Subgroup, and occured in two broadly distinct styles. This first style of early silicification may be termed ‘capping’. It is distinguished by being relatively unselective in the lithologies replaced, pervasive, and concentrated in metre-scale mesoscopic alteration zones that are parallel to seawater-accessible diastematic interfaces. Clear examples of such interfaces are provided by the tops of volcanic piles and the walls of early seafloor fissures (Chapter 2, 7). All lithologies appear vulnerable to capping silicification, which is observed in intrusive to extrusive, felsic to mafic rocks. It preferentially affected permeable and porous rocks, however, such as pyroclastic deposits and pillowed flows, whilst leaving impermeable rocks, such as the centers of lava flows, relatively unaltered.

Capping silicifation is common in greenstone belts, and has long been attributed to hydrothermal fluids (e.g. in the Pilbara by Barley, 1984). Geochemical, textural and fluid inclusions studies (de Vries and Touret, 2007) have firmly established a role for hydrothermal fluids in Archaean seafloor alteration. Zones are thought to represent quenching interfaces between circulating fluids and Archaean bottomwater. Here, sharp drops in temperature and solubility stripped silica from fluids through precipitation and replacement, in agreement with laboratory and theoretical findings (Fournier and Rowe, 1977a, b; Fournier and Potter, 1982; Fournier, 1983; Fournier and Marshall, 1983; Gunnarsson and Arnorsson, 2000). So conducive were such zones to silicification that they frequently became self-sealing (e.g. Gibson et al., 1983; Hofmann and Bolhar, 2007; Hofmann and Harris, 2008).

The Coonterunah carbonate-tephra sequence is bounded at the base and top by capping silification several meters thick. The basal silicified veneer is concentrated in the top of the underlying tholeiitic volcanic pile, with the degree of silicification dissipating into the basal ~5 meters of tephra. The top veneer is a silicified cap on ~ 65 m of overlying doleritic gabbro, that likely also contributed to silicification of ~8 meters of immediately overlying limonitized ferruginous chert.

The second style of early silicifaction, which was lithologically highly selective, non-pervasive and confined to smaller (~ cm) scales, may be termed

'selective'. In the field, selective silification is often not readily distinguishable from capping silicification, except when it is replacing cm-scale bands of carbonate in laminated magnetite-carbonate units (Figure 9) or manifesting as chert pebbles in pebbly wackes (Figure 7 (a)). Zones of selective silicification are in some cases bound by mm-scale quartz veins oblique to bedding.

Much of the laminated Coonterunah carbonate outcrop bears evidence of selective silicification (Figure 9, 10), which can occur along well-defined silicification fronts (Figure 12), in which the degree of carbonate silicification varies gradually from none to complete.

Unlike capping silicification, meta-chert after carbonate occasionally – but not always - bears volumetrically minor quantities of small Ca-Mg silicate crystals, spatially progressing to tremolite-actinolite (Figure 11) with increasing grade. Selective silicification of Coonterunah carbonate is similar to the early silicification that affected the dolomite lithofacies of the Strelley Pool Chert (Chapter 2). Euhedral ~100 μm sparry dolomite rhombs in selective silicification zones after dolomite in both the Coonterunah Subgroup- and Strelley Pool Chert sedimentary carbonates (Figure (c, d)) attest to a probable interplay between early silicifying and dolomitizing fluids, as discussed later.

3.2. Metamorphism

As indicated by epidote-chlorite in metamafics, all Coonturunah rocks have been metamorphosed to at least lower greenschist facies, probably in response to post-depositional hydrothermal alteration and burial during early tilting to sub-vertical. In addition, two prominent later metamorphic gradients can be distinguished on the basis of structural, textural and mineralogical evidence. The older (M_1, Chapter 2) is a ~ 100 – 350 m thermal metamorphic gradient increasing towards the intrusive contact with the ~3.48 Ga (Buick et al., 1995) Carlindi Granitoid complex to the north. The fabric associated with contact metamorphism varies from hornfels to a strong contact-parallel foliation, now with a sub-vertical dip. Peak assemblages are defined by chlorite-actinolite-epidote in meta-basalts, -dolerites and -gabbros, tremolite- or actinolite-

quartz in metachert-carbonates, and cummingtonite- or grunerite-quartz in ferruginous metachert-carbonates. M_1 contact metamorphism occurred at low but poorly constrained pressures of ~2 kbar, compatible with plutonic intrusion from below.

Overprinting this is a regional fabric (M_7) associated with metamorphic grades increasing westward. The M_7 schistosity is sub-parallel to bedding for most of the strike length of the Coonterunah Subgroup, and culminates in lower amphibolite facies assemblages associated with the ~ 2.88 Ga (Baker et al., 2002) Pilgangoora Syncline fold (D_7) closure that marks the west-northwestward extent of volcano-sedimentary outcrop. Highest grade assemblages associated with M_7 are defined by hornblende-oligoclase in meta-mafics, and a single localized occurrence of almandine garnet, andesine plagioclase and ferrotschermakite amphibole in an orthogneiss rock with probable acidic volcanic protolith. Widespread renewed plutonism accompanied M_7, including garnet pegmatite dykes intruded along D_7 fold cleavage planes.

3.2.1. Peak Metamorphism of Carbonate-Magnetite Outcrop

Although low grades of metamorphism impede quantitative geothermobarometry, some constraints can be placed upon the system through consideration of the CaO-MgO-CO_2 sub-system for carbonates (Flowers and Helgeson, 1983) and the $AlO_{1.5}$-CaO-FeO-MgO±H_2O system for mafic rocks (Spear, 1995).

Dolomite and calcite are texturally equilibrated, and tightly clustered in Ca-Mg-Fe space (Figure 13). Carbonate mineral compositions in dolomitic (lower bulk Ca/Mg) and calcitic (higher bulk Ca/Mg) samples are similar. The lack of ankerite and/or siderite after magnetite, meanwhile, rules out post-peak carbonate metasomatism through reactions such as (Demchuk et al., 2003):

$$2\ Mt + 6\ CO_2 = 6\ Sid + O_2$$

$$2\ Fe_3O_4 + 6\ CO_2 = 6\ FeCO_3 + O_2 \qquad (1)$$

Calcite and dolomite compositions therefore likely reflect peak metamorphism. $CaMg_{-1}$ carbonate-carbonate exchange thermometry, though imprecise at greenschist facies conditions, indicates maximum temperatures of ~ 350 - 400 ºC (Goldsmith et al.,

1962; Rosenberg, 1967; Essene, 1983; Tribble et al., 1995) (Figure 14). Although meta-mafic assemblages likewise provide notoriously inaccurate greenschist geothermometers (Alt, 1995b; Alt et al., 1996), simplified 'pseudosections' through the system $AlO_{1.5}$-CaO-K_2O-FeO-MgO-CO_2-H_2O-SiO_2 for mafics (Figure 15 - 17) and P-T diagrams for the CaO-MgO-CO_2-H_2O-SiO_2 system for metachert-carbonate (Figure 18, 19) help constrain metamorphic conditions. The absence of metamorphic hornblende in proximate (< 20 m) and conformable meta-basalts and lack of tremolite at metachert-carbonate contacts are compatible with this rough maximum temperature estimate.

At higher grade, the presence of protolith carbonate is suggested by the widespread presence of small (~10 μm typical) needles and prisms of the tremolite-actinolite series. Both tremolite [$Ca_2Mg_5Si_8O_{22}(OH)_2$] and actinolite are variably in meta-chert, and are readily distinguished by systematic variation in the degree of pleochroism and birifringence (Figures 11 (a – d)). These Fe-Mg amphiboles would have formed in meta-carbonates that experienced partial pre-metamorphic silicification. Diopside and forsterite are nowhere present in meta-carbonates. Talc is relatively rare in Coonterunah meta-cherts (Figure 11 (e)), especially when compared to the lithologically similar overlying Strelley Pool Chert carbonates. This probably reflects lower pressures accompanying shallower metamorphism of the latter.

3.2.2. Silica Mobility and Metamorphism

The occurrence of calcite and dolomite is restricted to localized occurrences at low grade, and it is only rarely observed in association with Ca-Mg±Fe amphiboles at higher grade. In pure carbonates, dolomite is stable up to ~ 600 ºC, above which it breaks down to calcite and periclase:

$$Dol = Cc + Per + CO_2$$

$$CaMg[CO_3]_2 = CaCO_3 + MgO + CO_2 \quad (2)$$

Calcite breaks down to lime at temperatures in excess of 1200 ºC:

$$Cc = CaO + CO_2$$

$$CaCO_3 = CaO + CO_2 \quad (3)$$

If only minor silicification occurred, calcite remains present and stable until the stability field of wollastonite is reached:

$$Cc + Qtz = Wol + CO_2$$

$$CaCO_3 + SiO_2 = CaSiO_3 + CO_2 \quad (4)$$

In siliceous carbonates, additional calcite would be expected to form in talc and tremolite forming reactions:

$$3Dol + 4Qtz + H_2O = Ta + 3Cc + 3CO_2$$

$$3CaMg[CO_3]_2 + 4SiO_2 + H_2O = Mg_6Si_8O_{20}(OH)_4 + 3CaCO_3 + 3CO_2 \quad (5)$$

$$5Dol + 4Qtz + H_2O = Tr + 3Cc + 7CO_2$$

$$5CaMg[CO_3]_2 + 4SiO_2 + H_2O = Ca_2Mg_5Si_8O_{22}(OH)_2 + 3CaCO_3 + 7CO_2 \quad (6)$$

Alternatively, tremolite may form through the calcite-consuming reaction:

$$5Ta + 12Cc + 8Qtz = 6Tr + 4H_2O + 12CO_2$$

$$5Mg_6Si_8O_{20}(OH)_4 + 12CaCO_3 + 8SiO_2$$
$$= 6Ca_2Mg_5Si_8O_{22}(OH)_2 + 4H_2O + 12CO_2 \quad (7)$$

However, textural evidence for reaction (7), in the form of talc-amphibole or calcite-amphibole, is lacking. In light of reactions (1 – 6), the absence of carbonate at higher metamorphic grades suggests that silica remobilization and carbonate removal accompanied metamorphism.

In ferruginous Coonterunah cherts at higher metamorphic grade, grunerite-cummingtonite $[Fe_7Si_8O_{22}(OH)_2]$-$[(Mg,Fe)_7Si_8O_{22}(OH)_2]$ accompanies amphiboles of the tremolite-actinolite series, both occurring in S_0-parallel foliations (Figure 11 (b, f)).

3.2.3. Oxidation and Late Silicification

‘Late silicification’ refers to both precipitative and replacive silicification that ensued after peak metamorphism. Post-metamorphic cryptocrystalline silicification is readily distinguished from granular or sugary Archaean meta-chert that contains exhibits recrystallized mega-quartz (Knauth, 1994a). Much of it is under geomorphological control, being most pronounced on ridge crests and absent in freshly eroded river cuttings. It occurs on Tertiary ferricrete-silcrete plateaux, and like them, can be ascribed to alteration by oxygenated Cenozoic ground- and river- water. It is occasionally accompanied by fine haematization of pre-existing iron minerals. The style of silicification and accompanying haematite is commonly encountered throughout the Pilbara region.

Very high fluid:rock ratios in open high-throughput hydrothermal systems would have to be maintained to achieve oxidation of magnetite to haematite with anoxic waters (Catling and Moore, 2003). In consequence, certain occurrences of Pilbara haematite have been put forward as evidence for oxygenated Archaean bottom-waters (Hoashi et al., 2009; Kato et al., 2009). This argument is inapplicable to haematite in the Coonterunah Group, however, which is demonstrably post-metamorphic. All observed haematite occurs as fine reddish granular microcrystalline dusting in close association with magnetite-altering goethite and limonite in unsilicified carbonate outcrops, or as a jasperitic coating on quartz in (unmetamorphosed) chert in earthy dark-red bands in banded haematite (see also Figure 4 (e)). This hematite must have formed subsequent to greenschist-facies metamorphism under sub-hydrothermal conditions, as metamorphism and hydrothermalism would cause recrystallization to haematite of coarse grey specular habit (Kolb et al., 1973; Vorob'yeva and Mel'nik, 1977; Sapieszko and Matijevic, 1979; Diakonov et al., 1994; Sugimoto et al., 1996; Savelli et al., 1999).

A possible silicified and haematized lateral analogue of the magnetite-carbonate unit described here is shown in Figures 4 (d - e). It bears five mesobands of similar thickness, displaying textural similarities with the better preserved laminated magnetite-carbonate. Although the lack of overlying and underlying outcrop makes stratigraphic correlation difficult, it occupies a similar stratigraphic position relative to

overlying and underlying volcanic units, and is also immediately overlain by a cryptically banded black chert.

3.2.4. Alteration & Metamorphism Summary

In summary, all textural evidence is compatible with peak metamorphic temperatures between ~ 350 – 400 ºC for the sedimentary carbonate outcrop. Carbonate laminae had a pre-metamorphic aragonite-dolomite or calcite-dolomite protolith. Magnetite laminae had a ferric oxide or ferri-oxihydroxide protolith, such as goethite or magnetite.

Metamorphic assemblages are compatible with early replacive carbonate silicification, in line with good field evidence. Bedded calcium carbonate and dolomite, exposed to multiple episodes of silicification and metamorphism, were evidently fairly common constituents of Coonterunah sedimentary protoliths.

4. Geochemistry

4.1. Methodology

Samples of four carbonate mesobands, four metapelites and one biomodal tephra unit were analysed using inductively-coupled plasma (ICP) and x-ray fluorescence (XRF) techniques (Table 4 – 7). Geochemical analysis was performed by the Washington State University GeoAnalytical Lab using in-house procedures for XRF (Johnson et al., 1999) and ICP (http://www.sees.wsu.edu/Geolab/note/icpms.html). Chondrite normalizations (subscripted 'CN' hereafter) were calculated using data in Sun and McDonough (1989), and shale normalizations (Post-Archaean Australian Shale, 'PAAS', subscripted 'SN' hereafter) were calculated using data in Nance and Taylor (1976).

4.2. Metapelite and Tuff Analyses

Other than varying amounts of quartz (SiO_2 = 41.6 – 60.9 wt.%), partly reflecting varying degrees of silicification, biotite-chlorite-quartz pelites are texturally and compositionally homogeneous. They are highly ferruginous, with 17.8 – 27.9 wt.%

FeO (as total iron oxide) and only 3.4 - 5.9 wt.% MgO. Al_2O_3 accounts for 10.7 - 16.8 wt.%, and alkaline and alkali earth element concentrations were low, in agreement with the absence of feldspars observed petrologically. Bimodal tuff contains 9.9 wt.% total iron oxide, 3.5 wt.% CaO, and 2.4 wt.% Na_2O, but is in other respects geochemically similar to chlorite-quartz-biotite pelites.

Eu anomalies are sub-chondritic, LREE are enriched, MREE and HREE are flat, and there are no positive La or Y/Ho anomalies (Figure 18). Zr concentrations are in the range 150 – 450 ppm. Eu/Eu* ratios and relative Hf, La, Th, Nb, Sc, Ti, Y and Zr concentrations indicate a differentiated provinance, compatible with continental- or even passive-margin- rather than oceanic- island arc volcanism (Figure 21).

4.3. Carbonate Rock Analyses

Other than the Fe, Ca, Mg and Mn expected from magnetite-carbonate rocks, major element concentrations are low to nil. SiO_2 attains maximum concentrations of 3.3 wt.% in limonite-altered magnetite mesobands and ~1 wt.% in carbonate mesobands. Al_2O_3 and TiO_2 make up less than 0.1 and 0.01 wt.%, respectively, whilst K_2O is at or below detection limits ($\leq$ 0.0001 wt.%). P_2O_5 concentrations reach 0.05 and 0.08 wt.% in carbonate and magnetite mesobands, respectively, although ICP/XRF analysis provides poor resolution for this oxide. Carbonate mesobands contain ~ 5 – 7 ppm Na, which is absent from magnetite mesobands, consistent with individual mineral analyses.

Trace (including rare earth)-element concentrations are highest in the most calcitic sample, intermediate in dolomitic mesobands, and lowest in the magnetite mesobands (Table 5, Figure 22, 23).

REE patterns are very similar in all carbonates analyzed (Table 5, Figure 24). A prominent La anomaly is observed, with La/La* = 1.3 – 1.5 ($La/La^* = [La/(3Pr - 2Ce)]_{SN}$). Except for this positive La anomaly, LREE are highly depleted, with $(Ce/Sm)_{SN} < 1$. Ce is non-anomalous, with $Pr/Pr^* \approx 1$ ($Pr/Pr^* = [Pr/(Ce/2 + Nd/2)]_{SN}$).

Eu anomalies are strongly superchondritic, with Eu/Eu* = 1.6 - 1.7 ($Eu/Eu^* = [Eu/(Sm * Gd)^{0.5}]_{CN}$), but lowest in the magnetite mesoband. Positive Gd anomalies,

thought somewhat obscured by large Eu anomalies, are indicated by $(Gd/Tb)_{SN}$ = 1.05 – 1.10 and Gd/Gd* = 1.20 – 1.27 [Gd* = (Sm/3 + 2Tb/3)]. A strong positive Y anomaly is present, as indicated by high Y/Ho ratios of 47 - 55. Otherwise, $HREE_{SN}$ and $HREE_{CN}$ profiles are fairly flat.

Small but distinct negative Yb anomalies are also observed. Although Yb^{2+} speciation is thought to require temperatures and/or reducing conditions unattainable to most geological systems (Bau, 1991), depletion is also present in analyses of other carbonates (Wildeman and Haskin, 1973; Boynton, 1984; Lee et al., 2004), and Precambrian carbonates in particular (Kamber and Webb, 2001; Tsikos et al., 2001; Yamamoto et al., 2004; Spier et al., 2007). The issue is presently not understood, and further research is needed.

4.4. Analysis of Geochemical Results

REE systematics in intercalated meta-pelites and tuffs, both of which offer far more receptive adsorption surfaces than would carbonates, show no indication of hydrothermal, metasomatic or Phanerozoic seawater overprinting. This is a strong indication of early geochemical closure.

Precipitating calcium carbonate surfaces are quite conducive to adsorption (Comans and Middelburg, 1987; Papadopoulos and Rowell, 1989; Morse and Mackenzie, 1990; Stipp and Hochella, 1991, 1992; Stipp et al., 1992; Wang and Xu, 2001; Paikaray et al., 2005), whilst extremely large water:rock ratios are required to subsequently alter their geochemical signature (Banner et al., 1988). Ancient carbonates therefore offer excellent seawater proxies (Nothdurft et al., 2004).

Although Fe-dolomite and calcite of purported hydrothermal origin exists in the Pilbara (Kitajima et al., 2001), the Al, Cr, Fe, K, Na, Ni, Rb, Si and/or Ti enrichments observed in hydrothermally precipitated Archaean carbonates (Veizer et al., 1989b) are absent in the samples examined. Instead, the majority of trace element concentrations, including Ba, Co, Cu, Na, U and Zn, are similar to those observed in modern marine calcite and dolomite (Veizer, 1983) (Figure 22). Na concentrations, in particular, indicate precipitation from a saline fluid not dissimilar from modern seawater (Churnet

and Misra, 1981), while high Fe and Mn concentrations are typical of Archaean limestones (Veizer et al., 1989a).

The lack of a clay fraction, suggesting negligible clastic contamination, accounts for the very low Al, K, Si and Ti concentrations. Other immobile elements insoluble in aqueous solution, such as Cr (~ 0.2 ppm), Hf (< 0.04 ppm), Nb (< 0.06 ppm), Sc (< 0.1 ppm), Th (< detection limit), Y (<4 ppm), and Zr (< 2 ppm), also exhibit low concentrations. These concentrations are much (~ 10 – 100x) lower, for instance, than those reported from Archaean marine shelf carbonates from the South African Pongola and Australian Hamersley Groups (Veizer et al., 1990), which also have distinctly higher (~ 10x – 100x) concentrations of more mobile Ba and Rb, but similarly low (< 4 ppm) V and Zr concentrations. Pelagic micrite commonly contains lower abundances of these elements compared to other carbonates (e.g. Nader et al., 2006).

On the other hand, compared to Archaean benthic shelf precipitates, Coonterunah carbonates contain relatively high amounts of more soluble micronutrient metals, with ~ 2 – 5x as much Cu (10 – 50 ppm), Ni (2 – 7 ppm), Sr (42 – 72 ppm) and Zn (10 – 20 ppm) – specific enrichments shared with carbonate of microbial origin (Kamber and Webb, 2007; Algeo and Maynard, 2008). These high concentrations are outside the range of trace-metal poor carbonate cements (e.g. Clayton, 1986). Elevated concentrations of biologically conservative but redox-sensitive U and V (Algeo and Maynard, 2008) and highly sub-chondritic Th/U ratios (~ 0.5 – 1.3 compared to chondritic values of ~ 4) are compatible with oxygenated seawater at the site of precipitation (Bau and Alexander, 2009), but far from conclusive.

4.5. Discussion of Geochemistry

In comparison to many other carbonates of various ages, REE concentrations in Coonterunah carbonates are high (Figure 24), but well below (≤ 0.1x) those of strongly enriched hydrothermal carbonates (Belka, 1998; Hecht et al., 1999). REE concentrations are about an order of magnitude higher than Holocene carbonates from the Heron Reef (Webb and Kamber, 2000), carbonates from the unconformably

overlying Strelley Pool chert (van Kranendonk et al., 2003), and dolomite intercalated with Euro Basalt from the Kelly Group (Yamamoto et al., 2004). Of all Archaean carbonates, REE abundances are similar to only the most enriched samples from the Late Archaean microbial Campbellrand carbonate (Kamber and Webb, 2001). This may seem surprising in light of the fact that the Coonterunah carbonates have no discernable aluminous clastic component. However, similarly high REE abundances are in fact typical of fine-grained post-Archaean micrites, and a general correlation between ΣREE and micrite content is observed in, for instance, Devonian reefal carbonates (Nothdurft et al., 2004).

Except for higher Eu and Gd anomalies and unusually low clastic contamination, REE patterns are similar to those of Archaean sedimentary carbonate and banded-iron formation (Figure 25); that is, signatures are typical of chemical sediments precipitated from Archaean ocean water. The positive La anomaly is encountered in both modern (de Baar et al., 1991; Bau and Dulski, 1996) and ancient (Yamamoto et al., 2004) seawater, and is ascribed to the lanthanide tetrad effect (Masuda et al., 1987; Kawabe et al., 1998), as are the lesser and more rarely preserved positive Gd and Er anomalies (Alibert and Mcculloch, 1993). La, Gd and Er anomalies are generally absent in hydrothermal and metasomatic carbonates (Bau and Moller, 1992). The negative Ce anomaly which would be expected from oxygenated post-Archaean marine alteration (Alibo and Nozaki, 1999) is absent.

The strongly positive Eu anomaly is thought to result from high Eu concentrations in Archaean hydrothermal fluids (Bau, 1991) which provided an important flux to early oceans (Michard and Albarede, 1986; Derry and Jacobsen, 1990). High Eu/Sm ratios are suggestive of chemical precipitation below 200ºC (Bau, 1993). LREE depletion and superchondiritic Y/Ho ratios are compatible with open ocean deposition free from terrigenous contamination (Nothdurft et al., 2004).

The positive Y anomaly, also encountered in marine waters of all ages, is commonly ascribed to Y/Ho fractionation associated with relatively enhanced scavenging of Ho during removal by sinking particulate matter from the surface to deep -ocean (Nozaki et al., 1997). If so, somewhat lower Y/Ho ratios would be

expected from a young Coonterunah ocean. An alternative, or rather additional, explanation is that preferential complexation with CO_3^{2-} inhibits scavenging through particulate surface sorption of La, Y, Gd and Lu, leaving the water column relatively enriched in these elements. Ferrioxyhydroxide surfaces, precipitating in surface waters, provide for particularly efficient scavenging (Quinn et al., 2004). Both the extent of REE scavenging and the degree of fractionation strongly increase with CO_3^{2-} concentrations (Bau, 1999; Quinn et al., 2006). Yttrium concentrations and anomalies increase markedly with increasing relative carbonate-to-magnetite abundance, suggesting that some Y/Ho fractionation may indeed be induced by Archaean Y^{3+}-CO_3^{2-} complexation (Luo and Byrne, 2004) resulting from high pCO_2.

On the basis of our geochemical analyses, we conclude that Coonterunah micrite sampled typical Archaean ocean water, preserved a geochemical signature that was not compromised by subsequent diagenesis, hydrothermal alteration, metasomatism, metamorphism, or interaction with Phanerozoic seawater. We further conclude that micrite precipitated under high [CO_3^{2-}] in the presence of oxygen. In the context of Precambrian precipitation, we attribute greater Coonterunah Eu/Eu* anomalies to a secular decrease in the relative importance of hydrothermal influx to Earth's oceans over geological time (see also Isua Discussion in Chapter 4). Complexation with organic ligands in productive Archaean surface water would explain the unusually pronounced positive Gd anomalies (Lee and Byrne, 1993).

5. Isotopes

5.1. Methodology

The freshest surface samples of metapelites and sedimentary carbonates were selected (red arrows, statigraphic column, Figure 3) for $\delta^{18}O_{carb}$, $\delta^{13}C_{carb}$ and $\delta^{13}C_{org}$ isotopic analysis. Three samples of unequivocally metasomatic carbonate alteration were also analyzed: one associated with a late strike-slip fault off-setting Coonterunah units along strike from the prominent carbonate unit, and two others from two different carbonated alteration zones of Coucal Formation tholeiitic basalt, immediately

overlying the sampling site. One sample of a partially silicified carbonate (Figure 9 (d)) and four tuffaceous tephra units were also analyzed.

Exterior weathering was removed with a diamond saw. Samples destined for microanalysis were then drilled lamina by lamina with a 1 mm Dremel drill, while samples destined for bulk analysis were coarsely crushed, and fragments etched in concentrated HCl to remove surface contamination. Etched fragments were then finely crushed in an agate puck mill. Kerogen was isolated by decarbonation with concentrated HCl, and analysed by combustion in a Costech elemental analyzer coupled to a Finnigan MAT 253 isotope-ratio mass-spectrometer. Carbonate was analysed by reaction with HPO_4 at 80 °C using a third-generation Kiel device coupled to a Finnigan Delta-plus isotope-ratio mass-spectrometer. Results were standardized using standard statistical methods (Coplen et al., 2006), and are expressed in δ-notation as per mille (‰) values relative to the PDB standard.

5.2. Results

5.2.1. Carbonate Isotopes

Carbonate isotope analyses are plotted on Figure 27 - 29. $\delta^{18}O_{carb}$ analyses of the prominent 32-cm thick laminated carbonate unit (Table 7) ranged between -19.36 ± 0.02 and -16.00 ± 0.03 ‰, with an average of -17.8 ± 1.0 ‰. Inter-laminar variation was tighter but statistically significant, with intra-sample laminae analyses falling between -18.38 ± 0.07 and -16.55 ± 0.04 ‰. In comparison to oxygen isotopes, $\delta^{13}C_{carb}$ analyses of the 32-cm thick laminated carbonate show less lateral variability, ranging from -3.41 ± 0.02 to -2.70 ± 0.01 ‰ with an average of -3.04 ± 0.22 ‰. This is similar to the inter-laminar range between -3.41 ± 0.02 and -2.80 ± 0.01 ‰. Dolomitic carbonate obtained from a pervasively silicified sample carried similar carbon and oxygen signatures, with $\delta^{18}O_{carb}$ = -17.07 ± 0.92 ‰ and $\delta^{13}C_{carb}$ = -2.95 ± 0.13 ‰. More calcitic samples ($\delta^{18}O_{carb}$ = -18.93 ± 0.05 ‰ and $\delta^{13}C_{carb}$ = -3.13 ± 0.01) were somewhat more depleted, showing isotopic displacements of $\Delta^{18}O_{carb} \approx$ -1.0 ‰ and $\Delta^{13}C_{carb} \approx$ -0.5 ‰ relative to the averaged dolomitic samples.

With one exception, analyses of three cm-scale inter-laminated carbonate/pelite (Table 10) were similar, with two of the samples yielding $\delta^{18}O_{carb}$ = –17.71 ± 0.05 ‰, $\delta^{13}C_{carb}$ = -2.48 ± 0.02 ‰ and $\delta^{18}O_{carb}$ = -16.11 ± 0.03 ‰, $\delta^{13}C_{carb}$ = -3.34 ± 0.03 ‰, similar to those obtained for the more prominent carbonate outcrop. The third carbonate/pelite yielded $\delta^{18}O_{carb}$ = –13.35 ± 0.03 ‰, $\delta^{13}C_{carb}$ = -2.03 ± 0.11 ‰, making it the least fractionated of any laminated carbonate analyzed.

Metasomatic carbonate samples (Table 11) had highly variable oxygen and carbon isotope signatures, with two samples bearing $\delta^{18}O_{carb}$ ≈ - 16.9 to -16.6 ‰ , $\delta^{13}C_{carb}$ = +0.7 to +1.6 ‰, and a third bearing $\delta^{18}O_{carb}$ ≈ -7.7 ‰, $\delta^{13}C_{carb}$ ≈ -5.0 ‰, distinctly different from those obtained from any laminated carbonate.

5.2.2. Kerogen Isotopes

Laminae analyzed from calcitic samples bore variable, but high, amounts of kerogen, with sample averages in the range of 0.20 – 0.46 wt.% carbon (Table 12). Dolomitic laminae and samples were distinctly less kerogenous (Table 12), frequently at or below detection limits (< 0.05 wt.%). Carbonate-hosted kerogen yielded an average of $\delta^{13}C_{c_{org}}$ = -26.10 ± 2.38 ‰ (Figure 28). Petrographic examination of (early) metachert after carbonate±grunerite did occasionally reveal kerogen, but in insufficient quantities for isotopic analysis. No kerogen could be obtained from chert bands in (late) haematitic banded chert, and none was observed petrographically.

Most metapelites (Table 13) yielded little to no analyzable carbon, with the most carbonaceous sample (~0.03 wt.%) yielding $\delta^{13}C_{c_{org}}$ = -26.14 ± 0.23 ‰, similar to carbonate-hosted kerogen.

5.3. Discussion of Isotopic Results

5.3.1. Archaean Ocean Water

$\delta^{18}O_{carb}$ isotopes reveal ~3.4 ‰ of lateral variability and ~1.9 ‰ of laminar variability, indicating that the carbonate isotopes have suffered minimal closed-system intra-laminar re-equilibration. The slight fractionation observed between calcitic and dolomitic samples agrees well with that predicted from the equilibrium fractionation of both oxygen and carbon (Sheppard and Schwarcz, 1970) at T ≈ 350 - 400ºC:

$$10^3 \cdot \ln \alpha_{dol\text{-}cc} = 0.45\ (10^6\ T^{-2}) - 0.40 \quad (8)$$

$$10^3 \cdot \ln \alpha_{dol\text{-}cc} \approx 0.594$$

Giving $\alpha^{O}_{dol\text{-}cc} = 1.000594$ or $\Delta^{18}O_{dol\text{-}cc} = +0.59$ ‰

$$10^3 \cdot \ln \alpha^{C}_{dol\text{-}cc} = 0.18\ (10^6\ T^{-2}) + 0.17 \quad (9)$$

$$10^3 \cdot \ln \alpha^{C}_{dol\text{-}cc} \approx 0.567$$

Giving $\alpha^{C}_{dol\text{-}cc} = 1.000567$ or $\Delta^{18}O_{dol\text{-}cc} = +0.57$ ‰

The $\delta^{18}O_{carb}$ values of -17.8 ± 1.0 ‰ imply depleted $\delta^{18}O$ in seawater or pore-fluids. These values fit the general trend of increasing $\delta^{18}O_{carb}$ since Early Archaean times, the origin of which remains contentious (Muehlenbachs and Clayton, 1976a, b; Veizer et al., 1989a; Veizer et al., 1989b; Knauth, 1992, 1994b; Shields and Veizer, 2002; Robert and Chaussidon, 2006; Jaffres et al., 2007; Shields, 2007). Carbonate carbon isotopes are much less vulnerable than oxygen to water-rock interaction (Banner, 1995). The analyses suggest laminated carbonates have incurred only limited isotopic exchange between minerals and/or organic matter, and suffered little from post-depositional thermal processes. $\delta^{18}O_{carb}$ - $\delta^{13}C_{carb}$ values are clustered, rather than describing positively sloped linear arrays that would indicate isotopic re-equilibration during diagenesis (Dickson and Coleman, 1980), although some isotopic re-equilibration with deep Archaean pore-water (Patterson and Walter, 1994) cannot be ruled out. Thus, the micritic carbonate should, to first order, reflect the average composition of dissolved CO_2 in the ocean water it formed from. The constitution of this dissolved inorganic carbon ('D.I.C.') will depend largely on surface ocean pH, pCO_2 and temperature (Emrich and Vogel, 1970; Deines et al., 1974; Veizer, 1992).

Although several factors other than $\delta^{13}C_{DIC}$ potentially influence the pre-depositional $\delta^{13}C_{carb}$ signature (Talbot, 1990; Li and Ku, 1997; Lamb et al., 2002; Leng and Marshall, 2004; Xu et al., 2006), effects due to temperature, precipitation rates and $[CO_3^{2-}]$ were likely small and constant (Romanek et al., 1992; Spero et al., 1997).

$\delta^{13}C_{carb}$ values of -3.04 ± 0.22 ‰ are ~3 to 6 ‰ lighter than those of more recent deep-sea limestones (Milliman, 1974). However, discontinuous alternating magnetite and carbonate depositional events suggests surface- rather than deep- ocean control on precipitation, in which case $\delta^{13}C_{carb}$ values represent surface ocean $\delta^{13}C_{DIC}$. Isotopic values are compatible with stratified surface waters whose isotopic composition is controlled by organic export (Deuser, 1970), and see minimal mixing with deeper waters at the time of carbonate precipitation (Kaufman et al., 1991; Grotzinger and Knoll, 1995; Kaufman and Knoll, 1995).

5.3.2. Organic Matter

Under equilibrium carbonate-kerogen isotopic exchange (Chapter 3), an average of ~ 0.4 wt.% C_{org} with $\delta^{13}C_{org} \approx$ -26 ‰ equilibrating with ~ 99.6 wt.% calcite with $\delta^{13}C_{carb} \approx$ -3 ‰ at T ≈ 350 ºC would require pre-metamorphic kerogen as depleted as $\delta^{13}C_{org} \approx$ -42 ‰, while carbonate isotopics would undergo negligible shift. In carbonate systems at these low temperatures, however, reduced carbon-carbonate isotopic exchange is kinetically inhibited (Chapter 3), and kerogen $\delta^{13}C_{org}$ values must therefore be viewed as maxima. Similar isotopic ratios to chert-hosted kerogen (Chapter 6) further suggest that kerogen has experienced little isotopic re-equilibration with carbonate.

These carbon isotope signatures in organic detritus are compatible with a variety of autotrophic pathways and microbial clades, including both ferrous iron and oxygenic photosynthesis.

6. Protolith Identification

6.1. Magnetite precursor

Apart from the unusual carbonate association, magnetite laminae are texturally and geochemically indistinguishable from those observed in magnetite-BIFs ('oxide facies') of similar metamorphic grade, for which a ferric oxy-hydroxide precursor is widely favoured (see Chapter 2B). Before accepting this interpretation, however, the unusual bulk composition and mineralogy of the host rock calls for alternate precursors to magnetite to be considered.

6.1.1. Metamorphic Magnetite?

Natural ankerites do not exceed 37 mol.% $FeCO_3$ (~ 20 wt.% Fe) (Warne et al., 1981) and therefore cannot give rise to pure magnetite bands. Siderite may thermally decompose to magnetite through two different reactions (French and Eugster, 1965; Yui, 1966; French, 1971; Weidner, 1972; Frost, 1979):

$$6FeCO_3 + O_2 = 2Fe_3O_4 + 6CO_2 \quad (10)$$

$$6FeCO_3 = 2Fe_3O_4 + 6C + 5O_2 \quad (11)$$

In the absence of reduced carbon, the siderite-magnetite transition reaction (10) can occur at low temperatures, determined by the partial pressure of CO_2. The magnetite-siderite assemblage is stable up to temperatures of $T \approx 80$, 200 and 340 ºC at $\log(fCO_2) \approx -3$, 0 and +3 respectively. The formation of magnetite + fluid without reduced carbon from siderite through this mechanism would require oxygen to be buffered above the graphite-fluid buffer (to $\log(fO_2) \approx -25$ to -24 at $P \approx 2000$ bars, $T \approx$ 350 - 400 ºC). However, the haematite-magnetite buffer is far out of reach of the assemblages here considered, with no evidence for fO_2^{HM}-buffering accompanying metamorphism here or anywhere else in the field area. All Coonterunah haematite observed, including that in assocation with magnetite, is of post-metamorphic origin (see section on oxidation and haematization, and also Chapter 2). Even if appeals to the existence of an unusual pre-metamorphic siderite-haematite assemblage were made, this would have either required exactly molar amounts of haematite and siderite to be present, or have left some evidence of either of these main-stage reactants:

$$Fe_2O_3 + FeCO_3 = Fe_3O_4 + CO_2 \quad (12)$$

With regards to reaction (11), the very lowest temperature at which siderite can be expected to form magnetite in the absence of external fO_2 buffering is 455 - 465 ºC (French and Rosenberg, 1965), although this figure is obtained from open-system degassing at atmospheric pressure under ideal laboratory conditions. Decarbonation reactions have positive slopes in P-T space (Holloway, 1977; Holloway, 1981), and siderite degassing forms no exception. Minimum sealed-tube laboratory temperatures of 475 ºC (Weidner, 1968, 1972) can prudently be taken as a safe minimum for this natural system, which exceeds that of meta-carbonate peak metamorphism.

Magnetite textures show no evidence for ankerite, siderite or haematite pseudomorphism, and the copious quantities of reduced carbon that would accompany reaction (11) (calculation in Chapter 3) are not observed: small amounts of reduced carbon are present, but in association with Ca-Mg carbonate minerals rather than magnetite. This reduced carbon is probably sufficient to provide buffering capabilities, in which case reaction (10) could also not have occurred. It is concluded that magnetite was not formed upon metamorphism of one or more iron-bearing carbonate phase(s).

6.1.2. Diagenetic Magnetite?

The presence of well-preserved flame structures shows that magnetite did not form diagenetically as dispersed metastable magnetite from solution through half-reactions such as (Lapteva, 1958):

$$3Fe^{2+} + 4H_2O = Fe_3O_4 + 8H^+ + 2e^- \quad (13)$$

It is also unlikely that siderite or ferruginous silicates were a diagenetic precursor to magnetite. Firstly, this would have required high-fO_2 pore-waters, commonly considered improbable during Archaean deep sediment diagenesis. Oxidation fronts in modern hydrothermal systems are clearly visible in volcanic systems (Alt and Bach, 2003), and basalt-seawater reactions affect at least the top 200-300m of modern ocean crust, with deeper alteration not uncommon (Mottl and Wheat, 1994; Alt, 1995a; Staudigel et al., 1996; Wheat and Mottl, 2000; Humphris et al.,

2003). However, there is no evidence for any oxidative seafloor alteration of Coonterunah volcanic rocks with high-fO_2 bottomwater- or hydrothermal- fluids, strongly disfavouring anything other than the commonly accepted reducing Archaean porewater.

Furthermore, during diagenesis, three-carbonate-phase assemblages in the system Ca-Fe-Mg-fluid are invariant, and bulk chemistry would have resulted in alternating dolomite-ankerite-siderite, ankerite-calcite or ankerite-siderite mesobands, at odds with observed equilibrium dolomite-calcite-magnetite assemblages in both kinds of mesobands (consider the bulk compositions in ternary diagram, Figure 13). Thus it seems most likely that magnetite mesobands formed through benthic or pelagic precipitation, and are either primary or derived from amorphous ferric oxy-hydroxide precursors, such as goethite or ferrihydrite.

6.2. Carbonate Precursor

6.2.1. Calcium Carbonate

Ca/Mg ratios (Table 1, 2) establish that calcitic samples cannot represent metamorphosed pure dolomite or Mg-calcite, while those of the most dolomitic samples are compatible with only the very most calcic of naturally occuring dolomite (Reeder, 1983). Clearly, variable amounts of either aragonite or calcite must have been present prior to metamorphism.

Aragonite dissolves more readily than calcite at higher pressures experienced in deepwater environments (Lasemi and Sandberg, 1984; Burton and Walter, 1987b), and generally grows much slower in supersaturated calcium bicarbonate solutions (de Choudens-Sanchez and Gonzalez, 2009) but faster at higher temperatures (Burton and Walter, 1987a). The precipitation of aragonite is much less sensitive to Mg concentrations than that of calcite (Berner, 1975).

The identification of calcium carbonate precursors is challenging even in young rocks (Palmer et al., 1988; Dickson, 2002; Palmer and Wilson, 2004), and much more so in metamorphosed rocks of Archaean age. Several lines of evidence favour a calcitic over an aragonitic interpretation, but cannot be considered definitive. Consideration of

the partitioning behaviour of Sr argues against an aragonite precursor to calcite and dolomite (Kinsman, 1969; Kinsman and Holland, 1969; Katz et al., 1972; Lorens, 1981). Sr is positively correlated with calcite, and occurs in concentrations an order of magnitude below those of analogous contemporary limestones and dolomites, and two orders of magnitude below those of modern aragonite precipitates (Veizer, 1983). Comparison of Cu, Na and U concentrations in the latter also favour a calcite, rather than aragonite, carbonate precursor.The low concentrations of Sr are likely due to interference with Mn^{2+} (Brand and Veizer, 1980), which was likely highly concentrated in anoxic Archaean oceans (Kirschvink et al., 2000), also born out by very high Mn concentrations (Figure 22). Sr concentrations are similar to those of shallow marine Late Archaean and Early Proterozoic microbial calcite (Kamber and Webb, 2001), interpreted as an early diagenetic carbonate directly precipitated from seawater (Beukes, 1987; Sumner, 1997a).

Both calcite and dolomite bear the distinctive geochemical stamp of Archaean seawater. Overall sedimentological homogeneity and a complete lack of sedimentary textures associated with mechanical transport rule out an epigenetic origin, while the presence of flame structures (Figure 6 (a, b)) indicative of soft-sediment deformation necessitate a pre-diagenetic origin. Diagenetic crystals are absent. Thus, it can be concluded that the precursor carbonate was a primary precipitate, in keeping with the ubiquitous evidence for large-scale primary precipitation of both aragonite and calcite, independently of stromatolites, in the Precambrian (Grotzinger, 1989; Grotzinger, 1994).

It remains to be determined whether precipitation occurred *in situ*, directly on the sediment-water interface, or from suspension antecedent to settling. Pelagic (biological) carbonate precipitation in modern open oceans is slower than benthic production, but occurs over much larger areas, easily in excess of the entire lateral extent of Coonterunah sediments (Milliman, 1995). Clues to abiotic benthic carbonate precipitation, such as botryoidal, crystal fan, digitate, herringbone, radial-fibrous, tufa, and/or stromatolitic- fabrics and structures (Chafetz and Folk, 1984; Bensen, 1994; Jones and Kahle, 1995; Bartley et al., 2000; Fouke et al., 2000; Sumner and Grotzinger,

2000; Winefield, 2000; Sumner, 2002) are lacking in the Coonterunah carbonates, and lamination associated with Archaean and post-Archaean seafloor precipitation is typically isopachous, microlaminar (usually ~ 1 – 3 μm) and traceable only on the cm-scale (Panieri et al., 2008), in contrast to the km-scale mm-thick laminae reported here.

Could some uniquely Archaean benthic or earliest diagenetic microbe-sediment interaction be responsible? By supersaturating ambient seawater with respect to carbonate, several biological mechanisms are frequently implicated in the 'passive' precipitation of seafloor carbonate, and are thought to be particularly important in the aphotic zone (Chafetz and Buczynski, 1992).

A deep aphotic (> 120 m) depositional environment disqualifies possible photoautotrophic pathways (both anoxygenic and oxygenic photosynthesis), while the absence of authigenic pyrite and bioenergetic preclusion of nitrification as a nitrate source rule out heterotrophic contenders (dissimilatory nitrate reduction and dissimilatory sulphate reduction followed by H_2S removal), thereby exhausting all anaerobic CO_2-producing metabolic pathways known to be capable of causing carbonate precipitation (Castanier et al., 1999).

The only viable electron acceptor left unconsidered is ferric iron, which was readily available in the form of magnetite or its ferri-oxyhydroxide precursor. In the latter case, magnetite could even represent a metabolic waste-product (Lovley et al., 1987). However, only indirect evidence for ferric heterotrophic precipitation of carbonate minerals other than siderite exists (Hendry, 1993). Textural evidence in the Coonterunah carbonates also strongly disfavours an appreciable carbonate-forming metabolic role for magnetite or its pre-diagenetic precursor, as all observable relationships between these minerals are evidently depositional rather than diagenetic. Furthermore, extraordinarily high Archaean deep-water $[Ca^{2+}]/[HCO_3^-][OH^-]$ ratios would be needed, and kinetic hindrances from the precipitation-inhibiting effect of the ferrous iron released through all such reactions (Meyer, 1984; Sumner and Grotzinger, 1996) would somehow need to be overcome. Hence it seems most likely that precursor carbonate consisted of a micritic calcium carbonate ooze or mud that slowly settled from suspension after precipitation in the water column.

6.2.2. Dolomite

The areal extent of dolomite requires a large regional source of Mg^{2+}, and the geological setting rules out reflux dolomitization through groundwater-flow (Jones and Rostron, 2000; Jones and Xiao, 2005). The occurrence of dolomite varies laterally but does not exhibit a pronounced lamina-to-lamina or mesoband-to-mesoband variation. That is, relative to the total carbonate inventory (= dolomite + calcite + rhodocrosite), the proportion of dolomite is constant in individual outcrops (Table 1, 2), while the fraction of total carbonate as dolomite varies from ~51 mol.% (~49 wt.%) in the most calcitic sample collected, to ~86 mol.% (~85 wt.%) in the most dolomitic (Table 1, 2). More dolomitic outcrop is distinctly better preserved. The degree of dolomitization remains constant within individual fault blocks, although relatively calcitic outcrop is insufficiently continuous to rule out a tectonic control on dolomitization (Davies and Smith Jr., 2006). Only one continuous carbonate outcrop having exposed contact with underlying substrate was found, so substrate-permeability control on dolomitization cannot be ruled out as an alternative explanation.

The constant degree of dolomitization at the individual outcrop level argues against a non-mimetic origin, with a local, rather than pelagic, control on the dolomite/calcite ratio. A pelagic origin for dolomite would have been surprising, as kinetic considerations hinder its precipitation from open ocean water (Hsü, 1966; Leeder, 1999). Early reports of ambient precipitation under high pCO_2 alkaline conditions (Chilingar et al., 1967) have yet to be repeated, and synthetic precipitates in seawater-like media (Arvidson and Mackenzie, 1999) have required temperatures far in excess of an inferred Archaean temperate climate (Hren et al., in press; Blake et al., in press).

It has long been recognized that carbonates affected by mimetic dolomitization maintain their original $\delta^{13}C_{carb}$ and $\delta^{18}O_{carb}$ ratios (Epstein et al., 1963; Degens and Epstein, 1964; Weber, 1965; O'Neil and Epstein, 1966) and trace-element geochemistry (Bau and Alexander, 2006), accounting for the consistent isotopic results.

Rare instances of laminated primary lacustrine dolomite would seem to provide a poor analogue, as such dolomite accounts for less than 10% of the total laminar carbonate inventory (Warren, 1990) (compare with Table 1, 2). Disordered proto-dolomite, the precursor to primary dolomite, is far too vulnerable to survive diagenesis (e.g. Sinha and Smykatz-Kloss, 2003). Dolomite spars, rarely preserved, lack the visible curvature of saddle dolomite, thereby discounting deep burial dolomitization. Therefore, the Coonterunah dolomite probably represents a benthic replacement of precursor calcite.

This is in good agreement with geochemistry. Metapelite petrology suggests weathering of acid-intermediate tuff to chlorite rather than kaolinite, K-feldspar or K-mica, which calls for seawater with $a_{Mg^{2+}}/a_{H^+}$ over $\sim 10^5$ (Helgeson, 1967), while elevated Zn concentrations in both metapelites and volcanoclastics would be well-explained by typical dolomitizing fluids (Bustillo et al., 1992).

Were hydrothermal fluids implicated in dolomitization (Katz and Matthews, 1977; Machel and Lonnee, 2002; Davies and Smith Jr., 2006, 2007; Friedman, 2007), or did dolomitization come about through hydraulic circulation of sea-water at close to ambient temperatures, in the manner responsible for most dolomite formation today (Machel, 2004)? The occurrence of dolomite is limited to laminated carbonate, and neither overlying nor underlying volcanoclastic rocks show any evidence of hydrothermal dolomitization in the field or through the microscope. Trace element concentrations and REE anomalies decrease, rather than increase, with the degree of dolomitization. Furthermore, hydrothermal fluids would have been expected to leave a distinctive geochemical imprint on phyllosilicate-rich volcaniclastics and metapelites. Instead, these preserve remarkably intact igneous signatures (REE concentrations, Figure 18): Eu anomalies are negative rather than positive, and no superchondritic La or Y/Ho ratios are visible.

Thus, dolomite evidently formed through mimetic dolomitization of precursor calcium carbonate in the presence of ambient Archaean seawater or derived porewaters. As this style of dolomitization is inhibited in very deep and/or cold seawater (Holland

and Zimmerman, 2002), Coonterunah deposition probably did not occur at abyssal depths.

7. Speculative Model

7.1. Precipitation of Magnetite Precursor

Having eliminated a possible diagenetic, metamorphic or hydrothermal origin, there remain but four possible ways to precipitate a ferric oxy-hydroxide precursor to magnetite in an Archaean ocean:

(i) Abiotic photolytic oxidation (Cairns-Smith, 1978; Braterman et al., 1983):

$$2Fe^{2+} + 6H_2O + h\upsilon \rightarrow 2Fe(OH)_3 + H_2 + 4H^+ \quad (14)$$

(ii) Abiotic oxidation with free oxygen, following oxygenic photosynthesis:

$$CO_2 + H_2O + h\upsilon \rightarrow CH_2O + O_2 \quad (15)$$

$$4Fe^{2+} + O_2 + 10H_2O \rightarrow 4Fe(OH)_3 + 8H^+ \quad (16)$$

$$\Delta^{13}C_{c_{org}\text{ - DIC}} \approx -23\ ‰;\ \delta^{13}C_{c_{org}} \approx -26\ ‰$$

(iii) Aerobic chemolithoautotrophy, following oxygenic photosynthesis (Cloud, 1968; Cloud, 1973; Emerson and Revsbech, 1994a, b; Konhauser et al., 2002):

$$12Fe^{2+} + O_2 + 2CO_2 + 32H_2O \rightarrow 12Fe(OH)_3 + 2CH_2O + 24H^+ \quad (17)$$

$$\Delta^{13}C_{c_{org}\text{ - DIC}} \approx -5 \text{ to } -15\ ‰;\ \delta^{13}C_{c_{org}} \approx -8 \text{ to } -18\ ‰$$

(iv) Anoxygenic anaerobic ferrous photoautotrophy (Garrels et al., 1973; Baur, 1978; Hartman, 1984; Walker, 1987; Widdel et al., 1993; Ehrenreich and Widdel, 1994; Zerkle et al., 2005; Croal et al., 2009):

$$4Fe^{2+} + CO_2 + 11H_2O + h\upsilon \rightarrow 4Fe(OH)_3 + CH_2O + 8H^+ \quad (18)$$

$$\Delta^{13}C_{c_{org}\text{ - DIC}} \approx -23\ ‰;\ \delta^{13}C_{HCO_3^-} \approx -26\ ‰$$

Photolytic ferrous iron oxidation (reaction (14)) is inhibited in the presence of dissolved silica, and can no longer be considered a tenable model for the Archaean

(e.g. Hamade et al., 2000). Carbon isotopes in carbonate-hosted kerogen are compatible with both oxygenic and ferrous-iron photosynthesis.

With the exception of oxygenic photosynthesis (reaction (15)), it should be noted that all other candidate reactions generate high acidity. In order to precipitate the iron in banded-iron formation, without appealing to oxygenic photosynthesis, the efficient and continual sinking of ferric precipitates (Jamieson, 1995) would have maintained extremely acidic Archaean surface oceans. In addition to conflicting with geological evidence, in the form of widespread Archaean peri-tidal carbonate, such a system would have rapidly become bioenergetically self-limiting.

Oxygenic photosynthesizers, whose soluble waste product (O_2) and carbon source (CO_2) are in direct contact with the atmospheric reservoir, face no comparable handicap. Oxygenic photosynthesis gives rise to steep pH gradients in modern surface oceans, where [H^+] concentrations are up to an order of magnitude lower than in the sub-photic zone. This pH gradient is even more pronounced in stratified water bodies, such as the Black Sea (Codispoti et al., 1991; Basturk et al., 1994; Hiscock and Millero, 2006; Yakushev et al., 2006).

Although no geological evidence exists to sway the argument either way, and current scientific consensus stands in opposition (e.g. Canfield, 2005; Olson, 2006), a dominant role for oxygenic over anoxygenic photosynthesis seems to be the most parsimonious explanation for the Coonterunah micrite-BIF.

7.2. Precipitation of Carbonate Precursor

The origin of micrite is controversial, and has been ascribed to both biotic and abiotic processes. While shallow marine micritic ‘whitings’ may result from the stirring of bottom carbonate muds, sub-tidal ‘whitings’ are attributed to spontaneous precipitation from supersaturated seawater, possibly through oxygenic photosynthesis (Cloud, 1962; Broecker and Takahashi, 1966; Stockman et al., 1967; Bathurst, 1971; Bathurst, 1974; Neumann and Land, 1975; Ellis and Milliman, 1985; Shinn et al., 1989). All studies agree that micrites result from sporadic supersaturation with respect to carbonate in the sruface ocean.

Calcite equilibria are governed by the following reactions (Plummer et al., 1978; Busenberg and Plummer, 1986; Chou et al., 1988, 1989):

$CaCO_3(s) + H^+ = Ca^{2+} + HCO_3^-$ (forward rate: k_1, back: k_{-1}) (19)

$CaCO_3(s) + H_2CO_3^* = Ca^{2+} + 2\ HCO_3^-$ (forward rate: k_2, back: k_{-2}) (20)

$CaCO_3(s) = Ca^{2+} + CO_3^{2-}$ (forward rate: k_3, back: k_{-3}) (21)

Irrespective of whether precipitation occurs within cellular diffusive sublayers or in surrounding seawater, alternating layering of magnetite and carbonate precipitate necessitate intermittent supersaturation of calcite, in which case precipitation can be assumed to occur sufficiently far from equilibrium to allow back reactions (k_{+1}, k_{+2}, k_{+3}) to be ignored. Overlooking activity corrections:

$$\dot{d}[CaCO_3] = k_{-1}[Ca^{2+}][HCO_3^-]) + k_{-2}[Ca^{2+}][HCO_3^-]^2 + k_{-3}[Ca^{2+}][CO_3^{2-}] \quad (22)$$

It will immediately be seen that under higher pCO_2 regimes with constant pH, calcite precipitation is greatly facilitated (Figure 29, 30). At the time of calcite precipitation, surface oceans must have been sheltered from the inhibiting effects of underlying waters concentrated in ferrous iron, supporting the notion of a stratified surface ocean with transient O_2 production. Facultative aerobes, which sequester iron efficiently, would be unaffected by such Eh-stratification (Reid et al., 1993; Braun and Killmann, 1999) and would thus avoid iron limitations affecting modern phytoplankton production (Kolber et al., 1994). Oxygenic photosynthesis can occur over widespread conditions of salinity, alkalinity and cation concentrations (Guerrero and de Wit, 1992).

At steady state, calcite precipitation can compensate for the drawdown of CO_2 resulting from oxygenic photosynthesis (reaction 15 above):

$$Ca^{2+} + 2\ HCO_3^- \rightarrow CaCO_3 + CO_2 + H_2O \quad (23)$$

During Phanerozoic oxygenic photosynthesis, reactions (15) and (23) can result in the net reaction (McConnaughey, 1991; McConnaughey and Falk, 1991; McConnaughey et al., 1994; Yates and Robbins, 1998):

$$Ca^{2+} + 2\ HCO_3^- \rightarrow CaCO_3 + CH_2O + O_2 \qquad (24)$$

This assumes that CO_2 drawdown compensates for combined respiration, autotrophy and carbonate export, as it commonly is today in regions experiencing low terrestrial influx (Smith and Veeh, 1989). Such biologically mediated carbonate precipitation is common in modern stratified alkaline lakes (Kempe and Kazmierczak, 1990; Wright, 1990), and can result in seasonal planar laminations (Dickman, 1985). Compared to these Phanerozoic settings, the steady-state encapsulated by reaction (22) would have been more easily maintained under higher Archaean $[H_2CO_3]$, $[H_2CO_3]$, $[Ca^{2+}]$ and $[HCO_3^-]$, which would have ensured low CO_2 drawdown. It is further reasonable to expect that elevated Archaean temperatures, in the absence of atmospheric ozone and presence of high CO_2 and perhaps CH_4 (Rye et al., 1995; Catling et al., 2001; Ohmoto et al., 2004), would have been greatly conducive to thermal stratification. These features, in turn, may have considerably boosted the saturation state of calcium carbonate through evapoconcentration (Garrels, 1987). Calcite retrosolubility insures much readier precipitation in warmer waters.

As evidenced by empirical (Mayer, 1994b; Mayer, 1994a) and laboratory (Churchill et al., 2004) studies, carbonate mineral surfaces are unusually good adsorbers of organic matter, and a strong relationship between organic matter and calcium carbonate precipitation is commonly observed (Greenfield, 1963; Dalrymple, 1965; Monty, 1965; Golubic, 1973; Krumbein and Cohen, 1974; Golubic, 1976; Krumbein and Cohen, 1977; Krumbein et al., 1977; Krumbein, 1978, 1979; Lyons, 1984; Pratt, 1984; Kocurko, 1986; Slaughter and Hill, 1991; Chafetz and Buczynski, 1992). Organic detritus bearing the signature of photoautotrophy accompanied carbonate irrigation.

Regular magnetite-carbonate alternations hint at external periodic forcing (c.f. Eichler, 1976), and annual ocean destratification suggests itself through

sedimentological similarities with stratitified lakes and epeiric seas. The oxygenated upper ocean would have been devoid of electron donors (Fe^{2+}, H_2S) - not to mention lethal - to obligatory anaerobic anoxygenic photosynthesizers. The base of the photic zone, while inaccessible to oxygenic bacteria, may well have been accessible to the ~ 420 – 520 nm absorbance carotenoids (Kappler et al., 2006) of Fe^{2+}-oxidizing bacteria, however. If so, annual die-offs of these and other obligate anaerobes would have accompanied seasonal destratification, as happens in some lakes (Pfennig, 1977).

In sudden contact with warmer, more alkaline and oxygenated waters, ferrous iron exhibits very rapid oxidation kinetics (e.g. Lasaga, 1997)(Reaction (16) above). Since low activation energies accompanying large free energy changes tend to favour abiotic over biotic processes, much of the iron precipitation may have ensued without enzymatic catalysis. In addition to having the effect of rapidly stripping any oxygen (and other electron acceptors, notably nitrate and nitrite, albeit these would need to be microbially mediated), the introduction of more acidic deep-water and precipitation of ferric iron would have rapidly de-alkalinized surface waters, putting an abrupt end to carbonate precipitation. Disparate settling rates largely due to differences in aggregation behaviour (Jamieson, 1995; Jackson and Burd, 1998; Jones et al., 1998; Winterwerp and Kranenburg, 2002) through a > 200 m water-column would have ensured discontinuous boundaries between any co-precipitated $CaCO_3$ and ferri-oxyhydroxide.

In addition to Eh-gradients, pronounced pH-gradients typify seasonally or permanently stratified water bodies with surficial H^+-reducing oxygenic photosynthesis and deep anoxia, such as the Black Sea (Hiscock and Millero, 2006; Yakushev et al., 2006). The major restorative flux in the Black Sea results from the upward diffusive export of acidity in the form of sulphide (Anderson and Schiff, 1987; Calvert and Karlin, 1991), which was likely absent from Archaean oceans (Walker and Brimblecomb, 1985; Canfield and Teske, 1996; Canfield and Raiswell, 1999; Canfield et al., 2000; Huston et al., 2001; Shen et al., 2003; Philippot et al., 2007). Instead, the Archaean downward export and burial of ferric iron in the form of insoluble oxyhydroxides, magnetite and haematite (compare Anderson and Schiff, 1987; Peine et

al., 2000; Sobolev and Roden, 2002) was tantamount to the sequestration of photic-zone derived alkalinity – a mechanism that would remain in place until both dissolved iron- and manganese- activities were reduced to below the buffering capacity of siderite (see below).

7.3. Dolomitization

A similar style of lateral variability in the degree of dolomitization is observed in Precambrian platform carbonates, such as in the Campbellrand Platform (Beukes, 1987). The pure dolomite-iron oxide association is exceedingly rare in sedimentary rocks, however, as these minerals are more-or-less confined to shallow and deep facies, respectively. The association has been observed at the base of iron-ore deposits in the Hamersley Basin at Mount Tom Price in the Dales Gorge Member of the Brockman Iron Formation (Taylor et al., 2001), and in the Amazonas Craton 'itabirites' of the ~ 2.76 Ga Carajás Formation (Guedes et al., 2003) and the ~ 2.4 – 2.6 Ga Cauê Formation, Quadrilátero Ferrífero, Minas Gerais (Ver´ýssimo et al., 2002; Spier et al., 2003; Spier et al., 2007; Spier et al., 2008). In all three cases, the origin of dolomite has been ascribed to a hydrothermal replacement of chert (Taylor et al., 2001; Beukes et al., 2002; Guedes et al., 2003). As we discuss in the accompanying paper (Harnmeijer & Buick, in prep.), this interpretation is at odds with the textural and geochemical evidence, and the lateral transition to deeper cherty-BIFs is not a facies change, but a consequence of enhanced silicification, particularly of pre-dolomite calcium carbonate, at depth.

In comparison to Coonterunah carbonate-BIF, Proterozoic dolomite-BIFs have similar trace- and rare-earth-element distributions and $\delta^{13}C_{carb}$ values, while $\delta^{18}O_{carb}$ values are compatible with the secular temporal increase in $\delta^{18}O_{seawater}$ observed in Precambrian carbonate generally (Figures 24, 29).

In addition to Si, fluids (< 405 ºC) circulating through mafic piles gain Ca at the expense of Mg (Mottl and Holland, 1978; Mottl, 1983b, a; Bowers and Taylor, 1985; Mottl and Wheat, 1994; Alt and Bach, 2003). In marked contrast, the interaction of seawater with felsic rocks can be expected to produce Mg^{2+}-rich fluids (Baker and de

Groot, 1983) and raise Mg/Ca ratios. In addition to promoting dolomitization, elevated fluid Mg/Ca ratios inhibit silicification by increasing silica solubility (Laschet, 1984) and forming ions of $MgH_3SiO_4^+$ (Williams and Crerar, 1985; Williams et al., 1985), and also stabilize the presence of calcite by inhibiting dissolution (Sjoberg, 1978; Morse and Berner, 1979; Mucci and Morse, 1990). In consequence, dolomite is commonly associated with felsic volcanics (Baker and de Groot, 1983; Herrmann and Hill, 2001). On the rare occasions when localized Archaean dolomitization is mapped, it is frequently associated with greenstone belt felsic volcanics. Examples include the Rio del Velhas Greenstone Belt, São Fransisco Craton (Baars, 1997), the Barberton's Hooggenoeg Formation (Rouchon et al., 2009). Dolomitic Carajás BIFs directly overlie the felsic-dominated volcano-sedimentary Grão Pará Group, while sericitized meta-felsic units of the Batalal Formation underlie dolomitic Cauê BIFs.

The chert and silicified basalt cap underlying the Coonterunah tephra and carbonate sequence would have ensured chemical isolation from siliceous fluids equilibrated with underlying mafic assemblages, and would would also have provided thermal insolation (Shibuya et al., 2007), although higher Archaean surface heat heat flow may well have assisted dolomitization kinetics. We propose that deposition of bimodal tuffs and tuffaceous wackes led to an altered diagenetic flow regime characterised by reaction-controlled interstitial water profiles (Hesse, 1990) and ambient temperatues (rather than the more usual basalt-equilibrated hydrothermal fluid regime) that allowed for efficient mimetic dolomitization.

Although dolomite formation is notoriously sluggish, it yields far more enduring rocks. Calcite and aragonite, on the other hand, are highly vulnerable to dissolution. In marine environments between pH = 6 and 9, calcite dissolution rates are 1 to 2.5 orders of magnitude faster than those for dolomite (Morse and Arvidson, 2002). In modern oceans, an estimated 75-95% of deep pelagic carbonate is dissolved at the sediment-water interface (Adelseck and Berger, 1975).

It is worth noting that an increasingly prominent role for microbial mediation is recognized in contemporary dolomite formation (Vasconcelos et al., 1995; Vasconcelos and McKenzie, 1997; Wright, 1999; Moreira et al., 2004; Wright and

Wacey, 2004), but poor preservation makes is impossible to determine whether biology was responsible for Coonterunah dolomitization.

7.4. Steady-State Surface Ocean Productivity

By introducing an assumption about the isotopic composition of the dissolved carbon influx into Archaean surface ocean(s), $\delta^{13}C_w$, the fraction of organic carbon export, f_{org}, can be estimated (Kump and Arthur, 1999) very roughly using the speculative model outlined above. Phanerozoic riverine fluxes carry compositions of $\delta^{13}C_w \approx -4$ ‰ (Des Marais and Moore, 1984; Kump, 1991), but abundant geological evidence for widespread subaqeous and subaerial volcanism, and against substantial local terrigenous delivery, make a mantle value of $\delta^{13}C_w = -5$ ‰ (Chapter 3) a more appropriate choice for the Coonterunah depositional basin, giving:

$$f_{org} = (\delta^{13}C_w - \delta^{13}C_{carb}) / (\Delta^{13}C_{org\text{-}carb}) \qquad (25)$$
$$f_{org} \approx 8.70 \cdot 10^{-2}$$

Using the thinnest carbonate laminae between minimally recrystallized magnetite laminae, we estimate average carbonate laminar thicknesses in the range of $z \approx 0.1 - 0.2$ mm ($\bar{z} = 0.15$ mm), which is similar to measured laminar thicknesses in 'normal' BIFs (e.g. Gole, 1981; Gole and Klein, 1981). Assuming that fractions r_w and r_b are respired in the water- and sediment- columns respectively, and fraction r_m is devolatilized during metamorphism, total seasonal surface productivity P [g C_{org} m^{-2} $season^{-1}$] can now be estimated using total organic carbon (TOC, ≈ 0.33 wt.%) in an average carbonate lamina of thickness $\bar{z} = 0.15$ mm and density ρ_{carb}:

$$P \cdot f_{org} \cdot (1-r_w) \cdot (1-r_b) \cdot (1-r_m) = (100 \cdot TOC) \cdot \rho_{carb} \cdot z \qquad (26)$$
$$P \approx 15 \cdot (1-r_w) \cdot (1-r_b) \cdot (1-r_m)$$

In addition, equation (24) above and the molar mass ratio $M_{c_{org}}/M_{carb}$ also allow for estimation of the total seasonal surface productivity P from the amount of calcium

carbonate precipitated, assuming a 1:1 molar ratio of calcite production to photosynthesis and negligible dissolution:

$$P = d[CaCO_3]/dt = \rho_{carb} \cdot z \cdot M_{c_{org}}/M_{carb}$$

$$P \approx 49 \text{ g } C_{org} \text{ m}^{-2} \text{ season}^{-1} \quad (27)$$

This demi-annual figure is comparable to that offshore from modern productive margins (Loubere and Fariduddin, 1999), and would suggest a combined burial efficiency and metamorphic survival $[(1-r_w)\cdot(1-r_b)\cdot(1-r_m)]$ of ~32% of surface carbon exported, which seems reasonable for reducing environments that are limited in electron acceptors.

8. The Case of Missing Micrite

From trace-metal compositional trends in Archaean, Proterozoic and Phanerozoic carbonates, a secular increase in marine alkali metal ratios K_2O/Al_2O_3 and K/Rb over time has been postulated (Veizer and Garrett, 1978). Early Archaean Coonterunah samples extend this trend, which has been ascribed to increasing fluxes of continental material to the oceans through time.

Ancient basinal limestone is rare, and where present is usually associated with stromatolites. The oldest substantial (> 50 m) alkali earth-carbonate outcrops are all dolomite-dominated, and come from the ~ 3.36 Ga Chitradurga Group, Dharwarr-Singhbhum Block, India (Beckinsale et al., 1980; Radhakrishna and Naqvi, 1986; Rao and Naqvi, 1995), the ~2.7 – 2.9 Ga Michipicoten (Wawa) Greenstone Belt, Superior Province (Ayres et al., 1985; Veizer et al., 1989a), and the ~2.7 Ga Wabigoon Greenstone Belt, Superior Province (Wilks and Nisbet, 1985, 1988). Lesser limestone outcrop has been mapped in association with dolomite in the ~2.74 – 2.96 Ga Uchi Greenstone Belt, Superior Province (Hofmann et al., 1985), the ~2.7 – 2.8 Ga 'Upper Greenstones' of Zimbabwe (Nisbet, 1987), the ~2.7 Ga Abitibi Greenstone Belt (Ayres et al., 1985; Jensen, 1985; Roberts, 1987), and the ~2.7 Ga Yellowknife Supergroup, Slave Province (Henderson, 1975, 1981).

The observed paucity of ancient limestone has found frequent use in arguments for a secular increase in Ca/Mg ratios over geological time (Veizer, 1978; Veizer and Garrett, 1978; Sochava and Podkovyrov, 1995), which along with increasing Al/Fe ratios has likewise come to be ascribed to increases in terrestrial input to the oceans (Ronov and Migdisov, 1970, 1971 1971; Veizer, 1978).

The occurrence of marine micrite is also thought to have increased through geological time, with a sudden increase following the Archaean-Proterozoic transition (Robbins and Blackwelder, 1992; Yates and Robbins, 1998; Sumner, 2002). The preservation of pelagic marine micrite requires sub-tidal sediment-starved basins (Eriksson, 1983). However, non-epiclastic micrite is conspicuously absent from potentially suitable Archaean sections, such as Zimbabwe's 2.6 Ga Bulawayo greenstone belt and Australia's 2.6 Ga Carawine Formation (Sumner, 2000), and the literature does not record any instances of Archaean marine carbonate muds elsewhere.

Both aragonite and calcite crusts and micrites are absent from the deeper basinward facies in Campbellrand-Malmani, with micrite restricted exclusively to peri-tidal facies (Sumner and Grotzinger, 2004). Near-slope deep-water facies of the Wittenoon-Carawine Formation bear only Carawine-derived peri-platform oozes (Simonson et al., 1993).

Although Proterozoic micrite is common (e.g. Grotzinger, 1986, 1989; Knoll and Swett, 1990; Fairchild, 1991; Sami and James, 1994, 1996; Turner et al., 1997; Bartley et al., 2000; Turner et al., 2000), evidence for a pelagic origin is equivocal (Knoll and Swett, 1990; Sami and James, 1994; Turner et al., 1997). The well-preserved basinal micrites of the 1.8 Ga Pethei Group in northwestern Canada, where shallow platform micrite is much less common and associated with stromatolites rather than pelagic precipitation (Sami and James, 1993, 1994), perhaps provide the first unambiguous example of abundant marine micrite. So-called 'cap carbonates' of Neoproterozoic age also commonly contain abundant micritic mud, and also show similar carbon isotope ratios of $\delta^{13}C_{carb} \approx -1$ to -5 (Tucker, 1986; Singh, 1987; Fairchild, 1993; Kennedy, 1996; Hoffman et al., 1998; Myrow and Kaufman, 1999; Prave, 1999).

In short, there is no definitive evidence for the stability of soft calcium carbonate oozes on anything other than shallow platforms for 1.7 billion years subsequent to deposition of Coonterunah micrite. Factors controlling the kinetics of aragonite and calcite precipitation are complex, and include temperature, silica, Fe^{2+}, SO_4^{2-}, PO_4^{3-}, HCO_3^- and Ca^{2+} concentrations, Mg/Ca ratios, pH, the presence of organic ligands, and microbial diversity (Meyer, 1984; Inskeep and Bloom, 1986; Morse, 1997; Castanier et al., 1999; Bosak and Newman, 2003; Lopez et al., 2009). Regardless, Archaean surface ocean conditions were highly favourable to the precipitation of carbonates. This is also born out by geological evidence, in the form of a wide variety of (usually partly to completely silicified) peri-tidal carbonates.

Because of a strong and non-linear response to temperature (Lopez et al., 2009), higher inferred Archaean surface ocean temperatures (e.g. Knauth and Lowe, 2003) would favour rapid calcite formation. With regards to silica inhibition, concentrations in excess of 250 ppm dissolved silica are required to inhibit calcite precipitation below pH = 9 (Garcia-Ruiz, 2000), much higher than the solubilities of any SiO_2 species below 100 ºC (Figure 30) and thus much higher than could have been reached in Archaean surface oceans. Ferrous iron, the most effective commonly occuring cationic inhibitor of calcite formation (Meyer, 1984; Dromgoole and Walter, 1990a, b; Sumner and Grotzinger, 1996; Sumner, 1997b), appears to have been confined to deeper Archaean waters (Sumner, 1997b). The paucity of ferruginous precipitates in the shallow marine Strelley Pool Chert overlying the Coonterunah carbonates stands in support of this. Sulphate, another potent inhibitor, was likely restricted to localized marginal marine settings (Buick and Dunlop, 1990; Grotzinger and Kasting, 1993; Grotzinger, 1994). An Archaean sulphate control on dolomitization could account for the observation that some of the few Strelley Pool Chert lithofacies not to bear silicified gypsum are dolomitic ones (Buick and Barnes, 1984). Phosphate concentrations, already expected to be low in the more productive photic zone, would face further restrictions in basinal settings devoid of terrestrial clastic input. PO_4^{3-} concentrations may affect relative rates of aragonite and calcite precipitation (Berner and Morse, 1974; Berner et al., 1978; Dekanel and Morse, 1978; Mucci, 1986; Walter

and Burton, 1986), but not inhibit it altogether. High Archaean pCO_2 would have ensured high carbonate and bicarbonate concentrations, irrespective of (reasonable) pH (Figure 30).

Precambrian marine [Ca^{2+}] concentrations and Ca/Mg ratios are controversial (Kazmierczak and Kempe, 2004). There exist good theoretical arguments for the rapid initial alkalinization of the Hadaean ocean (Morse and Mackenzie, 1998), and some workers argue for sodic Archaean oceans (Maisonneuve, 1982; Kempe and Degens, 1985; Grotzinger and Kasting, 1993). It has long been known (e.g. Haedden, 1903) that chemical weathering of alkaline (Na-, K-, Ca- and Mg-) silicates in the presence of CO_2 produces alkaline solutions, and waters derived from feldspathic igneous rocks, as expected from continental weathering, are dominated by Na^+ and Ca^{2+} cations (Wedepohl, 1969; Nesbitt and Young, 1982; Fedo et al., 1995). The weathering of oceanic-crust-like material, on the other hand, is likely dominated by reactions such as the following:

$$Mg_2SiO_4 + 4CO_2 + 4H_2O \rightarrow 2Mg^{2+} + 4HCO_3^- + H_4SiO_{4(aq)} \qquad (28)$$

The nature of clays so formed will largely be controlled by the nature of the fluid, rather than bulk chemistry. Findings of chlorite-weathering of K-feldspar in Coonterunah and Isua rocks (Chapter 4) suggest that the standard view of smectite and K-mica formation from feldspar weathering (e.g. Corcoran and Mueller, 2004) may not be appropriate to Archaean marine weathering, calling for diagenetic pore-water activity ratios on the order of $Mg^{2+}/H^+ \approx 10^5$.

Pore-water studies indicate that open cold-water circulation causes Si and Mg^{2+} (and sometimes Ca^{2+}) stripping from modern sea-water (Wheat and Mottl, 1994; Elderfield et al., 1999; Wheat and Mottl, 2000; Humphris et al., 2003). Despite such Mg-stripping, present-day lower ocean crust may still act as a net oceanic Mg^{2+} source (Bach et al., 2001) through the low-temperature alteration of serpentinites, which may contribute up to the equivalent of 85% of the present fluvial flux (Snow and Dick, 1995). The controversial nature of the Archaean oceanic crust makes it difficult to infer

to what extent Archaean seawater alteration of ultramafic oceanic crust would have affected geochemical cycling.

It is thus hard to rule out the possibility that Archaean oceans may have experienced far higher Mg^{2+} influxes than today. Like today, however, the vertical and lateral distribution profiles of marine Mg^{2+} must have been fairly featureless, suggesting that if concentrations were incapable of inhibiting calcite formation anywhere they would have been so generally. A similar argument applies for the availability of Ca^{2+}, although here the issue at hand – the possibility of widespread surficial $CaCO_3$ precipitation – is obviously paramount.

In summary, the more compelling question is not "how did the Coonterunah carbonates form?", but rather, "why are there so few old rocks like it?"

9. Synthesis: Banded-Iron Formation

> "[…] if any [iron formation] represents sedimentary material of radically different composition which has suffered gross chemical transformation into [iron formation] after deposition, then some example should by now have been found and described where some vestige of the precursor which has locally escaped modification can be shown to grade laterally into [iron formation]"
>
> (Trendall and Blockley, 2004)

Canonical banded-iron formation presents a curious association of redox-insensitive silica and redox-sensitive iron (Chapter 2B). While historically attention has principally been focused on the iron-bearing minerals, it is the intimate association with chert that makes banded-iron formations so deeply unusual. Silica is not responsive to changes in redox conditions, and in fluids relevant to marine systems is highly insoluble up to pH = 9, above which it exhibits rapidly increasing solubility with increased alkalinity. The kinetic behaviour of silica in aqueous solutions is highly temperature sensitive, with solubility increasing with temperature and precipitation rates increasing by about 3 orders of magnitude between 0 and 200 ºC (Rimstidt and

Barnes, 1980). Silica readily comes out of solution upon cooling, but solubility shows low pressure dependence (Dixit et al., 2001). Kinetics at neutral pH are approximately an order of magnitude faster than at pH = 5, and much more sensitive to silica supersaturation (Icopini et al., 2005; Conrad et al., 2007).

Iron, in marked contrast, can be solubilized only under conditions of increasing acidity and severe anoxia, and becomes *more* soluble as temperature and salinity decreases (Kester et al., 1975; Liu and Millero, 2002).

Textural and other sedimentological similarities with Recent limestones have led some to propose that BIFs are diagenically altered carbonate (Lepp and Goldich, 1964; Kimberley, 1974; Dimroth, 1975). A specific hydrothermal-volcanogenic origin for BIF-hosted chert has also been proposed (Hughes, 1976; Simonson, 1985; Simonson, 1987). With regards to the Fe-mineral endowment, however, these models resort to either a replacive or a diagenetic origin. Other than being at odds with a plethora of evidence for a primary origin for ferruginous laminations and the minerals within them (e.g. McLennan, 1976 and references therein), a secondary origin for *both* iron and silica cannot account for the alternating banding.

Based on these and other geochemical considerations, together with geological evidence, it can be argued that conditions in Archaean basins were such that any micritic aragonite and calcite would either have dissolved, or silicified, and thus that the siliceous laminae in Archaean BIFs represent diagenically silicified carbonates.

9.1. Siderite Precipitation

As discussed above, the calcite - magnetite and low-Fe-dolomite - magnetite associations are rare in sedimentary rocks (Table 15, 16). This is curious, as transgressive and regressive sequences, where preserved, bear shallower carbonate facies carbonates and deeper BIF facies (Peter, 2003; Klein, 2005). The more familiar siderite-chert association, with or without magnetite, stands in conspicuous contrast. What little Ca and Mg BIFs contain usually resides in siderite and lesser ankerite. Siderite is found in transgressive sequences overlying alkali earth carbonates and underlying magnetite-chert ‘oxide facies’ BIF (e.g. James, 1955; Dimroth, 1968;

Trendall and Blockley, 1970; Dimroth and Chauvel, 1973; Klein and Bricker, 1977; Ewers and Morris, 1981; Ewers, 1983; Rao and Naqvi, 1995).

Interpretations for the origin(s) of BIF-siderite vary. Isotopically light carbon in BIF-hosted siderite and ankerite is commonly ascribed to the remineralization of isotopically light organic matter detritus, later incorporated into carbonate (Walker, 1984; Baur et al., 1985; Nealson and Myers, 1990; Brown, 2006; Raiswell, 2006; Pecoits et al., 2009). On the basis of textural evidence, some siderite has been interpreted as a precipitate or micrite (Beukes and Klein, 1992), as in the case of the Early Archaean ~3.45 Ga Panorama Formation of the Warrawoona Group (van Kranendonk et al., 2003; Bolhar et al., 2005) and ~ 3.415 Ga Buck Reef Chert of the Onverwacht Group (Lowe, 1994; Lowe and Byerley, 1999; Tice and Lowe, 2004, 2006), and the Palaeoproterozoic ~ 2.5 Ga Dales Gorge Member of the Brockman Iron Formation (Kaufman et al., 1990) and ~ 2.3 Ga Kuruman Iron Formation (Klein and Beukes, 1989a; Beukes et al., 1990), although the latter also contains siderite of demonstrably diagenetic origin (Kaufman, 1996). Some Early Archaean ankerite, without siderite, is interpreted to have precipitated directly in marginal marine sabkha and reef-like environments, such as the Dresser and Strelley Pool Chert formations (Buick and Dunlop, 1990; Lowe, 1994; Allwood et al., 2008).

Between 0 and 40 ºC, equilibrated siderite is enriched relative to co-precipitated calcite by $\Delta^{13}C_{sid\text{-}cc} \approx +6$ to +4 ‰ in the laboratory (Bottinga, 1968; Golyshev et al., 1981; Zhang et al., 2001; Deines, 2004; Jimenez-Lopez and Romanek, 2004), and also in rocks where siderite precipitation precedes or accompanies that of calcite (e.g. Uysal et al., 2000). Paradoxically, Palaeoproterozoic BIF-siderite is isotopically depleted to $\delta^{13}C_{sid} \approx -3$ to -11 ‰ (Ohmoto et al., 2004; Ohmoto et al., 2006), while calcite-dolomite both within and without banded-iron formations shows a remarkably restricted range, between $\delta^{13}C_{carb} \approx -3$ to +1 ‰ (Figure 29). Evidently, siderite was precipitated from a DIC source that was 6 to 18 ‰ more depleted than the calcite-dolomite source. This conclusion is inescapable, holding true irrespective of ocean hydrochemistry. Appeals to isotopically depleted hydrothermal carbon (e.g. Beukes et al., 1990) are incompatible with analyses from a broad array of conduit- and axial-

hydrothermal fluids (Ohmoto, 1972; DesMarais, 1996; Charlou et al., 2002; Douville et al., 2002).

The presence of siderite in BIFs can be adequately explained by precipitation induced by the hugely alkalinity-generating respiration of organic matter using ferric iron reduction. Iron reduction has played an established role in the precipitation of siderite in Phanerozoic ironstone in certain marine environments where organic matter rain rates are high in relation to porewater sulphate (Spears, 1989; Kholodov and Butuzova, 2004b, a, 2008) and some modern reducing environments (Postma, 1981, 1982; Sawicki et al., 1995). Siderite is readily generated through iron-reduction in the laboratory (Zhang et al., 2001; Romanek et al., 2003).

Although contemporary analogues to iron-dominated, low-sulphide benthic biogeochemical systems are scarce, alkalinity production is indeed encountered where these criteria are met (Howell, 1976; Psenner, 1988; Dillon et al., 1997; Van Cappellen et al., 1998; Blodau et al., 1999; Peine et al., 2000; Koschorreck and Tittel, 2002, 2007).

Three alkalinity-producing reactions involving ferric iron as an electron acceptor are known (Andrews et al., 1991), and are listed along with ensuing isotopic shift ($\Delta^{13}C_{c_{product}} - {}_{c_{reactant}}$) and expected $\delta^{13}C_{HCO_3^-}$ produced from respiration of organic detritus with $\delta^{13}C^{i}{}_{c_{org}} \approx -26‰$.

(i) Methanogenesis by acetate fermentation (Whiticar et al., 1986) coupled with methanotrophic iron reduction. This is equivalent to the anaerobic microbial oxidation of organic matter using Fe^{3+} (Alperin and Reeburgh, 1985):

$$CH_3COOH \rightarrow CH_4 + CO_2 \qquad (29a)$$

$$8Fe(OH)_3 + CH_4 \rightarrow 6H_2O + 8Fe^{2+} + HCO_3^- + 15OH^- \qquad (29b)$$

$$\Delta^{13}C_{HCO_3^-} - {}_{c_{org}} \approx -34\ ‰;\ \delta^{13}C_{HCO_3^-} \approx -60\ ‰$$

(ii) Methanogenesis accompanied by iron reduction (Coleman, 1985):

$$4\ Fe(OH)_3 + 13\ CH_2O + H_2O \rightarrow 4\ Fe^{2+} + 6\ CH_4 + 7\ HCO_3^- + OH^- \qquad (30)$$

$$\Delta^{13}C_{HCO_3^-} - {}_{c_{org}} \approx +26 \text{ to } +36\ ‰;\ \delta^{13}C_{HCO_3^-} \approx 0 \text{ to } +10\ ‰$$

(iii) Anaerobic oxidation of organic matter through iron reduction:

$$4\ Fe(OH)_3 + CH_2O + H_2O \rightarrow 4\ Fe^{2+} + HCO_3^- + 7\ OH^- \quad (31)$$

$$\Delta^{13}C_{HCO_3^-} - {}_{c_{org}} \approx 0\ ‰;\ \delta^{13}C_{HCO_3^-} \approx -26\ ‰$$

Some observations concerning these reactions are in order. It must first be recognized that in real systems the situation is complicated by the paired fluxing of methanogenesis-derived isotopically light CH_4 and heavy dissolved carbon to the site of methanotrophy, which can result in the steady-state production of DIC isotopically similar to original organic matter (Raiswell, 1987) despite on-going methanogenesis. Reaction (30) is inapplicable as a dominant pathway, as it would have produced siderite that is isotopically enriched relative to seawater, which is at odds with all geochemical evidence. If reactions (29, 31) in fact played a role in shallow BIF diagenesis, certain geological trends would be expected. In particular, since reactions producing less alkalinity also produce isotopically lighter dissolved carbon, correlations between the *amount* of carbonate produced with both associated $\delta^{13}C_{carb}$ and $\delta^{13}C_{org}$ should result: the former positive, the latter negative. As ferric iron is the only candidate electron acceptor, these trends should anti-correlate with the amount of unmetabolized ferric iron remaining.

For reactions (29) and (31), seawater mixing would be required to precipitate siderite with $\delta^{13}C_{sid} \approx -5$ to -11‰ using microbially-produced alkalinity. Although the $\delta^{13}C_{DIC}$ compositions of Archaean marine (deep) waters are not known, substantial deviations far from our inferred surface $\delta^{13}C_{DIC} \approx -3$ ‰ seem unlikely, particularly under a high pCO_2 atmosphere. Adopting a magmatic $\delta^{13}C_{DIC} \approx -5$ ‰ for Archaean deep-water at T ≈ 5 ºC, precipitation pathways (29) and (31) would need to invoke 78 to 89 % and 43 to 71 % seawater DIC components, respectively, and be capable of inducing precipitation of ~ 4.5 - 9.0 and ~ 1.7 - 3.4 moles of siderite per mole of organic carbon respired. Stoichiometric considerations therefore favour reaction (31). On a mole-per-mole of carbon basis, reaction (31) is also the most potent generator of

alkalinity, and probably out-competes all other common electron acceptors (Kuivila and Murray, 1984; Lovley, 1987; Grassian, 2005), including sulphate, reduction of which is demonstrably capable of causing carbonate precipitation in geological environments (e.g. Clayton, 1986) (Table 14). No Archaean isotopic evidence exists for an appreciable role for methanogenesis in any environment. Reaction (31) therefore presents the most likely candidate for the origin of siderite in BIFs, therefore:

$$Fe^{2+} + CO_3^{2-} \rightarrow FeCO_3 \quad (32)$$

$$K_{FeCO_3} = K_{FeCO_3}(T) = [Fe^{2+}][CO_3^{2-}] \quad (33)$$

Since greatest alkalinity is required to produce the isotopically heaviest siderite, and further organic processing by the likes of reactions (29) can account for isotopically lighter siderite as diagensis proceeds, consideration can be restricted to metabolically induced precipitation of siderite with $\delta^{13}C_{sid} \approx -5$. Reaction (31) can be separated into metabolic (*a, b*) and seawater (*x, y*) components:

$$a\ Fe^{2+} + x\ Fe^{2+} + b\ CO_3^{2-} + y\ CO_3^{2-} \rightarrow z\ FeCO_3 \quad (34)$$

Where $a = (1 - x)$ and $b = (1 - y)$ when normalized to molar siderite production, $z = 1$. By assumption, metabolic fraction b has $\delta^{13}C \approx -26$ ‰, seawater fraction y has $\delta^{13}C_{DIC} \approx -5$ ‰. Siderite produced is fractionated to an equilibrium value of $\delta^{13}C_{sid} \approx -5$ ‰, which corresponds to equilibration with $\delta^{13}C_{DIC} \approx -10$ ‰. In that case, $y \approx (5.2) \cdot b$. Now, assuming that $[Fe^{2+}]$ and $[CO_3^{2-}]$ are large compared to iron and carbonate production, the limit to equation (33) allows estimation of deep-water ferrous iron and carbonate activities:

$$[Fe^{2+}][CO_3^{2-}]^{-1} \rightarrow \sim 6 \quad (35)$$

$$[Fe^{2+}] \approx (6 \cdot K_{FeCO_3})^{0.5} \quad (36)$$

$$[CO_3^{2-}] \approx (K_{FeCO_3} / 6)^{0.5} \quad (37)$$

This results in estimated iron concentrations of ~16 μM for Proterozoic bottom-waters at 5 ºC, and would constrain Archaean pCO_2 as a function of deep-water pH (Figure

31). The pH of $CaCO_3$-buffered surface waters would then be controlled by $[Ca^{2+}]$ influx, presumably from continental weathering through carbonate equibria (19 - 21) above, supplemented with the (temperature-dependent) equilibria:

$$K_{CO_2} = K_{CO_2}(T) = [H_2CO_3]\,(pCO_2)^{-1} \quad (38)$$

$$K_{H_2CO_3} = K_{H_2CO_3}(T) = [H^+]\,[HCO_3^-]\,[H_2CO_3]^{-1} \quad (39)$$

$$K_{HCO_3^-} = K_{HCO_3^-}(T) = [H^+]\,[CO_3^{2-}]\,[HCO_3^-]^{-1} \quad (40)$$

Like all respiration that makes use of a solid-state electron acceptor, the oxidation of organic matter with ferric iron requires either grain-contact or chelation (Megonigal et al., 2004; Fortin and Langley, 2005). Ferric iron likely represented the most potent, if not the only, electron acceptor in the Archaean benthic environment, which may in part account for the lack of organic coatings and general sterility of BIF-hosted primary magnetite and haematite. By this reasoning, the association of shallower sideritic BIF facies with lower $\delta^{13}C_{carb}$ and lower magnetite contents is no surprise - in fact, just such diagenetic $\delta^{13}C_{carb}$ – ferric iron trends are seen in Phanerozoic ironstones (e.g. Hangari et al., 1980).

A positive correlation between magnetite content and $\delta^{13}C_{org}$ in associated kerogen has been used to argue against a metabolic and/or diagenetic origin for siderite. In fact, this correlation is also seen in modern sediments bearing primary magnetite (e.g. Andrews et al., 1991), and the reported 'oxide-facies' values ($\delta^{13}C_{org} \approx -26 \pm 4‰$) are highly typical of pelagic production in stratified oceans, and have remained remarkably constant throughout the Archaean and well into the Palaeoproterozoic. Lighter $\delta^{13}C_{org}$ values in sideritic BIFs are readily explained by greater overlying surface ocean productivity and respiration involving consortia of fermenters and anaerobic ferric-iron-reducing methanotrophy (Beal et al., 2009).

9.2. Silicification of Carbonate

Silicification can preserve textures at and below the micron scale (Akahane et al., 2004), whereas texturally destructive dolomitization results from the strong tendency of authigenic dolomite tendency towards macrocrystallinity (Swett, 1965; Bustillo and Alonso-Zarza, 2007), thereby accounting for more irregular interlaminar boundaries in Coonterunah micrite-BIF when compared to those of cherty banded-iron formation of similar grade.

Calcium carbonates are highly amenable to silicification, as shown by replacement in a extraordinarily broad array of geological environments and periods (Siever, 1962; Walker, 1962; Hesse, 1987b, 1989b; Noble and Van Stempvoort, 1989; Fairchild et al., 1991; Kuehn and Rose, 1992; Spotl and Wright, 1992; Misik, 1993; Ulmerscholle et al., 1993; Knauth, 1994b; Mazzullo, 1994; Whittle and Alsharhan, 1994; Gardner and Hendry, 1995; Penela and Barragan, 1995; GarciaGarmilla and Elorza, 1996; Arenas et al., 1999; Thiry, 1999; Bartley et al., 2000; Chetty and Frimmel, 2000; Goedert et al., 2000; Packard et al., 2001; Alonso-Zarza et al., 2002; Bustillo et al., 2002; Eliassen and Talbot, 2003; Slack et al., 2004; Holail et al., 2005; Henchiri and Slim-S'Himi, 2006; MacKenzie and Craw, 2007; Lakshtanov and Stipp, 2009).

Mechanisms of carbonate silicification are poorly understood, and few laboratory simulations – let alone under Archaean conditions - have been attempted. Replacement is surface-area controlled, resulting in an inverse relationship between silicification and carbonate grain-size fraction (Kastner et al., 1977; Williams and Crerar, 1985). Perhaps for this reason, in mixed carbonates, carbonate mud is the most readily silicified constituent (e.g. Meyers, 1977; Geeslin and Chafetz, 1982). Higher P_{CO_2} also enhances carbonate silicification, perhaps through prevention of calcium carbonate buffering (Lovering and Patten, 1962).

Silica precipitation can involve different pseudomorphs, and can also occur directly through a gel stage. In near-surface environments, precipitation from aqueous solution usually occurs in the form of amorphous silica or opal-A. Opal-CT formation occurs in sediments of pre-Miocene age, and also forms diagenetically (Weaver and Wise, 1973; Bohrmann et al., 1990; Bohrmann et al., 1994), perhaps in response to

greater water depths (Knauth, 1979; but see Gao and Land, 1991), where it is the most common diagenetic precursor to quartz (Flörke et al., 1976).

Much of the silica after carbonate in the sedimentary record, however, appears to have precipitated directly as chalcedony or quartz (Walker, 1962; Jacka, 1974; Hatfield, 1975; Meyers, 1977; Maliva and Siever, 1988b; McBride, 1988; Knauth, 1992; Hendry and Trewin, 1995). During early diagenetic silicification with high [Si] porewaters, carbonate mud comes to be replaced by microcrystalline (< 5 - 20 μm in diameter, also called 'microquartz' (Folk and Pittman, 1971)) or to cryptocrystalline quartz, rather than mega-quartz (Jacka, 1974; Hatfield, 1975; Hesse, 1987a). As evidenced by sequential fabric changes during rim-to-core silicification of carbonate ooids, high [Si] concentrations generally result in replacement by cryptocrystalline quartz rather than other silica fabrics (Choquette, 1955; Swett, 1965; Chanda et al., 1976; Chanda et al., 1977). Where estimates have been possible, silicification is found to be rapid (McBride, 1988), commonly reaching completion during the early stages of diagenesis (Hesse, 1972; Jacka, 1974; Namy, 1974; Meyers, 1977; Meyers and James, 1978; Geeslin and Chafetz, 1982).

The composition of carbonates exerts a strong control on silicification, which is a highly selective process (Maliva, 2001). Geological evidence suggests that calcite is more amenable to silicification than aragonite (e.g. Holdaway and Clayton, 1982; Woo et al., 2008), although one of the few laboratory studies found little difference between Mg-calcite, aragonite and aragonite replacement rates (Klein and Walter, 1995).

Marine silicification of mixed dolomite-calcium carbonate assemblages, meanwhile, shows preferential and faster silicification of the latter, frequently leaving dolomite altogether untouched (e.g. Knauth, 1979; Whittle and Alsharhan, 1994; Penela and Barragan, 1995). Hydrothermal silicification also preferentially replaces undolomitized (or less dolomitized) calcite over pure dolomite (e.g. Kuehn and Rose, 1992; Packard et al., 2001). Indeed, precursor carbonate dolomitization and silicification commonly go hand-in-hand (Geeslin and Chafetz, 1982; Laschet, 1984; Keheila and Elayyat, 1992; Alonso-Zarza et al., 2002)(see also Strelley Pool Chert,

Chapter 2C), since the former causes the necessary de-alkalinization of porewater that enables precipitation of the latter:

$$CaCO_3 + Mg^{2+} + HCO_3^- \rightarrow CaMg(CO_3)_2 + H^+ \quad (41)$$

$$H_4SiO_{4(aq)} = H_3SiO_4^- + H^+ \quad (42)$$

$$H_4SiO_{4(aq)} = Si_2O_6(OH)_6^{2-} + 4H_2O + 2H^+ \quad (43)$$

$$H_4SiO_{4(aq)} \rightarrow SiO_2 + 2H_2O \quad (44)$$

In the absence of dolomitization, several other mechanisms greatly enhance the ability of silica to precipitate in the presence of calcium carbonate (Greenwood, 1973; Kastner et al., 1977; Kitano et al., 1979; Williams and Crerar, 1985; Williams et al., 1985). For instance, during the potentially important transformation from opal-A to opal-CT, which is strongly temperature-dependent and inhibited by the presence of clay minerals, carbonate dissolution-silicification becomes autocatalytic by providing the necessary hydroxyl ions (Kastner, 1983):

$$CaCO_3 \rightarrow Ca^{2+} + CO_3^{2-} \quad (45)$$

$$CO_3^{2-} + H_2O \rightarrow OH^- + HCO_3^- \quad (46)$$

The thermodynamic drive towards replacive silicification of carbonate depends on the proclivity of available dissolved silica to precipitate, together with the tendency of carbonate towards dissolution.

9.2.1 Silica precipitation

Silicification is the most pronounced form of alteration to have affected Early Archaean outcrop, selectively conferring upon it a profound preservation bias (Chapter 1). Contemporary chert formation, which is common, takes place through intraformational redistribution (dissolution and reprecipitation) of biogenic silica, particularly siliceous sponge spicules, radiolarian tests and diatom frustules. Silica biosynthesis evolved no earlier than ~ 750 Ma (Bengston, 1994). Decoupled Archaean carbon and silica cycles would have allowed for silica-saturated or even super-saturated Archaean bottomwaters (Maliva et al., 1989; Siever, 1992), in strong contrast

to today (Ragueneau et al., 2000). Silica concentrations of 20 - 120 ppm have been estimated for Precambrian oceans (Holland, 1984). Thus thermodynamically unhindered, Archaean pre- and syn-diagenetic silicification was vigorous and widespread, although there also exists ample evidence for late silicification in the Precambrian (e.g. Maliva, 2001).

Silica shuttling through adsorption onto precipitation ferric oxide surfaces (Fischer and Knoll, 2009) poses an efficient delivery mechanism. Shuttling would have been assisted by the strong control of pH on silica adsorption (Swedlund and Webster, 1999; Davis et al., 2002), with silica adsorbing efficiently in shallow alkaline waters and desorbing rapidly in acidic Archaean deep water, thereby maintaining a silica gradient and prohibiting the build-up of silica in shallow waters.

A direct role for Archaean biota in silicification can be ruled out. Most experimental evidence for such a role is negative (Yee et al., 2003; Konhauser et al., 2004). Although microbes may provide an interface for silicification (Benning et al., 2004a; Benning et al., 2004b), their role becomes appreciable only under extremely acidic (pH ~ 3) conditions (Amores and Warren, 2007). However, dead organic matter may have indirectly stimulated silicification, as such relationships are frequently seen in Proterozoic carbonates with chert nodules and lenses (Knoll and Simonson, 1981; Knoll, 1985)

Both low-temperature and hydrothermal reactions have been implicated as a cause of Archaean silicification (Hanor and Duchac, 1990). In modern shallow-shallow environments, silicification is often brought about through the rapid decrease in alkalinity (Kuznetsov and Skobeleva, 2005b, a), for instance through mixing of low-pH water with silica-saturated water in coastal depressions (Umeda, 2003), through intermittent supply, and after periodic dehydration (Hinman and Lindstrom, 1996). Groundwater silicification, in particular, can give rise to regionally extensive alteration (Thiry and Millot, 1987; Thiry et al., 1988a; Thiry et al., 1988b; Thiry and Ribet, 1999).

The potential for silicification increases markedly with water depth (Maliva and Siever, 1988a), and silicification of deep-sea carbonate is consequently a common modern phenomenon (e.g. Rex, 1969; Winterer et al., 1970; Heath and Moberly, 1971;

Weaver and Wise, 1972; Wise and Kelts, 1972), despite the fact that eukaryotic bioturbation severely reduces porewater silica concentrations (Gehlen et al., 1993).

It is well established in laboratory (Lewin, 1961; Iler, 1979; Delmas et al., 1982) and field (Millot, 1970; Parron et al., 1976; Thiry, 1981) studies that the surface adsorption of Fe^{2+} and other cations decreases both silica solubility and solution rates.

9.2.2. Hydrothermal Silicification

The replacement of carbonate by silica has long been recognized as a characteristic feature of hydrothermal systems (Schwartz, 1959; Keith et al., 1978; Hutchinson, 1982; Rimstidt and Cole, 1983; Hesse, 1989a). Measured in terms of convective heat transfer, present diffusive hydrothermal flow across the seafloor is 5 to 10x more significant than the focused flow occurring through discrete conduits (Lowell et al., 1995). Most of this is seawater was modified by fluid path leaching during chemical reactions with subsurface rocks (Skinner and Barton, 1973; Halbach et al., 1997).

Silica leaching is particularly efficient in basalts (James et al., 2003), giving rise to hot silica-supersaturated fluids. Modern mafic hydrothermal systems are further characterized by pronounced depletions in O_2, Mg^{2+} and SO_4^{2-}, and enrichment in H^+ (Seyfried, 1987; James et al., 2003). An average pH of 3.5 was obtained from a recent compilation of 20 marine hydrothermal systems (Butterfield et al., 2003). These acidic conditions are maintained through uptake of hydroxyl ions into phyllosilicates, $Mg(OH)_2$ fixation during seawater-rock interactions, and Ca^{2+} leaching (Alt and Bach, 2003; Halbach et al., 2003), with magmatic CO_2 and SO_2 possibly giving rise to additional acidity (Butterfield et al., 2003). Ca-bearing phases are particularly vulnerable to alteration by the resulting hot and acidic silica-supersaturated fluids (Duchac and Hanor, 1987; Seyfried, 1987; Hanor and Duchac, 1990; Toulkeridis et al., 1998; Seyfried et al., 1999; James et al., 2003), which causes a pronounced preferential replacement of carbonate minerals (e.g. Slack et al., 2004). Analyses of ankerite intercalated in Pilbara Euro Basalt pillows show significant silicifation (5 – 10 wt.%, Yamamoto et al., 2004).

9.2.3. Carbonate Dissolution

Many factors effect carbonate dissolution rates (Eisenlohr et al., 1999). In modern oceans, the ready dissolution of calcium carbonate is driven by its unusual retrograde solubility, the undersaturated state of bottom waters, and the production of carbonic acid (and to a far lesser extent, ammonia and sulphide) during organic matter oxidation (Emerson and Bender, 1981; Archer et al., 1989; Berelson et al., 1990; Berelson et al., 1994; Steinsund and Hald, 1994). Experiments have consistently shown that suspended carbonate dissolves faster than sediment plugs (Keir, 1980, 1983), and that smaller size fractions dissolve more readily, with log dissolution rate ∝ reciprocal diameter (Morse, 1978; Keir, 1980; Walter and Morse, 1984).

Sufficiently far from equilibrium, where back reactions (19 - 21) above can neglected, calcium carbonate dissolution rates (mol cm^{-2} s^{-1}) are described by:

$$\text{Dissolution rate} = k_1[H^+] + k_2[H_2CO_3^*] + k_3 \quad (47)$$

While net silicification of carbonate proceeds as follows:

$$CaCO_3 + H_4SiO_{4(aq)} \rightarrow SiO_2 + Ca^{2+} + 2\ H_2O + CO_3^{2-} \quad (48)$$

Assuming rates for silica precipitation are also applicable to replacement, reaction (48) will display fourth-order kinetics (Icopini et al., 2005):

$$\text{Silicification rate} = k_4[H_4SiO_4]^4 \quad (49)$$

Where the rate constant is a strong function of pH:

$$k_4 = -\ m \log [H^+] + \log k_0 \quad (50)$$

and rate constant co-efficient *m* in equation (50) itself also varies as a function of $[H^+]$. The concentation of Archaean silicic acid, $[H_4SiO_4]$, will depend on water temperature, and whether Archaean oceans were supersaturated with respect to quartz, opal-CT, or amorphous silica. Concentrations do not change appreciably between pH = 5 and pH = 9, and (unlike Ca^{2+} and Fe^{2+}) are independent of pCO_2 (Figure 29). Between 0 and 100 ºC, the solubility of quartz increases by an order of magnitude, from ~0.1 to 1.0 mM,

while that of amorphous silica increases from ~1.1 to 6.5 mM. Under these circumstances, respective silica precipitation rates will be around ~10^{-12} and ~$0.25 \cdot 10^{-7}$ mmol sec^{-1} between pH = 6 and 9. In contact with seawater, Archaean silicification of calcite (V_{mol} = 33.93 cm^3 mol^{-1}) using cold waters saturated with respect to amorphous silica (or hot waters saturated with respect to any phase of silica) would occur on timescales on the order of 10 - 100 years. Solutions buffered by ferrous iron cause rapid dissolution of calcium carbonate grains, and precipitation of a ferric oxide coating on carbonate grains (Castano and Garrels, 1950).

9.3. Geochemical Evidence

Few geochemical techniques are capable of elucidating widespread silicification of precursor carbonate, since this process would be expected to lead to the simple dilution of trace elements, including more immobile REEs, Y, Zr, Hf, Th, Sc and Al (Dostal and Strong, 1983), and anomalies imparted by fractionation in aqueous media are carried by magnetite or Ca-Mg carbonate rather than silica. Field studies attest to these elements' immobility during both hydrothermal- (Duchac and Hanor, 1987) and diagenetic- (Murray et al., 1992) silicification.

Similar diagenetic $\delta^{18}O_{SiO_2}$ values in carbonate-replacing cherts from shallow-marine carbonates and cherts in deep-marine banded-iron formation (compare Becker and Clayton, 1976; Knauth and Lowe, 1978b; Perry et al., 1978b; Katrinak, 1987; Hoefs, 1992; Knauth and Lowe, 2003) are compatible with a similar origin for both. $\delta^{18}O_{SiO_2}$ values in early silicified carbonate from Barberton's Onverwacht Group range from -14.5 to -8.5 $‰_{PDB}$ (Knauth and Lowe, 1978a), while the least thermally processed cherts at Isua give $\delta^{18}O_{SiO_2}$ = -10.2 $‰_{PDB}$ (Perry et al., 1978a). Lamellar $\delta^{18}O$ analyses of Hamersley banded-iron formation show similar values ($\delta^{18}O_{SiO_2} \leq$ -8.2 $‰_{PDB}$) in partially equilibrated iron-oxide-rich bands (Becker and Clayton, 1976; Ohmoto et al., 2006), while the isotopic range of iron-oxide-poor bands tends towards more isotopically depleted, diagenetic-like values (-19.3 $‰_{PDB} \leq \delta^{18}O_{SiO_2}$) (Ohmoto et al., 2006), compatible with the interpretation that a chert component formed after iron

oxide. Carbonates without chert examined in these studies typically equilibrated with higher $\delta^{18}O$ fluids (Becker and Clayton, 1976), compatible with the replacement hypothesis put forward here.

As laboratory experiments show no Y/Ho fractionation during adsorption on silica (Kosmulski, 1997), it is noteworthy that Early Archaean cherts appear to carry chondritic to slightly sub-chondritic, rather than Archaean seawater-like, Y/Ho ratios (Minami et al., 1998). Ge/Si ratios in BIFs also support the view that iron and silica are sourced from different reservoirs (Hamade et al., 2003; Slack et al., 2004; Frei and Polat, 2007).

Two measures to aid investigation of BIF diagenesis can be introduced (M_x is molecular weight of molecule x):

Precursor CaO (wt.%), $\mathfrak{D}_{CaO}$ =

CaO in (present calcite + pre-dolomitization calcite + pre-silicification calcite)

$$\mathfrak{D}_{CaO} = M_{CaO}\cdot(W_{CaO}/M_{CaO} - W_{MgO}/M_{MgO} + 2\,W_{MgO}/M_{MgO}) + 100\cdot(\rho_{cc}/\rho_{qtz}\cdot W_{SiO_2})\,/(\rho_{cc}/\rho_{qtz}\cdot W_{SiO_2} + (100 - W_{SiO_2})) \quad (51)$$

Degree of Silicification (molar), ς =

(moles of quartz) / (moles of precursor calcite)

$$\varsigma = (W_{SiO_2} / M_{SiO_2})\,(P_{CaO}\,M_{CaO})^{-1} \quad (52)$$

This simple first-order analysis assumes that all silica was formed through replacement of carbonate. Evidence that silicification of carbonate occurred very early in Early Archaean shallow environments comes from the lack of correlation between $\delta^{18}O_{carb}$ and the degree of silicification, ς, in the Stelley Pool Chert (Figure 33(a), using data in (Lindsay et al., 2005)), as corroborated by textural and structural relations in neptunian fissures sourcing material from the Strelley Pool Chert (Geological Introduction, Chapter 2). Clear evidence for progressive diagenetic silicification in both shelf carbonates and BIFs (Figure 34 (b)), meanwhile, can be deduced from analysis of

Pangola Shelf rocks (using data in Veizer et al., 1990)) and magnetite-calcite rocks associated with BIFs of the Mooidraai Formation (using data in Tsikos et al., 2001).

The combined diagenetic effect of carbonate silicification and dissolution can be represented as the resultant of two vectors in CaO+MgO – FeO* – SiO_2 chemical space (Figure 32). For isovolumetric silicification, the slope of the silicification vector will depend on the density contrast between the carbonate phase replaced and the silica phase precipitated, which will depend on the phases involved (Table 15). Appreciable clockwise trends away from the (CaO + MgO) – (SiO_2) parallel would be expected, for instance, for replacement of either aragonite or calcite by opal-A ($\rho_{opal\text{-}A}$ / ρ_{cc} = 2.01 / 2.71 ≈ 0.74), while only minimal density changes are incurred during silicification directly to α-quartz ($\rho_{\alpha\text{-}quartz}$ = 2.65 g cm^{-3}). As any opaline phases would ultimately have transformed to α-quartz, this will not alter our analysis.

Results for a variety of Early Archaean carbonates and all known Ca-Mg carbonate-bearing BIFs for which data could be found are plotted in Figure 33, the latter unfortunately restricted to the Palaeoproterozoic (Mooidraai data refers to the same rocks plotted in Figure 34 (b)). Magnetite-barren carbonates of non-hydrothermal origin plot close to the calcite - quartz and Fe-dolomite – quartz joins. Compositional trends in magnetite-bearing Palaeoproterozoic Ca-Mg carbonates, meanwhile, reveal diagenetic reactions to form greenalite and minnesotaite:

$$CaCO_3 + 3Fe^{2+} + 2H_4SiO_4 + 6OH^- \rightarrow$$
$$Fe_3Si_2O_5(OH)_4 + Ca^{2+} + CO_3^{2-} + 5H_2O \quad (53)$$

$$CaCO_3 + 3Fe^{2+} + 4H_4SiO_4 + 6OH^- \rightarrow$$
$$Fe_3Si_4O_{10}(OH)_2 + Ca^{2+} + CO_3^{2-} + 10H_2O \quad (54)$$

Trends captured by reactions (53) and (54) may perhaps also be explained by the formation of quartz and a ferruginous mineral, such as siderite or magnetite:

$$CaCO_3 + 3Fe^{2+} + H_4SiO_4 + 3HCO_3^- + 3OH^- \rightarrow$$
$$3FeCO_3 + 2SiO_2 + Ca^{2+} + CO_3^{2-} + 5H_2O \quad (55)$$

$$CaCO_3 + 3Fe^{2+} + 4H_4SiO_4 + 3HCO_3^- + 3OH^- \rightarrow$$
$$3FeCO_3 + 4SiO_2 + Ca^{2+} + CO_3^{2-} + 1H_2O \quad (56)$$

Although different Early Archaean bottom- and pore-water chemistry would have caused marked differences with Palaeoproterozoic BIF diagenesis (as attested, for instance, by the apparent non-primary origin of some Palaeoproterozoic magnetite in Figure 33), the little available data on Ca-Mg carbonate-bearing BIFs show that the amount of chert tends to increase at the cost of Ca-Mg carbonate during diagenesis.

9.4. Preliminary Geological Evidence

In a pilot study, a selection of BIFs were examined for fluid-inclusion evidence of carbonate silicification in chert bands. BIFs were examined from: (i) the ~3.7 – 3.8 Ga Isua Supracrustal Belt (Chapter 4); (ii) outcrop of > 3.4 Ga Swaziland Supergroup in the Vredefort impact-structure; (iii) the ~3.0 Ga Gorge Creek Group (Chapter 2C); (iv) the ~2.593 Ga Marra Mamba Iron Formation at the base of the Hamersley Group; and (v) the ~ 2.46 Ga Kuraman Iron Formation in the upper Transvaal Supergroup. All were found to contain small (1 – 5 μm) bleb-like oval inclusions (Figure 35) that optically resemble fluid inclusions in carbonate silicification zones of the Pilgangoora Belt described above (see also Chapter 2C). Exhaustive microprobe analysis of several Isua samples confirmed the absence of a crystaline phase. Inclusions are enclosed within quartz grains, and distinctly smaller and less entrained in more metamorphosed BIFs examined, consistent with the behaviour of CO_2-H_2O inclusions in quartz (Kerrich, 1976).

10. Conclusions

Coonterunah carbonates were deposited and lithified in a chemical environment dominated by Archaean seawater rather than basalt-equilibrated hydrothermal fluids. High Mg^{2+} concentrations suggest an important role for serpentinization in the regulation of Early Archaean seawater chemistry. Kerogen and carbonate $\delta^{13}C$ isotopes are compatible with precipitation in a stratified surface ocean in which photoautotrophy

occurred. High copper concentrations sampled from the surface ocean and the absence of diagenetic pyrite attest to a limited role for sulphur cycling in the Early Archaean benthic environment.

Geochemical and sedimentological features of Coonterunah carbonate fit very well with a pelagic micrite origin, and alternating discontinuous lamination with magnetite strongly favours precipitation under the control of changes in surface ocean chemistry. Figure 36 and 37 schematically summarize the key biogeochemical cycles in Archaean benthic and pelagic environments discussed. The mechanisms by which alternating precipitation occurs remains speculative, and many alternative models may be envisaged. Seasonal destratification of a transiently oxidized surface ocean is favored, as this mechanism provides for the conditions ammenable to *both* ferric iron *and* Ca-carbonate precipitation.

Coonterunah carbonate, already technically a BIF (>15 wt.% FeO) in its unsilicified form, represents canonical oxide-facies BIF when silicified, and may present a possible window into BIF-formation. Figure 38 aims to give an overview of a generalized Archaean marine environment with reference to BIF genesis.

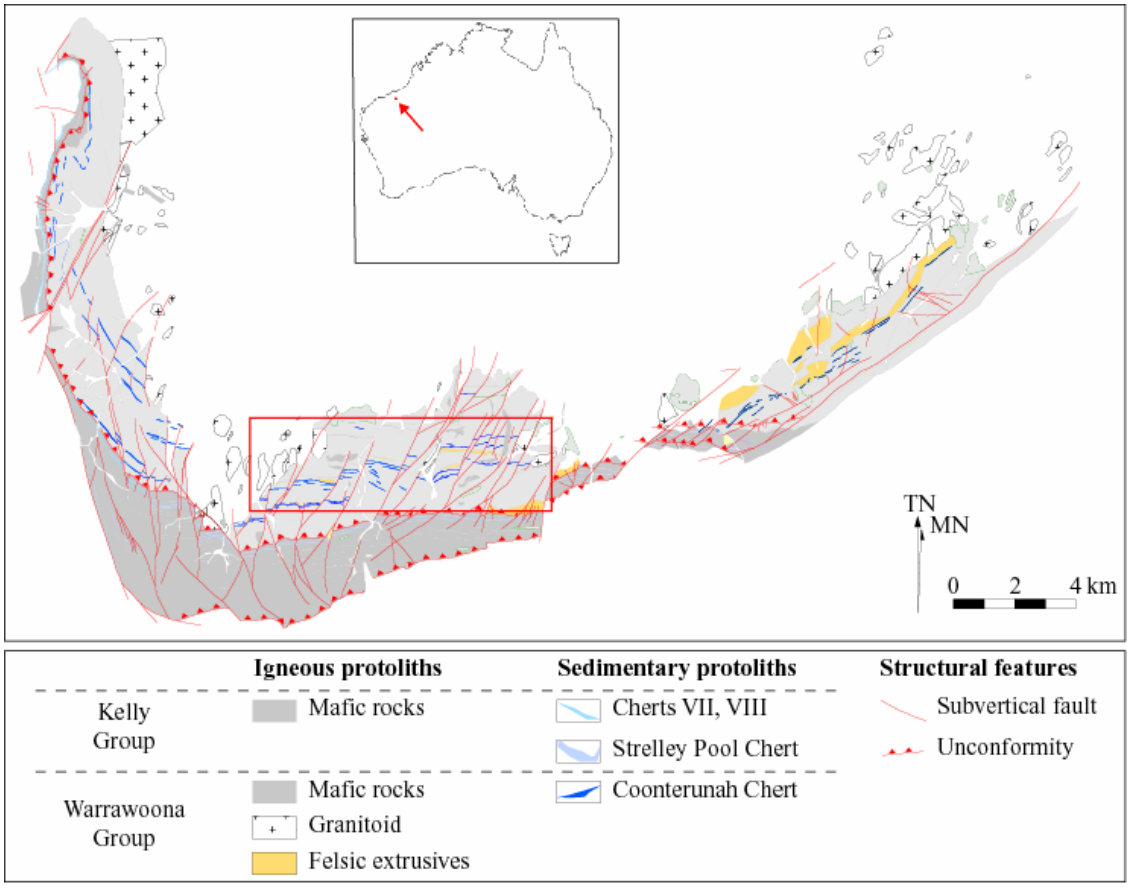

Figure 1: Geological map of Pilgangoora Belt, with regional location shown in inset. Box shows outline of study area (Figure 2).

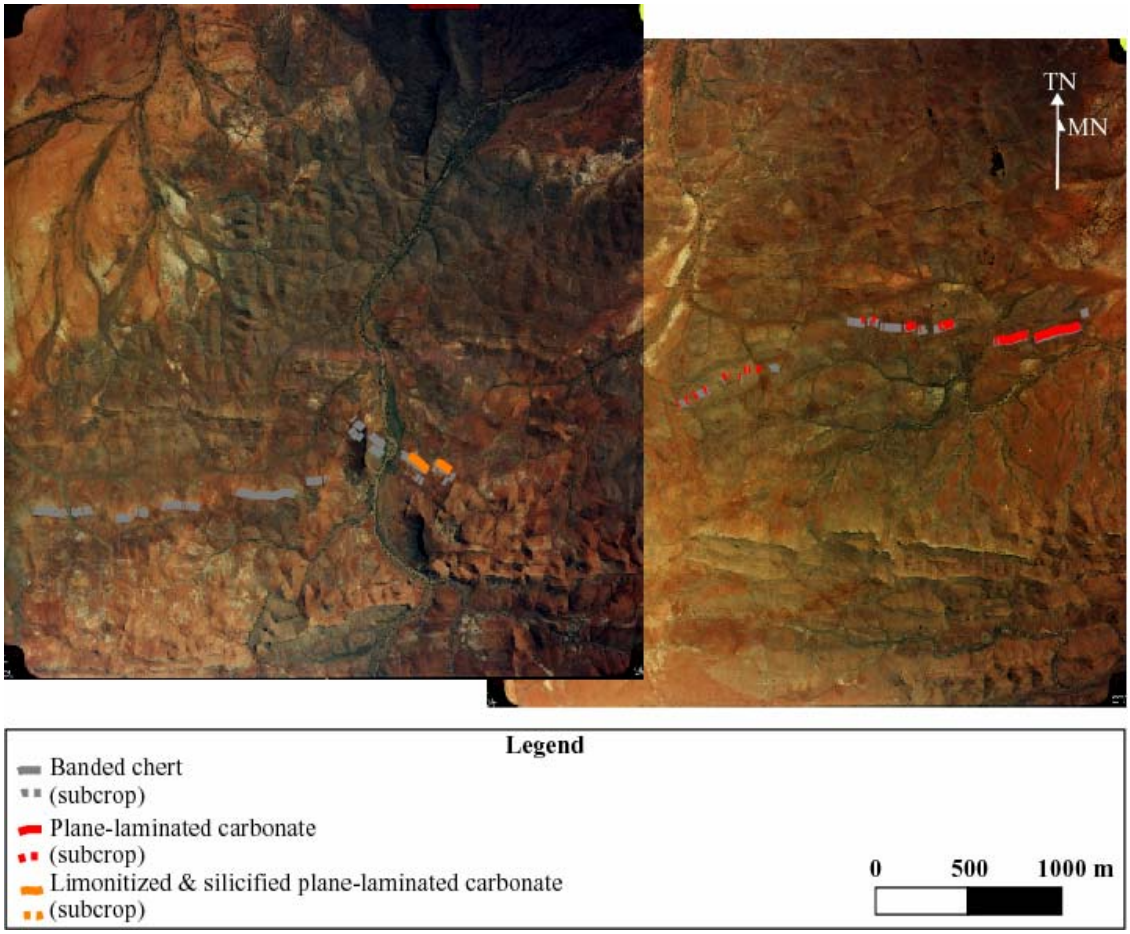

Figure 2: Aerial photograph of micritic-BIF outcrop in Coonterunah Subgroup.

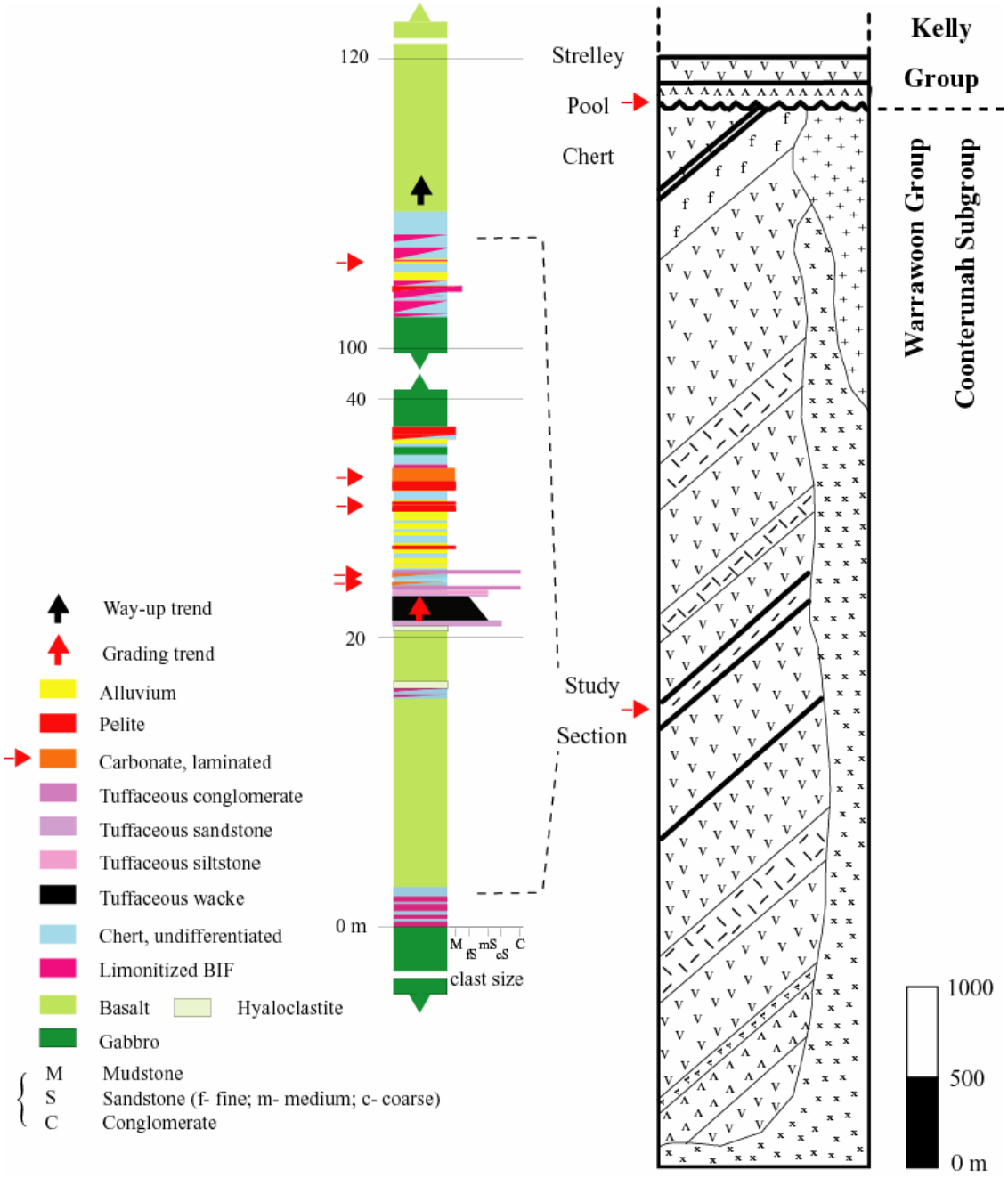

Figure 3: Stratigraphic column of tephra-carbonate sequence in lower section of Coucal Formation in Coonterunah Subgroup, Warrawoona Group.

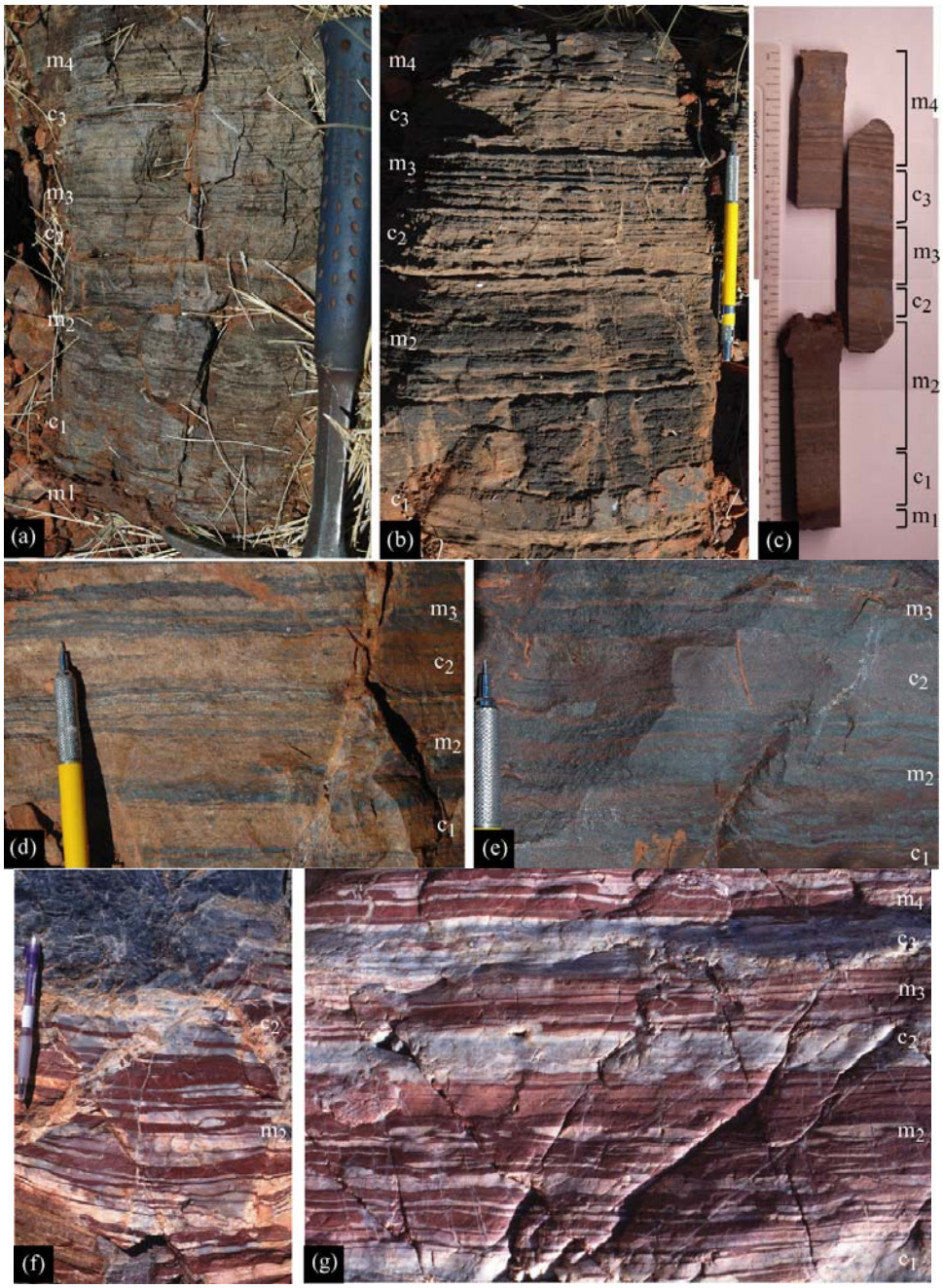

Figure 4: Outcrop photographs of Coonterunah sedimentary units, magnetite ($m_1 – m_4$) and carbonate ($c_1 – c_3$) mesobands labelled. (a): Calcitic phase. Alternating calcite and magnetite laminae. (b): Dolomitic phase. Alternating dolomite/calcite and magnetite laminae. C1 mesoband partially silicified. (c): Slabs through dolomitic phase. (d, e): Early-silicified phase with alternating laminae of actinolite-bearing sugary metachert and magnetite (d), metamorphosed to cummingtonite along contact interfaces at higher grade (e). (f, g): Late-silicified phase. Alternating laminae of milky-white chert and jasperitic chert. Carbonate has been pervasively silicified, and magnetite has been oxidized to fine haematite.

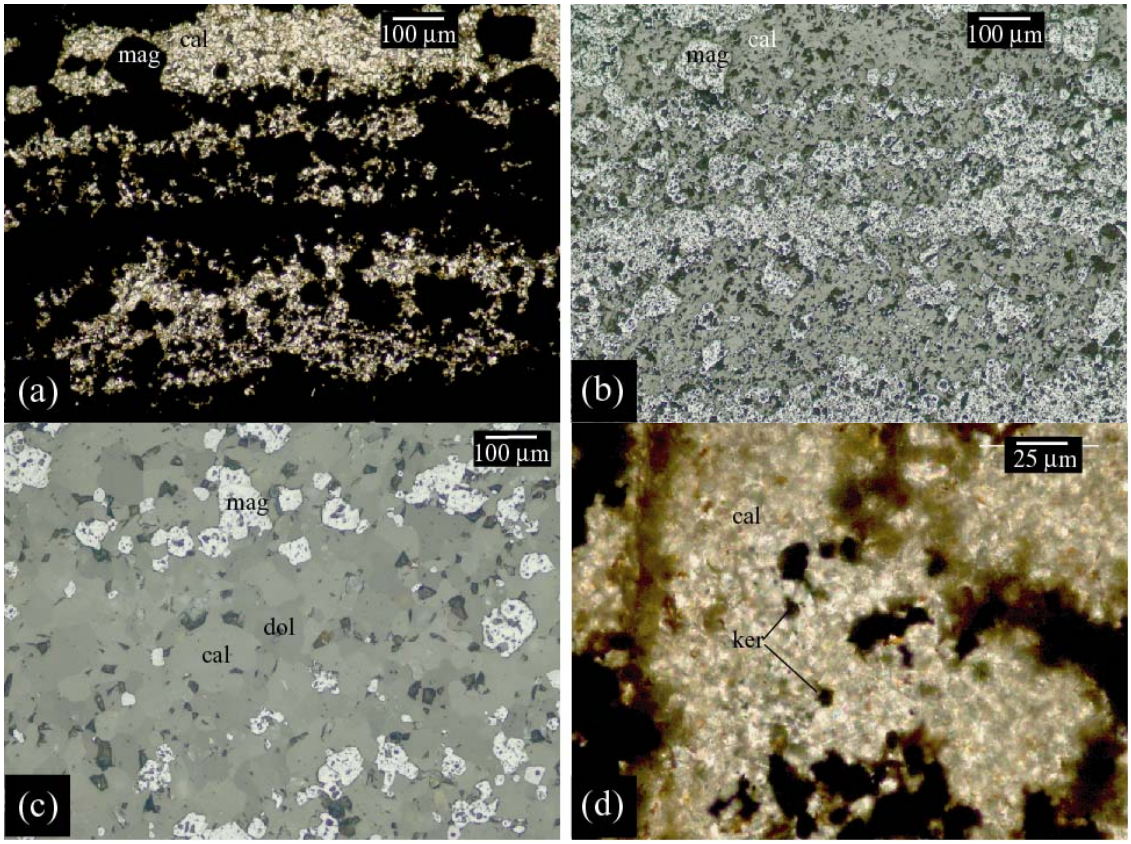

Figure 5: Thin-section photomicrographs of prominent 32cm carbonate unit. (a, b): Plane-polarized (a) and reflected-light (b) images of alternating magnetite and calcite laminations. (c): Reflected light image of alternating dolomite/calcite and magnetite laminations. (d): Plane-polarized image of greenish-black amoebal kerogen in calcite lamellae in limestone phase.

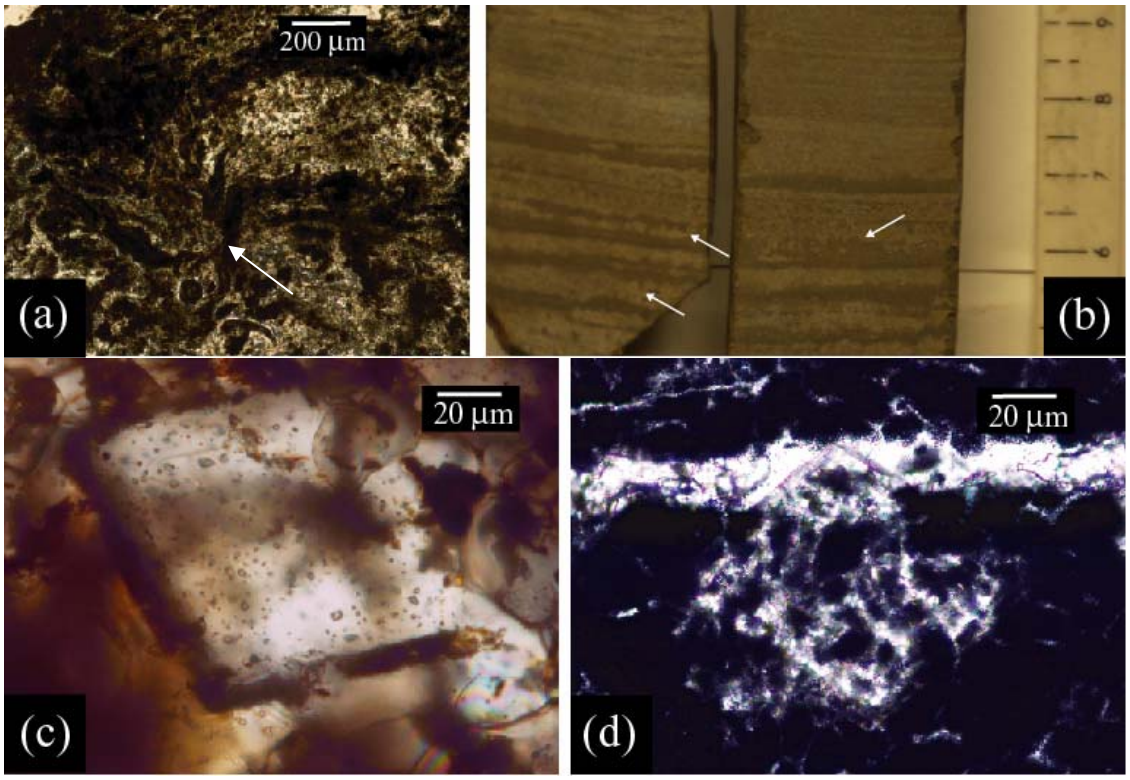

Figure 6: (a, b): Thin-section and slab photographs of soft-sediment deformation and flame structures. (c, d): Thin-section photographs of sparry dolomite in silicified micrite-BIF (c) and silicified laminated carbonate lithofacies of Strelley Pool Chert, Kelly Group (d) for comparison.

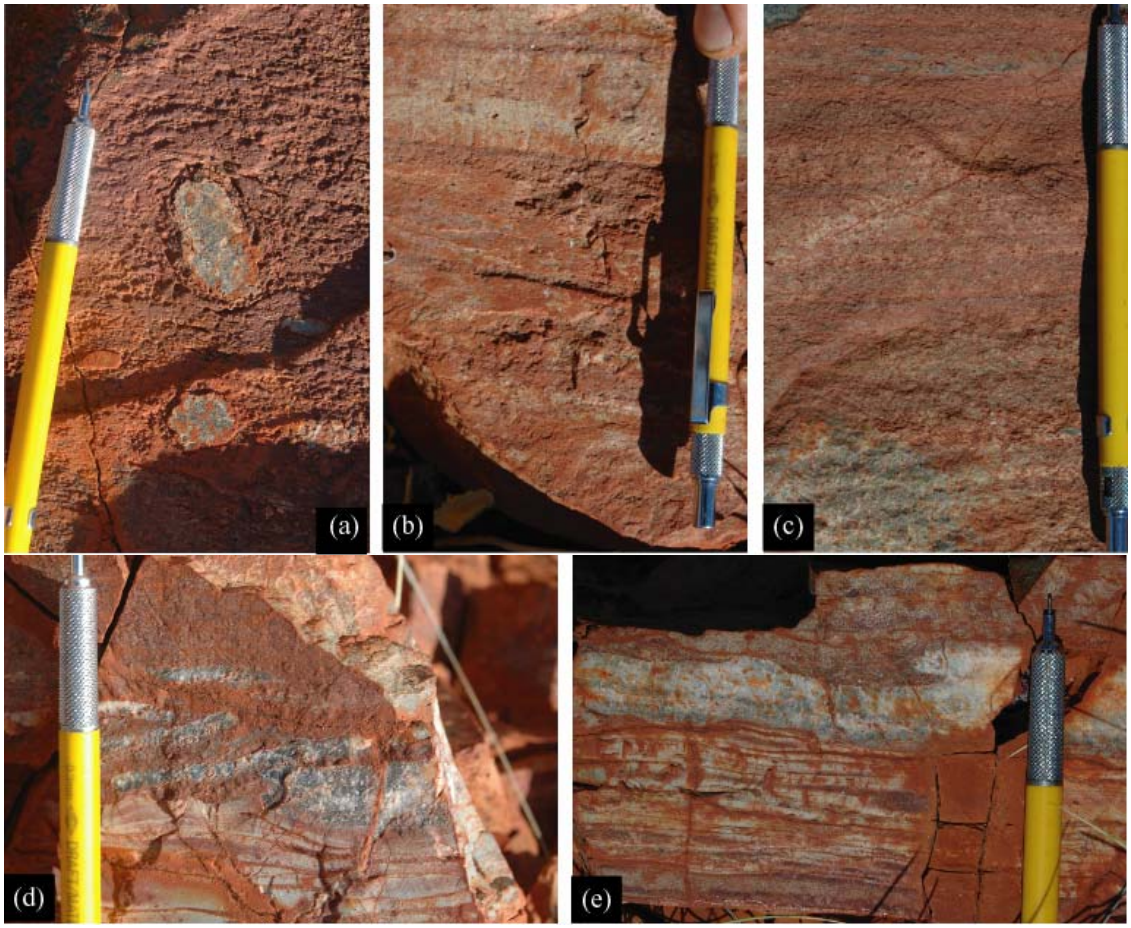

Figure 7 (a - e). Outcrop photographs of Coonterunah volcanoclastics, pencil points in younging direction. (a): Chert clasts in pebbly tuffaceous wacke. (b): Graded tuffaceous wacke-siltstone. (c): Alternating light- and dark planar banded tuffaceous wacke. (d): Tabular silicified hydraulic breccia, loading underlying silicified tuff. (e): Soft sediment deformation structure in tuffaceous wacke impinging on meta-chert. Note gentle undulations in underlying silicified tuff.

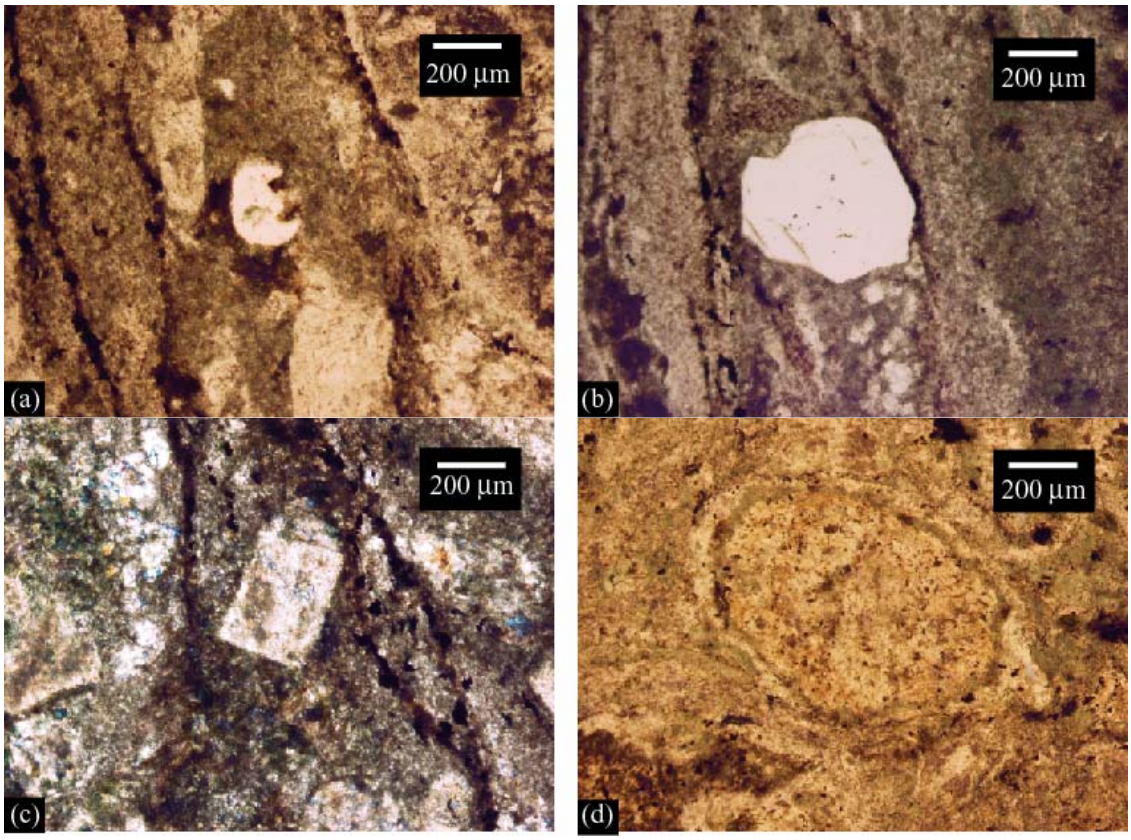

Figure 8: Thin-section photographs of Coonterunah volcanoclastics. (a, b): Well-rounded recrystallized beta-quartz phenocrysts in alternating planar layers of chloritized (a) and sericitized (b) eutaxitic glassy groundmass. (c): Block sericite-altered albite-feldspar phenocryst in chlorite-altered glassy groundmass rich in opaque oxides. (d): Mildly flattened ellipsoidal quartz-muscovite-chlorite amygdale in chloritized glassy groundmass.

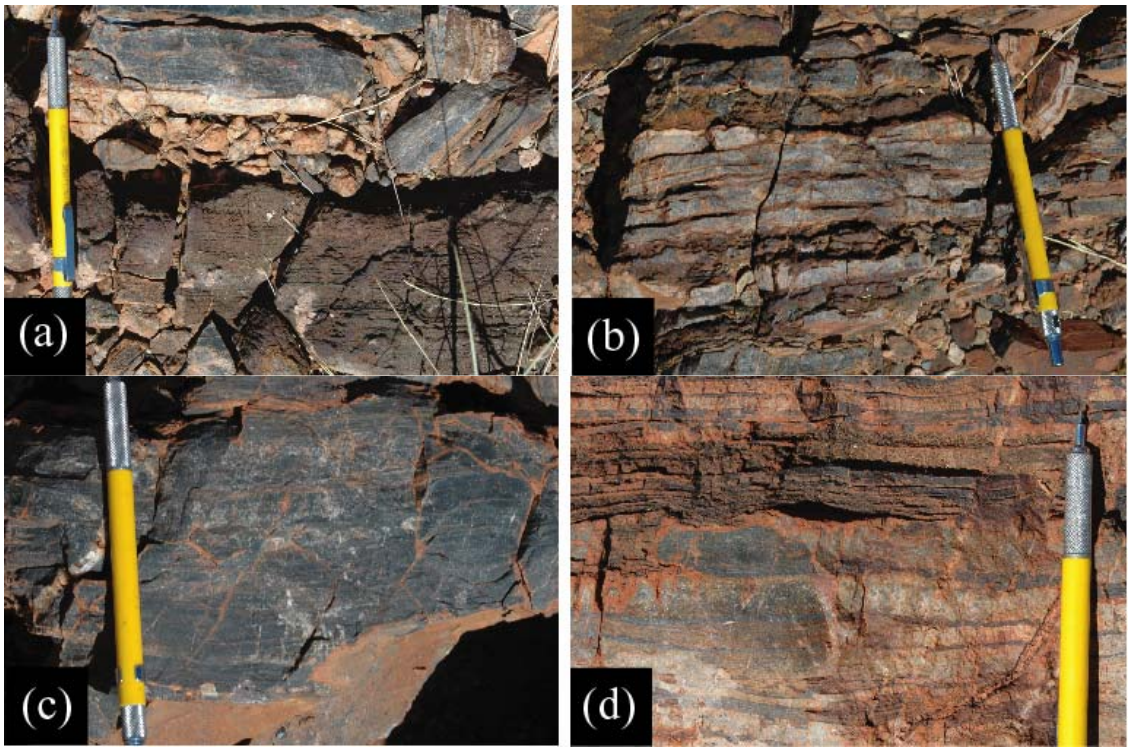

Figure 9: Outcrop photographs of carbonate silicification in Coucal Formation. (a): Prominent laminated carbonate unit overlain by banded metachert. Note ~15 mm thick talc alteration zone at lower contact with carbonate. (b): Partially silicified carbonate unit, ~30 m laterally westwards of photograph (a). Note talc zones at metachert/carbonate contacts, and orange weathering zones after magnetite. (c): Tremolite-bearing banded meta-chert – possibly a thoroughly silicified carbonate. (d): Ferruginous metachert with remnant unchertified carbonate. Niote sugary texture in metachert.

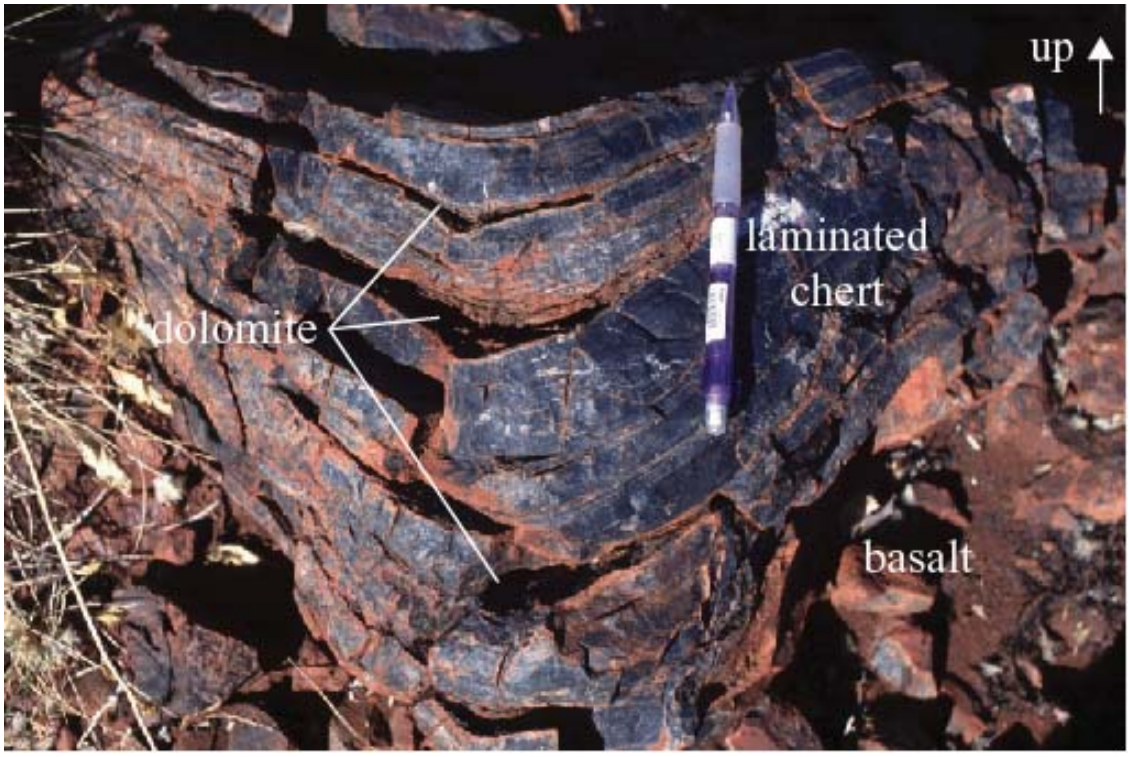

Figure 10: Interflow metachert sediment atop basaltic subcrop in the Coucal Formation, showing precursor dolomite along central axis of minimal compaction.

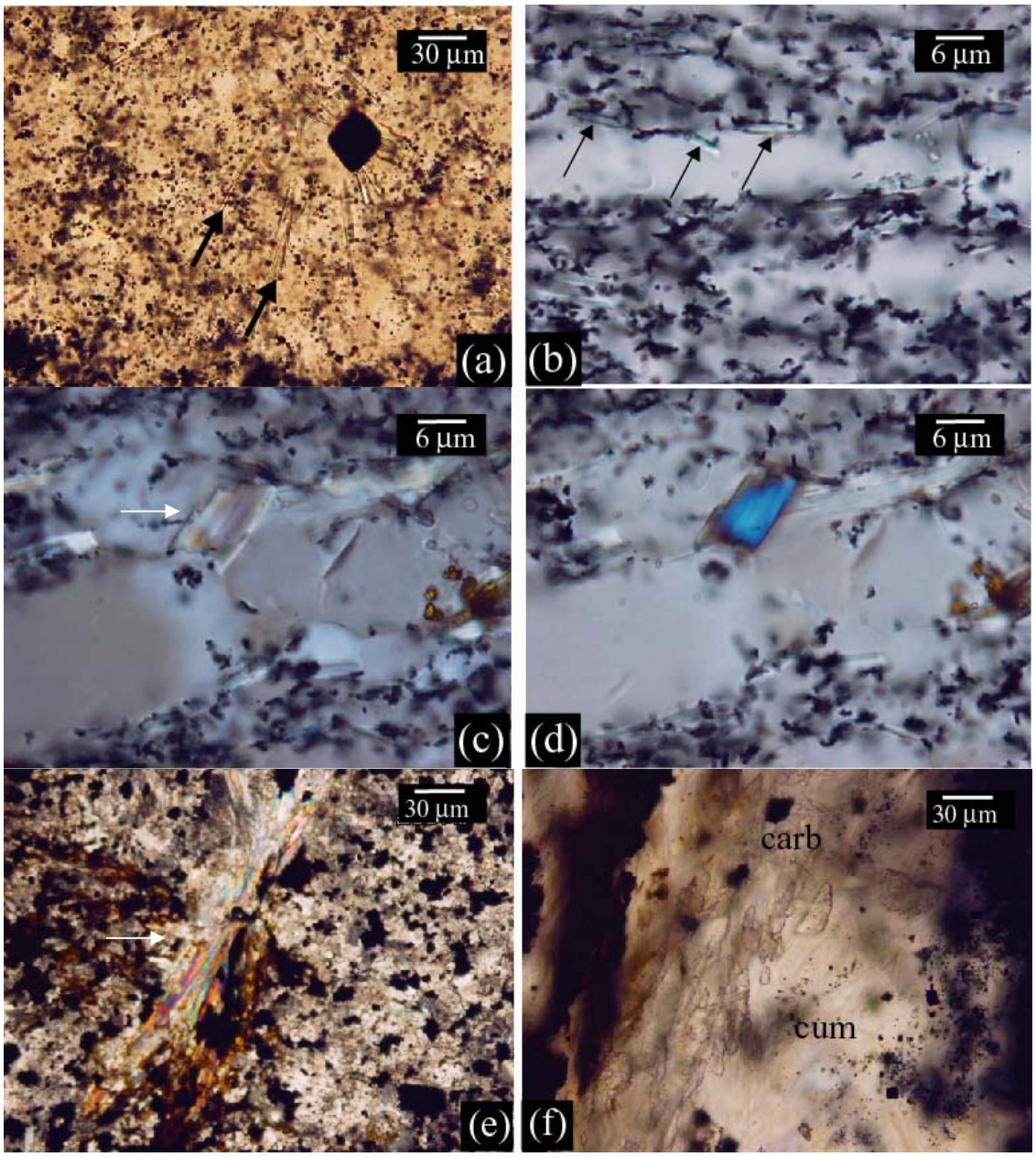

Figure 11: Photomicrographs of Ca-Mg±Fe amphibole in Coucal formation metachert. (a): Laths of pale green-yellow lightly pleochroic actinolite fringing magnetite in magnetite-carbonate metachert. (b - d): Apleochroic tremolite showing upper first-order and lower second-order birifringence. This elongate acicular habit is the most commonly occuring style of amphibole growth in metacherts, and is typical of growth at low metamorphic grades. Rusty-brown granular goethite in center-right of (c) and (d). (e): Feathery talc after dolomite and quartz in low-grade ferruginous magnetite-metachert. (f): Cummingtonite growth in a dolomite-magnetite-chert assemblage in ferruginous magnetite-metachert.

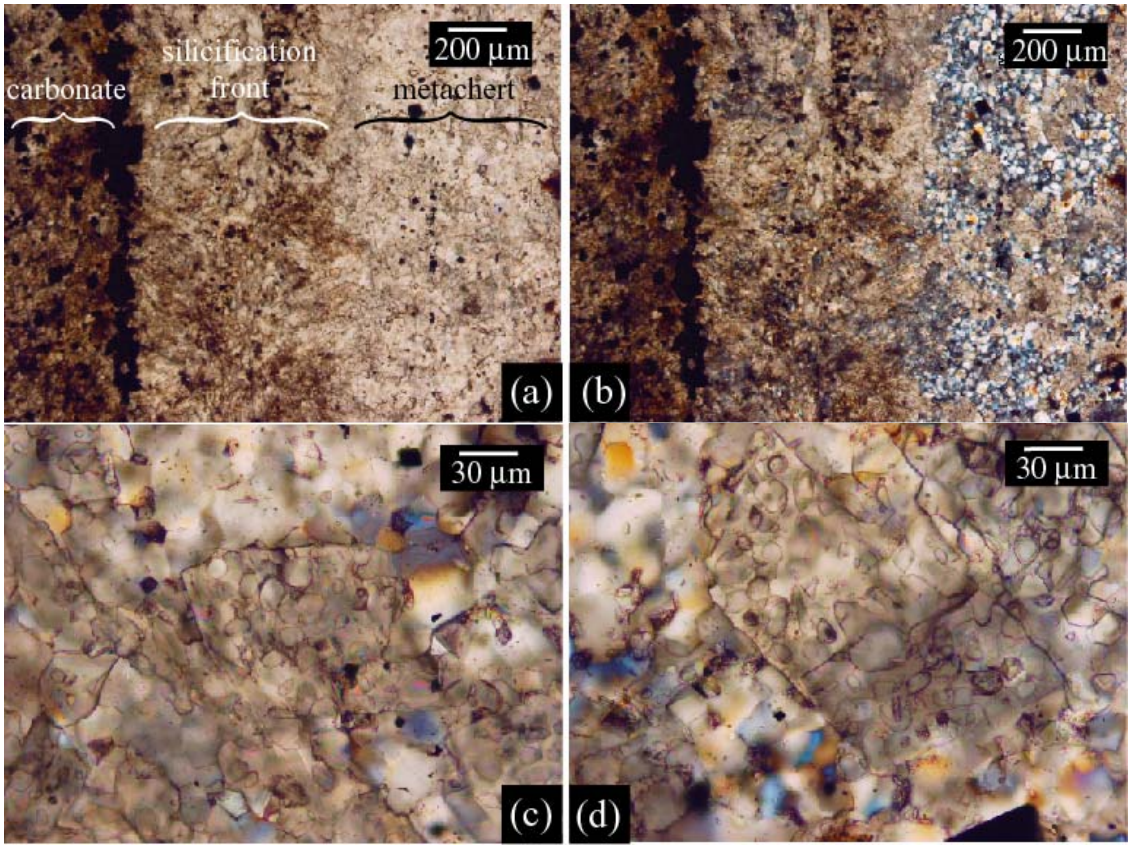

Figure 12: Photomicrographs of carbonate silicification textures. (a, b): Silicification front in Coonterunah metacarbonate. (c, d): Partially silicified skeletal dolomite within silicification front.

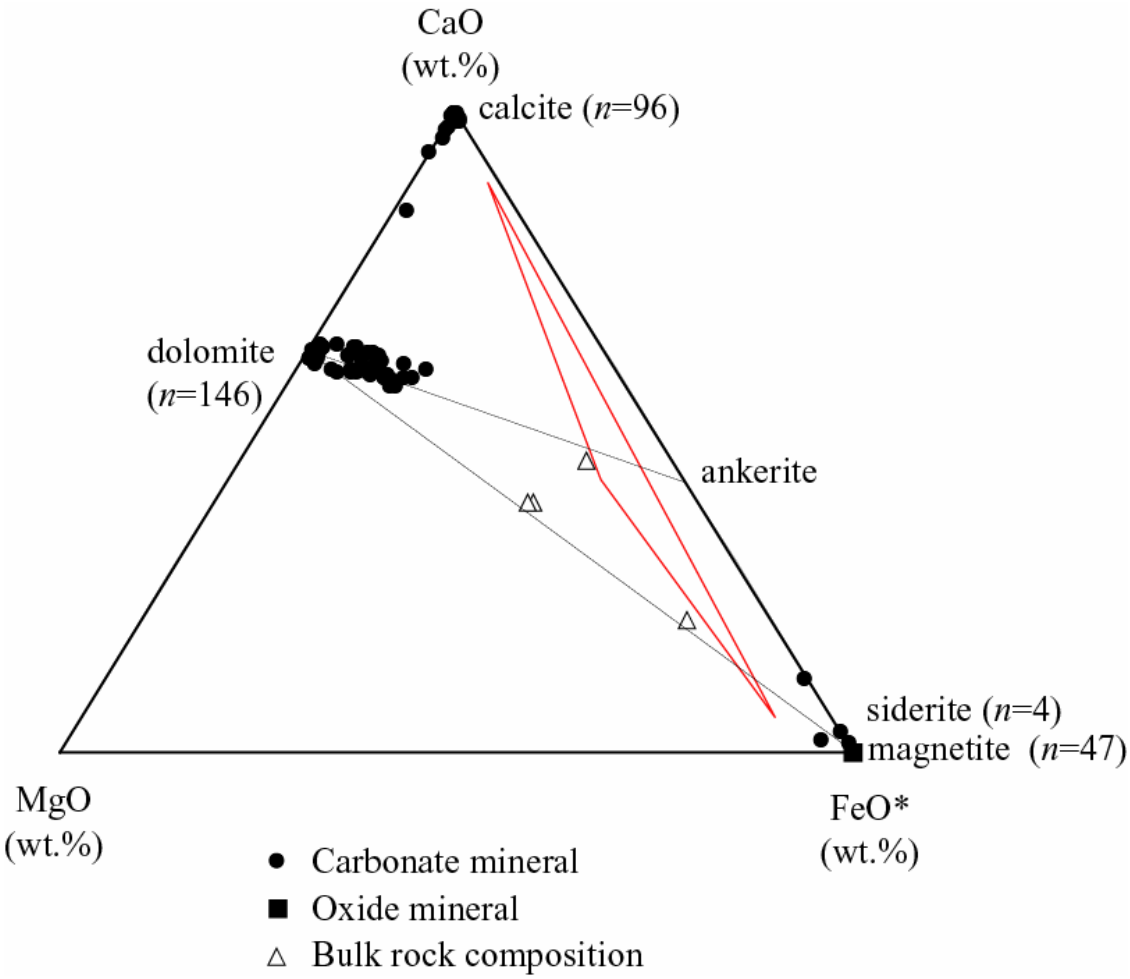

Figure 13: CaO – FeO* - MgO ternary diagram (oxide wt.%, not molar) of individual mineral and bulk proto-BIF analyses. Filled circles = individual carbonate analysis; filled squares = individual oxide analyses; open triangles = bulk rock compositions. Red triangle shows univariant field calculated for siderite-calcite-ankerite equilibrium assemblage at T = 400 ºC. (FeO* = total iron calculated as $Fe^{II}O$).

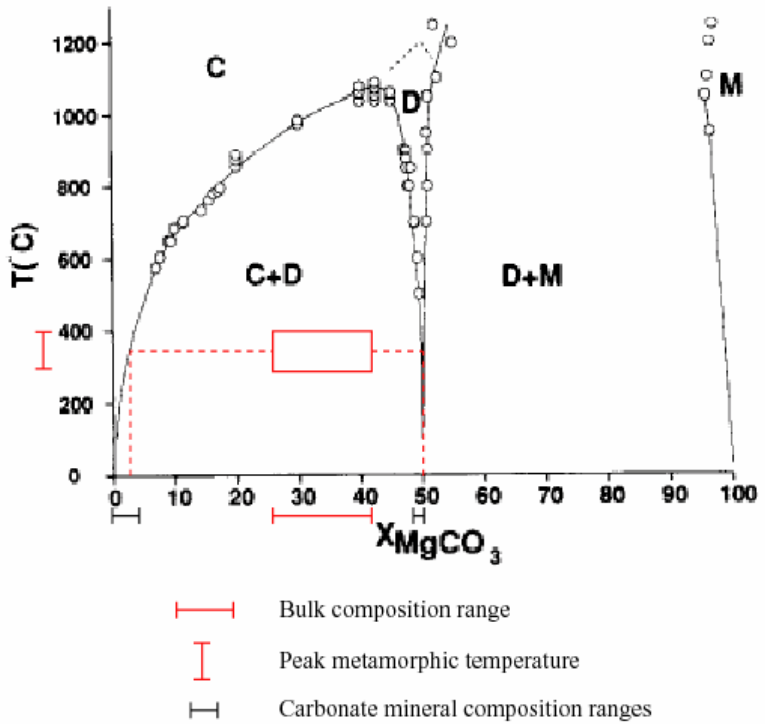

Figure 14: Subsolvus relations for $CaCO_3$-$MgCO_3$ binary join (Tribble et al., 1995), with Coonterunah micrite-BIF mineral and bulk compositions superimposed.

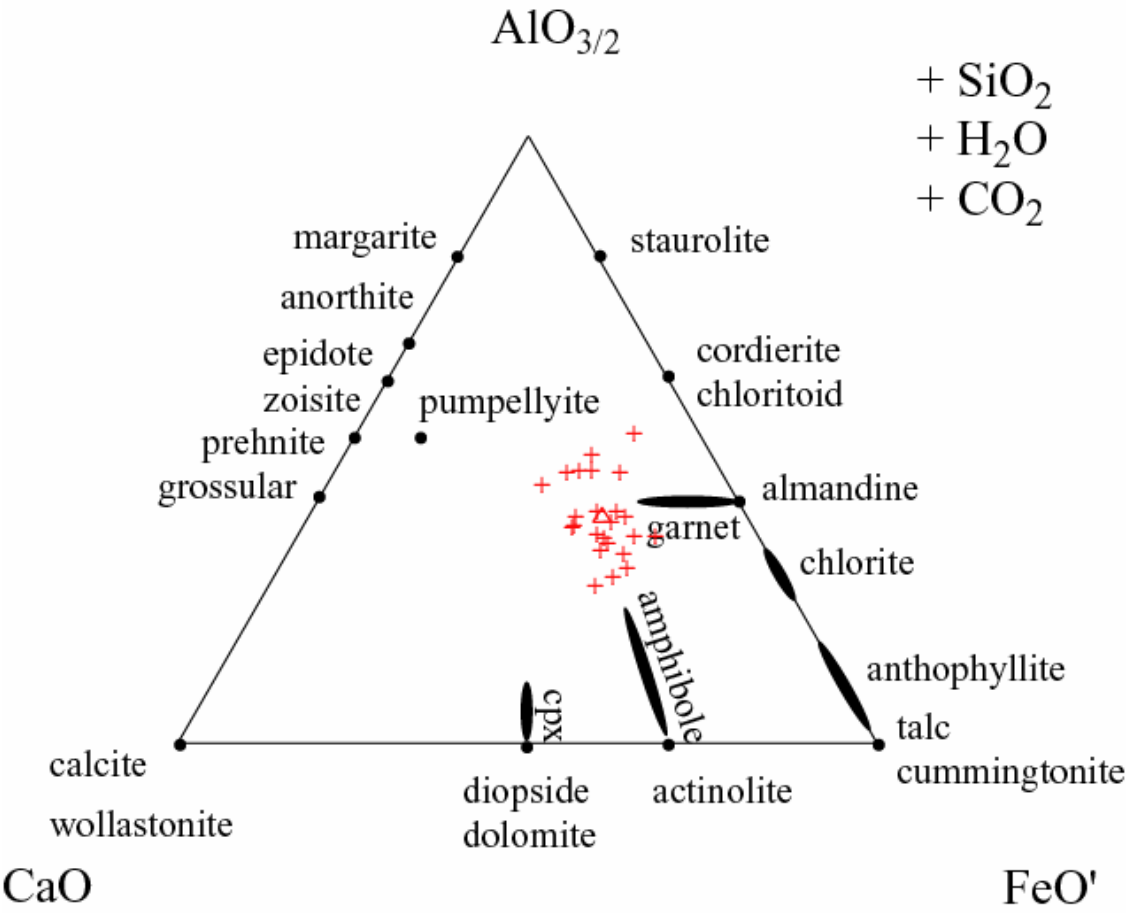

Figure 15: Ternary ACF phase diagram (Spear, 1995) of Coonterunah basalt. Relevant mineral compositions are also plotted. Triangle shows average composition. FeO' = FeO + MgO.

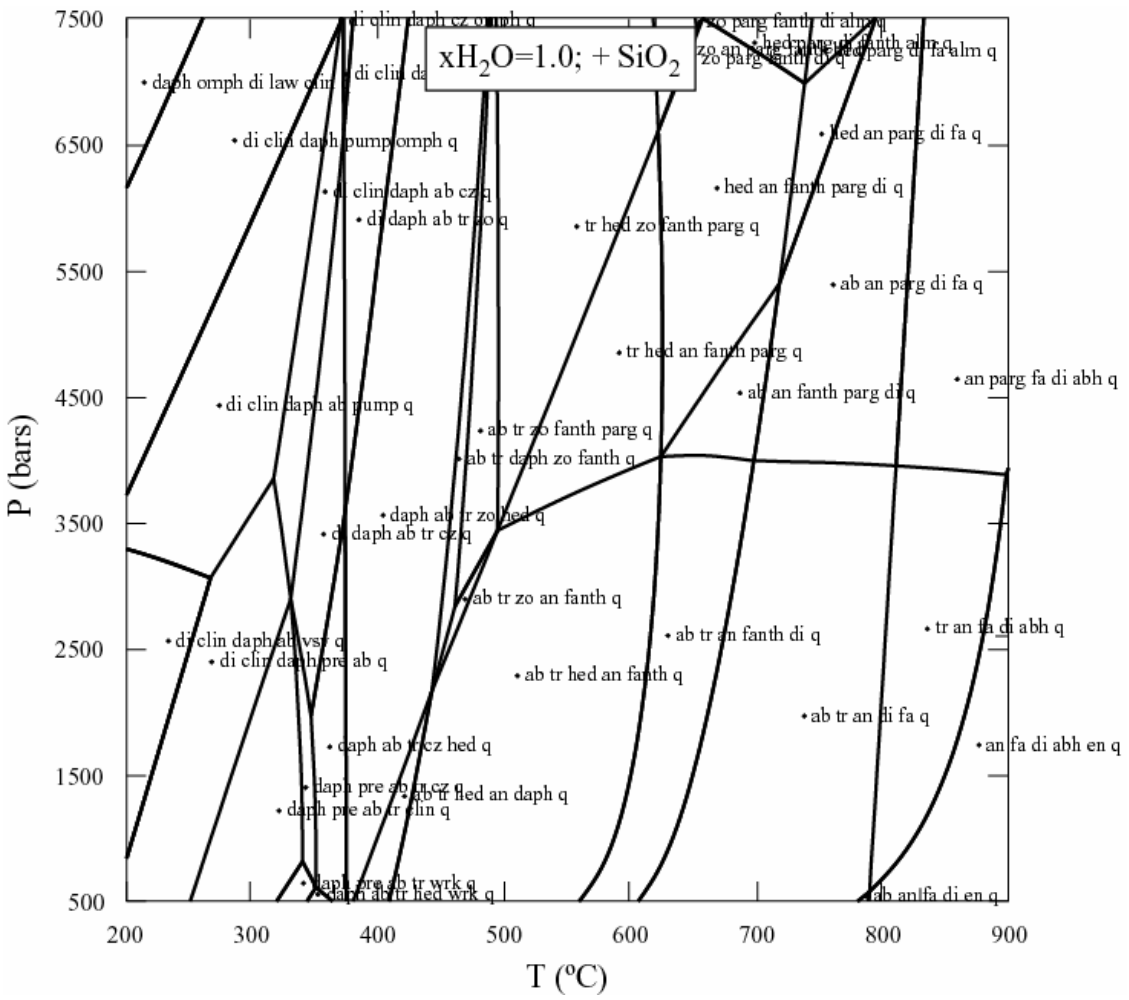

Figure 16: Simplified P-T pseudosection calculated for the system ACFMS using the thermodynamic dataset of Holland and Powell (1998) at xH_2O = 1.0 for averaged Coonterunah basalt (triangle, Figure 12).

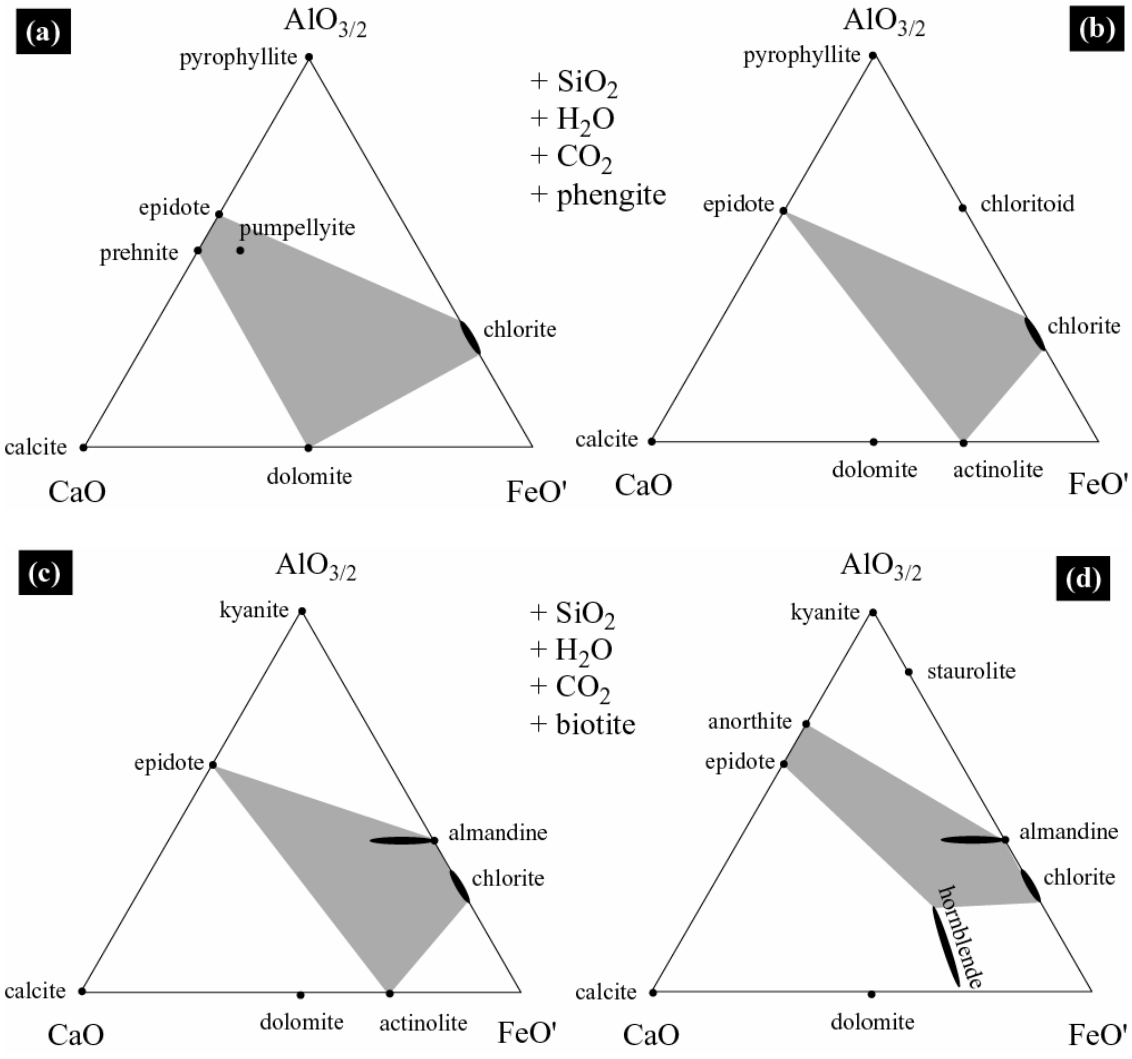

Figure 17: Ternary ACF' stability diagrams of Pilgangoora Belt mafic assemblages undergoing progressive metamorphism, with compositional field indicated in grey. FeO' = FeO + MgO.

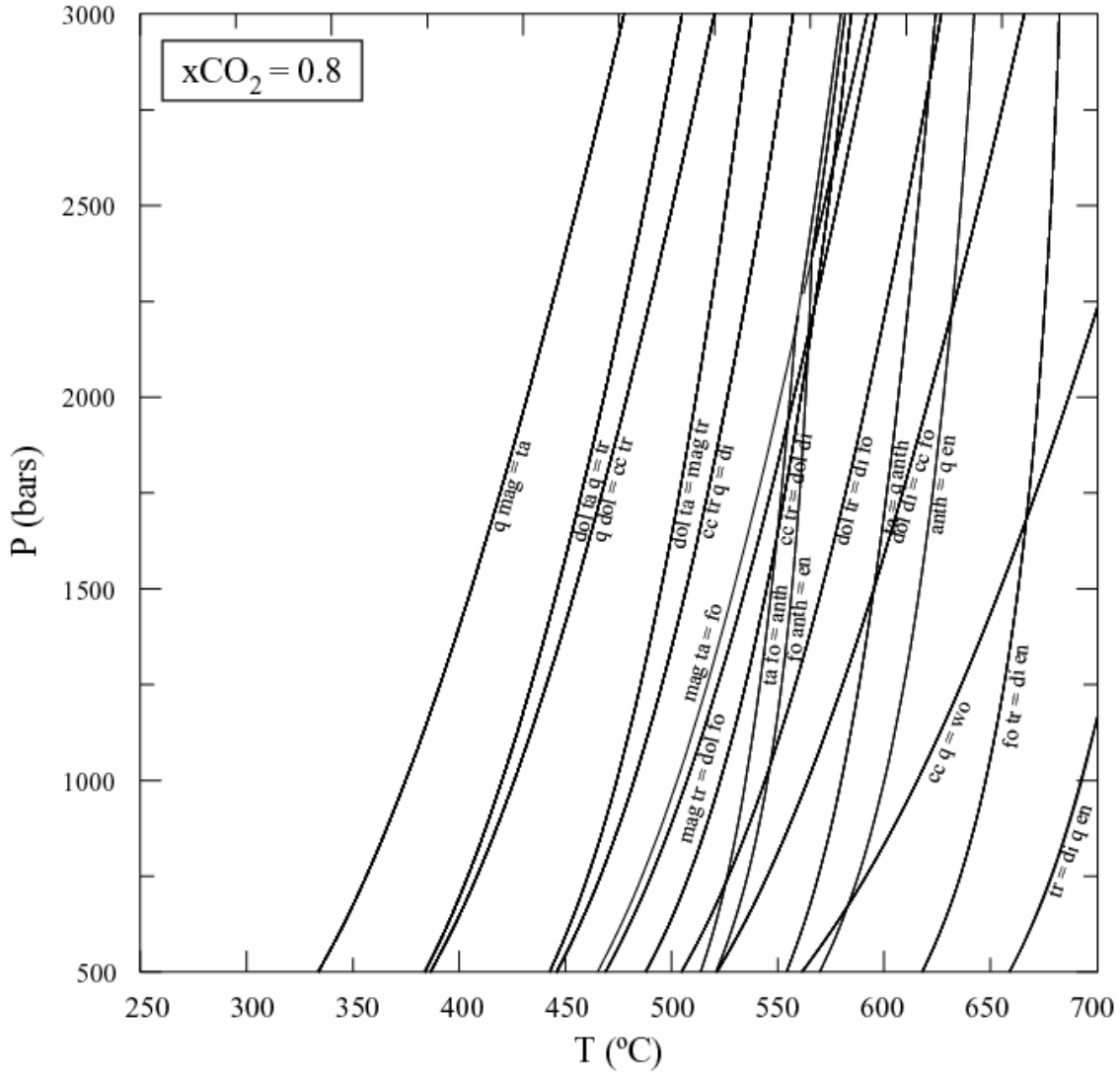

Figure 18: P – T diagram calculated for the system CMS using the thermodynamic dataset of Holland and Powell (1998) at $xCO_2 = 0.8$.

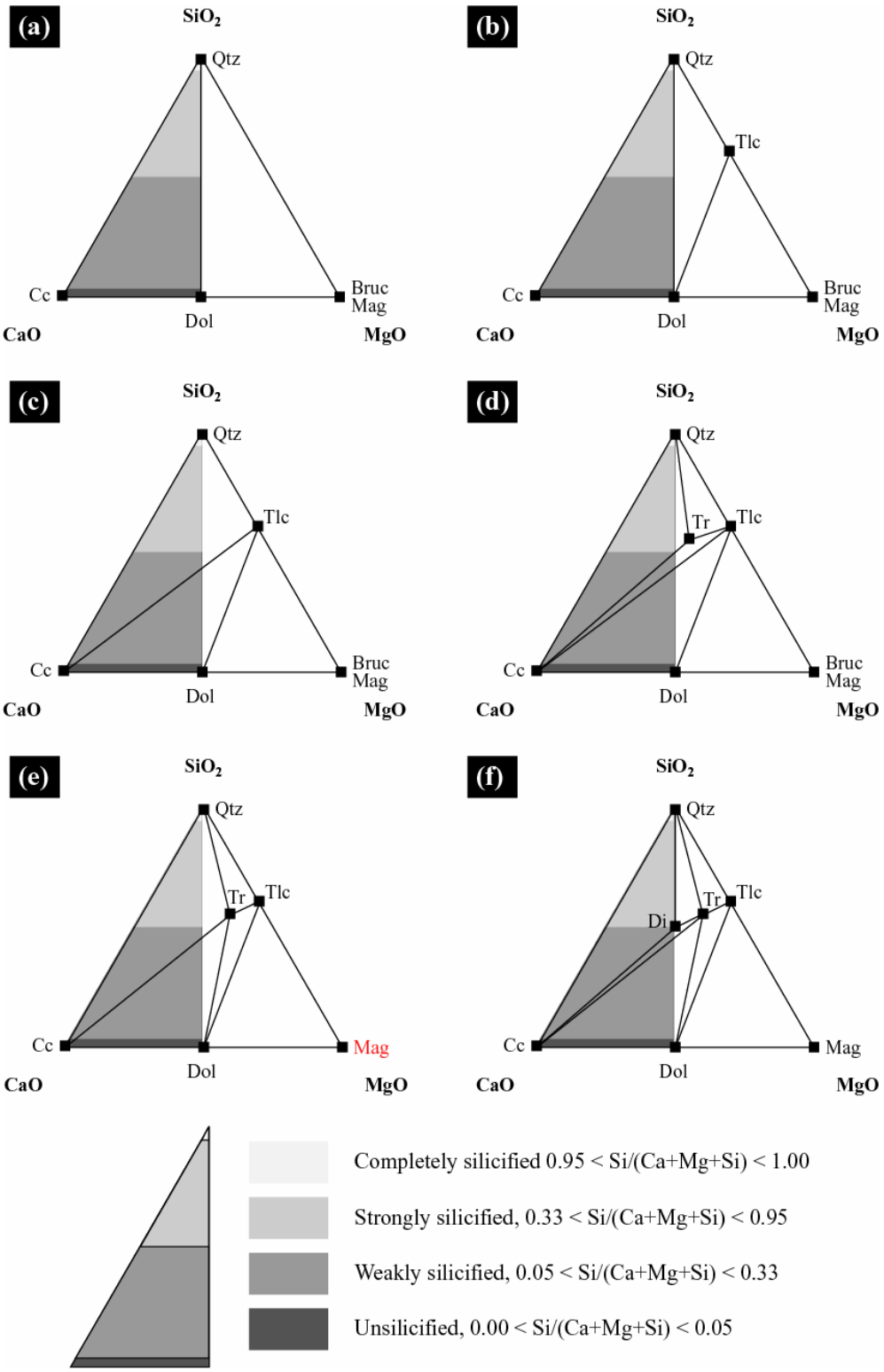

Figure 19: Ternary CMS stability diagrams of variably chertified Pilgangoora Belt carbonate assemblages undergoing progressive metamorphism. Degree of pre-metamorphic silicification indicated by grey shading.

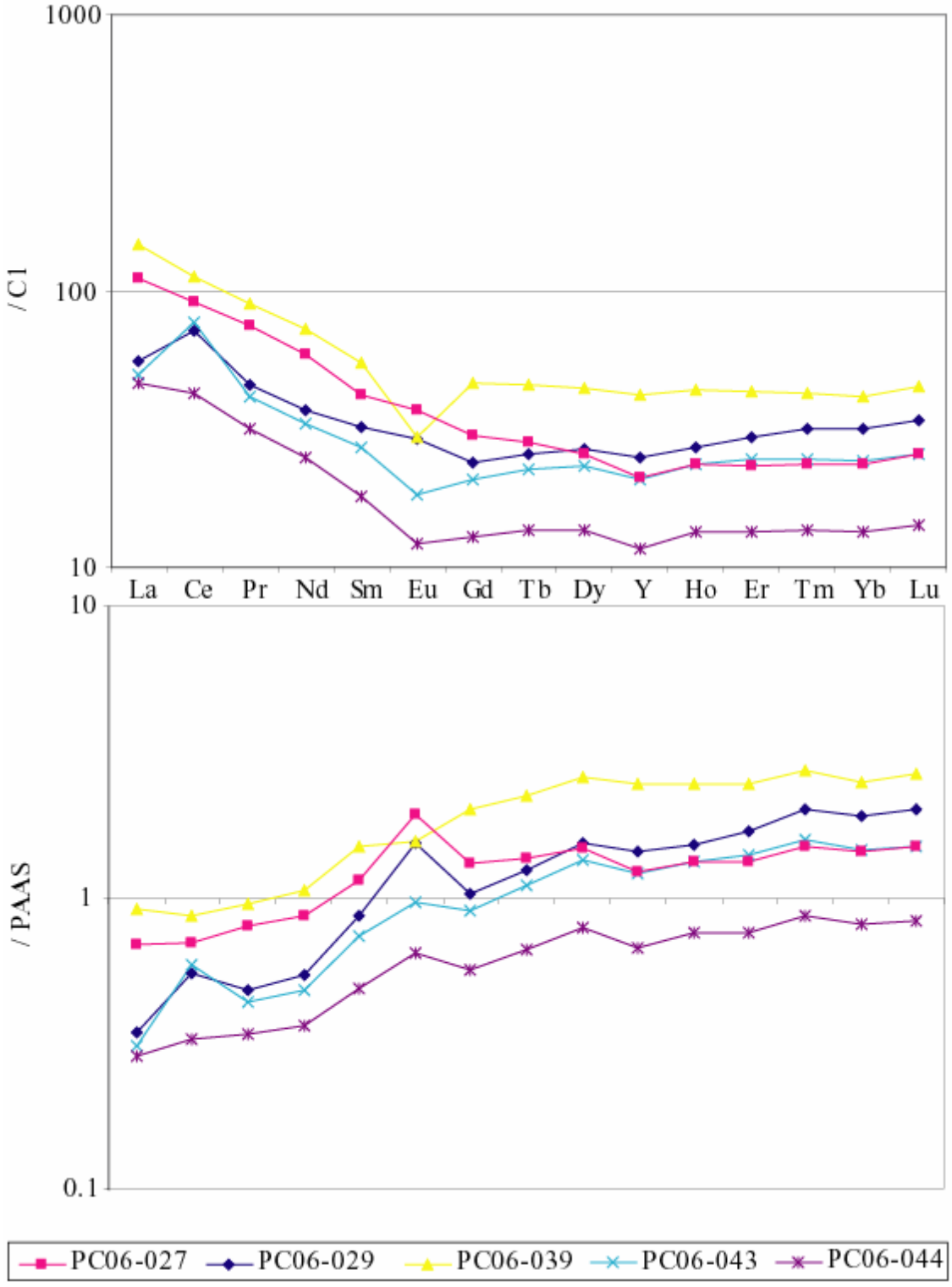

Figure 20: Chondrite (‘C1’)- and Post-Archaean average shall (‘PAAS’)- normalized REE distributions in Coucal volcanoclastic samples.

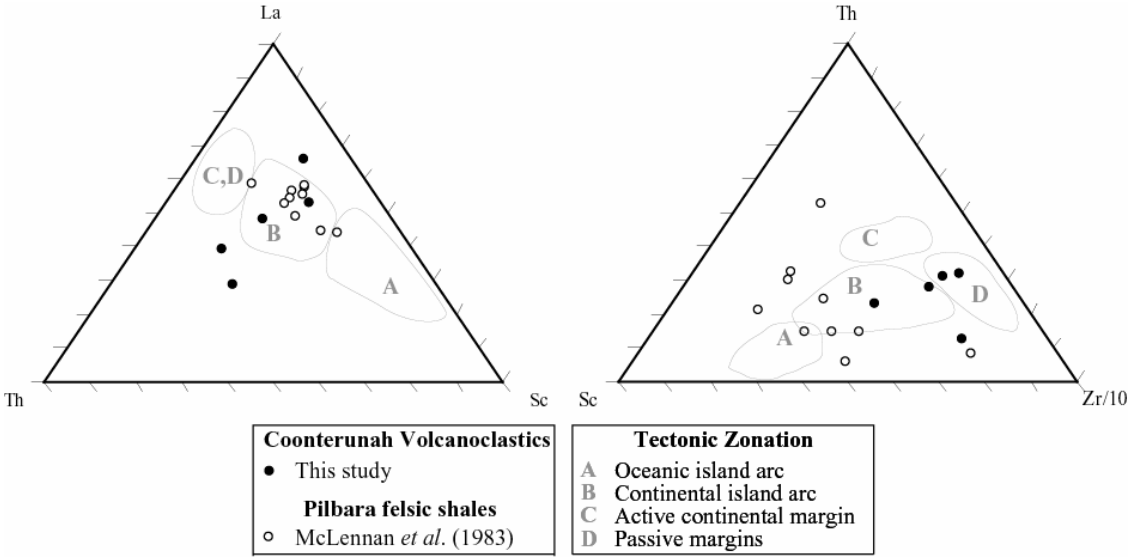

Figure 21: Ternary La-Sc-Th (a) and Th-0.1Zr-Sc (b) discrimination diagrams showing Coonterunah volcanoclastics. Also shown are continentally-derived compositions of TTG-weathering shales from the younger Gorge Creek Group (McLennan et al., 1983).

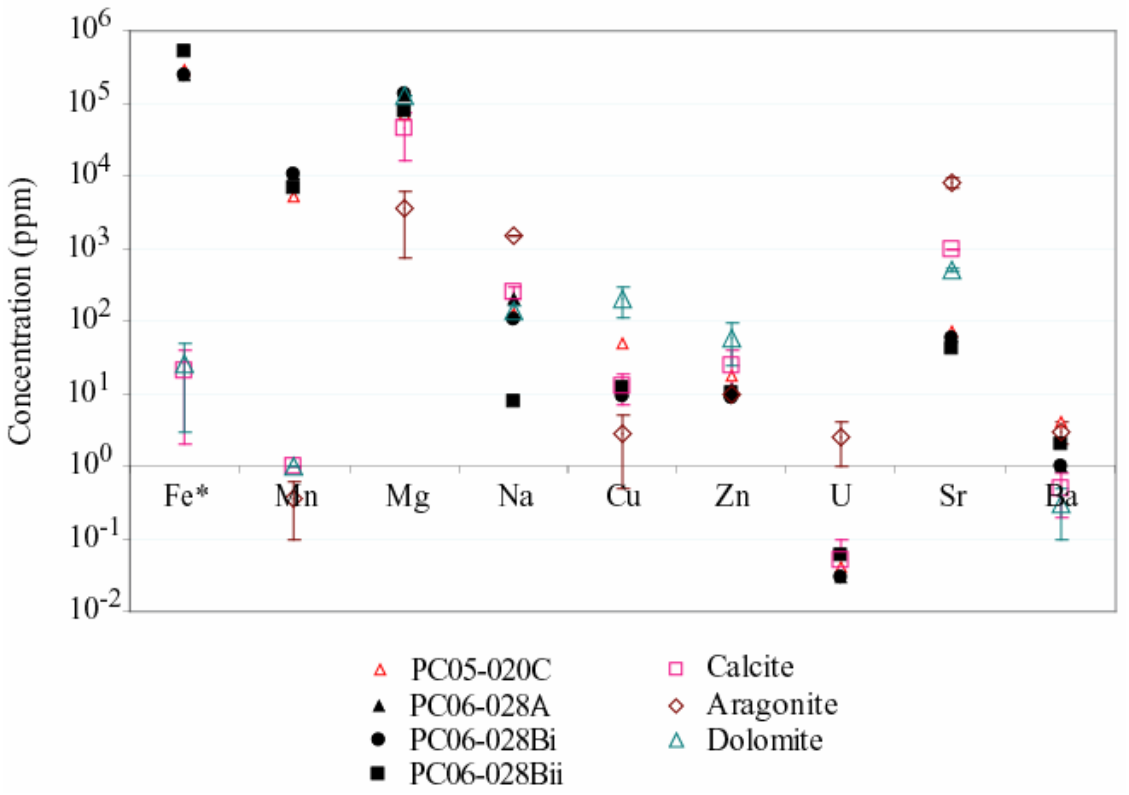

Figure 22: Carbonate mesoband trace element concentrations, compared to averages (symbols) and ranges (bars) contemporary aragonite, calcite and dolomite (Veizer, 1983). Note that dilution due to magnetite was not taken into account.

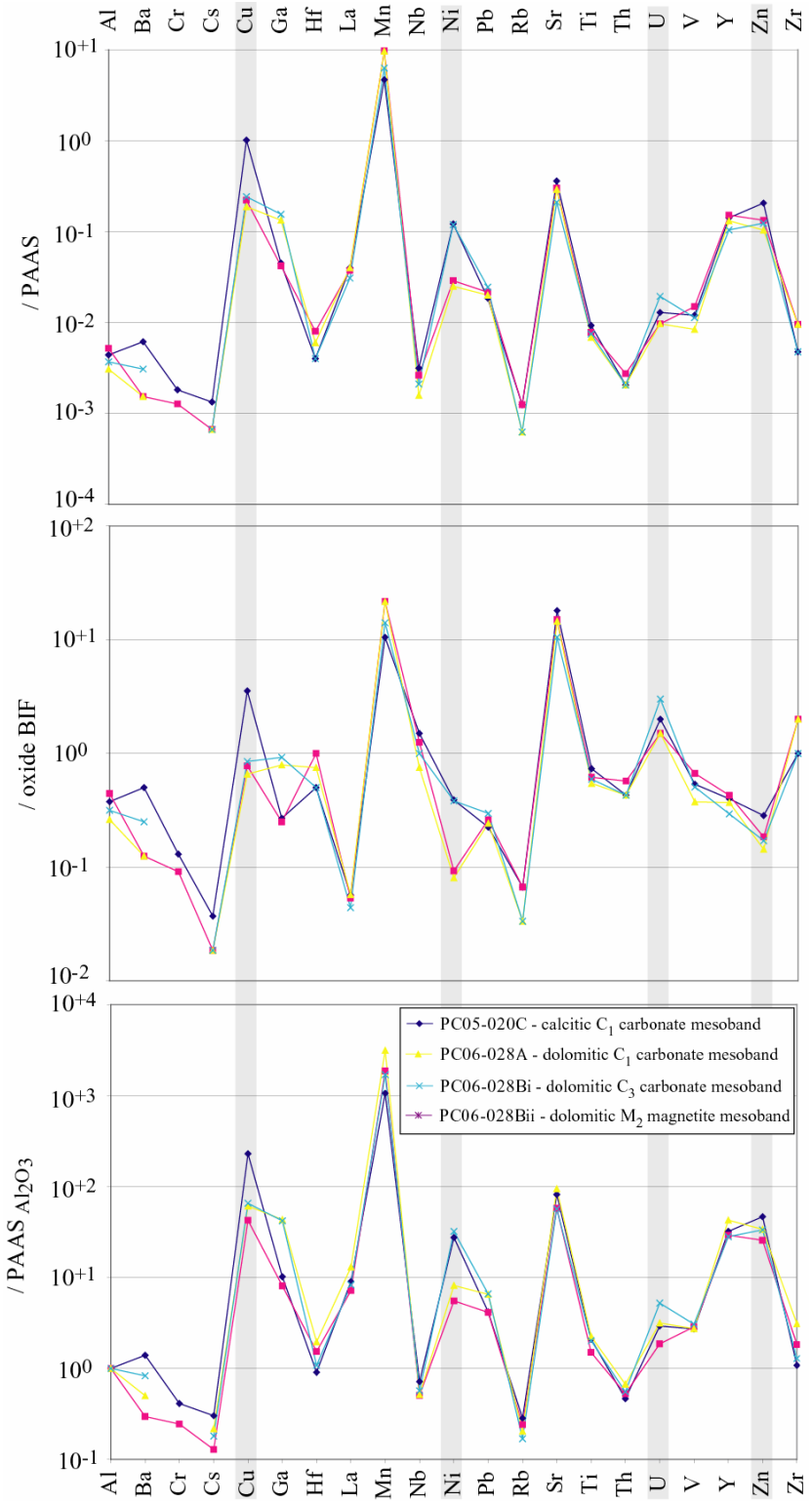

Figure 23: Comparative trace-element diagram showing trace element concentrations normalized to PAAS (top), oxide-BIF (middle) and PAAS/Al_2O_3 (bottom). Redox-sensitive and/or micronutritive trace elements Cu, Ni, U and Zn are shaded.

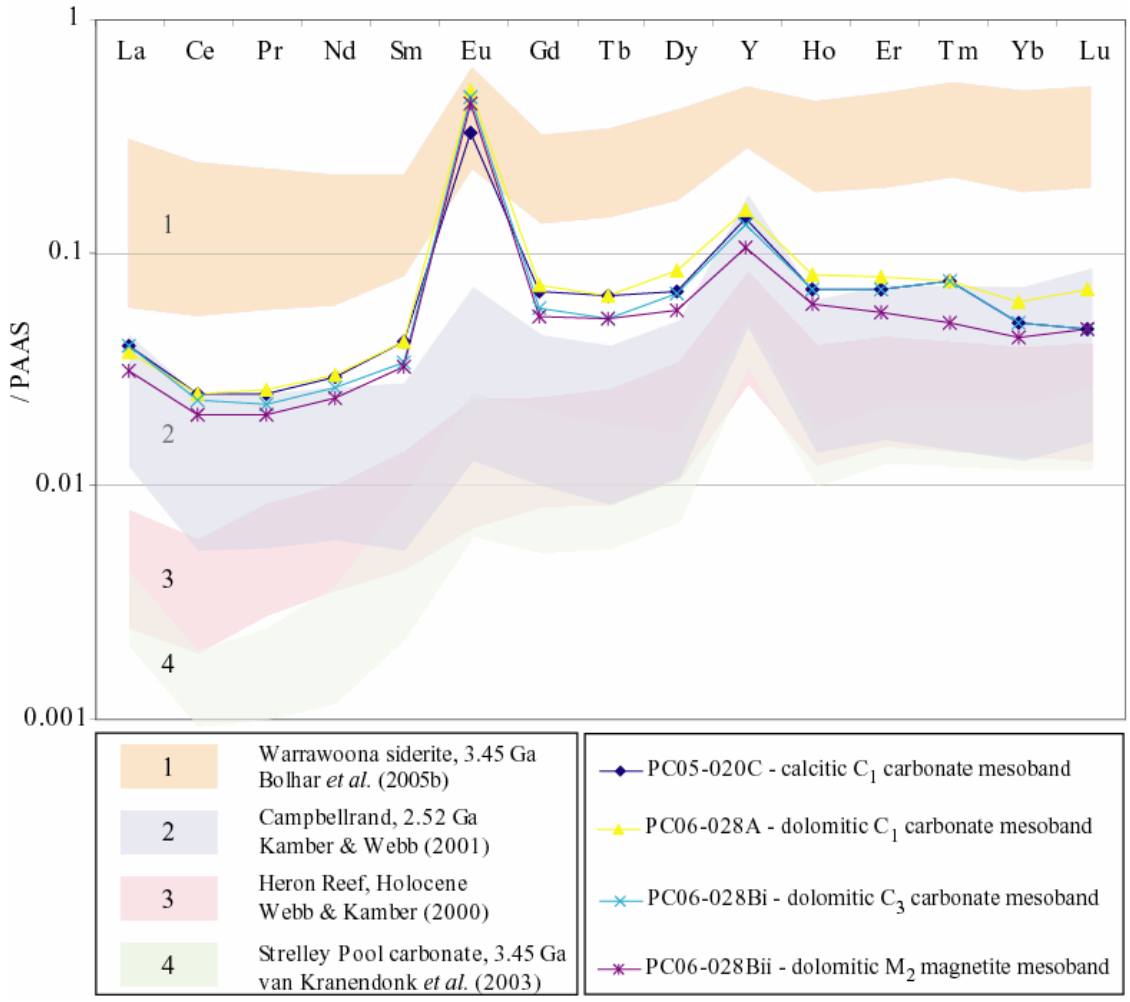

Figure 24: PAAS-normalized REE distributions in Coucal micrite-BIF mesobands, compared to shaded REE distribution ranges in (1) Warrawoona siderite (Bolhar et al., 2005), (2) 2.52 Ga Campbellrand platform carbonates (Kamber and Webb, 2001), (3) Holocene Heron Reef carbonates (Webb and Kamber, 2000), and (4) 3.45 Ga Strelley Pool Chert ankerite (van Kranendonk et al., 2003).

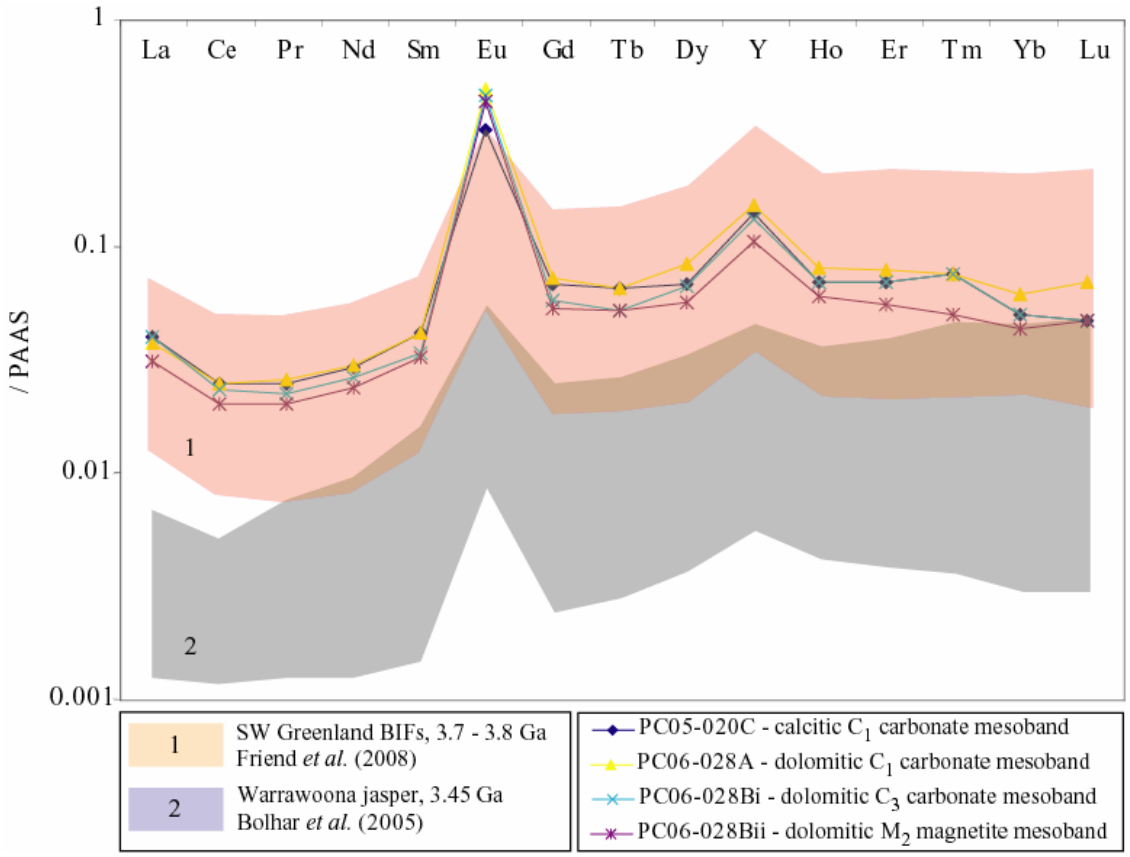

Figure 25: PAAS-normalized REE distributions in Coucal micrite-BIF mesobands, compared to shaded REE distribution ranges in (1) 3.7 – 3.8 Ga BIF-like chemical sediments in southwest Greenland (Friend et al., 2008), and (2) 3.45 Ga Warrawoona jasper bands (Bolhar et al., 2005).

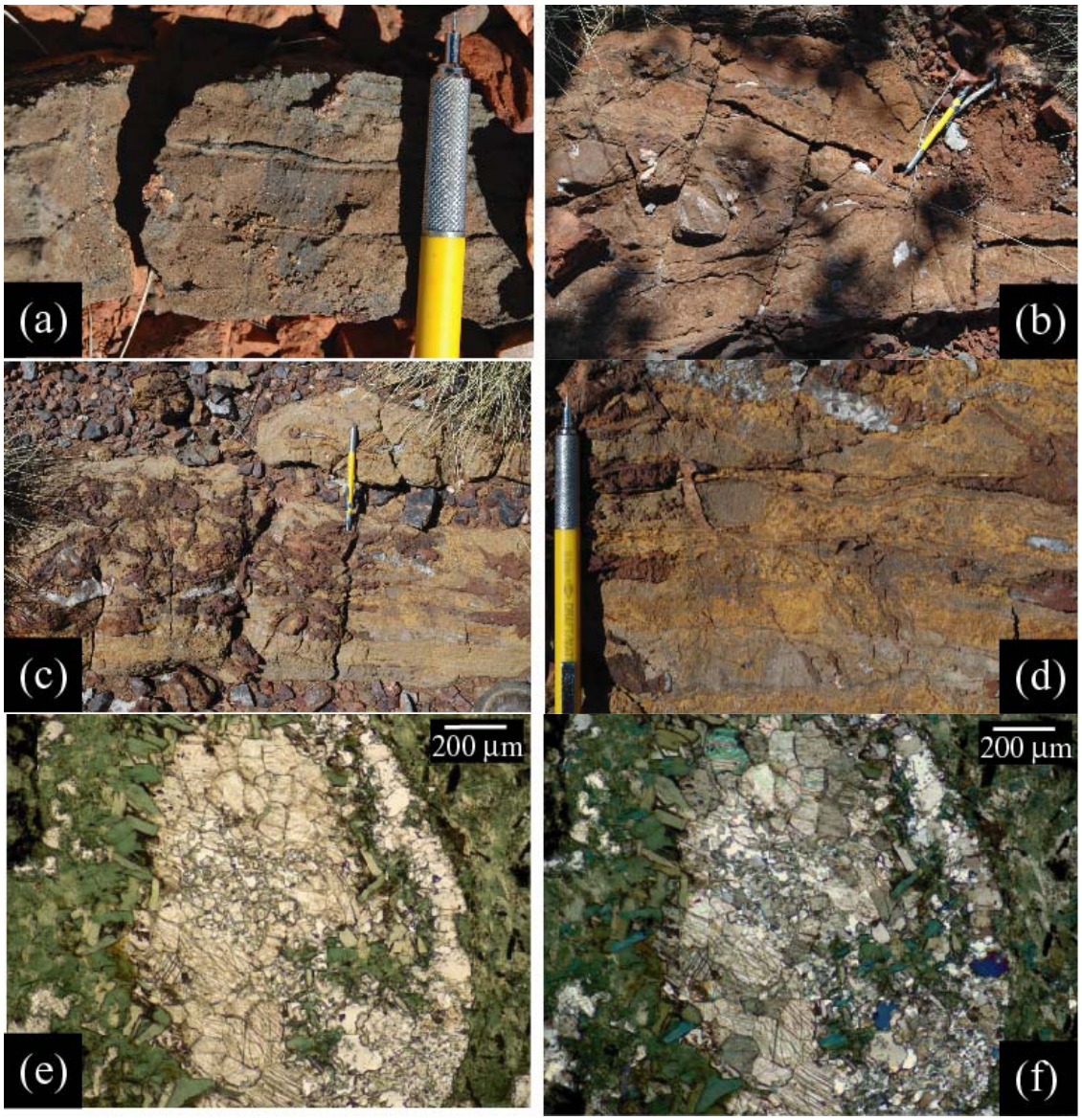

Figure 26: Outcrop and thin-section photographs of Coucal Formation carbonate alteration, metasomatism and metamorphism. (a): Recrytallized limestone, planar lamination obliterated a metamorphic massive texture. (b): Fault-plane associated metasomatic ankerite. (c, d) Heavily calcretized and limonized planar carbonate. (e – f): Thin-section plane-polarized (e) and cross-polarized (f) photomicrographs of ankerite-filled vesicle in tholeittic metabasalt.

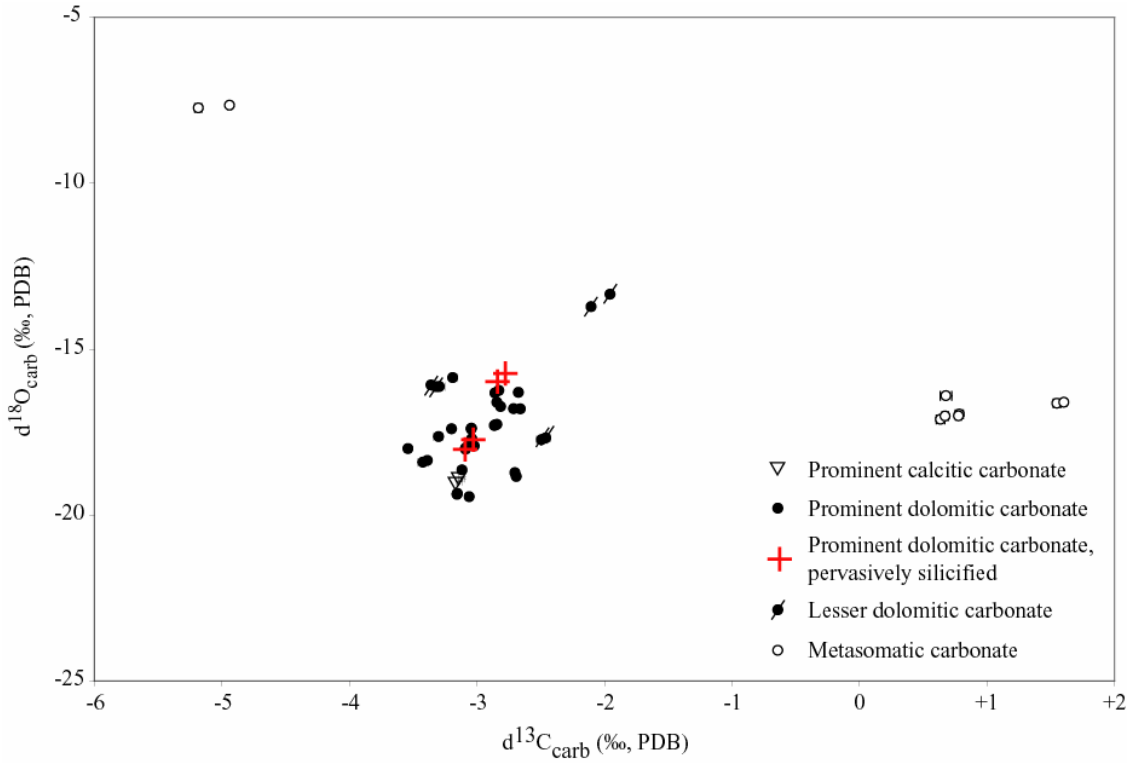

Figure 27: $\delta^{13}C_{carb}$ - $\delta^{18}O_{carb}$ diagram of sedimentary and metasomatic carbonate analyses.

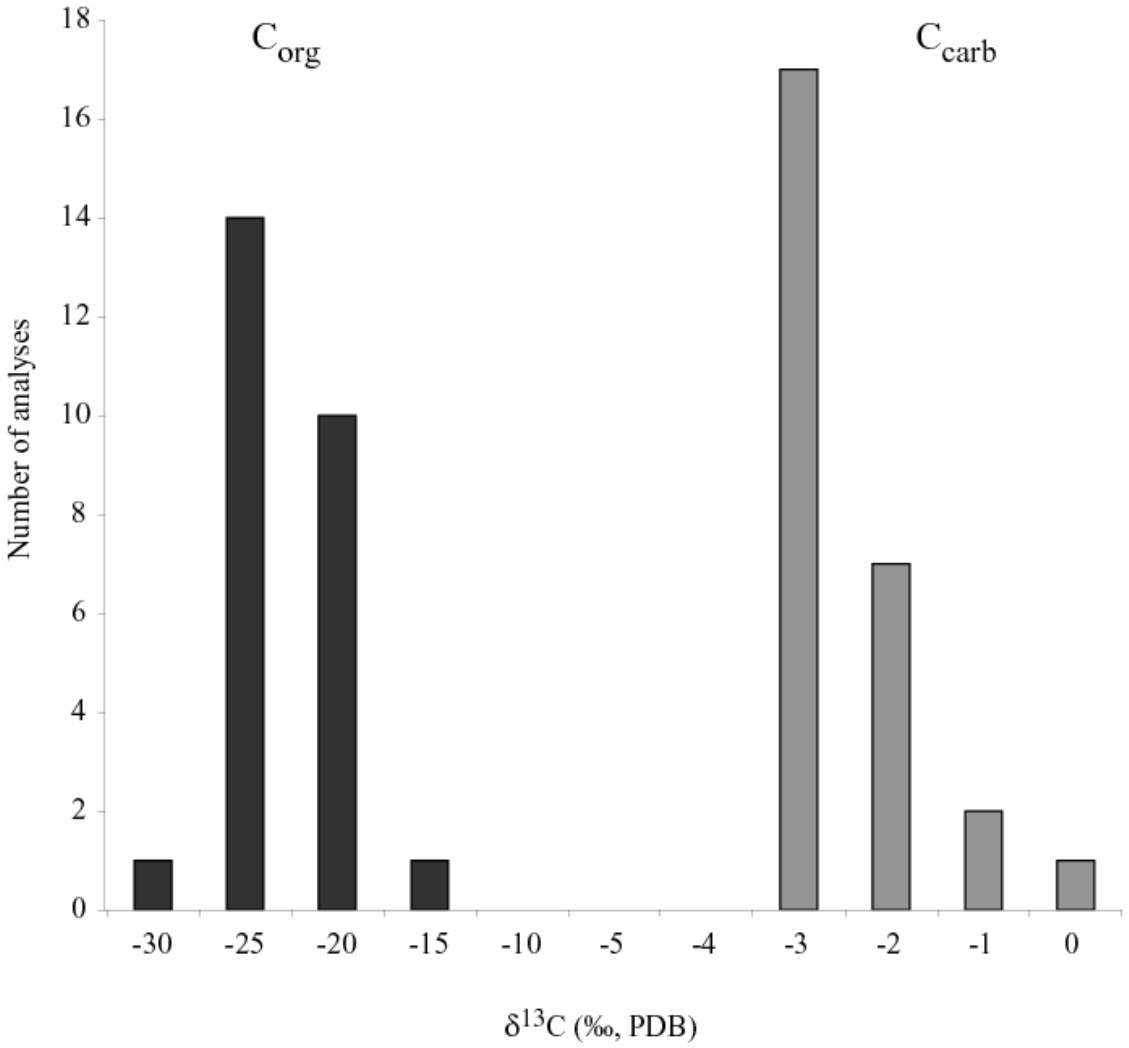

Figure 28: Histrogram showing statistical distribution of carbonate-hosted kerogen $\delta^{13}C_{org}$ and carbonate $\delta^{13}C_{carb}$ analyses.

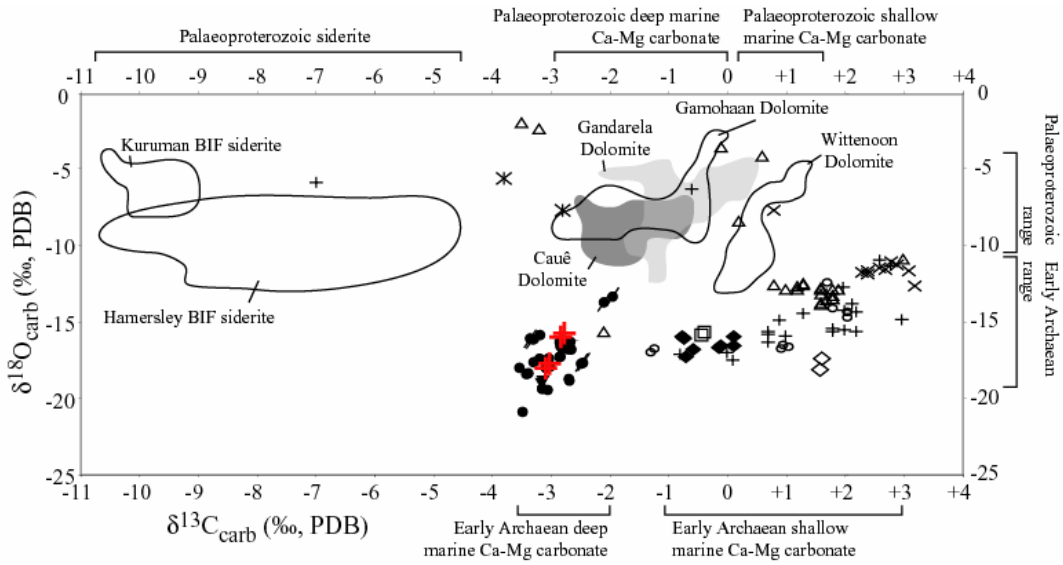

Shallow marine sedimentary calcite and dolomite					
Early Archaean	Pilbara Supergroup	Strelley Pool Chert	Pilgangoora Belt	◇ Sparry dolomite (drillcore) □ Laminated carbonate (neptunian breccia) ○ Laminated carbonate (outcrop)	This study
				+ Laminated carbonate (neptunian breccia and outcrop)	Lindsay *et al.* (2005)
			North Pole Dome	× Laminated carbonate	
		McPhee Formation	Marble Bar	* Laminated carbonate	Veizer *et al.* (1989)
	Swaziland Supergroup	(various localities)		△ Assorted bedded carbonate	
Palaeo-proterozoic	Hamersley Group	(various localities)		◯ Wittenoon Dolomite	Veizer *et al.* (1990)
Basinal marine calcitic and dolomitic BIF					
Early Archaean	Pilbara Supergroup	Coonterunah Subgroup, Pilgangoora Belt	Double Bar Fm.	◆ Sparry dolomite (drillcore)	This study
			Coucal Fm.	▼ Prominent calcitic carbonate ● Prominent dolomitic carbonate + Prominent dolomitic carbonate, pervasively silicified Lesser dolomitic carbonate	
Palaeo-proterozoic	Minas Supergroup	Quadrilátero Ferrífero		⬤ Cauê Dolomite	Spier *et al.* (2007)

Figure 29: $\delta^{13}C_{carb}$ - $\delta^{18}O_{carb}$ diagram comparing Precambrian BIF- and non-BIF carbonate in this and other studies. Pilbara Block: calcitic and dolomitic chert from Strelley Pool Chert peritidal sediments collected in the Pilgangoora Belt and North Pole Dome (Lindsay et al., 2005) and McPhee Formation dolomitic chert in the Marble Bar Belt (Veizer et al., 1989a); Kaapvaal Craton: various calcitic and dolomitic sedimentary cherts (Veizer et al., 1989a); Transvaal Basin: BIF-siderite from the Kuruman Formation and non-BIF dolomite from the Gomahaan Formation (Beukes and Klein, 1990; Klein and Beukes, 1989); Hamersley Basin: non-BIF dolomite from Wittenoon Formation and assorted Hamersley BIF-siderite (Veizer et al., 1990); Quadrilátero Ferrífero, Minas Supergroup: non-BIF dolomite from the Gandarela Formation (Bekker et al., 2003; Sial et al., 2000) and BIF-dolomite from the Cauê Formation (Spier et al., 2007).

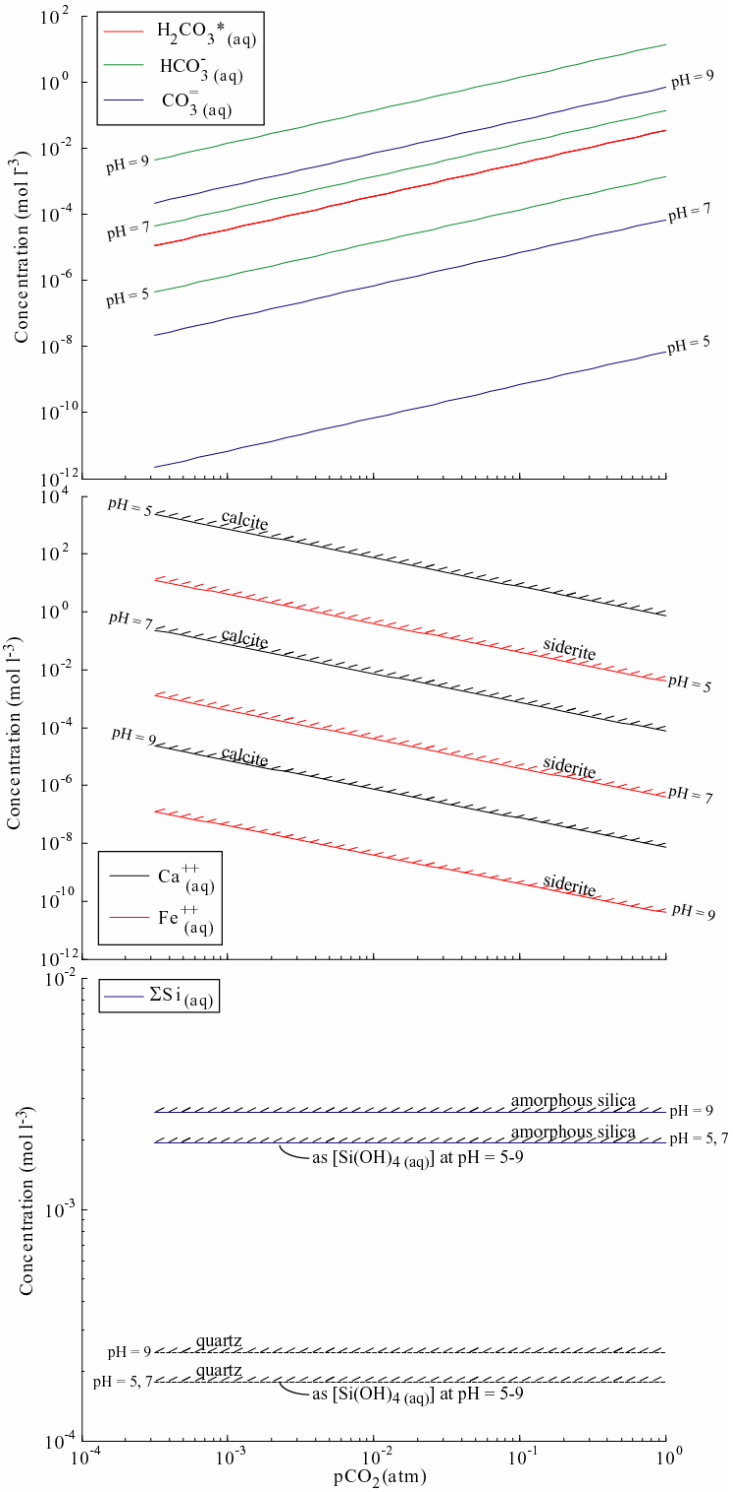

Figure 30: Thermochemical diagram showing calculated speciation at pH = 5, 7 and 9 as a function of pCO_2 at 25 ºC. (a): DIC speciation (data in Stumm and Morgan, 1996). (b) Calcite and siderite stability (data in Stumm and Morgan, 1996). (c): Silica speciation (data in Gunnarsson and Arnorsson, 2000).

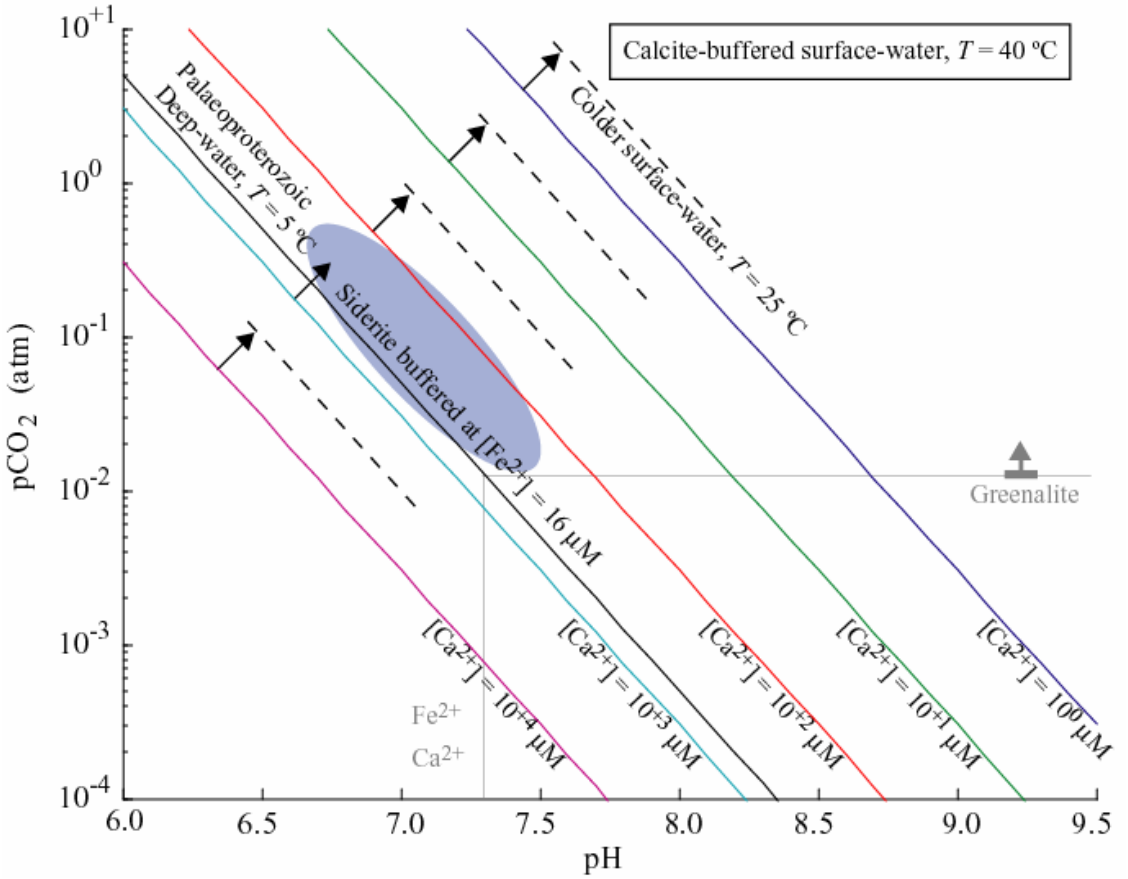

Figure 31: Thermochemical pCO_2 – pH diagram showing Archaean deep siderite-buffered seawater at 5 ºC (calculation in text) and surface calcite-buffered seawater at different Ca^{2+} concentrations at 40 ºC (solid lines) and 25 ºC (dashed lines). Also shown are the stability field of greenalite. Inferred composition for Archaean surface water is shaded.

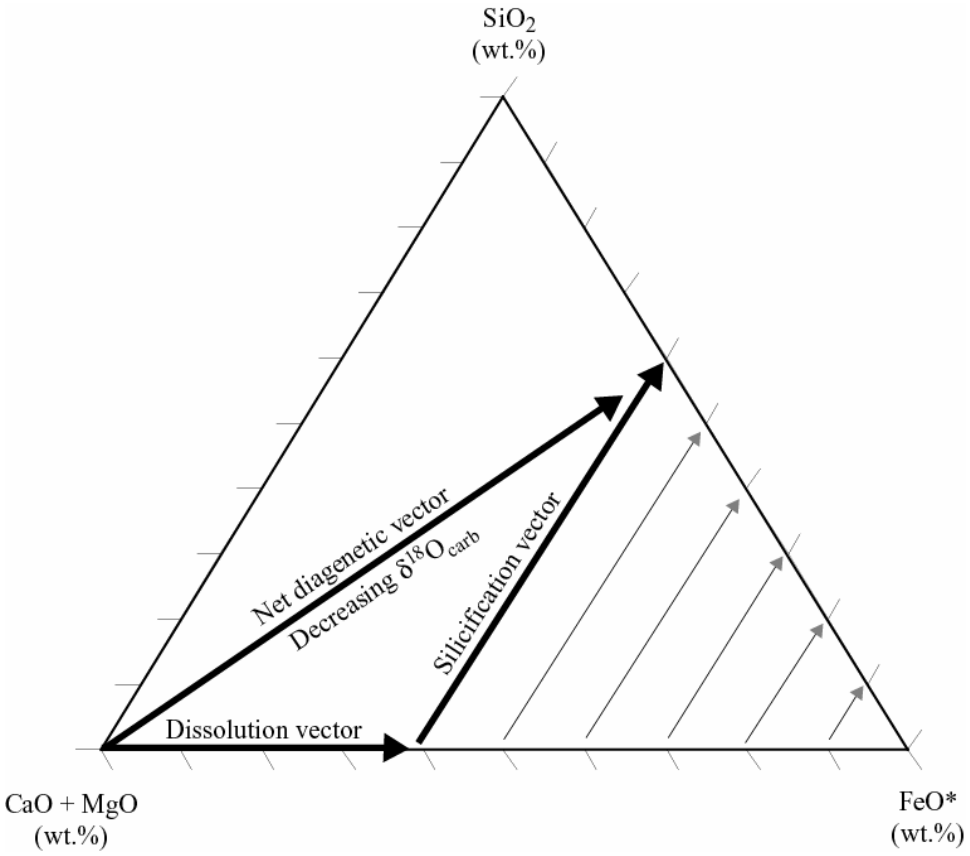

Figure 32: Ternary CaO+MgO – SiO_2 – FeO* diagram illustrating diagenesis of Ca-Mg carbonates in the presence of high-activity $Fe^{2+}_{(aq)}$ and $H_4SiO_{4(aq)}$ porewaters.

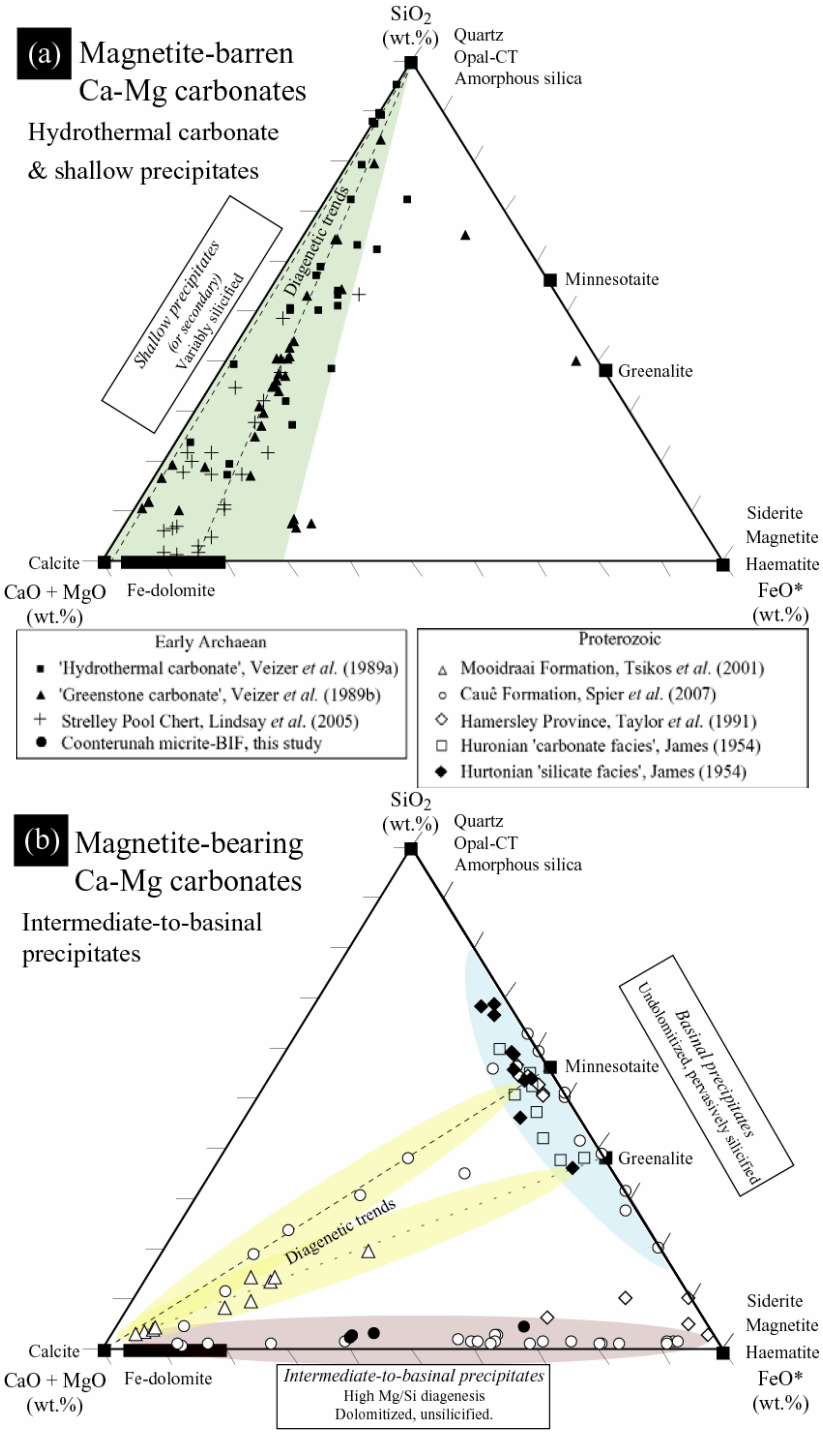

Figure 33: Ternary diagrams showing compositions of (a) Early Archaean variably silicified greenstone-belt carbonates (Veizer et al., 1989a) and carbonate interpreted to be of secondary hydrothermal origin (Veizer et al., 1989b), and (b) Precambrian ferruginous carbonates (Tsikos et al., 2001), carbonate-bearing BIFs (this study and Spier et al., 2007), and carbonates barren of iron (this study and Veizer et al., 1989a; Veizer et al., 1989b). Inferred diagenetic trends are also shown.

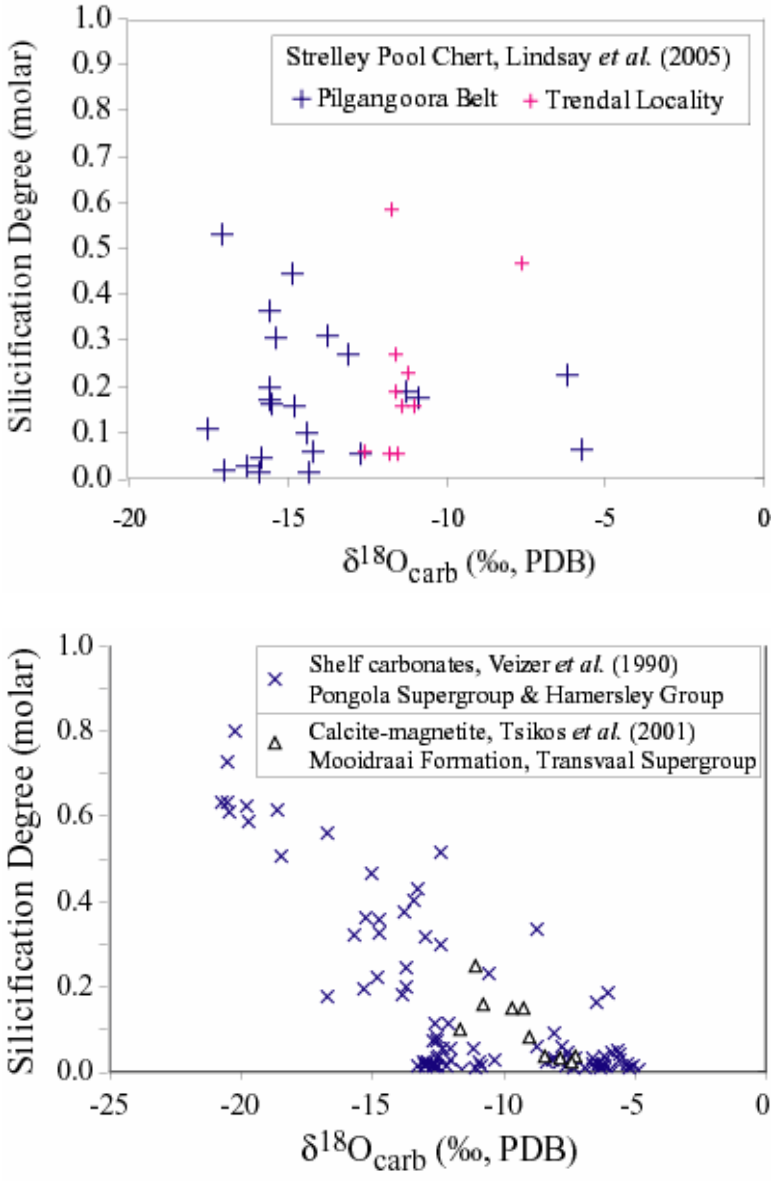

Figure 34: Degree of molar silicification, ς, versus $\delta^{18}O_{carb}$ in (a) the Strelley Pool Chert (Lindsay et al., 2005) and (b) shelf carbonates from the Mesoarchaean Pongola Supergroup and the Palaeoproterozoic Hamersley Group (Veizer et al., 1990) and ferruginous limestone from the Palaeoproterozoic Mooidraai Formation. Data from Tsikos (2001). A clear diagenetic trend is evident in (b).

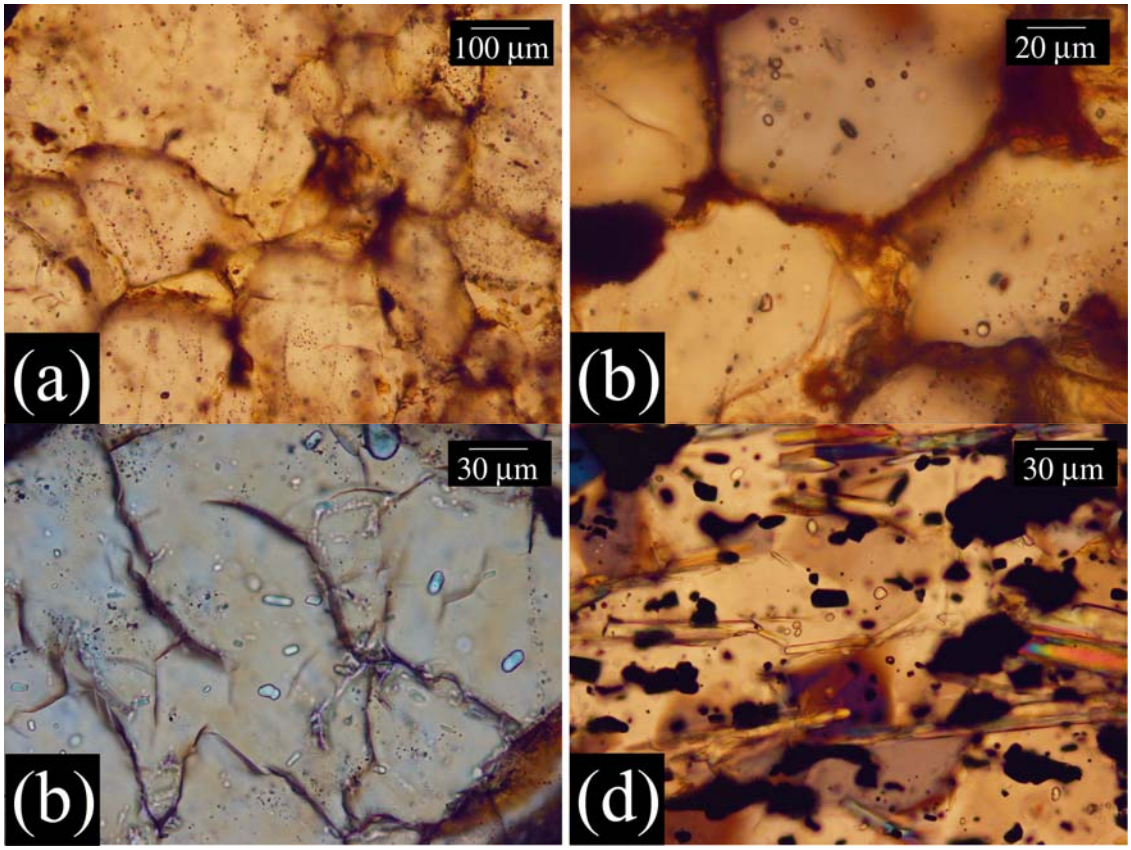

Figure 35: Photomicrographs of fluid inclusions in BIF chert bands. (a, b): Marra Mamba Iron Formation. (c): Gorge Creek Group. (d): Quartz-grunerite-magnetite BIF from northeast Isua Supracrustal Belt (Chapter 4).

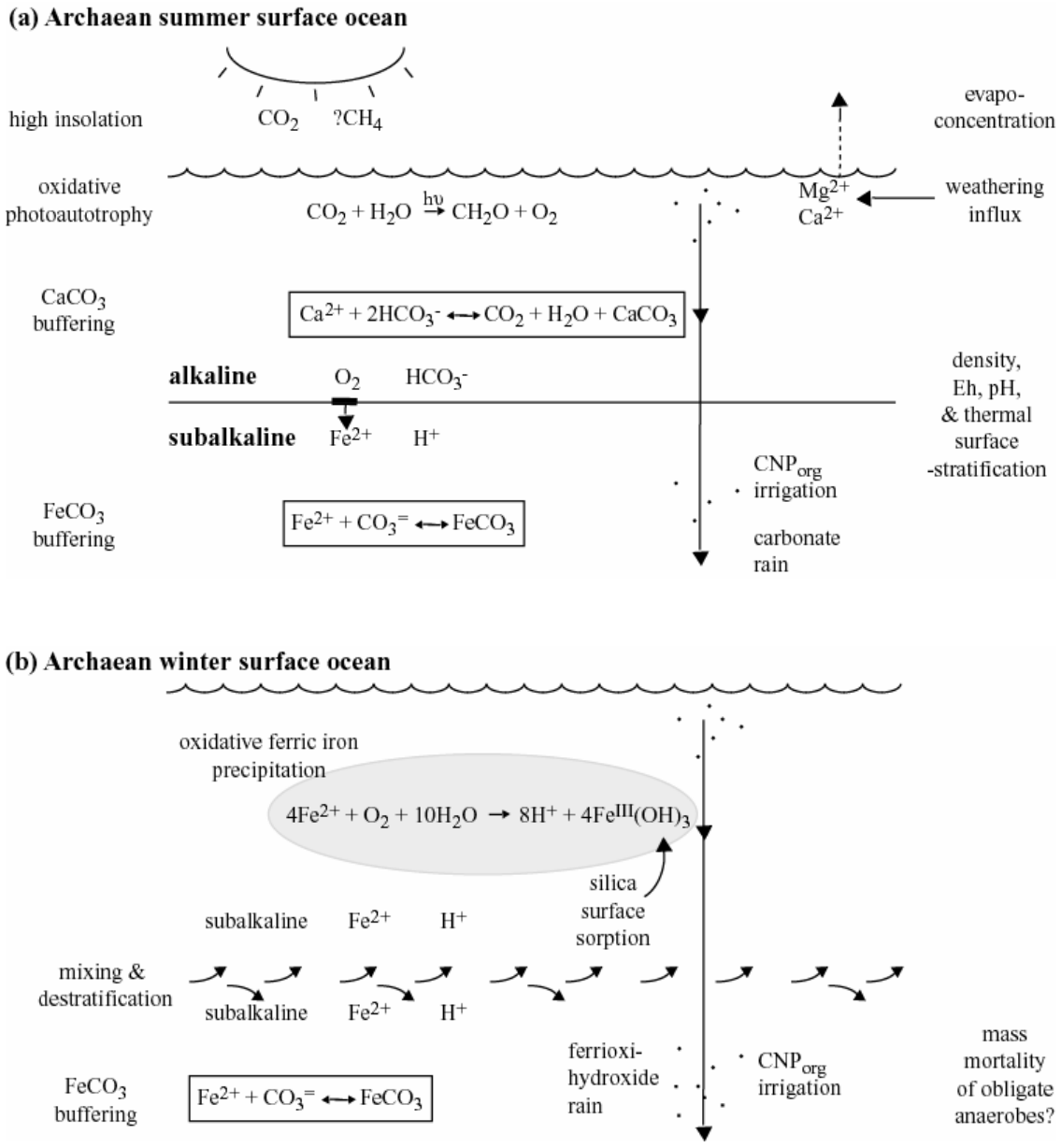

Figure 36: Schematic diagrams of Early Archaean pelagic environments. (a): Stratified surface ocean. (b): Destratified surface ocean.

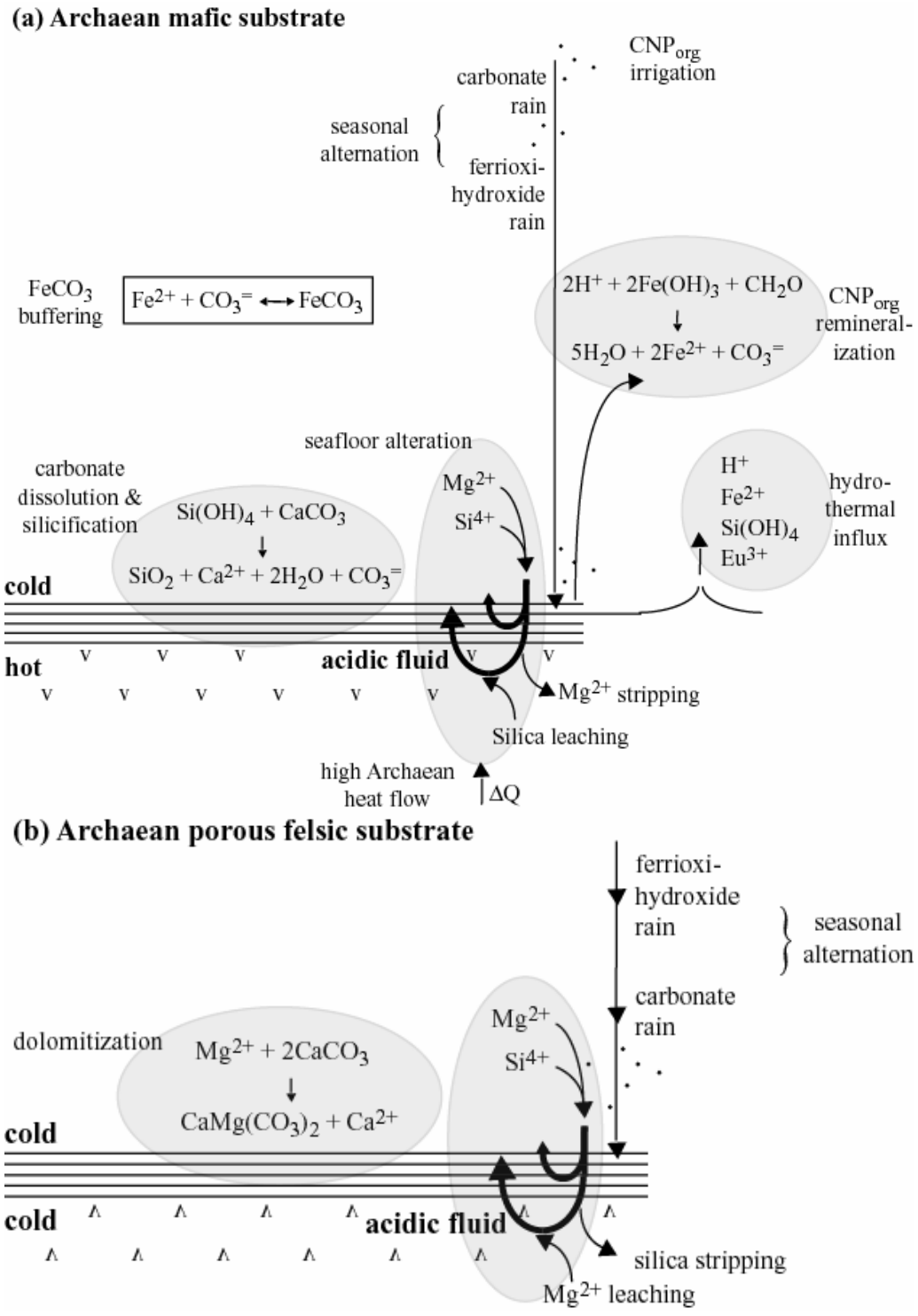

Figure 37: Schematic diagrams of Early Archaean benthic environments. (a): Canonical Archaean greenstone belt hot mafic substrate. (b): Benthic environment on permeable felsic substrate, as in the case of the Coucal Formation..

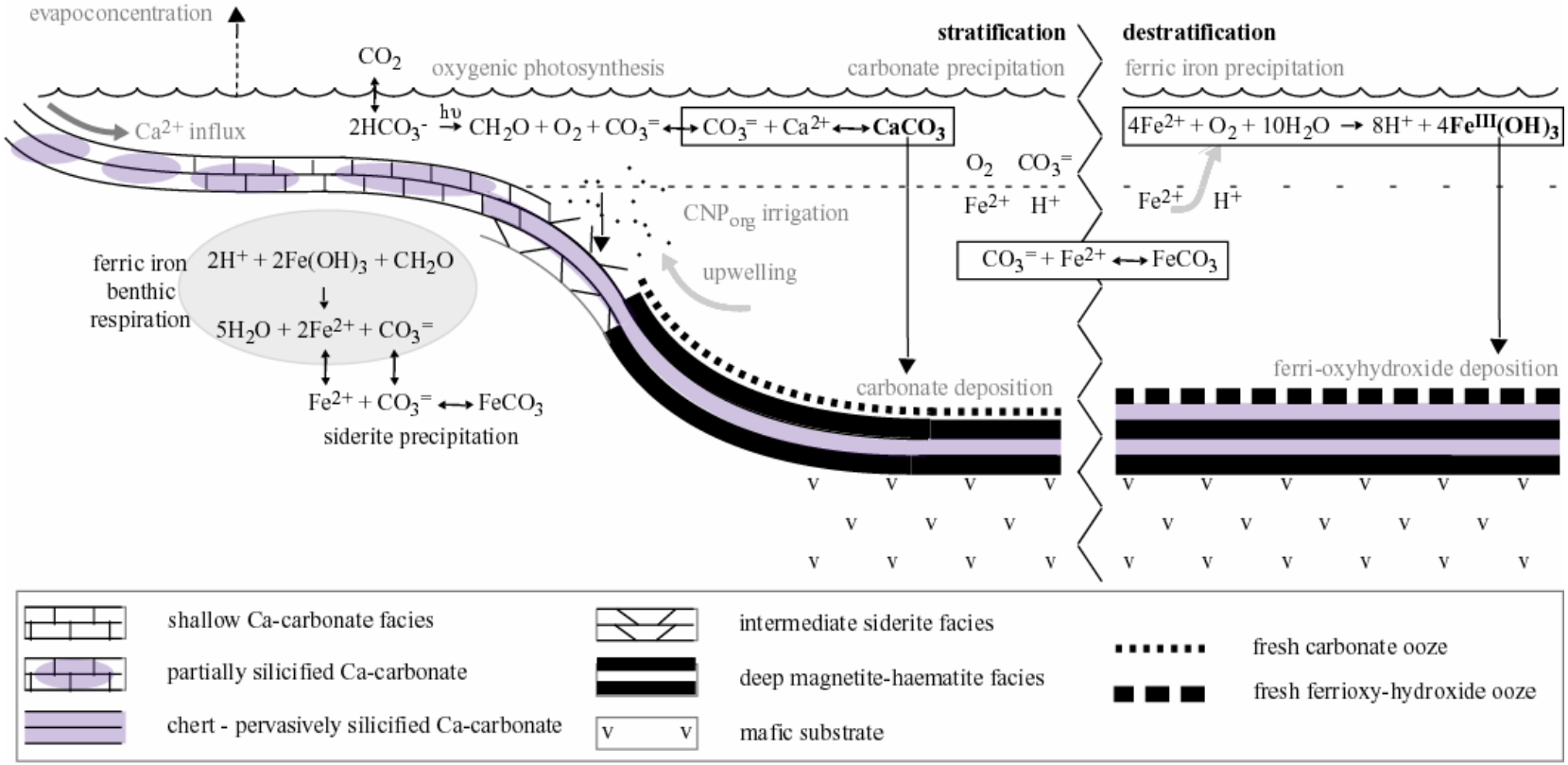

Figure 38: Schematic diagram of hypothetical Early Archaean marine environment, showing facies relationships between CaMg carbonate, siderite, magnetite and carbonate silicification.

Table 1: Molar distribution of magnetite and carbonate phases.

Sample	**Units**	**PC05-020C**	**PC06-028A**	**PC06-028Bi**	**PC06-028Bii**
Lithology		Calcitic	Dolomitic	Dolomitic	Dolomitic
Mesoband		C_1	C_1	C_3	M_2
Fe_3O_4	Mol%	15.69	13.10	12.90	33.13
$[Ca_{0.5}Mg_{0.5}](CO_3)$	Mol%	43.07	73.75	75.16	55.43
$CaCO_3$	Mol%	40.37	11.38	10.22	10.08
$MnCO_3$	Mol%	0.87	1.76	1.72	1.36
Sum	*Mol%*	*99.13*	*98.24*	*98.28*	*98.64*
Ca/Mg	***Molar***	*2.87*	*1.31*	*1.27*	*1.36*
% of carbonate as dolomite	***Molar***	*51.09*	*84.88*	*86.29*	*82.89*
% of carbonate as rhodochrosite	***Molar***	*1.03*	*2.07*	*1.47*	*2.03*

Table 2: Mass distribution of magnetite and carbonate phases.

Sample	**Units**	**PC05-020C**	**PC06-028A**	**PC06-028Bi**	**PC06-028Bii**
Lithology		Calcitic	Dolomitic	Dolomitic	Dolomitic
Mesoband		C_1	C_1	C_3	M_2
Fe_3O_4	Wt%	30.93	27.14	26.82	55.00
$[Ca_{0.5}Mg_{0.5}](CO_3)$	Wt%	33.81	60.85	62.22	36.64
$CaCO_3$	Wt%	34.41	10.20	9.18	7.24
$MnCO_3$	Wt%	0.85	1.81	1.78	1.12
Sum	*Wt%*	*99.15*	*98.19*	*98.22*	*98.88*
% of carbonate as dolomite	***Weight***	48.95	83.52	85.02	81.43
% of carbonate as rhodochrosite	***Weight***	1.24	2.49	2.43	2.49

Table 3: Individual mineral microprobe analyses (atomic proportions)

Pt#	Mineral	Fe	Mn	Mg	Ca	Ba	Sr
1	Dolomite	0.0131	0.0171	0.6512	0.8186	0.0001	0
2	Dolomite	0.0137	0.014	0.6798	0.7923	0.0001	0.0001
3	Dolomite	0.0125	0.0144	0.6449	0.8272	0.001	0
4	Dolomite	0.0169	0.0173	0.6661	0.7996	0.0002	0
5	Calcite	0.0021	0.0139	0.0177	1.4658	0	0.0005
6	Calcite	0.0038	0.011	0.0477	1.4371	0.0003	0.0001
7	Dolomite	0.0147	0.0201	0.6555	0.8098	0	0
8	Dolomite	0.0135	0.0203	0.6453	0.8209	0	0
9	Dolomite	0.0116	0.0162	0.682	0.7901	0	0.0001
10	Dolomite	0.0208	0.0177	0.6602	0.801	0	0.0003
11	Dolomite	0.0124	0.0177	0.653	0.8168	0	0.0001
12	Dolomite	0.0202	0.0195	0.6678	0.7925	0	0
13	Dolomite	0.0207	0.0208	0.6371	0.8215	0	0
14	Dolomite	0.0176	0.0174	0.672	0.7928	0	0.0002
15	Dolomite	0.014	0.019	0.6612	0.8058	0	0
16	Dolomite	0.0126	0.0148	0.6809	0.7916	0.0001	0
17	Dolomite	0.0087	0.0198	0.6616	0.8099	0	0
18	Calcite	0.0037	0.0135	0.0093	1.4731	0.0002	0.0002
19	Calcite	0.0019	0.0122	0.0103	1.4753	0.0004	0
20	Calcite	0.0021	0.0139	0.1311	1.3522	0.0006	0.0002
21	Calcite	0.0003	0.0206	0.0084	1.4708	0	0
22	Calcite	0.0187	0.021	0.2788	1.1811	0.0002	0.0002
23	Rhodochroi	0.0307	0.7471	0.0624	0.6562	0	0.0036
24	Calcite	0.0115	0.0142	0.0171	1.4569	0.0001	0.0002
25	Rhodochroi	0.0407	0.4411	0.0558	0.9553	0.0004	0.0067
26	Calcite	0.017	0.0348	0.0092	1.4387	0.0003	0
27	Calcite	0.002	0.0202	0.0212	1.4565	0	0.0001
28	Dolomite	0.0145	0.0145	0.6681	0.8023	0.0006	0.0001
29	Dolomite	0.0961	0.0323	0.5475	0.8238	0	0.0004
30	Dolomite	0.0462	0.0404	0.6434	0.7698	0.0002	0
31	Dolomite	0.0577	0.0533	0.5885	0.8006	0	0
32	Dolomite	0.1035	0.0274	0.5839	0.7852	0	0

Table 3 (cont'd): Individual mineral microprobe analyses (atomic proportions).

Pt#	Mineral	Fe	Mn	Mg	Ca	Ba	Sr
33	Dolomite	0.0557	0.0514	0.5911	0.8016	0.0001	0
34	Dolomite	0.1503	0.0323	0.5458	0.7716	0	0
35	Dolomite	0.0644	0.0423	0.5804	0.8129	0	0
36	Dolomite	0.085	0.0311	0.5845	0.7991	0.0001	0.0002
37	Dolomite	0.1646	0.0344	0.5026	0.7983	0	0
38	Dolomite	0.1078	0.0305	0.5432	0.8186	0	0
39	Dolomite	0.1418	0.0292	0.559	0.7699	0	0.0001
40	Dolomite	0.0734	0.0464	0.5729	0.8071	0.0001	0.0001
41	Dolomite	0.0763	0.0272	0.6137	0.7827	0	0.0001
42	Dolomite	0.1039	0.0451	0.551	0.7998	0.0002	0
43	Dolomite	0.1242	0.04	0.5589	0.7769	0	0
44	Dolomite	0.0906	0.0461	0.5388	0.824	0.0003	0.0003
45	Dolomite	0.1299	0.0302	0.552	0.7879	0	0
46	Dolomite	0.1012	0.0295	0.5422	0.8269	0	0.0003
47	Dolomite	0.1564	0.025	0.5227	0.796	0	0
48	Dolomite	0.1433	0.0294	0.4983	0.829	0	0.0001
49	Dolomite	0.1429	0.0277	0.5479	0.7814	0.0001	0
50	Dolomite	0.1793	0.0278	0.4671	0.8258	0	0
51	Dolomite	0.1248	0.0321	0.5591	0.7837	0.0004	0
52	Dolomite	0.0599	0.0402	0.5757	0.8241	0	0
53	Dolomite	0.0973	0.0378	0.581	0.7837	0	0.0001
54	Dolomite	0.0366	0.0276	0.6056	0.8301	0	0
55	Dolomite	0.0753	0.04	0.6108	0.7738	0.0001	0
56	Dolomite	0.085	0.0395	0.5532	0.8223	0	0
57	Dolomite	0.083	0.0351	0.6071	0.7745	0.0003	0
58	Dolomite	0.1073	0.0429	0.5545	0.7954	0	0
59	Dolomite	0.1282	0.0264	0.5536	0.7917	0	0.0001
60	Dolomite	0.0622	0.0487	0.5679	0.8211	0	0
61	Dolomite	0.1171	0.0274	0.5623	0.7928	0.0004	0
62	Calcite	0.0073	0.0349	0.0035	1.4542	0.0001	0
63	Dolomite	0.0133	0.0446	0.6663	0.7758	0	0

Table 4: Major element oxide concentrations (wt.%) in carbonate samples. ('LOI' = loss on ignition)

Sample	**PC05-020C**	**PC06-028A**	**PC06-028Bi**	**PC06-028Bii**
Lithology	Calcitic	Dolomitic	Dolomitic	Dolomitic
Mesoband	C_1	C_1	C_3	M_2
SiO_2	1.93	1.56	1.21	3.26
TiO_2	0.009	0.008	0.007	0.007
Al_2O_3	0.08	0.10	0.06	0.07
FeO*	28.12	24.11	24.09	51.22
MnO	0.514	1.069	1.059	0.691
MgO	7.22	12.69	13.12	8.01
CaO	28.87	23.11	23.22	15.21
Na_2O	0.013	0.020	0.011	0.001
K_2O	0.002	0.002	0.000	0.000
P_2O_5	0.050	0.056	0.051	0.077
L.O.I.	29.68	33.52	33.81	20.09
Σ	*96.49*	*96.24*	*96.64*	*98.63*

Table 5: Trace element ICP concentrations (ppm) in carbonate samples.

Sample	**PC05-020C**	**PC06-028A**	**PC06-028Bi**	**PC06-028Bii**
Lithology	Calcitic	Dolomitic	Dolomitic	Dolomitic
Mesoband	C_1	C_1	C_3	M_2
La	1.51	1.42	1.52	1.17
Ce	1.96	1.97	1.86	1.6
Pr	0.22	0.23	0.2	0.18
Nd	0.93	0.96	0.84	0.76
Sm	0.23	0.23	0.19	0.18
Eu	0.36	0.55	0.51	0.48
Gd	0.32	0.34	0.27	0.25
Tb	0.05	0.05	0.04	0.04
Dy	0.3	0.37	0.29	0.25
Y	3.82	4.10	3.54	2.81
Ho	0.07	0.08	0.07	0.06
Er	0.2	0.23	0.2	0.16
Tm	0.03	0.03	0.03	0.02
Yb	0.14	0.17	0.14	0.12
Lu	0.02	0.03	0.02	0.02
∑REE	*6.34*	*6.66*	*6.18*	*5.29*
Sc	0.1	0.1	0.0	0
V	1.8	2.2	1.3	1.7
Cr	0.2	0.1	0.0	0
Ni	6.7	1.6	1.4	6.5
Cu	50.6	11.1	9.4	12.1
Ga	0.90	0.84	2.66	3.10
Zn	17.5	11.3	8.8	10.5
Cs	0.02	0.01	0.01	0.01
Pb	0.37	0.43	0.4	0.49
Zr	1	2	2	1
Hf	0.02	0.04	0.03	0.02
Nb	0.06	0.05	0.03	0.04
Ta	0	0	0	0
Th	0.03	0.04	0.03	0.03
U	0.04	0.03	0.03	0.06
Rb	0.2	0.2	0.1	0.1
Sr	72	60	58	42
Ba	4	1	1	2

Table 6: Major element oxide concentrations (wt.%) in pelitic and volcanoclastic samples. ('LOI' = loss on ignition).

Sample	**PC06-027**	**PC06-027R**	**PC06-029**	**PC06-039**	**PC06-043**	**PC06-044**
Lithology	Metapelite bio-chl	Metapelite bio-chl	Metapelite bio-chl	Tuffaceous wacke	Metapelite bio-chl	Metapelite bio-chl
SiO_2	41.90	41.90	41.58	56.70	56.45	60.90
TiO_2	0.648	0.647	0.492	0.670	0.368	0.389
Al_2O_3	15.48	15.46	14.49	16.75	10.69	10.03
FeO*	25.55	25.58	27.86	9.91	20.92	17.77
MnO	0.312	0.311	0.193	0.152	0.162	0.151
MgO	5.93	5.90	4.73	4.45	3.41	3.33
CaO	0.31	0.27	0.37	3.53	0.09	0.13
Na_2O	0.184	0.181	0.017	2.437	0.013	0.009
K_2O	0.132	0.133	0.057	0.654	0.313	0.122
P_2O_5	0.104	0.103	0.058	0.075	0.049	0.085
L.O.I.	6.02	6.02	6.17	3.86	4.77	4.25
Σ	*96.56*	*96.51*	*96.02*	*99.18*	*97.23*	*97.16*

Table 7: Trace element concentrations (ppm) in volcanoclastic samples.

Sample	**PC06-027**	**PC06-027R**	**PC06-029**	**PC06-039**	**PC06-043**	**PC06-044**
Lithology	Metapelite bio-chl	Metapelite bio-chl	Metapelite bio-chl	Tuffaceous wacke	Metapelite bio-chl	Metapelite bio-chl
La	26.33		13.20	35.06	11.86	10.93
Ce	55.85		44.24	69.45	47.14	26.28
Pr	7.14		4.32	8.49	3.94	3.03
Nd	27.73		17.38	34.08	15.39	11.62
Sm	6.400		489	8.43	4.17	2.75
Eu	2.14		1.70	1.72	1.06	0.71
Gd	6.15		4.89	9.53	4.25	2.66
Tb	1.06		0.96	1.72	0.85	0.51
Dy	6.48		6.78	11.4	5.9	3.5
Y	33.11		39.03	66	33	18.29
Ho	1.34		1.53	2.5	1.3	1
Er	3.84		4.92	7.16	4.06	2.22
Tm	0.60		0.81	1.09	0.63	0.35
Yb	4.02		5.36	7.03	4.11	2.27
Lu	0.65		0.87	1.14	0.65	0.36
∑REE	*182.84*		*150.88*	*265.19*	*138.02*	*86.21*
Sc	14.9		9.9	14.2	6	5.5
V	88	87	38	40	27	37
Cr	24	24	17	13	15	10
Ni	122	123	87	3	82	77
Cu	4	5	5	16	3	2
Ga	22	24	21	22	16	15
Zn	216	217	164	70	125	115
Cs	0.46		0.56	0.58	0.30	0.12
Pb	2.15		3.04	4.57	2.38	1.37
Zr	238		315	435	231	146
Hf	6.8		9.32	11	7	4.16
Nb	11.45		15.91	15	12	7.2
Ta	1.15		1.58	1	1	0.82
Th	10.18		15	9	11	6
U	2.04		2.88	3	2	1.59
Rb	7.1		2.6	17.3	2.3	1.4
Sr	12		3	108	4	2
Ba	33		15	100	21	12

Table 8: Bulk and laminar $\delta^{13}C_{carb}$ and $\delta^{18}O_{carb}$ analyses of prominent 32-cm thick laminated carbonate unit. (B*xx*[c/m] refers to carbonate/magnetite lamina *xx* mm from base of sample PC06-028, 'rep' = replica)

Sample	**Analysis**	**Mass**	**CO_2**	**CO_2**	**± 1σ**	**$\delta^{13}C_{carb}$**	**± 1σ**	**$\delta^{18}O_{carb}$**	**± 1σ**
		(mg)	(µg)	(wt.%)	(‰, PDB)	(‰, PDB)			
B55[c]	rep1	0.11	47.86	42.0		-3.12	0.03	-18.65	0.04
B63[c]	rep1	0.19	70.01	36.5		-3.09	0.03	-17.99	0.03
	rep2	0.19	64.47	34.9		-3.06	0.02	-17.89	0.04
	mean			*35.7*	*1.1*	*-3.08*	*0.02*	*-17.94*	*0.05*
B75[c]	rep1	0.19	62.17	32.4		-3.54	0.03	-18.00	0.02
B79[c]	rep1	0.73	86.94	11.9		-3.05	0.03	-17.41	0.02
	rep2	0.54	84.79	15.7		-3.04	0.02	-17.39	0.03
	mean			*13.8*	*2.7*	*-3.04*	*0.00*	*-17.40*	*0.01*
B80[m]	rep1	0.26	53.09	20.6		-3.30	0.04	-17.64	0.03
	rep2	0.31	59.24	18.9		-3.20	0.03	-17.41	0.04
	mean			*19.8*	*1.2*	*-3.25*	*0.07*	*-17.52*	*0.05*
B82[c]	rep1	0.30	72.48	24.0		-2.81	0.02	-16.73	0.02
	rep2	0.17	49.24	28.8		-2.84	0.02	-16.60	0.03
	rep3	1.27	86.63	6.8		-2.67	0.02	-16.30	0.02
	mean			*19.9*	*11.6*	*-2.78*	*0.09*	*-16.55*	*0.04*
B87[c]	rep1	0.26	76.32	28.9		-2.66	0.02	-16.80	0.04
	rep2	0.14	55.70	38.7		-2.71	0.02	-16.80	0.03
	mean			*33.8*	*6.9*	*-2.69*	*0.04*	*-16.80*	*0.05*
B89[c]	rep1	0.17	36.93	21.3		-3.39	0.02	-18.36	0.04
	rep2	0.12	23.39	20.0		-3.42	0.05	-18.41	0.05
	mean			*20.7*	*1.0*	*-3.41*	*0.02*	*-18.38*	*0.07*
B90[c]	rep1	0.22	62.32	27.9		-2.85	0.01	-17.28	0.03
	rep2	0.14	55.24	38.4		-2.86	0.02	-17.31	0.04
	rep3	0.30	68.17	23.0		-2.84	0.02	-17.27	0.01
	mean			*29.8*	*7.9*	*-2.85*	*0.01*	*-17.28*	*0.05*
PC05-020C	rep1	0.40	64.45	16.0		-3.12	0.02	-18.89	0.04
	rep2	0.58	69.99	12.1		-3.14	0.02	-18.98	0.03
	mean			*14.0*	*2.7*	*-3.13*	*0.01*	*-18.93*	*0.05*
PC06-026	rep1	1.74	112.91	6.5		-3.29	0.04	-16.13	0.02
	rep2	1.01	106.77	10.6		-3.19	0.03	-15.86	0.02
	mean			*8.5*	*2.9*	*-3.24*	*0.07*	*-16.00*	*0.03*
PC06-028A	rep1	0.67	42.09	6.3		-3.06	0.02	-19.45	0.02
PC06-028B-i	rep1	0.71	74.74	10.6		-3.15	0.01	-19.35	0.04
	rep2	0.43	68.96	15.9		-3.16	0.02	-19.38	0.03
	mean			*13.2*	*3.8*	*-3.16*	*0.00*	*-19.36*	*0.02*
PC06-028B-ii	rep1	1.27	50.09	3.9		-3.04	0.01	-17.76	0.04
	rep2	1.28	47.12	3.7		-3.02	0.02	-17.92	0.04
	mean			*3.8*	*0.2*	*-3.03*	*0.01*	*-17.84*	*0.06*
PC06-053	rep1	0.51	72.85	14.2		-2.70	0.02	-18.73	0.03
	rep2	0.30	70.28	23.7		-2.69	0.01	-18.84	0.03
	mean			*18.9*	*6.7*	*-2.70*	*0.01*	*-18.78*	*0.04*
Average				*21.1*	*11.2*	*-3.04*	*0.22*	*-17.80*	*1.00*

Table 9: Bulk $\delta^{13}C_{carb}$ and $\delta^{18}O_{carb}$ analyses of silicified prominent 32-cm thick carbonate unit. ('rep' = replica)

Sample	**Analysis**	**Mass**	**CO_2**	**CO_2**	**± 1σ**	**$\delta^{13}C_{carb}$**	**± 1σ**	**$\delta^{18}O_{carb}$**	**± 1σ**
		(mg)	(µg)	(wt.%)		(‰, PDB)		(‰, PDB)	
PC03-078	rep1	3.68	39.74	1.1		-3.04	0.03	-17.70	0.05
	rep2	2.73	36.37	1.3		-2.83	0.03	-16.25	0.05
	rep3	5.60	31.31	0.6		-3.09	0.03	-18.02	0.05
	rep4	8.04	34.95	0.4		-2.86	0.03	-16.33	0.05
	mean			*0.9*	*0.4*	*-2.95*	*0.13*	*-17.07*	*0.92*

Table 10: Bulk $\delta^{13}C_{carb}$ and $\delta^{18}O_{carb}$ analyses of lesser cm-scale interlaminated carbonate/chlorite schist units. ('rep' = replica)

Sample	**Analysis**	**Mass**	**CO_2**	**CO_2**	**± 1σ**	**$\delta^{13}C_{carb}$**	**± 1σ**	**$\delta^{18}O_{carb}$**	**± 1σ**
		(mg)	(µg)	(wt.%)		(‰, PDB)		(‰, PDB)	
PC06-031	rep1	0.41	43.65	10.6		-2.49	0.04	-17.73	0.04
	rep2	2.00	48.00	2.4		-2.46	0.04	-17.68	0.03
	mean			*6.5*	*5.8*	*-2.48*	*0.02*	*-17.71*	*0.05*
PC06-041	rep1	2.31	67.17	2.9		-3.36	0.03	-16.08	0.01
	rep2	1.69	67.52	4.0		-3.32	0.03	-16.13	0.03
	mean			*3.4*	*0.8*	*-3.34*	*0.03*	*-16.11*	*0.03*
PC06-045	rep1	4.56	115.40	2.5		-1.96	0.01	-13.35	0.02
	rep2	2.72	121.12	4.5		-2.10	0.02	-13.72	0.01
	mean			*3.5*	*1.4*	*-2.03*	*0.11*	*-13.54*	*0.03*
Average				***4.5***	***1.8***	***-2.62***	***0.67***	***-15.78***	***2.10***

Table 11: Metasomatic and vein carbonate $\delta^{13}C_{carb}$ and $\delta^{18}O_{carb}$ analyses. ('rep' = replica)

Sample	**Analysis**	**Mass**	**CO_2**	**CO_2**	**± 1σ**	**$\delta^{13}C_{carb}$**	**± 1σ**	**$\delta^{18}O_{carb}$**	**± 1σ**
		(mg)	(µg)	(wt.%)		(‰, PDB)		(‰, PDB)	
PC05-021	rep1	1.49	38.94	2.6		1.55	0.03	-16.63	0.03
	rep2	0.42	32.87	7.8		1.60	0.02	-16.61	0.03
	mean			*5.2*	*3.6*	*1.58*	*0.04*	*-16.62*	*0.04*
PC06-022	rep1	0.41	36.65	8.9		-4.94	0.01	-7.65	0.03
	rep2	0.82	39.98	4.9		-5.19	0.03	-7.74	0.04
	mean			*6.9*	*2.9*	*-5.06*	*0.17*	*-7.69*	*0.05*
PC06-025	rep1	7.86	63.04	0.8		0.68	0.05	-16.40	0.01
	rep2	6.55	64.60	1.0		0.64	0.03	-17.12	0.05
	rep3	6.38	63.52	1.0		0.67	0.03	-17.02	0.05
	rep4	0.27	25.59	9.4		0.78	0.03	-16.96	0.04
	rep5	0.45	33.77	7.6		0.78	0.02	-17.02	0.01
	mean			*3.9*	*4.2*	*0.71*	*0.07*	*-16.90*	*0.29*

Table 12: Laminated carbonate-hosted kerogen $\delta^{13}C_{org}$ analyses. ('blk' = bulk analysis, 'lam' = laminar analysis)

Sample	**Lithology**	**Analysis**	**Mass**	**C_{org}**	**$\delta^{13}C_{org}$**	**± 1σ**
			(mg)	(wt.%)	(‰, PDB)	
PC05-020A	Calcitic	blk	5.0	0.93	-28.77	0.12
PC05-020B	Calcitic	lam1	27.8	0.22	-25.34	0.12
		lam2	24.1	0.25	-27.34	0.12
		lam3	24.6	0.28	-26.49	0.65
		lam4	15.2	0.33	-24.29	0.35
		lam5	15.2	1.21	-29.63	0.35
		mean		*0.46*	*-26.61*	*0.22*
PC05-020C	Calcitic	lam1	32.0	0.21	-27.21	0.12
		lam2	14.4	0.16	-27.67	0.12
		lam3	21.0	0.12	-27.03	0.65
		lam4	23.2	0.25	-26.26	0.35
		lam5	22.5	0.23	-26.33	0.35
		lam6	24.4	0.27	-27.11	0.35
		mean		*0.20*	*-26.94*	*0.54*
Average	*Calcitic*			*0.33*	*-26.78*	*0.58*
PC06-031	Dolomitic	blk	1.6	0.06	-23.28	0.18
PC06-041	Dolomitic	blk	1.1	0.08	-26.80	0.18
Average	*Dolomitic*			*0.07*	*-25.14*	*2.38*

Table 13: Metapelite-hosted kerogen $\delta^{13}C_{org}$ analyses. ('rep' = replica)

Sample	**Analysis**	**Mass**	**C_{org}**	**± 1σ**	**$\delta^{13}C_{org}$**	**± 1σ**
		(mg)	(wt.%)		(‰, PDB)	
PC06-024B	rep1	37.3	0.009		-17.22	0.20
	rep2	57.3	0.007		-15.21	0.20
	mean		*0.008*	*0.002*	*-16.21*	*1.42*
PC06-024I	rep1	17.9	0.007		-21.88	0.20
	rep2	17.9	0.007		-22.17	0.20
	mean		*0.007*	*0.003*	*-22.03*	*0.21*
PC06-027	rep1	4.7	0.025		-24.05	0.20
	rep2	20.4	0.006		-22.23	0.20
	mean		*0.015*	*0.013*	*-23.14*	*1.29*
PC06-029	rep1	11.0	0.010		-25.74	0.20
	rep2	12.8	0.008		-25.42	0.20
	mean		*0.009*	*0.001*	*-25.58*	*0.22*
PC06-040	rep1	33.0	0.003		-24.58	0.13
	rep2	42.1	0.003		-24.17	0.13
	mean		*0.003*	*0.001*	*-24.37*	*0.29*
PC06-044	rep1	3.1	0.032		-25.97	0.13
	rep2	3.2	0.030		-26.30	0.13
	mean		*0.031*	*0.001*	*-26.14*	*0.23*
Average			*0.01*	*0.01*	*-22.72*	*3.4*

Table 14: Densities of BIF-forming minerals.

Mineral	**Density, ρ**
	(g cm-3)
Aragonite	2.93
Calcite	2.71
Dolomite	2.84
Siderite	3.87
Goethite	4.27
Magnetite	5.15
Haematite	5.28
Amorphous silica	<1.7
Opal-A	1.71
Opal-CT	2.01
α-Quartz	2.65

Table 15: Summary of Archaean precipitation.

	Ion(s)		**Setting**	**Peri-tidal**	**Platform**	**Slope**	**Basin**	
			Substrate				*Hot mafic flows*	*Cold felsic tuff*
Primary precipitate	Carbonate	Ca^{2+}	Calcite	√	√			(√)
		Ca^{2+}, Mg^{2+}	Dolomite	√	√	Some		√
		Ca^{2+}, Mg^{2+}, Fe^{2+}	Ankerite	√	Some	Some		
		Fe^{2+}	Siderite			√	Some	
	Oxi	Fe^{2+}, Fe^{3+}	Magnetite				√	√
		Fe^{3+}	Haematite				√	
	Silica	Si^{4+}	Chert	√	√	√	√	
		Si^{4+}	Obvious carbonate silicification	√	√			√

Table 16: Geochemical and mineralogical comparisons between Phanerozoic ironstone, Coonterunah carbonate, and Archaean seawater, BIF, and canonical carbonate.

Feature	*Archaean Seawater*	*Canonical Archaean greenschist metasediment*			*Phanerozoic Ironstone*
		Oxide-BIF	*Carbonate*	*Coonterunah*	
Chert	High [Si]	Yes	No	No	No
Magnetite	High [Fe]	Yes	No	Yes	Yes
Dolomite	Low [Mg]?	No	Yes	Yes	No
$Apatite_{Auth}$	Low [P]?	Rare	Yes	Yes	Yes
$Pyrite_{Auth}$	Low [S]	Sometimes	No	No	No
C_{org}	Life?	No	Yes	Yes	Yes
Na	Saline	n/a	Enriched	Enriched	n/a
La/La*	Positive	Positive	Positive	Positive	Positive
Ce/Ce*	Unity	Unity	Unity	Unity	Negative
Eu/Eu*	Positive	Positive	Positive	Positive	Null
Y/Ho	Positive	Positive	Positive	Positive	Positive
LREE	Depleted	Depleted	Depleted	Depleted	Depleted

References

Adelseck, C. G. and Berger, W. H., 1975. On the dissolution of planktonic foraminifera and associated microfossils during settling and on the sea floor. In: Sliter, W. V., Be, A. W. H., and Berger, W. H. Eds.), *Dissolution of deep-sea carbonates*. Cushman Foundation.

Akahane, H., Furuno, T., Miyajima, H., Yoshikawa, T., and Yamamoto, S., 2004. Rapid wood silicification in hot spring water: an explanation of silicification of wood during the Earth's history. *Sediment Geol* **169**, 219-228.

Algeo, T. J. and Maynard, J. B., 2008. Trace-metal covariation as a guide to water-mass conditions in ancient anoxic marine environments. *Geosphere* **4**, 872-887.

Alibert, C. and Mcculloch, M. T., 1993. Rare-Earth Element and Neodymium Isotopic Compositions of the Banded Iron-Formations and Associated Shales from Hamersley, Western-Australia. *Geochimica Et Cosmochimica Acta* **57**, 187-204.

Alibo, D. S. and Nozaki, Y., 1999. Rare earth elements in seawater: Particle association, shale-normalization, and Ce oxidation. *Geochim. Cosmochim. Acta* **63**, 363-372.

Allwood, A. C., Walter, M. R., Burch, I. A., and Kamber, B. S., 2008. 3.43 billion-year-old stromatolite reef from the Pilbara Craton of Western Australia: ecosystem-scale insights to early life on Earth. *Precamb. Res.* **158**, 198-227.

Alonso-Zarza, A. M., Sanchez-Moya, Y., Bustillo, M. A., Sopena, A., and Delgado, A., 2002. Silicification and dolomitization of anhydrite nodules in argillaceous terrestrial deposits: an example of meteoric-dominated diagenesis from the Triassic of central Spain. *Sedimentology* **49**, 303-317.

Alperin, M. J. and Reeburgh, W. S., 1985. Inhibition Experiments on Anaerobic Methane Oxidation. *Appl. Environ. Microbiol.* **50**, 940-945.

Alt, J. C., 1995a. Subseafloor processes in mid-ocean ridge hydrothermal systems. In: Humphris, S. E., Zierenberg, R. A., Mullineaux, L. S., and Thomson, R. E. Eds.), *Seafloor Hydrothermal Systems: Physical, Chemical, Biological and Geological Interactions*. American Geophysical Union, Washington, D.C.

Alt, J. C., 1995b. Subseafloor processes in mid-ocean ridge hydrothermal systems. In: Humphris, S. E., Zierenberg, R. A., Mullineaux, L. S., and Thomsen, H. S. Eds.), *Seafloor hydrothermal systems: physical, chemical, biological, and geological interactions*. American Geophysical Union.

Alt, J. C. and Bach, W., 2003. Alteration of oceanic crust: subsurface rock-water interactions. In: Halbach, P. E., Tunnicliffe, V., and Hein, J. R. Eds.), *Energy and Mass Transfer in Marine Hydrothermal Systems*. Dahlem University Press, Berlin.

Alt, J. C., Laverne, C., Vanko, D., Tartarotti, P., Teagle, D. A. H., Bach, W., Zuleger, E., Erzinger, E., Erzinger, J., and Honnorez, J., 1996. Hydrothermal alteration of a section of upper oceanic crust in the Eastern Equatorial Pacific: a synthesis of results from site 504 (DSDP/ODP Legs 69, 70, and 83, and ODP Legs 111, 137,140, AND 148). In: Alt, J. C., Kinoshita, H., Stokking, L. B., and Michael, P. J. Eds.), *Proceedings of the Ocean Drilling Program, Scientific Results*.

Amores, D. R. and Warren, L. A., 2007. Identifying when microbes biosilicify: The interconnected requirements of acidic pH, colloidal SiO2 and exposed microbial surface. *Chem. Geol.* **240**, 298-312.

Anderson, R. F. and Schiff, S. L., 1987. Alkalinity Generation and the Fate of Sulfur in Lake-Sediments. *Can. J. Fish. Aquat. Sci.* **44**, 188-193.

Andrews, J. E., Turner, M. S., Nabi, G., and Spiro, B., 1991. The Anatomy of an Early Dinantian Terraced Floodplain - Paleoenvironment and Early Diagenesis. *Sedimentology* **38**, 271-287.

Archer, D., Emerson, S., and Reimers, C., 1989. Dissolution of Calcite in Deep-Sea Sediments - Ph and O-2 Microelectrode Results. *Geochim. Cosmochim. Acta* **53**, 2831-2845.

Arenas, C., Zarza, A. M. A., and Pardo, G., 1999. Dedolomitization and other early diagenetic processes in Miocene lacustrine deposits, Ebro Basin (Spain). *Sediment Geol* **125**, 23-45.

Arvidson, R. S. and Mackenzie, F. T., 1999. The dolomite problem: Control of precipitation kinetics by temperature and saturation state. *Am. J. Sci.* **299**, 257-288.

Ayres, L. D., Thurston, P. C., Card, K. D., and Weber, W., 1985. *Archean Supracrustal Sequences: An Introduction and Perspective*. Geological Association of Canada.

Baars, F. J., 1997. The São Francisco craton. In: De Wit, D. W. and Ashwal, L. D. Eds.), *Greenstone Belts*. Oxford University.

Bach, W., Alt, J. C., Niu, Y., and Humpris, S. E., 2001. The geochemical consequences of late-stage low-grade alteration of lower ocean crust at the SW Indian Ridge: Results from ODP Hole 735B (Leg 176). *Geochim. Cosmochim. Acta* **65**, 3267-3287.

Baker, D. E. L., Seccombe, P. K., and Collins, W. J., 2002. Structural history and timing of gold mineralization in the northern East Strelley Belt, Pilbara Craton, Western Australia. *Economic Geology* **97**, 775-785.

Baker, J. H. and de Groot, P. A., 1983. Proterozoic seawater - felsic volcanics interaction W. Bergslagen, Sweden. Evidence for high REE mobility and implications for 1.8 Ga seawater compositions. *Contrib. Mineral. Petrol.* **82**, 119-130.

Banner, J. L., 1995. Application of the Trace-Element and Isotope Geochemistry of Strontium to Studies of Carbonate Diagenesis. *Sedimentology* **42**, 805-824.

Banner, J. L., Hanson, G. N., and Meyers, W. J., 1988. Rare-Earth Element and Nd Isotopic Variations in Regionally Extensive Dolomites from the Burlington-Keokuk Formation (Mississippian) - Implications for Ree Mobility During Carbonate Diagenesis. *J Sediment Petrol* **58**, 415-432.

Barley, M. E., 1984. Volcanism and hydrothermal alteration, Warrawoona Group, East Pilbara. In: Muhling, J. R., Groves, D. I., and Blake, T. S. Eds.), *Archaean and Proterozoic basins of the the Pilbara, Western Australia: evolution and mineralization potential*. University of Western Austrlia, Perth.

Bartley, J. K., Knoll, A. H., Grotzinger, J. P., and Sergeev, V. N., 2000. Lithification and fabric genesis in precipitated stromatolites and associated peritidal

carbonates, Mesoproterozoic Billyakh Group, Siberia. *SEPM Special Publications* **67**, 59-73.

Basturk, O., Saydam, C., Salihoglu, I., Eremeeva, L. V., Konovalov, S. K., Stoyanov, A., Dimitrov, A., Cociasu, A., Dorogan, L., and Altabet, M., 1994. Vertical Variations in the Principle Chemical-Properties of the Black-Sea in the Autumn of 1991. *Mar. Chem.* **45**, 149-165.

Bathurst, R. G., 1974. Marine Diagenesis of Shallow-Water Calcium-Carbonate Sediments. *Annu Rev Earth Pl Sc* **2**, 257-274.

Bathurst, R. G. C., 1971. *Carbonate sediments and their diagenesis*. Elsevier, Amsterdam, New York,.

Bau, M., 1991. Rare-Earth Element Mobility During Hydrothermal and Metamorphic Fluid Rock Interaction and the Significance of the Oxidation-State of Europium. *Chem. Geol.* **93**, 219-230.

Bau, M., 1993. Effects of Syn-Depositional and Postdepositional Processes on the Rare-Earth Element Distribution in Precambrian Iron-Formations. *Eur J Mineral* **5**, 257-267.

Bau, M., 1999. Scavenging of dissolved yttrium and rare earths by precipitating iron oxyhydroxide: Experimental evidence for Ce oxidation, Y-Ho fractionation, and lanthanide tetrad effect. *Geochim. Cosmochim. Acta* **63**, 67-77.

Bau, M. and Alexander, B., 2006. Preservation of primary REE patterns without Ce anomaly during dolomitization of Mid-Paleoproterozoic limestone and the potential re-establishment of marine anoxia immediately after the "Great Oxidation Event". *S Afr J Geol* **109**, 81-86.

Bau, M. and Alexander, B., 2009. Distribution of high field strength elements (Y, Zr, REE, Hf, Ta, Th, U) in adjacent magnetite and chert bands and in reference standards FeR-3 and FeR-4 from the Temagami iron-formation, Canada, and the redox level of the Neoarchean ocean. *Precamb. Res.* **174**, 337-346.

Bau, M. and Dulski, P., 1996. Distribution of yttrium and rare-earth elements in the Penge and Kuruman iron-formations, Transvaal Supergroup, South Africa. *Precamb. Res.* **79**, 37-55.

Bau, M. and Moller, P., 1992. Rare-Earth Element Fractionation in Metamorphogenic Hydrothermal Calcite, Magnesite and Siderite. *Mineralogy and Petrology* **45**, 231-246.

Baur, M. E., 1978. Thermodynamics of heterogeneous iron-carbon systems: implications for the terrestrial primitive reducing atmosphere. *Chem. Geol.* **22**, 189-206.

Baur, M. E., Hayes, J. M., Studley, S. A., and Walter, M. R., 1985. Millimeter-Scale Variations of Stable Isotope Abundances in Carbonates from Banded Iron-Formations in the Hamersley Group of Western-Australia. *Economic Geology* **80**, 270-282.

Beal, E. J., House, C. H., and Orphan, V. J., 2009. Manganese- and iron-dependent marine methane oxidation. *Science* **325**, 184-187.

Becker, R. H. and Clayton, R. N., 1976. Oxygen Isotope Study of a Precambrian Banded Iron-Formation, Hamersley Range, Western-Australia. *Geochim. Cosmochim. Acta* **40**, 1153-1165.

Beckinsale, R. D., Drury, S. A., and Holt, R. W., 1980. 3,360-Myr Old Gneisses from the South Indian Craton. *Nature* **283**, 469-470.

Bekker, A., Karhu, J. A., Eriksson, K. A., and Kaufman, A. J., 2003. Chemostratigraphy of Paleoproterozoic carbonate successions of the Wyoming Craton: tectonic forcing of biogeochemical change? *Precamb. Res.* **120**, 279-325.

Belka, Z., 1998. Early Devonian Kess-Kess carbonate mud mounds of the eastern Anti-Atlas (Morocco), and their relation to submarine hydrothermal venting. *Journal of Sedimentary Research* **68**, 368-377.

Bengston, S., 1994. The advent of the animal skeleton. In: Bengston, S. (Ed.), *Early life on Earth*. Columbia University Press, New York.

Benning, L. G., Phoenix, V. R., Yee, N., and Konhauser, K. O., 2004a. The dynamics of cyanobacterial silicification: An infrared micro-spectroscopic investigation. *Geochim. Cosmochim. Acta* **68**, 743-757.

Benning, L. G., Phoenix, V. R., Yee, N., and Tobin, M. J., 2004b. Molecular characterization of cyanobacterial silicification using synchrotron infrared micro-spectroscopy. *Geochim. Cosmochim. Acta* **68**, 729-741.

Bensen, J., 1994. Carbonate deposition, Pyramid Lake subbasin, Nevada: 1. Sequence of formation and elevational distribution of carboante deposits (tufas). *Palaeogeogr. Palaeoclimatol. Palaeoecol.* **109**, 55-89.

Berelson, W. M., Hammond, D. E., Mcmanus, J., and Kilgore, T. E., 1994. Dissolution Kinetics of Calcium-Carbonate in Equatorial Pacific Sediments. *Global Biogeochem Cy* **8**, 219-235.

Berelson, W. M., Hammond, D. E., Oneill, D., Xu, X. M., Chin, C., and Zukin, J., 1990. Benthic Fluxes and Pore Water Studies from Sediments of the Central Equatorial North Pacific - Nutrient Diagenesis. *Geochim. Cosmochim. Acta* **54**, 3001-3012.

Berner, R. A., 1975. The role of magnesium in the crystal growth of calcite and aragonite from sea water. **39**, 489-504.

Berner, R. A. and Morse, J. W., 1974. Dissolution Kinetics of Calcium-Carbonate in Sea-Water .4. Theory of Calcite Dissolution. *Am. J. Sci.* **274**, 108-134.

Berner, R. A., Westrich, J. T., Graber, R., Smith, J., and Martens, C. S., 1978. Inhibition of Aragonite Precipitation from Super-Saturated Seawater - Laboratory and Field-Study. *Am. J. Sci.* **278**, 816-837.

Beukes, N., Gutzmer, J., and Mukhopadhyay, D. K., 2002. The geology and genesis of high-grade hematite iron ore deposits. *Transactions of the Institute of Mining and Metallurgy, Section B: Applied Earth Science* **112**, 18-25.

Beukes, N. and Klein, C., 1992. Models for iron-formation deposition, *The Proterozoic biosphere: a multidisciplinary study*. Cambridge University Press.

Beukes, N. J., 1987. Facies relations, depositional environments and diagenesis in a major early Proterozoic stromatolitic carbonate platform to basinal sequence, Campbellrand Subgroup, Transvaal Supergroup, southern Africa. *Sediment Geol* **54**, 1-46.

Beukes, N. J. and Klein, C., 1990. Geochemistry and Sedimentology of a Facies Transition - from Microbanded to Granular Iron-Formation - in the Early Proterozoic Transvaal Supergroup, South-Africa. *Precamb. Res.* **47**, 99-139.

Beukes, N. J., Klein, C., Kaufman, A. J., and Hayes, J. M., 1990. Carbonate petrography, kerogen distribution, and carbon and oxygen isotope variations in an early Proterozoic transition from limestone to iron-formation deposition, Transvaal Supergroup, South Africa. *Economic Geology* **85**, 663-689.

Blodau, C., Peine, A., Hoffmann, S., and Peiffer, S., 1999. Organic matter diagenesis in acidic mine lakes. *Acta Hydrochim. Hydrobiol.* **28**, 123-135.

Bohrmann, G., Abelmann, A., Gersonde, R., Hubberten, H., and Kuhn, G., 1994. Pure Siliceous Ooze, a Diagenetic Environment for Early Chert Formation. *Geology* **22**, 207-210.

Bohrmann, G., Kuhn, G., Abelmann, A., Gersonde, R., and Futterer, D., 1990. A Young Porcellanite Occurrence from the Southwest Indian Ridge. *Mar Geol* **92**, 155-163.

Bolhar, R., Van Kranendonk, M. J., and Kamber, B. S., 2005. A trace element study of siderite-jasper banded iron formation in the 3.45 Ga Warrawoona Group, Pilbara Craton - Formation from hydrothermal fluids and shallow seawater. *Precamb. Res.* **137**, 93-114.

Bosak, T. and Newman, D. K., 2003. Microbial nucleation of calcium carbonate in the Precambrian. *Geology* **31**, 577-580.

Bottinga, Y., 1968. Calculation of Fractionation Factors for Carbon and Oxygen Isotopic Exchange in the System Calcite-Carbon Dioxide-Water. *J. Phys. Chem.* **72**, 800.

Bowers, T. S. and Taylor, H. P., 1985. An Integrated Chemical and Stable-Isotope Model of the Origin of Midocean Ridge Hot-Spring Systems. *J Geophys Res-Solid* **90**, 2583-2606.

Boynton, W. V., 1984. Cosmochemistry of the rare earth elements: meteorite studies. In: Henderson, P. (Ed.), *Rare Earth Element Geochemistry,*. Elsevier, Amsterdam.

Brand, U. and Veizer, J., 1980. Chemical Diagenesis of a Multicomponent Carbonate System .1. Trace-Elements. *J Sediment Petrol* **50**, 1219-1236.

Braterman, P. S., Cairns-Smith, A. G., and Sloper, R. W., 1983. Photo-oxidation of hydrated Fe^{2+} - significance for banded iron formations. *Nature* **303**, 163-164.

Braun, V. and Killmann, H., 1999. Bacterial solutions to the iron-supply problems. *Trends in Biochemical Sciences* **24**, 104-109.

Broecker, W. S. and Takahashi, T., 1966. Calcium Carbonate Precipitation on Bahama Banks. *J. Geophys. Res.* **71**, 1575-&.

Brown, D. A., 2006. Microbial mediation of iron mobilization and deposition in iron formations since the early Precambrian. *Geological Society of America Memoir* **198**, 239-256.

Buick, R. and Barnes, K. R., 1984. Cherts in the Warrawoona Group: Early Archaean silicified sediments deposited in shallow-water environments. In: Muhling, J. R., Groves, D. I., and Blake, T. S. Eds.), *Archaean and Proterozoic basins of the the Pilbara, Western Australia: evolution and mineralization potential*. University of Western Austrlia, Perth.

Buick, R. and Dunlop, J. S. R., 1990. Evaporitic sediments of early Archaean age from the Warrawoona Group, North Pole, Western Australia. *Sedimentology* **37**, 247-277.

Buick, R., Thornett, J. R., McNaughton, N. J., Smith, J. B., Barley, M. E., and Savage, M., 1995. Record of emergent continental crust ~3.5 billion years ago in the Pilbara Craton of Australia. *Nature* **375**, 574-577.

Burton, E. A. and Walter, L. M., 1987a. Relative Precipitation Rates of Aragonite and Mg Calcite from Seawater - Temperature or Carbonate Ion Control. *Geology* **15**, 111-114.

Burton, E. A. and Walter, L. M., 1987b. Relative precipitation rates of aragonite and Mg calcite from seawater: temperature or carbonate ion control? *Geology* **15**, 111-114.

Busenberg, E. and Plummer, L. N., 1986. The Solubility of Baco3(Cr) (Witherite) in Co2-H2o Solutions between 0-Degrees and 90-Degrees-C, Evaluation of the

Association Constants of Bahc3+(Aq) and Baco3(Aq) between 5-Degrees and 80-Degrees-C, and a Preliminary Evaluation of the Thermodynamic Properties of Ba-2+(Aq). *Geochim. Cosmochim. Acta* **50**, 2225-2233.

Bustillo, M. and Alonso-Zarza, A. M., 2007. Overlapping of pedogenesis and meteoritc diagenesis in distal allucial and shallow lacustrine deposits in the Madrid Miocene Basin, Spain. *Sediment Geol* **198**, 255-271.

Bustillo, M., Fort, R., and Ordonez, S., 1992. Genetic-Implications of Trace-Element Distributions in Carbonate and Noncarbonate Phases of Limestones and Dolostones from Western Cantabria, Spain. *Chem. Geol.* **97**, 273-283.

Bustillo, M. A., Arribas, M. E., and Bustillo, M., 2002. Dolomitization and silicification in low-energy lacustrine carbonates (Paleogene, Madrid Basin, Spain). *Sediment Geol* **151**, 107-126.

Butterfield, D. A., Seyfried, W. E., and Lilley, M. D., 2003. Composition and evolution of hydrothermal fluids. In: Halbach, P. E., Tunnicliffe, V., and Hein, J. R. Eds.), *Energy and Mass Transfer in Marine Hydrothermal Systems*. Dahlem University Press, Berlin.

Cairns-Smith, A. G., 1978. Precambrian solution photochemistry, inverse segragation, and banded iron formations. *Nature* **276**, 807-808.

Calvert, S. E. and Karlin, R. E., 1991. Relationships between sulphur, organic carbon and iron in the modern sediments of the Black Sea. *Geochim. Cosmochim. Acta* **55**, 2483-2490.

Canfield, D. E., 2005. The early history of atmospheric oxygen: Homage to Robert A. Garrels. *Annu Rev Earth Pl Sc* **33**, 1-36.

Canfield, D. E., Habicht, K. S., and Thamdrup, B., 2000. The Archean sulfur cycle and the early history of atmospheric oxygen. *Science.* **288**, 658-661.

Canfield, D. E. and Raiswell, R., 1999. The evolution of the sulfur cycle. *American Journal of Science.* **299**, 679-723.

Canfield, D. E. and Teske, A., 1996. Late Proterozoic rise in atmosphere oxygen concentration inferred from phylogenetic and sulfur-isotope studies. *Nature* **382**, 127-132.

Castanier, S., Le Metayer-Levrel, G., and Perthuisot, J. P., 1999. Ca-carbonates precipitation and limestone genesis - the microbiogeologist point of view. *Sediment Geol* **126**, 9-23.

Castano, J. R. and Garrels, R. M., 1950. Experiments on the deposition of iron with special reference to the Clinton iron ore deposits. *Economic Geology* **45**, 755-770.

Catling, D. C. and Moore, J. A., 2003. The nature of coarse-grained crystalline hematite and its implications for the early environment of Mars. *Icarus* **165**, 277-300.

Catling, D. C., Zahnle, K. J., and McKay, C. P., 2001. Biogenic methane, hydrogen escape, and the irreversible oxidation of early Earth. *Science* **293**, 839-843.

Chafetz, H. S. and Buczynski, C., 1992. Bacterially induced lithification of microbial mats. *Palaios* **7**, 277-293.

Chafetz, H. S. and Folk, R. L., 1984. Travertines: depositional morphology and the bacterially constructed constituents. *J Sediment Petrol* **54**, 289-316.

Chanda, S. K., Bhattacharyya, A., and Sakar, S., 1977. Deformation of ooids by compaction: implications for lithification. **88**, 1577-1585.

Chanda, S. K., Bhattacharyya, A., and Sarkar, A., 1976. Early diagenetic chert nodules in Bhander Limestone, Maihar, Satna District, Madhya Pradesh, India. *J Geol* **84**, 213-224.

Charlou, J. L., Donval, J. P., Fouquet, Y., Jean-Baptiste, P., and Holm, N., 2002. Geochemistry of high H-2 and CH4 vent fluids issuing from ultramafic rocks at the Rainbow hydrothermal field (36 degrees 14 ' N, MAR). *Chem. Geol.* **191**, 345-359.

Chetty, D. and Frimmel, H. E., 2000. The role of evaporites in the genesis of base metal sulphide mineralisation in the Northern Platform of the Pan-African Damara Belt, Namibia: geochemical and fluid inclusion evidence from carbonate wall rock alteration. *Miner Deposita* **35**, 364-376.

Chilingar, G. V., Bissel, H. J., and Fairbridge, R. W., 1967. *Carbonate rocks*. Elsevier Pub. Co., Amsterdam, New York,.

Choquette, P. W., 1955. A petrographic study of the State College siliceous oolite. **63**, 337-347, 3 Figs., 1 Tab., 1 Pl.

Chou, L., Garrels, R. M., and Wollast, R., 1988. Comparative-Study of the Dissolution Kinetics and Mechanisms of Carbonates in Aqueous-Solutions. *Chem. Geol.* **70**, 77-77.

Chou, L., Garrels, R. M., and Wollast, R., 1989. Comparative-Study of the Kinetics and Mechanisms of Dissolution of Carbonate Minerals. *Chem. Geol.* **78**, 269-282.

Churchill, H., Teng, H., and Hazen, R. M., 2004. Correlation of pH-dependent surface interaction forces to amino acid adsorption: Implications for the origin of life. *Am. Mineral.* **89**, 1048-1055.

Churnet, H. G. and Misra, K. C., 1981. Genetic-Implications of the Trace-Element Distribution Pattern in the Upper Knox Carbonate Rocks, Copper Ridge District, East Tennessee. *Sediment Geol* **30**, 173-194.

Clayton, C. J., 1986. The chemical environment of flint formation in Upper Cretaceous chalks. In: Sieveking, G. d. G. and Hart, M. B. Eds.), *The scientific study of flint and chert : proceedings of the Fourth International Flint Symposium held at Brighton Polytechnic, 10-15 April 1983*. Cambridge University Press, Cambridge [Cambridgeshire] ; New York.

Cloud, P., 1962. Environment of calcium carbonate deposition west of Andros Island, Bahamas, *United States Geological Survey Professional Paper*.

Cloud, P., 1973. Paleoecological Significance of Banded Iron-Formation. *Economic Geology* **68**, 1135-1143.

Cloud, P. E., 1968. Atmospheric and Hydrospheric Evolution on Primitive Earth. *Science* **160**, 729-&.

Codispoti, L. A., Friederich, G. E., Murray, J. W., and Sakamoto, C. M., 1991. Chemical Variability in the Black-Sea - Implications of Continuous Vertical Profiles That Penetrated the Oxic Anoxic Interface. *Deep-Sea Res* **38**, S691-S710.

Coleman, M. L., 1985. Geochemistry of Diagenetic Non-Silicate Minerals - Kinetic Considerations. *Philos T Roy Soc A* **315**, 39-56.

Comans, R. N. J. and Middelburg, J. J., 1987. Sorption of Trace-Metals on Calcite - Applicability of the Surface Precipitation Model. *Geochim. Cosmochim. Acta* **51**, 2587-2591.

Condie, K. C., 1997. *Plate tectonics and crustal evolution*. Butterworth-Heinemann, Oxford.

Conrad, C. F., Icopini, G. A., Yasuhara, H., Bandstra, J. Z., Brantley, S. L., and Heaney, P. J., 2007. Modeling the kinetics of silica nanocolloid formation and precipitation in geologically relevant aqueous solutions. *Geochim. Cosmochim. Acta* **71**, 531-542.

Coplen, T. B., Brand, W. A., Gehre, M., Groning, M., Meijer, H. A. J., Toman, B., and Verkouteren, R. M., 2006. New guidelines for delta C-13 measurements. *Anal. Chem.* **78**, 2439-2441.

Corcoran, P. L. and Mueller, P. A., 2004. Aggressive Archaean weathering. In: Eriksson, K. A., Altermann, W., Nelson, D. R., Mueller, P. A., and Catuneanu, O. Eds.), *The Precambrian Earth: Tempos and Events*. Elsevier, Amsterdam.

Croal, L. R., Jiao, Y., Kappler, A., and Newman, D. K., 2009. Phototrophic Fe(II) oxidation in an atmosphere of H-2: implications for Archean banded iron formations. *Geobiol.* **7**, 21-24.

Dalrymple, D. W., 1965. Calcium carbonate deposition associated with blue-green algal mats, Baffin Bay, Texas. **10**, 187-200, 7 Figs.

Davies, G. R. and Smith Jr., L. B., 2006. Structurally controlled hydrothermal dolomite reservoir facies: An overview. *American Association of Petroleum Geologists Bulletin* **90**, 1641-1690.

Davies, G. R. and Smith Jr., L. B., 2007. Structurally controlled hydrothermal dolomite reservoir facies: An

overview: Reply. *American Association of Petroleum Geologists Bulletin* **91**, 1342-1344.

Davis, C. C., Chen, H. W., and Edwards, M., 2002. Modeling silica sorption to iron hydroxide. *Environ. Sci. Technol.* **36**, 582-587.

de Baar, H. J. W., Schijf, J., and Byrne, R. H., 1991. Solution Chemistry of the Rare-Earth Elements in Seawater. *European Journal of Solid State and Inorganic Chemistry* **28**, 357-373.

de Choudens-Sanchez, V. and Gonzalez, L. A., 2009. Calcite and aragonite precipitation under controlled instantaneous supersaturation: elucidating the role of CaCO3 saturation state and Mg/Ca ratio on calcium carbonate polymorphism. *Journal of Sedimentary Research* **79**, 363-376.

de Vries, S. T. and Touret, J. L. R., 2007. Early Archaean hydrothermal fluids; a study of inclusions from the similar to 3.4 Ga Buck Ridge Chert, Barberton Greenstone Belt, South Africa. *Chem. Geol.* **237**, 289-302.

Degens, E. T. and Epstein, S., 1964. Oxygen and carbon isotope ratios in coexisting calcites and dolomites from recent and ancient sediments. *Geochim. Cosmochim. Acta* **28**, 23-44.

Deines, P., 2004. Carbon isotope effects in carbonate systems. *Geochim. Cosmochim. Acta* **68**, 2659-2679.

Deines, P., Langmuir, D., and Harmon, R. S., 1974. Stable Carbon Isotope Ratios and Existence of a Gas-Phase in Evolution of Carbonate Ground Waters. *Geochim. Cosmochim. Acta* **38**, 1147-1164.

Dekanel, J. and Morse, J. W., 1978. Chemistry of Ortho-Phosphate Uptake from Seawater on to Calcite and Aragonite. *Geochim. Cosmochim. Acta* **42**, 1335-1340.

Delmas, A.-B., Garcia-Hernandez, J., and Pedro, G., 1982. Discussion sur les conditions et les mecanismes de formation du quartz a 25 C en milieu ouvert. Analyse reactionelle par voie cinetique. *Sci. Geol. Bull.* **35**, 81-91.

Demchuk, I. G., Krupenin, M. R., and Sazonov, V. N., 2003. Mechanism of multistage sideritization in the Bakal ore field (The South Urals). *Zapiski Vserossijskogo mineralogiceskogo obs^estva* **132**, 86-93.

Derry, L. A. and Jacobsen, S. B., 1990. The Chemical Evolution of Precambrian Seawater - Evidence from Rees in Banded Iron Formations. *Geochim. Cosmochim. Acta* **54**, 2965-2977.

Des Marais, D. J. and Moore, J. G., 1984. Carbon and Its Isotopes in Mid-Oceanic Basaltic Glasses. *Earth Planet. Sci. Lett.* **69**, 43-57.

DesMarais, D. J., 1996. Stable light isotope biogeochemistry of hydrothermal systems. *Ciba F Symp* **202**, 83-98.

Deuser, W. G., 1970. C-13 in Black-Sea Waters and Implications for Origin of Hydrogen Sulfide. *Science* **168**, 1575-&.

Diakonov, I., Khodakovsky, I., Schott, J., and Sergeeva, E., 1994. Thermodynamic Properties of Iron-Oxides and Hydroxides .1. Surface and Bulk Thermodynamic Properties of Goethite (Alpha-Feooh) up to 500-K. *Eur J Mineral* **6**, 967-983.

Dickman, M., 1985. Seasonal Succession and Microlamina Formation in a Meromictic Lake Displaying Varved Sediments. *Sedimentology* **32**, 109-118.

Dickson, J. A. D., 2002. Fossil echinoderms as monitor of the Mg/Ca ratio of Phanerozoic oceans. *Science* **298**, 1222-1224.

Dickson, J. A. D. and Coleman, M. L., 1980. Changes in carbon and oxygen isotope composition during limestone diagenesis. *Sedimentology* **27**.

Dillon, P. J., Evans, H. E., and Girard, R., 1997. Hypolimnetic alkalinity generation in two dilute, oligotrophic lakes in Ontario, Canada. *Water Air Soil Pollut.* **99**, 373-380.

Dimroth, E., 1968. Sedimentary textures, diagenesis, and sedimentary environment of certain Precambrian ironstones. *Jahrbuch für Geologie und Paläontologie* **130**.

Dimroth, E., 1975. Paleo-environment of iron-rich sedimentary rocks. *Geol. Rundschau* **64**, 751-767.

Dimroth, E. and Chauvel, J. J., 1973. Petrography of Sokoman Iron Formation in Part of Central Labrador-Trough, Quebec, Canada. *Geol Soc Am Bull* **84**, 111-134.

Dixit, S., Van Cappellen, P., and van Bennekom, A. J., 2001. Processes controlling solubility of biogenic silica and pore water build-up of silicic acid in marine sediments. *Mar. Chem.* **73**, 333-352.

Dostal, J. and Strong, D. F., 1983. Trace-Element Mobility During Low-Grade Metamorphism and Silicification of Basaltic Rocks from Saint-John, New-Brunswick. *Can. J. Earth Sci.* **20**, 431-435.

Douville, E., Charlou, J. L., Oelkers, E. H., Bienvenu, P., Colon, C. F. J., Donval, J. P., Fouquet, Y., Prieur, D., and Appriou, P., 2002. The rainbow vent fluids (36 degrees 14 ' N, MAR): the influence of ultramafic rocks and phase separation on trace metal content in Mid-Atlantic Ridge hydrothermal fluids. *Chem. Geol.* **184**, 37-48.

Dromgoole, E. L. and Walter, L. M., 1990a. Inhibition of Calcite Growth-Rates by Mn-2+ in Cacl2 Solutions at 10-Degrees-C, 25-Degrees-C, and 50-Degrees-C. *Geochim. Cosmochim. Acta* **54**, 2991-3000.

Dromgoole, E. L. and Walter, L. M., 1990b. Iron and Manganese Incorporation into Calcite - Effects of Growth-Kinetics, Temperature and Solution Chemistry. *Chem. Geol.* **81**, 311-336.

Duchac, K. C. and Hanor, J. S., 1987. Origin and timing of the metasomatic silicification of an early Archean komatiite sequence, Barberton Mountain Land, South Africa. *Precamb. Res.* **37**, 125-146.

Ehrenreich, A. and Widdel, F., 1994. Anaerobic Oxidation of Ferrous Iron by Purple Bacteria, a New-Type of Phototrophic Metabolism. *Appl. Environ. Microbiol.* **60**, 4517-4526.

Eichler, J., 1976. Origin of the Precambrian banded iron-formations, *Handbook of strata-bound and stratiform ore deposits*. Elsevier Scientific Pub. Co., Amsterdam ; New York.

Einsele, G., 2000. *Sedimentary basins : evolution, facies, and sediment budget*. Springer, Berlin ; New York.

Eisenlohr, B., Meteva, K., Gabrov, F., and Dreybrodt, W., 1999. The inhibiting action of intrinsic impurities in natural calcium carbonate minerals to their dissolution

kinetics in aqueous H2O–CO2 solutions. *Geochim. Cosmochim. Acta* **63**, 989-1001.

Elderfield, H., Wheat, C. G., Mottl, M. J., Monnin, C., and Spiro, B., 1999. Fluid and geochemical transport through oceanic crust: A transect across the easten flank of the Juan de Fuca Ridge. *Earth and Planetary Science Letters* **172**, 151-165.

Eliassen, A. and Talbot, M. R., 2003. Diagenesis of the mid-Carboniferous Minkinfjellet Formation, central Spitsbergen, Svalbard. *Norw J Geol* **83**, 319-331.

Ellis, J. P. and Milliman, J. D., 1985. Calcium-Carbonate Suspended in Arabian Gulf and Red-Sea Waters - Biogenic and Detrital, Not Chemogenic. *J Sediment Petrol* **55**, 805-808.

Emerson, D. and Revsbech, N. P., 1994a. Investigation of an Iron-Oxidizing Microbial Mat Community Located near Aarhus, Denmark - Field Studies. *Appl. Environ. Microbiol.* **60**, 4022-4031.

Emerson, D. and Revsbech, N. P., 1994b. Investigation of an Iron-Oxidizing Microbial Mat Community Located near Aarhus, Denmark - Laboratory Studies. *Appl. Environ. Microbiol.* **60**, 4032-4038.

Emerson, S. and Bender, M., 1981. Carbon Fluxes at the Sediment-Water Interface of the Deep-Sea - Calcium-Carbonate Preservation. *Journal of Marine Research* **39**, 139-162.

Emrich, K. and Vogel, J. C., 1970. Carbon Isotope Fractionation During Precipitation of Calcium Carbonate. *Earth Planet. Sci. Lett.* **8**, 363-&.

Epstein, S., Graf, D. I., and Degens, E. T., 1963. *Isotopic and cosmic chemistry*. North-Holland Publishing Company, Amsterdam.

Eriksson, K. A., 1983. Siliciclastic-hosted iron-formations in the early Archaean Barberton and Pilbara sequences. *Journal of the Geological Society of Australia* **30**, 473-482.

Eriksson, K. A., Krapez, B., and Fralick, P. W., 1997. Sedimentological aspects. In: de Wit, M. J. and Ashwal, L. D. Eds.), *Greenstone Belts*. Oxford Science, Oxford.

Eriksson, P. G., Catuneanu, O., Sarkar, S., and Tirsgaard, H., 2005. Patterns of sedimentation in the Precambrian. *Sediment Geol* **176**, 17-42.

Eriksson, P. G., Condie, K. C., Tirsgaard, H., Mueller, W. U., Altermann, W., Miall, A. D., Aspler, L. B., Catuneanu, O., and Chiarenzelli, J. R., 1998. Precambrian clastic sedimentation systems. *Sediment Geol* **120**, 5-53.

Essene, E. J., 1983. Solid solutions and solvi among metamorphic carbonates with applications to geologic thermobarometry. In: Reeder, R. J. (Ed.), *Carbonates: Mineralogy and Chemistry*. Mineralogical Society of America, Blacksburg, Virginia.

Ewers, W. E., 1983. Chemical factors in the deposition and diagenesis of banded-iron formation. In: Trendall, A. F. and Morris, E. P. Eds.), *Iron-formation: Facts and problems*. Elsevier, Amsterdam; New York.

Ewers, W. E. and Morris, R. C., 1981. Studies of the Dales-Gorge-Member of the Brockman-Iron-Formation, Western Australia. *Economic Geology* **76**, 1929-1953.

Fairchild, I. J., 1991. Origins of carbonate in Neoproterozoic stromatolites and the identification of modern analogues. *Precamb. Res.* **53**, 281-299.

Fairchild, I. J., 1993. Balmy shores and icy wastes: the paradox of carbonates with glacial deposits in Neoproterozoic times. *Sedimentology Review* **1**, 1-15.

Fairchild, I. J., Knoll, A. H., and Swett, K., 1991. Coastal Lithofacies and Biofacies Associated with Syndepositional Dolomitization and Silicification (Draken Formation, Upper Riphean, Svalbard). *Precamb. Res.* **53**, 165-197.

Fedo, C. M., Nesbitt, H. W., and Young, G. M., 1995. Unraveling the Effects of Potassium Metasomatism in Sedimentary-Rocks and Paleosols, with Implications for Paleoweathering Conditions and Provenance. *Geology* **23**, 921-924.

Fischer, W. W. and Knoll, A. H., 2009. An iron shuttle for deepwater silica in Late Archean and early Paleoproterozoic iron formation. *GSA Bulletin* **121**, 222-235.

Fisher, R. V. and Schmincke, H.-U., 1984. *Pyroclastic rocks*. Springer-Verlag, Berlin ; New York.

Flörke, O. W., Hollmann, R., von Rad, U., and Rösch, H., 1976. Intergrowth and twinning in opal-CT lepispheres. *Contrib. Mineral. Petrol.* **58**, 235-242.

Flowers, G. C. and Helgeson, H. C., 1983. Equilibrium and Mass-Transfer During Progressive Metamorphism of Siliceous Dolomites. *Am. J. Sci.* **283**, 230-286.

Folk, R. L. and Pittman, J. S., 1971. Length-slow chalcedony: a new testament for vanished evaporites. *J Sediment Petrol* **41**, 1045-1058.

Fortin, D. and Langley, S., 2005. Formation and occurrence of biogenic iron-rich minerals. *Earth-Sci Rev* **72**, 1-19.

Fouke, B. W., Farmer, J. D., Des Marais, D. J., Pratt, L., Sturchio, N. C., Burns, P. C., and Discipulo, M. K., 2000. Depositional facies and aqueous-solid geochemistry of travertine-depositing hot springs (Angel Terrace, Mammoth Hot Springs, Yellowstone National Park, U.S.A.). *Journal of Sedimentary Research* **70**, 565-585.

Fournier, R. O., 1983. A Method of Calculating Quartz Solubilities in Aqueous Sodium-Chloride Solutions. *Geochim. Cosmochim. Acta* **47**, 579-586.

Fournier, R. O. and Marshall, W. L., 1983. Calculation of Amorphous Silica Solubilities at 25-Degrees-C to 300-Degrees-C and Apparent Cation Hydration Numbers in Aqueous Salt-Solutions Using the Concept of Effective Density of Water. *Geochim. Cosmochim. Acta* **47**, 587-596.

Fournier, R. O. and Potter, R. W., 1982. An Equation Correlating the Solubility of Quartz in Water from 25-Degrees-C to 900-Degrees-C at Pressures up to 10,000 Bars. *Geochim. Cosmochim. Acta* **46**, 1969-1973.

Fournier, R. O. and Rowe, J. J., 1977a. Solubility of Amorphous Silica in Water at High-Temperatures and High-Pressures. *Am. Mineral.* **62**, 1052-1056.

Fournier, R. O. and Rowe, J. J., 1977b. Solubility of Amorphous Silica in Water at High-Temperatures and High-Pressures. *Transactions-American Geophysical Union* **58**, 822-822.

Frei, R. and Polat, A., 2007. Source heterogeneity for the major components of similar to 3.7 Ga Banded Iron Formations (Isua Greenstone Belt, Western Greenland):

Tracing the nature of interacting water masses in BIF formation. *Earth Planet. Sci. Lett.* **253**, 266-281.

French, B. M., 1971. Stability relations of siderite (FeCO3): thermal decomposition in equilibrium with graphite. *Am. J. Sci.* **271**, 37-78.

French, B. M. and Eugster, H. P., 1965. Experimental control of oxygen fugacities by graphite-gas equilibriums. *J. Geophys. Res.* **70**, 1529-1539.

French, B. M. and Rosenberg, P. E., 1965. Siderite (FeCO3): thermal decomposition in equilibrium with graphite. *Science* **147**, 1283-1284.

Friedman, G. M., 2007. Structurally controlled hydrothermal dolomite reservoir facies: An overview: Discussion. *American Association of Petroleum Geologists Bulletin* **91**, 1339-1341.

Friend, C. R. L., Nutman, A. P., Bennett, V. C., and Norman, M. D., 2008. Seawater-like trace element signatures (REE+Y) of Eoarchaean chemical sedimentary rocks from southern West Greenland, and their corruption during high-grade metamorphism. *Contrib. Mineral. Petrol.* **155**, 229-246.

Frost, B. R., 1979. Mineral Equilibria Involving Mixed-Volatiles in a C-O-H Fluid Phase - Stabilities of Graphite and Siderite. *Am. J. Sci.* **279**, 1033-1059.

Gao, G. Q. and Land, L. S., 1991. Nodular Chert from the Arbuckle Group, Slick Hills, Sw Oklahoma - a Combined Field, Petrographic and Isotopic Study. *Sedimentology* **38**, 857-870.

GarciaGarmilla, F. and Elorza, J., 1996. Dolomitization and synsedimentary salt tectonics: The Upper Cretaceous Cueva Formation at El Ribero, northern Spain. *Geol Mag* **133**, 721-&.

Garcia-Ruiz, J. M., 2000. Geochemical scenarios for the precipitation of biomimetic inorganic carbonates, *Carbonate sedimentation and diagenesis in an evolving Precambrian world*.

Gardner, R. A. M. and Hendry, D. A., 1995. Early Silica Diagenetic Fabrics in Late Quaternary Sediments, South-India. *Journal of the Geological Society* **152**, 183-192.

Garrels, R. M., 1987. A Model for the Deposition of the Microbanded Precambrian Iron Formations. *Am. J. Sci.* **287**, 81-106.

Garrels, R. M., Perry, E. A., and Mackenzi.Ft, 1973. Genesis of Precambrian Iron-Formations and Development of Atmospheric Oxygen. *Economic Geology* **68**, 1173-1179.

Geeslin, J. H. and Chafetz, H. S., 1982. Ordovician Aleman ribbon cherts: an example of silicification prior to carbonate lithification. *Journal of Sedimentary Research* **52/4**, 1283-1293, 12 Figs.

Gehlen, M., Vanraaphorst, W., and Wollast, R., 1993. Kinetics of Silica Sorption on North-Sea Sediments. *Chem. Geol.* **107**, 359-361.

Gibson, H. L., Watkinson, D. H., and Comba, C. D. A., 1983. Silicification - Hydrothermal Alteration in an Archean Geothermal System within the Amulet Rhyolite Formation, Noranda, Quebec. *Economic Geology* **78**, 954-971.

Goedert, J. L., Peckmann, J., and Reitner, J., 2000. Worm tubes in an allochtonous cold-seep carbonate from lower Oligocene rocks of Western Washington. *J. Paleontol.* **74**, 929-999.

Goldsmith, J. R., Graf, D. I., Witters, J., and Northrop, D. A., 1962. Studies in the system CaCO3-MgCO3-FeCO3: 1. Phase relations; 2. A method for major element spectrochemical analysis; 3. Compositions of some ferroan dolomites. *J Geol* **70**, 659-688.

Gole, M. J., 1981. Archean Banded Iron-Formations, Yilgarn-Block, Western Australia. *Economic Geology* **76**, 1954-1974.

Gole, M. J. and Klein, C., 1981. Banded Iron-Formations through Much of Precambrian Time. *J Geol* **89**, 169-183.

Golubic, S., 1973. The relationship between blue-green algae and carbonate deposits. **9**, 434-472.

Golubic, S., 1976. Organisms that build stromatolites. Elsevier, Amsterdam.

Golyshev, S. I., Padalko, N. L., and Pechenkin, S. A., 1981. Fractionation of Stable Isotopes of Carbon and Oxygen in Carbonate Systems. *Geokhimiya*, 1427-1441.

Grassian, V., 2005. *Environmental Catalysis*. CRC.

Greenfield, L. J., 1963. Metabolism and concentration of calcium and magnesium and precipitation of calcium carbonate by a marine bacterium. **109**, 23-45.

Greenwood, R., 1973. Cristobalite; its relationship to chert formation in selected samples from the Deep Sea Drilling Project. *Journal of Sedimentary Research* **43**, 700-708.

Grotzinger, J. P., 1986. Cyclicity and paleoenvironmental dynamics, Rocknest Platform, northwest Canada. *Geol Soc Am Bull* **97**, 1208-1231.

Grotzinger, J. P., 1989. Facies and evolution of Precambrian carbonate depositional systems: emergence of the modern platform archetype. *Controls on Carbonate Platform and Basin Development, SEPM Special Publication* **44**, 79-105.

Grotzinger, J. P., 1994. Trends in Precambrian carbonate sediments and their implication for understanding evolution. In: Bengston, S. (Ed.), *Early Life on Earth*. Columbia University Press, New York.

Grotzinger, J. P. and Kasting, J. F., 1993. New Constraints on Precambrian Ocean Composition. *J Geol* **101**, 235-243.

Grotzinger, J. P. and Knoll, A. H., 1995. Anomalous carbonate precipitates: is the Precambrian the key to the Permian? *Palaios* **10**, 578-596.

Groves, D. I., Dunlop, J. S. R., and Buick, R., 1981. An Early Habitat of Life. *Sci. Am.* **245**, 64-73.

Guedes, S. C., Rosière, C. A., and Barley, M. E., 2003. The association of carbonate alteration of banded iron formation with the Carajás high-grade hematite deposits. *Applied Earth Science: IMM Transactions section B* **112**, 26-30(5).

Guerrero, M. C. and de Wit, R., 1992. Microbial mats in the inland saline lakes of Spain. *Limnetica* **8**, 197-204.

Gunnarsson, I. and Arnorsson, S., 2000. Amorphous silica solubility and the thermodynamic properties of H4SiO4 degrees in the range of 0 degrees to 350 degrees C at P-sat. *Geochim. Cosmochim. Acta* **64**, 2295-2307.

Halbach, P., Hansmann, W., Koppel, V., and Pracejus, B., 1997. Whole-rock and sulfide lead-isotope data from the hydrothermal JADE field in the Okinawa back-arc trough. *Miner Deposita* **32**, 70-78.

Halbach, P. E., Fouquet, Y., and Herzig, P., 2003. Moineralization and compositional patterns in deep-sea hydrothermal systems. In: Halbach, P. E., Tunnicliffe, V., and Hein, J. R. Eds.), *Energy and Mass Transfer in Marine Hydrothermal Systems*. Dahlem University Press, Berlin.

Hamade, T., Konhauser, K. O., Raiswell, R., Goldsmith, S., and Morris, R. C., 2003. Using Ge/Si ratios to decouple iron and silica fluxes in Precambrian banded iron formations. *Geology* **31**, 35-38.

Hamade, T., Phoenix, V. R., and Konhauser, K. O., 2000. Photochemical and microbiological mediated precipitation of iron and silica*10th Annual V.M. Goldschmidt Conference*, Oxford, England.

Hangari, K. M., Ahmad, S. N., and Perry, E. C., 1980. Carbon and Oxygen Isotope Ratios in Diagenetic Siderite and Magnetite from Upper Devonian Ironstone, Wadi-Shatti District, Libya. *Economic Geology* **75**, 538-545.

Hanor, J. S. and Duchac, K. C., 1990. Isovolumetric Silicification of Early Archean Komatiites - Geochemical Mass Balances and Constraints on Origin. *J Geol* **98**, 863-877.

Hartman, H., 1984. The evolution of photosynthesis and microbial mats: A speculation on the banded iron formations. In: Cohen, Y. (Ed.), *Microbial mats, stromatolites : based on the proceedings of the Integrated Approach to the Study of Microbial Mats*. A.R. Liss, New York.

Hatfield, C. B., 1975. Replacement of Fossils by Length-Slow Chalcedony and Associated Dolomitization. *J Sediment Petrol* **45**, 951-952.

Heath, G. R. and Moberly, R., 1971. Cherts from the western Pacific, Leg 7, Deep Sea Drilling Project. In: Winterer, E. L. (Ed.), *Initial Reports of the Deep Sea Drilling Project*.

Hecht, L., Freiberger, R., Gilg, H. A., Grundmann, G., and Kostitsyn, Y. A., 1999. Rare earth element and isotope (C, O, Sr) characteristics of hydrothermal carbonates: genetic implications for dolomite-hosted talc mineralization at Gopfersgrun (Fichtelgebirge, Germany). *Chem. Geol.* **155**, 115-130.

Heinrichs, T. K. and Reimer, T. O., 1977. Sedimentary Barite Deposit from Archean Fig Tree Group of Barberton Mountain Land (South-Africa). *Economic Geology* **72**, 1426-1441.

Helgeson, H. C., 1967. Solution chemistry and metamorphism. In: Abelson, P. H. (Ed.), *Researches in geochemistry*. John Wiley & Sons.

Henchiri, M. and Slim-S'Himi, N., 2006. Silicification of sulphate evaporites and their carbonate replacements in Eocene marine sediments, Tunisia: two diagenetic trends. *Sedimentology* **53**, 1135-1159.

Henderson, J. B., 1975. Archean Stromatolites in Northern Slave Province, Northwest-Territories, Canada. *Can. J. Earth Sci.* **12**, 1619-1630.

Henderson, J. B., 1981. Archean basin evolution in the Slave Province, Canada. In: Kröner, A. (Ed.), *Precambrian plate tectonics*. Elsevier, Amsterdam.

Hendry, J. P., 1993. Calcite Cementation During Bacterial Manganese, Iron and Sulfate Reduction in Jurassic Shallow Marine Carbonates. *Sedimentology* **40**, 87-106.

Hendry, J. P. and Trewin, N. H., 1995. Authigenic Quartz Microfabrics in Cretaceous Turbidites - Evidence for Silica Transformation Processes in Sandstones. *Journal of Sedimentary Research Section a-Sedimentary Petrology and Processes* **65**, 380-392.

Herrmann, W. and Hill, A. P., 2001. The Origin of Chlorite-Tremolite-Carbonate Rocks Associated with the Thalanga Volcanic-Hosted Massive Sulfide Deposit, North Queensland, Australia. *Economic Geology* **96**, 1149-1173.

Hesse, R., 1972. Selective Silicification of Ooids in Graywackes of Gault Formation, Early Cretaceous, East Alps. *American Association of Petroleum Geologists Bulletin* **56**, 626-&.

Hesse, R., 1987a. Selective and Reversible Carbonate Silica Replacements in Lower Cretaceous Carbonate-Bearing Turbidites of the Eastern Alps. *Sedimentology* **34**, 1055-1077.

Hesse, R., 1987b. Selective and reversible carbonate-silica replacements in Lower Cretaceous carbonate-bearing turbidites of the Eastern Alps. **34**, 1055-1077, 15 Figs.

Hesse, R., 1989a. Silica Diagenesis - Origin of Inorganic and Replacement Cherts. *Earth-Sci Rev* **26**, 253-284.

Hesse, R., 1989b. Silica diagenesis: origin of inorganic and replacement cherts. *Earth-Science Reviews* **26**, 253-284.

Hesse, R., 1990. Early diagenetic pore water/sediment interaction: modern offshore basins. In: McIlreath, I. A. and Morrow, D. W. Eds.), *Diagenesis*. Goscience Canada, Ottawa.

Hinman, N. W. and Lindstrom, R. F., 1996. Seasonal changes in silica deposition in hot spring systems. *Chemical Geology* **132**, 237-246.

Hiscock, W. T. and Millero, F. J., 2006. Alkalinity of the anoxic waters in the Western Black Sea. *Deep-Sea Res Pt Ii* **53**, 1787-1801.

Hoashi, M., Bevacqua, D. C., Otake, T., Watanabe, Y., Hickman, A. H., Utsunomiya, S., and Ohmoto, H., 2009. Primary hematite formation in an oxygenated deep sea 3.46 billion years ago. *Geochim. Cosmochim. Acta* **73**, A538-A538.

Hoefs, J., 1992. The stable isotope composition of sdimentary iron oxides with special reference to banded iron formation. In: Clauer, N. and Claudhuri, S. Eds.), *Lecture notes in earth sciences*. Springer-Verlag, Berlin; New York.

Hoffman, P. F., Kaufman, A. J., Halverson, G. P., and Schrag, D. P., 1998. A Neoproterozoic snowball Earth. *Science* **281**, 1342-1346.

Hofmann, A. and Bolhar, R., 2007. Carbonaceous cherts in the Barberton greenstone belt and their significance for the study of early life in the Archean record. *Astrobiology* **7**, 355-388.

Hofmann, A. and Harris, C., 2008. Silica alteration zones in the Barberton greenstone belt: A window into the subseafloor processes 3.5-3.3 Ga ago. *Chem. Geol.* **257**, 224-242.

Hofmann, H. J., Thurston, P. C., and Wallace, H., 1985. Archean stromatolites from Uchi Greenstone Belt, northwestern Ontario. In: Ayres, L. D., Thurston, P. C., Card, K. D., and Weber, W. Eds.), *Evolution of Archean Supracrustal Sequences*. Geological Association of Canada.

Holail, H. H. M., Shaaban, M. M. N., Mansour, A. S., and Rifai, I., 2005. Diagenesis of the middle eocene upper dammam subformation, Qatar: Petrographic and isotopic evidence. *Carbonate Evaporite* **20**, 72-81.

Holdaway, H. K. and Clayton, C. J., 1982. Preservation of shell microstructure in silicified brachiopods from the Upper Cretaceous Wilmington Sands of Devon. *Geol Mag* **119**, 371-382.

Holland, H. D., 1984. *The chemical evolution of the atmosphere and oceans*. Princeton University Press, Princeton, N.J.

Holland, H. D. and Zimmerman, H., 2002. The Dolomite Problem Revisited. In: Krauskopf, K. B. (Ed.), *Frontiers in Geochemistry: Global Inorganic Geochemistry*. Bellwether.

Holland, T. J. B. and Powell, R., 1998. An internally consistent thermodynamic data set for phases of petrological interest. *J Metamorph Geol* **16**, 309-343.

Holloway, J. R., 1977. Fugacity and activity of molecular species in supercritical fluids. In: Fraser, D. G. (Ed.), *Thermodynamics in Geology*. Reidel, Dordecht, the Netherlands.

Holloway, J. R., 1981. Volumes and Compositions of Supercritical Fluids. In: Hollister, L. S. and Crawford, M. L. Eds.), *Fluid Inclusions: Petrologic Applications*. Mineralogical Association of Canada.

Howell, J. A., 1976. Effects of Influent Substrate Concentration on Kinetics of Natural Microbial Populations in Continuous Culture. *Water Res.* **10**, 271-271.

Hsü, J., 1966. Origin of dolomite in sedimentary sequences: a critical analysis. **2**, 133-138, 2 Figs.

Hughes, C. J., 1976. Volcanogenic cherts in the Late Precambrian Conception Group, Avalon Peninsula, Newfoundland. *Can. J. Earth Sci.* **13**, 512-519.

Humphris, S. E., Halbach, M., and Juniper, K., 2003. Low-temperature alteration: fluxes and mineralization. In: Halbach, P. E., Tunnicliffe, V., and Hein, J. R. Eds.), *Energy and Mass Transfer in Marine Hydrothermal Systems*. Dahlem University Press, Berlin.

Huston, D. L., Brauhart, C. W., Drieberg, S. L., Davidson, G. J., and Groves, D. I., 2001. Metal leaching and inorganic sulfate reduction in volcanic-hosted massive sulfide mineral systems: evidence from the paleo-Archean Panorama district, Western Australia. *Geology* **29**, 687-690.

Hutchinson, R. W., 1982. Syn-depositional hydrothermal processes and Precambrian sulphide deposits. In: Hutchinson, R. W., Spence, C. D., and Franklin, J. M. Eds.), *Precambrian Sulfide Deposits*. Geological Association of Canada.

Icopini, G. A., Brantley, S. L., and Heaney, P. J., 2005. Kinetics of silica oligomerization and nanocolloid formation as a function of pH and ionic strength at 25 degrees C. *Geochim. Cosmochim. Acta* **69**, 293-303.

Iler, R. K., 1979. *The chemistry of silica: solubility, polymerization, colloid and surface properties, and biochemistry*. Wiley, New York.

Inskeep, W. P. and Bloom, P. R., 1986. Kinetics of Calcite Precipitation in the Presence of Water-Soluble Organic-Ligands. *Soil Sci. Soc. Am. J.* **50**, 1167-1172.

Jacka, A. D., 1974. Replacement of fossils by length-slow chalcedony and associated dolomitization. **44/2**, 421-427.

Jackson, G. A. and Burd, A. B., 1998. Aggregation in the marine environment. *Environ. Sci. Technol.* **32**, 2805-2814.

Jaffres, J. B. D., Shields, G. A., and Wallmann, K., 2007. The oxygen isotope evolution of seawater: A critical review of a long-standing controversy and an improved geological water cycle model for the past 3.4 billion years. *Earth-Sci Rev* **83**, 83-122.

James, H. L., 1954. Sedimentary facies of iron formation. *Economic Geology* **49**, 235-293.

James, H. L., 1955. Zones of Regional Metamorphism in the Precambrian of Northern Michigan. *Geol Soc Am Bull* **66**, 1455-1488.

James, R. H., Allen, D. E., and Seyfried, W. E., 2003. An experimental study of alteration of oceanic crust and terrigenous sediments at moderate temperatures

(51 to 350 degrees C): Insights as to chemical processes in near-shore ridge-flank hydrothermal systems. *Geochim. Cosmochim. Acta* **67**, 681-691.

Jamieson, E. J., 1995. Precipitation and characteristics of iron (III) oxyhydroxides from acid liquors. Ph.D. thesis, Murdoch University.

Jensen, L. S., 1985. Stratigraphy and petrogenesis of Archean metavolcanic sequences, southwestern Abitibi Subprovince, Ontario. In: Ayres, L. D., Thurston, P. C., Card, K. D., and Webber, W. Eds.), *Evolution of Archean supracrustal sequences*. Geological Association of Canada.

Jimenez-Lopez, C. and Romanek, C. S., 2004. Precipitation kinetics and carbon isotope partitioning of inorganic siderite at 25 degrees C and 1 atm. *Geochim. Cosmochim. Acta* **68**, 557-571.

Johnson, D. M., Hooper, P. R., and Conrey, R. M., 1999. XRF Analysis of Rocks and Minerals for Major and Trace Elements on a Single Low Dilution Li-tetraborate Fused Bead. *Adv. X-Ray Anal.* **41**, 843-867.

Jones, B. and Kahle, C. F., 1995. Origins of endogenetic micrite in karst terrains: a case study from the Cayman Islands. **65**, 283-293.

Jones, G. D. and Rostron, B. J., 2000. Analysis of fluid flow constraints in regional-scale reflux dolomitization: constant versus variable-flux hydrogeological models. *B Can Petrol Geol* **48**, 230-245.

Jones, G. D. and Xiao, Y. T., 2005. Dolomitization, anhydrite cementation, and porosity evolution in a reflux system: Insights from reactive transport models. *Aapg Bull* **89**, 577-601.

Jones, S. E., Jago, C. F., Bale, A. J., Chapman, D., Howland, R. J. M., and Jackson, J., 1998. Aggregation and resuspension of suspended particulate matter at a seasonally stratified site in the southern North Sea: physical and biological controls. *Cont Shelf Res* **18**, 1283-1309.

Kamber, B. S. and Webb, G. E., 2001. The geochemistry of late Archaean microbial carbonate: Implications for ocean chemistry and continental erosion history. *Geochim. Cosmochim. Acta* **65**, 2509-2525.

Kamber, B. S. and Webb, G. E., 2007. Transition metal abundances in microbial carbonate: a pilot study based on in situ LA-ICP-MS analysis. *Geobiol.* **5**, 375-389.

Kappler, A., Pasquero, C., Konhauser, K. O., and Newman, D. K., 2006. Deposition of banded iron formations by anoxygenic phototrophic Fe(II)-oxidizing bacteria. *Geology* **33**, 865-868.

Kastner, M., 1983. Opal-A to Opal-CT transformation: A kinetic study. In: Iijima, A. and Hein, J. R. Eds.), *Siliceous Deposits in the Pacific Region*. Elsevier Scientific Pub. Co., Amsterdam ; New York.

Kastner, M., Keene, J. B., and Gieskes, J. M., 1977. Diagenesis of Siliceous Oozes .1. Chemical Controls on Rate of Opal-a to Opal-Ct Transformation - Experimental-Study. *Geochim. Cosmochim. Acta* **41**, 1041-&.

Kato, Y., Suzuki, K., Nakamura, K., Hickman, A. H., Nedachi, M., Kusakabe, M., Bevacqua, D. C., and Ohmoto, H., 2009. Hematite formation by oxygenated groundwater more than 2.76 billion years ago. *Earth Planet. Sci. Lett.* **278**, 40-49.

Katrinak, K., 1987. Stable isotope studies of cherts from the Archean Swaziland Supergroup of South Africa. M.Sc., Arizona State University.

Katz, A. and Matthews, A., 1977. The dolomitization of CaCO3: an experimental study. *Geochim. Cosmochim. Acta* **41**, 297-304.

Katz, A., Sass, E., Starinsky, A., and Holland, H. D., 1972. Strontium behaviour in the aragonite-calcite transformation. **36**, 481-496.

Kaufman, A. J., 1996. Geochemical and mineralogic effects of contact metamorphism on banded iron-formation: An example from the Transvaal Basin, South Africa. *Precamb. Res.* **79**, 171-194.

Kaufman, A. J., Hayes, J. M., and Klein, C., 1990. Primary and diagenetic controls of isotopic compositions of iron-formation carbonates. *Geochim. Cosmochim. Acta* **54**, 3461-3473.

Kaufman, A. J., Hayes, J. M., Knoll, A. H., and Germs, G. J. B., 1991. Isotopic compositions of carbonates and organic carbon from upper Proterozoic

successions in Namibia: stratigraphic variation and the effects of diagenesis and metamorphism. *Precamb. Res.* **49**, 3101-327.

Kaufman, A. J. and Knoll, A. H., 1995. Neoproterozoic variations in the C-isotopic compositions of seawater: stratigraphic and biogeochemical implications. *Precamb. Res.* **73**, 27-49.

Kawabe, I., Toriumi, T., Ohta, A., and Miura, N., 1998. Monoisotopic REE abundances in seawater and the origin of seawater tetrad effect. *Geochem J* **32**, 213-229.

Kazmierczak, J. and Kempe, S., 2004. Calcium build-up in the Precambrian Sea, *Cellular Origin, Life in Extreme Habitats and Astrobiology*. Springer.

Keheila, E. A. and Elayyat, A., 1992. Silicification and Dolomitization of the Lower Eocene Carbonates in the Eastern Desert between Sohag and Qena, Egypt. *J Afr Earth Sci* **14**, 341-349.

Keir, R. S., 1980. Dissolution Kinetics of Biogenic Calcium Carbonates in Seawater. *Geochim. Cosmochim. Acta* **44**, 241-252.

Keir, R. S., 1983. Variation in the Carbonate Reactivity of Deep-Sea Sediments - Determination from Flux Experiments. *Deep-Sea Res* **30**, 279-296.

Keith, T. E. C., White, D. E., and Beeson, M. H., 1978. Hydrothermal alteration and self-sealing in Y-7 and Y-8 drill holes in northern part of Upper Geyser Basin, Yellowstone National Park, Wyoming, U.S. *Geological Survey Professional Papers* **1054-A**, 26.

Kempe, S. and Degens, E. T., 1985. An early soda ocean? *Chem. Geol.* **53**, 95-108.

Kempe, S. and Kazmierczak, J., 1990. Calcium carbonate supersaturation and the formation of in situ calcified stromatolites, *Facets of modern biogeochemistry*. Springer, Berlin.

Kennedy, M. J., 1996. Stratigraphy, sedimentology, and isotopic geochemistry of Australian Neoproterozoic postglacial cap dolostones: Deglaciation, delta C-13 excursions, and carbonate precipitation. *Journal of Sedimentary Research* **66**, 1050-1064.

Kerrich, R., 1976. Some Effects of Tectonic Recrystallization on Fluid Inclusions in Vein Quartz. *Contrib. Mineral. Petrol.* **59**, 195-202.

Kester, D. R., Byrne, R. H., and Liang, Y. J., 1975. Redox Reactions and Solution Complexes of Iron in Marine Systems. *ACS Symp. Ser.*, 56-79.

Kholodov, V. N. and Butuzova, G. Y., 2004a. Problems of siderite formation and iron ore epochs: Communication 1. Types of siderite-bearing iron ore deposits. *Lithol Miner Resour*+ **39**, 389-411.

Kholodov, V. N. and Butuzova, G. Y., 2004b. Problems of siderite formation and iron ore epochs: Communication 2. General issues of the precambrian and phanerozoic ore accumulation. *Lithol Miner Resour*+ **39**, 489-508.

Kholodov, V. N. and Butuzova, G. Y., 2008. Siderite formation and evolution of sedimentary iron ore deposition in the Earth's history. *Geol Ore Deposit*+ **50**, 299-319.

Kimberley, M. M., 1974. Origin of iron ore by diagenetic replacement of calcareous oolite. *Nature* **250**, 319-320.

Kinsman, D. J., 1969. Modes of formation, sedimentary associations, and diagnostic features of shallow-water and supratidal evaporites. **53**, 830-840, 2 Figs.

Kinsman, D. J. J. and Holland, H. D., 1969. The co-precipitation of cations with CaCO3 -IV. The co-precipitation of Sr2+ with aragonite between 16° and 96°. **33**, 1-17, 1 Fig.

Kirschvink, J. L., Gaidos, E. J., Bertani, L. E., Beukes, N. J., Gutzmer, J., Maepa, L. N., and Steinberger, R. E., 2000. Paleoproterozoic snowball Earth: extreme climatic and geochemical global change and its biological consequences. *Proceedings of the National Academy of Science USA* **97**, 1400-1405.

Kitajima, K., Maruyama, S., Utsunomiya, S., and Liou, J. G., 2001. Seafloor hydrothermal alteration at an Archaean mid-ocean ridge. *J Metamorph Geol* **19**, 581-597.

Kitano, Y., Okumura, M., and Idogaki, M., 1979. Behavior of Dissolved Silica in Parent Solution at the Formation of Calcium-Carbonate. *Geochem J* **13**, 253-260.

Klein, C., 2005. Some Precambrian banded iron-formations (BIFs) from around the world: Their age, geologic setting, mineralogy, metamorphism, geochemistry, and origin. *Am. Mineral.* **90**, 1473-1499.

Klein, C. and Beukes, N. J., 1989a. Geochemistry and sedimentology of a facies transition from limestone to iron-formation deposition in the early Proterozoic Transvaal Supergroup, South Africa. *Economic Geology* **84**, 1733-1774.

Klein, C. and Beukes, N. J., 1989b. Geochemistry and Sedimentology of a Facies Transition from Limestone to Iron-Formation Deposition in the Early Proterozoic Transvaal Supergroup, South-Africa. *Economic Geology* **84**, 1733-1774.

Klein, C. and Bricker, O. P., 1977. Some Aspects of Sedimentary and Diagenetic Environment of Proterozoic Banded Iron-Formation. *Economic Geology* **72**, 1457-1470.

Klein, R. T. and Walter, L. M., 1995. Interactions between Dissolved Silica and Carbonate Minerals - an Experimental-Study at 25-50-Degrees-C. *Chem. Geol.* **125**, 29-43.

Knauth, L. P., 1979. A model for the origin of chert in limestone. *Geology* **7**, 274-277.

Knauth, L. P., 1992. Origin and diagenesis of cherts: an isotopic perspective, *Lecture notes in earth sciences ;*. Springer-Verlag, Berlin ; New York.

Knauth, L. P., 1994a. Petrogenesis of chert. In: Heaney, P. J., Prewitt, C. T., and Gibbs, G. V. Eds.), *Silica: Physical Behavior, Geochemistry and Materials Applications*. Mineralogical Society of America, Washington D.C.

Knauth, L. P., 1994b. Petrogenesis of Chert. *Rev Mineral* **29**, 233-258.

Knauth, L. P. and Lowe, D. R., 1978a. Oxygen Isotope Geochemistry of Cherts from Onverwacht Group (3.4 Billion Years), Transvaal, South-Africa, with Implications for Secular Variations in Isotopic Composition of Cherts. *Earth Planet. Sci. Lett.* **41**, 209-222.

Knauth, L. P. and Lowe, D. R., 1978b. Oxygen isotope geochemistry of cherts from the Onverwacht Group (3.4 billion years), Transvaal, South Africa, with

implications for secular variations in the isotopic composition of cherts. *Earth and Planetary Science Letters* **41**, 209-222.

Knauth, L. P. and Lowe, D. R., 2003. High Archean climatic temperature inferred from oxygen isotope geochemistry of cherts in the 3.5 Ga Swaziland Supergroup, South Africa. *Geol Soc Am Bull* **115**, 566-580.

Knoll, A. H., 1985. Exceptional preservation of photosynthetic organisms in silicified carbonates and silicified peats. *Phil. Trans. R. Soc. Lond.* **311**, 111-122.

Knoll, A. H. and Simonson, B., 1981. Early Proterozoic microfossils and penecontemporaneous quartz cementation in the Sokoman Iron Formation, Canada. *Science* **211**, 478-480.

Knoll, A. H. and Swett, K., 1990. Carbonate Deposition During the Late Proterozoic Era - an Example from Spitsbergen. *Am. J. Sci.* **290A**, 104-132.

Kocurko, M. J., 1986. Interaction of organic matter and crystallization of High-Magnesium calcite, south Louisiana. **38**, 13-21, 10 Figs.

Kolb, E. D., Caporaso, A. J., and Laudise, R. A., 1973. Hydrothermal Growth of Hematite and Magnetite. *J. Cryst. Growth* **19**, 242-246.

Kolber, Z. S., Barber, R. T., Coale, K. H., Fitzwater, S. E., Greene, R. M., Johnson, K. S., Lindley, S., and Falkowski, P. G., 1994. Iron Limitation of Phytoplankton Photosynthesis in the Equatorial Pacific-Ocean. *Nature* **371**, 145-149.

Konhauser, K., Jones, B., Phoenix, V., Ferris, G., and Renaut, R., 2004. The microbial role in hot spring silicification. *Ambio* **33**, 552-558.

Konhauser, K. O., Hamade, T., Raiswell, R., Morris, R. C., Ferris, F. G., Southam, G., and Canfield, D., 2002. Could bacteria have formed the Precambrian banded iron formations? *Geology* **30**, 1079-1082.

Koschorreck, M. and Tittel, J., 2002. Benthic photosynthesis in an acidic mining lake (pH 2.6). *Limnol. Oceanogr.* **47**, 1197-1201.

Koschorreck, M. and Tittel, J., 2007. Natural alkalinity generation in neutral lakes affected by acid mine drainage. *J. Environ. Qual.* **36**, 1163-1171.

Kosmulski, M., 1997. Adsorption of Trivalent Cations on Silica. *J. Colloid Interface Sci.* **195**, 395-403.

Krumbein, W. E., 1978. Algal mats and their lithification, Collingwood.

Krumbein, W. E., 1979. Photolithotrophic and chemoorganotrophic activity of bacteria and algae as related to beachrock formation and degradation (Gulf of Aqaba). **1**, 139-203.

Krumbein, W. E. and Cohen, C., 1977. Primary production, mat formation and lithification: contribution oxygenic and facultative anoxygenic cyanobacteria. Springer, Berlin.

Krumbein, W. E. and Cohen, Y., 1974. Biogene, klastische und evaporitische Sedimentation in einem mesothermen monomiktischen ufernahen See (Golf von Aqaba). **63**, 1035-1065, 15 Figs., 1 Tab.

Krumbein, W. E., Cohen, Y., and Shilo, M., 1977. Solar Lake (Sinai). 4. Stromatolite cyanobacterial mats. **22**, 635-665.

Kuehn, C. A. and Rose, A. W., 1992. Geology and Geochemistry of Wall-Rock Alteration at the Carlin Gold Deposit, Nevada. *Econ. Geol.* **87**, 1697-1721.

Kuivila, K. M. and Murray, J. W., 1984. Organic matter diagenesis in freshwater sediments: The alkalinity and total CO_2 balance and methane production in the sediments of Lake Washington. *Limnol. Oceanogr.* **29**, 1218-1230.

Kump, L. R., 1991. Interpreting Carbon-Isotope Excursions - Strangelove Oceans. *Geology* **19**, 299-302.

Kump, L. R. and Arthur, M. A., 1999. Interpreting carbon-isotope excursions: carbonates and organic matter. *Chem. Geol.* **161**, 181-198.

Kusky, T. P. and Hudleston, P. J., 1999. Growth and demise of an Archean carbonate platform, Steep Rock Lake, Ontario, Canada. *Can. J. Earth Sci.* **36**, 565-584.

Kuznetsov, V. G. and Skobeleva, N. M., 2005a. Silicification of carbonate rocks in the Yurubcha-Tokhomo zone, Siberian Platform: A possible model of silica geochemistry in the Proterozoic. *Doklady Earth Sciences* **400**, 5-7.

Kuznetsov, V. G. and Skobeleva, N. M., 2005b. Silicification of riphean carbonate sediments (Yurubcha-Tokhomo zone, Siberian Craton). *Lithology and Mineral Resources* **40**, 552-563.

Lakshtanov, L. Z. and Stipp, S. L. S., 2009. Silica influence on calcium carbonate precipitation*Goldschmidt Conference Abstract*.

Lamb, A. L., Leng, M. J., Lamb, H. F., Telford, R. J., and Mohammed, M. U., 2002. Climatic and non-climatic effects on the delta O-18 and delta C-13 compositions of Lake Awassa, Ethiopia, during the last 6.5 ka. *Quaternary Sci Rev* **21**, 2199-2211.

Lapteva, O. N., 1958. On the dependence of the redox potential of a ferric-ferrous solution on the Ph value. *Zh. Anal. Khim.* **31**.

Lasaga, A. C., 1997. *Kinetic Theory in the Earth Sciences*. Princeton University Press, Princeton, New Jersey.

Laschet, C., 1984. On the origin of cherts. *Facies* **10**, 257-290, 19 Figs.

Lasemi, Z. and Sandberg, P. A., 1984. Transformation of Aragonite-Dominated Lime Muds to Microcrystalline Limestones. *Geology* **12**, 420-423.

Lee, J. H. and Byrne, R. H., 1993. Complexation of trivalent rare earth elements (Ce, Eu, Gd, Tb, Yb) by carbonate ions. *Geochemica et Cosmochimica Acta* **57**, 295-302.

Lee, S. G., Kim, Y., Chae, B. G., Koh, D. C., and Kim, K. H., 2004. The geochemical implication of a variable Eu anomaly in a fractured gneiss core: application for understanding Am behavior in the geological environment. *Appl Geochem* **19**, 1711-1725.

Leeder, M. R., 1999. *Sedimentology and sedimentary basins : from turbulence to tectonics*. Blackwell Science, Oxford ; Malden, MA.

Leng, M. J. and Marshall, J. D., 2004. Palaeoclimate interpretation of stable isotope data from lake sediment archives. *Quaternary Sci Rev* **23**, 811-831.

Lepp, H. and Goldich, S. S., 1964. Origin of Precambrian iron formations. *Economic Geology* **59**, 1025-1060.

Lewin, J. C., 1961. The dissolution of silica from diatom walls. *Geochim. Cosmochim. Acta* **21**, 182–198.

Li, H. C. and Ku, T. L., 1997. delta C-13-delta O-18 covariance as a paleohydrological indicator for closed-basin lakes. *Palaeogeogr. Palaeoclimatol. Palaeoecol.* **133**, 69-80.

Lindsay, J. F., Brasier, M. D., McLoughlin, N., Green, O. R., Fogel, M., Steele, A., and Mertzman, S. A., 2005. The problem of deep carbon - An Archean paradox. *Precamb. Res.* **143**, 1-22.

Liu, X. W. and Millero, F. J., 2002. The solubility of iron in seawater. *Mar. Chem.* **77**, 43-54.

Lopez, O., Zuddas, P., and Faivre, d., 2009. The influence of temperature and seawater composition on calcite cryustal growth mechanisms and kinetics: Implications for Mg incorporation in calcite lattice. *Geochim. Cosmochim. Acta* **73**, 337-347.

Lorens, R. B., 1981. Sr, Cd, Mn and Co distribution coefficients in calcite as a function of calcite precipitation rate. **45**, 553-561.

Loubere, P. and Fariduddin, M., 1999. Quantitative estimation of global patterns of surface ocean biological productivity and its seasonal variation on timescales from centuries to millennia. *Global Biogeochem Cy* **13**, 115-133.

Lovering, T. G. and Patten, L. E., 1962. The Effect of Co2 at Low Temperature and Pressure on Solutions Supersaturated with Silica in the Presence of Limestone and Dolomite. *Geochim. Cosmochim. Acta* **26**, 789-&.

Lovley, D. R., 1987. Organic-Matter Mineralization with the Reduction of Ferric Iron - a Review. *Geomicrobiol. J.* **5**, 375-399.

Lovley, D. R., Stolz, J. F., Nord, G. L., and Phillips, E. J. P., 1987. Anaerobic Production of Magnetite by a Dissimilatory Iron-Reducing Microorganism. *Nature* **330**, 252-254.

Lowe, D. R., 1983. Restricted shallow-water sedimentation of early Archean stromatolitic and evaporitic strata of the Strelley Pool Chert, Pilbara Block, Western Australia. *Precambrian Res.* **19**, 239-283.

Lowe, D. R., 1994. Abiological Origin of Described Stromatolites Older Than 3.2 Ga. *Geology* **22**, 387-390.

Lowe, D. R. and Byerley, G. R., 1999. Stratigraphy of the west-central part of the Barberton Greenstone Belt, South Africa. In: Lowe, D. R. and Byerly, G. R. Eds.), *Geologic Evolution of the Barberton Greenstone Belt, South Africa*. Geological Society of America.

Lowe, D. R. and Knauth, L. P., 1977. Sedimentology of the Onverwacht Group (3.4 billion years), Transvaal, South Africa, and its bearing on the characteristics and evolution of the early Earth. *J. Geol.* **85**, 699-723.

Lowe, D. R. and Nocita, B. W., 1996. Stratigraphy and sedimentology of the Mapepe Formation: sedimentation in an evolving foreland basin. In: Lowe, D. R. and Byerley, G. R. Eds.), *Geologic evolution of the Barberton Greenstone Belt, South Africa*.

Lowell, R. P., Rona, P. A., and von Herzen, R. P., 1995. Seafloor hydrothermal systems. *J. Geophys. Res.* **100**, 327-352.

Luo, Y. R. and Byrne, R. H., 2004. Carbonate complexation of yttrium and the rare earth elements in natural waters. *Geochim. Cosmochim. Acta* **68**, 691-699.

Lyons, W. B., 1984. Calcification of cyanobacterial mats in Solar Lake, Sinai. **12**, 623-626.

Machel, H. G., 2004. Concepts and models of dolomitization: a critical reappraisal. In: Braithwaite, C. J. R., Rizzi, G., and Darke, G. Eds.), *the Geometry and Petrogenesis of dolomite Hydrocarbon Reservoirs*. Geological Society, London.

Machel, H. G. and Lonnee, J., 2002. Hydrothermal dolomite - a product of poor definition and imagination. *Sediment Geol* **152**, 163-171.

MacKenzie, D. J. and Craw, D., 2007. Contrasting hydrothermal alteration mineralogy and geochemistry in the auriferous Rise & Shine Shear Zone, Otago, New Zealand. *New Zeal J Geol Geop* **50**, 67-79.

Maisonneuve, J., 1982. The composition of the Precambrian ocean waters. *Sediment. Geol.* **31**, 1-11.

Maliva, R. G., 2001. Silicification in the Belt Supergroup (Mesoproterozoic), Glacier National Park, Montana, USA. *Sedimentology* **48**, 887-896.

Maliva, R. G., Knoll, A. H., and Siever, R., 1989. Secular change in chert distribution: a reflection of evolving biological participation in the silica cycle. *Palaios* **4**, 519-532.

Maliva, R. G. and Siever, R., 1988a. Mechanism and Controls of Silicification of Fossils in Limestones. *J Geol* **96**, 387-398.

Maliva, R. G. and Siever, R., 1988b. Pre-Cenozoic Nodular Cherts - Evidence for Opal-Ct Precursors and Direct Quartz Replacement. *Am. J. Sci.* **288**, 798-809.

Masuda, A., Kawakami, O., Dohmoto, Y., and Takenaka, T., 1987. Lanthanide Tetrad Effects in Nature - 2 Mutually Opposite Types, W and M. *Geochem J* **21**, 119-124.

Mayer, L. M., 1994a. Relationships between Mineral Surfaces and Organic-Carbon Concentrations in Soils and Sediments. *Chem. Geol.* **114**, 347-363.

Mayer, L. M., 1994b. Surface area control of organic carbon accumulation in continental shelf sediments. *Geochim. Cosmochim. Acta.* **58**, 1271-1284.

Mazzullo, S. J., 1994. Lithification and Porosity Evolution in Permian Periplatform Limestones, Midland Basin, Texas. *Carbonate Evaporite* **9**, 151-171.

McBride, E. F., 1988. Silicification of Carbonate Pebbles in a Fluvial Conglomerate by Groundwater. *J Sediment Petrol* **58**, 862-867.

McConnaughey, T., 1991. Calcification in Chara-Corallina - Co2 Hydroxylation Generates Protons for Bicarbonate Assimilation. *Limnol. Oceanogr.* **36**, 619-628.

McConnaughey, T. A. and Falk, R. H., 1991. Calcium-Proton Exchange During Algal Calcification. *Biological Bulletin* **180**, 185-195.

McConnaughey, T. A., Labaugh, J. W., Rosenberry, D. O., Striegl, R. G., Reddy, M. M., Schuster, P. F., and Carter, V., 1994. Carbon Budget for a Groundwater-Fed Lake - Calcification Supports Summer Photosynthesis. *Limnol. Oceanogr.* **39**, 1319-1332.

McLennan, S. M., 1976. Paleo-Environment of Iron-Rich Sedimentary Rocks. *Geologische Rundschau* **65**, 1126-1129.

McLennan, S. M., Taylor, S. R., and Eriksson, K. A., 1983. Geochemistry of Archean Shales from the Pilbara Supergroup, Western-Australia. *Geochim. Cosmochim. Acta* **47**, 1211-1222.

Megonigal, J. P., Hines, M. E., and Visscher, P. T., 2004. Anaerobic Metabolism: Linkages to Trace Gases and Aerobic Processes. In: Schlesinger, W. H. (Ed.), *Biogeochemistry*. Elsevier-Pergamon, Oxford.

Meyer, H. J., 1984. The Influence of Impurities on the Growth-Rate of Calcite. *J. Cryst. Growth* **66**, 639-646.

Meyers, W. J., 1977. Chertification in the Mississippian Lake Valley Formation, Sacramento Mountains, New Mexico. **24**, 75-105.

Meyers, W. J. and James, A. T., 1978. Stable isotopes of cherts and carbonate cements in the Lake Valley Formation (Mississippian), Sacramento Mountains, New Mexico. **25**, 105-124.

Michard, A. and Albarede, F., 1986. The Ree Content of Some Hydrothermal Fluids. *Chemical Geology* **55**, 51-60.

Milliman, 1995. Calcium carbonate sedimentation in the global ocean: linkages between neritic and pelagic environments. *Oceanography* **8**, 92-94.

Milliman, J. D., 1974. *Marine carbonates*. Springer-Verlag, Berlin.

Millot, G., 1970. *Geology of clay minerals. Weathering, sedimentology, geochemistry*. Springer, New York.

Minami, M., Masuda, A., Takahashi, K., Adachi, M., and Shimizu, H., 1998. Y-Ho fractionation and lanthanide tetrad effect observed in cherts. *Geochem J* **32**, 405-419.

Misik, M., 1993. Carbonate Rhombohedra in Nodular Cherts - Mesozoic of the West Carpathians. *J Sediment Petrol* **63**, 275-281.

Monty, C., 1965. Recent algal stromatolites in the Windward Lagoon, Andros Island, Bahamas. **88/5-6**, 269-276.

Moreira, D., Walter, L. M., Vasconcelos, C., McKenzie, J. A., and McCall, P. J., 2004. Role of sulfide oxidation in dolomitization: sediment and pore-water geochemistry of a hypersaline lagoon system. *Geology* **32**, 701-704.

Morse, J. W., 1978. Dissolution Kinetics of Calcium-Carbonate in Sea-Water .6. Near-Equilibrium Dissolution Kinetics of Calcium Carbonate-Rich Deep-Sea Sediments. *Am. J. Sci.* **278**, 344-353.

Morse, J. W. and Arvidson, R. S., 2002. The dissolution kinetics of major sedimentary carbonate minerals. *Earth-Sci Rev* **58**, 51-84.

Morse, J. W. and Berner, R. A., 1979. The chemistry of calcium carbonate in the deep oceans. In: Jenne, E. (Ed.), *Chemical modelling - speciation, sorption, solubility and kinetics in aqueous systems*. American Chemical Society, Washington, D.C.

Morse, J. W. and Mackenzie, F. T., 1990. *Geochemistry of sedimentary carbonates*. Elsevier [Science Publishers B.V.] ;

[Elsevier Science Publishing Co., Inc., distributors for the United States and Canada], Amsterdam, The Neth.

New York, N.Y.

Morse, J. W. and Mackenzie, F. T., 1998. Hadean ocean carbonate geochemistry. *Aquat Geochem* **4**, 301-319.

Morse, J. W., Wang, Q., Mai, Y.T., 1997. Influence of temperature and Mg:Ca ratio on $CaCO_3$ precipitates from seawater. *Geology* **25**, 85-87.

Mottl, M. J., 1983a. Hydrothermal processes at seafloor spreading centers: application of basalt-seawater experimental results. In: Rona, P. A., Bostrom, K., Laubier, L., and Smith, K. L. Eds.), *Hydrothermal Processes at Seafloor Spreading Centers,*. Plenum, New York.

Mottl, M. J., 1983b. Metabasalts, Axial Hot Springs, and the Structure of Hydrothermal Systems at Mid-Ocean Ridges. *Geol Soc Am Bull* **94**, 161-180.

Mottl, M. J. and Holland, H. D., 1978. Chemical Exchange During Hydrothermal Alteration of Basalt by Seawater .1. Experimental Results for Major and Minor Components of Seawater. *Geochim. Cosmochim. Acta* **42**, 1103-1115.

Mottl, M. J. and Wheat, C. G., 1994. Hydrothermal Circulation through Midocean Ridge Flanks - Fluxes of Heat and Magnesium. *Geochimica Et Cosmochimica Acta* **58**, 2225-2237.

Mucci, A., 1986. Growth kinetics and composition of magnesian calcite overgrowths precipitated from seawater: quantitative influence of orthophosphate ions. **50**, 2235-2265.

Mucci, A. and Morse, J. W., 1990. Chemistry of Low-Temperature Abiotic Calcites - Experimental Studies on Coprecipitation, Stability, and Fractionation. *Rev Aquat Sci* **3**, 217-254.

Muehlenbachs, K. and Clayton, R. N., 1976a. Oxygen Isotope Composition of Oceanic-Crust and Its Bearing on Seawater. *J. Geophys. Res.* **81**, 4356-4369.

Muehlenbachs, K. and Clayton, R. N., 1976b. Oxygen Isotope Composition of Oceanic-Crust and Its Bearing on Sea-Water. *Eos T Am Geophys Un* **57**, 411-412.

Mueller, W., Chown, E. H., and Potvin, R., 1994. Substorm Wave Base Felsic Hydroclastic Deposits in the Archean Lac-Des-Vents Volcanic Complex, Abitibi Belt, Canada. *J Volcanol Geoth Res* **60**, 273-300.

Murray, R. W., Tenbrink, M. R. B., Gerlach, D. C., Russ, G. P., and Jones, D. L., 1992. Rare-Earth, Major, and Trace-Element Composition of Monterey and DSDP Chert and Associated Host Sediment - Assessing the Influence of Chemical Fractionation During Diagenesis. *Geochimica Et Cosmochimica Acta* **56**, 2657-2671.

Myrow, P. M. and Kaufman, A. J., 1999. A newly discovered cap carbonate above Varanger-age glacial deposits in Newfoundland, Canada. *Journal of Sedimentary Research* **69**, 784-793.

Nader, F. H., Abdel-Rahman, A. F. M., and Haidar, A. T., 2006. Petrographic and chemical traits of Cenomanian platform carbonates (central Lebanon): implications for depositional environments. *Cretac. Res.* **27**, 689-706.

Nakamura, K. and Kato, Y., 2002. Carbonate minerals in the Warrawoona Group, Pilbara Craton: Implications for continental crust, life, and global carbon cycle in the Early Archean. *Resour Geol* **52**, 91-100.

Nakamura, K. and Kato, Y., 2004. Carbonatization of oceanic crust by the seafloor hydrothermal activity and its significance as a CO2 sink in the Early Archean. *Geochim. Cosmochim. Acta* **68**, 4595-4618.

Namy, J. N., 1974. Early diagenetic cherts in the Marble Falls Group (Pennsylvanian) of central Texas. *J Sediment Petrol* **56**, 495-500.

Nance, W. B. and Taylor, S. R., 1976. Rare-Earth Element Patterns and Crustal Evolution .1. Australian Post-Archean Sedimentary-Rocks. *Geochim. Cosmochim. Acta* **40**, 1539-1551.

Nealson, K. H. and Myers, C. R., 1990. Iron Reduction by Bacteria - a Potential Role in the Genesis of Banded Iron Formations. *Am. J. Sci.* **290A**, 35-45.

Nesbitt, H. W. and Young, G. M., 1982. Early Proterozoic climates and plate motions inferred from major element chemistry of lutites. *Nature* **299**, 715-717.

Neumann, A. C. and Land, L. S., 1975. Lime Mud Deposition and Calcareous Algae in Bight of Abaco, Bahamas - Budget. *J Sediment Petrol* **45**, 763-786.

Nisbet, E. G., 1987. *The young earth: An introduction to Archaean geology*. Allen & Unwin, Boston.

Noble, J. P. A. and Van Stempvoort, D. R., 1989. Early burial quartz authigenesis in Silurian platform carbonates, New Brunswick, Canada. **59/1**, 65-76, 20 Figs.

Nothdurft, L. D., Webb, G. E., and Kamber, B. S., 2004. Rare earth element geochemistry of Late Devonian reefal carbonates, canning basin, Western Australia: Confirmation of a seawater REE proxy in ancient limestones. *Geochim. Cosmochim. Acta* **68**, 263-283.

Nozaki, Y., Zhang, J., and Amakawa, H., 1997. The fractionation between Y and Ho in the marine environment. *Earth Planet. Sci. Lett.* **148**, 329-340.

Ohmoto, H., 1972. Systematics of Sulfur and Carbon Isotopes in Hydrothermal Ore-Deposits. *Economic Geology* **67**, 551-&.

Ohmoto, H., Watanabe, K., Yamaguchi, K., Naraoka, H., Haruna, M., Kakegawa, T., Hayashi, K., and Kato, Y., 2006. Chemical and biological evaluation of early Earth: constraints from banded iron formations. *Geological Society of America Memoir* **198**, 239-256.

Ohmoto, H., Watanabe, Y., and Kumazawa, K., 2004. Evidence from massive siderite beds for a CO2-rich atmosphere before, 1.8 billion years ago. *Nature* **429**, 395-399.

Olson, J. M., 2006. Photosynthesis in the Archean Era. *Photosynth. Res.* **88**, 109-117.

O'Neil, J. R. and Epstein, S., 1966. Oxygen Isotope Fractionation in System Dolomite-Calcite-Carbon Dioxide. *Science* **152**, 198-&.

Packard, J. J., Al-Aasm, I., Samson, I., Berger, Z., and Davies, J., 2001. A devonian hydrothermal chert reservoir: the 225 bcf Parkland field, British Columbia, Canada. *Aapg Bull* **85**, 51-84.

Paikaray, S., Banerjee, S., and Mukherji, S., 2005. Sorption behavior of heavy metal pollutants onto shales and correlation with shale geochemistry. *Environ Geol* **47**, 1162-1170.

Palmer, T. J., Hudson, J. D., and Wilson, M. A., 1988. Paleoecological Evidence for Early Aragonite Dissolution in Ancient Calcite Seas. *Nature* **335**, 809-810.

Palmer, T. J. and Wilson, M. A., 2004. Calcite precipitation and dissolution of biogenic aragonite in shallow Ordovician calcite seas. *Lethaia* **37**, 417-427.

Panieri, G., Lugli, S., Manzi, V., Palinska, K. A., and Roveri, M., 2008. Microbial communities in Messinian evaporite deposits of the Vena del Gesso (northern Apennines, Italy). *Stratigraphy* **5**, 343-352.

Papadopoulos, P. and Rowell, D. L., 1989. The Reactions of Copper and Zinc with Calcium-Carbonate Surfaces. *J Soil Sci* **40**, 39-48.

Parron, C., Nahon, D., Fritz, B., Paquet, H., and Millot, G., 1976. Desilicification et quartzification par alteration des gres albiens du Gard. Modeles geochmiques de la genese des dalles quartzitiques et silcretes. *Sci. Geol. Bull.* **29**, 273-284.

Patterson, W. P. and Walter, L. M., 1994. Syndepositional Diagenesis of Modern Platform Carbonates - Evidence from Isotopic and Minor Element Data. *Geology* **22**, 127-130.

Pecoits, E., Gingras, M. K., Barley, M. E., Kappler, A., Posth, N. R., and Konhauser, K., 2009. Petrography and geochemistry of the Dales Gorge banded iron

formation: Paragenetic sequence, source and implications for palaeo-ocean chemistry. *Precamb. Res.* **172**, 163-187.

Peine, A., Tritschler, A., Kusel, K., and Peiffer, S., 2000. Electron flow in an iron-rich acidic sediment - evidence for an acidity-driven iron cycle. *Limnol. Oceanogr.* **45**, 1077-1087.

Penela, A. J. M. and Barragan, G., 1995. Silicification of Carbonate Clasts in a Marine-Environment (Upper Miocene, Vera Basin, Se Spain). *Sediment Geol* **97**, 21-32.

Perry, E. C., Ahmad, S. N., and Swulius, T. M., 1978a. Oxygen Isotope Composition of 3,800 My Old Metamorphosed Chert and Iron Formation from Isukasia, West-Greenland. *J Geol* **86**, 223-239.

Perry, E. C. J., Ahmad, S. N., and Swulius, T. M., 1978b. The oxygen isotope composition of 3,800 m.y. old metamorphosed chert and iron formation from Isukasia, west Greenland. *Journal; of Geology* **86**, 223-239.

Peter, J. M., 2003. Ancient iron formations: their genesis and use in the exploration fro stratiform base metal sulphide deposits, with examples from the Bathurst Mining Camp. In: Lentz, D. R. (Ed.), *Geochemistry of sediments and sedimentary rocks : evolutionary considerations to mineral deposit-forming environments*. Geological Association of Canada, St. John's, Nfld.

Pfennig, N., 1977. Phototrophic green and purple bacteria: a comparative systematic survey. *Annu. Rev. Microbiol.* **31**, 275-290.

Philippot, P., Van Zuilen, M., Lepot, K., Thomazo, C., Farquhar, J., and Van Kranendonk, M. J., 2007. Early Archaean microorganisms preferred elemental sulfur, not sulfate. *Science* **317**, 1534-1537.

Plummer, L. N., Wigley, T. M. L., and Parkhurst, D. L., 1978. Kinetics of Calcite Dissolution in Co2-Water Systems at 5-Degrees-C to 60-Degrees-C and 0.0 to 1.0 Atm Co2. *Am. J. Sci.* **278**, 179-216.

Postma, D., 1981. Formation of Siderite and Vivianite and the Pore-Water Composition of a Recent Bog Sediment in Denmark. *Chem. Geol.* **31**, 225-244.

Postma, D., 1982. Pyrite and Siderite Formation in Brackish and Fresh-Water Swamp Sediments. *Am. J. Sci.* **282**, 1151-1183.

Pratt, B. R., 1984. Epiphyton and Renalcis - Diagenetic microfossils from calcification of coccoid blue-green algae. **54/3**, 947-971, 14 Figs.

Prave, A. R., 1999. Two diamictites, two cap carbonates, two $\delta^{13}C$ excursions, two rifts: the Neoproterozoic Kingston Peak Formation, Death Valley, California. *Geology* **27**, 339-342.

Psenner, R., 1988. Alkalinity Generation in a Soft-Water Lake - Watershed and in-Lake Processes. *Limnol. Oceanogr.* **33**, 1463-1475.

Quinn, K. A., Byrne, R. H., and Schijf, J., 2004. Comparative scavenging of yttrium and the rare earth elements in seawater: Competitive influences of solution and surface chemistry. *Aquat Geochem* **10**, 59-80.

Quinn, K. A., Byrne, R. H., and Schijf, J., 2006. Sorption of yttrium and rare earth elements by amorphous ferric hydroxide: Influence of solution complexation with carbonate. *Geochim. Cosmochim. Acta* **70**, 4151-4165.

Radhakrishna, B. P. and Naqvi, S. M., 1986. Precambrian Continental-Crust of India and Its Evolution. *J Geol* **94**, 145-166.

Ragueneau, O., Treguer, P., Leynaert, A., Anderson, R. F., Brzezinski, M. A., DeMaster, D. J., Dugdale, R. C., Dymond, J., Fischer, G., Francois, R., Heinze, C., Maier-Reimer, E., Martin-Jezequel, V., Nelson, D. M., and Queguiner, B., 2000. A review of the Si cycle in the modem ocean: recent progress and missing gaps in the application of biogenic opal as a paleoproductivity proxy. *Global and Planetary Change* **26**, 317-365.

Raiswell, R., 1987. Non-steady state microbial diagenesis and the origin of concretions and nodular limestones. In: Marshall, J. D. (Ed.), *Diagenesis of sedimentary sequences*.

Raiswell, R., 2006. An evaluation of diagenetic recycling as a source of iron for banded iron formations. *Geological Society of America Memoir* **198**, 223-237.

Rao, T. G. and Naqvi, S. M., 1995. Geochemistry, Depositional Environment and Tectonic Setting of the Bifs of the Late Archean Chitradurga Schist Belt, India. *Chem. Geol.* **121**, 217-243.

Reeder, R. J., 1983. Crystal chemistry of the rhombohedral carbonates. In: Reeder, R. J. (Ed.), *Carbonates: Mineralogy and Chemistry*. Mineralogical Society of America, Blacksburg, Virginia.

Reid, R. T., Live, D. H., Faulkner, D. J., and Buttler, A., 1993. A siderophore from a marine bacterium with an exceptional ferric ion affinity constant. *Nature* **366**, 455-458.

Rex, R. W., 1969. X-ray mineralogy studies - Leg 1, Deep Sea Drilling

Project. In: Ewing, M. (Ed.), *Initial Reports of the Deep Sea Drilling Project*.

Rimstidt, J. D. and Barnes, H. L., 1980. The Kinetics of Silica-Water Reactions. *Geochim. Cosmochim. Acta* **44**, 1683-1699.

Rimstidt, J. D. and Cole, D. R., 1983. Geothermal mineralization, I. The mechanism of formation of the Beowawe, Nevada, siliceous sinter deposit. *Am. J. Sci.* **283**, 861-875.

Robbins, L. L. and Blackwelder, P. L., 1992. Biochemical and Ultrastructural Evidence for the Origin of Whitings - a Biologically Induced Calcium-Carbonate Precipitation Mechanism. *Geology* **20**, 464-468.

Robert, F. and Chaussidon, M., 2006. A palaeotemperature curve for the Precambrian oceans based on silicon isotopes in cherts. *Nature* **443**, 969-972.

Roberts, R. G., 1987. Ore Deposit Models 11: Archean Lode Gold Deposits. *Geosci Can* **14**, 37-52.

Romanek, C. S., Grossman, E. L., and Morse, J. W., 1992. Carbon Isotopic Fractionation in Synthetic Aragonite and Calcite - Effects of Temperature and Precipitation Rate. *Geochim. Cosmochim. Acta* **56**, 419-430.

Romanek, C. S., Zhang, C. L. L., Li, Y. L., Horita, J., Vali, H., Cole, D. R., and Phelps, T. J., 2003. Carbon and hydrogen isotope fractionations associated with dissimilatory iron-reducing bacteria. *Chem. Geol.* **195**, 5-16.

Ronov, A. B. and Migdisov, A. A., 1970, 1971. Evolution of the chemical composition of rocks.

Rose, N. M., Rosing, M. T., and Bridgwater, D., 1996. The origin of metacarbonate rocks in the Archaean Isua supracrustal belt, West Greenland. *Am. J. Sci.* **296**, 1004-1044.

Rosenberg, P. E., 1967. Subsolidus relations in the system CaCO3-MgCO3-FeCO3 between 350 C and 550 C. *Am. Mineral.* **52**, 787-796.

Rouchon, V., Orberger, B., Hoffman, A., and Pinti, D. L., 2009. Diagenetic Fe-carbonates in Paleoarchean felsic sedimentary rocks (Hooggenoeg Formation, Barberton greenstone belt, South Africa): Implications for CO2 sequestration and the chemical budget of seawater. *Precamb. Res.* **172**, 255-278.

Rye, R., Kuo, P. H., and Holland, H. D., 1995. Atmospheric carbon dioxide concentrations before 2.2 billion years ago. *Nature* **378**, 603-605.

Sami, T. T. and James, N. P., 1993. Evolution of an Early Proterozoic Foreland Basin Carbonate Platform, Lower Pethei Group, Great Slave Lake, North-West Canada. *Sedimentology* **40**, 403-430.

Sami, T. T. and James, N. P., 1994. Peritidal Carbonate Platform Growth and Cyclicity in an Early Proterozoic Foreland Basin, Upper Pethei Group, Northwest Canada. *J Sediment Res B* **64**, 111-131.

Sami, T. T. and James, N. P., 1996. Synsedimentary cements as Paleoproterozoic platform building blocks, Pethei Group, northwestern Canada. *Journal of Sedimentary Research* **66**, 209-222.

Sapieszko, R. S. and Matijevic, E., 1979. Preparation of well-defined colloidal particles by thermal decomposition of metal chelates. *J. Colloid Interface Sci.* **74**, 405-422.

Savelli, C., Marani, M., and Gamberi, F., 1999. Geochemistry of metalliferous, hydrothermal deposits in the Aeolian arc (Tyrrhenian Sea). *J Volcanol Geoth Res* **88**, 305-323.

Sawicki, J. A., Brown, D. A., and Beveridge, T. J., 1995. Microbial Precipitation of Siderite and Protoferrihydrite in a Biofilm. *Can Mineral* **33**, 1-6.

Schwartz, G. M., 1959. Hydrothermal alteration. *Economic Geology* **54**, 161-183.

Seyfried, W. E., 1987. Experimental and Theoretical Constraints on Hydrothermal Alteration Processes at Midocean Ridges. *Annu Rev Earth Pl Sc* **15**, 317-335.

Seyfried, W. E., Ding, K., Berndt, M. E., and Chen, X., 1999. Experimental and Theoretical Controls on the Composition of Mid-Ocean Ridge Hydrothermal Fluids. *Reviews in Economic Geology* **8**, 181-200.

Shen, Y., Knoll, A. H., and Walter, M. R., 2003. Evidence for low sulphate and anoxia in a mid-Proterozoic marine basin. *Nature* **423**, 632-635.

Sheppard, S. M. and Schwarcz, H. P., 1970. Fractionation of Carbon and Oxygen Isotopes and Magnesium between Coexisting Metamorphic Calcite and Dolomite. *Contrib. Mineral. Petrol.* **26**, 161-&.

Shibuya, T., Kitajima, K., Komiya, T., Terabayashi, M., and Maruyama, S., 2007. Middle archean ocean ridge hydrothermal metamorphism and alteration recorded in the cleaverville area, pilbara craton, western australia. *J Metamorph Geol* **25**, 751-767.

Shields, G., 2007. The marine carbonate and chert isotope records and their implication for tectonics, life and climate on the early Earth. In: van Kranendonk, M., Smithies, R. H., and Bennett, V. C. Eds.), *Earth's oldest rocks*. Elsevier, Amsterdam ; London.

Shields, G. and Veizer, J., 2002. Precambrian marine carbonate isotope database: Version 1.1. *Geochem Geophy Geosy* **3**, -.

Shinn, E. A., Steinen, R. P., Lidz, B. H., and Swart, P. K., 1989. Whitings, a Sedimentologic Dilemma. *J Sediment Petrol* **59**, 147-161.

Sial, A. N., Ferreira, V. P., Dealmeida, A. R., Romano, A. W., Parente, C. V., Dacosta, M. L., and Santos, V. H., 2000. Carbon isotope fluctuations in Precambrian carbonate sequences of several localities in Brazil. *An. Acad. Bras. Cienc.* **72**, 539-558.

Siever, R., 1962. Silica Solubility, 0-Degrees-C-200-Degrees-C, and the Diagenesis of Siliceous Sediments. *J Geol* **70**, 127-150.

Siever, R., 1992. The Silica Cycle in the Precambrian. *Geochim. Cosmochim. Acta* **56**, 3265-3272.

Simonson, B. M., 1985. Sedimentology of cherts in the early Proterozoic Wishart Formation, Quebec - Newfoundland, Canada. *Sedimentology* **32**, 23-40.

Simonson, B. M., 1987. Early silica cementation and subsequent diagenesis in arenites from four Early Proterozoic Iron Formations of North America. *J Sediment Petrol* **57**.

Simonson, B. M., Schubel, K. A., and Hassler, S. W., 1993. Carbonate Sedimentology of the Early Precambrian Hamersley Group of Western-Australia. *Precamb. Res.* **60**, 287-335.

Singh, U., 1987. Ooids and cements from the Late Precambrian of the Flinders Ranges, South Australia. **57/1**, 117-127.

Sinha, R. and Smykatz-Kloss, W., 2003. Thermal characterization of lacustrine dolomites from the Sambhar Lake playa, Thar desert, India. *J Therm Anal Calorim* **71**, 739-750.

Sjoberg, E. L., 1978. Kinetics and mechanism of calcite dissolution in aqueous solutions at low temperatures. *Acta Univ. Stockholmiensism Stockholm Contr. Geology* **332**, 1-92.

Skinner, B. J. and Barton, P. B., 1973. Genesis of Mineral-Deposits. *Annu Rev Earth Pl Sc* **1**, 183-211.

Slack, J. F., Kelley, K. D., Anderson, V. M., Clark, J. L., and Ayuso, R. A., 2004. Multistage hydrothermal silicification and Fe-Tl-As-Sb-Ge-REE enrichment in the Red Dog Zn-Pb-Ag district, northern Alaska: Geochemistry, origin, and exploration applications. *Economic Geology* **99**, 1481-1508.

Slaughter, M. and Hill, R. J., 1991. The influence of organic matter in organogenic dolomitization. **61/2**, 296-303, 4 Figs., 2 Tabs.

Smith, S. V. and Veeh, H. H., 1989. Mass balance of biogeochemically active materials (C, N, P) in a hypersaline gulf. *Estuarine, Coastal and Shelf Science* **29**, 195-215.

Snow, J. E. and Dick, H. J. B., 1995. Pervasive mangesium loss by marine weathering of peridotite. *Geochim. Cosmochim. Acta* **59**, 4219-4235.

Sobolev, D. and Roden, E. E., 2002. Evidence for rapid microscale bacterial redox cycling of iron in circumneutral environments. *Anton Leeuw Int J G* **81**, 587-597.

Sochava, A. V. and Podkovyrov, V. N., 1995. The Compositional Evolution of Mesoproterozoic and Neoproterozoic Carbonate Rocks. *Precamb. Res.* **73**, 283-289.

Spear, F. S., 1995. *Metamorphic phase equilibria and pressure-temperature-time paths*. Mineralogical Society of America, Washington, D.C.

Spears, D. A., 1989. Aspects of incorporation into sediments with special reference to the Yorkshire ironstones. In: Young, T. P. and Taylor, W. E. G. Eds.), *Phanerozoic ironstones*. Geological Society, London.

Spero, H. J., Bijma, J., Lea, D. W., and Bemis, B. E., 1997. Effect of seawater carbonate concentration on foraminiferal carbon and oxygen isotopes. *Nature* **390**, 497-500.

Spier, C. A., de Oliveira, S. M. B., and Rosiere, C. A., 2003. Geology and geochemistry of the Aguas Claras and Pico Iron Mines, Quadrilatero Ferrifero, Minas Gerais, Brazil. *Miner Deposita* **38**, 751-774.

Spier, C. A., de Oliveira, S. M. B., Rosiere, C. A., and Ardisson, J. D., 2008. Mineralogy and trace-element geochemistry of the high-grade iron ores of the Aguas Claras Mine and comparison with the Capao Xavier and Tamandua iron ore deposits, Quadrilahero Ferrifero, Brazil. *Miner Deposita* **43**, 229-254.

Spier, C. A., de Oliveira, S. M. B., Sial, A. N., and Rios, F. J., 2007. Geochemistry and genesis of the banded iron formations of the Caue Formation, Quadrilatero Ferrifero, Minas Gerais, Brazil. *Precamb. Res.* **152**, 170-206.

Spotl, C. and Wright, V. P., 1992. Groundwater Dolocretes from the Upper Triassic of the Paris Basin, France - a Case-Study of an Arid, Continental Diagenetic Facies. *Sedimentology* **39**, 1119-1136.

Staudigel, H., Plank, T., While, B., and Schminke, H. U., 1996. Geochemical fluxes during seafloor alteration of the basaltic upper oceanic crust: DSDP Sites 417

and 418. In: Bebout, G. E., Scholl, D. W., Kirby, S. H., and Platt, J. P. Eds.), *Subduction Top to Bottom*. American Gephyiscal Union, Washington, D.C.

Steinsund, P. I. and Hald, M., 1994. Recent Calcium-Carbonate Dissolution in the Barents Sea - Paleoceanographic Applications. *Mar Geol* **117**, 303-316.

Stipp, S. L. and Hochella, M. F., 1991. Structure and Bonding Environments at the Calcite Surface as Observed with X-Ray Photoelectron-Spectroscopy (Xps) and Low-Energy Electron-Diffraction (Leed). *Geochim. Cosmochim. Acta* **55**, 1723-1736.

Stipp, S. L. and Hochella, M. F., 1992. Uptake of Cd2+ and Other Divalent-Cations by Calcite, Solid-State Diffusion and Solid-Solution Formation. *Abstr Pap Am Chem S* **203**, 178-Geoc.

Stipp, S. L., Hochella, M. F., Parks, G. A., and Leckie, J. O., 1992. Cd2+ Uptake by Calcite, Solid-State Diffusion, and the Formation of Solid-Solution - Interface Processes Observed with near-Surface Sensitive Techniques (Xps, Leed, and Aes). *Geochim. Cosmochim. Acta* **56**, 1941-1954.

Stockman, K. W., Ginsburg, R. N., and Shinn, E. A., 1967. Production of Lime Mud by Algae in South Florida. *J Sediment Petrol* **37**, 633-&.

Stumm, W. and Morgan, B., 1996. *Aquatic chemistry*. John Wiley & Sons, New York.

Sugimoto, T., Waki, S., Itoh, H., and Muramatsu, A., 1996. Preparation of monodisperse platelet-type hematite particles from a highly condensed beta-FeOOH suspension. *Colloid Surface A* **109**, 155-165.

Sumner, D. Y., 1997a. Carbonate precipitation and oxygen stratification in late Archean seawater as deduced from facies and stratigraphy of the Gamohaan and Frisco Formations, Transvaal Supergroup, South Africa. *American Journal of Science* **297**, 455-487.

Sumner, D. Y., 1997b. Carbonate precipitation and oxygen stratification in late Archean seawater as deduced from facies and stratigraphy of the Gamohaan and Frisco formations, Transvaal Supergroup, South Africa. *Am. J. Sci.* **297**, 455-487.

Sumner, D. Y., 2000. Microbial versus environmental influences on the morphology of Late Archean fenestrate microbialites. In: Riding, R. E. and Awramik, S. M. Eds.), *Microbial sediments*. Springer-Verlag, Berlin.

Sumner, D. Y., 2002. Decimetre-thick encrustations of calcite and aragonite on the sea-floor and implications for Neoarchaean and Neoproterozoic ocean chemistry. *Special Publications of the International Association of Sedimentologists* **33**, 107-120.

Sumner, D. Y. and Grotzinger, J. P., 1996. Were kinetics of Archean calcium carbonate precipitation related to oxygen concentration? *Geology* **24**, 119-122.

Sumner, D. Y. and Grotzinger, J. P., 2000. Late Archean aragonite precipitation: petrography, facies associations, and environmental significance. In: Grotzinger, J. P. and James, N. P. Eds.), *Carbonate sedimentation and diagenesis in the evolving Precambrian world*. Society for Sedimentary Geology.

Sumner, D. Y. and Grotzinger, J. P., 2004. Implications for Neoarchaean ocean chemistry from primary carbonate mineralogy of the Campbellrand-Malmani Platform, South Africa. *Sedimentology* **51**, 1273-1299.

Sun, S. S. and McDonough, W. F., 1989. Chemical and isotopic systematics of oceanic basalts: implications for mantle composition and processes. In: Saunders, A. D. and Norry, M. J. Eds.), *Magmatism in the Ocean Basins*.

Swedlund, P. J. and Webster, J. G., 1999. Adsorption and polymerisation of silicic acid on ferrihydrite, and its effect on arsenic adsorption. *Water Res.* **33**, 3413-3422.

Swett, K., 1965. Dolomitization Silicification and Calcitization Patterns in Cambro-Ordovician Oolites from Northwest Scotland. *J Sediment Petrol* **35**, 928-&.

Talbot, M. R., 1990. A Review of the Paleohydrological Interpretation of Carbon and Oxygen Isotopic-Ratios in Primary Lacustrine Carbonates. *Chem. Geol.* **80**, 261-279.

Taylor, D., Dalstra, H. J., Harding, A. E., Broadbent, G. C., and Barley, M. E., 2001. Genesis of high-grade hematite orebodies of the Hamersley province, Western Australia. *Economic Geology* **96**, 837-873.

Thiry, M., 1981. Sedimentation continentale et alterations associees: calcitations, ferruginisations et silicifications. Les Argiles Plastiques du Sparnacian de Bassin de Paris. *Sci. Geol. Mem.* **64**, 173.

Thiry, M., 1999. Diversity of continental silicification features: examples from the Cenozoic deposits in the Paris Basin and neighbouring basement. In: Thiry, M. and Simon-Coinçon, R. Eds.), *Palaeoweathering, palaeosurfaces, and related continental deposits*. Blackwell Science, Oxford; Malden, MA.

Thiry, M., Ayrault, M. B., and Grisoni, J. C., 1988a. Groundwater Silicification and Leaching in Sands - Example of the Fontainebleau Sand (Oligocene) in the Paris Basin. *Geol Soc Am Bull* **100**, 1283-1290.

Thiry, M., Ayrault, M. B., Grisoni, J. C., Menillet, F., and Schmitt, J. M., 1988b. The Fontainebleau Sandstones - Groundwater Silicification Related to the Geomorphologic Evolution of the Paris-Basin During Plio-Quaternary. *B Soc Geol Fr* **4**, 419-430.

Thiry, M. and Millot, G., 1987. Mineralogical Forms of Silica and Their Sequence of Formation in Silcretes. *J Sediment Petrol* **57**, 343-352.

Thiry, M. and Ribet, I., 1999. Groundwater silicification in Paris Basin limestones: Fabrics, mechanisms, and modeling. *Journal of Sedimentary Research* **69**, 171-183.

Tice, M. M. and Lowe, D. R., 2004. Photosynthetic microbial mats in the 3,416-Myr-old ocean. *Nature* **431**, 549-552.

Tice, M. M. and Lowe, D. R., 2006. The origin of carbonaceous matter in pre-3.0 Ga greenstone terrains: A review and new evidence from the 3.42 Ga Buck Reef Chert. *Earth-Sci Rev* **76**, 259-300.

Toulkeridis, T., Goldstein, S. L., Clauer, N., Kroner, A., Todt, W., and Schidlowski, M., 1998. Sm-Nd, Rb-Sr and Pb-Pb dating of silicic carbonates from the early Archaean Barberton Greenstone Belt, South Africa - Evidence for post-depositional isotopic resetting at low temperature. *Precamb. Res.* **92**, 129-144.

Trendall, A. F. and Blockley, J. G., 1970. *The iron formations of the Precambrian Hamersley Group, Western Australia, with special reference to the associated crocidolite*.

Trendall, A. F. and Blockley, J. G., 2004. Precambrian iron-formation. In: Eriksson, K. A., Altermann, W., Nelson, D. R., Mueller, P. A., and Catuneanu, O. Eds.), *The Precambrian Earth: Tempos and Events*. Elsevier, Amsterdam.

Tribble, J. S., Arvidson, R. S., Lane, M., and Mackenzie, F. T., 1995. Crystal-Chemistry, and Thermodynamic and Kinetic-Properties of Calcite, Dolomite, Apatite, and Biogenic Silica - Applications to Petrologic Problems. *Sediment Geol* **95**, 11-37.

Tsikos, H., Moore, J. M., and Harris, C., 2001. Geochemistry of the Palaeoproterozoic Mooidraai Formation: Fe-rich limestone as end member of iron formation deposition, Kalahari Manganese Field, Transvaal Supergroup, South Africa. *J Afr Earth Sci* **32**, 19-27.

Tucker, M. E., 1986. Formerly Aragonitic Limestones Associated with Tillites in the Late Proterozoic of Death-Valley, California. *J Sediment Petrol* **56**, 818-830.

Turner, E. C., James, N. P., and Narbonne, G. M., 1997. Growth dynamics of Neoproterozoic calcimicrobial reefs, Mackenzie Mountains, northwest Canada. *Journal of Sedimentary Research* **67**, 437-450.

Turner, E. C., James, N. P., and Narbonne, G. M., 2000. Taphonomic control on microstructure in early neoproterozoic reefal stromatolites and thrombolites. *Palaios* **15**, 87-111.

Ulmerscholle, D. S., Scholle, P. A., and Brady, P. V., 1993. Silicification of Evaporites in Permian (Guadalupian) Back-Reef Carbonates of the Delaware Basin, West Texas and New-Mexico. *J Sediment Petrol* **63**, 955-965.

Umeda, M., 2003. Precipitation of silica and formation of chert-mudstone-peat association in Miocene coastal environments at the opening of the Sea of Japan. *Sedimentary Geology* **161**, 249-268.

Uysal, I. T., Golding, S. D., and Glikson, M., 2000. Petrographic and isotope constraints on the origin of authigenic carbonate minerals and the associated

fluid evolution in Late Permian coal measures, Bowen Basin (Queensland), Australia. *Sediment Geol* **136**, 189-206.

Van Cappellen, P., Viollier, E., Roychoudhury, A., Clark, L., Ingall, E., Lowe, K., and Dichristina, T., 1998. Biogeochemical cycles of manganese and iron at the oxic-anoxic transition of a stratified marine basin (Orca Basin, Gulf of Mexico). *Environ. Sci. Technol.* **32**, 2931-2939.

van Kranendonk, M., Webb, G. E., and Kamber, B., 2003. Geological and trace element evidence for a marine sedimentary environment of deposition and biogenicity of 3.45 Ga stromatolitic carbonates in the Pilbara Craton, and support for a reducing Archaean ocean. *Geobiol.* **1**, 91-108.

Vasconcelos, C. and McKenzie, J. A., 1997. Microbial mediation of modern dolomite precipitation and diagenesis under anoxic conditions (Lagoa Vermelha, Rio De Janeiro, Brazil). *Journal of Sedimentary Research* **67**, 378-390.

Vasconcelos, C., McKenzie, J. A., Bernasconi, S., Grujic, D., and Tien, A. J., 1995. Microbial mediation as a possible mechanism for natural dolomite formation at low temperatures. *Nature* **377**, 220-222.

Veizer, J., 1978. Secular Variations in Composition of Sedimentary Carbonate Rocks, II. Fe, Mn, Ca, Mg, Si and Minor Constituents. *Precamb. Res.* **6**, 381-413.

Veizer, J., 1983. Chemical diagenesis of carbonates: theory and application of trace element technique, *Stable isotopes in sedimentary geology: Society of Economic Paleontologists and Mineralogists Short Course 10.*

Veizer, J., 1992. Depositional and diagenetic history of limestones: Stable and radiogenic isotopes. In: Clauer, N. and Chaudhuri, S. Eds.), *Lecture notes in earth sciences ;*. Springer-Verlag, Berlin ; New York.

Veizer, J., Clayton, R. N., Hinton, R. W., von Brunn, V., Mason, T. R., Buck, S. G., and Hoefs, J., 1990. Geochemistry of Precambrian carbonates: 3 - Shelf seas and non-marine environments of the Archean. *Geochim. Cosmochim. Acta* **54**, 2717-2729.

Veizer, J. and Garrett, D. E., 1978. Secular Variations in Composition of Sedimentary Carbonate Rocks .1. Alkali-Metals. *Precamb. Res.* **6**, 367-380.

Veizer, J., Hoefs, J., Lowe, D. R., and Thurston, P. C., 1989a. Geochemistry of Precambrian carbonates: II. Archean greenstone belts and Archean sea water. *Geochim. Cosmochim. Acta* **53**, 859-871.

Veizer, J., Hoefs, J., Ridler, R. H., Jensen, L. S., and Lowe, D. R., 1989b. Geochemistry of Precambrian Carbonates: I. Archean Hydrothermal Systems. *Geochim. Cosmochim. Acta* **53**, 845-857.

Ver´ýssimo, C. U. V., Schrank, A., Pires, F. R. M., Hasui, Y., Zanardo, A., and Parente, C. V., 2002. Geochemical study of the itabirite iron ores of the Alegria mine—Quadril´atero Ferr´ýfero, Minas Gerais, Brazil. *Australasian Institute of Mining and Metallurgy*, 95–103.

Viljoen, M. J. and Viljoen, R. P., 1969. The geological and geochemical significance of the upper formations of the Onverwacht Group. *Geological Society of South Africa Special Publications* **2**, 113-152.

Vorob'yeva, K. A. and Mel'nik, Y. P., 1977. Experimental Investigation of System Fe2o3-H2o at T=100-200degreesc and P up to 9 Kbar. *Geokhimiya*, 1121-1128.

Walker, J. C. G., 1984. Suboxic diagenesis in banded iron formations. *Nature* **309**, 340-342.

Walker, J. C. G., 1987. Was the Archaean biosphere upside down? *Nature* **329**, 710-712.

Walker, J. C. G. and Brimblecomb, P., 1985. Iron and sulfur in the pre-biologic ocean. *Precamb. Res.* **28**, 205-222.

Walker, T. R., 1962. Reversible Nature of Chert-Carbonate Replacement in Sedimentary Rocks. *Geol Soc Am Bull* **73**, 237-242.

Walter, L. M. and Burton, E. A., 1986. The Effect of Ortho-Phosphate on Carbonate Mineral Dissolution Rates in Seawater. *Chem. Geol.* **56**, 313-323.

Walter, L. M. and Morse, J. W., 1984. Reactive surface area of skeletal carbonates during dissolution: effect of grain size. **54/4**, 1081-1090, 5 Figs., 4 Tabs.

Wang, Y. F. and Xu, H. F., 2001. Prediction of trace metal partitioning between minerals and aqueous solutions: A linear free energy correlation approach. *Geochim. Cosmochim. Acta* **65**, 1529-1543.

Warne, D. S. J., Morgan, D. J., and Milodowski, A. E., 1981. Thermal analysis studies of the dolomite, ferroan dolomite, ankerite series. Part 1. Iron content recognition and determination by variable atmorphere DTA. *Thermochim. Acta* **51**, 105-111.

Warren, J. K., 1990. Sedimentology and Mineralogy of Dolomitic Coorong Lakes, South-Australia. *J Sediment Petrol* **60**, 843-858.

Weaver, F. M. and Wise, S. W., 1973. Origin of Cristobalite-Rich Tertiary Sediments in Atlantic and Gulf Coastal-Plain. *American Association of Petroleum Geologists Bulletin* **57**, 1840-1840.

Weaver, F. M. and Wise, S. W. J., 1972. Ultramorphology of deep sea cristobalitic chert. **237/73**, 56-57, 3 Figs.

Webb, G. E. and Kamber, B. S., 2000. Rare earth elements in Holocene reefal microbialites: A new shallow seawater proxy. *Geochim. Cosmochim. Acta* **64**, 1557-1565.

Weber, J. N., 1965. Oxygen Isotope Fractionation between Coexisting Calcite and Dolomite in Freshwater Upper Carboniferous Freeport Formation. *Nature* **207**, 972-&.

Wedepohl, K. H., 1969. Composition and abundance of common igneous rocks. In: Wedepohl, K. H. (Ed.), *The Handbook of Geochemistry*. Springer-Verlag, Berlin.

Weidner, J. R., 1968. Phase equilibria in a portion of the system Fe-C-O from 250. to 10000 bars and 400 °C to 1200 °C and its petrologic significance, Pennsylvania State University.

Weidner, J. R., 1972. Equilibria in the system Fe-C-O part I: siderite-magnetite-carbon-vapor equilibrium from 500 to 10,000 bars. *Am. J. Sci.* **272**, 735-751.

Wheat, C. G. and Mottl, M. J., 1994. Hydrothermal circulation, Juan de Fuca Ridge eastern flank: Factors controlling basement water composition. *Journal of Geophysical Research* **100**, 12527-12555.

Wheat, C. G. and Mottl, M. J., 2000. Composition of pore and spring waters from Baby Bare: Global implications of geochemical fluxes from a ridge flank hydrothermal system. *Geochim. Cosmochim. Acta* **64**, 629-642.

Whiticar, M. J., Faber, E., and Schoell, M., 1986. Biogenic Methane Formation in Marine and Fresh-Water Environments - Co2 Reduction Vs Acetate Fermentation Isotope Evidence. *Geochim. Cosmochim. Acta* **50**, 693-709.

Whittle, G. L. and Alsharhan, A. S., 1994. Dolomitization and Chertification of the Early Eocene Rus Formation in Abu-Dhabi, United-Arab-Emirates. *Sediment Geol* **92**, 273-285.

Widdel, F., Schnell, S., Heising, S., Ehrenreich, A., Assmus, B., and Schink, B., 1993. Ferrous iron oxidation by anoxygenic phototrophic bacteria. *Nature* **362**, 834-835.

Wildeman, T. R. and Haskin, L. A., 1973. Rare-Earths in Precambrian Sediments. *Geochim. Cosmochim. Acta* **37**, 419-438.

Wilks, M. E. and Nisbet, E. G., 1985. Archean Stromatolites from the Steep Rock Group, Northwestern Ontario, Canada. *Can. J. Earth Sci.* **22**, 792-799.

Wilks, M. E. and Nisbet, E. G., 1988. Stratigraphy of the Steep Rock Group, Northwest Ontario - a Major Archean Unconformity and Archean Stromatolites. *Can. J. Earth Sci.* **25**, 370-391.

Williams, L. A. and Crerar, D. A., 1985. Silica Diagenesis .2. General Mechanisms. *Journal of Sedimentary Petrology* **55**, 312-321.

Williams, L. A., Parks, G. A., and Crerar, D. A., 1985. Silica Diagenesis .1. Solubility Controls. *J Sediment Petrol* **55**, 301-311.

Winefield, P. R., 2000. Development of Late Paleoproterozoic aragonitic seafloor cements in the McArthur Group, northern Australia, *Carbonate sedimentation and diagenesis in an evolving Precambrian world*.

Winterer, E. L., Riedel, W. R., Bronnima.P, Gealy, E. L., Heath, R., Kroenke, L., Martini, E., Moberly, R., Resig, J., and Worsley, T., 1970. Main Geological and Geophysical Results of Dsdp-Leg-7 (Guam to Honolulu). *Geophysics* **35**, 1172-&.

Winterwerp, J. C. and Kranenburg, C., 2002. *Fine sediment dynamics in the marine environment*. Elsevier, Amsterdam, Netherlands ; New York.

Wise, S. W. and Kelts, K. R., 1972. Inferred Diagenetic History of Weakly Silicified Deep-Sea Chalk. *American Association of Petroleum Geologists Bulletin* **56**, 1906-&.

Woo, K. S., Choi, D. W., and Lee, K. C., 2008. Silicification of cave corals from some lava tube caves in the Jeju Island, Korea: Implications for speleogenesis and a proxy for paleoenvironmental change during the Late Quaternary. *Quaternary International* **176-177**, 82-95.

Wright, D. T., 1999. The role of sulphate-reducing bacteria and cyanobacteria in dolomite formation in distal ephemeral lakes of the Coorong region, South Australia. *Sediment Geol* **126**, 147-157.

Wright, D. T. and Wacey, D., 2004. Sedimentary dolomite: a reality check. In: Braithwaite, C. J. R., Rizzi, G., and Darke, G. Eds.), *The geometry and petrogenesis of dolomite hydrocarbon reservoirs*. Geological Society of London, London.

Wright, P. V., 1990. Lacustrine carbonates. In: Tucker, J. and Wright, P. V. Eds.), *Carbonate sedimentology*. Blackwell Scientific, Oxford.

Xu, H., Ai, L., Tan, L. C., and An, Z. S., 2006. Stable isotopes in bulk carbonates and organic matter in recent sediments of Lake Qinghai and their climatic implications. *Chem. Geol.* **235**, 262-275.

Yakushev, E. V., Chasovnikov, V. K., Debolskaya, E. I., Egorov, A. V., Makkaveev, P. N., Pakhomova, S. V., Podymov, O. I., and Yakubenko, V. G., 2006. The northeastern Black Sea redox zone: Hydrochemical structure and its temporal variability. *Deep-Sea Res Pt Ii* **53**, 1769-1786.

Yamamoto, K., Itoh, N., Matsumoto, T., Tanaka, T., and Adachi, M., 2004. Geochemistry of Precambrian carbonate intercalated in pillows and its host basalt: implications for the REE composition of circa 3.4 Ga seawater. *Precamb. Res.* **135**, 331-344.

Yates, K. K. and Robbins, L. L., 1998. Production of carbonate sediments by a unicellular green alga. *Am. Mineral.* **83**, 1503-1509.

Yee, N., Phoenix, V. R., Konhauser, K. O., Benning, L. G., and Ferris, F. G., 2003. The effect of cyanobacteria on silica precipitation at neutral pH: implications for bacterial silicification in geothermal hot springs. *Chemical Geology* **199**, 83-90.

Yui, S., 1966. Decomposition of siderite to magnetite at lower oxygen fugacities: a thermodynamical interpretation and geological implications. *Economic Geology* **61**, 768-776.

Zerkle, A. L., House, C. H., and Brantley, S. L., 2005. Biogeochemical signatures through time as inferred from whole microbial genomes. *Am. J. Sci.* **305**, 467-502.

Zhang, C. L., Horita, J., Cole, D. R., Zhou, J. Z., Lovley, D. R., and Phelps, T. J., 2001. Temperature-dependent oxygen and carbon isotope fractionations of biogenic siderite. *Geochim. Cosmochim. Acta* **65**, 2257-2271.

6. Sedimentary Carbon Isotopes From the 3.52 Ga Coonterunah Subgroup

1. Introduction

Despite much scientific effort, it is still unclear how long the Earth has been inhabited by living organisms. This uncertainty stems from two main problems: the scarcity of suitable low-grade metasedimentary facies in the early geological record, and the ambiguity of even the best-preserved relics of early life-forms. The first is partly due to the dearth of early Archean rocks in general (the older things are, the rarer they become) and partly because the vagaries of geologic history have subjected most very ancient rocks to considerable metamorphism and deformation, obliterating or obscuring any biological relics they might contain. The second results from the apparent simplicity of early organisms, rendering their physical remains and traces of their activities vulnerable, and difficult to distinguish from inorganic mimics. Hence, microfossils and stromatolites provide compelling evidence for life back to around 3.0 Ga (billion years) ago, but before that, all purported physical records of biological activity have been questioned, by one expert or another, on the grounds of syngenicity or biogenicity.

The carbon isotope record is somewhat more robust, but becomes controversial before about 3.45 Ga, the age of the oldest very low-grade sedimentary rocks in Australia's Warrawoona Group and South Africa's Onverwacht Group. Specifically, debate has focussed on the age and origin of carbonaceous matter in the Isua and Akilia areas of Greenland. These upper-amphibolite to granulite facies rocks are older than 3.7 Ga and contain massive carbonates and graphitic gneisses that show carbon isotopic fractionations not inconsistent with a biological origin followed by later metamorphic resetting (Schidlowski, 1988). However, the carbonates have recently been reinterpreted as metasomatic derivatives of ultramafic igneous rocks, not sediments (Rose *et al.*, 1996), and hence their isotopic values reflect abiotic processes only. Graphite yields a wide range of $\delta^{13}C_{org}$ values, from as heavy as -3‰ in ankerite-quartz-cummingtonite schist (Ueno *et al.*, 2002) to as light as -45‰ from minute inclusions in apatite crystals (Mojzsis *et al.*, 1996). To explain this spread, it has been

argued that the heavier values represent metamorphically reset biological ratios, whereas the lighter values are closer to an original autotrophic signature (Schidlowski *et al*., 1979; Ueno *et al.*, 2002). But it is now evident that much of the graphite thus far reported at Isua was produced abiotically (van Zuilen *et al*., 2002) and doubtful whether any graphite at all occurs at Akilia (Lepland *et al*., 2005; Moorbath, 2005). The most likely Isua graphite to be both biological and ancient (~3.8 Ga) is moderately abundant (TOC = 0.1-0.9 wt.%), resides in turbiditic metasediments that are not associated with metasomatic carbonate and ranges in $\delta^{13}C_{org}$ from –20 to -14‰ (Rosing, 1999). However, meteoritic organic carbon from carbonaceous chondrites and tarry residues from prebiotic synthesis experiments show a similar range of values. Moreover, the absence of a reliable sedimentary $\delta^{13}C_{carb}$ record makes it is impossible to prove that the total isotopic fractionation reflects biological autotrophy (Buick, 2001).

Here we present $\delta^{13}C$ analyses of organic and carbonate carbon from a recently discovered succession of slightly younger and better preserved sedimentary rocks from the Pilbara Craton in Australia. These yield much less equivocal data which extend the incontrovertible record of life on Earth back to the first billion years of this planet's history.

2. Geological Setting

The rocks examined here belong to the Coonterunah Group, the basal stratigraphic unit in Archean Pilbara Craton of northwestern Australia (Figure 1). The ~5.5 km thick succession, truncated at the base by slightly younger granitoid intrusions, is dominated by tholeiitic basalts with subordinate felsic volcanics and volcanogenic sediments, magnesian and komatiitic basalts, and synvolcanic gabbroic intrusions (Buick *et al*., 1995; Green *et al.*, 2000). From the widespread presence of pillows, sparse amygdales in basalts, rare breccias in dacites and paucity of clastic sediments, the depositional environment was apparently deep marine. Dacites and rhyolites from near the top of the succession have been dated by SHRIMP U-Pb in zircon techniques as 3515-3517 Ma old (Buick *et al.*, 1995). The metamorphic grade

varies along the exposed strike length of ~75 km from mid-greenschist facies to lower amphibolite facies (Green *et al*., 2000), with a tectonic fabric only developed in the higher-grade areas. In most areas, deformation has consisted of nothing more than early open folding, followed by block faulting and subsequent tilting to the present subvertical bedding planes. Following the erosional unconformity and subsequent deposition of the very low-grade and minimally deformed Warrawoona Group at ~3.4 Ga, very little has disturbed their repose (Buick *et al.*, 1995). Thus, they are the oldest known low-grade rocks on Earth and as such, are an excellent place to search for isotopic records of early life.

Ferruginous chert beds (Figure 2 (a)) form thin (~0.3m thick) layers between basalt flows and thick (10-30m) units between different volcanic lithologies. They have white and red or black banding on a centimeter scale and a poorly defined lamination on a millimeter scale. The layering is planar to undulating with diffuse boundaries, showing no evidence of clastic sedimentary structures or textures. However, the chert is clearly sedimentary and not secondary as the laminae drape topographic highs on underlying basalt flows, thickening into troughs and thinning over ridges (Figure 2 (b)). At a microscopic scale, all layers are predominantly composed of equigranular microquartz, with the colored bands and laminae containing varying amounts (up to 25%) of very fine-grained (~0.1 mm) hematite or magnetite. Laterally gradational contacts indicate that the hematitic layers are secondary modifications of originally magnetitic bands. Trace amounts of organic carbon exist in the magnetitic layers, but TOC is generally too low for successful extraction by acid digestion without risk of modern contamination. No detrital clastic grains have been observed in thin-sections. Thus, the cherts are best interpreted as interflow sediments resembling banded iron-formation that were deposited during times of volcanic quiescence under very low energy conditions with miniscule levels of clastic sedimentation. Their intimate association with surrounding volcanic rocks indicates that they formed in the same environmental setting; *i.e.* in deep marine conditions.

Associated with some of the chert beds are thin (5-30 cm) beds of massive to plane-laminated (2-5 mm) carbonate. In most places, these have been secondarily

silicified during Tertiary weathering, resulting in lenses and pods within layers of amorphous brown silcrete, with interfingering contacts and grain overgrowths showing that the carbonate was indeed the primary phase. The carbonate is now quite coarse grained (0.5-1 mm) and composed of equant grey-brown crystals, but this is almost certainly the result of metamorphic recrystallization and it was presumably finer originally. Along some contacts with adjacent siliceous beds, carbonate is interlayered with quartz-grunerite-magnetite laminae, gradually passing into quartz-magnetite chert. The present mineralogy of the carbonate layers is ferroan dolomite and calcite, identified through microprobe analysis. As in the cherts, no evidence of clastic sedimentary structures or textures has been observed, and on the microscopic scale, no detrital mineral grains have been found in thin-sections of the carbonate rocks. So, the depositional environment of the carbonates is best interpreted as similar to the interbedded cherts and volcanics; *i.e.* low energy chemical sediments formed in a deep-water submarine setting. Unlike the older Isua carbonates from Greenland, there are no cross-cutting carbonate veins and adjacent mafic igneous igneous rocks show only very limited carbonate alteration.

3. Methods

Surface samples were collected from minimally metamorphosed parts of the Coonterunah Group, as far as possible from igneous intrusions and cross-cutting faults. Exterior weathering was removed with a diamond saw and the rocks were then coarsely crushed. Fragments were etched in HCl and HF to remove any surface contamination and then finely crushed, in a steel puck mill for carbonates and by agate pestle and mortar for cherts. Kerogen was isolated from powders with higher TOC by demineralizing with HF and then removing secondary fluorides with H_3BO_3, a modification of the technique of Robl and Davis (1993). Some carbonates were reacted under vacuum with HPO_4 in sealed quartz-glass Y-tubes at 100°C for 24 hours, while others were reacted and analysed at 80 °C using a Kiel-III carbonate mass-spectrometer. Cherts were decarbonated with warm concentrated HCl. Some cherts and kerogen isolates were combusted under vacuum in sealed quartz-glass bombs with

CuO at 800°C for 4 hours, with the resulting CO_2 was purified cryogenically in a vacuum gas-distillation line and analysed on a Nuclide isotope-ratio mass-spectrometer. Others were analysed in a Thermo Finnigan MAT 253. Results are expressed in $\delta^{13}C$ or $\delta^{18}O$ notation as per mille (‰) values relative to the PDB standard. For oxygen isotopes in carbonates, values were calculated using a published calcite fractionation factor at the appropriate temperature.

4. Results

$\delta^{13}C_{org}$ values are tabulated in Table 1. It is evident that there is a major mode centered about -25‰ and a spread skewed towards heavier values from -20‰ to -5‰. The tight clustering of values around the major mode (-25.4‰, corrected for replicates) indicates that it is of primary significance, because low-grade metamorphism has inconsistent isotopic resetting effects depending on local conditions and tends to smear the distribution between original sedimentary and bulk earth values. Moreover, for high TOC samples where a $\delta^{13}C_{org}$ value could be obtained from isolated kerogen, all fall within the major modal population, suggesting that metamorphic resetting has only influenced kerogen-poor samples. Thus, the most reasonable interpretation is that the major mode represents mildly reset original values and therefore is an approximate indicator of the bulk $\delta^{13}C_{org}$ deposited during sedimentation. If so, it is roughly equivalent to the values observed in modern sediments where carbon isotopic fractionation is controlled by RuBisCO-modulated carbon-fixation. Though the spread in values around this particular mode gets as light as -31‰, it is unlikely that the original values were very much lighter than this, as maturational hydrocarbon expulsion probably did not shift values by much more than a couple of parts per mille, even given the extremely low TOC percentages (Buick *et al*., 1998). The minor light mode may highlight microbial remineralization of organic matter during diagenesis and the heavy outliers may represent metamorphic resetting (see Discussion).

Carbonates show a much narrower range of isotopic values than kerogen. $\delta^{13}C_{carb}$ ranges between -1‰ and -4‰, with a mean of 2.9‰ (Table 2). Values are strongly skewed towards lighter values. This tighter distribution probably reflects the

much higher amounts of carbonate in the samples compared with organic carbon. In such circumstances, metamorphic resetting is likely to have been minimal. Diagenetic alteration may have been significant, because the carbonate beds are thin and volumetrically minor within the stratigraphic succession. Interactions between sedimentary carbonates and diagenetic fluids can be monitored in very low-grade terrains by $\delta^{18}O$ values. In the Coonterunah carbonates, these range from -7‰ to -20‰ about a mean of -17.1‰. Though it is unknown exactly what marine Archean $\delta^{18}O$ values were, it seems likely that they became lighter back through time (Veizer *et al*., 1989). Diagenetic alteration in most sedimentary environments, excluding evaporitic basins, resets the marine signature to even lighter values. This would suggest that the closest Coonterunah $\delta^{18}O$ value to contemporary seawater was around -7‰ and that the lighter values represent diagenetic fluid-rock interaction. If so, then original $\delta^{13}C_{carb}$ values were probably not altered much during diagenesis, as lighter $\delta^{18}O$ values are not correlated with either extremity of the $\delta^{13}C_{carb}$ distribution (Figure 3, inset). So, while diagenetic and metamorphic fluid-rock interactions may have occurred, they do not appear to have substantially modified $\delta^{13}C_{carb}$.

$\Delta^{13}C$ ($\delta^{13}C_{carb}$ - $\delta^{13}C_{org}$) is an approximate measure of the fractionation between oxidized and reduced carbon species. Given the minor uncertainty about exact original isotopic compositions because of the effects of diagenesis and metamorphism, this is a more appropriate measure to use than the precise fractionation ε_{TOC}. As $\delta^{13}C_{carb}$ values form a single homogeneous population, their mean of -2.9‰ can be used in the calculation. For $\delta^{13}C_{org}$, the corrected mean of values clustered around the major mode (-25.6‰) is used, as this most closely represents the original material deposited. Hence, bulk $\Delta^{13}C$ is 22.7‰, very similar to the modern marine value of ~22‰. Though diagenesis and metamorphism have probably reduced the Coonterunah $\Delta^{13}C$ value, this was probably only by a few per mille. This is shown in the few kerogenous carbonates in which $\Delta^{13}C$ can be determined for individual samples (Table 3), where any re-equilibration between reduced and oxidized carbon species should be most pronounced. Collectively, these indicate a mean $\Delta^{13}C$ of 23.4‰, closely comparable to the bulk $\Delta^{13}C$ value. This confirms the validity of the latter value and demonstrates

that, for most samples, diagenetic and metamorphic isotopic homogenization has been limited.

5. Discussion

An integral problem in any paleobiological study of particularly ancient rocks is assessing whether the feature under examination, be it isotopes or organisms, is indigenous and syngenetic. Any rock with an extremely long geologic history has had ample opportunity for post-depositional contamination, and where contents of the material in question are extremely low, the chances of modern adulteration are high. Both of these problems have been encountered in previous organic and isotopic studies of the ~3.8 Ga gniesses of Greenland, with modern organic contaminants, once thought to be syngenetic, occurring abundantly in surface rocks, and massive carbonates, formerly believed to be sedimentary, forming metasomatically near ultramafic igneous rocks. In the case of the Coonterunah rocks, however, such difficulties were not encountered. The Coonterunah carbonates show sedimentary lamination, are interbedded with siliceous sedimentary facies and are kilometres removed from any source of ultramafic metasomatism. The kerogen in the Coonterunah cherts is clearly indigenous because it can be extracted by acid digestion, yielding similar isotopic values to *in situ* treatments that have been carefully manipulated to exclude the possibility of surface contamination. Moreover, carbonate samples also contain kerogen clearly embedded in metamorphosed ferroan dolomite and calcite crystals (Figure 2(c)), indicating its premetamorphic emplacement.

The spread of $\delta^{13}C_{org}$ values provides further evidence for the ancient origin of the Coonterunah organic matter, because if it were modern superficial contamination or ancient post-metamorphic adulteration, it should have a homogeneous isotopic composition. Instead, the isotopic diversity is best interpreted as representing either metamorphic resetting or metabolic disparity. As $\delta^{13}C_{org}$ ranges between -47‰ and -5‰ with a mode around -25‰, a purely biological explanation would have to invoke three distinct mechanisms of isotopic fractionation. The -25‰ mode could be the product of oxygenic photosynthesis by cyanobacteria using RuBisCO which imparts a

~25‰ total fractionation from dissolved CO_2, as seen here. Some of this primary production could then have been remineralized by methanogenic Archaea, which have a cellular biomass markedly lighter than the consumed organic matter, yielding the few values between -37‰ and -47‰. The heavy values between -15‰ and -5‰ could be the result of anoxygenic photosynthesis by green or purple sulphur bacteria, an autotrophic process with a smaller associated isotopic fractionation than its oxygenic equivalent. However, the range and extremity of heavy values observed make this rather unlikely as no form of photosynthesis yields organic matter heavier than dissolved CO_2, which would have been around -10‰ for carbonates near 0‰ (Des Marais, 1997). Instead, it is more plausible that differing degrees of maturational decarbonation of light hydrocarbons and metamorphic re-equilibration with heavy carbonates were responsible for the spread of heavy values. Though attempts were made to sample only lower grade rocks, the regional metamorphic grade, mid-greenschist to lower amphibolite facies, is right at the point where profound isotopic adjustments start to occur (Hayes *et al.*, 1983; Des Marais *et al.*, 1992; Des Marais, 1997). It is unlikely that the population around the mode of -25‰ also represents metamorphically reset kerogen that was originally very much lighter, of similar isotopic composition to the light subpopulation near -40‰, as the major modal cluster is large and distinct, without a skewed tail trailing towards the lighter mode.

The carbonates show a distinct similarity to younger Archean carbonates associated with BIFs. A trend in $\delta^{13}C_{carb}$ values from close to 0‰ to lighter values to -4‰ is evident in the Hamersley Group (Kaufman *et al.*, 1990), where it has been attributed to deposition in deeper water below a redox chemocline with increasing proportions of bicarbonate derived from recycled light organic matter. As the Coonterunah carbonates were apparently deposited in a similar environment and are associated with magnetite-grunerite cherts, a similar origin could be invoked. A metamorphic origin for the trend is unlikely, as the carbonates contain little kerogen and have many orders of magnitude more of the oxidized species than the reduced, providing a robust buffer to isotopic re-equilibration. If so, the initial oceanic $\delta^{13}C_{carb}$ ratio was probably around the heaviest $\delta^{13}C_{carb}$ value observed, about -1‰. This would

accord with estimates of near 0‰ obtained from somewhat younger Archaean shallow-marine carbonates (Veizer *et al*., 1989).

It is possible to erect a set of criteria for recognizing biogenic signatures in carbon isotopes very early in Earth's history when abiotic contributions may have been more significant than now. These are listed in order of increasing rigour, with only criterion 5, where both reduced and oxidized species are congruently preserved together, representing the highest likelihood of biogenicity. As most of the criteria are based on statistical parameters, sample numbers ($n > 10$) and sizes (CO_2 yield > 0.3 μmoles) have to be sufficiently large for robust analysis.

1. Organic negativity - because carbonaceous chondritic meteorites, mantle-derived diamonds and prebiotic organic syntheses all produce solid organic carbon with $\delta^{13}C_{org}$ values in the range -15‰ to 0‰, values should be lighter than this range (<-15‰), especially at low TOC (<0.1%);
2. Kerogen consistency - because abiogenic organic carbon tends to be broadly spread about a mean, the standard deviation should be low (<5) indicating high kurtosis;
3. Carbonate coherence - because biogenic fractionations over the past 800 Ma have ranged between 22‰ and 32‰ (Hayes *et al*., 1999) but inorganic carbonates and organics are generally fractionated less than this, the gross bulk fractionation between $\delta^{13}C_{org}$ and $\delta^{13}C_{carb}$ ($\Delta^{13}C$) from a single suite of rocks should be >20‰;
4. Complementary skewness - because metamorphic re-equilibration tends to skew the isotopic distribution to one side of the mean, if any skewness occurs, it should be positive around $\delta^{13}C_{org}$ modes and negative for $\delta^{13}C_{carb}$;
5. Fractionation congruency - because metamorphic resetting should be most evident in rocks with coexisting kerogen and carbonate, the standard deviation for the population of individual sample $\Delta^{13}C$ values should be low (<5).

The Coonterunah isotopic values satisfy all 5 of these criteria, so they evidently indicate biogenic carbon isotopic fractionation. It is thus reasonable to consider the

sorts of metabolic processes that might have been operative in early Archean ecosystems. The $\Delta^{13}C$ fractionation clearly represents autotrophic carbon-fixation which, given its magnitude and moderate metamorphic resetting, probably signifies the Calvin-Benson cycle using the enzyme ribulose-bisphosphate carboxylase-oxygenase (RuBisCO). This, however, need not have been oxygenic photosynthesis; indeed, it need not have been photosynthesis at all. Many forms of autotrophy employ this mechanism for carbon fixation, and so other geochemical evidence (*e.g.* Hayes, 1983; Buick, 1992; Brocks *et al*., 1999) is needed before oxygenic photosynthesis can be recognized. The minor modes in the $\delta^{13}C_{org}$ distribution may also represent distinct metabolic processes. The light mode possibly indicates methanogenesis, as values lighter than -40‰ are beyond the range of fractionation imparted by any form of photosynthesis but are characteristic of biogenic methane production. Given the sparse data, it is impossible to determine whether this methanogenesis relied on the heterotrophic breakdown of primary autotrophic production (organic recycling) or autotrophic redox reactions involving simple gas species (chemolithotrophy). It does not necessarily also imply oxidative methylotrophy as a means of fixing the light methane isotopic signature into biomass, because one class of methanogens, the methylotrophic methanogens which split methyl groups from simple methylated molecules to produce methane (Summons *et al.*, 1999). The heavy mode, as mentioned above, probably does not reflect the activities of green or purple sulfur bacteria metabolizing photosynthetically, which tend to produce organic matter lighter than -10‰. Given the broad spread of values and their extreme enrichment in ^{13}C, this mode is more likely to represent metamorphosed organic matter initially derived from other sources.

The secular distribution of sedimentary carbon isotope values for rocks older than 1 Ga is plotted in Figure 4. It can be seen that the Coonterunah kerogens and carbonates are not too dissimilar to those from other early Archaean successions. The carbonates are a bit lighter than those from shallow marine facies, such as the ~3.46 Ga Warrawoona Group, but are similar to those derived from deeper-water BIF successions. This difference is also manifest in mineralogy, with the shallow marine

carbonates dominatly composed of dolomite, whereas the deeper water facies, including the Coonterunah carbonates, are calcitic. The Coonterunah kerogens are a bit heavier than most comparable early Archaean organic carbon, though not markedly so. This may reflect their higher metamorphic grade than most, but as the coexisting kerogen-carbonate pairs show little sign of metamorphic re-equilibration, this may instead be a primary environmental or biological indicator. As there are several other deep-water successions represented in the early Archaean carbon isotope record, it seems unlikely to be a simple factor of depositional environment. It could possibly indicate lower levels of dissolved CO_2 in the water mass, as isotopic discrimination during microbial autotrophy diminishes with CO_2 availability (*e.g.* Calder & Parker, 1978; Des Marais *et al.*, 1989). It might also indicate a greater input of biomass from non-cyanobacterial microbial autotrophs (*e.g.* Ruby *et al.*, 1987; Des Marais *et al.*, 1989). Lastly, it may simply reflect lower levels of methanogenic recycling than in other Archaean successions (*e.g.* Hayes, 1983; 1994), though the presence of an apparently methanogenic light mode in the Coonterunah kerogen data would suggest otherwise. Regardless, a rather more refined instrument than carbon isotopes is needed to resolve the problem.

When comparing the Coonterunah with the ~3.8 Ga Itsaq data, it is striking that organic polymodality is a common feature. If the Itsaq data does indeed, in whole or in part, represent biological activity, then this perhaps reveals that early Archaean microbial ecosystems had more complex isotopic partitioning than occurs in younger settings. At present, carbon isotopic signatures are overwhelmingly dominated by biomass generated by oxygenic photosynthesis, producing unimodal isotopic signatures. As the secondary modes in Archaean isotopic distributions possibly represent diverse autotrophic and heterotrophic pathways, this suggests that biomass generation and recycling was not so simple. As many of these possible pathways are anaerobic or microaerophilic, this scenario would accord with the model of a less oxygenated early Earth that is widely, but not universally, upheld.

At present, it seems unlikely that older incontrovertible carbon isotope evidence for the existence of primordial life will be found in rocks that are currently known. All

more ancient successions lack coexisting sedimentary carbonates and kerogen, though they may have one or the other. Moreover, they have all suffered greater metamorphism and deformation, beyond the degree where substantial resetting of carbon isotopic values applies. Morphological evidence for life is very unlikely to survive such conditions. Though it is not inconceivable that older low-grade rocks will be discovered; indeed the Coonterunah Group was not recognized as being older and better preserved than other Pilbara greenstones until 1995; the co-occurrence of sedimentary carbonates and kerogens is not overly common in Archean successions generally. Though many Archean terrains are still poorly mapped and dated, it is likely that particularly ancient low-grade successions remain to be discovered only in cratons that are generally mildly metamorphosed and very old. Thus, this Coonterunah data might be as old as it gets. If so, it would be unfortunate for science, because most of the really interesting questions about the early evolution of life lie in the preceding billion years of Earth's history, when life itself began, diversified and developed the complex metabolic pathways already in evidence by the dawn of the biogeochemical record.

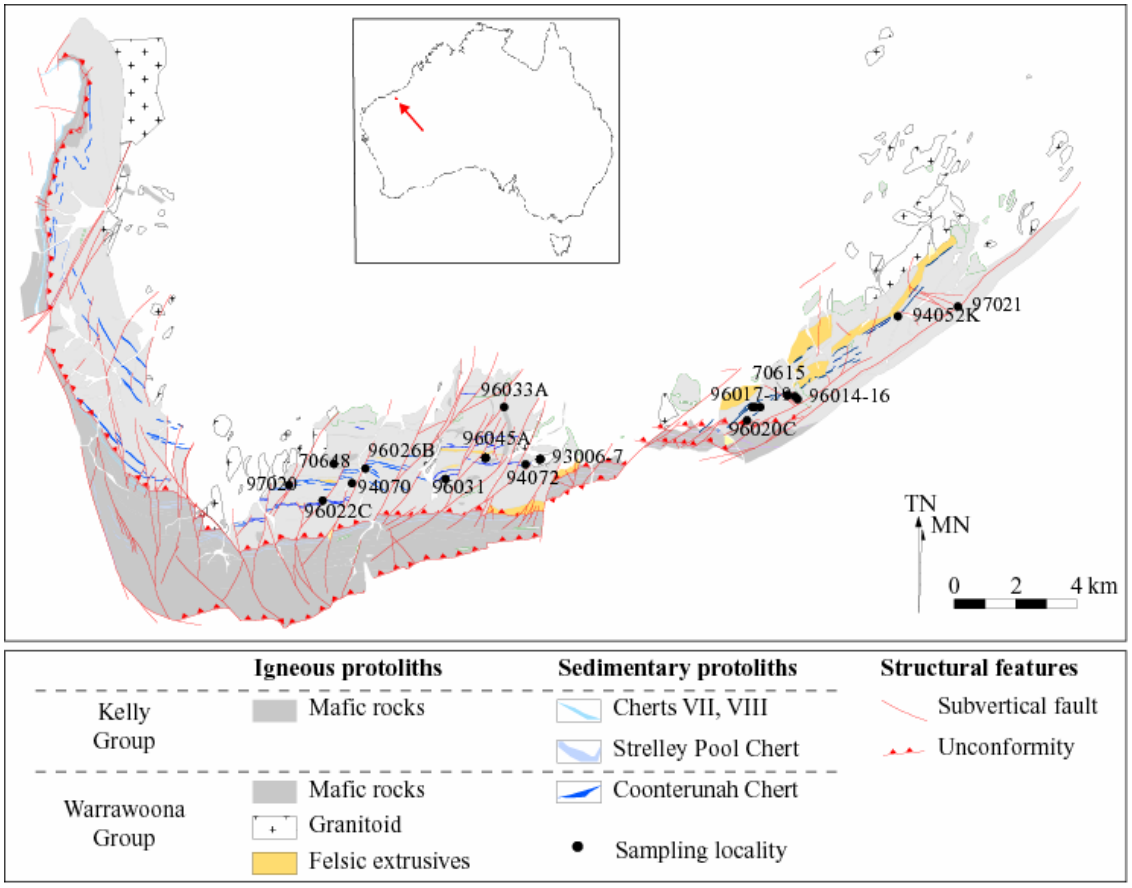

Figure 1: Geological map of the Pilgangoora Belt and Coonterunah Subgroup, showing sample sites.

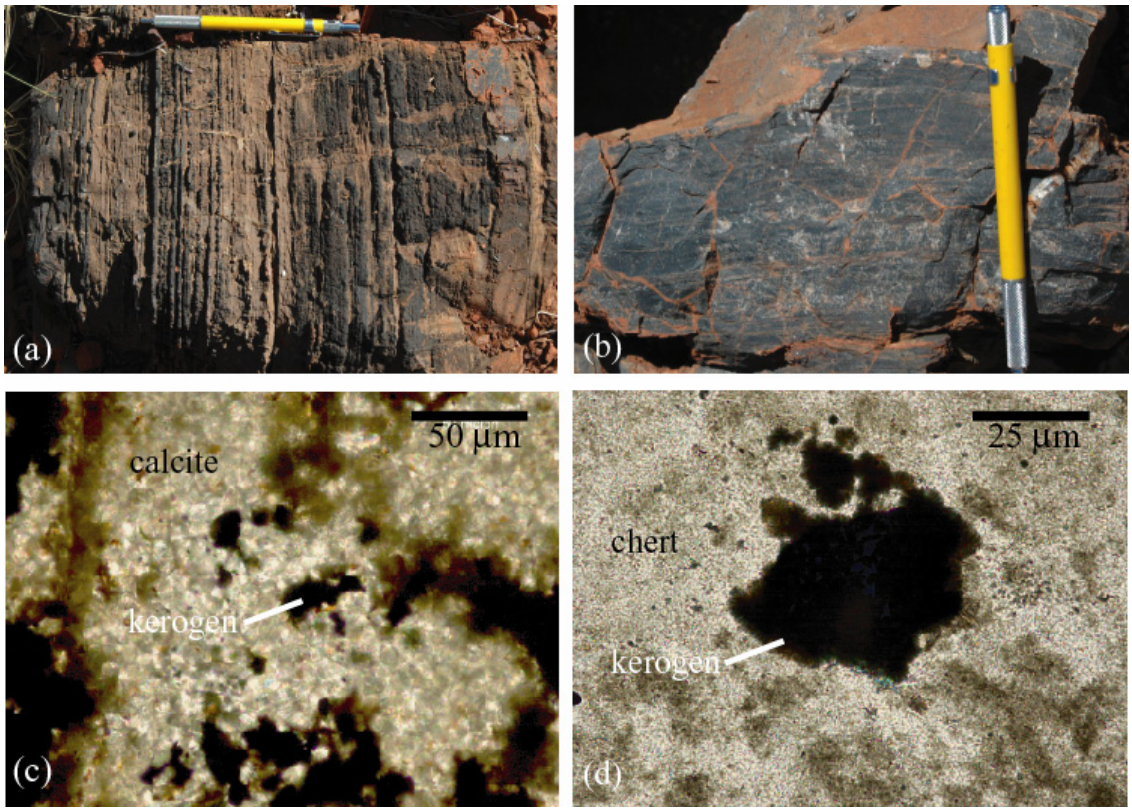

Figure 2: (a): Laminated carbonate in outcrop. (b): Banded chert in outcrop. (c): Thin-section of laminated carbonate. (d): Thin-section of chert-hosted kerogen**.**

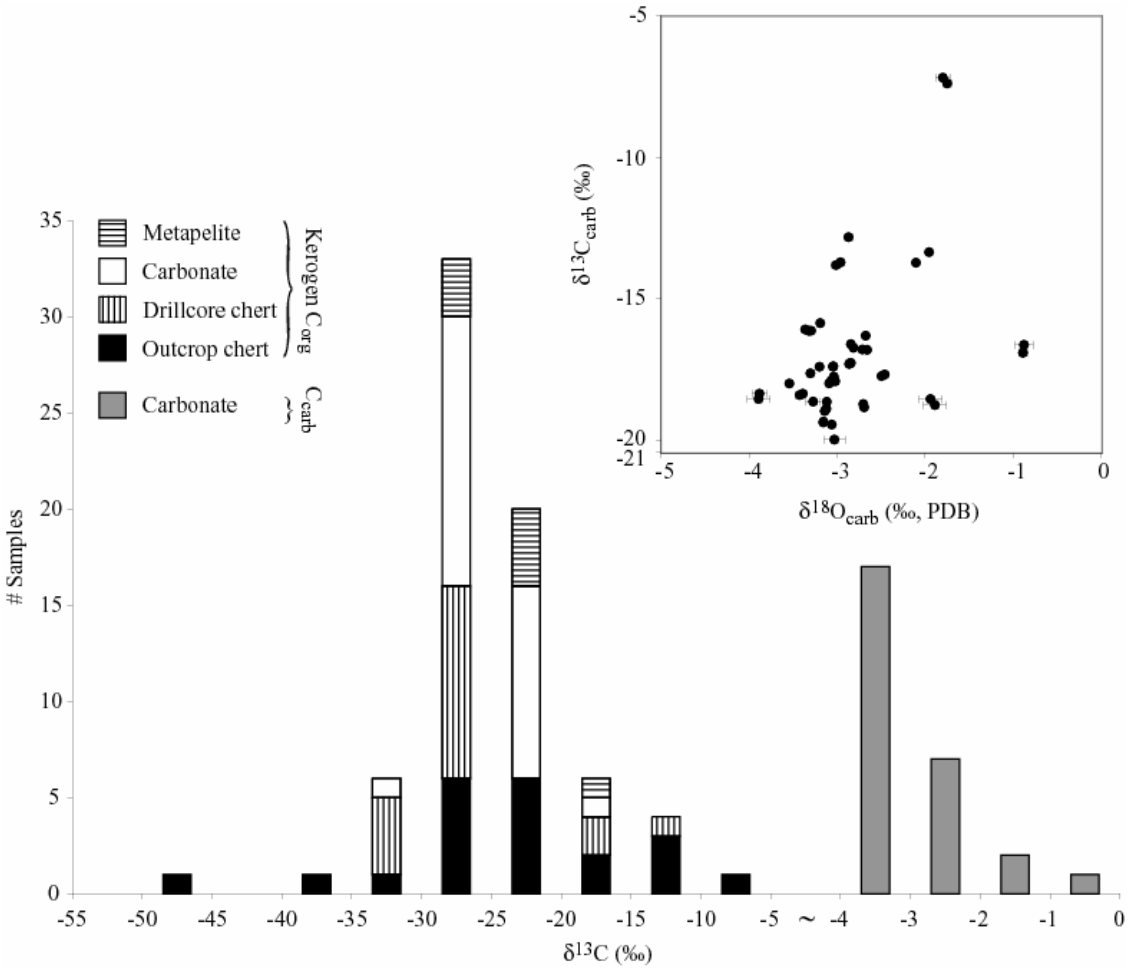

Figure 3: Carbon isotopic data from Coonterunah Subgoup. Inset shows cross-plot of $\delta^{18}O_{carb}$ vs. $\delta^{13}C_{carb}$.

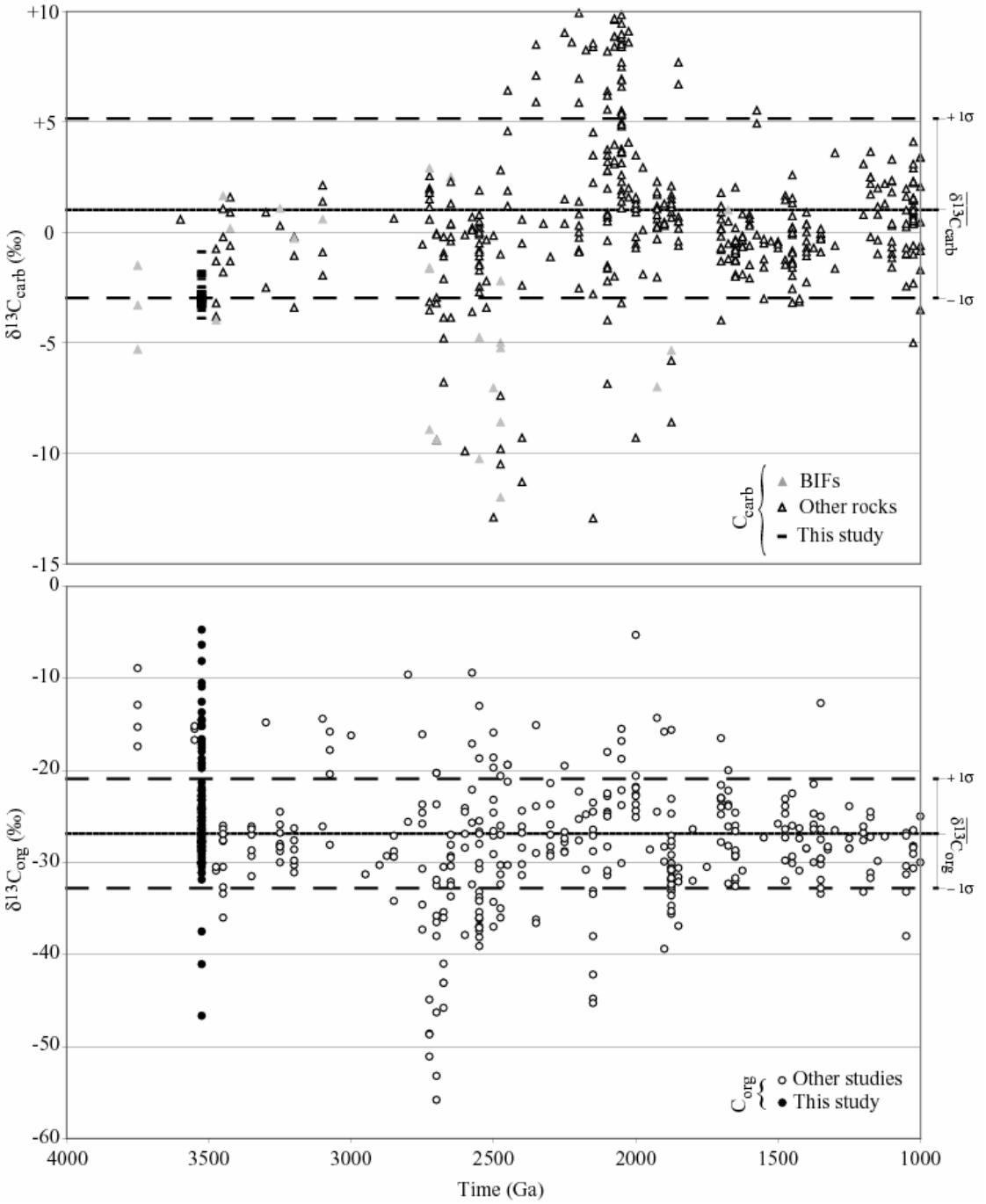

Figure 4: Secular trends in carbon isotopes before 1 Ga.

Table 1: Coonterunah kerogen $\delta^{13}C_{org}$ data. Suffix "K**"** in sample label indicates macerated kerogen, others are decarbonated whole-rock analyses, suffix "rep" indicates replicate analysis, suffix "lam" indicated microdremel laminar analysis. Laminar analyses are treated as distinct samples in calculation of averages.

Rock-type	Sample	Size (mg)	CO_2 yield (µmoles)	$\delta^{13}C_{org}$ (‰, VPDB)	± σ (‰)	Sample average (‰)
Chert-hosted kerogen	70615	249.6	2.9	-8.13	0.05	**-7.25**
	70615 rep1	196.3	1.11	-6.36	0.11	
	70615K	1.2	0.38	-22.76	0.11	**-22.76**
	70648	207	0.57	-27.52	0.11	**-27.52**
	70648K	0.4	0.58	-27.66	0.12	**-27.66**
	93007	200.5	0.36	-27.91	0.11	**-27.91**
	94052K	1.4	31.99	-28.87	0.08	**-28.87**
	94053 5sec	200.1	0.60	-30.50	0.09	**-30.56**
	94053 10sec	195.4	0.72	-31.11	0.07	
	94053 15sec	221.9	1.37	-31.86	0.08	
	94053 20sec	220.3	1.23	-29.06	0.08	
	94053 25sec	199.9	0.88	-30.29	0.07	
	96014	205.4	1.47	-22.8	0.06	**-22.80**
	96016	218.6	2.2	-14.48	0.11	**-14.48**
	96017B	208.3	14.87	-4.72	0.08	**-4.72**
	96018	197.3	1.27	-27.3	0.08	**-27.30**
	96019A	99.2	0.81	-12.55	0.08	**-11.53**
	96019A rep1	196.7	1.47	-10.5	0.07	
	96020C	105.7	0.49	-22.09	0.08	**-20.93**
	96020C rep1	201.7	0.82	-19.76	0.07	
	96022C	213.5	2.7	-10.92	0.08	**-10.92**
	96031	206	0.61	-25.42	0.11	
	96031 rep1	202.6	0.58	-24.31	0.16	**-24.87**
	97020A*	225.3	7.13	-46.66	0.08	**-46.66**
	97020B*	200.0	4.93	-41.07	0.04	**-39.29**
	97020B rep1	220.6	3.73	-37.50	0.07	
	97021*	204.5	9.78	-19.5	0.09	**-19.50**
	PC03-104	0.8	20.70	-23.78	0.38	**-23.78**
	PC03-119	2.8	0.20	-23.96	0.13	**-23.59**
	PC03-119 rep1	9.9	0.31	-23.22	0.13	
	PC04-005	13.1	1.77	-25.07	0.37	**-25.27**
	PC04-005 rep1	6.1	1.06	-26.01	0.37	
	PC04-005 rep2	10.0	0.94	-24.75	0.37	
	PC04-113	6.3	2.59	-17.95	0.38	**-17.16**
	PC04-113 rep1	19.4	6.95	-16.61	0.38	
	PC04-113 rep2	14.7	5.32	-16.91	0.38	
	Mean			***-23.33***	***9.21***	***-22.97***

Table 1 (cont'd).

Rock-type	Sample	Size (mg)	CO_2 yield (µmoles)	$\delta^{13}C_{org}$ (‰, VPDB)	± σ (‰)	Sample average (‰)
Carbonate-hosted kerogen	93006K	9.9	0.98	-26.65	0.08	**-24.88**
	93006K rep1	11.4	1.12	-23.1	0.04	
	96045AK	17.2	2.19	-24.27	0.09	**-23.57**
	96045AK rep1	12.4	4.72	-22.87	0.07	
	96045BK	4.2	7.24	-28.77	0.06	**-28.77**
	PC05-020A blk	5.0	3.90	-28.77	0.12	**-28.77**
	PC05-020B lam1	27.8	5.10	-25.34	0.12	**-25.34**
	PC05-020B lam2	24.1	5.17	-27.34	0.12	**-27.34**
	PC05-020B lam3	24.6	5.76	-26.49	0.65	**-26.49**
	PC05-020B lam4	15.2	4.22	-24.29	0.35	**-24.29**
	PC05-020B lam5	15.2	15.53	-29.63	0.35	**-29.63**
	PC05-020C lam1	32.0	5.57	-27.21	0.12	**-27.21**
	PC05-020C lam2	14.4	1.93	-27.67	0.12	**-27.67**
	PC05-020C lam3	21.0	2.08	-27.03	0.65	**-27.03**
	PC05-020C lam4	23.2	4.83	-26.26	0.35	**-26.26**
	PC05-020C lam5	22.5	4.37	-26.33	0.35	**-26.33**
	PC05-020C lam6	24.4	5.46	-27.11	0.35	**-27.11**
	PC05-020C lam7	8.0	0.68	-24.53	0.09	**-24.53**
	PC05-020C lam8	10.0	0.76	-23.24	0.09	**-23.24**
	PC05-021 lam1	5.7	2.29	-25.17	0.12	**-25.17**
	PC05-021 lam2	11.7	2.12	-31.13	0.12	**-31.13**
	PC05-021 lam3	5.5	2.28	-24.08	0.65	**-24.08**
	PC05-021 lam4	2.9	1.54	-24.20	0.35	**-24.20**
	PC05-021 lam5	0.6	0.31	-22.64	0.09	**-22.64**
	PC05-021 lam6	1.0	0.29	-21.32	0.09	**-21.32**
	PC06-031 lam1	8.3	0.62	-19.22	0.18	**-19.22**
	PC06-031 lam2	1.6	0.35	-23.28	0.18	**-23.28**
	PC06-041 blk	3.1	0.29	-25.53	0.18	**-26.16**
	PC06-041 blk rep1	1.1	0.29	-26.80	0.18	
	Mean			***-25.53***	***2.58***	***-25.60***

Table 1 (cont'd).

Rock-type	Sample	Size (mg)	CO_2 yield (µmoles)	$\delta^{13}C_{org}$ (‰, VPDB)	± σ (‰)	Sample average (‰)
	155.00m	9.2	0.26	-30.10	0.51	**-30.10**
	155.00m rep1	8.9	0.29	-30.10	0.51	
	157.60m	18.9	15.52	-28.29	0.51	**-28.03**
	157.60m rep1	18.2	16.05	-28.30	0.51	
	157.60m rep2	18.9	15.52	-27.80	0.51	
	157.60m rep3	18.2	16.05	-27.73	0.51	
	158.70m	21.0	12.41	-28.40	0.51	**-28.38**
	158.70m rep1	16.1	9.60	-28.14	0.51	
	158.70m rep2	21.0	12.41	-28.28	0.51	
	158.70m rep3	16.1	9.60	-28.70	0.51	
	160.40m	15.8	14.36	-28.54	0.51	**-28.29**
	160.40m rep1	17.5	14.86	-28.74	0.51	
	160.40m rep2	15.8	14.36	-27.98	0.51	
	160.40m rep3	17.5	14.86	-27.91	0.51	
	160.70m	23.5	24.59	-28.22	0.51	**-27.33**
	160.70m rep1	23.5	24.59	-26.45	0.51	
	162.40m	18.9	16.10	-27.80	0.51	**-27.76**
	162.40m rep1	18.9	16.10	-27.72	0.51	
	163.40m rep2	9.0	11.28	-27.62	0.51	
	163.40m rep3	18.3	20.06	-27.83	0.51	
	163.40m rep4	9.0	11.28	-28.45	0.51	
	163.40m rep5	18.3	20.06	-27.13	0.51	
	163.70m	17.2	15.77	-27.71	0.51	**-27.77**
	163.70m rep1	17.5	15.08	-27.72	0.51	
	163.70m rep2	17.2	15.77	-27.77	0.51	
	163.70m rep3	17.5	15.08	-27.88	0.51	
	169.45m	9.1	0.61	-27.43	0.51	**-28.36**
	169.45m rep1	10.8	4.88	-28.23	0.51	
	169.45m rep2	10.8	4.88	-29.41	0.51	
	170.75m	12.0	10.06	-29.25	0.51	**-28.59**
	170.75m rep1	11.2	1.58	-27.01	0.51	
	170.75m rep2	12.4	1.69	-26.84	0.51	
	170.75m rep3	12.0	10.06	-28.63	0.51	
	170.75m rep4	11.2	1.58	-29.90	0.51	
	170.75m rep5	12.4	1.69	-29.89	0.51	
	288.55m	7.7	0.40	-30.08	0.51	**-30.09**
	288.55m rep1	5.5	0.27	-30.10	0.51	
	310.53m	2.0	0.21	-30.11	0.51	**-30.09**
	310.53m rep1	3.4	0.53	-30.06	0.51	
	311.64m	3.6	0.56	-13.70	0.51	**-14.12**
	311.64m rep1	3.7	0.54	-14.55	0.51	
	312.32m	1.7	0.40	-17.56	0.51	**-16.39**
	312.32m rep1	2.8	0.52	-15.21	0.51	
	313.37m	2.4	0.36	-18.72	0.51	**-16.67**
	313.37m rep1	6.5	0.49	-14.62	0.51	
	Mean			***-26.78***	***4.30***	***-26.09***

Table 1 (cont'd).

Rock-type	Sample	Size (mg)	CO_2 yield (µmoles)	$\delta^{13}C_{org}$ (‰, VPDB)	± σ (‰)	Sample average (‰)
Metapelite-hosted kerogen	PC06-024B	37.3	0.93	-17.22	0.20	**-16.21**
	PC06-024B rep1	57.3	1.02	-15.21	0.20	
	PC06-024I	17.9	0.34	-21.88	0.20	**-22.03**
	PC06-024I rep1	17.9	0.35	-22.17	0.20	
	PC06-027	4.7	0.32	-24.05	0.20	**-23.14**
	PC06-027 rep1	20.4	0.32	-22.23	0.20	
	PC06-029	11.0	0.28	-25.74	0.20	**-25.58**
	PC06-029 rep1	12.8	0.30	-25.42	0.20	
	PC06-031	8.3	0.62	-19.22	0.13	**-21.25**
	PC06-031 rep1	1.6	0.35	-23.28	0.13	
	PC06-040	33.0	0.30	-24.58	0.13	**-24.37**
	PC06-040 rep1	42.1	0.35	-24.17	0.13	
	PC06-041	3.1	0.29	-25.53	0.13	**-26.16**
	PC06-041 rep1	1.1	0.29	-26.80	0.13	
	PC06-044	3.1	0.27	-25.97	0.13	**-26.14**
	PC06-044 rep1	3.2	0.27	-26.30	0.13	
	Mean			***-23.11***	***3.36***	***-23.11***

Table 2: Coonterunah carbonate $\delta^{13}C_{carb}$ and $\delta^{18}O_{carb}$ data.

Sample	Size (mg)	CO_2 (μmoles)	$\delta^{13}C_{carb}$ (‰)	±1σ (‰)	$\delta^{18}O_{carb}$ (‰, PDB)	±1σ (‰)	Sample average (‰)	
							$\delta^{13}C_{carb}$	$\delta^{18}O_{carb}$
93006	2.90	10.36	-1.94	0.13	-18.55	0.11	-1.92	-18.66
93006 rep1	3.20	12.80	-1.89	0.13	-18.76	0.15		
94070	4.70	25.06	-3.03	0.12	-19.98	0.11	-3.03	-19.98
94072	2.90	15.95	-3.89	0.13	-18.54	0.14	-3.89	-18.54
94072 rep1	3.10	18.10	-3.88	0.08	-18.36	0.14	-3.89	-18.45
96026B	15.00	75.20	-1.75	0.05	-7.38	0.13	-1.78	-7.28
96026B rep1	13.10	62.83	-1.80	0.08	-7.18	0.09		
96033A	15.50	77.41	-3.27	0.08	-18.64	0.09	-3.27	-18.64
96033B	15.80	84.71	-2.96	0.04	-13.71	0.08		
96033B rep1	20.40	20.40	-2.87	0.04	-12.82	0.09	-2.92	-13.27
96045A	23.60	52.96	-0.88	0.10	-16.63	0.1	-0.89	-16.77
96045A rep1	28.40	28.40	-0.89	0.05	-16.91	0.13		
96045B	10.30	48.27	-3.01	0.05	-13.81	0.09	-3.01	-13.81
B55W	0.11	47.86	-3.12	0.03	-18.65	0.04	-3.12	-18.65
B63W	0.19	70.01	-3.09	0.03	-17.99	0.03	-3.08	-17.94
B63W rep1	0.19	64.47	-3.06	0.02	-17.89	0.04		
B75W	0.19	62.17	-3.54	0.03	-18.00	0.02	-3.54	-18.00
B79W	0.73	86.94	-3.05	0.03	-17.41	0.02	-3.04	-17.40
B79W rep1	0.54	84.79	-3.04	0.02	-17.39	0.03		
B80D	0.26	53.09	-3.30	0.04	-17.64	0.03	-3.25	-17.52
B80D rep1	0.31	59.24	-3.20	0.03	-17.41	0.04		
B82W	0.30	72.48	-2.81	0.02	-16.73	0.02	-2.78	-16.55
B82W rep1	0.17	49.24	-2.84	0.02	-16.60	0.03		
B82W rep2	1.27	86.63	-2.67	0.02	-16.30	0.02		
B87W	0.26	76.32	-2.66	0.02	-16.80	0.04	-2.69	-16.80
B87W rep1	0.14	55.70	-2.71	0.02	-16.80	0.03		
B89W	0.17	36.93	-3.39	0.02	-18.36	0.04	-3.41	-18.38
B89W rep1	0.12	23.39	-3.42	0.05	-18.41	0.05		
B90W	0.22	62.32	-2.85	0.01	-17.28	0.03	-2.85	-17.28
B90W rep1	0.14	55.24	-2.86	0.02	-17.31	0.04		
B90W rep2	0.30	68.17	-2.84	0.02	-17.27	0.01		
PC05-020C	0.40	64.45	-3.12	0.02	-18.89	0.04	-3.13	-18.93
PC05-020C rep1	0.58	69.99	-3.14	0.02	-18.98	0.03		
PC06-026	1.74	112.91	-3.29	0.04	-16.13	0.02	-3.24	-16.00
PC06-026 rep1	1.01	106.77	-3.19	0.03	-15.86	0.02		
PC06-028A	0.67	42.09	-3.06	0.02	-19.45	0.02	-3.06	-19.45
PC06-028B-i	0.71	74.74	-3.15	0.01	-19.35	0.04	-3.16	-19.36
PC06-028B-i rep1	0.43	68.96	-3.16	0.02	-19.38	0.03		
PC06-028B-ii	1.27	50.09	-3.04	0.01	-17.76	0.04	-3.03	-17.84
PC06-028B-ii rep1	1.28	47.12	-3.02	0.02	-17.92	0.04		
PC06-031	0.41	43.65	-2.49	0.04	-17.73	0.04	-2.48	-17.71
PC06-031 rep1	2.00	48.00	-2.46	0.04	-17.68	0.03		
PC06-041	2.31	67.17	-3.36	0.03	-16.08	0.01	-3.34	-16.11
PC06-041 rep1	1.69	67.52	-3.32	0.03	-16.13	0.03		
PC06-045	4.56	115.40	-1.96	0.01	-13.35	0.02	-2.03	-13.54
PC06-045 rep1	2.72	121.12	-2.10	0.02	-13.72	0.01		
PC06-053	0.51	72.85	-2.70	0.02	-18.73	0.03	-2.70	-18.78
PC06-053 rep1	0.30	70.28	-2.69	0.01	-18.84	0.03		

Table 3: Coonterunah $\Delta^{13}C$ data.

Sample	**$\delta^{13}C_{org}$** (‰)	**$\delta^{13}C_{carb}$** (‰)	**$\Delta^{13}C$** (‰)
96006K	-26.65	-1.89	24.76
96006K rep1	-23.1	-1.94	21.16
96045AK	-24.27	-0.88	23.39
96045AK rep1	-22.87	-0.89	21.98
96045BK	-28.77	-2.94	25.83
PC05-020 avg	-26.52	-3.13	23.39
Mean (n=5)	*-25.36*	*-1.94*	*23.42*
Bulk analyses	*-25.12*	*-2.91*	*22.75*

References

Brocks, J.J., Logan, G.R., Buick, R. & Summons, R.E. (1999) *Science* **285**, 1033-1036.

Buick, R. (1992) *Science* **255**, 74-77.

Buick, R. (2001) in *Palaeobiology II*, eds. Briggs, D.E.G. & Crowther, P.R. (Blackwell, Oxford), pp. 13-21.

Buick, R., Des Marais, D.J. & Knoll, A.H. (1995) *Chem. Geol.* **123**, 153-171.

Buick, R., Rasmussen, B. & Krapez, B. (1998) *AAPG Bull.* **82**, 50-69.

Buick, R., Thornett, J.R., McNaughton, N.J., Smith, J., Barley, M.E. & Savage, M. (1995) *Nature* **375**, 574-577.

Calder, J.A. & Parker, P.L. (1978) *Geochim. Cosmochim. Acta* **37**, 133-140.

Des Marais, D.J. (1997) *Org. Geochem.* **27**, 185-193.

Des Marais, D.J., Cohen, Y., Nguyen, H., Cheatham, M., Cheatham, T. & Munoz, E. (1989) in *Microbial Mats: Physiological Ecology of Benthic Microbial Communities*, eds. Cohen, Y. & Rosenberg, E. (American Society for Microbiology, Washington), pp. 191-205.

Des Marais, D.J., Strauss, H., Summons, R.E. & Hayes, J.M. (1992) *Nature* **359**, 605-609.

Eiler, J.M., Mojzsis, S.J. & Arrhenius, G. (1997) *Nature* **386**, 665.

Green, M.J., Sylvester, P.J. & Buick, R. (2000) *Tectonophys* **322**, 69-88.

Hayes, J.M. (1983) in *Earth's Earliest Biosphere*, ed. Schopf, J.W. (Princeton Univ. Press, Princeton), pp. 291-301.

Hayes, J.M. (1994) in *Early Life on Earth Nobel Symposium*, ed. Bengtson, S. (Columbia Univ. Press, New York), pp. 220-236.

Hayes, J.M., Kaplan, I.R. & Wedeking, K. (1983) in *Earth's Earliest Biosphere*, ed. Schopf, J.W. (Princeton Univ. Press, Princeton), pp. 93-134.

Hayes, J.M., Strauss, H. & Kaufman, A.J. (1999) *Chem. Geol.* **161**, 103-125.

Kaufman, A.J., Hayes, J.M. & Klein, C. (1990) *Geochim. Cosmochim. Acta* **54**, 3461-3473.

Lepland, A., van Zuilen, M.A., Arrhenius, G., Whitehouse, M.J. & Fedo, C.M. (2005)

Geology **33**, 77-79.

Lowe, D.R. (1994) *Geology* **22**, 387-390.

Mojzsis, S.J., Arrhenius, G., McKeegan, K.D., Harrison, T.M., Nutman, A.P. & Friend, C.R.L. (1996) *Nature* **384**, 55-59.

Moorbath, S. (2005) *Nature* **434**, 155.

Robl, T.L. & Davis, B.H. (1993) *Org. Geochem.* **20**, 249-255.

Rose, N.M., Rosing, M.T. & Bridgwater, D. (1996) *Am. J. Sci.* **296**, 1004-1044.

Rosing, M.T., Rose, N.M., Bridgwater, D. & Thomsen, H.S. (1996) *Geology* **24**, 43-46.

Rosing, M.T. (1999) *Science* **283**, 674-676.

Ruby, E.G., Jannasch, H.W. & Deuser, W.G. (1987) *App. Microbiol.* **53**, 1940-1943.

Schidlowski, M. (1988) *Nature* **333**, 313-318.

Schidlowski, M., Appel, P.W.U., Eichmann, R. & Junge, E. (1979) *Geochim. Cosmochim. Acta* **43**, 189-199.

Summons, R.E., Franzmann, P.D. & Nichols P.D. (1998) *Org. Geochem*. **28**, 465-475.

Ueno, Y., Yurimoto, H., Yoshioka, H., Komiya, T. & Maruyama, S. (2002) *Geochim. Cosmochim. Acta* **66**, 1257-1268.

van Zuilen, M.A., Lepland, A. & Arrhenius G. (2002) *Nature* **418**, 627-630.

Veizer, J., Hoefs, J., Lowe, D.R. & Thurston P.C. (1989) *Geochim. Cosmochim. Acta* **53**, 859-871.

7. Early Archaean Oncoidal Trace Fossils

1. Introduction

Prudence is warranted when considering the early evolution of the biosphere. Evidence for early Archaean life is highly ambiguous, however. Purported microfossils (Schopf and Packer, 1987; Schopf et al., 2002) are, to say the least, controversial (Brasier et al., 2002; Brasier et al., 2005). Although seemingly compelling, structures of purported stromatolitic origin (Lowe, 1980; Hofmann et al., 1999; Allwood et al., 2006) remain open to non-biological interpretations in the absence of microfossil or microbial palimpsest proof of biogenic accretion (Buick et al., 1981; Lowe, 1994; Grotzinger and Rothman, 1996; Grotzinger and Knoll, 1999). For microtubules and pitted microfabrics in Archean basalts and silicified sandstones that have been interpreted as endolithic microborings (Furnes et al., 2004; Banerjee et al., 2006; Brasier et al., 2006; Wacey et al., 2006), it is often difficult to establish their biogenic origin and ancient age (McLoughlin et al., 2007). Chemical evidence of life is also susceptible to ambiguity (e.g. contamination, abiotic non-equilibrium processes: Chapter 3). Isotopically depleted graphite at Isua (Rosing, 1999) may have arisen through the non-biological decarbonation of siderite (van Zuilen et al., 2002; van Zuilen et al., 2003) or through non-equilibrium thermodynamics (Chapter 3). Isotopically depleted kerogen at Barberton and in the Pilbara could be the product of ancient Fischer-Tropsch-type synthesis (Ueno et al., 2001; Brasier et al., 2002; Ueno et al., 2003; Ueno et al., 2004; Brasier et al., 2005). Although sulphur isotopic evidence is more persuasive of biological processing (Shen et al., 2001), debate continues

regarding the type of ancient sulphur cycling and the isotopic fractionation incurred (Philippot et al., 2007; Ueno et al., 2008; Shen et al., 2009).

2. Oncoids

Biogenic coated grains are a common feature in many modern environments ranging from marshes, streams and freshwater lakes to inter- and sub-tidal marine settings (Flügel, 1982). Such biogenic concretions are termed 'oncoids' and are characterized by concentric growth of alternating organic and mineral laminae that have inconsistent thickness and trancating relationships, unlike the abiotically precipitated concentric laminae in ooids and pisoids. Oncoids form by adhesion of fine grains of sediment to the mucilaginous surface of microbial biofilms growing on the surface of larger sediment grains, commonly after carbonate precipitation through metabolic alkalinity production. Because commonly associated with photosynthesis, a depositional depth between 0 and 100 m is often assumed for modern marine oncoids. Homogeneous concentric overgrowth – whether phototrophic or chemotrophic - on all sides of an oncoid requires consistent nodule turning, which is facilitated by a sloping substrate, waves and/or tidal currents.

Although a rich diversity of oncoid growth forms are encountered today, only spongiostromate and micritic forms existed prior to the Neoproterozoic-Cambrian transition. Hitherto, the oldest known oncoid occurrence came from the late Palaeoproterozoic of South Africa (Schaefer et al., 2001; Gutzmer et al., 2002).

3. Geological Settings

3.1. Barberton

Barberton oncoids were discovered near the top of the >3453 ± 3 Ma (Armstrong et al., 1990) H3C carbonaceous sedimentary chert unit in Barberton's Hooggenoeg Formation, which lies in the Onverwacht Group near the base of the Swaziland Supergroup. The oncoids occur on the western limb of the Onverwacht anticline, ~2 km west of the fold hinge (Figure 1). In this location, the H3C chert overlies a patchily metasomatized volcanic pile of unvariolitic pillowed basalt, with random komatiitic spinifex texture developed immediately below the conformably overlying chert. The chert itself, ~15 m thick, consists of a ~10 m basal unit of variably silicified volcanogenic lithofacies, dominated by silicified mafic ash. Black chert occurs with increasing prominence towards the top of the H3C, forming the top ~5 m. Komatiitic basalt of the H4 member conformably overlies the oncoid-bearing black chert. The presence of chlorite ± epidote ± actinolite in associated basalts indicates that Barberton oncoids were metamorphosed to greenschist facies conditions.

3.2. Pilbara

Oncoids have been discovered from two seperate formations in the Pilbara Supergroup. The ~3.48 Ga Dresser Formation in the North Pole Dome of the Pilbara Craton contains oncoids in shallow-marine silicified sediments deposited in a tidal flat/evaporite pond environment (Groves et al., 1981; Buick and Dunlop, 1990). The oncoids occur in massive lenticular beds of stromatoloidal intraclastic rudite up to 1.5

metres thick, together with multilaminate curved clasts of extremely tabular aspect that are interpreted as desiccated and ripped-up microbial mats. Such beds concordantly overlie stromatolites (Buick et al., 1981) and concordantly underlie dolomitic banded chert that is unsilicified carbonate in subsurface drill-cores (Philippot et al., 2007).

The Pilbara's Pilgangoora Syncline preserves an angular unconformity (Buick et al., 1995) between ~3.52 Ga underlying deep-marine mafic and felsic volcanics, chemical precipitates and rarely preserved volcanoclastics of the Coonterunah Group and overlying shallow marine and intermittently sub-aerial (Lowe, 1983) sedimentary units of the Strelley Pool Chert ('SPC') and higher volcanic units of the ~3.35 Ga (Banerjee et al., 2007) Kelly Group. Extending downwards from and perpendicular to the sub-vertically dipping Coonterunah-Kelly unconformity are several suites of irregularly spaced ancient Neptunian fissures (Figure 2, 3, see also Chapter 2B). These fissures developed in response to crustal flexure associated with doming induced by the intermittent intrusion of several granitoid suites of varying age and depth. Doming, which commenced with intrusion of the 3.468 Ga ± 4 Carlindi batholith, led to shoaling of the Kelly depositional system during fissuring. Fissures are commonly irregularly spaced on the order of ~100s m apart (e.g. Figure 3). Fissure formation and infill dates to the time of SPC sedimentation: clastic fissure material is demonstrably derived from the overlying seafloor, being identical to material in particular lithofacies of the overlying SPC (Harnmeijer & Buick, in prep.). Where well-preserved, fissures vary in depth between 250 and 750 m, with a width of 3-5 m in contact with SPC. Fissures thin gradually downwards, commonly abruptly shrinking entirely from a width of 1-2 m

within the lowest 10 m. The presence of pumpellyite restricts Pilbaran oncoid metamorphism to sub-greenschist facies conditions.

Oncoids have been observed in younger Neptunian fissures elsewhere (Cavalazzi et al., 2007), where their distinctively high porosity and resultant low density (Verrecchia et al., 1997) restricts their occurrence to the upper levels, as also observed in the Pilbara.

4. Descriptions

Oncoids at all locales are preserved in breccia. Early and pervasive silicification allowed exceptionally good preservation and minimal compression, as shown by the lack of a preferred elongation direction in Barberton (Figure 4) and Pilbara (Figure 5) oncoids. No branching, columnar or lobate growth forms are present, and all lack evidence of radial microfabrics. With the exception of organically cemented agglomerations that numerically comprise ~5% of Barberton oncoids (Figure 4 (a, b)), all are unattached.

Pilbara oncoids vary between 0.5 and 2 mm, are not grain-supported and volumetrically comprise 10-15% of the rock. The larger and less sorted Barberton oncoid grains are of pisoid size, mostly ranging between 0.5 and 5 mm although smaller disrupted clasts abound, and being nearly grain-supporting, their host rock may fairly be termed an ‘oncolite’ (Catalov, 1983).

Oncoid outer surfaces at all locales are smooth, defined by laminar fabric and are subspherical to ovoidal in shape, suggesting growth in a relatively high-energy

environment. Diagenesis likely occurred in low intertidal to shallow subtidal settings, compatible with inferred depositional environments for their host lithofacies (Lowe, 1983; Lowe and Byerley, 1999). But even today, such environments rarely preserve oncoids (Flügel, 2004).

Cortical lamellae consist of well-defined alternating light-dark couplets, occasionally singular but more commonly multiple (up to five, seven and eight in oncoids from the Dresser, Strelley Pool Chert and Hooggenoeg Formations, respectively). Light lamellae are usually 2 to 3 times thicker than dark ones, ranging from 0.02-0.06mm compared to 0.01-0.02mm for dark lamellae. Though mostly of nearly uniform thickness, many vary laterally in thickness by up to 100%. They are generally smooth but may be gently undulose to slightly wrinkly. Individual lamellae are frequently discontinuous, non-concentric and with occasional micro-unconformities in denser fabric. A tendency towards increased sphericity during growth is also apparent. These features are strongly suggestive of biogenic accretion around a clastic nucleus. Barberton oncoid agglomerations, furthermore, show renewed growth after reworking and transport.

Only silica casts and fluid inclusions remain of minerals entrained within the finely dispersed wispy kerogenous lamellae, giving rise to high reflectance (Figure 5 (f)). Crystal sizes range from ~0.5 to 5 μm, with a dominant mode around ~1 μm. Minerals interfacial angles are well preserved (Figure 3 (e)), allowing cubic sulphide and octahedral magnetite habits to be ruled out. The trigonal rhombohedral crystals of

dolomite or calcite are more likely. Unfortunately, no chemical remnants could be discovered with either SEM or WDS microprobe imaging.

Nuclei at all locations are distinct, with nucleus shape determining overall oncoid grain shape. Lamellar coatings are typically distributed asymmetrically about the nuclear core, although this phenomenon is cryptic in thinly coated grains. With few exceptions, Pilbara oncoid nuclei now comprise coarse drusy quartz (likely Tertiary), commonly bearing ~10 μm carbonate inclusions and occasional similarly sized anhedral Fe-dolomite grains. Nuclear pseudomorph crystal shapes, dominantly euhedral, are highly variable. A diverse array of lithic fragments evidently seeded oncoid growth.

Barberton oncoid nuclei are pervasively sericitized but are usually less coarsely silicified, allowing determination of lithic fragment identity. Although highly variable, many of these nuclei are derived from mafic volcanics. In contrast to their Pilbara counterparts, a majority of Barberton nuclei are distinctly rounded, resembling mafic vitric arenite grains. Also present are variably textured shards, ranging from blocky-equant to irregular and elongate cuspate forms. Pseudomorphs after feldspar laths are common.

5. Interpretation

In order to rule out a non-biological origin, the oncoids must be distinguished from superficially similar structures. The alternate term ‘oncoloid’ has been employed for coated particles resembling oncoids, but of either non-biological or unknown origin

(Dahanayake and Krumbein, 1986). Alternatives to biogenic oncoids include ooids, vadoids, vesicles, spherules and accretionary lapilli. The degree of preservation is sufficiently good to allow these candidates to be ruled out.

The oncoids reported here are distinctly non-spherical and non-ellipsoidal, and often exhibit kinked cortices. There is no dominant flattening direction, and cortical angularities suggest very little flattening whatsoever occurred. Lamellae are frequently irregular and nonconcentric, unlike smaller and more regular ooids and vadoids (Lyell, 1859; Kalkowsky, 1908; Flügel, 1982). This leaves biological encrustation as the most likely growth mechanism.

6. Isotopes

Kerogen was isolated by dissolving samples in concentrated HF, combusted in a Costech elemental analyzer and then analyzed by a Thermo-Finnigan MAT 253 isotope-ratio mass-spectrometer (Table 1). Barberton oncolite yields $\delta^{13}C_{PDB}$ = -24.5 ± 0.1‰. Pilbara oncoids are insufficiently kerogenous for individual lamellar analysis, but bulk oncoid sample yielded $\delta^{13}C_{PDB}$ = -32.1 ± 0.9‰. Relative to kerogen analysed from the overlying SPC adjacent to fissure walls, chert-hosted kerogen in 5 Pilbaran fissures is distinctly isotopically depleted by an average of 8.3‰ (range between 5 and 12‰).

7. Conclusion

Trace fossils occur in the form of abundant well-preserved oncoids associated with the Dresser Formation, H3C Hoogenoeg Member and Neptunian fissures extending below the Strelley Pool Chert. Multi-laminar microstromatoloidal films, preserved as nitrogenous kerogen, coat a diversity of lithic fragments of shallow marine affinity. The oncoids bear evidence for multiple stages of growth during sedimentary processing, with instances of smaller reworked oncoids organically cemented into aggregate complexes.

Individual kerogenous laminae entrain abundant coated microscopic (1-5 μm) crystals, now thoroughly silicified, whose interfacial angles are suggestive of a carbonate precursor, likely formed as a precipitate associated with metabolic alkalinity production. The conspicuous absence of oncoidal sulphide suggests that sulphur metabolism may have been of only local significance during early Archaean times (Shen and Buick, 2004), leaving oxygenic photoautotrophy/respiration and/or ferric chemoheterotrophy as the likely responsible metabolic pathways. Carbon isotope analysis supports this interpretation: oncoidal kerogen from the H3C chert carries $\delta^{13}C_{PDB}$ = -24.5 ± 0.1 ‰, typical of both early Archaean deep-marine benthic carbon (Chapter 5, 6) and modern organic marine detritus that was biosynthesized through photoautotrophy. Fissure-hosted kerogen, on the other hand, is distinctly depleted with $\delta^{13}C_{PDB}$ = -32.1 ± 0.9 ‰, in the range of other Pilbaran fissures which carry $\delta^{13}C_{PDB}$ between -32 and -36 ‰. This lighter carbon may be indicative of a methanogenic component in biomass (Chapter 8).

We conclude that microbial communities capable of complex biofilm aggregation in high-energy depositional environments were already well developed in a diverse array of marine settings near the beginning of sedimentation on both the Kaapvaal and Pilbara Cratons at ~3.4 Ga. Our findings represent amongst the oldest unambiguous trace fossil evidence for life on Earth, and pre-date the next-oldest known occurrence of oncoids (Schaefer et al., 2001; Gutzmer et al., 2002) by over one billion years.

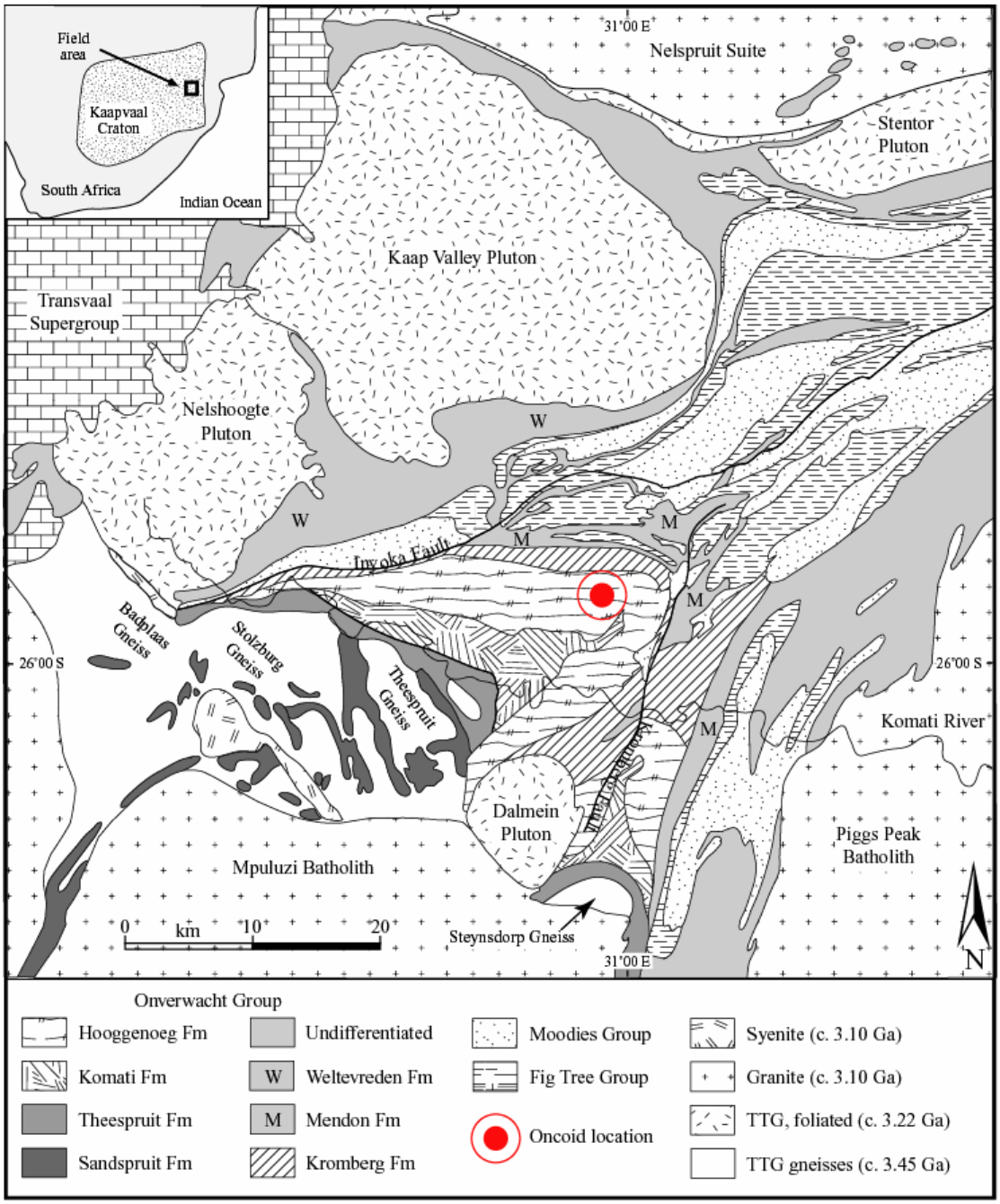

Figure 1: Geological map showing Hooggenoeg Formation in Barberton Greenstone Belt, South Africa (after Kamo and Davis, 1994; Lowe and Byerley, 1999; Hofmann and Bolhar, 2007). Inset shows location of study area in South Africa.

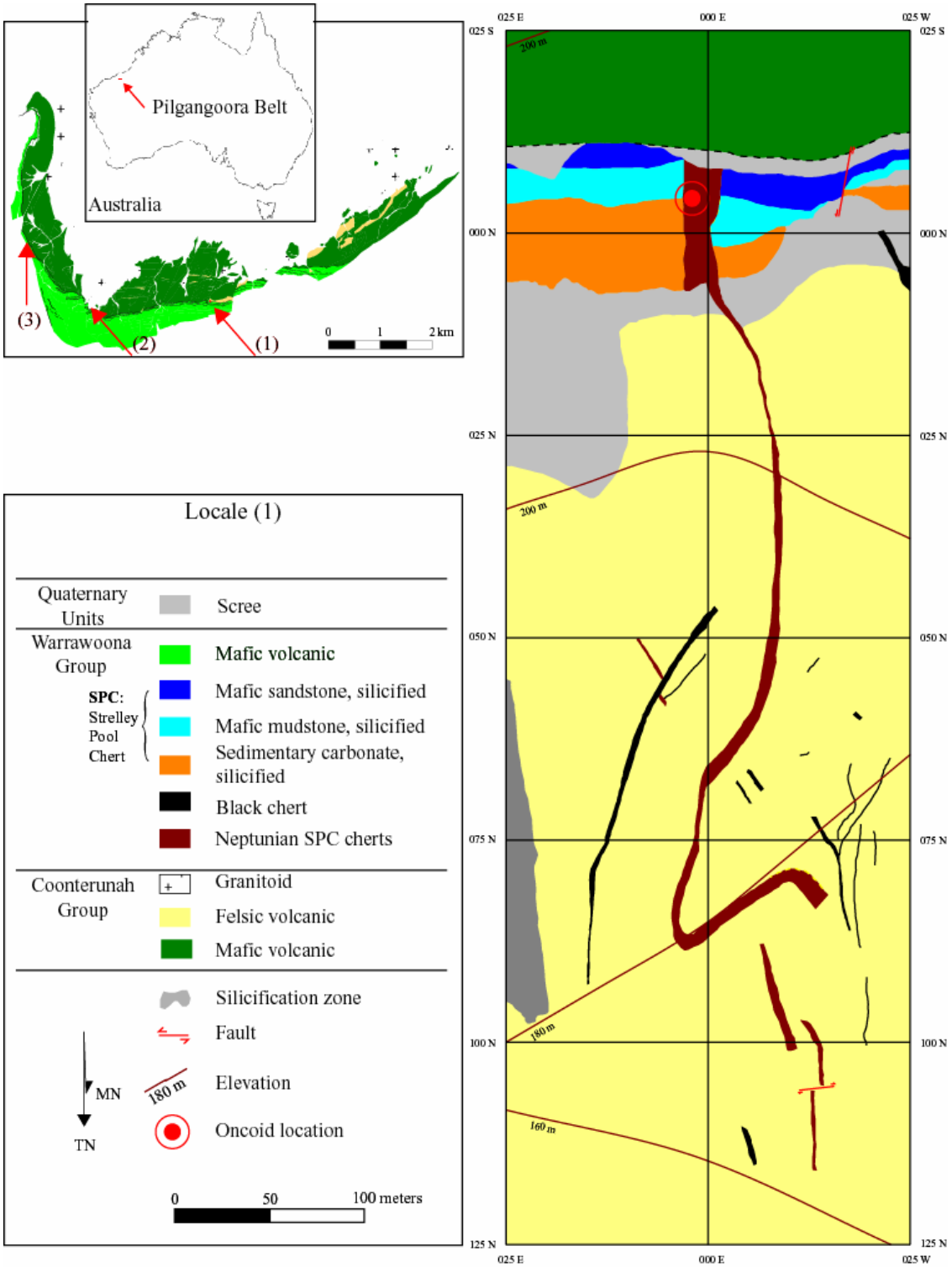

Figure 2: Geological map showing location of Pilbaran oncoid sample at fissure locale (1). Inset show three Early Archaean Neptunian fissure complexes in Pilgangoora area, Pilbara Craton, northwest Australia.

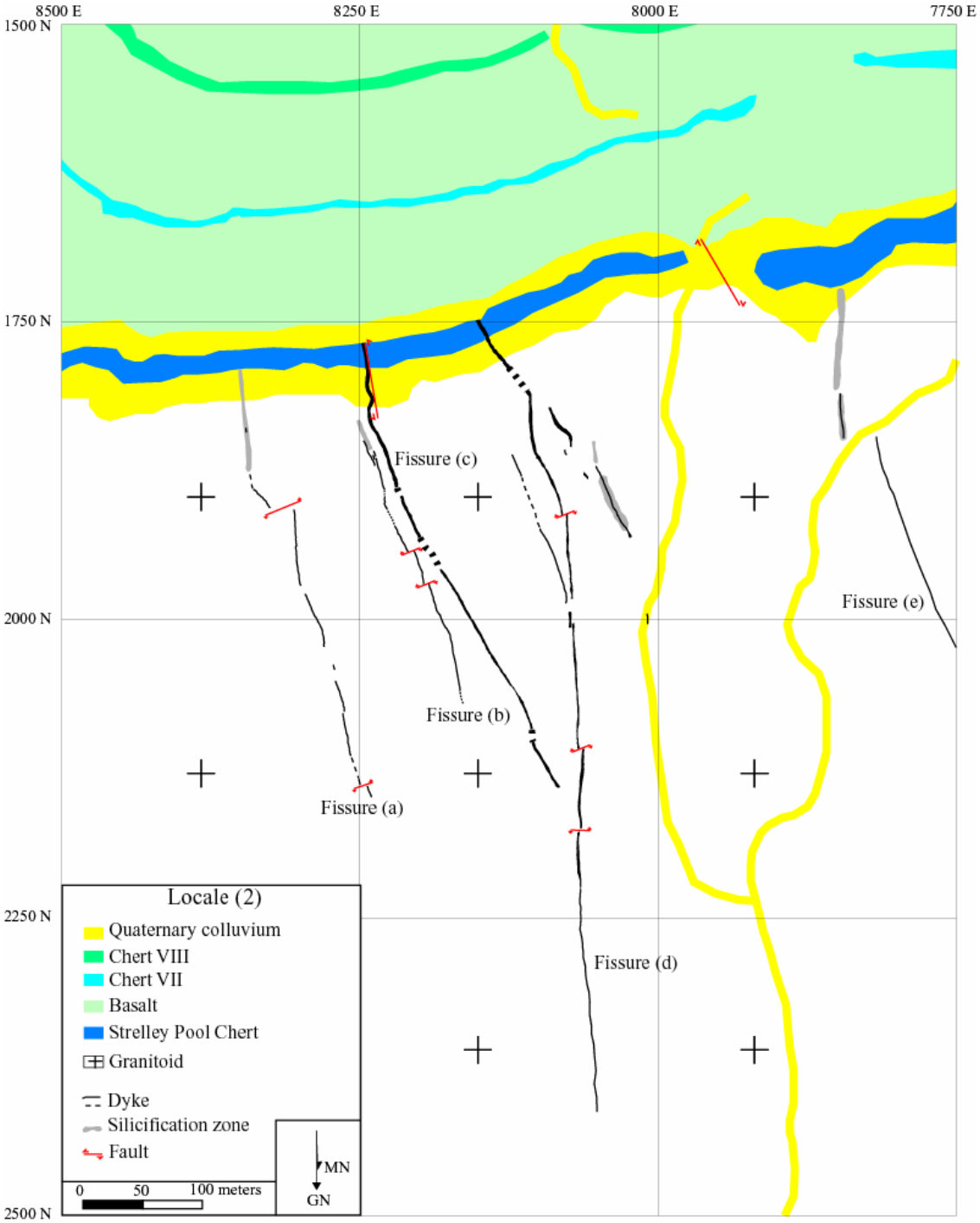

Figure 3: Geological map of Early Archaean Pilbaran fissure complex, locale (2) of Figure (1).

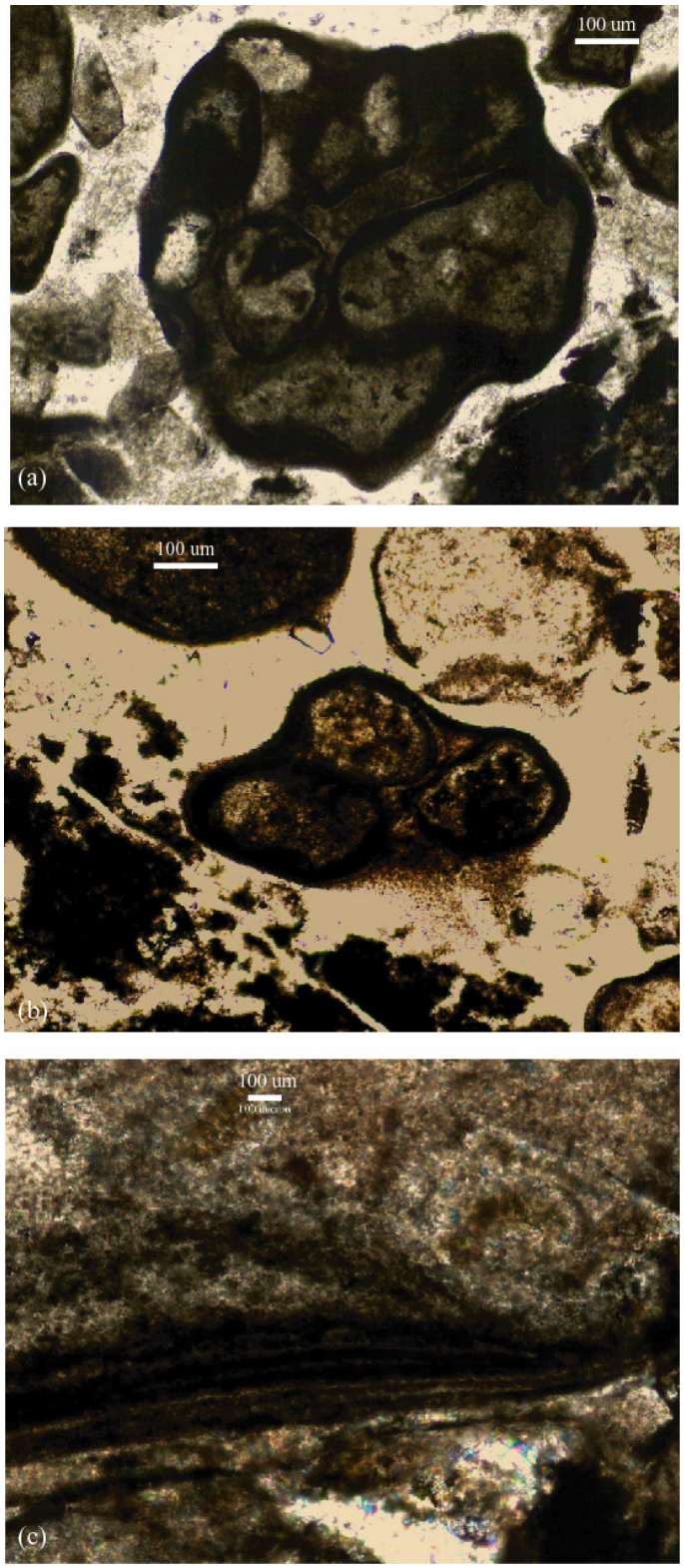

Figure 4: Plane-polarized photographs of (a, b) selected Barberton oncoid agglomerations and (c) detail of microstromatolitic kerogenous laminae.

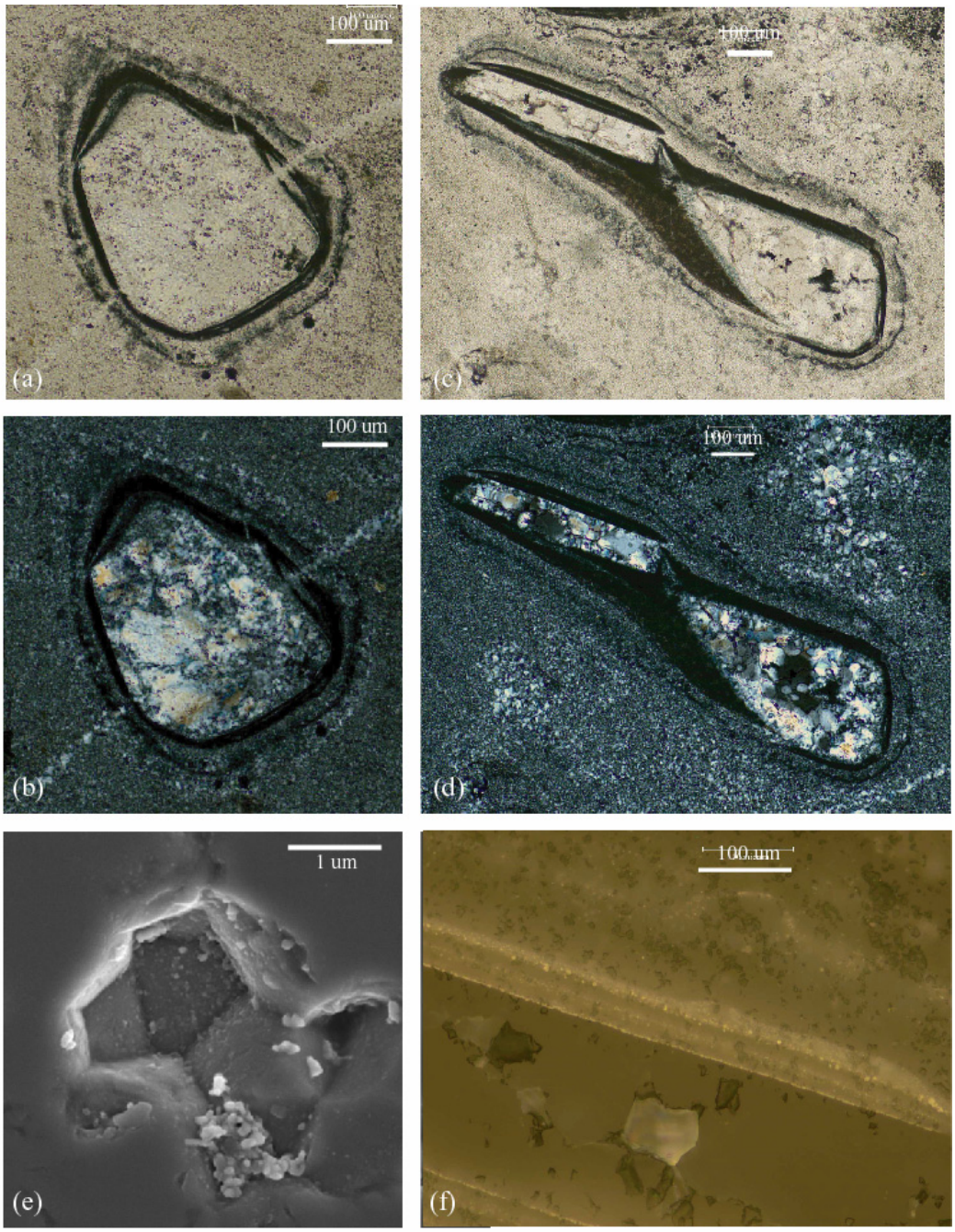

Figure 5: (a, c) plane-polarized, (b, d) cross-polarized, (e) SEM, and (f) reflected-light photographs of selected Pilbara oncoids. Note internal laminar reflections (f) associated with (e) individual probable carbonate minerals.

Table 1: Carbon isotope data from Barberton and Pilbara oncoid samples, and Pilbara Neptunian Fissures.

Unit	Member / Locale	Lithology	*n*	$\delta^{13}C_{PDB}$ (‰)	± 1σ (‰)	Oncoids ?
Barberton Hooggenoeg	H3C	Black chert breccia	1	-24.5	0.1	√
Pilbara Strelley Pool Chert	Fissure 1	Bedded black chert*	1	-31.5	0.4	X
		Fissure chert breccia	2	-32.1	0.9	√
	Fissure 2(a)	Bedded black chert	2	-25.6	3.0	X
		Fissure chert breccia	3	-33.5	1.7	X
	Fissure 2(c)	Bedded black chert	1	-30.2	0.2	X
		Fissure chert breccia	1	-35.8	0.1	X
	Fissure 2(d)	Bedded black chert	2	-25.8	0.4	X
		Fissure chert breccia	2	-34.8	1.2	X

* Designates SPC sample collected immediately adjacent to Neptunian Fissure.

References

Allwood, A. C., Walter, M. R., Kamber, B. S., Marshall, C. P., and Burch, I. W., 2006. Stromatolite reef from the Early Archaean era of Australia. *Nature* **441**, 714-718.

Armstrong, F. A. J., Compston, W., de Wit, D. W., and Williams, I. S., 1990. The stratigraphy of the 3.5-3.2 Ga Barberton Greenstone Belt revisted: a single zircon ion microprobe study. *Earth and Planetary Science Letters* **101**, 90-106.

Banerjee, D. M., Simonetti, A., Furnes, H., Muehlenbachs, K., Staudigel, H., Heaman, L. M., and van Kranendonk, M., 2007. Direct dating of Archean microfossil ichnofossils. *Geology* **35**, 487-490.

Banerjee, N. R., Furnes, H., Muehlenbachs, K., Staudigel, H., and de Wit, M., 2006. Preservation of similar to 3.4-3.5 Ga microbial biomarkers in pillow lavas and hyaloclastites from the Barberton Greenstone Belt, South Africa. *Earth Planet. Sci. Lett.* **241**, 707-722.

Brasier, M., McLoughlin, N., Green, O., and Wacey, D., 2006. A fresh look at the fossil evidence for early Archaean cellular life. *Philos T R Soc B* **361**, 887-902.

Brasier, M. D., Green, O. R., Jephcoat, A. P., Kleppe, A. K., Van Kranendonk, M., Lindsay, J. F., Steele, A., and Grassineau, N. V., 2002. Questioning the evidence for Earth's oldest fossils. *Nature* **416**, 76-81.

Brasier, M. D., Green, O. R., Lindsay, J. F., McLoughlin, N., Steele, A., and Stoakes, C., 2005. Critical testing of earth's oldest putative fossil assemblage from the similar to 3.5 Ga Apex Chert, Chinaman Creek, western Australia. *Precamb. Res.* **140**, 55-102.

Buick, R. and Dunlop, J. S. R., 1990. Evaporitic sediments of early Archaean age from the Warrawoona Group, North Pole, Western Australia. *Sedimentology* **37**, 247-277.

Buick, R., Dunlop, J. S. R., and Groves, D. I., 1981. Stromatolite Recognition in Ancient Rocks - an Appraisal of Irregularly Laminated Structures in an Early

Archean Chert-Barite Unit from North-Pole, Western-Australia. *Alcheringa* **5**, 161-181.

Buick, R., Thornett, J. R., McNaughton, N. J., Smith, J. B., Barley, M. E., and Savage, M., 1995. Record of emergent continental crust ~3.5 billion years ago in the Pilbara Craton of Australia. *Nature* **375**, 574-577.

Catalov, G. A., 1983. Triassic Oncoids from Central Balkanides (Bulgaria). In: Peryt, T. M. (Ed.), *Coated Grains*. Springer-Verlag, Berlin.

Cavalazzi, B., Barbieri, R., and Ori, G. G., 2007. Chemosynthetic microbialites in the Devonian carbonate mounds of Hamar Laghdad (Anti-Atlas, Morocco). *Sediment Geol* **200**, 73-88.

Dahanayake, K. and Krumbein, W. E., 1986. Microbial Structures in Oolytic Iron Formations. *Miner Deposita* **21**, 85-94.

Flügel, E., 1982. *Microfacies analysis of limestones*. Springer-Verlag, Berlin ; New York.

Flügel, E., 2004. *Microfacies of carbonate rocks : analysis, interpretation and application*. Springer, Berlin ; New York.

Furnes, H., Banerjee, N. R., Muehlenbachs, K., Staudigel, H., and de Wit, M., 2004. Early life recorded in archean pillow lavas. *Science* **304**, 578-581.

Grotzinger, J. P. and Knoll, A. H., 1999. Stromatolites in Precambrian carbonates: evolutionary mileposts or environmental dipsticks? *Annual Reviews of Earth and Planetary Science* **27**, 313-358.

Grotzinger, J. P. and Rothman, H. D., 1996. An abiotic model for stromatolite morphogenesis. *Nature* **383**, 423-425.

Groves, D. I., Dunlop, J. S. R., and Buick, R., 1981. An Early Habitat of Life. *Sci. Am.* **245**, 64-73.

Gutzmer, J., Schaefer, M. O., and Beukes, N. J., 2002. Red bed-hosted oncolitic manganese ore of the Paleoproterozoic Soutpansberg Group, Bronkhorstfontein, South Africa. *Economic Geology* **97**, 1151-1166.

Hofmann, A. and Bolhar, R., 2007. Carbonaceous cherts in the Barberton greenstone belt and their significance for the study of early life in the Archean record. *Astrobiology* **7**, 355-388.

Hofmann, H. J., Grey, K., Hickman, A. H., and Thorpe, R. I., 1999. Origin of 3.45 Ga coniform stromatolites in Warrawoona Group, Western Australia. *Geol Soc Am Bull* **111**, 1256-1262.

Kalkowsky, E., 1908. Oolith and Stromatolith im norddeutschen Buntsandstein. *Deutsch. Geol. Gesell. Zeitschr.* **60**, 68-125.

Kamo, S. L. and Davis, D. W., 1994. Reassessment of Archean Crustal Development in the Barberton Mountain Land, South-Africa, Based on U-Pb Dating. *Tectonics* **13**, 167-192.

Lowe, D. R., 1980. Stromatolites 3400-Myr old from the Archean of Western Australia. *Nature* **284**, 441-443.

Lowe, D. R., 1983. Restricted shallow-water sedimentation of early Archean stromatolitic and evaporitic strata of the Strelley Pool Chert, Pilbara Block, Western Australia. *Precambrian Res.* **19**, 239-283.

Lowe, D. R., 1994. Abiological Origin of Described Stromatolites Older Than 3.2 Ga. *Geology* **22**, 387-390.

Lowe, D. R. and Byerley, G. R., 1999. Stratigraphy of the west-central part of the Barberton Greenstone Belt, South Africa. In: Lowe, D. R. and Byerly, G. R. Eds.), *Geologic Evolution of the Barberton Greenstone Belt, South Africa*. Geological Society of America.

Lyell, C., 1859. *A manual of elementary geology : or, The ancient changes of the earth and its inhabitants as illustrated by geological monuments*. D. Appleton, New York.

McLoughlin, N., Brasier, M. D., Wacey, D., Green, O. R., and Perry, R. S., 2007. On biogenicity criteria for endolithic microborings on early earth and beyond. *Astrobiology* **7**, 10-26.

Philippot, P., Van Zuilen, M., Lepot, K., Thomazo, C., Farquhar, J., and Van Kranendonk, M. J., 2007. Early Archaean microorganisms preferred elemental sulfur, not sulfate. *Science* **317**, 1534-1537.

Rosing, M. T., 1999. ^{13}C-depleted carbon microparticles in >3700-Ma sea-floor sedimentary rocks from west Greenland. *Science* **283**, 74-76.

Schaefer, M. O., Gutzmer, J., and Beukes, N. J., 2001. Late Paleoproterozoic Mn-rich oncoids: Earliest evidence for microbially mediated Mn precipitation. *Geology* **29**, 835-838.

Schopf, J. W., Kudryavtsev, A. B., Agresti, D. G., Wdowiak, T. J., and Czaja, A. D., 2002. Laser-Raman imagery of Earth's earliest fossils. *Nature* **416**, 73-76.

Schopf, J. W. and Packer, B. M., 1987. Early Archean (3.3-billion to 3.5-billion-year-old) microfossils from Warrawoona Group, Australia. *Science* **237**, 70-73.

Shen, Y., Buick, R., and Canfield, D. E., 2001. Isotopic evidence for microbial sulphate reduction in the early Archaean era. *Nature* **410**, 77-81.

Shen, Y., Farquhar, J., Masterson, A., and Kaufman, A. J., 2009. Evaluating the biogenicity of early Archaean sulphur cycling using quadruple isotope systematics. *Earth Planet. Sci. Lett.* **279**, 383-291.

Shen, Y. N. and Buick, R., 2004. The antiquity of microbial sulfate reduction. *Earth-Sci Rev* **64**, 243-272.

Ueno, Y., Isozaki, Y., Yurimoto, H., and Maruyama, S., 2001. Carbon isotopic signatures of individual Archean microfossils(?) from Western Australia. *Int Geol Rev* **43**, 196-212.

Ueno, Y., Ono, S., Rumble, D., and Maruyama, S., 2008. Quadruple sulfur isotope analysis of ca. 3.5 Ga Dresser Formation: New evidence for microbial sulfate reduction in the early Archean. *Geochim. Cosmochim. Acta* **72**, 5675-5691.

Ueno, Y., Yoshioka, H., Isozaki, Y., and Maruyama, S., 2003. Origin of 13C-depleted kerogen in ca. 3.5 Ga hydrothermal silica dikes from Western Australia*Goldschmidt*.

Ueno, Y., Yoshioka, H., Maruyama, S., and Isozaki, Y., 2004. Carbon isotopes and petrography of kerogens in similar to 3.5-Ga hydrothermal silica dikes in the North Pole area, Western Australia. *Geochim. Cosmochim. Acta* **68**, 573-589.

van Zuilen, M. A., Lepland, A., and Arrhenius, G., 2002. Reassessing the evidence for the earliest traces of life. *Nature* **418**, 627-630.

van Zuilen, M. A., Lepland, A., Teranes, J., Finarelli, J., Wahlen, M., and Arrhenius, G., 2003. Graphite and carbonates in the 3.8 Ga old Isua Supracrustal Belt, southern West Greenland. *Precamb. Res.* **126**, 331-348.

Verrecchia, E. P., Freytet, P., Julien, J., and Baltzer, F., 1997. The unusual hydrodynamical behaviour of freshwater oncolites. *Sediment Geol* **113**, 225-243.

Wacey, D., McLoughlin, N., Green, O. R., Parnell, J., Stoakes, C., and Brasier, M., 2006. The ~3.4 billion-year-old Strelley Pool Sandstone: a new window into early life on Earth. *International Journal of Astrobiology* **5**, 333-342.

8. Concluding Synthesis

Due to a dearth of preserved evidence, questions about Early Archaean biogeochemical cycling are highly under-determined (Chapter 1). This has two consequences. The first is that the diversity of explanatory models admissible into the scientific arena is large. The second is that new discoveries of Early Archaean meta-sedimentary outcrop potentially carry greater significance than do those of younger rocks deposited under conditions that are better understood.

Three hitherto unreported settings of Early Archaean marine sedimentation carrying potential geobiological significance were described in this thesis: ~3.7 – 3.8 Ga deep-marine metaturbidites from the Isua Supracrustal Belt in southwest Greenland, ~3.52 Ga deep-marine micritic banded-iron formation from the Coonterunah Subgroup in the Pilbara's Pilgangoora Belt in northwest Australia, and ~3.45 Ga shallow marine and intermittently sub-aerially exposed neptunian fissures cutting the Kelly-Warrawoona Group erosional unconformity, also in the Pilgangoora Belt. All three environments contain appreciable quantities of syn-sedimentary reduced carbon compounds with isotopic fractionations outside the range of equilibrium processes, but similar to those associated with autotrophic metabolism (Chapter 2).

1. Fischer-Tropsch-Type Synthesis

The origin of ancient of reduced carbon need not necessarily be biological. Hydrocarbons of an impressively complex and diverse nature can be produced abiologically through chemical processes known as Fischer-Tropsch-type ('FTT') reactions (Figure 1). FTT synthesis, *sensu strictu*, is the process whereby CO is converted to hydrocarbon gas by reaction with H_2 (compare Fischer, 1935):

$$n\,CO + (2n+1)\,H_2 \rightarrow C_nH_{(2n+2)} + n\,H_2O$$

Industrial FTT synthesis is performed under H_2O-free conditions to maximize CH_4 production, whereas geologically relevant experiments generally include an aqueous phase. The presence of a vapour phase significantly enhances the potential for

organic synthesis of chain hydrocarbons (McCollom et al., 1999). FTT synthesis has yielded a wide range of compounds in the laboratory (Lancet and Anders, 1970; Yuen et al., 1990; McCollom et al., 1999; Rushdi and Simoneit, 2001; Voglesonger et al., 2001; McCollom, 2003; McCollom and Seewald, 2003a, b; Foustoukos and Seyfried, 2004; McCollom, 2004; Rushdi and Simoneit, 2004; McCollom and Seewald, 2006). As a result, it has been suggested as a potential non-biological mechanism for the formation of simple organics in various (astro-)geological environments, including hydrothermal vents (Sherwood-Lollar et al., 1993; Berndt et al., 1996; Shock and Schulte, 1998; Horita and Berndt, 1999; Holm and Charlou, 2001; Riedel et al., 2001; Brasier et al., 2002; Charlou et al., 2002; Kennedy et al., 2002; Sherwood-Lollar et al., 2002; Ueno et al., 2003; van Kranendonk et al., 2003; Foustoukos and Seyfried, 2004; Simoneit, 2004; Simoneit et al., 2004; Ueno et al., 2004; Bjonnes and Lindsay, 2005; Brasier et al., 2005; Lindsay et al., 2005a; van Kranendonk, 2006), cooling volcanic gases (Zolotov and Shock, 1999), igneous rocks (Salvi and Williams-Jones, 1997; Potter et al., 2004), serpentinizing systems (Szatmari, 1989; Abrajano et al., 1990; Charlou et al., 1998; Kelley and Fruh-Green, 1999; Fruh-Green et al., 2003; Sleep et al., 2004; Kelley et al., 2005; Schulte et al., 2006), interplanetary dust particles (Llorca and Casanova, 1998; Zolotov and Shock, 2001) and carbonaceous chondrites (Hartman et al., 1993; Zolotov and Shock, 2001).

Despite this, empirical evidence for the non-biological formation of hydrocarbons (discounting simple C_1 compounds such as methane) through FTT synthesis in geological systems on Earth remains scarce. Theoretical calculations (Shock, 1990) suggest that n-alkanes and PAHs can form metastably under ~ 250 °C. Both the possible temperature range and energetic drive for hydrocarbon formation increase with a lower fO_2 and higher CO/CO_2 ratios (Zolotov and Shock, 2000; Rushdi and Simoneit, 2001). The rate of FTT synthesis is greatly accelerated by, or requires, the presence of a metal catalyst. Mineral phases that catalyze FTT reactions include Co, ThO_2, ZnO, Ru and Rh (Roper, 1983), magnetite (Fe_3O_4), brucite ($Mg(OH)_2$), Ni-Fe alloys such as awaruite ($Ni_{2-3}Fe$), Cr- and Fe- bearing chromite minerals (Foustoukos and Seyfried, 2004), and montmorillonite (McCollom et al., 1999) (Figure 1). The

extreme sensitivity of successful FTT experimentation to *P, T, fO_2* and catalyst conditions suggests that the ability of a given geological environment to support FTT synthesis would be largely controlled by the host rock composition.

Experiments on the isotopic signature imparted on the reaction produces of FTT reactions exhibit widely differing results. Some laboratory experiments indicate a modest fractionation of 11 - 35 ‰ depletion in ^{12}C relative to precursor CO (Yuen et al., 1990), whereas others (e.g. McCollom and Seewald, 2006) report a higher and narrower range of ^{12}C depletion on the order of 30 - 36 ‰. For both alkanes and alkenes ($C_1 < C_n < C_4$), a fractionation between 40 and 48 ‰ was recently reported in both open-system and steady-state experiments (Taran et al., 2007). Fractionations relative to CH_4 fell well under 12 ‰ for most synthesized compounds, with the majority of hydrocarbons depleted by 0 to 5 ‰ relative to methane.

As an open-system process, it is difficult to place constraints on the occurrence of FTT reactions using geological criteria. What's more, potential FTT reactions occur in the very same kinds of environments in which evidence for early metabolism may be sought, as both processes are associated with the dissipation of energy in the presence of steady flows of COH-fluids and thermochemical discontinuities. However, if Early Archaean kerogen is of microbial origin, systematic variations in isotopic behaviour may be expected to follow changes in microbial ecology in different depositional environments, which should not accompany abiotic kerogen.

2. Metamorphism and $\delta^{13}C_{org}$

Reduced carbon did not maintain isotopic closure during metamorphism, and no appreciable differences in the thermal maturation behaviour of organic matter from fluvial, shallow and deep-marine environments could be discerned (Figure 2). Schistose graphitic black meta-chert horizons from lower amphibolite-facies sub-aqueously deposited felsic schists (Kohler and Anhaeusser, 2002) collected from the Kaapvaal Craton's Bien Venue Formation, Fig Tree Group give $\delta^{13}C_{org} = -18.8 \pm 0.1$ ‰, while a value of $\delta^{13}C_{org} = -28.8 \pm 0.1$ ‰ from a sample of black chert interstratified with terrigenous clastic sediments in sub-greenschist facies rocks from

the Central Domain is probably representative of protolithic Fig Tree kerogen (Walsh and Lowe (1999) give $\delta^{13}C_{org}$ = -33.6, -26.0 and -30.3 ‰ for three Fig Tree samples).

Early Archaean marine kerogen behaved similarly under metamorphism. Lower amphibolite-facies graphite from the marine Coonterunah Subgroup's Coucal Formation gives a rather uniform $\delta^{13}C_{org}$ = -16.5 ± 0.5 ‰, with lowest grade kerogen at lower greenschist facies showing $\delta^{13}C$ = -23.8 ± 0.2 ‰. A similar fractionation appears to have accompanied metamorphism of kerogen associated with Chert VII and Chert VIII in the Euro Basalt Formation, which taken together show a range of $\delta^{13}C$ = -19.7 to -23.2 ‰ in the highest grade (lower amphibolite-facies at western Pilgangoora Belt closure) rocks from which kerogen could be isolated, systematically approaching and reaching SPC-like values of $\delta^{13}C$ = -29.5 to -32.9 ‰ eastward along strike, and maintaining this ratio for the remaining third of the strike-length of the belt at and below talc-forming metamorphic grade. Two highly recrystallized kerogenous black meta-cherts analyzed from a shallow (~ 25 m) dyke-like structure underneath Chert VII in the upper greenschist facies zone of the belt both give $\delta^{13}C$ = -17.0 ± 0.2 ‰.

All in all, Early Archaean kerogen appears to display little variation in its isotopic evolution during metamorphism, ranging from isotopically light ($\delta^{13}C$ = -29.5 to -37.1 ‰, see below) in all environments at lowest grades to < -20 ‰ at the highest (Figure 2). This is not what would be expected from kerogen of abiotic origin, which would be expected to vary greatly in different environments. Furthermore, meteorite studies suggest that FTT kerogen undergoes highly variable stepwise pyrolysis of labile fractions (Shimoyama, 1997; Kitajima et al., 2002; Septhon et al., 2004; Busemann et al., 2007), although this carbonaceous matter may present an imperfect analogue to Early Archaean kerogen.

3. Carbon Cycling

$\delta^{13}C_{carb\text{-}org}$ correlations between shallow-water and pelagic deep carbonate provide a powerful palaeo-oceanographical tool (Magaritz and Issar, 1973; Weisset et al., 1998; Immenhauser et al., 2002; Immenhauser et al., 2003; Panchuk et al., 2005). Like today, Early Archaean marine sedimentary $\delta^{13}C_{carb}$ would have depended on

temperature-dependent carbonate-DIC isotopic equilibria and DIC availability, the latter controlled by reservoir size and autotrophic production (Hayes, 1993). Carbonate-DIC isotopic equilibria also depend on the type of carbonate precipitated and the dissolved carbonate concentration. Under modern surface ocean conditions, calcite and aragonite precipitate with enrichments over seawater DIC of about +1.0 and +2.7 ‰, respectively (Romanek et al., 1992). Higher $[CO_3^{2-}]$ solutions precipitate isotopically lighter carbonates, through the linear relationship: -0.060 ± 0.015 ‰ (μmol $[CO_3^{2-}]$ $kg^{-1})^{-1}$ (McCrea, 1950; Spero et al., 1997).

Two mechanisms produce opposing effects on the isotopic differential, $\Delta^{13}C_{n\text{-}o} = \delta^{13}C_{\text{nearshore DIC}} - \delta^{13}C_{\text{open ocean DIC}}$, between partially restricted shallow water masses (e.g. on submerged platforms) and the open ocean. On the one hand, cellular $\delta^{12}C$ uptake during vigorous primary production leads to relative enrichment in near-shore surface $\delta^{13}C_{DIC}$ (Swart and Eberli, 2005). Consequently, organic matter removal affects precipitated $\delta^{13}C_{carb}$ (Magaritz, 1989) such that increases in organic matter export are accompanied by increases in $\delta^{13}C_{carb}$ (Shackleton, 1985).

On the other hand, $\delta^{12}C_{CO_2}$ input from the respiration of marine and terrestrial organic matter during water-mass residence can have the opposing effect of reducing $\delta^{13}C_{DIC}$ and $\delta^{13}C_{carb}$ (Patterson and Walter, 1994). Near-shore $\delta^{13}C_{DIC}$ depletions are also observed to result from the disequilibrium influx of atmospheric CO_2 into highly alkaline waters (Herczeg and Fairbanks, 1987; Lazar and Erez, 1992).

3.1. A Eulittoral to Basinal Trend

A compilation of pertinent Early Archaean and Proterozoic carbonate isotope compositions is shown in Chapter 5, Figure 29. Early Archean shallow marine sedimentary laminated carbonates from the ~3.45 Ga Strelley Pool Chert (from several belts across the eastern Pilbara) and Barberton's ~3.47 Ga (Armstrong et al., 1991) Onverwacht Group have similar isotopic compositions, and show linear positive correlations in their carbon and oxygen isotopes, with values ranging from $(\delta^{13}C, \delta^{18}O)_{carb}$ = (+3.0 ‰, -11.0 ‰) to (+1.0 ‰, -17.0 ‰), with a few lower outlying $\delta^{13}C_{carb}$

values obtained from the SPC in the Pilgangoora Belt. This linear trend can be attributed to isotopic equilibration with pore-waters during progressive diagenesis, although high evaporation rates may very well have played a role in increasing $\delta^{18}O_{carb}$ (Adlis et al., 1988) in the Strelley Pool Chert palaeoreef.

Compared to these shallow marine carbonates, the slightly older 3.52 Ga deep-marine carbonates from the Coonterunah Subgroup, interpreted in Chapter 5 as likely pelagic surface precipitates, are much more isotopically depleted, clustering at ($\delta^{13}C$, $\delta^{18}O)_{carb}$ = (-3.0 ± 1.0 ‰, -17.8 ± 0.2 ‰). These $\delta^{13}C_{carb}$ values are similar to the most depleted samples of Palaeoproterozoic basinal fine-laminated Ca-Mg carbonates in banded-iron formation, which likely formed in the same way, but in equilibrium with higher Palaeozoic $\delta^{18}O_{seawater}$. Partially silicified dolomitic spar in chert from Double Bar Formation drillcore shows values intermediate ($\delta^{13}C_{carb}$ = -0.9 to +0.1 ‰) between these shallow and deep marine end-members, perhaps reflecting transitional water depths and/or intermediate productivity. These values suggest significant differences in DIC compositions between Early Archaean littoral environments, with $\Delta^{13}C_{n\text{-}o}$ = $\delta^{13}C_{nearshore\ DIC}$ - $\delta^{13}C_{open\ ocean\ DIC}$ ≈ +4.0 to +6.0 ‰. (The exact figure depends on details of Early Archaean carbonate diagenesis, which could be ascertained through a comprehensive fluid-inclusion study).

Like today, Archaean primary productivity probably would have been higher in near-shore environments than in the surface waters overlying basins such as that into which the Coonturunah micrite-BIF settled. This assumption is born out by evidence for greater C_{org} sequestration in the form of higher TOC (wt.%) kerogenous bedded cherts and cementing matrix cherts deposited in shallower environments of the Barberton's Hooggenoeg Formation and the Pilbara's Strelley Pool Chert, compared with the C_{org}-poor carbonates and cherts of the deep-water Coonterunah Subgroup and Isua meta-turbidites.

The least metamorphosed concordant metachert- and carbonate-hosted kerogen from the Strelley Pool Chert (from both fresh outcrop and drillcore samples) and the upper reaches of neptunian fissures ranges isotopically between $\delta^{13}C_{org}$ ≈ - 29 and - 32 ‰, similar to analytical results obtained by other workers (Lindsay et al., 2005b).

More depleted values of $\delta^{13}C_{org}$ = - 34.7 to -37.1 ‰ are obtained from less metamorphosed (prehnite-pumpellyite facies) sedimentary kerogen in black metachert from the Barberton Hoogenoeg H_4C Member, which appears to be representative of Hoogenoeg kerogen generally (e.g. Walsh and Lowe, 1999). (On the basis of field evidence, very depleted kerogen ($\delta^{13}C_{org}$ = -37.1 to -39.1 ‰) in black and white banded chert from the H_2C Member was inferred to be of post-sedimentary origin (cross-cutting relationships are shown in Chapter 2C, Figure 4 (d, e)), as also concluded by Hofmann and Bolhar (2007)).

In contrast to this light matrix carbon in shallow-marine cherts, kerogenous oncolite breccia from the H_3C Member is distinctly enriched at $\delta^{13}C_{org}$ = - 24.0 to -26.4 ‰. Textural evidence for continuous tumbling and rapid cementation (Chapter 7) is compatible with the interpretation of this range as representative of minimally processed Early Archaean photoautotrophy. Indeed, oncolite kerogen is isotopically similar to kerogen from both black chert ($\delta^{13}C_{org}$ = -23.8 ± 0.2 ‰) and pelagic carbonate precipitate ($\delta^{13}C$ = -26.1 ± 2.4 ‰) in the deep-marine Coucal Formation, both of which may have sequestered surface ocean particulate organic matter with only a minimal contribution from more isotopically depleted benthic biota. Black chert from the Coonterunah Subgroup's uppermost Double Bar Formation contains kerogen in the range $\delta^{13}C_{org}$ = -27.3 to -30.2 ‰, intermediate between shallow and deep-marine kerogen.

The pre-metamorphic isotopic signature of ~lower-amphibolite facies graphite, $\delta^{13}C_{org}$ = -17.5, in deep-water Isua metaturbidites is harder to extrapolate. This value is similar to analyses from the only other pre-3.8 Ga meta-turbidite outcrop (Rosing, 1999), and is distinctly more fractionated than metasomatically-derived carbon from a graphitic vein ($\delta^{13}C_{org}$ = -12.6 ± 0.1 ‰) cross-cutting leached banded-iron formation immediately overlying the meta-turbidite rocks. In addition to graphite, most Isua meta-turbidites contain small amounts of recrystallized siderite, ferroan calcite and/or ankerite. This carbonate is not texturally associated with graphite, and there are no relationships between TOC (wt.%), $\delta^{13}C_{carb}$ and carbonate (wt.%) (Figure 3). Thus, meta-turbidite graphite was likely not derived from fluids evolved from siderite

decarbonation reactions (van Zuilen et al., 2002; van Zuilen et al., 2003). Organic matter may have been delivered together with clastic material from shallower benthic settings, however.

The picture that emerges is one of organic export, rather than respiratory remineralization, control on surface-ocean $\delta^{13}C_{DIC}$. The low availability of soluble electron acceptors, notably oxygen, nitrate/nitrite and sulphate, at least in the sub-photic zones, can account for the lack of a water column remineralization flux. In the absence of insuperable competition from denitrifiers and sulphate-reducers (Lovley et al., 1982), sub-photic benthic remineralization would have been dominated by metabolic processes in which organic compounds serve as electron acceptors, namely fermentation and methanogenesis. Early Archaean organic matter degradation by consortia of fermenting and methanogenic prokaryotes (see below, Figure 5) would have resulted in higher fluxes of isotopically depleted CH_4 (and H_2) and lower fluxes of relatively isotopically enriched CO_2 than in the more familiar benthic systems that were to arise later.

4. Life in Ancient Seafloor Cracks and Degradation of Organic Matter

No single anaerobic microorganism has the capability to completely break down organic polymers into C_1 compounds, and highly specific substrate requirements are the microbiological rule (Fenchel et al., 1995). Step-wise organic matter degradation is performed by syntrophic consortia of prokaryotes, each of which are typically adapted to energy yields close to the theoretical thermodynamic threshold (~ 20 kJ mol^{-1}) allowing metabolism (Valentine, 2001). As a result, variations in micronutrient availability and other environmental conditions may greatly alter the fate of organic matter in sediments.

Kerogen in Pilgangoora neptunian fissures – at least one of which contains microstromatolitic oncoids - ranges from Strelley Pool Chert-like values of $\delta^{13}C_{org} \approx$ -29 to – 31 ‰ at shallow depths, to $\delta^{13}C_{org} \approx$ -34 to –36 ‰ at depth, the latter thereby representing the most isotopically depleted kerogen sampled in the Pilgangoora Belt. Less highly metamorphosed kerogen from similar structures at North Pole Dome gives

$\delta^{13}C_{org} \approx$ -38.6 ‰, similar to 'hydrothermal dyke' kerogen from the same structures analyzed by Ueno et al. (2003). Neptunian organic matter occasionally shows an intimate association with disseminated magnetite of highly variable grain-size (<1 to ~10 μm), hinting at the operation of metabolic pathways using ferric iron. Like the magnetite in the basal Strelley Pool Chert conglomerate-sandstone, neptunian magnetite is likely derived from the erosion of Coonterunah Subgroup material, such as sedimentary magnetite-metachert. Minerals with ferric iron are otherwise rare in the Strelley Pool Chert lithofacies assemblages, particularly when compared to basinal Coonterunah sediments.

A texturally similar association between kerogen and sulphide minerals is commonly encountered in shallow-marine bedded black cherts of the Kelly Group, raising the possibility that oxidized species of sulphur acted as electron acceptors during chemoheterotrophy. Abundant diagenetic gypsum pseudomorphs in silicified lutites of the uppermost beds of the Strelley Pool Chert and in overlying Euro Basalt Formation cherts are compatible with the presence of some SO_4^{2-} in contemporary seawater, and disseminated pyrite of likely diagenetic origin is also common in some of the same rocks. The oxidized metabolic precursor(s) to pyrite may have formed through photosynthetic oxidation of volcanically-derived sulphur compounds.

The ~ 6 ‰ ^{12}C depletion of deep neptunian kerogen over that in bedded cherts requires a mechanism for both isotopic fractionation and carbon fixation (compare Hayes et al., 1987). The most natural explanation for the observed isotopic shift is the enhanced metabolic processing of SPC-derived seafloor organic detritus through coupled fermentation, acetogenesis and methanogenesis. Biomass $\delta^{13}C$ of methylotrophic (Summons et al., 1998) and methanogenic (Londry et al., 2008) Archaea can exhibit significant (up to $\Delta^{13}C \approx$ -20.9 and -24.8 ‰, respectively) depletions with respect to their carbon source, with the degree of fractionation strongly dependent on substrate type and increasing markedly with substrate availability. In addition to providing for efficient entrapment of organic matter through protection from hydraulic stirring, neptunian fissures would have acted as conduits for concentrated granitoid weathering products, heated fluids, and substrates (CO_2, CH_4,

H_2, methanol, acetate) released through organic matter degradation. Highly insoluble H_2 ($K_{H_2} \approx 7.8 \cdot 10^{-4}$ atm^{-1}), in particular, may have been a rate-limiting electron donor in bedded sediments compared to fissure environments. In comparison, vertically oriented neptunian fissures offered a relatively nutritive environment that would have sustained a larger, and more isotopicaly depleted, methanogenic biomass. This inference is also supported by apparently isotopically lighter organic matter being sequestered in shallow- compared to deep- marine Early Archaean environments (Figure 2). An opposite trend to this is observed in modern systems, where CO_2 draw-down from a smaller Phanerozoic atmospheric reservoir leads to dis-equilibrium fractionation and thus isotopically enriched POC in more shallow and productive environments (Hollander and McKenzie, 1991).

The lack of very depleted biomass ($\delta^{13}C < 50$ ‰) shows that little or none of the methane produced through these processes was recycled through the anaerobic oxidation of methane ('AOM'), suggesting that the inorganic terminal electron acceptors sulphate (Orphan et al., 2001) and ferrihydrite (Beal et al., 2009) were absent from deeper sites of methane genesis. Key metabolic steps would have followed the sequence (Figure 5):

- Hydrolysis of polymers;
- Primary fermentation of monomers into low molecular weight products such as alcohols and volatile fatty acids;
- Limited anaerobic hetrotrophy using inorganic terminal electron acceptors sulphate and ferric iron minerals such as magnetite;
- Secondary fermentation of smaller volatile fatty acids;
- Primary fermentation products mineralized to CH_4 and CO_2;
- Use of secondary fermentation products for acetogenesis;
- Acetotrophic and hydrogenotrophic methanogenesis to produce isotopically light biomass, CO_2 and CH_4.

Most non-fermenting prokaryotes are incapable of using typical monomers released during polymer hydrolysis, as a result of which fermenters dominate even

modern high-SO_4^{2-} sediments (Devereux et al., 1996). Fermenters are remarkably versatile, and can degrade sugars, amino acids, purines, pyrimidines, acetylene, many aromatic hydrocarbons, and organic acids with up to C_{18} chain lengths (Schink and Stams, 2002). All branched-chain, aromatic and $>C_2$ fatty acids require secondary fermentation prior to becoming accessible to methanogenic bacteria (Schmitz et al., 2001). Acetogens comprise a diverse group of obligately anaerobic bacteria that make use of the acetyl-CoA pathway both as a terminal electron acceptor in energy conservation and reductive synthesis (Drake, 1994), and like fermenters display a wide range of catabolic capabilities.

Methanogenesis completes catabolism of organic detritus in the absence of electron acceptors. Early Archaean methanogenesis would have benefited from high atmospheric H_2 concentrations inferred by some for the early Earth (Tian et al., 2005; but see Catling, 2006). In addition to hydrogen, methanogens require a unique suite of micronutrients that includes Co, Fe, Na, Ni, V and Zn (Jarrell and Kalmokoff, 1988), all of which appear to have been present in high concentrations in the Early Archaean surface marine environment (see Chapter 5, micrite geochemistry). Acetotrophic methanogenesis yields methane with $\delta^{13}C$ = -65 to -50 ‰, compared to extremely depleted $\delta^{13}C$ = -110 to -60 ‰ by hydrogenotrophic methanogenesis (Whiticar et al., 1986), although methane produced under conditions of substrate limitation is far less fractionated (Fuchs et al., 1979). The former process tends to occur at shallower depths, progressively transitioning to the latter (Hornibrook et al., 1997; Chasar et al., 2000; Hornibrook et al., 2000).

5. A Stratified Archaean Ocean?

High overall sedimentary Fe/Al abundances, widespread ferruginous chemical precipitates, and the chamosite- and stilpnomelane-dominated mineralogy of metamorphosed deep-sea feldspar-weathering clays all suggest high bottom-water Fe^{2+} concentrations. Evidence for the mobility of iron in solution is conspicuously absent from Early Archaean peri-tidal sediments, however, lending credence to the Eh- and pH- stratified model explored in Chapter 5.

High volcanic outgassing rates almost certainly ensured an early high-pCO_2 atmosphere, continually equilibrating with surface oceans consequently high in dissolved inorganic carbon ($\sum$DIC). In the presence of high inorganic carbon concentrations, CO_2 remineralized from organic matter consequently seems to have represented an insignificant source of isotopically light carbon. For such an ocean to have its surface chemistry controlled by organic export rates implies a large standing biomass pool and efficient nutrient cycling.

6. Conclusion

At the time of the earliest recorded sedimentation, a diverse and abundant biosphere was already well established in a variety of environmental settings. If evolution was able to gain a foothold on and within these fragmented and volcanically active slivers of greenstone belt crust, then there exists every reason to anticipate the ubiquity of life in habitable zones elsewhere.

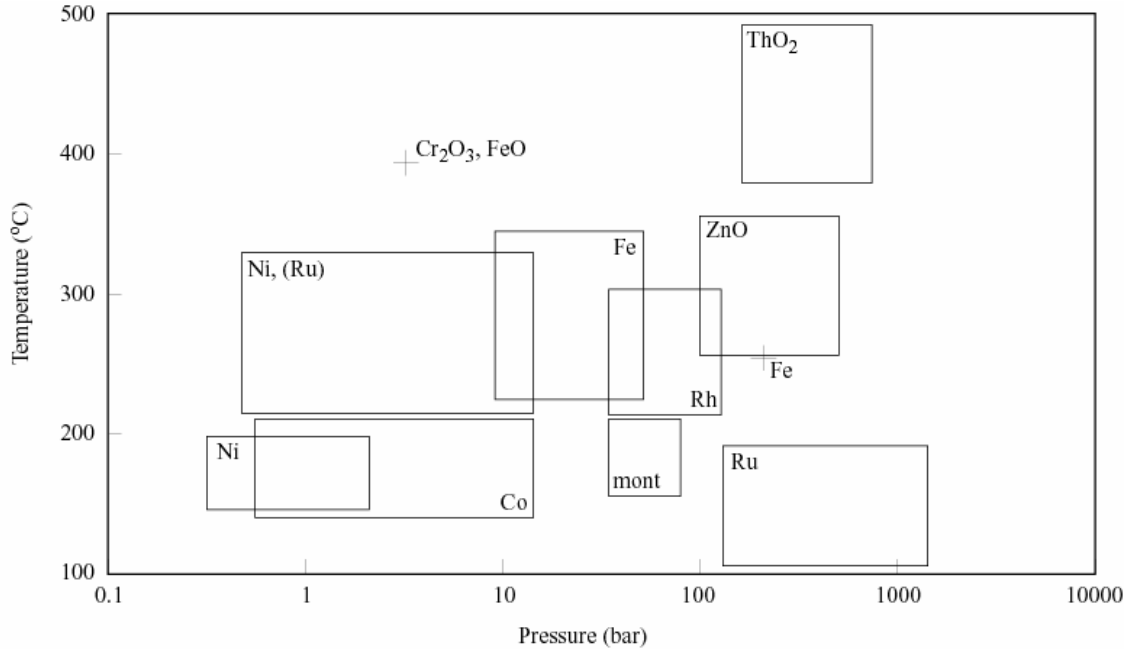

Figure 1: Selected P-T ranges of catalysts successfully applied in industrial FTT synthesis (after Roper, 1983 and references therein).

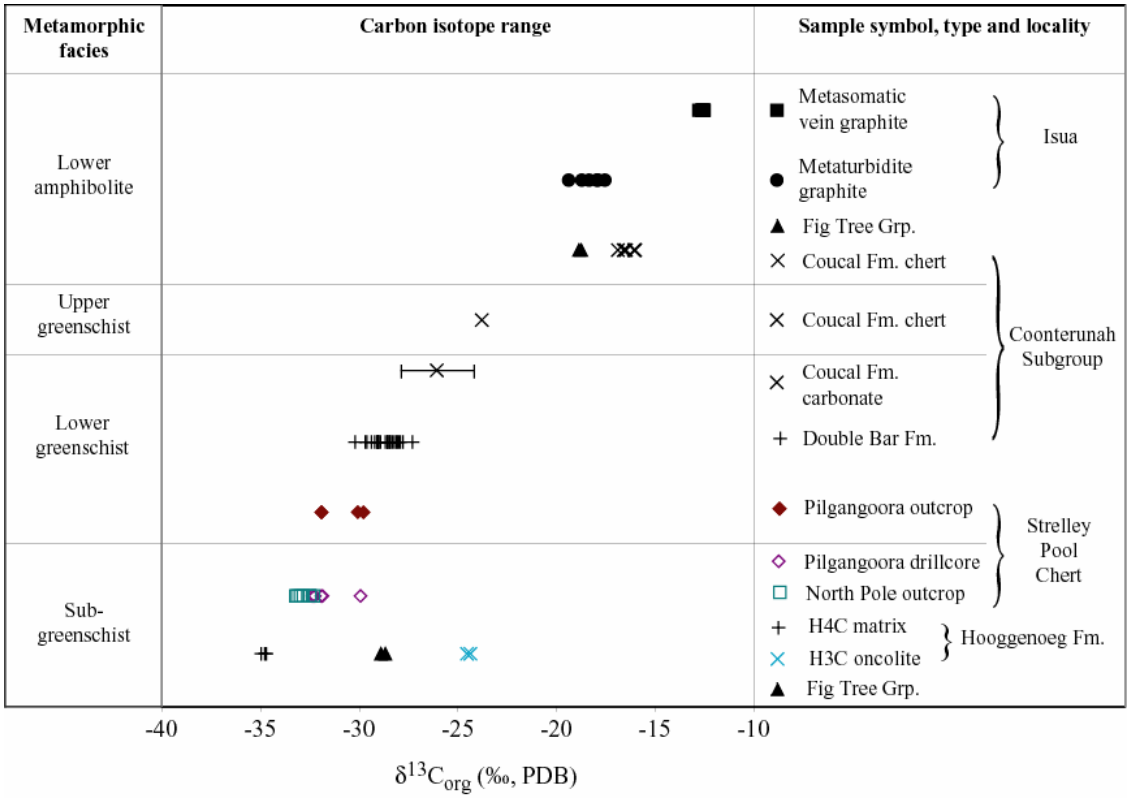

Figure 2: Carbon isotopes of kerogen and graphite from Early Archaean rocks at different metamorphic grade.

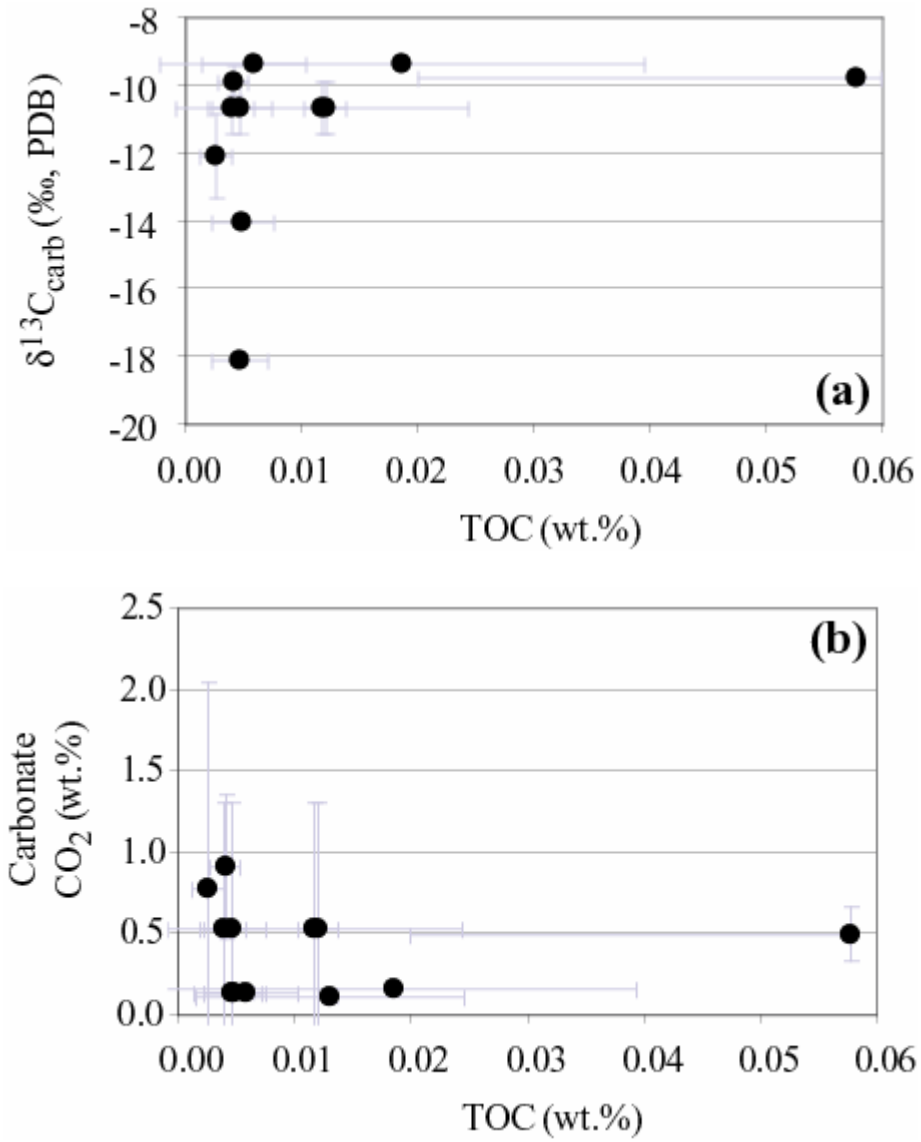

Figure 3: Isua metaturbidite graphite and carbonate are unrelated.

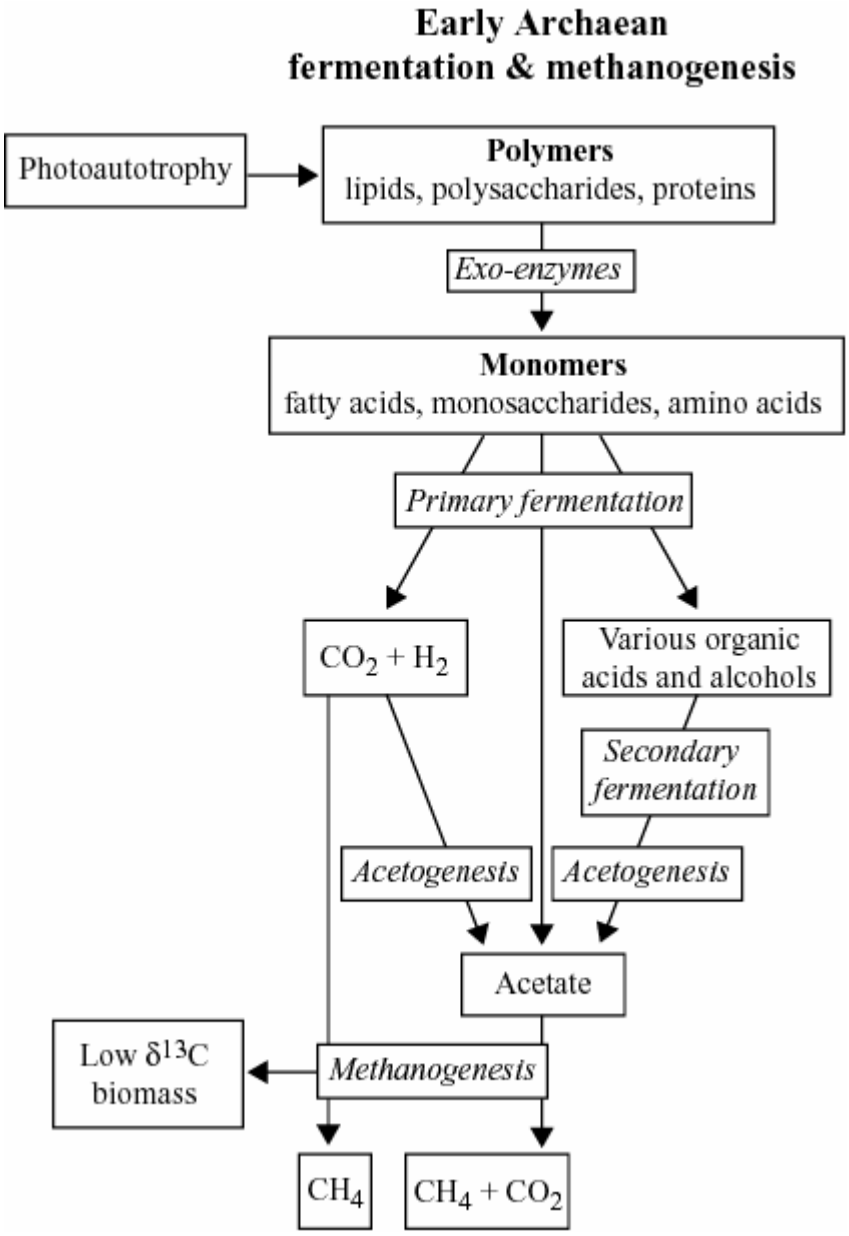

Figure 4: Flow diagram of inferred metabolic reactions in Early Archaean sediments.

References

Abrajano, T. A., Sturchio, N. C., Kennedy, B. M., Lyon, G. L., Muehlenbachs, K., and Bohlke, J. K., 1990. Geochemistry of Reduced Gas Related to Serpentinization of the Zambales Ophiolite, Philippines. *Appl Geochem* **5**, 625-630.

Adlis, D. S., Grossman, E. L., Yancey, T. E., and McLerran, R. D., 1988. Isotope stratigraphy and paleodepth changes of Pennsylvanian cyclical sedimentary deposits. *Palaios* **3**, 487-506.

Armstrong, F. A. J., Compston, W., De Wit, D. W., and Williams, I. S., 1991. The stratigraphy of the 3.5-3.2 Ga Barberton Greenstone Belt revisited: a single ziton ion microprobe study. *Earth Planet. Sci. Lett.* **101**, 90-106.

Beal, E. J., House, C. H., and Orphan, V. J., 2009. Manganese- and iron-dependent marine methane oxidation. *Science* **325**, 184-187.

Berndt, M. E., Allen, D. E., and Seyfried, W. E., 1996. Reduction of CO2 during serpentinization of olivine at 300 degrees C and 500 bar. *Geology* **24**, 351-354.

Bjonnes, E. and Lindsay, J. F., 2005. The depositional setting of Earth's earliest sedimentary rocks. *Lunar and Planetary Science* **XXXVI**.

Brasier, M. D., Green, O. R., Jephcoat, A. P., Kleppe, A. K., Van Kranendonk, M., Lindsay, J. F., Steele, A., and Grassineau, N. V., 2002. Questioning the evidence for Earth's oldest fossils. *Nature* **416**, 76-81.

Brasier, M. D., Green, O. R., Lindsay, J. F., McLoughlin, N., Steele, A., and Stoakes, C., 2005. Critical testing of earth's oldest putative fossil assemblage from the similar to 3.5 Ga Apex Chert, Chinaman Creek, western Australia. *Precamb. Res.* **140**, 55-102.

Busemann, H. O. D., Alexander, C. M., and Nittler, L. R., 2007. Characterization of insoluble organic matter in primitive meteorites by microRaman spectroscopy. *Meteorit Planet Sci* **42**, 1387-1416.

Catling, D. C., 2006. Comment on "A hydrogen-rich early Earth atmosphere". *Science* **311**, -.

Charlou, J. L., Donval, J. P., Fouquet, Y., Jean-Baptiste, P., and Holm, N., 2002. Geochemistry of high H-2 and CH4 vent fluids issuing from ultramafic rocks at the Rainbow hydrothermal field (36 degrees 14 ' N, MAR). *Chem. Geol.* **191**, 345-359.

Charlou, J. L., Fouquet, Y., Bougault, H., Donval, J. P., Etoubleau, J., Jean-Baptiste, P., Dapoigny, A., Appriou, P., and Rona, P. A., 1998. Intense CH4 plumes generated by serpentinization of ultramafic rocks at the intersection of the 15 degrees 20 ' N fracture zone and the Mid-Atlantic Ridge. *Geochim. Cosmochim. Acta* **62**, 2323-2333.

Chasar, L. S., Chanton, J. P., Glaser, P. H., and Siegel, D. I., 2000. Methane concentration and stable isotope distribution as evidence of rhizospheric processes: Comparison of a fen and bog in the Glacial Lake Agassiz Peatland complex. *Ann Bot-London* **86**, 655-663.

Devereux, R., Hines, M. E., and Stahl, D. A., 1996. S cycling: Characterization of natural communities of sulfate-reducing bacteria by 16S rRNA sequence comparisons. *Microb. Ecol.* **32**, 283-292.

Drake, H. L., 1994. Acetogenesis, acetogenic bacteria, and the acetyl-CoA "Wood/Lhungdahl" pathway: past and current perspectives. In: Drake, H. L. (Ed.), *Acetogenesis*. Chapman and Hall, New York.

Fenchel, T., Bernard, C., Esteban, G., Finlay, B. J., Hansen, P. J., and Iversen, N., 1995. Microbial Diversity and Activity in a Danish Fjord with Anoxic Deep-Water. *Ophelia* **43**, 45-100.

Fischer, F., 1935. Die Synthese der Treibstoffe (Kogasin) und Schmierole aus Kohlenoxyd und Wasserstoff bei gewohnlichem Druck. *Brennstoff-Chemie* **16**, 1-11.

Foustoukos, D. I. and Seyfried, W. E., 2004. Hydrocarbons in hydrothermal vent fluids: The role of chromium-bearing catalysts. *Science* **304**, 1002-1005.

Fruh-Green, G. L., Connolly, A. D., Plas, A., Kelley, D. S., and Grobety, B., 2003. Serpentinization of Oceanic Peridotites: Implications for Geochemical Cycles and Biological Activity, *The Subseafloor Biosphere at Mid-Ocean Ridges*.

Fuchs, G., Thauer, R. K., Ziegler, H., and Stichler, W., 1979. Carbon isotopic fractionation by Methanobacterium thermoautotrophicum. *Arch. Microbiol.* **12**, 135-139.

Hartman, H., Sweeney, M. A., Kropp, M. A., and Lewis, J. S., 1993. Carbonaceous Chondrites and the Origin of Life. *Origins Life Evol. Biosph.* **23**, 221-227.

Hayes, J. M., 1993. Factors Controlling C-13 Contents of Sedimentary Organic-Compounds - Principles and Evidence. *Mar Geol* **113**, 111-125.

Hayes, J. M., Takigiku, R., Ocampo, R., Callot, H. J., and Albrecht, P., 1987. Isotopic Compositions and Probable Origins of Organic-Molecules in the Eocene Messel Shale. *Nature* **329**, 48-51.

Herczeg, A. L. and Fairbanks, R. G., 1987. Anomalous Carbon Isotope Fractionation between Atmospheric Co2 and Dissolved Inorganic Carbon Induced by Intense Photosynthesis. *Geochim. Cosmochim. Acta* **51**, 895-899.

Hofmann, A. and Bolhar, R., 2007. Carbonaceous cherts in the Barberton greenstone belt and their significance for the study of early life in the Archean record. *Astrobiology* **7**, 355-388.

Hollander, D. J. and McKenzie, J. A., 1991. CO2 control on carbon-isotope fractionation during photosynthesis: A paleo-pCO2 barometer. *Geology* **19**, 929-932.

Holm, N. G. and Charlou, J. L., 2001. Initial indications of abiotic formation of hydrocarbons in the Rainbow ultramafic hydrothermal system, Mid-Atlantic Ridge. *Earth Planet. Sci. Lett.* **191**, 1-8.

Horita, J. and Berndt, M. E., 1999. Abiogenic methane formation and isotopic fractionation under hydrothermal conditions. *Science* **285**, 1055-1057.

Hornibrook, E. R. C., Longstaffe, F. J., and Fyfe, W. S., 1997. Spatial distribution of microbial methane production pathways in temperate zone wetland soils: Stable carbon and hydrogen isotope evidence. *Geochim. Cosmochim. Acta* **61**, 745-753.

Hornibrook, E. R. C., Longstaffe, F. J., and Fyfe, W. S., 2000. Evolution of stable carbon isotope compositions for methane and carbon dioxide in freshwater

wetlands and other anaerobic environments. *Geochim. Cosmochim. Acta* **64**, 1013-1027.

Immenhauser, A., Della Porta, G., Kenter, J. A. M., and Bahamonde, J. R., 2003. An alternative model for positive shifts in shallow-marine carbonate delta C-13 and delta O-18. *Sedimentology* **50**, 953-959.

Immenhauser, A., Kenter, J. A. M., Ganssen, G., Bahamonde, J. R., Van Vliet, A., and Saher, M. H., 2002. Origin and significance of isotope shifts in Pennsylvanian carbonates (Asturias, NW Spain). *Journal of Sedimentary Research* **72**, 82-94.

Jarrell, K. F. and Kalmokoff, M. L., 1988. Nutritional-Requirements of the Methanogenic Archaebacteria. *Can. J. Microbiol.* **34**, 557-576.

Kelley, D. S. and Fruh-Green, G. L., 1999. Abiogenic methane in deep-seated mid-ocean ridge environments: Insights from stable isotope analyses. *Journal of Geophysical Research-Solid Earth* **104**, 10439-10460.

Kelley, D. S., Karson, J. A., Fruh-Green, G. L., Yoerger, D. R., Shank, T. M., Butterfield, D. A., Hayes, J. M., Schrenk, M. O., Olson, E. J., Proskurowski, G., Jakuba, M., Bradley, A., Larson, B., Ludwig, K., Glickson, D., Buckman, K., Bradley, A. S., Brazelton, W. J., Roe, K., Elend, M. J., Delacour, A., Bernasconi, S. M., Lilley, M. D., Baross, J. A., Summons, R. T., and Sylva, S. P., 2005. A serpentinite-hosted ecosystem: The lost city hydrothermal field. *Science* **307**, 1428-1434.

Kennedy, M. J., Pevear, D. R., and Hill, R. J., 2002. Mineral surface control of Organic Carbon in Black Shale. *Science* **295**, 657-660.

Kitajima, K., Nakamura, E., Takaoka, N., and Murae, T., 2002. Evaluating the thermal metamorphism of CM chondrites by using the pyrolytic behavior of carbonaceous macromolecular matter. *Geochim. Cosmochim. Acta* **66**, 163-172.

Kohler, E. A. and Anhaeusser, C. R., 2002. Geology and geodynamic setting of Archaean silicic metavolcaniclastic rocks of the Bien Venue Formation, Fig Tree Group, northeast Barberton greenstone belt, South Africa. *Precamb. Res.* **116**, 199-235.

Lancet, M. S. and Anders, E., 1970. Carbon Isotope Fractionation in Fischer-Tropsch Synthesis and in Meteorites. *Science* **170**, 980-&.

Lazar, B. and Erez, J., 1992. Carbon Geochemistry of Marine-Derived Brines .1. C-13 Depletions Due to Intense Photosynthesis. *Geochim. Cosmochim. Acta* **56**, 335-345.

Lindsay, J. F., Brasier, M., McLoughlin, N., Green, O. R., Fogel, M., Steele, A., and Mertzman, S. A., 2005a. The problem of deep carbon - An Archean paradox. *Precamb. Res.* **143**, 1-22.

Lindsay, J. F., Brasier, M. D., McLoughlin, N., Green, O. R., Fogel, M., Steele, A., and Mertzman, S. A., 2005b. The problem of deep carbon - An Archean paradox. *Precamb. Res.* **143**, 1-22.

Llorca, J. and Casanova, I., 1998. Formation of carbides and hydrocarbons in chondritic interplanetary dust particles: A laboratory study. *Meteorit Planet Sci* **33**, 243-251.

Londry, K. L., Dawson, K. G., Grover, H. D., Summons, R. E., and Bradley, A. S., 2008. Stable isotope fractionation between substrates and products of Methanosarcina barkeri. *Org. Geochem.* **39**, 608-621.

Lovley, D. R., Dwyer, D. F., and Klug, M. J., 1982. Kinetic-Analysis of Competition between Sulfate Reducers and Methanogens for Hydrogen in Sediments. *Appl. Environ. Microbiol.* **43**, 1373-1379.

Magaritz, M., 1989. C-13 Minima Follow Extinction Events - a Clue to Faunal Radiation. *Geology* **17**, 337-340.

Magaritz, M. and Issar, A., 1973. Carbon and Oxygen Isotopes in Epigenetic Hydrothermal Rocks from Hamam-El-Farun, Sinai. *Chem. Geol.* **12**, 137-146.

McCollom, T. M., 2003. Formation of meteorite hydrocarbons from thermal decomposition of siderite (FeCO3). *Geochemica et Cosmochimica Acta* **67**, 311-317.

McCollom, T. M., 2004. Experimental study of potential sources of organic carbon in rocks from the Early Earth*Astrobiology Science Conference*. Cambridge, NASA/AIMS.

McCollom, T. M., Ritter, G., and Simoneit, B. R. T., 1999. Lipid synthesis under hydrothermal conditions by Fischer-Tropsch-type reactions. *Origins Life Evol. Biosph.* **29**, 153-166.

McCollom, T. M. and Seewald, J. S., 2003a. Experimental constraints on the hydrothermal reactivity of organic acids and acid anions: I. Formic acid and formate. *Geochim. Cosmochim. Acta* **67**, 3625-3644.

McCollom, T. M. and Seewald, J. S., 2003b. Experimental study of the hydrothermal reactivity of organic acids and acid anions: II. Acetic acid, acetate, and valeric acid. *Geochim. Cosmochim. Acta* **67**, 3645-3664.

McCollom, T. M. and Seewald, J. S., 2006. Carbon isotope composition of organic compounds produced by abiotic synthesis under hydrothermal conditions. *Earth Planet. Sci. Lett.* **243**, 74-84.

McCrea, J. M., 1950. On the isotopic chemistry of carbonates and a paleotemperature scale. *J. Chem. Phys.* **18**, 849-857.

Orphan, V. J., House, C. H., Hinrichs, K., McKeegan, K. D., and DeLong, E. F., 2001. Methane-consuming archaea revealed by directly coupled isotopic and phylogenetic analysis. *Science* **293**, 484-487.

Panchuk, K. M., Holmden, C., and Kump, L. R., 2005. Sensitivity of the epeiric sea carbon isotope record to local-scale carbon cycle processes: Tales from the Mohawkian Sea. *Palaeogeogr. Palaeoclimatol. Palaeoecol.* **228**, 320-337.

Patterson, W. P. and Walter, L. M., 1994. Depletion of C-13 in Seawater Sigma-Co2 on Modern Carbonate Platforms - Significance for the Carbon Isotopic Record of Carbonates. *Geology* **22**, 885-888.

Potter, J., Rankin, A. H., and Treloar, P. J., 2004. Abiogenic Fischer-Tropsch synthesis of hydrocarbons in alkaline igneous rocks; fluid inclusion, textural and isotopic evidence from the Lovozero complex, N.W Russia. *Lithos* **75**, 311-330.

Riedel, C., Schmid, M., Botz, R., and Theilen, F., 2001. The Grimsey hydrothermal field offshore North Iceland: crustal structure, faulting and related gas venting. *Earth Planet. Sci. Lett.* **193**, 409-421.

Romanek, C. S., Grossman, E. L., and Morse, J. W., 1992. Carbon Isotopic Fractionation in Synthetic Aragonite and Calcite - Effects of Temperature and Precipitation Rate. *Geochim. Cosmochim. Acta* **56**, 419-430.

Roper, M., 1983. Fischer-Tropsch Synthesis. In: Klein, W. (Ed.), *Catalysis in C1 Chemistry*. D. Reidel Publishing Company, Dordrecht.

Rosing, M. T., 1999. ^{13}C-depleted carbon microparticles in >3700-Ma sea-floor sedimentary rocks from west Greenland. *Science* **283**, 74-76.

Rushdi, A. I. and Simoneit, B. R. T., 2001. Lipid formation by aqueous Fischer-Tropsch-type synthesis over a temperature range of 100 to 400 degrees C. *Origins Life Evol. Biosph.* **31**, 103-118.

Rushdi, A. I. and Simoneit, B. R. T., 2004. Condensation reactions and formation of amides, esters, and nitriles under hydrothermal conditions. *Astrobiology* **4**, 211-224.

Salvi, S. and Williams-Jones, A. E., 1997. Fischer-Tropsch synthesis of hydrocarbons during sub-solidus alteration of the Strange Lake peralkaline granite, Quebec/Labrador, Canada. *Geochim. Cosmochim. Acta* **61**, 83-99.

Schink, B. and Stams, A. J. M., 2002. Syntrophism among prokaryotes. In: Dworkin, M. (Ed.),*The prokaryotes: an evolving electronic resource for the microbiological community*. Springer, New York.

Schmitz, R. A., Daniel, R., Deppenmeir, U., and Gottschalk, G., 2001. Syntrophism among prokaryotes. In: Dworkin, M. (Ed.),*The prokaryotes: an evolving electronic resource for the microbiological community*. Springer, New York.

Schulte, M., Blake, D., Hoehler, T., and Mccollom, T., 2006. Serpentinization and its implications for life on the early Earth and Mars. *Astrobiology* **6**, 364-376.

Septhon, M. A., Verchovsky, A. B., and Wright, I. P., 2004. Carbon and nitrogen isotope ratios in meteoritic organic matter: indicators of alteration processes on the parent asteroid. *International Journal of Astrobiology* **3**, 221-227.

Shackleton, 1985. Oceanic carbon isotope constraints on oxygen and carbon dioxide in the Cenozoic atmosphere. *Geophysical Monograph Series* **32**, 412-417.

Sherwood-Lollar, B., Frape, S. K., Weise, S. M., Fritz, P., Macko, S. A., and Welhan, J. A., 1993. Abiogenic methanogenesis in crystalline rocks. *Geochimica Cosmochimica Acta* **57**, 5087-5097.

Sherwood-Lollar, B., Westgate, T. D., Ward, J. A., Slater, G. F., and Lacrampe-Couloume, G., 2002. Abiogenic formation of alkanes in the Earth's crust as a minor source for global hydrocarbon reservoirs. *Nature* **416**, 522-524.

Shimoyama, A., 1997. Complex organics in meteorites. *Adv. Space Res.* **19**, 1045-1052.

Shock, E. L., 1990. Geochemical Constraints on the Origin of Organic-Compounds in Hydrothermal Systems. *Origins Life Evol. Biosph.* **20**, 331-367.

Shock, E. L. and Schulte, M. D., 1998. Organic synthesis during fluid mixing in hydrothermal systems. *Journal of Geophysical Research-Planets* **103**, 28513-28527.

Simoneit, B. R. T., 2004. Prebiotic organic synthesis under hydrothermal conditions: an overview. *Space Life Sciences: Steps toward Origin(S) of Life* **33**, 88-94.

Simoneit, B. R. T., Lein, A. Y., Peresypkin, V. I., and Osipov, G. A., 2004. Composition and origin of hydrothermal petroleum and associated lipids in the

sulfide deposits of the Rainbow Field (Mid-Atlantic Ridge at 36 degrees N). *Geochim. Cosmochim. Acta* **68**, 2275-2294.

Sleep, N. H., Meibom, A., Fridriksson, T., Coleman, R. G., and Bird, D. K., 2004. H-2-rich fluids from serpentinization: Geochemical and biotic implications. *Proc. Natl. Acad. Sci. U. S. A.* **101**, 12818-12823.

Spero, H. J., Bijma, J., Lea, D. W., and Bemis, B. E., 1997. Effect of seawater carbonate concentration on foraminiferal carbon and oxygen isotopes. *Nature* **390**, 497-500.

Summons, R. E., Franzmann, P. D., and Nichols, P. D., 1998. Carbon isotopic fractionation associated with methylotrophic methanogenesis. *Org. Geochem.* **28**, 465-475.

Swart, P. K. and Eberli, G., 2005. The nature of the delta C-13 of periplatform sediments: Implications for stratigraphy and the global carbon cycle. *Sediment Geol* **175**, 115-129.

Szatmari, P., 1989. Petroleum Formation by Fischer-Tropsch Synthesis in Plate-Tectonics. *Aapg Bulletin-American Association of Petroleum Geologists* **73**, 989-998.

Taran, Y., Kliger, G. A., and Sevastianov, S., 2007. Carbon isotope effects in the open-system Fischer-Tropsch synthesis. *Geochemica et Cosmochimica Acta* **71**, 4474-4487.

Tian, F., Toon, O. B., Pavlov, A. A., and De Sterck, H., 2005. A hydrogen-rich early Earth atmosphere. *Science* **308**, 1014-1017.

Ueno, Y., Yoshioka, H., Isozaki, Y., and Maruyama, S., 2003. Origin of 13C-depleted kerogen in ca. 3.5 Ga hydrothermal silica dikes from Western Australia*Goldschmidt*.

Ueno, Y., Yoshioka, H., Maruyama, S., and Isozaki, Y., 2004. Carbon isotopes and petrography of kerogens in similar to 3.5-Ga hydrothermal silica dikes in the North Pole area, Western Australia. *Geochim. Cosmochim. Acta* **68**, 573-589.

Valentine, D. L., 2001. Thermodynamic ecology of hydrogen-based syntrophy. In: Seckback, J. (Ed.), *Symbiosis: mechanism and model systems*. Kluwer, Dordrecht.

van Kranendonk, M., 2006. Volcanic degassing, hydrothermal circulation and the flourishing of life on Earth: A review of the evidence from c. 3490-3240 Ma rocks of the Pilbara Supergroup, Pilbara Craton, Western Australia. *Earth Science Review* **74**, 197-240.

van Kranendonk, M. J., Webb, G. E., Kamber, B., and Pirajno, F., 2003. Geological setting and biogenicity of 3.45 Ga stromatolitic cherts, east Pilbara, Australia. *Geochim. Cosmochim. Acta* **67**, A510-A510.

van Zuilen, M. A., Lepland, A., and Arrhenius, G., 2002. Reassessing the evidence for the earliest traces of life. *Nature* **418**, 627-630.

van Zuilen, M. A., Lepland, A., Teranes, J., Finarelli, J., Wahlen, M., and Arrhenius, G., 2003. Graphite and carbonates in the 3.8 Ga old Isua Supracrustal Belt, southern West Greenland. *Precamb. Res.* **126**, 331-348.

Voglesonger, K. M., Holloway, J. R., Dunn, E. E., Dalla-Betta, P. J., and O'Day, P. A., 2001. Experimental abiotic synthesis of methanol in seafloor hydrothermal systems during diking events. *Chem. Geol.* **180**, 129-139.

Walsh, M. M. and Lowe, D. R., 1999. Modes of accumulation of carbonaceous matter in the Early Archaean: A petrographic and geochemical study of the cabonaceous cherts of the Swaziland Supergroup. In: Lowe, D. R. and Byerly, G. R. Eds.), *Geologic Evolution of the Barberton Greenstone Belt, South Africa*. Geological Society of America.

Weisset, H. J., Lini, A., Follmi, K. B., and Kuhn, O., 1998. Correlation of Early Cretaceous carbon isotope stratigraphy and platform drowning events: a possible link? *Palaeogeogr. Palaeoclimatol. Palaeoecol.* **137**, 189-203.

Whiticar, M. J., Faber, E., and Schoell, M., 1986. Biogenic Methane Formation in Marine and Fresh-Water Environments - Co2 Reduction Vs Acetate Fermentation Isotope Evidence. *Geochim. Cosmochim. Acta* **50**, 693-709.

Yuen, G. U., Pecore, J. A., Kerridge, J. F., Pinnavaia, T. J., Rightor, E. G., Flores, J., Wedeking, K. W., Mariner, R., Des Marais, D. J., and Chang, S., 1990. Carbon isotopic fractionation in Fischer-Tropsch type reactions*LPSC XXI*.

Zolotov, M. and Shock, E., 1999. Abiotic synthesis of polycyclic aromatic hydrocarbons on Mars. *Journal of Geophysical Research-Planets* **104**, 14033-14049.

Zolotov, M. Y. and Shock, E. L., 2000. A thermodynamic assessment of the potential synthesis of condensed hydrocarbons during cooling and dilution of volcanic gases. *Journal of Geophysical Research-Solid Earth* **105**, 539-559.

Zolotov, M. Y. and Shock, E. L., 2001. Stability of condensed hydrocarbons in the solar nebula. *Icarus* **150**, 323-337.

BIBLIOGRAPHY

Abrajano, T. A., Sturchio, N. C., Kennedy, B. M., Lyon, G. L., Muehlenbachs, K., and Bohlke, J. K., 1990. Geochemistry of Reduced Gas Related to Serpentinization of the Zambales Ophiolite, Philippines. Appl Geochem 5, 625-630.

Adelseck, C. G. and Berger, W. H., 1975. On the dissolution of planktonic foraminifera and associated microfossils during settling and on the sea floor. In: Sliter, W. V., Be, A. W. H., and Berger, W. H. (Eds.), Dissolution of deep-sea carbonates. Cushman Foundation.

Adlis, D. S., Grossman, E. L., Yancey, T. E., and McLerran, R. D., 1988. Isotope stratigraphy and paleodepth changes of Pennsylvanian cyclical sedimentary deposits. Palaios 3, 487-506.

Aitken, B. G. and Echeverria, L. M., 1984. Petrology and Geochemistry of Komatiites and Tholeiites from Gorgona-Island, Colombia. Contrib. Mineral. Petrol. 86, 94-105.

Akahane, H., Furuno, T., Miyajima, H., Yoshikawa, T., and Yamamoto, S., 2004. Rapid wood silicification in hot spring water: an explanation of silicification of wood during the Earth's history. Sediment Geol 169, 219-228.

Algeo, T. J. and Maynard, J. B., 2008. Trace-metal covariation as a guide to water-mass conditions in ancient anoxic marine environments. Geosphere 4, 872-887.

Alibert, C. and Mcculloch, M. T., 1993. Rare-Earth Element and Neodymium Isotopic Compositions of the Banded Iron-Formations and Associated Shales from Hamersley, Western-Australia. Geochimica Et Cosmochimica Acta 57, 187-204.

Alibo, D. S. and Nozaki, Y., 1999. Rare earth elements in seawater: Particle association, shale-normalization, and Ce oxidation. Geochim. Cosmochim. Acta 63, 363-372.

Allaart, J.H., 1976. The pre-3760 m.y. old supracrustal rocks of the Isua area, central West Greenland, and the associated occurrence fo quartz-banded ironstone, In: The Early History of the Earth, B.F. Windley, ed., Wiley, London, p 177-189.

Allard, G. O., Caty, J.-L., and Gobeil, C., 1985. The Archean supracrustal rocks of the Chibougamau area. Geological Association of Canada.

Allen, J. F., 2002. Photosynthesis of ATP - electrons, proton pumps, rotors and poise. Cell 110, 349-360.

Allwood, A. C., Walter, M. R., Kamber, B. S., Marshall, C. , and Burch, I. W., 2006. Stromatolite reef from the Early Archaean era of Australia. Nature 441, 714-718.

Allwood, A. C., Walter, M. R., Burch, I. A., and Kamber, B. S., 2008. 3.43 billion-year-old stromatolite reef from the Pilbara Craton of Western Australia: ecosystem-scale insights to early life on Earth. Precamb. Res. 158, 198-227.

Alonso-Zarza, A. M., Sanchez-Moya, Y., Bustillo, M. A., Sopena, A., and Delgado, A., 2002. Silicification and dolomitization of anhydrite nodules in argillaceous terrestrial deposits: an example of meteoric-dominated diagenesis from the Triassic of central Spain. Sedimentology 49, 303-317.

Alperin, M. J. and Reeburgh, W. S., 1985. Inhibition Experiments on Anaerobic Methane Oxidation. Appl. Environ. Microbiol. 50, 940-945.

Alt, J.C., 1988, ‘Hydrothermal oxide and nontronite deposits on seamounts in the Eastern Pacific’, Marine Geology, 81, p 227-239.

Alt, J. C., 1995a. Subseafloor processes in mid-ocean ridge hydrothermal systems. In: Humphris, S. E., Zierenberg, R. A., Mullineaux, L. S., and Thomson, R. E. Eds.), Seafloor Hydrothermal Systems: Physical, Chemical, Biological and Geological Interactions. American Geophysical Union, Washington, D.C.

Alt, J. C., 1995b. Subseafloor processes in mid-ocean ridge hydrothermal systems. In: Humphris, S. E., Zierenberg, R. A., Mullineaux, L. S., and Thomsen, H. S. Eds.), Seafloor hydrothermal systems: physical, chemical, biological, and geological interactions. American Geophysical Union.

Alt, J. C. and Bach, W., 2003. Alteration of oceanic crust: subsurface rock-water interactions. In: Halbach, E., Tunnicliffe, V., and Hein, J. R. Eds.), Energy and Mass Transfer in Marine Hydrothermal Systems. Dahlem University Press, Berlin.

Alt, J. C., Laverne, C., Vanko, D., Tartarotti, , Teagle, D. A. H., Bach, W., Zuleger, E., Erzinger, E., Erzinger, J., and Honnorez, J., 1996. Hydrothermal alteration of a section of upper oceanic crust in the Eastern Equatorial Pacific: a synthesis of results from site 504 (DSDP/ODP Legs 69, 70, and 83, and ODP Legs 111, 137,140, and 148). In: Alt, J. C., Kinoshita, H., Stokking, L. B., and Michael, J. Eds.), Proceedings of the Ocean Drilling Program, Scientific Results.

Amores, D. R. and Warren, L. A., 2007. Identifying when microbes biosilicify: The interconnected requirements of acidic pH, colloidal SiO2 and exposed microbial surface. Chem. Geol. 240, 298-312.

Anderson, R. F. and Schiff, S. L., 1987. Alkalinity Generation and the Fate of Sulfur in Lake-Sediments. Can. J. Fish. Aquat. Sci. 44, 188-193.

Anbar, A. D., Zahnle, K., Arnold, G. L., and Mojzsis, S. J., 2001. Extraterrestrial iridium, sediment accumulation and the habitability of the early Earth's surface. J. Geophys. Res. 102 [E2], 3219-3237.

Andrews, J. E., Turner, M. S., Nabi, G., and Spiro, B., 1991. The Anatomy of an Early Dinantian Terraced Floodplain - Paleoenvironment and Early Diagenesis. Sedimentology 38, 271-287.

Appel, W.U., 1980, ‘On the Early Archaean Isua iron-formation, west Greenland’, Precambrian Research, 11, 73-98.

Appel, W.U., Fedo, C.M., Moorbath, S., Myers, J.S., 1998. Recognizable primary volcanic and sedimentary features in a low-strain domain of the highly deformed, oldest known (~3.7-3.8 Gyr) greenstone belt, Isua, Greenland. Terra Nova 10(2), 57-62.

Archer, D., Emerson, S., and Reimers, C., 1989. Dissolution of Calcite in Deep-Sea Sediments - Ph and O-2 Microelectrode Results. Geochim. Cosmochim. Acta 53, 2831-2845.

Archer, D., Emerson, S., and Smith, C. R., 1989. Direct Measurement of the Diffusive Sublayer at the Deep-Sea Floor Using Oxygen Microelectrodes. Nature 340, 623-626.

Archer, D. and Devol, A., 1992. Benthic Oxygen Fluxes on the Washington Shelf and Slope - a Comparison of Insitu Microelectrode and Chamber Flux Measurements. Limnolology Oceanography 37, 614-629.

Arenas, C., Zarza, A. M. A., and Pardo, G., 1999. Dedolomitization and other early diagenetic processes in Miocene lacustrine deposits, Ebro Basin (Spain). Sediment Geol 125, 23-45.

Armstrong, F. A. J., Compston, W., de Wit, D. W., and Williams, I. S., 1990. The stratigraphy of the 3.5-3.2 Ga Barberton Greenstone Belt revisted: a single zircon ion microprobe study. Earth and Planetary Science Letters 101, 90-106.

Armstrong, R.L., 1991. The persistent myth of crustal growth. Aus. J. of Earth Sci. 38, 613-630.

Arndt, N. T., Nelson, D. R., Compston, W., Trendall, A. F., and Thorne, A. M., 1991. The age of the Fortescue Group, Hamersley Basin, Western Australia, from ion microprobe zircon U-Pb results. Australian Journal of Earth Sciences 38, 261-281.

Arvidson, R. S. and Mackenzie, F. T., 1999. The dolomite problem: Control of precipitation kinetics by temperature and saturation state. Am. J. Sci. 299, 257-288.

Awramik, S. M., Schopf, J. W., and Walter, M. R., 1983. Filamentous Fossil Bacteria from the Archean of Western Australia. Precamb. Res. 20, 357-374.

Ayres, L. D., Thurston, C., Card, K. D., and Weber, W., 1985. Archean Supracrustal Sequences: An Introduction and Perspective. Geological Association of Canada.

Baars, F. J., 1997. The São Francisco craton. In: De Wit, D. W. and Ashwal, L. D. Eds.), Greenstone Belts. Oxford University.

Bach, W., Alt, J. C., Niu, Y., and Humpris, S. E., 2001. The geochemical consequences of late-stage low-grade alteration of lower ocean crust at the SW Indian Ridge: Results from ODP Hole 735B (Leg 176). Geochim. Cosmochim. Acta 65, 3267-3287.

Baglow, N., 1992, ‘Bindura’, Geological Survey of Zimbabwe Map, 1:100 000.

Baker, D. E. L., Seccombe, K., and Collins, W. J., 2002. Structural history and timing of gold mineralization in the northern East Strelley Belt, Pilbara Craton, Western Australia. Economic Geology 97, 775-785.

Baker, J. H. and de Groot, A., 1983. Proterozoic seawater - felsic volcanics interaction W. Bergslagen, Sweden. Evidence for high REE mobility and implications for 1.8 Ga seawater compositions. Contrib. Mineral. Petrol. 82, 119-130.

Baglow, N., 1992, 'Bindura', Geological Survey of Zimbabwe Map, 1:100 000.

Banerjee, N. R., Furnes, H., Muehlenbachs, K., Staudigel, H., and de Wit, M., 2006. Preservation of similar to 3.4-3.5 Ga microbial biomarkers in pillow lavas and hyaloclastites from the Barberton Greenstone Belt, South Africa. Earth Planet. Sci. Lett. 241, 707-722.

Banerjee, D. M., Simonetti, A., Furnes, H., Muehlenbachs, K., Staudigel, H., Heaman, L. M., and van Kranendonk, M., 2007. Direct dating of Archean microfossil ichnofossils. Geology 35, 487-490.

Banner, J. L., 1995. Application of the Trace-Element and Isotope Geochemistry of Strontium to Studies of Carbonate Diagenesis. Sedimentology 42, 805-824.

Banner, J. L., Hanson, G. N., and Meyers, W. J., 1988. Rare-Earth Element and Nd Isotopic Variations in Regionally Extensive Dolomites from the Burlington-Keokuk Formation (Mississippian) - Implications for Ree Mobility During Carbonate Diagenesis. J Sediment Petrol 58, 415-432.

Barbera, G., Lo Giudice, A., Mazzoleni, , Pappalardo, A., 2009. Combined statistical and petrological analysis of provenance and diagenetic history of mudrocks: Application to Alpine Tethydes shales (Sicily, Italy). Sediment Geol 213, 27-40.

Barley, M. E., Dunlop, J. S. R., Glover, J. E., and Groves, D. I., 1979. Sedimentary evidence for an Archaean shallow-water volcanic-sedimentary facies, eastern Pilbara Block, Western Australia. Earth Planet. Sci. Lett. 43, 74-84.

Barley, M. E., 1980. Evolution of Archaean calc-alkaline volcanics: a study of the Kelly Greenstone Belt and McPhee Dome, eastern Pilbara Block, Western Australia. Ph.D. thesis, University of Western Australia.

Barley, M. E. and Bickle, M. J., 1982. Komatiites in the Pilbara Block, Western Australia. In: Arndt, N. T. and Nisbet, E. G. Eds.), Komatiites. George Allen and Unwin, London, United Kingdom.

Barley, M. E., 1984. Volcanism and hydrothermal alteration, Warrawoona Group, East Pilbara. In: Muhling, J. R., Groves, D. I., and Blake, T. S. Eds.), Archaean and Proterozoic basins of the the Pilbara, Western Australia: evolution and mineralization potential. University of Western Austrlia, Perth.

Barley, M. E., Pickard, A. L., and Sylvester, J., 1997, 'Emplacement of a large igneous province as a possible cause of banded iron formation 2.45 billion years ago', Nature, 385, 55-58.

Baross, J. A. and Hoffman, S. E., 1985. Submarine Hydrothermal Vents and Associated Gradient Environments as Sites for the Origin and Evolution of Life. Origins Life Evol. Biosph. 15, 327-345.

Bartley, J. K., Knoll, A. H., Grotzinger, J. , and Sergeev, V. N., 2000. Lithification and fabric genesis in precipitated stromatolites and associated peritidal carbonates, Mesoproterozoic Billyakh Group, Siberia. SEPM Special Publications 67, 59-73.

Basturk, O., Saydam, C., Salihoglu, I., Eremeeva, L. V., Konovalov, S. K., Stoyanov, A., Dimitrov, A., Cociasu, A., Dorogan, L., and Altabet, M., 1994. Vertical Variations in the Principle Chemical-Properties of the Black-Sea in the Autumn of 1991. Mar. Chem. 45, 149-165.

Bathurst, R. G., 1974. Marine Diagenesis of Shallow-Water Calcium-Carbonate Sediments. Annu Rev Earth Pl Sc 2, 257-274.

Bathurst, R. G. C., 1971. Carbonate sediments and their diagenesis. Elsevier, Amsterdam, New York,.

Bau, M., 1991. Rare-Earth Element Mobility During Hydrothermal and Metamorphic Fluid Rock Interaction and the Significance of the Oxidation-State of Europium. Chem. Geol. 93, 219-230.

Bau, M. and Moller, , 1992. Rare-Earth Element Fractionation in Metamorphogenic Hydrothermal Calcite, Magnesite and Siderite. Mineralogy and Petrology 45, 231-246.

Bau, M., 1993. Effects of Syn-Depositional and Postdepositional Processes on the Rare-Earth Element Distribution in Precambrian Iron-Formations. Eur J Mineral 5, 257-267.

Bau, M., Moller, P. 1993. Rare-Earth Element Systematics of the Chemically Precipitated Component in Early Precambrian Iron Formations and the Evolution of the Terrestrial Atmosphere-Hydrosphere-Lithosphere System. Geochim. Cosmochim. Acta 57(10), 2239-2249.

Bau, M., 1996. Controls on the fractionation of isovalent trace elements in magmatic and aqueous systems: Evidence from Y/Ho, Zr/Hf, and lanthanide tetrad effect. Contrib. Mineral. Petrol. 123(3), 323-333.

Bau, M., Dulski, P., 1996. Distribution of yttrium and rare-earth elements in the Penge and Kuruman iron-formations, Transvaal Supergroup, South Africa. Precamb. Res. 79(1-2), 37-55.

Bau, M., Dulski, P., 1999. Comparing yttrium and rare earths in hydrothermal fluids from the Mid-Atlantic Ridge: implications for Y and REE behaviour during near-vent mixing and for the Y/Ho ratio of Proterozoic seawater. Chem. Geol. 155(1-2), 77-90.

Bau, M., 1999. Scavenging of dissolved yttrium and rare earths by precipitating iron oxyhydroxide: Experimental evidence for Ce oxidation, Y-Ho fractionation, and lanthanide tetrad effect. Geochim. Cosmochim. Acta 63, 67-77.

Bau, M. and Alexander, B., 2006. Preservation of primary REE patterns without Ce anomaly during dolomitization of Mid-Paleoproterozoic limestone and the potential re-establishment of marine anoxia immediately after the "Great Oxidation Event". S Afr J Geol 109, 81-86.

Bau, M. and Alexander, B., 2009. Distribution of high field strength elements (Y, Zr, REE, Hf, Ta, Th, U) in adjacent magnetite and chert bands and in reference

standards FeR-3 and FeR-4 from the Temagami iron-formation, Canada, and the redox level of the Neoarchean ocean. Precamb. Res. 174, 337-346.

Baur, M. E., 1978. Thermodynamics of heterogeneous iron-carbon systems: implications for the terrestrial primitive reducing atmosphere. Chem. Geol. 22, 189-206.

Baur, M. E., Hayes, J. M., Studley, S. A., and Walter, M. R., 1985. Millimeter-Scale Variations of Stable Isotope Abundances in Carbonates from Banded Iron-Formations in the Hamersley Group of Western-Australia. Economic Geology 80, 270-282.

Beal, E. J., House, C. H., and Orphan, V. J., 2009. Manganese- and iron-dependent marine methane oxidation. Science 325, 184-187.

Beaumont, V. and Robert, F., 1998. Nitrogen isotopic composition of organic matter from Precambrian cherts: new keys for nitrogen cycle evolution? Bulletin Societe geologique France 169, 211-220.

Beaumont, V. and Robert, F., 1999. Nitrogen isotope ratios of kerogens in Precambrian cherts: a record of the evolution of atmospheric chemistry? Precamb. Res. 96, 63-82.

Becker, R. H. and Clayton, R. N., 1976. Oxygen Isotope Study of a Precambrian Banded Iron-Formation, Hamersley Range, Western-Australia. Geochim. Cosmochim. Acta 40, 1153-1165.

Beckinsale, R. D., Drury, S. A., and Holt, R. W., 1980. 3,360-Myr Old Gneisses from the South Indian Craton. Nature 283, 469-470.

Bekker, A., Karhu, J. A., Eriksson, K. A., and Kaufman, A. J., 2003. Chemostratigraphy of Paleoproterozoic carbonate successions of the Wyoming Craton: tectonic forcing of biogeochemical change? Precamb. Res. 120, 279-325.

Belevtsev, Ya. N., Belevtsev, R. Ya., Siroshtan, R.I., 1982. The Krivoy Rog Basin. In: Trendall, A.F., Morris, R.C. (eds.), ‘Iron-formation: facts and problems’, Elsevier, Amsterdam, p 211-252.

Belka, Z., 1998. Early Devonian Kess-Kess carbonate mud mounds of the eastern Anti-Atlas (Morocco), and their relation to submarine hydrothermal venting. Journal of Sedimentary Research 68, 368-377.

Bell, K., Blenkinsop, J., and Moore, J. M., 1975. Evidence for a Proterozoic Greenstone Belt from Snow Lake, Manitoba. Nature 258, 698-701.

Belonoshko, A. and Saxena, S.K., 1991. A Molecular-Dynamics Study of the Pressure-Volume-Temperature Properties of Supercritical Fluids .2. CO2, CH4, CO, O2, and H2. Geochimica Et Cosmochimica Acta, 55(11): 3191-3208.

Bengston, S., 1994. The advent of the animal skeleton. In: Bengston, S. (Ed.), Early life on Earth. Columbia University Press, New York.

Benning, L. G., Phoenix, V. R., Yee, N., and Konhauser, K. O., 2004a. The dynamics of cyanobacterial silicification: An infrared micro-spectroscopic investigation. Geochim. Cosmochim. Acta 68, 743-757.

Benning, L. G., Phoenix, V. R., Yee, N., and Tobin, M. J., 2004b. Molecular characterization of cyanobacterial silicification using synchrotron infrared micro-spectroscopy. Geochim. Cosmochim. Acta 68, 729-741.

Bensen, J., 1994. Carbonate deposition, Pyramid Lake subbasin, Nevada: 1. Sequence of formation and elevational distribution of carboante deposits (tufas). Palaeogeogr. Palaeoclimatol. Palaeoecol. 109, 55-89.

Berelson, W. M., Hammond, D. E., Mcmanus, J., and Kilgore, T. E., 1994. Dissolution Kinetics of Calcium-Carbonate in Equatorial Pacific Sediments. Global Biogeochem Cy 8, 219-235.

Berelson, W. M., Hammond, D. E., Oneill, D., Xu, X. M., Chin, C., and Zukin, J., 1990. Benthic Fluxes and Pore Water Studies from Sediments of the Central Equatorial North Pacific - Nutrient Diagenesis. Geochim. Cosmochim. Acta 54, 3001-3012.

Berndt, M. E., Allen, D. E., and Seyfried, W. E., 1996. Reduction of CO2 during serpentinization of olivine at 300 degrees C and 500 bar. Geology 24, 351-354.

Berner, R. A., 1975. The role of magnesium in the crystal growth of calcite and aragonite from sea water. 39, 489-504.

Berner, R. A. and Morse, J. W., 1974. Dissolution Kinetics of Calcium-Carbonate in Sea-Water .4. Theory of Calcite Dissolution. Am. J. Sci. 274, 108-134.

Berner, R. A., Westrich, J. T., Graber, R., Smith, J., and Martens, C. S., 1978. Inhibition of Aragonite Precipitation from Super-Saturated Seawater - Laboratory and Field-Study. Am. J. Sci. 278, 816-837.

Berner, R. A., 1989. Biogeochemical cycles of carbon and sulfur and their effect on atmospheric oxygen over Phanerozoic time. Palaeogeography, Palaeoclimatology and Palaeoecology 73, 97-122.

Berner, R. A. and Lasaga, A. C., 1989. Modeling the Geochemical Carbon-Cycle. Sci. Am. 260, 74-81.

Bettenay, L. F., Bickle, M. J., Boulter, C. A., Groves, D. I., Morant, , Blake, T. S., and James, B. A., 1981. Evolution of the Shaw Batholith - an Archaean granitoid-gneiss dome in the eastern Pilbara, Western Australia. Geological Society of Australia Special Publication 7, 361-372.

Betts, J. N. and Holland, H. D., 1991. The oxygen content of ocean bottom waters, the burial efficiency of organic carbon, and the regulation of atmospheric oxygen. Palaeogeography; Palaeoclimatology; Palaeoecology 97, 5-18.

Beukes, N.J., 1973, ‘Precambrian iron-formations of southern Africa’, Economic Geology, 68, p 960-1024.

Beukes, N.J., 1983, ‘Paleoenvironmental setting of iron-formations in the depositional basin of the Transvaal Supergroup, South Africa’, In: Trendall, A.F., Morris, R.C. (eds.), ‘Iron-Formation: Facts and Problems’, Elsevier, New York, p 131-209.

Beukes, N. J., 1987. Facies relations, depositional environments and diagenesis in a major early Proterozoic stromatolitic carbonate platform to basinal sequence, Campbellrand Subgroup, Transvaal Supergroup, southern Africa. Sediment Geol 54, 1-46.

Beukes, N. J. and Klein, C., 1990. Geochemistry and Sedimentology of a Facies Transition - from Microbanded to Granular Iron-Formation - in the Early Proterozoic Transvaal Supergroup, South-Africa. Precamb. Res. 47, 99-139.

Beukes, N. J., Klein, C., Kaufman, A. J., and Hayes, J. M., 1990. Carbonate petrography, kerogen distribution, and carbon and oxygen isotope variations in an early Proterozoic transition from limestone to iron-formation deposition, Transvaal Supergroup, South Africa. Economic Geology 85, 663-689.

Beukes, N.J., Klein, C., 1992, 'Models for iron-formation deposition', In: Schopf, J.W. and Klein, C. (eds.), 'The Proterozoic Biosphere, a multidisciplinary study', Cambridge University Press, New York, p 147-152.

Beukes, N., Gutzmer, J., and Mukhopadhyay, D. K., 2002. The geology and genesis of high-grade hematite iron ore deposits. Transactions of the Institute of Mining and Metallurgy, Section B: Applied Earth Science 112, 18-25.

Bhatia, M.R., Crook, K.A.W., 1986. Trace-Element Characteristics of Graywackes and Tectonic Setting Discrimination of Sedimentary Basins. Contrib. Mineral. Petrol. 92(2), 181-193.

Bickle, M. J., Bettenay, L. F., Boulter, C. A., Groves, D. I., and Morant, , 1980. Horizontal tectonic interaction of an Archean gneiss belt and greenstones, Pilbara Block, Western Australia. Geology 8, 525-529.

Bickle, M. J., Morant, , Bettenay, L. F., Boulter, C. A., Blake, J. A., and Groves, D. I., 1985. Archean tectonics of the Shaw batholith, Pilbara Block, Western Australia: Structural and Metamorphic tests of the batholith concept. In: Ayres, L. D. (Ed.), Evolution of Archean Supracrustal Sequences.

Bidigare, R. R., Fluegge, A., Freeman, K. H., Hanson, K. L., Hayes, J. M., Hollander, D., Jasper, J. , King, L. L., Laws, E. A., Milder, J., Millero, F. J., Pancost, R., Popp, B. N., Steinberg, A., and Wakeham, S. G., 1997. Consistent fractionation of C-13 in nature and in the laboratory: Growth-rate effects in some haptophyte algae. Global Biogeochemical Cycles 11, 279-292.

Bidigare, R. R., Fluegge, A., Freeman, K. H., Hanson, K. L., Hayes, J. M., Hollander, D., Jasper, J. , King, L. L., Laws, E. A., Milder, J., Millero, F. J., Pancost, R., Popp, B. N., Steinberg, A., and Wakeham, S. G., 1999. Consistent fractionation of C-13 in nature and in the laboratory: Growth-rate effects in some haptophyte algae. Global Biogeochemical Cycles 13, 251-252.

Bjerrum, C.J., Canfield, D.E., 2002, ‘Ocean productivity before about 1.9 Gyr ago limited by phosphorus adsorption onto iron oxides’, Nature, 417, p 159-162.

Bjonnes, E. and Lindsay, J. F., 2005. The depositional setting of Earth's earliest sedimentary rocks. Lunar and Planetary Science XXXVI.

Blackburn, C. E., Bond, W. D., Breaks, F. W., Davis, D. W., Edwards, G. R., Poulson, K. H., Trowell, N. F., and Wood, J., 1985. Evolution of Archean volcanic-sedimentary sequences of the western Wabigoon subprovince and its margins: a review, Geological Association of Canada special paper. Geological Association of Canada, St. Johns, Nfld.

Blake, T. S., 1984. Evidence for stabilization of the Pilbara Block, Australia. Nature 307, 721-723.

Blake, T. S., 1993. Late Archaean crustal extension, sedimentary basin formation, flood basalt volcanism and continental rifting: the Nullagine and Mount Jope Supersequences, Western Australia. Precamb. Res. 60, 185-241.

Blake, T. S., Buick, R., Brown, S. J. A., and Barley, M. E., 2004. Stratigraphic geochronology of a late Archaean flood basalt province in the Pilbara Craton, Australia: constraints on basin evolution, mafic and felsic volcanism and continental drift rates. Precamb. Res. 133.

Blank, J.G., Delaney, J.R. and Desmarais, D.J., 1993. The Concentration and Isotopic Composition of Carbon in Basaltic Glasses from the Juan-De-Fuca Ridge, Pacific-Ocean. Geochimica Et Cosmochimica Acta, 57(4): 875-887.

Blewett, R. S., 2002. Archaean tectonic processes: a case for horizontal shortening in the North Pilbara Granite-Greenstone Terrane, Western Australia. Precamb. Res. 113, 87-120.

Blichert-Toft, J., Albarede, F., Rosing, M., Frei, R., Bridgwater, D., 1999. The Nd and Hf isotopic evolution of the mantle through the Archean. Results from the Isua supracrustals, West Greenland, and from the Birimian terranes of West Africa. Geochim. Cosmochim. Acta 63(22), 3901-3914.

Blodau, C., Peine, A., Hoffmann, S., and Peiffer, S., 1999. Organic matter diagenesis in acidic mine lakes. Acta Hydrochim. Hydrobiol. 28, 123-135.

Boak, J.L., Dymek, R.F., 1982. Metamorphism of the Ca-3800 Ma Supracrustal Rocks at Isua, West Greenland - Implications for Early Archean Crustal Evolution. Earth Planet. Sci. Lett. 59(1), 155-176.

Bohrmann, G., Abelmann, A., Gersonde, R., Hubberten, H., and Kuhn, G., 1994. Pure Siliceous Ooze, a Diagenetic Environment for Early Chert Formation. Geology 22, 207-210.

Bohrmann, G., Kuhn, G., Abelmann, A., Gersonde, R., and Futterer, D., 1990. A Young Porcellanite Occurrence from the Southwest Indian Ridge. Mar Geol 92, 155-163.

Bolhar, R., Kamber, B.S., Moorbath, S., Fedo, C.M., Whitehouse, M.J., 2004. Characterisation of early Archaean chemical sediments by trace element signatures. Earth Planet. Sci. Lett. 222(1), 43-60.

Bolhar, R., van Kranendonk, M. J., and Kamber, B. S., 2005. A trace element study of siderite-jasper banded iron formation in the 3.45 Ga Warrawoona Group, Pilbara Craton - Formation from hydrothermal fluids and shallow seawater. Precamb. Res. 137, 93-114.

Bolhar, R., Kamber, B.S., Moorbath, S., Whitehouse, M.J., Collerson, K.D., 2005a. Chemical characterization of earth's most ancient clastic metasediments from the Isua Greenstone Belt, southern West Greenland. Geochim. Cosmochim. Acta 69(6), 1555-1573.

Bolhar, R., Van Kranendonk, M.J., Kamber, B.S., 2005b. A trace element study of siderite-jasper banded iron formation in the 3.45 Ga Warrawoona Group, Pilbara Craton - Formation from hydrothermal fluids and shallow seawater. Precamb. Res. 137(1-2), 93-114.

Bosak, T. and Newman, D. K., 2003. Microbial nucleation of calcium carbonate in the Precambrian. Geology 31, 577-580.

Bottinga, Y., 1968. Calculation of Fractionation Factors for Carbon and Oxygen Isotopic Exchange in the System Calcite-Carbon Dioxide-Water. J. Phys. Chem. 72, 800.

Bottinga, Y., 1969. Carbon isotope fractionation between graphite, diamond and carbon dioxide. Earth and Planetary Science Letters, 5(5): 301-307.

Bowers, T. S. and Taylor, H. , 1985. An Integrated Chemical and Stable-Isotope Model of the Origin of Midocean Ridge Hot-Spring Systems. J Geophys Res-Solid 90, 2583-2606.

Bowring, S.A., Housh, T., 1995. The Earth's early evolution. Science 269(15 September), 1535-1540.

Bowring, S. A. and Williams, I. S., 1999. Priscoan (4.00-4.03 Ga) orthogneisses from northwestern Canada. Contrib. Mineral. Petrol. 134, 3-16.

Boyet, M., Blichert-Toft, J., Rosing, M., Storey, M., Telouk, , Albarede, F., 2003. 142Nd evidence for early Earth differentiation. Earth Planet. Sci. Lett. 214, 427-442.

Boynton, W. V., 1984. Cosmochemistry of the rare earth elements: meteorite studies. In: Henderson, (Ed.), Rare Earth Element Geochemistry,. Elsevier, Amsterdam.

Brand, U. and Veizer, J., 1980. Chemical Diagenesis of a Multicomponent Carbonate System .1. Trace-Elements. J Sediment Petrol 50, 1219-1236.

Brasier, M. D., Green, O. R., Jephcoat, A. , Kleppe, A. K., Van Kranendonk, M., Lindsay, J. F., Steele, A., and Grassineau, N. V., 2002. Questioning the evidence for Earth's oldest fossils. Nature 416, 76-81.

Brasier, M.D. et al., 2005. Critical testing of earth's oldest putative fossil assemblage from the similar to 3.5 Ga Apex Chert, Chinaman Creek, western Australia. Precambrian Research, 140(1-2): 55-102.

Brasier, M., McLoughlin, N., Green, O., and Wacey, D., 2006. A fresh look at the fossil evidence for early Archaean cellular life. Philos T R Soc B 361, 887-902.

Braterman, S., Cairns-Smith, A. G., and Sloper, R. W., 1983. Photo-oxidation of hydrated Fe2+ - significance for banded iron formations. Nature 303, 163-164.

Braun, V. and Killmann, H., 1999. Bacterial solutions to the iron-supply problems. Trends in Biochemical Sciences 24, 104-109.

Bridgwater, D., McGregor, V.R., 1974. Field work on the very early Precambrian rocks of the Isua area, southern West Greenland. Rap Grønlands Geol. Unders 65., 49–53.

Bridgwater, D. and Collerson, K. D., 1976. Major Petrological and Geochemical Characters of 3,600 My Uivak Gneisses from Labrador. Contrib. Mineral. Petrol. 54, 43-59.

Brocks, J. J., Logan, G. A., Buick, R., and Summons, R. E., 1999. Archean molecular fossils and the early rise of eukaryotes. Science 285, 1033-1036.

Broecker, W. S. and Takahashi, T., 1966. Calcium Carbonate Precipitation on Bahama Banks. J. Geophys. Res. 71, 1575-&.

Brown, D. A., 2006. Microbial mediation of iron mobilization and deposition in iron formations since the early Precambrian. Geological Society of America Memoir 198, 239-256.

Buick, R., Dunlop, J. S. R., and Groves, D. I., 1981. Stromatolite Recognition in Ancient Rocks - an Appraisal of Irregularly Laminated Structures in an Early Archean Chert-Barite Unit from North-Pole, Western-Australia. Alcheringa 5, 161-181.

Buick, R., 1984. Carbonaceous filaments from North Pole, Western Australia - are they fossil bacteria in Archean stromatolites? Precamb. Res. 24, 157-172.

Buick, R. and Barnes, K. R., 1984. Cherts in the Warrawoona Group: Early Archaean silicified sediments deposited in shallow-water environments. In: Muhling, J. R., Groves, D. I., and Blake, T. S. Eds.), Archaean and Proterozoic basins of the the Pilbara, Western Australia: evolution and mineralization potential. University of Western Austrlia, Perth.

Buick, R., 1985. Life and conditions in the Early Archaean: Evidence from 3500 m.y. old shallow-water sediments in the Warrawoona Group, North Pole, Western Australia. Ph.D. thesis, University of Western Australia.

Buick, R. and Dunlop, J. S. R., 1990. Evaporitic sediments of early Archaean age from the Warrawoona Group, North Pole, Western Australia. Sedimentology 37, 247-277.

Buick, R., 1992. The antiquity of oxygenic photosynthesis: evidence from stromatolites in sulphate-deficient Archaean lakes, Science 255, , 74-77.

Buick, R., Des Marais, D.J., and Knoll, A.H., 1995, Stable isotopic compositions of carbonates from the Mesoproterozoic Bangemall Group, northwestern Australia, Chemical Geology, 123, 153-171.

Buick, R., Thornett, J. R., McNaughton, N. J., Smith, J. B., Barley, M. E., and Savage, M., 1995. Record of emergent continental crust ~3.5 billion years ago in the Pilbara Craton of Australia. Nature 375, 574-577.

Buick, R., Rasmussen, B., and Krapez, B., 1998, Archean oil: evidence for extensive hydrocarbon generation and migration 2.5-3.5 Ga: AAPG Bulletin 82, 50-69.

Buick, R., Brauhart, C. W., Morant, , Thornett, J. R., Maniw, J. G., Archibald, N. J., Doepel, M. G., Fletcher, I. R., Pickard, A. L., Smith, J. B., Barley, M. E., McNaughton, N. J., and Groves, D. I., 2002. Geochronology and stratigraphic relationships of the Sulphur Springs Group and Strelley Granite: a temporally distinct igneous province in the Archaean Pilbara Craton, Australia. Precambrian Research 114, 87-120.

Burke, K. C. and Dewey, J. F., 1972. Orogeny in Africa. In: Dessauvagie, T. F. J. and Whiteman, A. J. Eds.), African Geology.

Burke, K., 1997. Foreword, Greenstone Belts. Clarendon Press.

Burkhardt, S., Riebesell, U., and Zondervan, I., 1999. Effects of growth rate, CO2 concentration, and cell size on the stable carbon isotope fractionation in marine phytoplankton. Geochim. Cosmochim. Acta 63, 3729-3741.

Burton, E. A. and Walter, L. M., 1987a. Relative Precipitation Rates of Aragonite and Mg Calcite from Seawater - Temperature or Carbonate Ion Control. Geology 15, 111-114.

Burton, E. A. and Walter, L. M., 1987b. Relative precipitation rates of aragonite and Mg calcite from seawater: temperature or carbonate ion control? Geology 15, 111-114.

Busemann, H. O. D., Alexander, C. M., and Nittler, L. R., 2007. Characterization of insoluble organic matter in primitive meteorites by microRaman spectroscopy. Meteorit Planet Sci 42, 1387-1416.

Busenberg, E. and Plummer, L. N., 1986. The Solubility of Baco3(Cr) (Witherite) in Co2-H2o Solutions between 0-Degrees and 90-Degrees-C, Evaluation of the Association Constants of Bahc3+(Aq) and Baco3(Aq) between 5-Degrees and 80-Degrees-C, and a Preliminary Evaluation of the Thermodynamic Properties of Ba-2+(Aq). Geochim. Cosmochim. Acta 50, 2225-2233.

Bustillo, M. and Alonso-Zarza, A. M., 2007. Overlapping of pedogenesis and meteoritc diagenesis in distal allucial and shallow lacustrine deposits in the Madrid Miocene Basin, Spain. Sediment Geol 198, 255-271.

Bustillo, M., Fort, R., and Ordonez, S., 1992. Genetic-Implications of Trace-Element Distributions in Carbonate and Noncarbonate Phases of Limestones and Dolostones from Western Cantabria, Spain. Chem. Geol. 97, 273-283.

Bustillo, M. A., Arribas, M. E., and Bustillo, M., 2002. Dolomitization and silicification in low-energy lacustrine carbonates (Paleogene, Madrid Basin, Spain). Sediment Geol 151, 107-126.

Butterfield, D. A., Seyfried, W. E., and Lilley, M. D., 2003. Composition and evolution of hydrothermal fluids. In: Halbach, E., Tunnicliffe, V., and Hein, J. R. Eds.), Energy and Mass Transfer in Marine Hydrothermal Systems. Dahlem University Press, Berlin.

Cairns-Smith, A. G., 1978. Precambrian solution photochemistry, inverse segragation, and banded iron formations. Nature 276, 807-808.

Cairns-Smith, A.G., 1982, ‘Genetic Takeover and the Mineral Origins of Life’, Cambridge University Press.

Calder, J.A., and Parker, L., 1978, Geochemical implications of induced changes in C13 fractionation by blue-green algae: Geochimica et Cosmochimica Acta, v. 37, 133-140.

Calvert, S. E. and Karlin, R. E., 1991. Relationships between sulphur, organic carbon and iron in the modern sediments of the Black Sea. Geochim. Cosmochim. Acta 55, 2483-2490.

Calvert, S. E., Bustin, R. M., and Pedersen, T. F., 1992. Lack of Evidence for Enhanced Preservation of Sedimentary Organic-Matter in the Oxygen Minimum of the Gulf of California. Geology 20, 757-760.

Calvert, S. E. and Pederson, T. F., 1992. Organic matter accumulation, remineralization and burial in an anoxic coastal sediment. In: Whelan, J. and Farrington, J. W. Eds.), Organic carbon accumulation and preservation in marine sediments: How important is Anoxia. Columbia University Press, New York.

Canfield, D. E., 1989. Sulfate reduction and oxic respiration in marine sediments: implications for organic carbon preservation in euxinic environments. Deep-Sea Res. 36, 121-138.

Canfield, D. E., 1993. Organic matter oxidation in marine sediments. In: Wollast, R., Chou, L., and Mackenzie, F. Eds.), Interactions of C,N,P, and S biogeochemical cycles. NATO-ARW.

Canfield, D. E., 1994. Factors influencing organic carbon preservation in marine sediments. Chem. Geol. 114, 315-329.

Canfield, D. E. and Teske, A., 1996. Late Proterozoic rise in atmosphere oxygen concentration inferred from phylogenetic and sulfur-isotope studies. Nature 382, 127-132.

Canfield, D. E. and Raiswell, R., 1999. The evolution of the sulfur cycle. American Journal of Science. 299, 679-723.

Canfield, D. E., Habicht, K. S., and Thamdrup, B., 2000. The Archean sulfur cycle and the early history of atmospheric oxygen. Science. 288, 658-661.

Canfield, D., 2005. The early history of atmospheric oxygen. Annual Review of Earth and Planetary Sciences 33, 1-36.

Carothers, W.W., Adami, L.H. and Rosenbauer, R.J., 1988. Experimental Oxygen Isotope Fractionation between Siderite-Water and Phosphoric-Acid Liberated CO2-Siderite. Geochimica Et Cosmochimica Acta, 52(10): 2445-2450.

Castanier, S., Le Metayer-Levrel, G., and Perthuisot, J. , 1999. Ca-carbonates precipitation and limestone genesis - the microbiogeologist point of view. Sediment Geol 126, 9-23.

Castano, J. R. and Garrels, R. M., 1950. Experiments on the deposition of iron with special reference to the Clinton iron ore deposits. Economic Geology 45, 755-770.

Catalov, G. A., 1983. Triassic Oncoids from Central Balkanides (Bulgaria). In: Peryt, T. M. (Ed.), Coated Grains. Springer-Verlag, Berlin.

Cates, N.L., Mojzsis, S.J., 2007. Pre-3750 Ma supracrustal rocks from the Nuvvuagittuq supracrustal belt, northern Quebec. Earth Planet. Sci. Lett. 255(1-2), 9-21.

Catling, D. C., Zahnle, K. J., and McKay, C. , 2001. Biogenic methane, hydrogen escape, and the irreversible oxidation of early Earth. Science 293, 839-843.

Catling, D. C. and Moore, J. A., 2003. The nature of coarse-grained crystalline hematite and its implications for the early environment of Mars. Icarus 165, 277-300.

Catling, D. C., 2006. Comment on "A hydrogen-rich early Earth atmosphere". Science 311.

Cavalazzi, B., Barbieri, R., and Ori, G. G., 2007. Chemosynthetic microbialites in the Devonian carbonate mounds of Hamar Laghdad (Anti-Atlas, Morocco). Sediment Geol 200, 73-88.

Chacko, T., Cole, D.R. and Horita, J., 2001. Equilibrium oxygen, hydrogen and carbon isotope fractionation factors applicable to geologic systems. Stable Isotope Geochemistry, 43: 1-81.

Chacko, T., Mayeda, T.K., Clayton, R.N. and Goldsmith, J.R., 1991. Oxygen and Carbon Isotope Fractionations between Co2 and Calcite. Geochimica Et Cosmochimica Acta, 55(10): 2867-2882.

Chafetz, H. S. and Buczynski, C., 1992. Bacterially induced lithification of microbial mats. Palaios 7, 277-293.

Chafetz, H. S. and Folk, R. L., 1984. Travertines: depositional morphology and the bacterially constructed constituents. J Sediment Petrol 54, 289-316.

Chanda, S. K., Bhattacharyya, A., and Sakar, S., 1977. Deformation of ooids by compaction: implications for lithification. 88, 1577-1585.

Chanda, S. K., Bhattacharyya, A., and Sarkar, A., 1976. Early diagenetic chert nodules in Bhander Limestone, Maihar, Satna District, Madhya Pradesh, India. J Geol 84, 213-224.

Charlou, J. L., Fouquet, Y., Bougault, H., Donval, J. , Etoubleau, J., Jean-Baptiste, , Dapoigny, A., Appriou, , and Rona, A., 1998. Intense CH4 plumes generated by serpentinization of ultramafic rocks at the intersection of the 15 degrees 20 ' N fracture zone and the Mid-Atlantic Ridge. Geochim. Cosmochim. Acta 62, 2323-2333.

Charlou, J. L., Donval, J. , Fouquet, Y., Jean-Baptiste, , and Holm, N., 2002. Geochemistry of high H-2 and CH4 vent fluids issuing from ultramafic rocks at the Rainbow hydrothermal field (36 degrees 14 ' N, MAR). Chem. Geol. 191, 345-359.

Chasar, L. S., Chanton, J. , Glaser, H., and Siegel, D. I., 2000. Methane concentration and stable isotope distribution as evidence of rhizospheric processes: Comparison of a fen and bog in the Glacial Lake Agassiz Peatland complex. Ann Bot-London 86, 655-663.

Chase, M.W., 1998. NIST-JANAF Thermochemical Tables, Fourth edition. Journal of Physical and Chemical Reference Data, Monograph 9.

Chetty, D. and Frimmel, H. E., 2000. The role of evaporites in the genesis of base metal sulphide mineralisation in the Northern Platform of the Pan-African Damara Belt, Namibia: geochemical and fluid inclusion evidence from carbonate wall rock alteration. Miner Deposita 35, 364-376.

Chilingar, G. V., Bissel, H. J., and Fairbridge, R. W., 1967. Carbonate rocks. Elsevier Pub. Co., Amsterdam, New York,.

Choquette, W., 1955. A petrographic study of the State College siliceous oolite. 63, 337-347, 3 Figs., 1 Tab., 1 Pl.

Chou, L., Garrels, R. M., and Wollast, R., 1988. Comparative-Study of the Dissolution Kinetics and Mechanisms of Carbonates in Aqueous-Solutions. Chem. Geol. 70, 77-77.

Chou, L., Garrels, R. M., and Wollast, R., 1989. Comparative-Study of the Kinetics and Mechanisms of Dissolution of Carbonate Minerals. Chem. Geol. 78, 269-282.

Chung, H.M., Gormlya, J.R. and Squiresa, R.M., 1988. Origin of gaseous hydrocarbons in subsurface environments: Theoretical considerations of carbon isotope distribution. Chemical Geology, 71(1-3): 97-104.

Churchill, H., Teng, H., and Hazen, R. M., 2004. Correlation of pH-dependent surface interaction forces to amino acid adsorption: Implications for the origin of life. Am. Mineral. 89, 1048-1055.

Churnet, H. G. and Misra, K. C., 1981. Genetic-Implications of the Trace-Element Distribution Pattern in the Upper Knox Carbonate Rocks, Copper Ridge District, East Tennessee. Sediment Geol 30, 173-194.

Clayton, R.N., Goldsmith, J.R., Karel, K.J., Mayeda, T.K. and Newton, R.C., 1975. Limits on Effect of Pressure on Isotopic Fractionation. Geochimica Et Cosmochimica Acta, 39(8): 1197-1201.

Clayton, C. J., 1986. The chemical environment of flint formation in Upper Cretaceous chalks. In: Sieveking, G. d. G. and Hart, M. B. Eds.), The scientific study of flint and chert : proceedings of the Fourth International Flint Symposium held at Brighton Polytechnic, 10-15 April 1983. Cambridge University Press, Cambridge.

Cloud, , 1962. Environment of calcium carbonate deposition west of Andros Island, Bahamas, United States Geological Survey Professional Paper.

Cloud , 1965, ‘Significance of the Gunflint (Precambrian) flora’, Science, 148, p 27-35.

Cloud, , 1973. Paleoecological Significance of Banded Iron-Formation. Economic Geology 68, 1135-1143.

Cloud, E., 1968. Atmospheric and Hydrospheric Evolution on Primitive Earth. Science 160, 729-&.

Cockell, C.S., 2002, 'Photobiological uncertainties in the Archaean and post-Archaean world', International Journal of Astrobiology, 1, p 31-38.

Codispoti, L. A., Friederich, G. E., Murray, J. W., and Sakamoto, C. M., 1991. Chemical Variability in the Black-Sea - Implications of Continuous Vertical Profiles That Penetrated the Oxic Anoxic Interface. Deep-Sea Res 38, S691-S710.

Coleman, M. L., 1985. Geochemistry of Diagenetic Non-Silicate Minerals - Kinetic Considerations. Philos T Roy Soc A 315, 39-56.

Collerson, K.D., Kamber, B.S., 1999. Evolution of the continents and the atmosphere inferred from Th-U-Nb systematics of the depleted mantle. Science 283, 1519-1522.

Collins, W. J., 1989. Polydiapirism of the Archean Mount Edgar Batholith, Pilbara Block, Western Australia. Precamb. Res. 43, 41-62.

Collins, W. J., Van Kranendonk, M. J., and Teyssier, C., 1998. Partial convective overturn of Archaean crust in the east Pilbara Craton, Western Australia: driving mechanisms and tectonic implications. Journal of Structural Geology 20, 1405-1424.

Comans, R. N. J. and Middelburg, J. J., 1987. Sorption of Trace-Metals on Calcite - Applicability of the Surface Precipitation Model. Geochim. Cosmochim. Acta 51, 2587-2591.

Condie, K.C., 1981, 'Archean Greenstone Belts', Elsevier, Amsterdam, 442 p

Condie, K.C., 1989. Geochemical Changes in Basalts and Andesites across the Archean-Proterozoic Boundary - Identification and Significance. Lithos 23(1-2), 1-18.

Condie, K. C., 1993. Chemical-Composition and Evolution of the Upper Continental-Crust - Contrasting Results from Surface Samples and Shales. Chem. Geol. 104, 1-37.

Condie, K. C., 1997. Plate tectonics and crustal evolution. Butterworth-Heinemann, Oxford.

Connolly, J.A.D., 1995. Phase-Diagram Methods for Graphitic Rocks and Application to the System C-O-H-Feo-Tio2sio2. Contributions to Mineralogy and Petrology, 119(1): 94-116.

Conrad, C. F., Icopini, G. A., Yasuhara, H., Bandstra, J. Z., Brantley, S. L., and Heaney, J., 2007. Modeling the kinetics of silica nanocolloid formation and precipitation in geologically relevant aqueous solutions. Geochim. Cosmochim. Acta 71, 531-542.

Coplen, T. B., Brand, W. A., Gehre, M., Groning, M., Meijer, H. A. J., Toman, B., and Verkouteren, R. M., 2006. New guidelines for delta C-13 measurements. Anal. Chem. 78, 2439-2441.

Corcoran, L. and Mueller, A., 2004. Aggressive Archaean weathering. In: Eriksson, K. A., Altermann, W., Nelson, D. R., Mueller, A., and Catuneanu, O. Eds.), The Precambrian Earth: Tempos and Events. Elsevier, Amsterdam.

Cowie, G. L., Calvert, S. E., Pedersen, T. F., Schulz, H., and von Rad, U., 1999. Organic content and preservational controls in surficial shelf and slope sediments from the Arabian Sea (Pakistan margin). Mar Geol 161, 23-38.

Croal, L. R., Jiao, Y., Kappler, A., and Newman, D. K., 2009. Phototrophic Fe(II) oxidation in an atmosphere of H-2: implications for Archean banded iron formations. Geobiol. 7, 21-24.

Dahanayake, K. and Krumbein, W. E., 1986. Microbial Structures in Oolytic Iron Formations. Miner Deposita 21, 85-94.

Dalrymple, D. W., 1965. Calcium carbonate deposition associated with blue-green algal mats, Baffin Bay, Texas. 10, 187-200.

Danielson, A., Moller, , Dulski, , 1992. The Europium Anomalies in Banded Iron Formations and the Thermal History of the Oceanic-Crust. Chem. Geol. 97(1-2), 89-100.

Darwin, C., 1871. The descent of man, and selection in relation to sex. D. Appleton and company, New York.

Dauphas, N., van Zuilen, M., Wadhwa, M., Davis, A.M., Marty, B., Janney, E., 2004. Clues from Fe isotope variations on the origin of early Archean BIFs from Greenland. Science 306(5704), 2077-2080.

Dauphas, N., Cates, N.L., Mojzsis, S., Busigny, V., 2007. Identification of chemical sedimentary protoliths using iron isotopes in the 3750 Ma Nuvvuagittuq supracrustal belt, Canada. Earth and Planet. Sci. Lett. 254(3-4), 358-376.

Davies, G. R. and Smith Jr., L. B., 2006. Structurally controlled hydrothermal dolomite reservoir facies: An overview. American Association of Petroleum Geologists Bulletin 90, 1641-1690.

Davies, G. R. and Smith Jr., L. B., 2007. Structurally controlled hydrothermal dolomite reservoir facies: An

overview: Reply. American Association of Petroleum Geologists Bulletin 91, 1342-1344.

Davis, C. C., Chen, H. W., and Edwards, M., 2002. Modeling silica sorption to iron hydroxide. Environ. Sci. Technol. 36, 582-587.

de Baar, H. J. W., Schijf, J., and Byrne, R. H., 1991. Solution Chemistry of the Rare-Earth Elements in Seawater. European Journal of Solid State and Inorganic Chemistry 28, 357-373.

de Choudens-Sanchez, V. and Gonzalez, L. A., 2009. Calcite and aragonite precipitation under controlled instantaneous supersaturation: elucidating the role of CaCO3 saturation state and Mg/Ca ratio on calcium carbonate polymorphism. Journal of Sedimentary Research 79, 363-376.

de Ronde, C.E.I., Channer, D.M., De, R., Faure, K., Bray, C.J., Spooner, E.T.C., 1997, ‘Fluid chemistry of Archaean seafloor hydrothermal vents: Implications for the

composition of circa 3.2 Ga seawater', Geochimica et Cosmochimica Acta, 61, p 4025-4042.

de Santis, R.D., Breedvelde, G.F.J. and J.M., Prausnitz, 1974. Thermodynamic Properties of Aqueous Gas-Mixtures at Advanced Pressures. Industrial & Engineering Chemistry, Process Design and Development, 13(4): 374-377.

de Vries, S. T. and Touret, J. L. R., 2007. Early Archaean hydrothermal fluids; a study of inclusions from the similar to 3.4 Ga Buck Ridge Chert, Barberton Greenstone Belt, South Africa. Chem. Geol. 237, 289-302.

de Wit, M. J. and Ashwal, L. D., 1997. Convergence towards divergent models of greenstone belts. In: de Wit, M. J. and Ashwal, L. D. Eds.), Greenstone Belts. Oxford Science, Oxford.

Degens, E. T. and Epstein, S., 1964. Oxygen and carbon isotope ratios in coexisting calcites and dolomites from recent and ancient sediments. Geochim. Cosmochim. Acta 28, 23-44.

Deines, , 2004. Carbon isotope effects in carbonate systems. Geochim. Cosmochim. Acta 68, 2659-2679.

Deines, , Langmuir, D., and Harmon, R. S., 1974. Stable Carbon Isotope Ratios and Existence of a Gas-Phase in Evolution of Carbonate Ground Waters. Geochim. Cosmochim. Acta 38, 1147-1164.

Deines, , 1980. The Carbon Isotopic Composition of Diamonds - Relationship to Diamond Shape, Color, Occurrence and Vapor Composition. Geochimica Et Cosmochimica Acta, 44(7): 943-961.

Dekanel, J. and Morse, J. W., 1978. Chemistry of Ortho-Phosphate Uptake from Seawater on to Calcite and Aragonite. Geochim. Cosmochim. Acta 42, 1335-1340.

Delmas, A.-B., Garcia-Hernandez, J., and Pedro, G., 1982. Discussion sur les conditions et les mecanismes de formation du quartz a 25 C en milieu ouvert. Analyse reactionelle par voie cinetique. Sci. Geol. Bull. 35, 81-91.

Demchuk, I. G., Krupenin, M. R., and Sazonov, V. N., 2003. Mechanism of multistage sideritization in the Bakal ore field (The South Urals). Zapiski Vserossijskogo mineralogiceskogo obs^estva 132, 86-93.

Derry, L. A. and Jacobsen, S. B., 1990. The Chemical Evolution of Precambrian Seawater - Evidence from Rees in Banded Iron Formations. Geochim. Cosmochim. Acta 54, 2965-2977.

Des Marais, D. J. and Moore, J. G., 1984. Carbon and Its Isotopes in Mid-Oceanic Basaltic Glasses. Earth Planet. Sci. Lett. 69, 43-57.

Des Marais, D.J., Cohen, Y., Nguyen, H., Cheatham, M., Cheatham, T. & Munoz, E., 1989, in Microbial Mats: Physiological Ecology of Benthic Microbial Communities, eds. Cohen, Y. & Rosenberg, E. (American Society for Microbiology, Washington), 191-205.

Des Marais, D.J., Strauss, H., Summons, R.E., and Hayes, J.M., 1992, Carbon isotope evidence for the stepwise oxidation of the Proterozoic environment: Nature, v. 359, 605-609.

Des Marais, D. J., 1996. Stable light isotope biogeochemistry of hydrothermal systems. Ciba F Symp 202, 83-98.

Des Marais, D.J., 1997, Isotopic evolution of the biogeochemical carbon cycle during the Proterozoic Eon, Organic Geochemistry 27, 185-193.

Deuser, W. G., 1970. C-13 in Black-Sea Waters and Implications for Origin of Hydrogen Sulfide. Science 168, 1575.

Devereux, R., Hines, M. E., and Stahl, D. A., 1996. S cycling: Characterization of natural communities of sulfate-reducing bacteria by 16S rRNA sequence comparisons. Microb. Ecol. 32, 283-292.

Diakonov, I., Khodakovsky, I., Schott, J., and Sergeeva, E., 1994. Thermodynamic Properties of Iron-Oxides and Hydroxides .1. Surface and Bulk Thermodynamic Properties of Goethite (Alpha-Feooh) up to 500-K. Eur J Mineral 6, 967-983.

Dickman, M., 1985. Seasonal Succession and Microlamina Formation in a Meromictic Lake Displaying Varved Sediments. Sedimentology 32, 109-118.

Dickson, J. A. D., 2002. Fossil echinoderms as monitor of the Mg/Ca ratio of Phanerozoic oceans. Science 298, 1222-1224.

Dickson, J. A. D. and Coleman, M. L., 1980. Changes in carbon and oxygen isotope composition during limestone diagenesis. Sedimentology 27.

Dillon, J., Evans, H. E., and Girard, R., 1997. Hypolimnetic alkalinity generation in two dilute, oligotrophic lakes in Ontario, Canada. Water Air Soil Pollut. 99, 373-380.

Dimarco, M. J. and Lowe, D. R., 1989a. Petrography and provenance of silicified early Archaean volcaniclastic sandstones, eastern Pilbara Block, Western Australia. Sedimentology 36, 821-836.

Dimarco, M. J. and Lowe, D. R., 1989b. Shallow-water volcaniclastic deposition in the early Archean Panorama Formation, Warrawoona Group, eastern Pilbara Block, Western Australia. Sediment Geol 64, 43-63.

Dimroth, E., 1968. Sedimentary textures, diagenesis, and sedimentary environment of certain Precambrian ironstones. Jahrbuch für Geologie und Paläontologie 130.

Dimroth, E., 1975. Paleo-environment of iron-rich sedimentary rocks. Geol. Rundschau 64, 751-767.

Dimroth, E. and Chauvel, J. J., 1973. Petrography of Sokoman Iron Formation in Part of Central Labrador-Trough, Quebec, Canada. Geol Soc Am Bull 84, 111-134.

Dixit, S., Van Cappellen, , and van Bennekom, A. J., 2001. Processes controlling solubility of biogenic silica and pore water build-up of silicic acid in marine sediments. Mar. Chem. 73, 333-352.

Dostal, J. and Strong, D. F., 1983. Trace-Element Mobility During Low-Grade Metamorphism and Silicification of Basaltic Rocks from Saint-John, New-Brunswick. Can. J. Earth Sci. 20, 431-435.

Douville, E., Bienvenu, , Charlou, J.L., Donval, J., Fouquet, Y., Appriou, , Gamo, T., 1999. Yttrium and rare earth elements in fluids from various deep-sea hydrothermal systems. Geochim. Cosmochim. Acta 63(5), 627-643.

Douville, E., Charlou, J. L., Oelkers, E. H., Bienvenu, , Colon, C. F. J., Donval, J. , Fouquet, Y., Prieur, D., and Appriou, , 2002. The rainbow vent fluids (36

degrees 14 ' N, MAR): the influence of ultramafic rocks and phase separation on trace metal content in Mid-Atlantic Ridge hydrothermal fluids. Chem. Geol. 184, 37-48.

Drake, H. L., 1994. Acetogenesis, acetogenic bacteria, and the acetyl-CoA "Wood/Lhungdahl" pathway: past and current perspectives. In: Drake, H. L. (Ed.), Acetogenesis. Chapman and Hall, New York.

Dromgoole, E. L. and Walter, L. M., 1990a. Inhibition of Calcite Growth-Rates by Mn-2+ in Cacl2 Solutions at 10-Degrees-C, 25-Degrees-C, and 50-Degrees-C. Geochim. Cosmochim. Acta 54, 2991-3000.

Dromgoole, E. L. and Walter, L. M., 1990b. Iron and Manganese Incorporation into Calcite - Effects of Growth-Kinetics, Temperature and Solution Chemistry. Chem. Geol. 81, 311-336.

Drummond, B. J., 1988. A review of crust/upper mantle structure in the Precambrian areas of Australia and implications for Precambrian crustal evolution. Precamb. Res. 40/41, 101-116.

Dunlop, J. S. R., 1976. The geology and mineralization of part of the North Pole barite deposits, Pilbara region, Western Australia. B.Sc (hons), University of Western Australia.

Dunlop, J. S. R., Muir, M. D., Milne, V. A., and Groves, D. I., 1978. A new microfossil assemblage from the Archaean of Western Australia. Nature 274, 676-678.

Dunn, S.R. and Valley, J.W., 1992. Calcite Graphite Isotope Thermometry - a Test for Polymetamorphism in Marble, Tudor Gabbro Aureole, Ontario, Canada. Journal of Metamorphic Geology, 10(4): 487-501.

Duchac, K. C. and Hanor, J. S., 1987. Origin and timing of the metasomatic silicification of an early Archean komatiite sequence, Barberton Mountain Land, South Africa. Precamb. Res. 37, 125-146.

Dymek, R.F., Klein, C., 1988. Chemistry, Petrology and Origin of Banded Iron-Formation Lithologies from the 3800-Ma Isua Supracrustal Belt, West Greenland. Precamb. Res. 39(4), 247-302.

Echeverria, L. M., 1980. Tertiary or Mesozoic Komatiites from Gorgona Island, Colombia - Field Relations and Geochemistry. Contrib. Mineral. Petrol. 73, 253-266.

Ehrenreich, A. and Widdel, F., 1994. Anaerobic Oxidation of Ferrous Iron by Purple Bacteria, a New-Type of Phototrophic Metabolism. Appl. Environ. Microbiol. 60, 4517-4526.

Eichler, J., 1976. Origin of the Precambrian banded iron-formations, Handbook of strata-bound and stratiform ore deposits. Elsevier Scientific Pub. Co., Amsterdam ; New York.

Eiler, J.M., Mojzsis, S.J. & Arrhenius, G., 1997, Nature 386, 665.

Einsele, G., 2000. Sedimentary basins : evolution, facies, and sediment budget. Springer, Berlin ; New York.

Eisenlohr, B., Meteva, K., Gabrov, F., and Dreybrodt, W., 1999. The inhibiting action of intrinsic impurities in natural calcium carbonate minerals to their dissolution kinetics in aqueous H2O–CO2 solutions. Geochim. Cosmochim. Acta 63, 989-1001.

Elderfield, H., 1988. The Oceanic Chemistry of the Rare-Earth Elements. Philosophical Transactions of the Royal Society of London Series a-Mathematical Physical and Engineering Sciences 325(1583), 105-126.

Elderfield, H., Wheat, C. G., Mottl, M. J., Monnin, C., and Spiro, B., 1999. Fluid and geochemical transport through oceanic crust: A transect across the easten flank of the Juan de Fuca Ridge. Earth and Planetary Science Letters 172, 151-165.

Emerson, S. R., 1985. Organic carbon preservation in marine sediments. In: Sundquist, E. T. and Broecker, W. S. Eds.), The Carbon Cycle and Atmospheric CO2: Natural Variations Archean to Present. Amer. Geophys. Union., Washington, D.C.

Emerson, S. E. and Hedges, J. H., 1988. Processes controlling the organic carbon content of open ocean sediments. Paleooceanography 3, 621-634.

Eriksson, K. A., 1982. Geometry and internal characteristics of Archaean submarine channel deposits, Pilbara Block, Western Australia. J Sediment Petrol 52, 383-393.

Ewers, W.E., Morris, R.C., 1981, 'Studies of the Dales Gorge Member of the Brockman Iron Formation, Western Australia', Economic Geology, 76, p 1929-1953.

Ewers, W.E., 1983, 'Chemical factors in the deposition and diagenesis of banded iron-formation', In: Trendall, A.F., Morris, R.C. (eds.), 'Banded iron-formation: Facts and problems', Elsevier, Amsterdam, p 491-512.

Eliassen, A. and Talbot, M. R., 2003. Diagenesis of the mid-Carboniferous Minkinfjellet Formation, central Spitsbergen, Svalbard. Norw J Geol 83, 319-331.

Ellis, J. and Milliman, J. D., 1985. Calcium-Carbonate Suspended in Arabian Gulf and Red-Sea Waters - Biogenic and Detrital, Not Chemogenic. J Sediment Petrol 55, 805-808.

Emerson, D. and Revsbech, N. , 1994a. Investigation of an Iron-Oxidizing Microbial Mat Community Located near Aarhus, Denmark - Field Studies. Appl. Environ. Microbiol. 60, 4022-4031.

Emerson, D. and Revsbech, N. , 1994b. Investigation of an Iron-Oxidizing Microbial Mat Community Located near Aarhus, Denmark - Laboratory Studies. Appl. Environ. Microbiol. 60, 4032-4038.

Emerson, S. and Bender, M., 1981. Carbon Fluxes at the Sediment-Water Interface of the Deep-Sea - Calcium-Carbonate Preservation. Journal of Marine Research 39, 139-162.

Emrich, K. and Vogel, J. C., 1970. Carbon Isotope Fractionation During Precipitation of Calcium Carbonate. Earth Planet. Sci. Lett. 8, 363-&.

Epstein, S., Graf, D. I., and Degens, E. T., 1963. Isotopic and cosmic chemistry. North-Holland Publishing Company, Amsterdam.

Eriksson, K. A., 1983. Siliciclastic-hosted iron-formations in the early Archaean Barberton and Pilbara sequences. Journal of the Geological Society of Australia 30, 473-482.

Eriksson, K. A., Krapez, B., and Fralick, W., 1994. Sedimentology of Archean Greenstone Belts - Signatures of Tectonic Evolution. Earth-Sci Rev 37, 1-88.

Eriksson, K. A., Krapez, B., and Fralick, W., 1997. Sedimentological aspects. In: de Wit, M. J. and Ashwal, L. D. Eds.), Greenstone Belts. Oxford Science, Oxford.

Eriksson, G., Catuneanu, O., Sarkar, S., and Tirsgaard, H., 2005. Patterns of sedimentation in the Precambrian. Sediment Geol 176, 17-42.

Eriksson, G., Condie, K. C., Tirsgaard, H., Mueller, W. U., Altermann, W., Miall, A. D., Aspler, L. B., Catuneanu, O., and Chiarenzelli, J. R., 1998. Precambrian clastic sedimentation systems. Sediment Geol 120, 5-53.

Essene, E. J., 1983. Solid solutions and solvi among metamorphic carbonates with applications to geologic thermobarometry. In: Reeder, R. J. (Ed.), Carbonates: Mineralogy and Chemistry. Mineralogical Society of America, Blacksburg, Virginia.

Ewers, W. E., 1983. Chemical factors in the deposition and diagenesis of banded-iron formation. In: Trendall, A. F. and Morris, E. Eds.), Iron-formation: Facts and problems. Elsevier, Amsterdam; New York.

Ewers, W. E. and Morris, R. C., 1981. Studies of the Dales-Gorge-Member of the Brockman-Iron-Formation, Western Australia. Economic Geology 76, 1929-1953.

Fairchild, I. J., 1991. Origins of carbonate in Neoproterozoic stromatolites and the identification of modern analogues. Precamb. Res. 53, 281-299.

Fairchild, I. J., 1993. Balmy shores and icy wastes: the paradox of carbonates with glacial deposits in Neoproterozoic times. Sedimentology Review 1, 1-15.

Fairchild, I. J., Knoll, A. H., and Swett, K., 1991. Coastal Lithofacies and Biofacies Associated with Syndepositional Dolomitization and Silicification (Draken Formation, Upper Riphean, Svalbard). Precamb. Res. 53, 165-197.

Fedo, C.M., Nesbitt, H.W., Young, G.M., 1995. Unraveling the Effects of Potassium Metasomatism in Sedimentary-Rocks and Paleosols, with Implications for Paleoweathering Conditions and Provenance. Geology 23(10), 921-924.

Fedo, C.M., 2000. Setting and origin for problematic rocks from the >3.7 Ga Isua Greenstone Belt, southern west Greenland: Earth's oldest coarse clastic sediments. Precamb. Res. 101, 69-78.

Fedo, C.M., Whitehouse, M.J., 2002a. Metasomatic origin of quartz-pyroxene rock, Akilia, Greenland, and implications for Earth's earliest life. Science 296, 1448-1452.

Fedo, C.M., Whitehouse, M.J., 2002b. The origin of a most contentious rock - Response. Science 298(5595), 961-962.

Fedo, C.M., Whitehouse, M.J., 2002c. Origin and significance of Archean quartzose rocks at Akilia, Greenland - Response. Science 298(5595).

Fenchel, T., Bernard, C., Esteban, G., Finlay, B. J., Hansen, J., and Iversen, N., 1995. Microbial Diversity and Activity in a Danish Fjord with Anoxic Deep-Water. Ophelia 43, 45-100.

Field, D., Clough, W.L., 1976. K/Rb ratios and metasomatism in metabasites from a Precambrian amphibolite–granulite transition zone. Journal of the Geological Society 132(3), 277-288.

Fischer, F., 1935. Die Synthese der Treibstoffe (Kogasin) und Schmierole aus Kohlenoxyd und Wasserstoff bei gewohnlichem Druck. Brennstoff-Chemie 16, 1-11.

Fischer, W. W. and Knoll, A. H., 2009. An iron shuttle for deepwater silica in Late Archean and early Paleoproterozoic iron formation. GSA Bulletin 121, 222-235.

Fisher, R. V. and Schmincke, H.-U., 1984. Pyroclastic rocks. Springer-Verlag, Berlin ; New York.

Flörke, O. W., Hollmann, R., von Rad, U., and Rösch, H., 1976. Intergrowth and twinning in opal-CT lepispheres. Contrib. Mineral. Petrol. 58, 235-242.

Flowers, G.C., 1979. Correction of Holloways (1977) Adaptation of the Modified Redlich-Kwong Equation of State for Calculation of the Fugacities of Molecular-Species in Supercritical Fluids of Geologic Interest. Contributions to Mineralogy and Petrology, 69(3): 315-318.

Flowers, G. C. and Helgeson, H. C., 1983. Equilibrium and Mass-Transfer During Progressive Metamorphism of Siliceous Dolomites. Am. J. Sci. 283, 230-286.

Floyd, A., Leveridge, B.E., 1987. Tectonic Environment of the Devonian Gramscatho Basin, South Cornwall - Framework Mode and Geochemical Evidence from Turbiditic Sandstones. Journal of the Geological Society 144, 531-542.

Flügel, E., 1982. Microfacies analysis of limestones. Springer-Verlag, Berlin ; New York.

Flügel, E., 2004. Microfacies of carbonate rocks : analysis, interpretation and application. Springer, Berlin ; New York.

Folk, R. L. and Pittman, J. S., 1971. Length-slow chalcedony: a new testament for vanished evaporites. J Sediment Petrol 41, 1045-1058.

Fortin, D. and Langley, S., 2005. Formation and occurrence of biogenic iron-rich minerals. Earth-Sci Rev 72, 1-19.

Fouke, B. W., Farmer, J. D., Des Marais, D. J., Pratt, L., Sturchio, N. C., Burns, C., and Discipulo, M. K., 2000. Depositional facies and aqueous-solid geochemistry of travertine-depositing hot springs (Angel Terrace, Mammoth Hot Springs, Yellowstone National Park, U.S.A.). Journal of Sedimentary Research 70, 565-585.

Fournier, R. O., 1983. A Method of Calculating Quartz Solubilities in Aqueous Sodium-Chloride Solutions. Geochim. Cosmochim. Acta 47, 579-586.

Fournier, R. O. and Marshall, W. L., 1983. Calculation of Amorphous Silica Solubilities at 25-Degrees-C to 300-Degrees-C and Apparent Cation Hydration Numbers in Aqueous Salt-Solutions Using the Concept of Effective Density of Water. Geochim. Cosmochim. Acta 47, 587-596.

Fournier, R. O. and Potter, R. W., 1982. An Equation Correlating the Solubility of Quartz in Water from 25-Degrees-C to 900-Degrees-C at Pressures up to 10,000 Bars. Geochim. Cosmochim. Acta 46, 1969-1973.

Fournier, R. O. and Rowe, J. J., 1977a. Solubility of Amorphous Silica in Water at High-Temperatures and High-Pressures. Am. Mineral. 62, 1052-1056.

Fournier, R. O. and Rowe, J. J., 1977b. Solubility of Amorphous Silica in Water at High-Temperatures and High-Pressures. Transactions-American Geophysical Union 58, 822-822.

Foustoukos, D. I. and Seyfried, W. E., 2004. Hydrocarbons in hydrothermal vent fluids: The role of chromium-bearing catalysts. Science 304, 1002-1005.

Fralick, , Davis, D. W., and Kissin, S. A., 2002. The age of the Gunflint Formation, Ontario, Canada: single zircon U-Pb age determinations from reworked volcanic ash. Can. J. Earth Sci. 39, 1085-1091.

Frei, R., Rosing, M., Waight, T.E., Ulfbeck, D.G., 2002. Hydrothermal-metasomatic and tectono-metamorphic processes in the Isua supracrustal belt (west Greenland): a multi-isotopic investigation of their effects on the Earth's oldest oceanic crustal sequence. Geochim. Cosmochim. Acta 66, 467-486.

Frei, R. and Polat, A., 2007. Source heterogeneity for the major components of similar to 3.7 Ga Banded Iron Formations (Isua Greenstone Belt, Western Greenland): Tracing the nature of interacting water masses in BIF formation. Earth Planet. Sci. Lett. 253, 266-281.

French, B.M. and Rosenberg, E., 1965. Siderite (FeCO3): thermal decomposition in equilibrium with graphite. Science, 147: 1283-1284.

French, B. M. and Eugster, H. , 1965. Experimental control of oxygen fugacities by graphite-gas equilibriums. J. Geophys. Res. 70, 1529-1539.

French, B. M., 1971. Stability relations of siderite (FeCO3): thermal decomposition in equilibrium with graphite. Am. J. Sci. 271, 37-78.

Friedman, G. M., 2007. Structurally controlled hydrothermal dolomite reservoir facies: An overview: Discussion. American Association of Petroleum Geologists Bulletin 91, 1339-1341.

Friend, C. R. L., Nutman, A. , Bennett, V. C., and Norman, M. D., 2008. Seawater-like trace element signatures (REE+Y) of Eoarchaean chemical sedimentary rocks from southern West Greenland, and their corruption during high-grade metamorphism. Contrib. Mineral. Petrol. 155, 229-246.

Fripp, R.E., 1976, 'Stratabound gold deposits in Archaean banded iron-formation, Rhodesia', Economic Geology, 71, p 58-75.

Froelich, N., Klinkhammer, G. , Bender, M. L., Luedtke, N. A., Heath, G. R., Cullen, D., Dauphin, , Hammond, D., Hartman, B., and Maynard, V., 1979. Early Oxidation of Organic-Matter in Pelagic Sediments of the Eastern Equatorial Atlantic - Suboxic Diagenesis. Geochim. Cosmochim. Acta 43, 1075-1090.

Frost, B.R., 1979. Mineral Equilibria Involving Mixed-Volatiles in a C-O-H Fluid Phase - Stabilities of Graphite and Siderite. American Journal of Science, 279(9): 1033-1059.

Frost, B.R., 1991. In: D.H. Lindsley (Editor), Oxide Minerals: petrologic and magnetic significance.

Frost, D.J. and Wood, B.J., 1995. Experimental Measurements of the Graphite C-O Equilibrium and Co2 Fugacities at High-Temperature and Pressure. Contributions to Mineralogy and Petrology, 121(3): 303-308.

Fruh-Green, G. L., Connolly, A. D., Plas, A., Kelley, D. S., and Grobety, B., 2003. Serpentinization of Oceanic Peridotites: Implications for Geochemical Cycles and Biological Activity, The Subseafloor Biosphere at Mid-Ocean Ridges.

Fryer, B.J., 1977. Rare-Earth Evidence in Iron-Formations for Changing Precambrian Oxidation-States. Geochim. Cosmochim. Acta 41(3), 361-367.

Fuchs, G., Thauer, R. K., Ziegler, H., and Stichler, W., 1979. Carbon isotopic fractionation by Methanobacterium thermoautotrophicum. Arch. Microbiol. 12, 135-139.

Furnes, H., Banerjee, N. R., Muehlenbachs, K., Staudigel, H., and de Wit, M., 2004. Early life recorded in archean pillow lavas. Science 304, 578-581.

Furnes, H., de Wit, M., Staudigel, H., Rosing, M., Muehlenbachs, K., 2007. A vestige of Earth's oldest ophiolite. Science 315(5819), 1704-1707.

Galimov, E. M., 2004. The pattern of delta C-13(org) versus HI/OI relation in recent sediments as an indicator of geochemical regime in marine basins: comparison of the Black Sea, Kara Sea, and Cariaco trench. Chem. Geol. 204, 287-301.

Ganeshram, R. S., Calvert, S. E., Pedersen, T. F., and Cowie, G. L., 1999. Factors controlling the burial of organic carbon in laminated and bioturbated sediments off NW Mexico: Implications for hydrocarbon preservation. Geochim. Cosmochim. Acta 63, 1723-1734.

Gao, G. Q. and Land, L. S., 1991. Nodular Chert from the Arbuckle Group, Slick Hills, Sw Oklahoma - a Combined Field, Petrographic and Isotopic Study. Sedimentology 38, 857-870.

Gao, S., Wedepohl, K.H., 1995. The Negative Eu Anomaly in Archean Sedimentary-Rocks - Implications for Decomposition, Age and Importance of Their Granitic Sources. Earth Planet. Sci. Lett. 133(1-2), 81-94.

GarciaGarmilla, F. and Elorza, J., 1996. Dolomitization and synsedimentary salt tectonics: The Upper Cretaceous Cueva Formation at El Ribero, northern Spain. Geol Mag 133, 721-&.

Garcia-Ruiz, J. M., 2000. Geochemical scenarios for the precipitation of biomimetic inorganic carbonates, Carbonate sedimentation and diagenesis in an evolving Precambrian world.

Gardner, R. A. M. and Hendry, D. A., 1995. Early Silica Diagenetic Fabrics in Late Quaternary Sediments, South-India. Journal of the Geological Society 152, 183-192.

Garrels, R. M., Perry, E. A., and Mackenzi.Ft, 1973. Genesis of Precambrian Iron-Formations and Development of Atmospheric Oxygen. Economic Geology 68, 1173-1179.

Garrels, R.M., 1987, ‘A model for the deposition of the micro-banded Precambrian iron-formations’, American Journal of Science, 287, p 81-106.

Garvin, J., Buick, R., Anbar, A. D., Arnold, G. L., and Kaufman, A. J., 2009. Isotopic Evidence for an Aerobic Nitrogen Cycle in the Latest Archean. Science 323, 1045-1048.

Geeslin, J. H. and Chafetz, H. S., 1982. Ordovician Aleman ribbon cherts: an example of silicification prior to carbonate lithification. Journal of Sedimentary Research 52/4, 1283-1293.

Gerlach, T.M. and Taylor, B.E., 1990. Carbon Isotope Constraints on Degassing of Carbon-Dioxide from Kilauea Volcano. Geochimica Et Cosmochimica Acta, 54(7): 2051-2058.

Gehlen, M., Vanraaphorst, W., and Wollast, R., 1993. Kinetics of Silica Sorption on North-Sea Sediments. Chem. Geol. 107, 359-361.

Glikson, A. Y., 1995. Asteroid/comet mega-impacts may have triggered major episodes of crustal evolution. Eos, Transactions, American Geophysical Union 76, 49, 54-55.

Glikson, A. Y. and Jahn, B.-M., 1985. REE and LIL elements, eastern Kaapvaal Shield, South Africa : evidence of crustal evolution by 3-stage melting. In: Ayers, L. D., Thurston, C., Card, K. D., and Weber, W. Eds.), Evolution of Archean Supracrustal Sequences. Geological Association of Canada.

Gibson, H. L., Watkinson, D. H., and Comba, C. D. A., 1983. Silicification - Hydrothermal Alteration in an Archean Geothermal System within the Amulet Rhyolite Formation, Noranda, Quebec. Economic Geology 78, 954-971.

Gnaneshwar, T., Naqvi, S.M., 1995, ‘Geochemistry, depositional environment and tectonic setting of the BIF’s of the Late Archaean Chitradurga Schist Belt, India’, Precambrian Research, 121, p 217-243.

Goedert, J. L., Peckmann, J., and Reitner, J., 2000. Worm tubes in an allochtonous cold-seep carbonate from lower Oligocene rocks of Western Washington. J. Paleontol. 74, 929-999.

Goldsmith, J. R., Graf, D. I., Witters, J., and Northrop, D. A., 1962. Studies in the system CaCO3-MgCO3-FeCO3: 1. Phase relations; 2. A method for major element spectrochemical analysis; 3. Compositions of some ferroan dolomites. J Geol 70, 659-688.

Gole, M. J., 1980. Mineralogy and Petrology of Very-Low-Metamorphic Grade Archean Banded Iron-Formations, Weld Range, Western-Australia. Am. Mineral. 65, 8-25.

Gole, M. J., 1981. Archean Banded Iron-Formations, Yilgarn-Block, Western Australia. Economic Geology 76, 1954-1974.

Gole, M. J. and Klein, C., 1981. Banded Iron-Formations through much of Precambrian time. J Geol 89, 169-183.

Golubic, S., 1973. The relationship between blue-green algae and carbonate deposits. 9, 434-472.

Golubic, S., 1976. Organisms that build stromatolites. Elsevier, Amsterdam.

Golyshev, S. I., Padalko, N. L., and Pechenkin, S. A., 1981. Fractionation of Stable Isotopes of Carbon and Oxygen in Carbonate Systems. Geokhimiya, 1427-1441.

Goodwin, A.M., 1973, ‘Archaean volcanogenic iron-formation of the Canadian shield’, Sci. Terre, 9, p 23-34.

Grassian, V., 2005. Environmental Catalysis. CRC.

Green, M.G., Sylvester, J., Buick, R., 2000. Growth and recycling of early Archaean continental crust: geochemical evidence from the Coonterunah and Warrawoona Groups, Pilbara Craton, Australia. Tectonophysics 322(1-2), 69-88.

Green, M. G., 2001. Early Archaean crustal evolution: evidence from ~3.5 billion year old greenstone successions in the Pilgangoora Belt, Pilbara Craton, Australia. Ph.D., University of Sydney.

Greenfield, L. J., 1963. Metabolism and concentration of calcium and magnesium and precipitation of calcium carbonate by a marine bacterium. 109, 23-45.

Greenwood, R., 1973. Cristobalite; its relationship to chert formation in selected samples from the Deep Sea Drilling Project. Journal of Sedimentary Research 43, 700-708.

Gross, G.A., 1965, ‘Geology of Iron Deposits in Canada, Volume 1. General Geology and Evaluation of Iron Deposits’, Geological Survey of Canada Economic Report, 22.

Gross G.A., 1983, ‘Tectonic systems and the deposition of iron-formation’, Precambrian Research, 20, p 171-187.

Grotzinger, J. , 1986. Cyclicity and paleoenvironmental dynamics, Rocknest Platform, northwest Canada. Geol Soc Am Bull 97, 1208-1231.

Grotzinger, J. , 1989. Facies and evolution of Precambrian carbonate depositional systems: emergence of the modern platform archetype. Controls on Carbonate Platform and Basin Development, SEPM Special Publication 44, 79-105.

Grotzinger, J. , 1994. Trends in Precambrian carbonate sediments and their implication for understanding evolution. In: Bengston, S. (Ed.), Early Life on Earth. Columbia University Press, New York.

Grotzinger, J. and Kasting, J. F., 1993. New Constraints on Precambrian Ocean Composition. J Geol 101, 235-243.

Grotzinger, J. and Knoll, A. H., 1995. Anomalous carbonate precipitates: is the Precambrian the key to the Permian? Palaios 10, 578-596.

Grotzinger, J. and Rothman, H. D., 1996. An abiotic model for stromatolite morphogenesis. Nature 383, 423-425.

Grotzinger, J. and Knoll, A. H., 1999. Stromatolites in Precambrian carbonates: evolutionary mileposts or environmental dipsticks? Annual Reviews of Earth and Planetary Science 27, 313-358.

Groves, D. I., Dunlop, J. S. R., and Buick, R., 1981. An Early Habitat of Life. Sci. Am. 245, 64-73.

Groves, D.I., Batt, W.D., 1984, ‘Spatial and temporal variations of Archean metallogenic associations in terms of evolution of granitoid-greenstone terrains with particular emphasis on Western Australia’, In: Kroner, A., Hanson, G.M., Goodwin, A.M. (eds.), ‘Archaean Geochemistry’, Springer-Verlag, Berlin, p 73-98.

Groves, D.I., Phillips, N., Ho, S.E., Houstoun, S.M., Standing, C.A., 1987, 'Craton-scale distribution of Archaean greenstone gold deposits: predictive capacity of the metamorphic model', Economic Geology, 82, p 2045-2058.

Gruau, G., Rosing, M., Bridgwater, D., Gill, R.C.O., 1996. Resetting of Sm-Nd systematics during metamorphism of >3.7 Ga rocks: implications for isotopic models of early earth differentiation. Chem. Geol. 133, 225-240.

Grundmanis, V. and Murray, J. W., 1982. Aerobic respiration in pelagic marine sediments. Geochem. Cosmochim. Acta 46, 1101-1120.

Guedes, S. C., Rosière, C. A., and Barley, M. E., 2003. The association of carbonate alteration of banded iron formation with the Carajás high-grade hematite deposits. Applied Earth Science: IMM Transactions section B 112, 26-30(5).

Guerrero, M. C. and de Wit, R., 1992. Microbial mats in the inland saline lakes of Spain. Limnetica 8, 197-204.

Gunnarsson, I. and Arnorsson, S., 2000. Amorphous silica solubility and the thermodynamic properties of H4SiO4 degrees in the range of 0 degrees to 350 degrees C at P-sat. Geochim. Cosmochim. Acta 64, 2295-2307.

Gutzmer, J., Schaefer, M. O., and Beukes, N. J., 2002. Red bed-hosted oncolitic manganese ore of the Paleoproterozoic Soutpansberg Group, Bronkhorstfontein, South Africa. Economic Geology 97, 1151-1166.

Halbach, , Hansmann, W., Koppel, V., and Pracejus, B., 1997. Whole-rock and sulfide lead-isotope data from the hydrothermal JADE field in the Okinawa back-arc trough. Miner Deposita 32, 70-78.

Halbach, E., Fouquet, Y., and Herzig, , 2003. Moineralization and compositional patterns in deep-sea hydrothermal systems. In: Halbach, E., Tunnicliffe, V., and Hein, J. R. Eds.), Energy and Mass Transfer in Marine Hydrothermal Systems. Dahlem University Press, Berlin.

Hales, B., Emerson, S. E., and Archer, D., 1994. Respiration and dissolution in the sediments of the western North Atlantic: estimates from models of in situ microelectrode measurements of porewater oxygen and pH. Deep-Sea Res. 41, 695-719.

Hall, D.L. and Bodnar, R.J., 1990. Methane in Fluid Inclusions from Granulites - a Product of Hydrogen Diffusion. Geochimica Et Cosmochimica Acta, 54(3): 641-651.

Hamade, T., Phoenix, V.R., Konhauser, K.O., 2000, 'Photochemical and microbiological mediated precipitation of iron and silica', In: Proceedings, 10th Annual V.M. Goldschmidt Conference, Oxford, England, p 475.

Hamade, T., Konhauser, K. O., Raiswell, R., Goldsmith, S., and Morris, R. C., 2003. Using Ge/Si ratios to decouple iron and silica fluxes in Precambrian banded iron formations. Geology 31, 35-38.

Hamann, S.D., Shaw, R.M., Lusk, J. and Batts, B.D., 1984. Isotopic Volume Differences - the Possible Influence of Pressure on the Distribution of Sulfur Isotopes between Sulfide Minerals. Australian Journal of Chemistry, 37(10): 1979-1989.

Hangari, K. M., Ahmad, S. N., and Perry, E. C., 1980. Carbon and Oxygen Isotope Ratios in Diagenetic Siderite and Magnetite from Upper Devonian Ironstone, Wadi-Shatti District, Libya. Economic Geology 75, 538-545.

Hanor, J. S. and Duchac, K. C., 1990. Isovolumetric Silicification of Early Archean Komatiites - Geochemical Mass Balances and Constraints on Origin. J Geol 98, 863-877.

Hardie, D. G., 2000. Metabolic control: a new solution to an old problem. Curr. Biol. 10, 757-759.

Harnmeijer, J., Orcutt, B., Devol, A., and Joye, S., 2005. Quantifying the role of manganese in biotic and abiotic nitrogen cycling. Geochim. Cosmochim. Acta 69, A581-A581.

Harrison, T.M., Blichert-Toft, J., Muller, W., Albarede, F., Holden, , Mojzsis, S.J., 2005. Heterogeneous Hadean hafnium: Evidence of continental crust at 4.4 to 4.5 Ga. Science 310, 1947-1950.

Hartman, H., 1984. The evolution of photosynthesis and microbial mats: A speculation on the banded iron formations. In: Cohen, Y. (Ed.), Microbial mats,

stromatolites : based on the proceedings of the Integrated Approach to the Study of Microbial Mats. A.R. Liss, New York.

Hartman, H., Sweeney, M. A., Kropp, M. A., and Lewis, J. S., 1993. Carbonaceous Chondrites and the Origin of Life. Origins Life Evol. Biosph. 23, 221-227.

Hartnett, H. E., 1998. Organic carbon input, degradation and preservation in continental margin sediments: an assesment of the role of a strong oxygen deficient zone. Ph.D., University of Washington.

Hartnett, H. E. and Devol, A. H., 2003. The role of a strong oxygen deficient zone in the preservation and degradation of organic matter: a carbon budget for the continental margins of NW Mexico and Washington. Geochim. Cosmochim. Acta 67, 247-264.

Hartnett, H. E., Keil, R. G., Hedges, J. I., and Devol, A. H., 1998. Influence of oxygen exposure time on organic carbon preservation in continental margin sediments. Nature 391, 572-536.

Hatfield, C. B., 1975. Replacement of Fossils by Length-Slow Chalcedony and Associated Dolomitization. J Sediment Petrol 45, 951-952.

Hayashi, T., Tanimizu, M., Tanaka, T., 2004. Origin of negative Ce anomalies in Barberton sedimentary rocks, deduced from La-Ce and Sm-Nd isotope systematics. Precamb. Res. 135(4), 345-357.

Hayes, J.M., Kaplan, I.R., and Wedeking, K.W., 1983, Precambrian Organic Geochemistry, Preservation of the Record, in Schopf, J.W., ed., Earth's Earliest Biosphere, 93-134.

Hayes, J. M., Takigiku, R., Ocampo, R., Callot, H. J., and Albrecht, , 1987. Isotopic Compositions and Probable Origins of Organic-Molecules in the Eocene Messel Shale. Nature 329, 48-51.

Hayes, J. M., 1993. Factors Controlling C-13 Contents of Sedimentary Organic-Compounds - Principles and Evidence. Mar Geol 113, 111-125.

Hayes, J.M., 1994, Global methanotrophy at the Archean-Proterozoic transition, in Bengtson, S., ed., Early Life on Earth, Volume 84: Nobel Symposium: Columbia U., New York, 220-236.

Hayes, J.M., Strauss, H., and Kaufman, A.J., 1999, The abundance of 13C in marine organic matter and isotopic fractionation in the global biogeochemical cycle of carbon during the past 800 Ma: Chemical Geology 161, 103-125.

Heath, G. R. and Moberly, R., 1971. Cherts from the western Pacific, Leg 7, Deep Sea Drilling Project. In: Winterer, E. L. (Ed.), Initial Reports of the Deep Sea Drilling Project.

Hecht, L., Freiberger, R., Gilg, H. A., Grundmann, G., and Kostitsyn, Y. A., 1999. Rare earth element and isotope (C, O, Sr) characteristics of hydrothermal carbonates: genetic implications for dolomite-hosted talc mineralization at Gopfersgrun (Fichtelgebirge, Germany). Chem. Geol. 155, 115-130.

Hedges, J. I., Hu, F. S., Devol, A. H., Hartnett, H. E., Tsamakis, E., and Keil, R. G., 1999. Sedimentary organic matter preservation: A test for selective degradation under oxic conditions. Am. J. Sci. 299, 529-555.

Hedges, J. I. and Keil, R. G., 1995. Sedimentary organic matter preservation: an assessment and speculative synthesis. Mar. Chem. 49, 81-115.

Heinrichs, T. K. and Reimer, T. O., 1977. Sedimentary Barite Deposit from Archean Fig Tree Group of Barberton Mountain Land (South-Africa). Economic Geology 72, 1426-1441.

Heising, S., Schink, B., 1998, 'Phototrophic oxidation of ferrous iron by a Rhodomicrobium vannielii strain', Microbiology, 144, p 2263-2269.

Heising, S., Richter, L., Ludwig, W., Schink, B., 1999, 'Chlorobium ferroxidans s noc., a phototrophic green sulfur bacterium that oxidizes ferrous iron in coculture with a "Geospirillum" s strain', Archives of Microbiology, 172, p 116-124.

Helgeson, H. C., 1967. Solution chemistry and metamorphism. In: Abelson, H. (Ed.), Researches in geochemistry. John Wiley & Sons.

Helly, J. J. and Levin, L. A., 2004. Global distribution of naturally occurring marine hypoxia on continental margins. Deep-Sea Res. Part I Oceanogr. Res. Pa 51, 1159-1168.

Henchiri, M. and Slim-S'Himi, N., 2006. Silicification of sulphate evaporites and their carbonate replacements in Eocene marine sediments, Tunisia: two diagenetic trends. Sedimentology 53, 1135-1159.

Henderson, J. B., 1975. Archean Stromatolites in Northern Slave Province, Northwest-Territories, Canada. Can. J. Earth Sci. 12, 1619-1630.

Henderson, J. B., 1981. Archean basin evolution in the Slave Province, Canada. In: Kröner, A. (Ed.), Precambrian plate tectonics. Elsevier, Amsterdam.

Hendry, J. , 1993. Calcite Cementation During Bacterial Manganese, Iron and Sulfate Reduction in Jurassic Shallow Marine Carbonates. Sedimentology 40, 87-106.

Hendry, J. and Trewin, N. H., 1995. Authigenic Quartz Microfabrics in Cretaceous Turbidites - Evidence for Silica Transformation Processes in Sandstones. Journal of Sedimentary Research Section a-Sedimentary Petrology and Processes 65, 380-392.

Henrichs, S. M. and Reeburgh, W., 1987. Anaerobic mineralization of marine sediment organic matter: Rates and the role of anaerobic porcesses in the oceanic carbon economy. Geomicrobiology J. 5, 191-237.

Herrmann, W. and Hill, A. , 2001. The Origin of Chlorite-Tremolite-Carbonate Rocks Associated with the Thalanga Volcanic-Hosted Massive Sulfide Deposit, North Queensland, Australia. Economic Geology 96, 1149-1173.

Herczeg, A. L. and Fairbanks, R. G., 1987. Anomalous Carbon Isotope Fractionation between Atmospheric Co2 and Dissolved Inorganic Carbon Induced by Intense Photosynthesis. Geochim. Cosmochim. Acta 51, 895-899.

Hesse, R., 1972. Selective Silicification of Ooids in Graywackes of Gault Formation, Early Cretaceous, East Alps. American Association of Petroleum Geologists Bulletin 56, 626.

Hesse, R., 1987a. Selective and Reversible Carbonate Silica Replacements in Lower Cretaceous Carbonate-Bearing Turbidites of the Eastern Alps. Sedimentology 34, 1055-1077.

Hesse, R., 1987b. Selective and reversible carbonate-silica replacements in Lower Cretaceous carbonate-bearing turbidites of the Eastern Alps. 34, 1055-1077, 15 Figs.

Hesse, R., 1989a. Silica Diagenesis - Origin of Inorganic and Replacement Cherts. Earth-Sci Rev 26, 253-284.

Hesse, R., 1989b. Silica diagenesis: origin of inorganic and replacement cherts. Earth-Science Reviews 26, 253-284.

Hesse, R., 1990. Early diagenetic pore water/sediment interaction: modern offshore basins. In: McIlreath, I. A. and Morrow, D. W. Eds.), Diagenesis. Goscience Canada, Ottawa.

Hessler, A.M., Lowe, D.R., 2006. Weathering and sediment generation in the Archean: An integrated study of the evolution of siliciclastic sedimentary rocks of the 3.2 Ga Moodies Group, Barberton greenstone belt, South Africa. Precamb. Res. 151(3-4), 185-210.

Hinman, N. W. and Lindstrom, R. F., 1996. Seasonal changes in silica deposition in hot spring systems. Chemical Geology 132, 237-246.

Hickman, A. H., 1972a. The North Pole barite deposits, Pilbara Goldfield. Geological Survey of Western Australia, Annual Report 1972, 57-60.

Hickman, A. H., 1972b. Precambrian structural geology of part of the Pilbara region. Geological Survey of Western Australia, Annual Report 1972, 68-73.

Hickman, A. H., 1975. Precambrian structural geology of part of the Pilbara region, Western Australia Geological Survey Annual Report. Geological Survey of Western Australia, Perth.

Hickman, A. H., 1983. Geology of the Pilbara Block and the environs. Australian Geological Survey.

Hickman, A. H., 1984. Archaean diapirism in the Pilbara Block, Western Australia. In: Kroner, A. and Greiling, R. Eds.), Precambrian Tectonics Illustrated. E. Schweizerbart'sche Verlagsbuchhandlung, Stuttgart, Germany.

Hiscock, W. T. and Millero, F. J., 2006. Alkalinity of the anoxic waters in the Western Black Sea. Deep-Sea Res Pt Ii 53, 1787-1801.

Hoashi, M., Bevacqua, D. C., Otake, T., Watanabe, Y., Hickman, A. H., Utsunomiya, S., and Ohmoto, H., 2009. Primary hematite formation in an oxygenated deep sea 3.46 billion years ago. Geochim. Cosmochim. Acta 73, A538-A538.

Hoefs, J., 1975. Ein Beitrag zur Isotopengeochemie das Kohlenstoffs in mamatischen Gesteinen. Fortschrift Mineralogie, 52: 475-478.

Hoefs, J., 1992. The stable isotope composition of sdimentary iron oxides with special reference to banded iron formation. In: Clauer, N. and Claudhuri, S. Eds.), Lecture notes in earth sciences. Springer-Verlag, Berlin.

Hoefs, M. J. L., Rijpstra, W. I. C., and Damste, J. S. S., 2002. The influence of oxic degradation on the sedimentary biomarker record I: Evidence from Madeira Abyssal Plain turbidites. Geochim. Cosmochim. Acta 66, 2719-2735.

Hoffman, E., 1988, 'United plates of America, the birth of a craton: Early Proterozoic assembly and growth of Laurentia', Ann. Rev. Earth Planet. Sci., 16, p 543-603.

Hoffman, F., Kaufman, A. J., Halverson, G. , and Schrag, D. , 1998. A Neoproterozoic snowball Earth. Science 281, 1342-1346.

Hofmann, H. J., Grey, K., Hickman, A. H., and Thorpe, R. I., 1999. Origin of 3.45 Ga coniform stromatolites in Warrawoona Group, Western Australia. Geol Soc Am Bull 111, 1256-1262.

Hofmann, A, Dirks, H. G. M., Jelsma, H. A., Matura, N., 2003, 'A tectonic origin for ironstone horizons in the Zimbabwe craton and their significance for greenstone belt geology', Journal of the Geological Society, London, 160, p 83-97.

Hofmann, A. and Bolhar, R., 2007. Carbonaceous cherts in the Barberton greenstone belt and their significance for the study of early life in the Archean record. Astrobiology 7, 355-388.

Hofmann, A. and Harris, C., 2008. Silica alteration zones in the Barberton greenstone belt: A window into the subseafloor processes 3.5-3.3 Ga ago. Chem. Geol. 257, 224-242.

Hofmann, H. J., Thurston, C., and Wallace, H., 1985. Archean stromatolites from Uchi Greenstone Belt, northwestern Ontario. In: Ayres, L. D., Thurston, C., Card, K.

D., and Weber, W. Eds.), Evolution of Archean Supracrustal Sequences. Geological Association of Canada.

Holail, H. H. M., Shaaban, M. M. N., Mansour, A. S., and Rifai, I., 2005. Diagenesis of the middle eocene upper dammam subformation, Qatar: Petrographic and isotopic evidence. Carbonate Evaporite 20, 72-81.

Holdaway, H. K. and Clayton, C. J., 1982. Preservation of shell microstructure in silicified brachiopods from the Upper Cretaceous Wilmington Sands of Devon. Geol Mag 119, 371-382.

Holland, H.D., 1973, 'The oceans: A possible source of iron in iron formations', Economic Geology, 68, p 1169-1172.

Holland, H. D., 1978. The chemistry of the atmosphere and oceans. Wiley, New York.

Holland, H. D., 1984. The chemical evolution of the atmosphere and oceans. Princeton University Press, Princeton, N.J.

Holland, H. D. and Zimmerman, H., 2002. The Dolomite Problem Revisited. In: Krauskopf, K. B. (Ed.), Frontiers in Geochemistry: Global Inorganic Geochemistry. Bellwether.

Holland, T. J. B. and Powell, R., 1998. An internally consistent thermodynamic data set for phases of petrological interest. J Metamorph Geol 16, 309-343.

Holland, H. D., 2002. Volcanic gases, black smokers, and the Great Oxidation Event. Geochemica et Cosmochimica Acta 66, 3811-3826.

Hollibaugh, J. T. and Azam, F., 1983. Microbial-Degradation of Dissolved Proteins in Seawater. Limnol. Oceanogr. 28, 1104-1116.

Holloway, J. R., 1977. Fugacity and activity of molecular species in supercritical fluids. In: Fraser, D. G. (Ed.), Thermodynamics in Geology. Reidel, Dordecht, the Netherlands.

Holloway, J. R., 1981. Volumes and Compositions of Supercritical Fluids. In: Hollister, L. S. and Crawford, M. L. Eds.), Fluid Inclusions: Petrologic Applications. Mineralogical Association of Canada.

Holloway, J.R., 1984. Graphite-CH4-H2O-CO2 Equilibria at Low-Grade Metamorphic Conditions. Geology, 12(8): 455-458.

Holm, N. G. and Charlou, J. L., 2001. Initial indications of abiotic formation of hydrocarbons in the Rainbow ultramafic hydrothermal system, Mid-Atlantic Ridge. Earth Planet. Sci. Lett. 191, 1-8.

Holmes, A., 1965. Principles of Physical Geology. Ronald Press, New York.

Hopkins, M., Harrison, T.M., Manning, C.E., 2008. Low heat flow inferred from >4 Gyr zircons suggests Hadean plate boundary interactions. Nature 456, 493-496.

Hoppe, H. G., 1993. Use of Fluorogenic Model Substrates for Extracellular Enzyme Activity (EEA) Measurement of Bacteria. In: Kemp, A. E., Shen, Y., Sherr, B., and Cole, D. R. Eds.), Handbook of Methods in Aquatic Microbial Ecology. Lewis.

Horita, J. and Berndt, M. E., 1999. Abiogenic methane formation and isotopic fractionation under hydrothermal conditions. Science 285, 1055-1057.

Horita, J., 2001. Carbon isotope exchange in the system CO2-CH4 at elevated temperatures. Geochimica Et Cosmochimica Acta, 65(12): 1907-1919.

Hornibrook, E. R. C., Longstaffe, F. J., and Fyfe, W. S., 1997. Spatial distribution of microbial methane production pathways in temperate zone wetland soils: Stable carbon and hydrogen isotope evidence. Geochim. Cosmochim. Acta 61, 745-753.

Hornibrook, E. R. C., Longstaffe, F. J., and Fyfe, W. S., 2000. Evolution of stable carbon isotope compositions for methane and carbon dioxide in freshwater wetlands and other anaerobic environments. Geochim. Cosmochim. Acta 64, 1013-1027.

Howell, J. A., 1976. Effects of Influent Substrate Concentration on Kinetics of Natural Microbial Populations in Continuous Culture. Water Res. 10, 271-271.

Hsü, J., 1966. Origin of dolomite in sedimentary sequences: a critical analysis. 2, 133-138.

Hughes, C. J., 1976. Volcanogenic cherts in the Late Precambrian Conception Group, Avalon Peninsula, Newfoundland. Can. J. Earth Sci. 13, 512-519.

Huizenga, J.M., 2001. Thermodynamic modelling of C-O-H fluids. Lithos, 55(1-4): 101-114.

Hunter, M., 1997, 'The tectonic setting of the Belingwe Greenstone Belt, Zimbabwe', Ph.D. thesis, University of Cambridge.

Humphris, S. E., Halbach, M., and Juniper, K., 2003. Low-temperature alteration: fluxes and mineralization. In: Halbach, E., Tunnicliffe, V., and Hein, J. R. Eds.), Energy and Mass Transfer in Marine Hydrothermal Systems. Dahlem University Press, Berlin.

Huston, D. L., Brauhart, C. W., Drieberg, S. L., Davidson, G. J., and Groves, D. I., 2001. Metal leaching and inorganic sulfate reduction in volcanic-hosted massive sulfide mineral systems: evidence from the paleo-Archean Panorama district, Western Australia. Geology 29, 687-690.

Hutchinson, R. W., 1982. Syn-depositional hydrothermal processes and Precambrian sulphide deposits. In: Hutchinson, R. W., Spence, C. D., and Franklin, J. M. Eds.), Precambrian Sulfide Deposits. Geological Association of Canada.

Icopini, G. A., Brantley, S. L., and Heaney, J., 2005. Kinetics of silica oligomerization and nanocolloid formation as a function of pH and ionic strength at 25 degrees C. Geochim. Cosmochim. Acta 69, 293-303.

Iler, R. K., 1979. The chemistry of silica: solubility, polymerization, colloid and surface properties, and biochemistry. Wiley, New York.

Immenhauser, A., Della Porta, G., Kenter, J. A. M., and Bahamonde, J. R., 2003. An alternative model for positive shifts in shallow-marine carbonate delta C-13 and delta O-18. Sedimentology 50, 953-959.

Immenhauser, A., Kenter, J. A. M., Ganssen, G., Bahamonde, J. R., Van Vliet, A., and Saher, M. H., 2002. Origin and significance of isotope shifts in Pennsylvanian carbonates (Asturias, NW Spain). Journal of Sedimentary Research 72, 82-94.

Ingram, B.L., Lin, J.C., 2002. Geochemical tracers of sediment sources to San Francisco Bay. Geology 30(6), 575-578.

Inskeep, W. and Bloom, R., 1986. Kinetics of Calcite Precipitation in the Presence of Water-Soluble Organic-Ligands. Soil Sci. Soc. Am. J. 50, 1167-1172.

Isley, A.E., 1995, 'Hydrothermal plumes and the delivery of iron to banded iron-formation', Journal of Geology, 103, p 169-185.

Isley, A.E., Abbott, D.H., 1999, 'Plume-related mafic volcanism and the deposition of banded iron formation', Journal of Geophysical Research, 104, p 15461-15477.

Jacka, A. D., 1974. Replacement of fossils by length-slow chalcedony and associated dolomitization. 44/2, 421-427.

Jackson, G. A. and Burd, A. B., 1998. Aggregation in the marine environment. Environ. Sci. Technol. 32, 2805-2814.

Jacobsen, S.B., Pimental-Klose, M.R., 1988, 'A Nd isotope study of the Hamersley and Michipicoten banded iron formations: The source of REE and Fe in Archaean oceans', Earth and Planetary Science Letters, 87, p 29-44.

Jaffres, J. B. D., Shields, G. A., and Wallmann, K., 2007. The oxygen isotope evolution of seawater: A critical review of a long-standing controversy and an improved geological water cycle model for the past 3.4 billion years. Earth-Sci Rev 83, 83-122.

Jahnke, R. A., 1990. Early diagenesis and recycling of biogenic debris at the seafloor, Santa Monica Basin, California. J. Mar. Res. 48, 413-436.

James H.L., 1954, 'Sedimentary facies of iron formation', Economic Geology, 49, p 235-293.

James, H.L., 1966, 'Chemistry of the iron-rich sedimentary rocks', In: Fleischer, M. (ed.), 'Data of Geochemistry', 6th edition, Paper 440-W, U.S. Govt. Printing Office, Washington D.C.

James, H.L., Trendall, A.F., 1982, 'Banded iron formation: distribution in time and paleoenvironmental significance', In: Holland, H.D., Schidlowski, M. (eds.), 'Mineral Deposits and the Evolution of the Biosphere', Springer-Verlag, New York, p 199-218.

James, H. L., 1954. Sedimentary facies of iron formation. Economic Geology 49, 235-293.

James, H. L., 1955. Zones of Regional Metamorphism in the Precambrian of Northern Michigan. Geol Soc Am Bull 66, 1455-1488.

James, R. H., Allen, D. E., and Seyfried, W. E., 2003. An experimental study of alteration of oceanic crust and terrigenous sediments at moderate temperatures

(51 to 350 degrees C): Insights as to chemical processes in near-shore ridge-flank hydrothermal systems. Geochim. Cosmochim. Acta 67, 681-691.

Jamieson, E. J., 1995. Precipitation and characteristics of iron (III) oxyhydroxides from acid liquors. Ph.D. thesis, Murdoch University.

Jarrell, K. F. and Kalmokoff, M. L., 1988. Nutritional-Requirements of the Methanogenic Archaebacteria. Can. J. Microbiol. 34, 557-576.

Javoy, M. and Pineau, F., 1991. The volatile record of a "popping" rock from the Mid-Atlantic Ridge at 14 degrees N: Chemical and isotopic composition of gas trapped in the vesicles. Earth and Planet. Sci. Lett., 107: 598-611.

Jensen, L. S., 1985. Stratigraphy and petrogenesis of Archean metavolcanic sequences, southwestern Abitibi Subprovince, Ontario. In: Ayres, L. D., Thurston, C., Card, K. D., and Webber, W. Eds.), Evolution of Archean supracrustal sequences. Geological Association of Canada.

Jimenez-Lopez, C. and Romanek, C. S., 2004. Precipitation kinetics and carbon isotope partitioning of inorganic siderite at 25 degrees C and 1 atm. Geochim. Cosmochim. Acta 68, 557-571.

Johnson, D. M., Hooper, R., and Conrey, R. M., 1999. XRF Analysis of Rocks and Minerals for Major and Trace Elements on a Single Low Dilution Li-tetraborate Fused Bead. Adv. X-Ray Anal. 41, 843-867.

Jones, B. and Kahle, C. F., 1995. Origins of endogenetic micrite in karst terrains: a case study from the Cayman Islands. 65, 283-293.

Jones, G. D. and Rostron, B. J., 2000. Analysis of fluid flow constraints in regional-scale reflux dolomitization: constant versus variable-flux hydrogeological models. B Can Petrol Geol 48, 230-245.

Jones, G. D. and Xiao, Y. T., 2005. Dolomitization, anhydrite cementation, and porosity evolution in a reflux system: Insights from reactive transport models. Aapg Bull 89, 577-601.

Jones, S. E., Jago, C. F., Bale, A. J., Chapman, D., Howland, R. J. M., and Jackson, J., 1998. Aggregation and resuspension of suspended particulate matter at a

seasonally stratified site in the southern North Sea: physical and biological controls. Cont Shelf Res 18, 1283-1309.

Joy, H.W. and Libby, W.F., 1960. Size effects among isotopic molecules. Journal of Chemical Physics, 33(4): 1276.

Kalkowsky, E., 1908. Oolith und Stromatolith im norddeutschen Buntsandstein. Zeitschrift der Deutschen geologischen Gesellschaft 60, 68-125.

Kamber, B. S. and Webb, G. E., 2001. The geochemistry of late Archaean microbial carbonate: Implications for ocean chemistry and continental erosion history. Geochim. Cosmochim. Acta 65, 2509-2525.

Kamber, B. S. and Webb, G. E., 2007. Transition metal abundances in microbial carbonate: a pilot study based on in situ LA-ICP-MS analysis. Geobiol. 5, 375-389.

Kamo, S. L. and Davis, D. W., 1994. Reassessment of Archean Crustal Development in the Barberton Mountain Land, South-Africa, Based on U-Pb Dating. Tectonics 13, 167-192.

Kappler, A., Pasquero, C., Konhauser, K. O., and Newman, D. K., 2006. Deposition of banded iron formations by anoxygenic phototrophic Fe(II)-oxidizing bacteria. Geology 33, 865-868.

Kasting, J.F., 1987, ‘Theoretical constraints on oxygen and carbon dioxide concentrations in the Precambrian atmosphere’, Precambrian Research, 34, p 205-229.

Kasting, J.F., Donahue, T.M., 1980, ‘The evolution of atmospheric oxygen’, Journal of Geophysical Research, 85, p 3255-3263.

Kastner, M., 1983. Opal-A to Opal-CT transformation: A kinetic study. In: Iijima, A. and Hein, J. R. Eds.), Siliceous Deposits in the Pacific Region. Elsevier Scientific Pub. Co., Amsterdam ; New York.

Kastner, M., Keene, J. B., and Gieskes, J. M., 1977. Diagenesis of Siliceous Oozes .1. Chemical Controls on Rate of Opal-a to Opal-Ct Transformation - Experimental-Study. Geochim. Cosmochim. Acta 41, 1041-&.

Kato, Y., Suzuki, K., Nakamura, K., Hickman, A. H., Nedachi, M., Kusakabe, M., Bevacqua, D. C., and Ohmoto, H., 2009. Hematite formation by oxygenated groundwater more than 2.76 billion years ago. Earth Planet. Sci. Lett. 278, 40-49.

Katrinak, K., 1987. Stable isotope studies of cherts from the Archean Swaziland Supergroup of South Africa. M.Sc., Arizona State University.

Katz, A. and Matthews, A., 1977. The dolomitization of CaCO3: an experimental study. Geochim. Cosmochim. Acta 41, 297-304.

Katz, A., Sass, E., Starinsky, A., and Holland, H. D., 1972. Strontium behaviour in the aragonite-calcite transformation. 36, 481-496.

Kaufman, A. J., Hayes, J. M., and Klein, C., 1990. Primary and diagenetic controls of isotopic compositions of iron-formation carbonates. Geochim. Cosmochim. Acta 54, 3461-3473.

Kaufman, A. J., Hayes, J. M., Knoll, A. H., and Germs, G. J. B., 1991. Isotopic compositions of carbonates and organic carbon from upper Proterozoic successions in Namibia: stratigraphic variation and the effects of diagenesis and metamorphism. Precamb. Res. 49, 3101-327.

Kaufman, A. J. and Knoll, A. H., 1995. Neoproterozoic variations in the C-isotopic compositions of seawater: stratigraphic and biogeochemical implications. Precamb. Res. 73, 27-49.

Kaufman, A. J., 1996. Geochemical and mineralogic effects of contact metamorphism on banded iron-formation: An example from the Transvaal Basin, South Africa. Precamb. Res. 79, 171-194.

Kawabe, I., Toriumi, T., Ohta, A., and Miura, N., 1998. Monoisotopic REE abundances in seawater and the origin of seawater tetrad effect. Geochem J 32, 213-229.

Kazmierczak, J. and Kempe, S., 2004. Calcium build-up in the Precambrian Sea, Cellular Origin, Life in Extreme Habitats and Astrobiology. Springer.

Keheila, E. A. and Elayyat, A., 1992. Silicification and Dolomitization of the Lower Eocene Carbonates in the Eastern Desert between Sohag and Qena, Egypt. J Afr Earth Sci 14, 341-349.

Kelley, D.S. and Fruh-Green, G.L., 1999. Abiogenic methane in deep-seated mid-ocean ridge environments: Insights from stable isotope analyses. Journal of Geophysical Research-Solid Earth, 104(B5): 10439-10460.

Keir, R. S., 1980. Dissolution Kinetics of Biogenic Calcium Carbonates in Seawater. Geochim. Cosmochim. Acta 44, 241-252.

Keir, R. S., 1983. Variation in the Carbonate Reactivity of Deep-Sea Sediments - Determination from Flux Experiments. Deep-Sea Res 30, 279-296.

Keith, T. E. C., White, D. E., and Beeson, M. H., 1978. Hydrothermal alteration and self-sealing in Y-7 and Y-8 drill holes in northern part of Upper Geyser Basin, Yellowstone National Park, Wyoming, U.S. Geological Survey Professional Papers 1054-A, 26.

Kelley, D. S. and Fruh-Green, G. L., 1999. Abiogenic methane in deep-seated mid-ocean ridge environments: Insights from stable isotope analyses. Journal of Geophysical Research-Solid Earth 104, 10439-10460.

Kelley, D. S., Karson, J. A., Fruh-Green, G. L., Yoerger, D. R., Shank, T. M., Butterfield, D. A., Hayes, J. M., Schrenk, M. O., Olson, E. J., Proskurowski, G., Jakuba, M., Bradley, A., Larson, B., Ludwig, K., Glickson, D., Buckman, K., Bradley, A. S., Brazelton, W. J., Roe, K., Elend, M. J., Delacour, A., Bernasconi, S. M., Lilley, M. D., Baross, J. A., Summons, R. T., and Sylva, S. , 2005. A serpentinite-hosted ecosystem: The lost city hydrothermal field. Science 307, 1428-1434.

Kempe, S. and Degens, E. T., 1985. An early soda ocean? Chem. Geol. 53, 95-108.

Kempe, S. and Kazmierczak, J., 1990. Calcium carbonate supersaturation and the formation of in situ calcified stromatolites, Facets of modern biogeochemistry. Springer, Berlin.

Kennedy, M. J., 1996. Stratigraphy, sedimentology, and isotopic geochemistry of Australian Neoproterozoic postglacial cap dolostones: Deglaciation, delta C-13

excursions, and carbonate precipitation. Journal of Sedimentary Research 66, 1050-1064.

Kennedy, M. J., Pevear, D. R., and Hill, R. J., 2002. Mineral surface control of Organic Carbon in Black Shale. Science 295, 657-660.

Kerrich, R., 1976. Some Effects of Tectonic Recrystallization on Fluid Inclusions in Vein Quartz. Contrib. Mineral. Petrol. 59, 195-202.

Kerrick, D.M., 1974. Review of Metamorphic Mixed-Volatile (H2o-Co2) Equilibria. American Mineralogist, 59(7-8): 729-762.

Kerrick, D.M. and Jacobs, G.K., 1981. A Modified Redlich-Kwong Equation for H2o, Co2, and H2o-Co2 Mixtures at Elevated Pressures and Temperatures. American Journal of Science, 281(6): 735-767.

Kester, D. R., Byrne, R. H., and Liang, Y. J., 1975. Redox Reactions and Solution Complexes of Iron in Marine Systems. ACS Sym Ser., 56-79.

Kharlashina, N.N. and Polyakov, V.B., 1992. The Effect of Pressure on the Equilibrium Isotope Fractionation in Minerals - Silicates, Calcite, Rutile. Geokhimiya, 2: 189-200.

Kholodov, V. N. and Butuzova, G. Y., 2004a. Problems of siderite formation and iron ore epochs: Communication 1. Types of siderite-bearing iron ore deposits. Lithol Miner Resour+ 39, 389-411.

Kholodov, V. N. and Butuzova, G. Y., 2004b. Problems of siderite formation and iron ore epochs: Communication 2. General issues of the precambrian and phanerozoic ore accumulation. Lithol Miner Resour+ 39, 489-508.

Kholodov, V. N. and Butuzova, G. Y., 2008. Siderite formation and evolution of sedimentary iron ore deposition in the Earth's history. Geol Ore Deposit+ 50, 299-319.

Kimberley, M. M., 1974. Origin of iron ore by diagenetic replacement of calcareous oolite. Nature 250, 319-320.

Kimberley, M.M., 1978, ‘Palaeoenvironmental classification of iron formations’, Economic Geology, 73, p 215-229.

Kinsman, D. J., 1969. Modes of formation, sedimentary associations, and diagnostic features of shallow-water and supratidal evaporites. 53, 830-840, 2 Figs.

Kinsman, D. J. J. and Holland, H. D., 1969. The co-precipitation of cations with CaCO3 -IV. The co-precipitation of Sr2+ with aragonite between 16° and 96°. 33, 1-17, 1 Fig.

Kirschvink, J. L., Gaidos, E. J., Bertani, L. E., Beukes, N. J., Gutzmer, J., Maepa, L. N., and Steinberger, R. E., 2000. Paleoproterozoic snowball Earth: extreme climatic and geochemical global change and its biological consequences. Proceedings of the National Academy of Science USA 97, 1400-1405.

Kitajima, K., Maruyama, S., Utsunomiya, S., and Liou, J. G., 2001. Seafloor hydrothermal alteration at an Archaean mid-ocean ridge. J Metamorph Geol 19, 581-597.

Kitano, Y., Okumura, M., and Idogaki, M., 1979. Behavior of Dissolved Silica in Parent Solution at the Formation of Calcium-Carbonate. Geochem J 13, 253-260.

Kitajima, K., Nakamura, E., Takaoka, N., and Murae, T., 2002. Evaluating the thermal metamorphism of CM chondrites by using the pyrolytic behavior of carbonaceous macromolecular matter. Geochim. Cosmochim. Acta 66, 163-172.

Kitchen, N.E. and Valley, J.W., 1995. Carbon-Isotope Thermometry in Marbles of the Adirondack Mountains, New-York. Journal of Metamorphic Geology, 13(5): 577-594.

Kiyokawa, S., 1983. Stratigraphy and structural evolution of a Middle Archaean greenstone belt, northwestern Pilbara Craton, Australia. Ph.D., University of Tokyo.

Klein, C., 1973. Changes in mineral assemblages with metamorphism of some Precambrian banded iron-formations, Economic Geology, 68, 1075-1088.

Klein, C. and Bricker, O. , 1977. Some Aspects of Sedimentary and Diagenetic Environment of Proterozoic Banded Iron-Formation. Economic Geology 72, 1457-1470.

Klein, C., 1983. Diagenesis and metamorphism of Precambrian banded iron-formation', In: Trendall, A.F., Morris, R.C. (eds.), 'Iron-formation: facts and problems', Elsevier, Amsterdam, p 417-460.

Klein, C. and Beukes, N. J., 1989a. Geochemistry and sedimentology of a facies transition from limestone to iron-formation deposition in the early Proterozoic Transvaal Supergroup, South Africa. Economic Geology 84, 1733-1774.

Klein, C. and Beukes, N. J., 1989b. Geochemistry and Sedimentology of a Facies Transition from Limestone to Iron-Formation Deposition in the Early Proterozoic Transvaal Supergroup, South-Africa. Economic Geology 84, 1733-1774.

Klein, C., Beukes, N.J., 1992, 'Proterozoic iron-formations', In: Condie, K.C. (ed.), 'Proterozoic Crustal Evolution', Elsevier, Amsterdam, p 383-418.

Klein, R. T. and Walter, L. M., 1995. Interactions between Dissolved Silica and Carbonate Minerals - an Experimental-Study at 25-50-Degrees-C. Chem. Geol. 125, 29-43.

Klein, C., 2005. Some Precambrian banded iron-formations (BIFs) from around the world: Their age, geologic setting, mineralogy, metamorphism, geochemistry, and origin. Am. Mineral. 90, 1473-1499.

Kloppenburg, A., White, S. H., and Zegers, T. E., 2001. Structural evolution of the Warrawoona Greenstone Belt and adjoining granitoid complexes, Pilbara Craton, Australia: implications for Archaean tectonic processes. Precamb. Res. 112, 107-147.

Knauth, L. , 1979. A model for the origin of chert in limestone. Geology 7, 274-277.

Knauth, L. , 1992. Origin and diagenesis of cherts: an isotopic perspective, Lecture notes in earth sciences ;. Springer-Verlag, Berlin ; New York.

Knauth, L. , 1994a. Petrogenesis of chert. In: Heaney, J., Prewitt, C. T., and Gibbs, G. V. Eds.), Silica: Physical Behavior, Geochemistry and Materials Applications. Mineralogical Society of America, Washington D.C.

Knauth, L. , 1994b. Petrogenesis of Chert. Rev Mineral 29, 233-258.

Knauth, L. and Lowe, D. R., 1978a. Oxygen Isotope Geochemistry of Cherts from Onverwacht Group (3.4 Billion Years), Transvaal, South-Africa, with Implications for Secular Variations in Isotopic Composition of Cherts. Earth Planet. Sci. Lett. 41, 209-222.

Knauth, L. and Lowe, D. R., 1978b. Oxygen isotope geochemistry of cherts from the Onverwacht Group (3.4 billion years), Transvaal, South Africa, with implications for secular variations in the isotopic composition of cherts. Earth and Planetary Science Letters 41, 209-222.

Knauth, L. and Lowe, D. R., 2003. High Archean climatic temperature inferred from oxygen isotope geochemistry of cherts in the 3.5 Ga Swaziland Supergroup, South Africa. Geol Soc Am Bull 115, 566-580.

Knoll, A. H. and Barghoorn, E. S., 1974. Ambient pyrite in Precambrian chert: new evidence and a theory. Proc. Nat. Acad. Sci. 71, 2329-2331.

Knoll, A. H., 1985. Exceptional preservation of photosynthetic organisms in silicified carbonates and silicified peats. Phil. Trans. R. Soc. Lond. 311, 111-122.

Knoll, A. H. and Simonson, B., 1981. Early Proterozoic microfossils and penecontemporaneous quartz cementation in the Sokoman Iron Formation, Canada. Science 211, 478-480.

Knoll, A. H. and Swett, K., 1990. Carbonate Deposition During the Late Proterozoic Era - an Example from Spitsbergen. Am. J. Sci. 290A, 104-132.

Kocurko, M. J., 1986. Interaction of organic matter and crystallization of High-Magnesium calcite, south Louisiana. 38, 13-21.

Kohler, E.A., Anhaeusser, C.R., 2002. Geology and geodynamic setting of Archaean silicic metavolcaniclastic rocks of the Bien Venue Formation, Fig Tree Group, northeast Barberton greenstone belt, South Africa. Precamb. Res. 116(3-4), 199-235.

Kolb, E. D., Caporaso, A. J., and Laudise, R. A., 1973. Hydrothermal Growth of Hematite and Magnetite. J. Cryst. Growth 19, 242-246.

Kolber, Z. S., Barber, R. T., Coale, K. H., Fitzwater, S. E., Greene, R. M., Johnson, K. S., Lindley, S., and Falkowski, G., 1994. Iron Limitation of Phytoplankton Photosynthesis in the Equatorial Pacific-Ocean. Nature 371, 145-149.

Konhauser, K. O., Hamade, T., Raiswell, R., Morris, R. C., Ferris, F. G., Southam, G., and Canfield, D., 2002. Could bacteria have formed the Precambrian banded iron formations? Geology 30, 1079-1082.

Konhauser, K., Jones, B., Phoenix, V., Ferris, G., and Renaut, R., 2004. The microbial role in hot spring silicification. Ambio 33, 552-558.

Koschorreck, M. and Tittel, J., 2002. Benthic photosynthesis in an acidic mining lake (pH 2.6). Limnol. Oceanogr. 47, 1197-1201.

Koschorreck, M. and Tittel, J., 2007. Natural alkalinity generation in neutral lakes affected by acid mine drainage. J. Environ. Qual. 36, 1163-1171.

Kosmulski, M., 1997. Adsorption of Trivalent Cations on Silica. J. Colloid Interface Sci. 195, 395-403.

Koziol, A.M., 2004. Experimental determination of siderite stability and application to Martian Meteorite ALH84001. American Mineralogist, 89(2-3): 294-300.

Krapez, B. and Barley, M. E., 1987. Archaean strike-slip faulting and related ensialic basins: evidence from the Pilbara Block, Australia. Geol. Mag. 124, 555-567.

Krapez, B., 1993. Sequence stratigraphy of the Archaean supracrustal belts of the Pilbara Block, Western Australia. Precamb. Res. 60, 1-45.

Krapez, B., Barley, M.E., Pickard, A.L., 2003, 'Hydrothermal and resedimented origins of the precursor sediments to banded iron formation: sedimentological evidence from the Early Palaeoproterozoic Brockman Supersequence of Western Australia, Sedimentology, 50(5), p 979-1011.

Kring, D. A. and Cohen, B. A., 2002. Cataclysmic bombardment throughout the inner solar system 3.9-4.0 Ga. J. Geophys. Res. 107, 41-46.

Kröner, A., 1981. Precambrian plate tectonics. Elsevier, Amsterdam.

Kröner, A., Hegner, E., Wendt, J. I., and Byerly, G. R., 1996. The oldest part of the Barberton granitoid-greenstone terrain, South Africa: evidence for crust formation between 3.5-3.7 Ga. Precamb. Res. 78, 105-124.

Krumbein, W. E., 1978. Algal mats and their lithification, Collingwood.

Krumbein, W. E., 1979. Photolithotrophic and chemoorganotrophic activity of bacteria and algae as related to beachrock formation and degradation (Gulf of Aqaba). 1, 139-203.

Krumbein, W. E. and Cohen, C., 1977. Primary production, mat formation and lithification: contribution oxygenic and facultative anoxygenic cyanobacteria. Springer, Berlin.

Krumbein, W. E. and Cohen, Y., 1974. Biogene, klastische und evaporitische Sedimentation in einem mesothermen monomiktischen ufernahen See (Golf von Aqaba). 63, 1035-1065, 15 Figs., 1 Tab.

Krumbein, W. E., Cohen, Y., and Shilo, M., 1977. Solar Lake (Sinai). 4. Stromatolite cyanobacterial mats. 22, 635-665.

Krumholz, L. R., McKinley, J. , Alrich, G. A., and Suflita, J. M., 1997. Confined subsurface microbial communities in Cretaceous rock. Nature 386, 64-66.

Kruner, A., Bryerly, G. R., and Lowe, D. R., 1991. Chronology of early Archaean granite-greenstone evolution in the Barberton Mountain Land, South Africa, based on precise dating by single zircon evaporation. Earth Planet. Sci. Lett. 103, 41-54.

Kuehn, C. A. and Rose, A. W., 1992. Geology and Geochemistry of Wall-Rock Alteration at the Carlin Gold Deposit, Nevada. Econ. Geol. 87, 1697-1721.

Kuivila, K. M. and Murray, J. W., 1984. Organic matter diagenesis in freshwater sediments: The alkalinity and total CO2 balance and methane production in the sediments of Lake Washington. Limnol. Oceanogr. 29, 1218-1230.

Kump, L. R., 1991. Interpreting Carbon-Isotope Excursions - Strangelove Oceans. Geology 19, 299-302.

Kump, L. R. and Arthur, M. A., 1999. Interpreting carbon-isotope excursions: carbonates and organic matter. Chem. Geol. 161, 181-198.

Kusky, T. and Hudleston, J., 1999. Growth and demise of an Archean carbonate platform, Steep Rock Lake, Ontario, Canada. Can. J. Earth Sci. 36, 565-584.

Kuznetsov, V. G. and Skobeleva, N. M., 2005a. Silicification of carbonate rocks in the Yurubcha-Tokhomo zone, Siberian Platform: A possible model of silica geochemistry in the Proterozoic. Doklady Earth Sciences 400, 5-7.

Kuznetsov, V. G. and Skobeleva, N. M., 2005b. Silicification of riphean carbonate sediments (Yurubcha-Tokhomo zone, Siberian Craton). Lithology and Mineral Resources 40, 552-563.

Lakshtanov, L. Z. and Stipp, S. L. S., 2009. Silica influence on calcium carbonate precipitationGoldschmidt Conference Abstract.

Lamb, A. L., Leng, M. J., Lamb, H. F., Telford, R. J., and Mohammed, M. U., 2002. Climatic and non-climatic effects on the delta O-18 and delta C-13 compositions of Lake Awassa, Ethiopia, during the last 6.5 ka. Quaternary Sci Rev 21, 2199-2211.

Lancet, M. S. and Anders, E., 1970. Carbon Isotope Fractionation in Fischer-Tropsch Synthesis and in Meteorites. Science 170, 980.

Lapteva, O. N., 1958. On the dependence of the redox potential of a ferric-ferrous solution on the Ph value. Zh. Anal. Khim. 31.

Lasaga, A. C., 1997. Kinetic Theory in the Earth Sciences. Princeton University Press, Princeton, New Jersey.

Lascelles, D. F., 2007, 'Black smokers and density currents: A uniformitarian model for the genesis of banded iron-formations', Ore Geology Reviews, 32, p 381-411.

Laschet, C., 1984. On the origin of cherts. Facies 10, 257-290.

Lasemi, Z. and Sandberg, A., 1984. Transformation of Aragonite-Dominated Lime Muds to Microcrystalline Limestones. Geology 12, 420-423.

Laws, E. A., Bidigare, R. R., and Popp, B. N., 1997. Effect of growth rate and CO2 concentration on carbon isotopic fractionation by the marine diatom Phaeodactylum tricornutum. Limnol. Oceanogr. 42, 1552-1560.

Laws, E. A., Popp, B. N., Bidigare, R. R., Kennicutt, M. C., and Macko, S. A., 1995. Dependence of Phytoplankton Carbon Isotopic Composition on Growth-Rate

and [Co2](Aq) - Theoretical Considerations and Experimental Results. Geochim. Cosmochim. Acta 59, 1131-1138.

Laws, E. A., Popp, B. N., Bidigare, R. R., Riebesell, U., and Burkhardt, S., 2001. Controls on the molecular distribution and carbon isotopic composition of alkenones in certain haptophyte algae. Geochem Geophy Geosy 2, -.

Laws, E. A., Thompson, A., Popp, B. N., and Bidigare, R. R., 1998. Sources of inorganic carbon for marine microalgal photosynthesis: A reassessment of delta C-13 data from batch culture studies of Thalassiosira pseudonana and Emiliania huxleyi. Limnol. Oceanogr. 43, 136-142.

Lazar, B. and Erez, J., 1992. Carbon Geochemistry of Marine-Derived Brines .1. C-13 Depletions Due to Intense Photosynthesis. Geochim. Cosmochim. Acta 56, 335-345.

Lee, J. H. and Byrne, R. H., 1993. Complexation of trivalent rare earth elements (Ce, Eu, Gd, Tb, Yb) by carbonate ions. Geochemica et Cosmochimica Acta 57, 295-302.

Lee, S. G., Kim, Y., Chae, B. G., Koh, D. C., and Kim, K. H., 2004. The geochemical implication of a variable Eu anomaly in a fractured gneiss core: application for understanding Am behavior in the geological environment. Appl Geochem 19, 1711-1725.

Leeder, M. R., 1999. Sedimentology and sedimentary basins : from turbulence to tectonics. Blackwell Science, Oxford ; Malden, MA.

Leng, M. J. and Marshall, J. D., 2004. Palaeoclimate interpretation of stable isotope data from lake sediment archives. Quaternary Sci Rev 23, 811-831.

Lenton, T. M., 2004. Clarifying Gaia: Regulation with or without Natural Selection. In: Schneider, S. H., Miller, J. R., Crist, E., and Boston, J. Eds.), Scientists debate Gaia. MIT Press.

Lepland, A., Arrhenius, G., Cornell, D., 2002, ‘Apatite in early Archean Isua supracrustal rocks, southern West Greenland: its origin, association with graphite and potential as a biomarker’, Precambrian Research, 118, p 221-241.

Lepp, H. and Goldich, S. S., 1964. Origin of Precambrian iron formations. Economic Geology 59, 1025-1060.

Levin, M., Thorlin, R., Kenneth, R. R., Taisaku, N., and Mercola, M., 2002. Assymmetries i H+/K+-ATPase and cell membrane potentials comprise a very early step in left-right patterning. Cell 111, 77-89.

Lewin, J. C., 1961. The dissolution of silica from diatom walls. Geochim. Cosmochim. Acta 21, 182–198.

Li, H. C. and Ku, T. L., 1997. delta C-13-delta O-18 covariance as a paleohydrological indicator for closed-basin lakes. Palaeogeogr. Palaeoclimatol. Palaeoecol. 133, 69-80.

Lindsay, J. F., Brasier, M. D., McLoughlin, N., Green, O. R., Fogel, M., Steele, A., and Mertzman, S. A., 2005. The problem of deep carbon - An Archean paradox. Precamb. Res. 143, 1-22.

Liu, X. W. and Millero, F. J., 2002. The solubility of iron in seawater. Mar. Chem. 77, 43-54.

Llorca, J. and Casanova, I., 1998. Formation of carbides and hydrocarbons in chondritic interplanetary dust particles: A laboratory study. Meteorit Planet Sci 33, 243-251.

Londry, K. L., Dawson, K. G., Grover, H. D., Summons, R. E., and Bradley, A. S., 2008. Stable isotope fractionation between substrates and products of Methanosarcina barkeri. Org. Geochem. 39, 608-621.

Lopez, O., Zuddas, , and Faivre, d., 2009. The influence of temperature and seawater composition on calcite cryustal growth mechanisms and kinetics: Implications for Mg incorporation in calcite lattice. Geochim. Cosmochim. Acta 73, 337-347.

Lorens, R. B., 1981. Sr, Cd, Mn and Co distribution coefficients in calcite as a function of calcite precipitation rate. 45, 553-561.

Lorenz, R.D., 2002, ‘Planets, life and the production of entropy’, International Journal of Astrobiology, 1, p 3-13.

Lovley, D. R., Dwyer, D. F., and Klug, M. J., 1982. Kinetic-Analysis of Competition between Sulfate Reducers and Methanogens for Hydrogen in Sediments. Appl. Environ. Microbiol. 43, 1373-1379.

Lowe, D.R., Knauth, L., 1977, 'Sedimentology of the Onverwacht Group (3.4 billion years), Transvaal, South Africa, and its bearing on the characteristics and evolution of the early earth', Journal of Geology, 85, p 699-723.

Lowe, D. R., 1980. Stromatolites 3400-Myr old from the Archean of Western Australia. Nature 284, 441-443.

Lowe, D. R., 1983. Restricted shallow-water sedimentation of early Archean stromatolitic and evaporitic strata of the Strelley Pool Chert, Pilbara Block, Western Australia. Precambrian Res. 19, 239-283.

Lowe, D. R., 1994. Abiological Origin of Described Stromatolites Older Than 3.2 Ga. Geology 22, 387-390.

Lowe, D. R. and Byerley, G. R., 1999. Stratigraphy of the west-central part of the Barberton Greenstone Belt, South Africa. In: Lowe, D. R. and Byerly, G. R. Eds.), Geologic Evolution of the Barberton Greenstone Belt, South Africa. Geological Society of America.

Loubere, and Fariduddin, M., 1999. Quantitative estimation of global patterns of surface ocean biological productivity and its seasonal variation on timescales from centuries to millennia. Global Biogeochem Cy 13, 115-133.

Lovering, T. G. and Patten, L. E., 1962. The Effect of Co2 at Low Temperature and Pressure on Solutions Supersaturated with Silica in the Presence of Limestone and Dolomite. Geochim. Cosmochim. Acta 26, 789-&.

Lovley, D. R., 1987. Organic-Matter Mineralization with the Reduction of Ferric Iron - a Review. Geomicrobiol. J. 5, 375-399.

Lovley, D. R., Stolz, J. F., Nord, G. L., and Phillips, E. J. , 1987. Anaerobic Production of Magnetite by a Dissimilatory Iron-Reducing Microorganism. Nature 330, 252-254.

Lowe, D. R., 1983. Restricted shallow-water sedimentation of early Archean stromatolitic and evaporitic strata of the Strelley Pool Chert, Pilbara Block, Western Australia. Precambrian Res. 19, 239-283.

Lowe, D. R., 1994. Abiological Origin of Described Stromatolites Older Than 3.2 Ga. Geology 22, 387-390.

Lowe, D. R. and Byerley, G. R., 1999. Stratigraphy of the west-central part of the Barberton Greenstone Belt, South Africa. In: Lowe, D. R. and Byerly, G. R. Eds.), Geologic Evolution of the Barberton Greenstone Belt, South Africa. Geological Society of America.

Lowe, D. R. and Knauth, L. , 1977. Sedimentology of the Onverwacht Group (3.4 billion years), Transvaal, South Africa, and its bearing on the characteristics and evolution of the early Earth. J. Geol. 85, 699-723.

Lowe, D. R. and Nocita, B. W., 1996. Stratigraphy and sedimentology of the Mapepe Formation: sedimentation in an evolving foreland basin. In: Lowe, D. R. and Byerley, G. R. Eds.), Geologic evolution of the Barberton Greenstone Belt, South Africa.

Lowell, R. , Rona, A., and von Herzen, R. , 1995. Seafloor hydrothermal systems. J. Geophys. Res. 100, 327-352.

Luo, Y. R. and Byrne, R. H., 2004. Carbonate complexation of yttrium and the rare earth elements in natural waters. Geochim. Cosmochim. Acta 68, 691-699.

Lyell, C., 1859. A manual of elementary geology : or, The ancient changes of the earth and its inhabitants as illustrated by geological monuments. D. Appleton, New York.

Lyons, W. B., 1984. Calcification of cyanobacterial mats in Solar Lake, Sinai. 12, 623-626.

Maas, R., Kinny, D., Williams, I.S., Froude, D.O., Compston, W., 1992. The Earths Oldest Known Crust - a Geochronological and Geochemical Study of 3900-4200 Ma Old Detrital Zircons from Mt Narryer and Jack Hills, Western-Australia. Geochim. Cosmochim. Acta 56(3), 1281-1300.

Machel, H. G., 2004. Concepts and models of dolomitization: a critical reappraisal. In: Braithwaite, C. J. R., Rizzi, G., and Darke, G. Eds.), the Geometry and Petrogenesis of dolomite Hydrocarbon Reservoirs. Geological Society, London.

Machel, H. G. and Lonnee, J., 2002. Hydrothermal dolomite - a product of poor definition and imagination. Sediment Geol 152, 163-171.

MacKenzie, D. J. and Craw, D., 2007. Contrasting hydrothermal alteration mineralogy and geochemistry in the auriferous Rise & Shine Shear Zone, Otago, New Zealand. New Zeal J Geol Geop 50, 67-79.

Magaritz, M., 1989. C-13 Minima Follow Extinction Events - a Clue to Faunal Radiation. Geology 17, 337-340.

Magaritz, M. and Issar, A., 1973. Carbon and Oxygen Isotopes in Epigenetic Hydrothermal Rocks from Hamam-El-Farun, Sinai. Chem. Geol. 12, 137-146.

Maisonneuve, J., 1982. The composition of the Precambrian ocean waters. Sediment. Geol. 31, 1-11.

Maliva, R. G., 2001. Silicification in the Belt Supergroup (Mesoproterozoic), Glacier National Park, Montana, USA. Sedimentology 48, 887-896.

Maliva, R. G., Knoll, A. H., and Siever, R., 1989. Secular change in chert distribution: a reflection of evolving biological participation in the silica cycle. Palaios 4, 519-532.

Maliva, R. G. and Siever, R., 1988a. Mechanism and Controls of Silicification of Fossils in Limestones. J Geol 96, 387-398.

Maliva, R. G. and Siever, R., 1988b. Pre-Cenozoic Nodular Cherts - Evidence for Opal-Ct Precursors and Direct Quartz Replacement. Am. J. Sci. 288, 798-809.

Margulis, L., Walker, J.C.G., Rambler, M., 1976, ‘Reassessment of the roles of oxygen and ultraviolet light in Precambrian evolution’, Nature, 264, p 620-624.

Marshall, C. et al., 2007. Structural characterization of kerogen in 3.4 Ga Archaean cherts from the Pilbara Craton, Western Australia. Precambrian Reasearch, 155: 1-23.

Martin, A., 1978, ‘The geology of the country around Que Que, Gwelo District’, Southern Rhodesia Geological Survey Bulletin, 83.

Martin, W. R. and Banta, G. T., 1992. The measurement of sediment irrigation rates: A comparison of the Br- tracer and 222Rn/226Ra disequilibrium techniques. Journal of Marine Research 50, 125-154.

Martin, H., 1994. Archean grey gneisses and the genesis of continental crust. In: Condie, K. C. (Ed.), Archean Crustal Evolution. Elsevier, Amsterdam ; New York.

Masuda, A., Kawakami, O., Dohmoto, Y., and Takenaka, T., 1987. Lanthanide Tetrad Effects in Nature - 2 Mutually Opposite Types, W and M. Geochem J 21, 119-124.

Matsuhisa, Y., Goldsmith, J.R. and Clayton, R.N., 1979. Oxygen Isotopic Fractionation in the System Quartz-Albite-Anorthite-Water. Geochimica Et Cosmochimica Acta, 43(7): 1131-1140.

Mattey, D., Carr, R.H., Wright, I. and Pillinger, C.T., 1984. Carbon Isotopes in Submarine Basalts. Earth and Planetary Science Letters, 70(2): 196-206.

Matthews, A., Goldsmith, J.R. and Clayton, R.N., 1983a. On the mechanisms and kinetics of oxygen isotope exchange in quartz and feldspars at elevated temperatures and pressures. Geological Society of America Bulletin, 94(3): 396-412.

Matthews, A., Goldsmith, J.R. and Clayton, R.N., 1983b. Oxygen isotope fractionation between zoisite and water. Geochemica et Cosmochimica Acta, 47(3): 645-654.

Matthews, A., Goldsmith, J.R. and Clayton, R.N., 1983c. Oxygen isotope fractionations involving pyroxenes; the calibration of mineral-pair geothermometers. Geochemica et Cosmochimica Acta, 47(3): 631-644.

Mayer, L. M., 1994a. Relationships between Mineral Surfaces and Organic-Carbon Concentrations in Soils and Sediments. Chem. Geol. 114, 347-363.

Mayer, L. M., 1994b. Surface area control of organic carbon accumulation in continental shelf sediments. Geochim. Cosmochim. Acta. 58, 1271-1284.

Mazzullo, S. J., 1994. Lithification and Porosity Evolution in Permian Periplatform Limestones, Midland Basin, Texas. Carbonate Evaporite 9, 151-171.

McBride, E. F., 1988. Silicification of Carbonate Pebbles in a Fluvial Conglomerate by Groundwater. J Sediment Petrol 58, 862-867.

McCollom, T.M., 2003. Formation of meteorite hydrocarbons from thermal decomposition of siderite (FeCO3). Geochemica et Cosmochimica Acta, 67(2): 311-317.

McCollom, T.M., 2004. Experimental study of potential sources of organic carbon in rocks from the Early Earth, Astrobiology Science Conference. Cambridge, NASA/AIMS, p 99.

McCollom, T. M., Ritter, G., and Simoneit, B. R. T., 1999. Lipid synthesis under hydrothermal conditions by Fischer-Tropsch-type reactions. Origins Life Evol. Biosph. 29, 153-166.

McCollom, T. M. and Seewald, J. S., 2003a. Experimental constraints on the hydrothermal reactivity of organic acids and acid anions: I. Formic acid and formate. Geochim. Cosmochim. Acta 67, 3625-3644.

McCollom, T. M. and Seewald, J. S., 2003b. Experimental study of the hydrothermal reactivity of organic acids and acid anions: II. Acetic acid, acetate, and valeric acid. Geochim. Cosmochim. Acta 67, 3645-3664.

McCollom, T. M. and Seewald, J. S., 2006. Carbon isotope composition of organic compounds produced by abiotic synthesis under hydrothermal conditions. Earth Planet. Sci. Lett. 243, 74-84.

McConnaughey, T., 1991. Calcification in Chara-Corallina - Co2 Hydroxylation Generates Protons for Bicarbonate Assimilation. Limnol. Oceanogr. 36, 619-628.

McConnaughey, T. A. and Falk, R. H., 1991. Calcium-Proton Exchange During Algal Calcification. Biological Bulletin 180, 185-195.

McConnaughey, T. A., Labaugh, J. W., Rosenberry, D. O., Striegl, R. G., Reddy, M. M., Schuster, F., and Carter, V., 1994. Carbon Budget for a Groundwater-Fed Lake - Calcification Supports Summer Photosynthesis. Limnol. Oceanogr. 39, 1319-1332.

McCrea, J. M., 1950. On the isotopic chemistry of carbonates and a paleotemperature scale. J. Chem. Phys. 18, 849-857.

McDonough, W.F., Frei, F.A., 1989. Rare Earth Elements in Upper Mantle Rocks, In: Reviews in Mineralogy, volume 21100-145.

McKay, D.S. et al., 1996. Search for past life on Mars: possible relic biogenic activity in martian meteorite ALH84001. Science, 273: 924-930.

McLennan, S.M., 1982. On the Geochemical Evolution of Sedimentary-Rocks. Chemical Geology 37(3-4), 335-350.

McLennan, S.M., Taylor, S.R., Kroner, A., 1983. Geochemical Evolution of Archean Shales from South-Africa .1. The Swaziland and Pongola Supergroups. Precamb. Res. 22(1-2), 93-124.

McLennan, S.M., Taylor, B.E., 1984. Archaean Sedimentary Rocks and Their Relation to the Composition of the Archaean Continental Crust, In: Archaean Geochemistry, A. Kroner, G.N. Hanson and A.M. Goodwin, eds., Springer, Berlin, p 47-72.

McLennan, S.M., Taylor, S.R., Mcgregor, V.R., 1984. Geochemistry of Archean Meta-Sedimentary Rocks from West Greenland. Geochim. Cosmochim. Acta 48(1), 1-13.

McLennan, S.M., 1993. Geochemical approaches to sedimentation, provenance, and tectonics, In: Processes Controlling the Composition of Clastic Sediments, M.J. Johnson and A.R. Basu, eds., Special Paper 284, Geological Society of America, Boulder, Colorado, p 21-39.

McLennan, S.M., Bock, B., Hemming, N.G., Hurowitz, J.A., Lev, S.M., McDaniel, D.K., 2004. The roles of provenance and sedimentary processes in the geochemistry of sedimentary rocks, In: Geochemistry of Sediments and Sedimentary Rocks: Evolutionary Considerations to Mineral Deposit-Forming Environments, 7-37.

McLoughlin, N., Brasier, M. D., Wacey, D., Green, O. R., and Perry, R. S., 2007. On biogenicity criteria for endolithic microborings on early earth and beyond. Astrobiology 7, 10-26.

McNaughton, N. J., Green, M. D., Compston, W., and Williams, I. S., 1988. Are anorthositic rocks basement to the Pilbara Craton? Geological Society of Australia Abstract 21, 272-273.

McSween, H.Y.J., 1997. Evidence for life in a martian meteorite? GSA Today, 7(7): 1-7.

McSween, H.Y.J. and Harvey, R., 1998. An evaporation model for formation of carbonates in the ALH84001 martian meteorite. International Geology Review, 40: 774-783.

McLennan, S. M., 1976. Paleo-Environment of Iron-Rich Sedimentary Rocks. Geologische Rundschau 65, 1126-1129.

McLennan, S. M., Taylor, S. R., and Eriksson, K. A., 1983. Geochemistry of Archean Shales from the Pilbara Supergroup, Western-Australia. Geochim. Cosmochim. Acta 47, 1211-1222.

Megonigal, J. , Hines, M. E., and Visscher, T., 2004. Anaerobic Metabolism: Linkages to Trace Gases and Aerobic Processes. In: Schlesinger, W. H. (Ed.), Biogeochemistry. Elsevier-Pergamon, Oxford.

Mel'nik, Y., 1982. Precambrian banded iron-formations, physicochemical conditions of formation. Developments in Precambrian Geology, 5. Elsevier, Amsterdam.

Meyer, H. J., 1984. The Influence of Impurities on the Growth-Rate of Calcite. J. Cryst. Growth 66, 639-646.

Meyers, W. J., 1977. Chertification in the Mississippian Lake Valley Formation, Sacramento Mountains, New Mexico. 24, 75-105.

Meyers, W. J. and James, A. T., 1978. Stable isotopes of cherts and carbonate cements in the Lake Valley Formation (Mississippian), Sacramento Mountains, New Mexico. 25, 105-124.

Michard, A. and Albarede, F., 1986. The REE Content of Some Hydrothermal Fluids. Chemical Geology 55, 51-60.

Milliman, 1995. Calcium carbonate sedimentation in the global ocean: linkages between neritic and pelagic environments. Oceanography 8, 92-94.

Milliman, J. D., 1974. Marine carbonates. Springer-Verlag, Berlin.

Millot, G., 1970. Geology of clay minerals. Weathering, sedimentology, geochemistry. Springer, New York.

Minami, M., Shimizu, H., Masuda, A., Adachi, M., 1995. Two Archean Sm-Nd ages of 3.2 and 2.5 Ga for the Marble Bar Chert, Warrawoona Group, Pilbara Block, Western Australia. Geochem J 29(6), 347-362.

Minami, M., Masuda, A., Takahashi, K., Adachi, M., and Shimizu, H., 1998. Y-Ho fractionation and lanthanide tetrad effect observed in cherts. Geochem J 32, 405-419.

Misik, M., 1993. Carbonate Rhombohedra in Nodular Cherts - Mesozoic of the West Carpathians. J Sediment Petrol 63, 275-281.

Mojzsis, S.J., Arrhenius, G., McKeegan, K.D., Harrison, T.M., Nutman, A., Friend, C.R.L., 1996. Evidence for life on earth before 3,800 million years ago. Nature 384(7 November), 55-59.

Mojzsis, S.J. and Harrison, T.M., 2000. Vestiges of a beginning: clues to the emergant biosphere recorded in the oldest known sedimentary rocks. GSA Today, 10(4): 1-6.

Mojzsis, S.J., Harrison, T.M., 2002, 'Origin and Significance of Archean Quartzose Rocks at Akilia, Greenland', Science, 298, p 917a.

Monty, C., 1965. Recent algal stromatolites in the Windward Lagoon, Andros Island, Bahamas. 88/5-6, 269-276.

Moorbath, S., Onions, R.K., Pankhurst, R.J., 1975. Evolution of Early Precambrian Crustal Rocks at Isua, West Greenland - Geochemical and Isotopic Evidence. Earth Planet. Sci. Lett. 27(2), 229-239.

Moorbath, S., 2005, Dating earliest life: Nature 434, 155.

Moore, J., J.M., 1977. Orogenic volcanism in the Proterozoic of Canada. Geological Association of Canada.

Moreira, D., Walter, L. M., Vasconcelos, C., McKenzie, J. A., and McCall, J., 2004. Role of sulfide oxidation in dolomitization: sediment and pore-water geochemistry of a hypersaline lagoon system. Geology 32, 701-704.

Morikiyo, T., 1984. Carbon Isotopic Study on Coexisting Calcite and Graphite in the Ryoke Metamorphic Rocks, Northern Kiso District, Central Japan. Contributions to Mineralogy and Petrology, 87(3): 251-259.

Morris, R., Horwitz, R., 1983, 'The origin of the iron-formation-rich Hamersley Group of Western Australia – Deposition on a platform', Precambrian Research, 21, p 273-197.

Morris, R., 1993, 'Genetic modelling for banded iron formation of the Hamersley Group, Pilbara craton, western Australia', Precambrian Research, 60, p 243-286.

Morse, J. W., 1978. Dissolution Kinetics of Calcium-Carbonate in Sea-Water .6. Near-Equilibrium Dissolution Kinetics of Calcium Carbonate-Rich Deep-Sea Sediments. Am. J. Sci. 278, 344-353.

Morse, J. W. and Arvidson, R. S., 2002. The dissolution kinetics of major sedimentary carbonate minerals. Earth-Sci Rev 58, 51-84.

Morse, J. W. and Berner, R. A., 1979. The chemistry of calcium carbonate in the deep oceans. In: Jenne, E. (Ed.), Chemical modelling - speciation, sorption, solubility and kinetics in aqueous systems. American Chemical Society, Washington, D.C.

Morse, J. W. and Mackenzie, F. T., 1990. Geochemistry of sedimentary carbonates. Elsevier.

Morse, J. W. and Mackenzie, F. T., 1998. Hadean ocean carbonate geochemistry. Aquat Geochem 4, 301-319.

Morse, J. W., Wang, Q., Mai, Y.T., 1997. Influence of temperature and Mg:Ca ratio on CaCO3 precipitates from seawater. Geology 25, 85-87.

Mottl, M. J., 1983a. Hydrothermal processes at seafloor spreading centers: application of basalt-seawater experimental results. In: Rona, A., Bostrom, K., Laubier, L., and Smith, K. L. Eds.), Hydrothermal Processes at Seafloor Spreading Centers,. Plenum, New York.

Mottl, M. J., 1983b. Metabasalts, Axial Hot Springs, and the Structure of Hydrothermal Systems at Mid-Ocean Ridges. Geol Soc Am Bull 94, 161-180.

Mottl, M. J. and Holland, H. D., 1978. Chemical Exchange During Hydrothermal Alteration of Basalt by Seawater .1. Experimental Results for Major and Minor Components of Seawater. Geochim. Cosmochim. Acta 42, 1103-1115.

Mottl, M. J. and Wheat, C. G., 1994. Hydrothermal Circulation through Midocean Ridge Flanks - Fluxes of Heat and Magnesium. Geochimica Et Cosmochimica Acta 58, 2225-2237.

Mucci, A., 1986. Growth kinetics and composition of magnesian calcite overgrowths precipitated from seawater: quantitative influence of orthophosphate ions. 50, 2235-2265.

Mucci, A. and Morse, J. W., 1990. Chemistry of Low-Temperature Abiotic Calcites - Experimental Studies on Coprecipitation, Stability, and Fractionation. Rev Aquat Sci 3, 217-254.

Muehlenbachs, K. and Clayton, R. N., 1976a. Oxygen Isotope Composition of Oceanic-Crust and Its Bearing on Seawater. J. Geophys. Res. 81, 4356-4369.

Muehlenbachs, K. and Clayton, R. N., 1976b. Oxygen Isotope Composition of Oceanic-Crust and Its Bearing on Sea-Water. Eos T Am Geophys Un 57, 411-412.

Mueller, W., Chown, E. H., and Potvin, R., 1994. Substorm Wave Base Felsic Hydroclastic Deposits in the Archean Lac-Des-Vents Volcanic Complex, Abitibi Belt, Canada. J Volcanol Geoth Res 60, 273-300.

Murray, J. W. and Kuivila, K. M., 1990. Organic matter diagenesis in the Northeast Pacific: Transition from aerobic red clay to sub-oxic hemipelagic sediments. Deep-Sea Res. 37, 59-80.

Murray, R. W., Tenbrink, M. R. B., Gerlach, D. C., Russ, G. , and Jones, D. L., 1992. Rare-Earth, Major, and Trace-Element Composition of Monterey and DSDP Chert and Associated Host Sediment - Assessing the Influence of Chemical Fractionation During Diagenesis. Geochimica Et Cosmochimica Acta 56, 2657-2671.

Murray, J. W., Codispoit, L. A., and Friederich, G. E., 1995. Oxidation-Reduction Environments: The suboxic Zone oin the Black Sea. In: Huang, C. , O'Melia, C.

R., and Morgan, J. J. Eds.), Aquatic Chemistry: Interfacian and Interspecies Processes. American Chemical Society, Washington, D.C.

Myers, J.S., Crowley, J.L., 2000. Vestiges of life in the oldest Greenland rocks? a review of early Archean geology in the Godthaabsfjord region, and reappraisal of field evidence for 3850 Ma life on Akilia. Precamb. Res. 103, 101-124.

Myers, J.S., 2001. Protoliths of the 3.8-3.7 Ga Isua greenstone belt, West Greenland. Precamb. Res. 105(2-4), 129-141.

Myrow, M. and Kaufman, A. J., 1999. A newly discovered cap carbonate above Varanger-age glacial deposits in Newfoundland, Canada. Journal of Sedimentary Research 69, 784-793.

Nader, F. H., Abdel-Rahman, A. F. M., and Haidar, A. T., 2006. Petrographic and chemical traits of Cenomanian platform carbonates (central Lebanon): implications for depositional environments. Cretac. Res. 27, 689-706.

Nakamura, K. and Kato, Y., 2002. Carbonate minerals in the Warrawoona Group, Pilbara Craton: Implications for continental crust, life, and global carbon cycle in the Early Archean. Resour Geol 52, 91-100.

Nakamura, K. and Kato, Y., 2004. Carbonatization of oceanic crust by the seafloor hydrothermal activity and its significance as a CO2 sink in the Early Archean. Geochim. Cosmochim. Acta 68, 4595-4618.

Namy, J. N., 1974. Early diagenetic cherts in the Marble Falls Group (Pennsylvanian) of central Texas. J Sediment Petrol 56, 495-500.

Nance, W.B., Taylor, S.R., 1976. Rare-Earth Element Patterns and Crustal Evolution .1. Australian Post-Archean Sedimentary-Rocks. Geochim. Cosmochim. Acta 40(12), 1539-1551.

Nealson, K. H. and Myers, C. R., 1990. Iron Reduction by Bacteria - a Potential Role in the Genesis of Banded Iron Formations. Am. J. Sci. 290A, 35-45.

Nelson, D. R., Trendall, A. F., de Laeter, J. R., Grobler, N. J., and Fletcher, I. R., 1992. A comparative study of the geochemical and isotopic systematics of late Archaean flood basalts from the Pilbara and Kaapvaal Cratons. Precamb. Res. 54, 231-256.

Nelson, D. R., Trendall, A. F., and Altermann, W., 1999. Chronological correlations between the Pilbara and Kaapvaal cratons. Precamb. Res. 97, 165-189.

Nelson, D. R., 2004. Earth's formation and first billion years. In: Eriksson, K. A., Altermann, W., Nelson, D. R., Mueller, A., and Catuneanu, O. Eds.), The Precambrian Earth: Tempos and Events. Elsevier, Amsterdam.

Nesbitt, H. W. and Young, G. M., 1982. Early Proterozoic climates and plate motions inferred from major element chemistry of lutites. Nature 299, 715-717.

Nesbitt, H.W., 2004. Petrogenesis of siliciclastic sediments and sedimentary rocks, In: Geochemistry of Sediments and Sedimentary Rocks: Evolutionary Considerations to Mineral Deposit-Forming Environments, 39-51.

Neumann, A. C. and Land, L. S., 1975. Lime Mud Deposition and Calcareous Algae in Bight of Abaco, Bahamas - Budget. J Sediment Petrol 45, 763-786.

Neumayr, , Ridley, J. R., McNaughton, N. J., Kinny, D., Barley, M. E., and Groves, D. I., 1998. Timing of gold mineralization in the Mt York district, Pilgangoora greenstone belt, and implications for the tectonic and metamorphic evolution of an area linking the western and eastern Pilbara craton. Precamb. Res. 88, 249-265.

Nijman, W., de Bruijne, K. C. H., and Valkering, M. E., 1998a. Growth fault control of early Archaean cherts, barite mounds and chert-barite veins, North Pole Dome, eastern Pilbara, Western Australia. Precamb. Res. 88, 25-52.

Nijman, W., Willigers, B. J. A., and Krikke, A., 1998b. Tensile and compressive growth structures: relationships between sedimentation, deformation and granite intrusion in the Archaean Coppin Gap greenstone belt, Eastern Pilbara, Western Australia. Precamb. Res. 88, 83-108.

Nisbet, E. G., 1987. The young earth: An introduction to Archaean geology. Allen & Unwin, Boston.

Nisbet, E.G., Martin, A., Bickle, M.J., Orpen, J.L., 1993. The Ngezi Group: komatiites, basalts and stromatolites on continental crust, In: Bickle, M.J., Nisbet, E.G. (eds.), ‘The Geology of the Belingwe Greenstone Belt, Zimbabwe’, Geological Society of Zimbabwe Special Publications, 2, p 121-165.

Noble, J. A. and Van Stempvoort, D. R., 1989. Early burial quartz authigenesis in Silurian platform carbonates, New Brunswick, Canada. 59/1, 65-76, 20 Figs.

Nothdurft, L. D., Webb, G. E., and Kamber, B. S., 2004. Rare earth element geochemistry of Late Devonian reefal carbonates, canning basin, Western Australia: Confirmation of a seawater REE proxy in ancient limestones. Geochim. Cosmochim. Acta 68, 263-283.

Nozaki, Y., Zhang, J., and Amakawa, H., 1997. The fractionation between Y and Ho in the marine environment. Earth Planet. Sci. Lett. 148, 329-340.

Nutman, A., Allaart, J.H., Bridgwater, D., Dimroth, E., Rosing, M., 1984. Stratigraphic and geochemical evidence for the depositional environment of the early Archaean Isua Supracrustal Belt, Southern West Greenland. Precamb. Res. 25, 365-396.

Nutman, A., Bridgwater, D., 1986. Early Archean Amitsoq Tonalites and Granites of the Isukasia Area, Southern West Greenland - Development of the Oldest-Known Sial. Contrib. Mineral. Petrol. 94(2), 137-148.

Nutman, A., McGregor, V.R., Friend, C.R.L., Bennett, V.C., Kinny, D., 1996. The Itsaq Gneiss Complex of southern west Greenland; The world's most extensive record of early crustal evolution (3900-3600 Ma). Precamb. Res. 78(1-3), 1-39.

Nutman, A., Mojzsis, S.J., Friend, C.R.L., 1997. Recognition of >=3850 Ma water-lain sediments in West Greenland and their significance for the early Archaean Earth. Geochim. Cosmochim. Acta 61(12), 2475-2484.

Nutman, A., Bennett, V.C., Friend, C.R.L., Norman, M.D., 1999. Meta-igneous (non-gneissic) tonalites and quartz-diorites from an extensive ca. 3800 Ma terrain south of the Isua supracrustal belt, southern West Greenland: constraints on early crust formation. Contrib. Mineral. Petrol. 137(4), 364-388.

Nutman, A. , Bennett, V. C., Friend, C. R. L., and Mcgregor, V. R., 2000. The early Archaean Itsaq Gneiss Complex of southern West Greenland: The importance of field observations in interpreting age and isotopic constraints for early terrestrial evolution. Geochim. Cosmochim. Acta 64, 3035-3060.

Ohmoto, H., 1972. Systematics of Sulfur and Carbon Isotopes in Hydrothermal Ore-Deposits. Economic Geology 67, 551-.

Ohmoto, H. and Kerrick, D., 1977. Devolatilization Equilibria in Graphitic Systems. American Journal of Science, 277(8): 1013-1044.

Ohmoto, H., Felder, R., 1987, 'Bacterial activity in the warmer, sulphate-bearing Archaean oceans', Nature, 328, p 244-246.

Ohmoto, H., Watanabe, Y., and Kumazawa, K., 2004. Evidence from massive siderite beds for a CO2-rich atmosphere before, 1.8 billion years ago. Nature 429, 395-399.

Ohmoto, H., Watanabe, K., Yamaguchi, K., Naraoka, H., Haruna, M., Kakegawa, T., Hayashi, K., and Kato, Y., 2006. Chemical and biological evaluation of early Earth: constraints from banded iron formations. Geological Society of America Memoir 198, 239-256.

Olson, D., Garrels, R. M., Berner, R. A., Armentano, T. V., Dyer, M. I., and Taalon, D. H., 1985. The natural carbon cycle. In: Trabalka, J. R. (Ed.), Atmospheric Carbon Dioxide and the Global Carbon Cycle. US De Energy, Washington, D.C.

Olson, J. M., 2006. Photosynthesis in the Archean Era. Photosynth. Res. 88, 109-117.

O'Neil, J. R. and Epstein, S., 1966. Oxygen Isotope Fractionation in System Dolomite-Calcite-Carbon Dioxide. Science 152, 198.

O'Neill, J., Maurice, C., Stevenson, R. K., Larocque, J., Cloquet, C., David, J., and Francis, D., 2007. The geology of the 3.8 Ga Nuvvuagittuq (Porpoise Cove) greenstone belt, northeastern Superior Province, Canada. In: van Kranendonk, M. J., Smithies, R. H., and Bennett, V. C. Eds.), Developments in Precambrian Geology.

Orphan, V. J., House, C. H., Hinrichs, K., McKeegan, K. D., and DeLong, E. F., 2001. Methane-consuming archaea revealed by directly coupled isotopic and phylogenetic analysis. Science 293, 484-487.

Pache, T., Brockamp, O., Clauer, N., 2008. Varied pathways of river-borne clay minerals in a near-shore marine region: A case study of sediments from the

Elbe- and Weser rivers, and the SE North Sea. Estuar. Coast. Shelf Sci. 78(3), 563-575.

Packard, J. J., Al-Aasm, I., Samson, I., Berger, Z., and Davies, J., 2001. A devonian hydrothermal chert reservoir: the 225 bcf Parkland field, British Columbia, Canada. Aapg Bull 85, 51-84.

Padgham, W. A., 1985. Observations and speculations on supracrustal successions in the Slave structural province. Geological Association of Canada.

Paikaray, S., Banerjee, S., and Mukherji, S., 2005. Sorption behavior of heavy metal pollutants onto shales and correlation with shale geochemistry. Environ Geol 47, 1162-1170.

Palmer, T. J., Hudson, J. D., and Wilson, M. A., 1988. Paleoecological Evidence for Early Aragonite Dissolution in Ancient Calcite Seas. Nature 335, 809-810.

Palmer, T. J. and Wilson, M. A., 2004. Calcite precipitation and dissolution of biogenic aragonite in shallow Ordovician calcite seas. Lethaia 37, 417-427.

Panchuk, K. M., Holmden, C., and Kump, L. R., 2005. Sensitivity of the epeiric sea carbon isotope record to local-scale carbon cycle processes: Tales from the Mohawkian Sea. Palaeogeogr. Palaeoclimatol. Palaeoecol. 228, 320-337.

Panieri, G., Lugli, S., Manzi, V., Palinska, K. A., and Roveri, M., 2008. Microbial communities in Messinian evaporite deposits of the Vena del Gesso (northern Apennines, Italy). Stratigraphy 5, 343-352.

Papadopoulos, and Rowell, D. L., 1989. The Reactions of Copper and Zinc with Calcium-Carbonate Surfaces. J Soil Sci 40, 39-48.

Paropkari, A. L., Babu, C. , and Mascarenhas, A., 1992. A critical evaluation of depositional parameters controlling variability of organic carbon in Arabian Sea sediments. Mar. Geol. 107, 213-226.

Parron, C., Nahon, D., Fritz, B., Paquet, H., and Millot, G., 1976. Desilicification et quartzification par alteration des gres albiens du Gard. Modeles geochmiques de la genese des dalles quartzitiques et silcretes. Sci. Geol. Bull. 29, 273-284.

Patterson, C., 1956. Age of meteorites and the earth. Geochim. Cosmochim. Acta 10, 230-237.

Patterson, W. and Walter, L. M., 1994. Depletion of C-13 in Seawater Sigma-Co2 on Modern Carbonate Platforms - Significance for the Carbon Isotopic Record of Carbonates. Geology 22, 885-888.

Patterson, W. and Walter, L. M., 1994. Syndepositional Diagenesis of Modern Platform Carbonates - Evidence from Isotopic and Minor Element Data. Geology 22, 127-130.

Pearce, J.A., Cann, J.R., 1973. Tectonic Setting of Basic Volcanic-Rocks Determined Using Trace-Element Analyses. Earth Planet. Sci. Lett. 19(2), 290-300.

Pecoits, E., Gingras, M. K., Barley, M. E., Kappler, A., Posth, N. R., and Konhauser, K., 2009. Petrography and geochemistry of the Dales Gorge banded iron formation: Paragenetic sequence, source and implications for palaeo-ocean chemistry. Precamb. Res. 172, 163-187.

Pedersen, T. F. and Calvert, S. E., 1990. What controls the formation of organic-carbon-rich sediments and sedimentary rocks? Amer. Assoc. Petrol. Geol. Bull. 74, 454-466.

Peine, A., Tritschler, A., Kusel, K., and Peiffer, S., 2000. Electron flow in an iron-rich acidic sediment - evidence for an acidity-driven iron cycle. Limnol. Oceanogr. 45, 1077-1087.

Penela, A. J. M. and Barragan, G., 1995. Silicification of Carbonate Clasts in a Marine-Environment (Upper Miocene, Vera Basin, Se Spain). Sediment Geol 97, 21-32.

Percival, J. A. and Card, K. D., 1983. Archean Crust as Revealed in the Kapuskasing Uplift, Superior Province, Canada. Geology 11, 323-326.

Perry, E. C. and Ahmad, S. N., 1977. Carbon isotope compostion of graphite and carbonate minerals from 3.8-Ga metamorphosed sediments, Isukasia, Greenland. Earth Planet. Sci. Lett. 36, 280-284.

Perry, E. C., Ahmad, S. N., and Swulius, T. M., 1978a. Oxygen Isotope Composition of 3,800 My Old Metamorphosed Chert and Iron Formation from Isukasia, West-Greenland. J Geol 86, 223-239.

Perry, E. C. J., Ahmad, S. N., and Swulius, T. M., 1978b. The oxygen isotope composition of 3,800 m.y. old metamorphosed chert and iron formation from Isukasia, west Greenland. Journal; of Geology 86, 223-239.

Peter, J. M., 2003. Ancient iron formations: their genesis and use in the exploration fro stratiform base metal sulphide deposits, with examples from the Bathurst Mining Cam In: Lentz, D. R. (Ed.), Geochemistry of sediments and sedimentary rocks : evolutionary considerations to mineral deposit-forming environments. Geological Association of Canada, St. John's, Nfld.

Pfennig, N., 1977. Phototrophic green and purple bacteria: a comparative systematic survey. Annu. Rev. Microbiol. 31, 275-290.

Pflug, H. D., 1978. Yeast-like microfossils detected in oldest sediments of the Earth. Naturwissenschaften 65, 611-615.

Pflug, H. D., 1979. Archean fossil finds resembling yeasts. Geologica et Palaeotologica 13, 1-8.

Pflug, H. D. and Jaeschke-Boyer, H., 1979. Combined structural and chemical analysis of 3,800-Myr-old microfossils. Nature 280, 483-486.

Phillips, G.N., Groves, D.I., Martyn, J.E., 1984, ‘An epigenetic origin for Archaean banded iron-formation-hosted gold deposits’, Economic Geology, 79, p 162-171.

Philippot, , Van Zuilen, M., Lepot, K., Thomazo, C., Farquhar, J., and Van Kranendonk, M. J., 2007. Early Archaean microorganisms preferred elemental sulfur, not sulfate. Science 317, 1534-1537.

Pickard, A.L., Barley, M.E., Krapez, B., 2004, ‘Deep-marine depositional setting of banded iron formation: sedimentological evidence from interbedded clastic sedimentary rocks in the early Palaeoproterozoic Dales Gorge Member of Western Australia, Sedimentary Geology, 170(1-2), p 37-62.

Pineau, F. and Mathez, E.A., 1990. Carbon Isotopes in Xenoliths from the Hualalai Volcano, Hawaii, and the Generation of Isotopic Variability. Geochimica Et Cosmochimica Acta, 54(1): 217-227.

Pinti, D. L. and Hashizume, K., 2001. N-15-depleted nitrogen in Early Archean kerogens: clues on ancient marine chemosynthetic-based ecosystems? A comment to Beaumont,V., Robert,F., 1999. Precambrian Res. 96, 62-82. Precamb. Res. 105, 85-88.

Pinti, D. L., Hashizume, K., Orberger, B., Gallien, J. , Cloquet, C., and Massault, M., 2007. Biogenic nitrogen and carbon in Fe-Mn-oxyhydroxides from an Archean chert, Marble Bar, Western Australia. Geochem Geophy Geosy 8.

Plummer, L. N., Wigley, T. M. L., and Parkhurst, D. L., 1978. Kinetics of Calcite Dissolution in Co2-Water Systems at 5-Degrees-C to 60-Degrees-C and 0.0 to 1.0 Atm Co2. Am. J. Sci. 278, 179-216.

Polat, A., Hofmann, A.W., Rosing, M.T., 2002. Boninite-like volcanic rocks in the 3.7-3.8 Ga Isua greenstone belt, West Greenland: geochemical evidence for intra-oceanic subduction zone processes in the early Earth. Chem. Geol. 184(3-4), 231-254.

Polat, A., Hofmann, A.W., Munker, C., Regelous, M., Appel, W.U., 2003. Contrasting geochemical patterns in the 3.7-3.8 Ga pillow basalt cores and rims, Isua greenstone belt, Southwest Greenland: implications for post magmatic alteration processes. Geochemica et Cosmochimica Acta 67(3), 441-457.

Polat, A., Frei, R., 2005. The origin of early Archean banded iron formations and of continental crust, Isua, southern West Greenland. Precamb. Res. 138(1-2), 151-175.

Polyakov, V.B. and Kharlashina, N.N., 1995a. The Use of Heat-Capacity Data to Calculate Carbon-Isotope Fractionation between Graphite, Diamond, and Carbon-Dioxide - a New Approach. Geochimica Et Cosmochimica Acta, 59(12): 2561-2572.

Polyakov, V.B. and Kharlashina, N.N., 1995b. Direct Calculation of Graphite and Diamond Beta-Factor Values by Use of Heat-Capacity Experimental-Data. Geokhimiya, 8: 1213-1227.

Postma, D., 1981. Formation of Siderite and Vivianite and the Pore-Water Composition of a Recent Bog Sediment in Denmark. Chem. Geol. 31, 225-244.

Postma, D., 1982. Pyrite and Siderite Formation in Brackish and Fresh-Water Swamp Sediments. Am. J. Sci. 282, 1151-1183.

Potter, J., Rankin, A. H., and Treloar, J., 2004. Abiogenic Fischer-Tropsch synthesis of hydrocarbons in alkaline igneous rocks; fluid inclusion, textural and isotopic evidence from the Lovozero complex, N.W Russia. Lithos 75, 311-330.

Pratt, B. R., 1984. Epiphyton and Renalcis - Diagenetic microfossils from calcification of coccoid blue-green algae. 54/3, 947-971.

Pratt, L. M., 1984. Influence of Paleoenvironmental Factors on Preservation of Organic-Matter in Middle Cretaceous Greenhorn Formation, Pueblo, Colorado. Aapg Bulletin-American Association of Petroleum Geologists 68, 1146-1159.

Prave, A. R., 1999. Two diamictites, two cap carbonates, two d13C excursions, two rifts: the Neoproterozoic Kingston Peak Formation, Death Valley, California. Geology 27, 339-342.

Prausnitz, 1969. Molecular Thermodynamics of Fluid-Phase Equilbria. Prentice-Hall, Englewood Cliffs, N.J., 156 p

Price, L.C., 1979. Aqueous Solubility of Methane at Elevated Pressures and Temperatures. American Association of Petroleum Geologists Bulletin, 63(9): 1527-1533.

Priest, F. G., 1984. Extracellular enzymes. Aspects of Microbiology 9, 1-79.

Psenner, R., 1988. Alkalinity Generation in a Soft-Water Lake - Watershed and in-Lake Processes. Limnol. Oceanogr. 33, 1463-1475.

Rasmussen, B., Buick, R., 1999. Redox state of the Archean atmosphere: evidence from detrital heavy minerals in ca. 3250-2750 Ma sandstones from the PIlbara Craton, Australia. Geology 27(2), 115-118.

Redlich, O. and Kwong, J.N.S., 1949. On the Thermodynamics of Solutions. V: An Equation of State. Fugacities of Gaseous Solutions. Chemical Review, 44: 233-244.

Reimers, C. E. and Jr., K. L. S., 1986. Reconciling measured and predicted fluxes of oxygen across the deep sea sediment-water interface. Limnol. Oceanogr 31, 305-318.

Reimers, C. E., K.M. Fischer, R. Mereweather, K.L. Smith, J., and Jahnke., R. A., 1986. Oxygen microprofiles measured in situ in deep ocean sediments.

Riding, R., 1999. The term stromatolite: towards an essential definition. Lethaia 32, 321-330.

Richet, Bottinga, Y., 1977. A review of hydrogen, carbon, nitrogen, oxygen, sulphur, and chlorine stable isotope fractionation among gaseous molecules. Annual Review of Earth and Planetary Science, 5: 65-110.

Riedel, C., Schmid, M., Botz, R., and Theilen, F., 2001. The Grimsey hydrothermal field offshore North Iceland: crustal structure, faulting and related gas venting. Earth Planet. Sci. Lett. 193, 409-421.

Rollinson, H., 2003. Metamorphic history suggested by garnet-growth chronologies in the Isua Greenstone Belt, West Greenland. Precamb. Res. 126(3-4), 181-196.

Romanek, C. S., Grossman, E. L., and Morse, J. W., 1992. Carbon Isotopic Fractionation in Synthetic Aragonite and Calcite - Effects of Temperature and Precipitation Rate. Geochim. Cosmochim. Acta 56, 419-430.

Roper, M., 1983. Fischer-Tropsch Synthesis. In: Klein, W. (Ed.), Catalysis in C1 Chemistry. D. Reidel Publishing Company, Dordrecht.

Ronov, A. B., 1990. Chemical Structure of the Earth's Crust and Chemical Balance of Major Elements. Izdatel'stvo, Moscow.

Rose, N.M., Rosing, M.T., Bridgwater, D., 1996. The origin of metacarbonate rocks in the Archaean Isua supracrustal belt, West Greenland. Am. J. Sci. 296(9), 1004-1044.

Rosenberg, E., 1967. Subsolidus relations in the system CaCO3-MgCO3-FeCO3 between 350 C and 550 C. American Mineralogist, 52: 787-796.

Rosing, M.T., Rose, N.M., Bridgwater, D., Thomsen, H.S., 1996. Earliest part of Earth's stratigraphic record: A reappraisal of the >3.7 Ga Isua (Greenland) supracrustal sequence. Geology 24(1), 43-46.

Rosing, M.T., 1999. 13C-depleted carbon microparticles in >3700-Ma sea-floor sedimentary rocks from west Greenland. Science 283(29 January), 74-76.

Ross, D.J.K., Bustin, R.M., 2009. Investigating the use of sedimentary geochemical proxies for paleoenvironment interpretation of thermally mature organic-rich strata: Examples from the Devonian-Mississippian shales, Western Canadian Sedimentary Basin. Chem. Geol. 260, 1-19.

Rouchon, V., Orberger, B., 2008. Origin and mechanisms of K-Si-metasomatism of ca. 3.4-3.3 Ga volcaniclastic deposits and implications for Archean seawater evolution: Examples from cherts of Kittys Gap (Pilbara craton, Australia) and Msauli (Barberton Greenstone Belt, South Africa). Precamb. Res. 165(3-4), 169-189.

Rusch, A., Huettel, M., Reimers, C. E., Taghon, G. L., and Fuller, C. M., 2003. Activity and distribution of bacterial populations in Middle Atlantic Bight shelf sands. FEMS Microbiol. Ecol. 44, 89-100.

Russell, M.J., Hall, A.J., 1996, 'The emergence of life from monosulphide bubbles at a submarine hydrothermal redox and pH front', Journal of the Geological Society, London, 153, p 1-25.

Quine, W. v. O., 1951. Two dogmas of empericism, From a logical point of view. Harvard University Press, Cambridge, Massachusetts.

Quinn, K. A., Byrne, R. H., and Schijf, J., 2004. Comparative scavenging of yttrium and the rare earth elements in seawater: Competitive influences of solution and surface chemistry. Aquat Geochem 10, 59-80.

Quinn, K. A., Byrne, R. H., and Schijf, J., 2006. Sorption of yttrium and rare earth elements by amorphous ferric hydroxide: Influence of solution complexation with carbonate. Geochim. Cosmochim. Acta 70, 4151-4165.

Radhakrishna, B. and Naqvi, S. M., 1986. Precambrian Continental-Crust of India and Its Evolution. J Geol 94, 145-166.

Ragueneau, O., Treguer, , Leynaert, A., Anderson, R. F., Brzezinski, M. A., DeMaster, D. J., Dugdale, R. C., Dymond, J., Fischer, G., Francois, R., Heinze, C., Maier-Reimer, E., Martin-Jezequel, V., Nelson, D. M., and Queguiner, B., 2000. A review of the Si cycle in the modem ocean: recent progress and missing gaps in

the application of biogenic opal as a paleoproductivity proxy. Global and Planetary Change 26, 317-365.

Raiswell, R., 1987. Non-steady state microbial diagenesis and the origin of concretions and nodular limestones. In: Marshall, J. D. (Ed.), Diagenesis of sedimentary sequences.

Raiswell, R., 2006. An evaluation of diagenetic recycling as a source of iron for banded iron formations. Geological Society of America Memoir 198, 223-237.

Rao, T. G. and Naqvi, S. M., 1995. Geochemistry, Depositional Environment and Tectonic Setting of the Bifs of the Late Archean Chitradurga Schist Belt, India. Chem. Geol. 121, 217-243.

Rasmussen, B., Fletcher, I. R., Brocks, J. J., and Kilburn, M. R., 2008. Reassessing the first appearance of eukaryotes and cyanobacteria. Nature 455, 1101-1209.

Reeder, R. J., 1983. Crystal chemistry of the rhombohedral carbonates. In: Reeder, R. J. (Ed.), Carbonates: Mineralogy and Chemistry. Mineralogical Society of America, Blacksburg, Virginia.

Reid, R. T., Live, D. H., Faulkner, D. J., and Buttler, A., 1993. A siderophore from a marine bacterium with an exceptional ferric ion affinity constant. Nature 366, 455-458.

Rex, R. W., 1969. X-ray mineralogy studies - Leg 1, Deep Sea Drilling

Project. In: Ewing, M. (Ed.), Initial Reports of the Deep Sea Drilling Project.

Rimstidt, J. D. and Barnes, H. L., 1980. The Kinetics of Silica-Water Reactions. Geochim. Cosmochim. Acta 44, 1683-1699.

Rimstidt, J. D. and Cole, D. R., 1983. Geothermal mineralization, I. The mechanism of formation of the Beowawe, Nevada, siliceous sinter deposit. Am. J. Sci. 283, 861-875.

Robbins, L. L. and Blackwelder, L., 1992. Biochemical and Ultrastructural Evidence for the Origin of Whitings - a Biologically Induced Calcium-Carbonate Precipitation Mechanism. Geology 20, 464-468.

Robert, F. and Chaussidon, M., 2006. A palaeotemperature curve for the Precambrian oceans based on silicon isotopes in cherts. Nature 443, 969-972.

Roberts, R. G., 1987. Ore Deposit Models 11: Archean Lode Gold Deposits. Geosci Can 14, 37-52.

Robl, T.L., and Davis, B.H., 1993, Comparison of the Hf-Hcl and Hf-Bf3 Maceration Techniques and the Chemistry of Resultant Organic Concentrates: Organic Geochemistry 20, 249-255.

Roedder, E., 1981. Are the 3.8 *109-y-old Isua objects microfossils, limonite-stained fluid inclusions, or neither? Nature 293, 459-462.

Romanek, C. S., Grossman, E. L., and Morse, J. W., 1992. Carbon Isotopic Fractionation in Synthetic Aragonite and Calcite - Effects of Temperature and Precipitation Rate. Geochim. Cosmochim. Acta 56, 419-430.

Romanek, C. S., Zhang, C. L. L., Li, Y. L., Horita, J., Vali, H., Cole, D. R., and Phelps, T. J., 2003. Carbon and hydrogen isotope fractionations associated with dissimilatory iron-reducing bacteria. Chem. Geol. 195, 5-16.

Ronov, A. B. and Migdisov, A. A., 1970, 1971. Evolution of the chemical composition of rocks.

Rose, N. M., Rosing, M. T., and Bridgwater, D., 1996. The origin of metacarbonate rocks in the Archaean Isua supracrustal belt, West Greenland. Am. J. Sci. 296, 1004-1044.

Rosenberg, E., 1967. Subsolidus relations in the system CaCO3-MgCO3-FeCO3 between 350 C and 550 C. Am. Mineral. 52, 787-796.

Rosing, M.T., Rose, N.M., Bridgwater, D., and Thomsen, H.S., 1996, Earliest part of Earth's stratigraphic record: A reappraisal of the >3.7 Ga Isua (Greenland) supracrustal sequence: Geology, 24, 43-46.

Rosing, M. T., 1999. 13C-depleted carbon microparticles in >3700-Ma sea-floor sedimentary rocks from west Greenland. Science 283, 74-76.

Rouchon, V., Orberger, B., Hoffman, A., and Pinti, D. L., 2009. Diagenetic Fe-carbonates in Paleoarchean felsic sedimentary rocks (Hooggenoeg Formation, Barberton greenstone belt, South Africa): Implications for CO2 sequestration and the chemical budget of seawater. Precamb. Res. 172, 255-278.

Ruby, E.G., Jannasch, H.J., and Deuser, W.G., 1987, Fractionation of stable carbon isotopes during chemoautotrophic growth of sulfur-oxidizing bacteria, Applied Environmental Microbiology 53, 1940-1943.

Rushdi, A. I. and Simoneit, B. R. T., 2001. Lipid formation by aqueous Fischer-Tropsch-type synthesis over a temperature range of 100 to 400 degrees C. Origins Life Evol. Biosph. 31, 103-118.

Rushdi, A. I. and Simoneit, B. R. T., 2004. Condensation reactions and formation of amides, esters, and nitriles under hydrothermal conditions. Astrobiology 4, 211-224.

Rye, R., Kuo, H., and Holland, H. D., 1995. Atmospheric carbon dioxide concentrations before 2.2 billion years ago. Nature 378, 603-605.

Salvi, S. and Williams-Jones, A. E., 1997. Fischer-Tropsch synthesis of hydrocarbons during sub-solidus alteration of the Strange Lake peralkaline granite, Quebec/Labrador, Canada. Geochim. Cosmochim. Acta 61, 83-99.

Sami, T. T. and James, N. , 1993. Evolution of an Early Proterozoic Foreland Basin Carbonate Platform, Lower Pethei Group, Great Slave Lake, North-West Canada. Sedimentology 40, 403-430.

Sami, T. T. and James, N. , 1994. Peritidal Carbonate Platform Growth and Cyclicity in an Early Proterozoic Foreland Basin, Upper Pethei Group, Northwest Canada. J Sediment Res B 64, 111-131.

Sami, T. T. and James, N. , 1996. Synsedimentary cements as Paleoproterozoic platform building blocks, Pethei Group, northwestern Canada. Journal of Sedimentary Research 66, 209-222.

Sapieszko, R. S. and Matijevic, E., 1979. Preparation of well-defined colloidal particles by thermal decomposition of metal chelates. J. Colloid Interface Sci. 74, 405-422.

Savelli, C., Marani, M., and Gamberi, F., 1999. Geochemistry of metalliferous, hydrothermal deposits in the Aeolian arc (Tyrrhenian Sea). J Volcanol Geoth Res 88, 305-323.

Sawicki, J. A., Brown, D. A., and Beveridge, T. J., 1995. Microbial Precipitation of Siderite and Protoferrihydrite in a Biofilm. Can Mineral 33, 1-6.

Schaefer, M. O., Gutzmer, J., and Beukes, N. J., 2001. Late Paleoproterozoic Mn-rich oncoids: Earliest evidence for microbially mediated Mn precipitation. Geology 29, 835-838.

Scheele, N. and Hoefs, J., 1992. Carbon Isotope Fractionation between Calcite, Graphite and Co2 - an Experimental-Study. Contributions to Mineralogy and Petrology, 112(1): 35-45.

Schidlowski, M., Appel, W.U., Eichmann, R. and Junge, E., 1979. Carbon isotope geochemistry of the 3.7 x 109-yr-old Isua sediments, west Greenland: implications for the Archaean carbon and oxygen cycles. Geochimica et Cosmochimica Acta, 43: 189-199.

Schidlowski, M., 1988. A 3800-million-year isotopic record of life from carbon in sedimentary rocks. Nature, 333(26 May): 313-318.

Schidlowski, M., 1993. The beginnings of life on Earth: evidence from the geological record. In: J.M. Greenberg, C.X. Mendoza-Gomez and V. Pirronello (Editors), The Chemistry of Life's Origins. Kluwer Academic Publishers, Netherlands, p 389-414.

Schidlowski, M., 2001. Carbon isotopes as biogeochemical recorders of life over 3.8 Ga of Earth history: evolution of a concept. Precambrian Research, 106(1-2): 117-134.

Schink, B. and Stams, A. J. M., 2002. Syntrophism among prokaryotes. In: Dworkin, M. (Ed.),The prokaryotes: an evolving electronic resource for the microbiological community. Springer, New York.

Schmitz, R. A., Daniel, R., Deppenmeir, U., and Gottschalk, G., 2001. Syntrophism among prokaryotes. In: Dworkin, M. (Ed.),The prokaryotes: an evolving electronic resource for the microbiological community. Springer, New York.

Schoenberg, R., Kamber, B. S., Collerson, K. D., and Moorbath, S., 2002. Tungsten isotope evidence from ~3.8-Gyr metamorphosed sediments for early meteorite bombardment of the Earth. Nature 418, 403-405.

Schopf, J. W., 1983. Earth's Earliest Biosphere: It's Origin and Evolution. Princeton University Press, Princeton, New Jersey.

Schopf, J. W. and Packer, B. M., 1987. Early Archean (3.3-billion to 3.5-billion-year-old) microfossils from Warrawoona Group, Australia. Science 237, 70-73.

Schopf, J. W., 1993. Microfossils of the early Archean Apex Chert: new evidence of the antiquity of life. Science 260, 640-646.

Schopf, J. W., Kudryavtsev, A. B., Agresti, D. G., Wdowiak, T. J., and Czaja, A. D., 2002. Laser-Raman imagery of Earth's earliest fossils. Nature 416, 73-76.

Schulte, M., Blake, D., Hoehler, T., and Mccollom, T., 2006. Serpentinization and its implications for life on the early Earth and Mars. Astrobiology 6, 364-376.

Schwartz, G. M., 1959. Hydrothermal alteration. Economic Geology 54, 161-183.

Schwerdner, W. M. and Lumbers, S., 1980. The Continental crust and its mineral deposits : the proceedings of a symposium held in honour of J. Tuzo Wilson held at Toronto, May, 1979, Geological Association of Canada special paper, Geological Association of Canada.

Septhon, M. A., Verchovsky, A. B., and Wright, I. , 2004. Carbon and nitrogen isotope ratios in meteoritic organic matter: indicators of alteration processes on the parent asteroid. International Journal of Astrobiology 3, 221-227.

Sethuram, K. and Moore, J. M., 1973. Petrology of Metavolcanic Rocks in Bishop-Corners-Donaldson-Area, Grenville-Province, Ontario. Can. J. Earth Sci. 10, 589-614.

Seyfried, W. E., 1987. Experimental and Theoretical Constraints on Hydrothermal Alteration Processes at Midocean Ridges. Annu Rev Earth Pl Sc 15, 317-335.

Seyfried, W. E., Ding, K., Berndt, M. E., and Chen, X., 1999. Experimental and Theoretical Controls on the Composition of Mid-Ocean Ridge Hydrothermal Fluids. Reviews in Economic Geology 8, 181-200.

Shackleton, 1985. Oceanic carbon isotope constraints on oxygen and carbon dioxide in the Cenozoic atmosphere. Geophysical Monograph Series 32, 412-417.

Sharp, Z.D., Papike, J.J. and Durakiewicz, T., 2003. The effect of thermal decarbonation on stable isotope compositions of carbonates. American Mineralogist, 88(1): 87-92.

Shaw, D.M., 1968. A review of K-Rb fractionation trends by covariance analysis. Geochim. Cosmochim. Acta 32, 573-601.

Shen, Y., Buick, R., and Canfield, D. E., 2001. Isotopic evidence for microbial sulphate reduction in the early Archaean era. Nature 410, 77-81.

Shen, Y., Knoll, A. H., and Walter, M. R., 2003. Evidence for low sulphate and anoxia in a mid-Proterozoic marine basin. Nature 423, 632-635.

Shen, Y. N. and Buick, R., 2004. The antiquity of microbial sulfate reduction. Earth-Sci Rev 64, 243-272.

Shen, Y., Farquhar, J., Masterson, A., and Kaufman, A. J., 2009. Evaluating the biogenicity of early Archaean sulphur cycling using quadruple isotope systematics. Earth Planet. Sci. Lett. 279, 383-291.

Sheppard, S. M. and Schwarcz, H. , 1970. Fractionation of Carbon and Oxygen Isotopes and Magnesium between Coexisting Metamorphic Calcite and Dolomite. Contrib. Mineral. Petrol. 26, 161.

Sherwood-Lollar, B., Frape, S. K., Weise, S. M., Fritz, , Macko, S. A., and Welhan, J. A., 1993. Abiogenic methanogenesis in crystalline rocks. Geochimica Cosmochimica Acta 57, 5087-5097.

Sherwood-Lollar, B., Westgate, T. D., Ward, J. A., Slater, G. F., and Lacrampe-Couloume, G., 2002. Abiogenic formation of alkanes in the Earth's crust as a minor source for global hydrocarbon reservoirs. Nature 416, 522-524.

Shibuya, T., Kitajima, K., Komiya, T., Terabayashi, M., and Maruyama, S., 2007. Middle archean ocean ridge hydrothermal metamorphism and alteration recorded in the cleaverville area, pilbara craton, western australia. J Metamorph Geol 25, 751-767.

Shields, G. and Veizer, J., 2002. Precambrian marine carbonate isotope database: Version 1.1. Geochem Geophy Geosy 3.

Shields, G.A., Webb, G.E., 2004. Has the REE composition of seawater changed over geological time? Chem. Geol. 204(1-2), 103-107.

Shields, G., 2007. The marine carbonate and chert isotope records and their implication for tectonics, life and climate on the early Earth. In: van Kranendonk, M., Smithies, R. H., and Bennett, V. C. Eds.), Earth's oldest rocks. Elsevier, Amsterdam.

Shimoyama, A., 1997. Complex organics in meteorites. Adv. Space Res. 19, 1045-1052.

Shinn, E. A., Steinen, R. , Lidz, B. H., and Swart, K., 1989. Whitings, a Sedimentologic Dilemma. J Sediment Petrol 59, 147-161.

Shock, E. L., 1990. Geochemical Constraints on the Origin of Organic-Compounds in Hydrothermal Systems. Origins Life Evol. Biosph. 20, 331-367.

Shock, E.L., 1992. Chemical Environments of Submarine Hydrothermal Systems. Origins of Life and Evolution of the Biosphere, 22(1-4): 67-107.

Shock, E. L. and Schulte, M. D., 1998. Organic synthesis during fluid mixing in hydrothermal systems. Journal of Geophysical Research-Planets 103, 28513-28527.

Sholkovitz, E.R., Landing, W.M., Lewis, B.L., 1994. Ocean Particle Chemistry - the Fractionation of Rare-Earth Elements between Suspended Particles and Seawater. Geochimica Et Cosmochimica Acta 58(6), 1567-1579.

Sial, A. N., Ferreira, V. , Dealmeida, A. R., Romano, A. W., Parente, C. V., Dacosta, M. L., and Santos, V. H., 2000. Carbon isotope fluctuations in Precambrian carbonate sequences of several localities in Brazil. An. Acad. Bras. Cienc. 72, 539-558.

Siever, R., 1962. Silica Solubility, 0-Degrees-C-200-Degrees-C, and the Diagenesis of Siliceous Sediments. J Geol 70, 127-150.

Siever, R., 1992. The Silica Cycle in the Precambrian. Geochim. Cosmochim. Acta 56, 3265-3272.

Simoneit, B. R. T., 2004. Prebiotic organic synthesis under hydrothermal conditions: an overview. Space Life Sciences: Steps toward Origin(S) of Life 33, 88-94.

Simoneit, B. R. T., Lein, A. Y., Peresypkin, V. I., and Osipov, G. A., 2004. Composition and origin of hydrothermal petroleum and associated lipids in the sulfide deposits of the Rainbow Field (Mid-Atlantic Ridge at 36 degrees N). Geochim. Cosmochim. Acta 68, 2275-2294.

Simonson, B. M., 1985. Sedimentology of cherts in the early Proterozoic Wishart Formation, Quebec - Newfoundland, Canada. Sedimentology 32, 23-40.

Simonson, B. M., 1987. Early silica cementation and subsequent diagenesis in arenites from four Early Proterozoic Iron Formations of North America. J Sediment Petrol 57.

Simonson, B. M., Schubel, K. A., and Hassler, S. W., 1993. Carbonate Sedimentology of the Early Precambrian Hamersley Group of Western-Australia. Precamb. Res. 60, 287-335.

Simonson, B.M., Hassler, S., 1996, 'Was the deposition of large Precambrian iron formations linked to major marine transgressions?', Journal of Geology, 104, p 665-676.

Simonson, B. M., Byerly, G. R., and Lowe, D. R., 2004. The Early Precambrian Stratigraphic Record of Large Extraterrestrial Impacts. In: Eriksson, K. A., Altermann, W., Nelson, D. R., Mueller, A., and Catuneanu, O. Eds.), The Precambrian Earth: Tempos and Events. Elsevier, Amsterdam.

Singh, U., 1987. Ooids and cements from the Late Precambrian of the Flinders Ranges, South Australia. 57/1, 117-127.

Sinha, R. and Smykatz-Kloss, W., 2003. Thermal characterization of lacustrine dolomites from the Sambhar Lake playa, Thar desert, India. J Therm Anal Calorim 71, 739-750.

Sleep, N. H., Meibom, A., Fridriksson, T., Coleman, R. G., and Bird, D. K., 2004. H-2-rich fluids from serpentinization: Geochemical and biotic implications. Proc. Natl. Acad. Sci. U. S. A. 101, 12818-12823.

Sjoberg, E. L., 1978. Kinetics and mechanism of calcite dissolution in aqueous solutions at low temperatures. Acta Univ. Stockholmiensism Stockholm Contr. Geology 332, 1-92.

Skinner, B. J. and Barton, B., 1973. Genesis of Mineral-Deposits. Annu Rev Earth Pl Sc 1, 183-211.

Slack, J. F., Kelley, K. D., Anderson, V. M., Clark, J. L., and Ayuso, R. A., 2004. Multistage hydrothermal silicification and Fe-Tl-As-Sb-Ge-REE enrichment in the Red Dog Zn-Pb-Ag district, northern Alaska: Geochemistry, origin, and exploration applications. Economic Geology 99, 1481-1508.

Slaughter, M. and Hill, R. J., 1991. The influence of organic matter in organogenic dolomitization. 61/2, 296-303, 4 Figs., 2 Tabs.

Smith, S. V. and Veeh, H. H., 1989. Mass balance of biogeochemically active materials (C, N, P) in a hypersaline gulf. Estuarine, Coastal and Shelf Science 29, 195-215.

Snow, J. E. and Dick, H. J. B., 1995. Pervasive mangesium loss by marine weathering of peridotite. Geochim. Cosmochim. Acta 59, 4219-4235.

Sobolev, D. and Roden, E. E., 2002. Evidence for rapid microscale bacterial redox cycling of iron in circumneutral environments. Anton Leeuw Int J G 81, 587-597.

Sochava, A. V. and Podkovyrov, V. N., 1995. The Compositional Evolution of Mesoproterozoic and Neoproterozoic Carbonate Rocks. Precamb. Res. 73, 283-289.

Spear, F. S., 1995. Metamorphic phase equilibria and pressure-temperature-time paths. Mineralogical Society of America, Washington, D.C.

Spears, D. A., 1989. Aspects of incorporation into sediments with special reference to the Yorkshire ironstones. In: Young, T. and Taylor, W. E. G. Eds.), Phanerozoic ironstones. Geological Society, London.

Spero, H. J., Bijma, J., Lea, D. W., and Bemis, B. E., 1997. Effect of seawater carbonate concentration on foraminiferal carbon and oxygen isotopes. Nature 390, 497-500.

Spier, C. A., de Oliveira, S. M. B., and Rosiere, C. A., 2003. Geology and geochemistry of the Aguas Claras and Pico Iron Mines, Quadrilatero Ferrifero, Minas Gerais, Brazil. Miner Deposita 38, 751-774.

Spier, C. A., de Oliveira, S. M. B., Rosiere, C. A., and Ardisson, J. D., 2008. Mineralogy and trace-element geochemistry of the high-grade iron ores of the Aguas Claras Mine and comparison with the Capao Xavier and Tamandua iron ore deposits, Quadrilahero Ferrifero, Brazil. Miner Deposita 43, 229-254.

Spier, C. A., de Oliveira, S. M. B., Sial, A. N., and Rios, F. J., 2007. Geochemistry and genesis of the banded iron formations of the Caue Formation, Quadrilatero Ferrifero, Minas Gerais, Brazil. Precamb. Res. 152, 170-206.

Spotl, C. and Wright, V. , 1992. Groundwater Dolocretes from the Upper Triassic of the Paris Basin, France - a Case-Study of an Arid, Continental Diagenetic Facies. Sedimentology 39, 1119-1136.

Staudigel, H., Plank, T., While, B., and Schminke, H. U., 1996. Geochemical fluxes during seafloor alteration of the basaltic upper oceanic crust: DSDP Sites 417 and 418. In: Bebout, G. E., Scholl, D. W., Kirby, S. H., and Platt, J. Eds.), Subduction Top to Bottom. American Gephyiscal Union, Washington, D.C.

Stein, R., 1990. Organic-Carbon Content Sedimentation-Rate Relationship and Its Paleoenvironmental Significance for Marine-Sediments. Geo-Marine Letters 10, 37-44.

Steinsund, I. and Hald, M., 1994. Recent Calcium-Carbonate Dissolution in the Barents Sea - Paleoceanographic Applications. Mar Geol 117, 303-316.

Stipp, S. L. and Hochella, M. F., 1991. Structure and Bonding Environments at the Calcite Surface as Observed with X-Ray Photoelectron-Spectroscopy (Xps) and Low-Energy Electron-Diffraction (Leed). Geochim. Cosmochim. Acta 55, 1723-1736.

Stipp, S. L. and Hochella, M. F., 1992. Uptake of Cd2+ and Other Divalent-Cations by Calcite, Solid-State Diffusion and Solid-Solution Formation. Abstr Pap Am Chem S 203, 178-Geoc.

Stipp, S. L., Hochella, M. F., Parks, G. A., and Leckie, J. O., 1992. Cd2+ Uptake by Calcite, Solid-State Diffusion, and the Formation of Solid-Solution - Interface Processes Observed with near-Surface Sensitive Techniques (Xps, Leed, and Aes). Geochim. Cosmochim. Acta 56, 1941-1954.

Stockman, K. W., Ginsburg, R. N., and Shinn, E. A., 1967. Production of Lime Mud by Algae in South Florida. J Sediment Petrol 37, 633..

Sugisaki, R. and Mimura, K., 1994. Mantle Hydrocarbons - Abiotic or Biotic. Geochimica Et Cosmochimica Acta, 58(11): 2527-2542.

Sugitani, K., Yamamoto, K., Wada, H., Binu-Lal, S.S., Yoneshige, M., 2002. Geochemistry of Archean carbonaceous cherts deposited at immature island-arc setting in the Pilbara Block, Western Australia. Sediment Geol 151(1-2), 45-66.

Sun, S.S., McDonough, W.F., 1989. Chemical and isotopic systematics of oceanic basalts: implications for mantle composition and processes, In: Magmatism in the Ocean Basins, A.D. Saunders and M.J. Norry, eds., Geological Society Special Publication 42313-345.

Stumm, W. and Morgan, B., 1996. Aquatic chemistry. John Wiley & Sons, New York.

Sugimoto, T., Waki, S., Itoh, H., and Muramatsu, A., 1996. Preparation of monodisperse platelet-type hematite particles from a highly condensed beta-FeOOH suspension. Colloid Surface A 109, 155-165.

Summons, R.E., Franzmann, D., and Nichols, D., 1998, Carbon isotopic fractionation associated with methylotrophic methanogenesis, Organic Geochemistry 28, 465-475.

Sumner, D. Y., 1997a. Carbonate precipitation and oxygen stratification in late Archean seawater as deduced from facies and stratigraphy of the Gamohaan and Frisco Formations, Transvaal Supergroup, South Africa. American Journal of Science 297, 455-487.

Sumner, D. Y., 1997b. Carbonate precipitation and oxygen stratification in late Archean seawater as deduced from facies and stratigraphy of the Gamohaan and Frisco formations, Transvaal Supergroup, South Africa. Am. J. Sci. 297, 455-487.

Sumner, D. Y., 2000. Microbial versus environmental influences on the morphology of Late Archean fenestrate microbialites. In: Riding, R. E. and Awramik, S. M. Eds.), Microbial sediments. Springer-Verlag, Berlin.

Sumner, D. Y., 2002. Decimetre-thick encrustations of calcite and aragonite on the sea-floor and implications for Neoarchaean and Neoproterozoic ocean chemistry. Special Publications of the International Association of Sedimentologists 33, 107-120.

Sumner, D. Y. and Grotzinger, J. , 1996. Were kinetics of Archean calcium carbonate precipitation related to oxygen concentration? Geology 24, 119-122.

Sumner, D. Y. and Grotzinger, J. , 2000. Late Archean aragonite precipitation: petrography, facies associations, and environmental significance. In: Grotzinger, J. and James, N. Eds.), Carbonate sedimentation and diagenesis in the evolving Precambrian world. Society for Sedimentary Geology.

Sumner, D. Y. and Grotzinger, J. , 2004. Implications for Neoarchaean ocean chemistry from primary carbonate mineralogy of the Campbellrand-Malmani Platform, South Africa. Sedimentology 51, 1273-1299.

Sun, S. S. and McDonough, W. F., 1989. Chemical and isotopic systematics of oceanic basalts: implications for mantle composition and processes. In: Saunders, A. D. and Norry, M. J. Eds.), Magmatism in the Ocean Basins.

Swart, K., Pillinger, C.T., Milledge, H.J. and Seal, M., 1983. Carbon Isotopic Variation within Individual Diamonds. Nature, 303(5920): 793-795.

Swart, K. and Eberli, G., 2005. The nature of the delta C-13 of periplatform sediments: Implications for stratigraphy and the global carbon cycle. Sediment Geol 175, 115-129.

Swedlund, J. and Webster, J. G., 1999. Adsorption and polymerisation of silicic acid on ferrihydrite, and its effect on arsenic adsorption. Water Res. 33, 3413-3422.

Swett, K., 1965. Dolomitization Silicification and Calcitization Patterns in Cambro-Ordovician Oolites from Northwest Scotland. J Sediment Petrol 35, 928.

Sylvester, J., 1994. Archean Granite Plutons. In: Condie, K. C. (Ed.), Archean Crustal Evolution. Elsevier, Amsterdam.

Szatmari, , 1989. Petroleum Formation by Fischer-Tropsch Synthesis in Plate-Tectonics. Aapg Bulletin-American Association of Petroleum Geologists 73, 989-998.

Takenouchi, S. and Kennedy, G.C., 1964. The binary system H2O-CO2 at high temperatures and pressures. American Journal of Science, 262: 1055-1074.

Talbot, M. R., 1990. A Review of the Paleohydrological Interpretation of Carbon and Oxygen Isotopic-Ratios in Primary Lacustrine Carbonates. Chem. Geol. 80, 261-279.

Taran, Y., Kliger, G. A., and Sevastianov, S., 2007. Carbon isotope effects in the open-system Fischer-Tropsch synthesis. Geochemica et Cosmochimica Acta 71, 4474-4487.

Tarney, J. and Windley, B. F., 1977. Chemistry, thermal gradients and evolution of the lower continental crust. Journal of the Geological Society of London 134, 153-172.

Taylor, S.R., McLennan, S.M., 1985, The Continental Crust: its Composition and Evolution, 312 p, Blackwell Scientific, Oxford.

Taylor, S.R., McLennan, S.M., 1995. The Geochemical Evolution of the Continental-Crust. Reviews of Geophysics 33(2), 241-265.

Taylor, D., Dalstra, H. J., Harding, A. E., Broadbent, G. C., and Barley, M. E., 2001. Genesis of high-grade hematite orebodies of the Hamersley province, Western Australia. Economic Geology 96, 837-873.

Terabayashi, M., Masada, Y., and Ozawa, H., 2003. Archean ocean-floor metamorphism in the North Pole area, Pilbara Craton, Western Australia. Precamb. Res. 127, 167-180.

Teske, A. , 2005. The deep subsurface biosphere is alive and well. Trends Microbiol. 13, 402-404.

Thamdrup, B. and Canfield, D., 2000. Benthic respiration in aquatic sediments. In: Sala, O. E., Jackson, R. B., Mooney, H. A., and Howarth, R. W. Eds.), Methods in Ecosystem Science. Springer, New York.

Thauer, R. K., Jungermann, K., and Decker, K., 1977. Energy conservation in anaerobic chemotrophic bacteria. Bacteriological Review 41, 100-180.

Thiry, M., 1981. Sedimentation continentale et alterations associees: calcitations, ferruginisations et silicifications. Les Argiles Plastiques du Sparnaciean de Bassin de Paris. Sci. Geol. Mem. 64, 173.

Thiry, M., 1999. Diversity of continental silicification features: examples from the Cenozoic deposits in the Paris Basin and neighbouring basement. In: Thiry, M. and Simon-Coinçon, R. Eds.), Palaeoweathering, palaeosurfaces, and related continental deposits. Blackwell Science, Oxford; Malden, MA.

Thiry, M., Ayrault, M. B., and Grisoni, J. C., 1988a. Groundwater Silicification and Leaching in Sands - Example of the Fontainebleau Sand (Oligocene) in the Paris Basin. Geol Soc Am Bull 100, 1283-1290.

Thiry, M., Ayrault, M. B., Grisoni, J. C., Menillet, F., and Schmitt, J. M., 1988b. The Fontainebleau Sandstones - Groundwater Silicification Related to the Geomorphologic Evolution of the Paris-Basin During Plio-Quaternary. B Soc Geol Fr 4, 419-430.

Thiry, M. and Millot, G., 1987. Mineralogical Forms of Silica and Their Sequence of Formation in Silcretes. J Sediment Petrol 57, 343-352.

Thiry, M. and Ribet, I., 1999. Groundwater silicification in Paris Basin limestones: Fabrics, mechanisms, and modeling. Journal of Sedimentary Research 69, 171-183.

Thurston, C., Ayres, L. D., Edwards, G. R., Gelinas, L., Ludden, J. N., and Verpaelst, , 1985. Archean bimodal volcanism. In: Ayres, L. D., Thurston, C., Card, K. D., and Weber, W. Eds.), Evolution of Archean Supracrustal Sequences. Geological Association of Canada.

Tian, F., Toon, O. B., Pavlov, A. A., and De Sterck, H., 2005. A hydrogen-rich early Earth atmosphere. Science 308, 1014-1017.

Tice, M. M. and Lowe, D. R., 2004. Photosynthetic microbial mats in the 3,416-Myr-old ocean. Nature 431, 549-552.

Tice, M. M. and Lowe, D. R., 2006. The origin of carbonaceous matter in pre-3.0 Ga greenstone terrains: A review and new evidence from the 3.42 Ga Buck Reef Chert. Earth-Sci Rev 76, 259-300.

Toulkeridis, T., Clauer, N., Kroner, A., 1996. Chemical variations in clay minerals of the Archaean Barberton Greenstone Belt (South Africa). Precamb. Res. 79(3-4), 195-207.

Toulkeridis, T., Goldstein, S. L., Clauer, N., Kroner, A., Todt, W., and Schidlowski, M., 1998. Sm-Nd, Rb-Sr and Pb-Pb dating of silicic carbonates from the early Archaean Barberton Greenstone Belt, South Africa - Evidence for post-depositional isotopic resetting at low temperature. Precamb. Res. 92, 129-144.

Towe, K.M., 1983, 'Precambrian atmospheric oxygen and banded iron formations: a delayed ocean model', Precambrian Research, 20, p 161-170.

Trendall, A. F. and Blockley, J. G., 1970. The iron formations of the Precambrian Hamersley Group, Western Australia, with special reference to the associated crocidolite.

Trendall, A. F., 1990. Pilbara Craton - Introduction, Geology and mineral resources of Western Australia. Western Australia Geological Survey, Perth.

Trendall, A. F. and Blockley, J. G., 2004. Precambrian iron-formation. In: Eriksson, K. A., Altermann, W., Nelson, D. R., Mueller, A., and Catuneanu, O. Eds.), The Precambrian Earth: Tempos and Events. Elsevier, Amsterdam.

Tribble, J. S., Arvidson, R. S., Lane, M., and Mackenzie, F. T., 1995. Crystal-Chemistry, and Thermodynamic and Kinetic-Properties of Calcite, Dolomite, Apatite, and Biogenic Silica - Applications to Petrologic Problems. Sediment Geol 95, 11-37.

Tsikos, H., Moore, J. M., and Harris, C., 2001. Geochemistry of the Palaeoproterozoic Mooidraai Formation: Fe-rich limestone as end member of iron formation deposition, Kalahari Manganese Field, Transvaal Supergroup, South Africa. J Afr Earth Sci 32, 19-27.

Tucker, M. E., 1986. Formerly Aragonitic Limestones Associated with Tillites in the Late Proterozoic of Death-Valley, California. J Sediment Petrol 56, 818-830.

Turner, E. C., James, N. , and Narbonne, G. M., 1997. Growth dynamics of Neoproterozoic calcimicrobial reefs, Mackenzie Mountains, northwest Canada. Journal of Sedimentary Research 67, 437-450.

Turner, E. C., James, N. , and Narbonne, G. M., 2000. Taphonomic control on microstructure in early neoproterozoic reefal stromatolites and thrombolites. Palaios 15, 87-111.

Tyler, I. M., 1990. Inliers of granite-greenstone terrane., Geology and Mineral Resources of Western Australia. .Western Australia Geological Survey.

Ueno, Y., Isozaki, Y., Yurimoto, H., and Maruyama, S., 2001. Carbon isotopic signatures of individual Archean microfossils(?) from Western Australia. Int Geol Rev 43, 196-212.

Ueno, Y., Yoshioka, H., Isozaki, Y., and Maruyama, S., 2003. Origin of 13C-depleted kerogen in ca. 3.5 Ga hydrothermal silica dikes from Western AustraliaGoldschmidt.

Ueno, Y., Yoshioka, H., Maruyama, S., and Isozaki, Y., 2004. Carbon isotopes and petrography of kerogens in similar to 3.5-Ga hydrothermal silica dikes in the North Pole area, Western Australia. Geochim. Cosmochim. Acta 68, 573-589.

Ueno, Y., Ono, S., Rumble, D., and Maruyama, S., 2008. Quadruple sulfur isotope analysis of ca. 3.5 Ga Dresser Formation: New evidence for microbial sulfate reduction in the early Archean. Geochim. Cosmochim. Acta 72, 5675-5691.

Ulmerscholle, D. S., Scholle, A., and Brady, V., 1993. Silicification of Evaporites in Permian (Guadalupian) Back-Reef Carbonates of the Delaware Basin, West Texas and New-Mexico. J Sediment Petrol 63, 955-965.

Umeda, M., 2003. Precipitation of silica and formation of chert-mudstone-peat association in Miocene coastal environments at the opening of the Sea of Japan. Sedimentary Geology 161, 249-268.

Uysal, I. T., Golding, S. D., and Glikson, M., 2000. Petrographic and isotope constraints on the origin of authigenic carbonate minerals and the associated fluid evolution in Late Permian coal measures, Bowen Basin (Queensland), Australia. Sediment Geol 136, 189-206.

Valentine, D. L., 2001. Thermodynamic ecology of hydrogen-based syntrophy. In: Seckback, J. (Ed.), Symbiosis: mechanism and model systems. Kluwer, Dordrecht.

Valley, J.W. and Oneil, J.R., 1981. C-13-C-12 Exchange between Calcite and Graphite - a Possible Thermometer in Grenville Marbles. Geochimica Et Cosmochimica Acta, 45(3): 411-419.

van Breugel, Y., Schouten, S., Paetzel, M., Nordeide, R., and Damste, J. S. S., 2005. The impact of recycling of organic carbon on the stable carbon isotopic composition of dissolved inorganic carbon in a stratified marine system (Kyllaren fjord, Norway). Org. Geochem. 36, 1163-1173.

van Cappellen, , Viollier, E., Roychoudhury, A., Clark, L., Ingall, E., Lowe, K., and Dichristina, T., 1998. Biogeochemical cycles of manganese and iron at the oxic-anoxic transition of a stratified marine basin (Orca Basin, Gulf of Mexico). Environ. Sci. Technol. 32, 2931-2939.

van Haaften, W. M. and White, S. H., 1998. Evidence for multiphase deformation in the Archean basal Warrawoona Group in the Marble Bar area, east Pilbara, Western Australia. Precamb. Res. 88, 53-66.

van Kranendonk, M., 2006. Volcanic degassing, hydrothermal circulation and the flourishing of life on Earth: A review of the evidence from c. 3490-3240 Ma rocks of the Pilbara Supergroup, Pilbara Craton, Western Australia. Earth Science Review 74, 197-240.

van Kranendonk, M. J., 1997. Results of field mapping, 1994-1996, in the North Shaw and Tambourah 1:100000 sheet areas, eastern Pilbara Craton, northwestern Australia. University of Newcastle/AGSO.

van Kranendonk, M. J. and Collins, W. J., 1998. Timing and tectonic significance of Late Archaean, sinistral strike-slip deformation in the Central Pilbara Structural Corridor, Pilbara Craton, Western Australia. Precamb. Res. 88, 207-232.

van Kranendonk, M. J., Hickman, A. H., Smithies, R. H., and Nelson, D. R., 2002. Geology and tectonic evolution of the Archean North Pilbara Terrain, Pilbara Craton, Western Australia. Economic Geology 97, 695-732.

van Kranendonk, M. J., 2000. Geology of the North Shaw 1:100 000 sheet: Western Australia Geological Survey. Western Australia Geological Survey, Perth.

van Kranendonk, M., Webb, G. E., and Kamber, B., 2003. Geological and trace element evidence for a marine sedimentary environment of deposition and biogenicity of 3.45 Ga stromatolitic carbonates in the Pilbara Craton, and support for a reducing Archaean ocean. Geobiol. 1, 91-108.

van Kranendonk, M. J., Webb, G. E., Kamber, B., and Pirajno, F., 2003. Geological setting and biogenicity of 3.45 Ga stromatolitic cherts, east Pilbara, Australia. Geochim. Cosmochim. Acta 67, A510-A510.

van Kranendonk, M., 2006. Volcanic degassing, hydrothermal circulation and the flourishing of life on Earth: A review of the evidence from c. 3490-3240 Ma rocks of the Pilbara Supergroup, Pilbara Craton, Western Australia. Earth Science Review 74, 197-240.

van Zuilen, M.A., Lepland, A. and Arrhenius, G., 2002. Reassessing the evidence for the earliest traces of life. Nature, 418: 627-630.

van Zuilen, M. A., Lepland, A., Teranes, J., Finarelli, J., Wahlen, M., and Arrhenius, G., 2003. Graphite and carbonates in the 3.8 Ga old Isua Supracrustal Belt, southern West Greenland. Precamb. Res. 126, 331-348.

van Zuilen, M., Kattathu, M., Wopenka, B., Lepland, A., Marti, K., and Arrhenius, G., 2005. Nitrogen and argon isotopic signatures in graphite from the 3.8-Ga-old Isua Supracrustal Belt, Southern West Greenland. Geochem. Cosmochem. Acta 69, 1241-1252.

Vasconcelos, C. and McKenzie, J. A., 1997. Microbial mediation of modern dolomite precipitation and diagenesis under anoxic conditions (Lagoa Vermelha, Rio De Janeiro, Brazil). Journal of Sedimentary Research 67, 378-390.

Vasconcelos, C., McKenzie, J. A., Bernasconi, S., Grujic, D., and Tien, A. J., 1995. Microbial mediation as a possible mechanism for natural dolomite formation at low temperatures. Nature 377, 220-222.

Veizer, J. and Hoefs, J., 1976. The nature of 18O/16O and 13C/12C secular trends in sedimentary carbonate rocks. Geochim. Cosmochim. Acta 40, 1387-1395.

Veizer, J., 1978. Secular Variations in Composition of Sedimentary Carbonate Rocks, II. Fe, Mn, Ca, Mg, Si and Minor Constituents. Precamb. Res. 6, 381-413.

Veizer J., 1983, ‘Geologic evolution of the Archean-Early Proterozoic Earth’, In: Schopf, J.W. (ed.), ‘Earth’s Earliest Biosphere’, Princeton University Press, New Jersey, p 240-259.

Veizer, J., 1983. Chemical diagenesis of carbonates: theory and application of trace element technique, Stable isotopes in sedimentary geology: Society of Economic Paleontologists and Mineralogists Short Course 10.

Veizer, J. and Garrett, D. E., 1978. Secular Variations in Composition of Sedimentary Carbonate Rocks .1. Alkali-Metals. Precamb. Res. 6, 367-380.

Veizer, J., Hoefs, J., Ridler, R. H., Jensen, L. S., and Lowe, D. R., 1989a. Geochemistry of Precambrian Carbonates: I. Archean Hydrothermal Systems. Geochim. Cosmochim. Acta 53, 845-857.

Veizer, J., Hoefs, J., Lowe, D. R., and Thurston, C., 1989b. Geochemistry of Precambrian carbonates: II. Archean greenstone belts and Archean sea water. Geochim. Cosmochim. Acta 53, 859-871.

Veizer, J., Clayton, R. N., Hinton, R. W., von Brunn, V., Mason, T. R., Buck, S. G., and Hoefs, J., 1990. Geochemistry of Precambrian carbonates: 3 - Shelf seas and non-marine environments of the Archean. Geochim. Cosmochim. Acta 54, 2717-2729.

Veizer, J., 1992. Depositional and diagenetic history of limestones: Stable and radiogenic isotopes. In: Clauer, N. and Chaudhuri, S. Eds.), Lecture notes in earth sciences ;. Springer-Verlag, Berlin.

Verrecchia, E. , Freytet, , Julien, J., and Baltzer, F., 1997. The unusual hydrodynamical behaviour of freshwater oncolites. Sediment Geol 113, 225-243.

Ver´ýssimo, C. U. V., Schrank, A., Pires, F. R. M., Hasui, Y., Zanardo, A., and Parente, C. V., 2002. Geochemical study of the itabirite iron ores of the Alegria mine—Quadril´atero Ferr´ýfero, Minas Gerais, Brazil. Australasian Institute of Mining and Metallurgy, 95–103.

Viljoen, M. J. and Viljoen, R. , 1969. The geological and geochemical significance of the upper formations of the Onverwacht Grou Geological Society of South Africa Special Publications 2, 113-152.

Voglesonger, K. M., Holloway, J. R., Dunn, E. E., Dalla-Betta, J., and O'Day, A., 2001. Experimental abiotic synthesis of methanol in seafloor hydrothermal systems during diking events. Chem. Geol. 180, 129-139.

Vorob'yeva, K. A. and Mel'nik, Y. , 1977. Experimental Investigation of System Fe2O3-H2O at T=100-200degreesc and P up to 9 Kbar. Geokhimiya, 1121-1128.

Wacey, D., McLoughlin, N., Green, O. R., Parnell, J., Stoakes, C., and Brasier, M., 2006. The ~3.4 billion-year-old Strelley Pool Sandstone: a new window into early life on Earth. International Journal of Astrobiology 5, 333-342.

Wada, H. and Suzuki, K., 1983. Carbon Isotopic Thermometry Calibrated by Dolomite-Calcite Solvus Temperatures. Geochimica Et Cosmochimica Acta, 47(4): 697-706.

Wakeham, S. G., Amann, R., Freeman, K. H., Hopmans, E. C., Jorgensen, B. B., Putnam, I. F., Schouten, S., Damste, J. S. S., Talbot, H. M., and Woebken, D., 2007. Microbial ecology of the stratified water column of the Black Sea as revealed by a comprehensive biomarker study. Org. Geochem. 38, 2070-2097.

Wakeham, S. G., Hopmans, E. C., Schouten, S., and Damste, J. S. S., 2004. Archaeal lipids and anaerobic oxidation of methane in euxinic water columns: a comparative study of the Black Sea and Cariaco Basin. Chem. Geol. 205, 427-442.

Walker, J. C. G., 1984. Suboxic diagenesis in banded iron formations. Nature 309, 340-342.

Walker, J. C. G., 1987. Was the Archaean biosphere upside down? Nature 329, 710-712.

Walker, J. C. G. and Brimblecomb, , 1985. Iron and sulfur in the pre-biologic ocean. Precamb. Res. 28, 205-222.

Walker, T. R., 1962. Reversible Nature of Chert-Carbonate Replacement in Sedimentary Rocks. Geol Soc Am Bull 73, 237-242.

Walsh, M. M. and Lowe, D. R., 1983. Filamentous microfossils from the 3.1-3.5 billion-year-old Swaziland Supergroup, Barberton Mountain Land, South Africa. Abstr. XIV Lunar & Planet. Sci. Conf. Houston, 814-815.

Walsh, M. M. and Lowe, D. R., 1985. Filamentous microfossils from the 3,500-Myr-old Onverwacht Group, Barberton Group, Barberton Mountain Land, South Africa. Nature 314, 530-532.

Walsh, M. M., 1992. Microfossils and possible microfossils from the Early Archean Onverwacht Group, Barberton Mountain Land, South Africa. Precamb. Res. 54, 271-293.

Walsh, M. M. and Lowe, D. R., 1999. Modes of accumulation of carbonaceous matter in the Early Archaean: A petrographic and geochemical study of the cabonaceous cherts of the Swaziland Supergrou In: Lowe, D. R. and Byerly, G. R. Eds.), Geologic Evolution of the Barberton Greenstone Belt, South Africa. Geological Society of America.

Walter, M. R., 1980. Palaeobiology of Archaean stromatolites. In: Glover, J. E. and Groves, D. I. Eds.), Extended Abstracts, Second International Archaean Symposium, Perth, Australia.

Walter, M. R., Buick, R., and Dunlop, J. S. R., 1980. Stromatolites 3,400-3,500 Myr Old from the North-Pole Area, Western-Australia. Nature 284, 443-445.

Walter, M.R., Hofmann, H.J., 1983, ‘The palaeontology and palaeoecology of Precambrian iron-formations’, In: Trendall, A.F., Morris, R.C. (eds.), ‘Iron-formation: facts and problems’, Elsevier, Amsterdam, p 373-400.

Walter, L. M. and Burton, E. A., 1986. The Effect of Ortho-Phosphate on Carbonate Mineral Dissolution Rates in Seawater. Chem. Geol. 56, 313-323.

Walter, L. M. and Morse, J. W., 1984. Reactive surface area of skeletal carbonates during dissolution: effect of grain size. 54/4, 1081-1090, 5 Figs., 4 Tabs.

Wang, Y. F. and Xu, H. F., 2001. Prediction of trace metal partitioning between minerals and aqueous solutions: A linear free energy correlation approach. Geochim. Cosmochim. Acta 65, 1529-1543.

Warne, D. S. J., Morgan, D. J., and Milodowski, A. E., 1981. Thermal analysis studies of the dolomite, ferroan dolomite, ankerite series. Part 1. Iron content recognition and determination by variable atmorphere DTA. Thermochim. Acta 51, 105-111.

Warren, J. K., 1990. Sedimentology and Mineralogy of Dolomitic Coorong Lakes, South-Australia. J Sediment Petrol 60, 843-858.

Weaver, F. M. and Wise, S. W., 1973. Origin of Cristobalite-Rich Tertiary Sediments in Atlantic and Gulf Coastal-Plain. American Association of Petroleum Geologists Bulletin 57, 1840-1840.

Weaver, F. M. and Wise, S. W. J., 1972. Ultramorphology of deep sea cristobalitic chert. 237/73, 56-57, 3 Figs.

Webb, G. E. and Kamber, B. S., 2000. Rare earth elements in Holocene reefal microbialites: A new shallow seawater proxy. Geochim. Cosmochim. Acta 64, 1557-1565.

Weber, J. N., 1965. Oxygen Isotope Fractionation between Coexisting Calcite and Dolomite in Freshwater Upper Carboniferous Freeport Formation. Nature 207, 972-&.

Wedepohl, K. H., 1969. Composition and abundance of common igneous rocks. In: Wedepohl, K. H. (Ed.), The Handbook of Geochemistry. Springer-Verlag, Berlin.

Wedepohl, K.H., Heinrichs, H., Bridgwater, D., 1991. Chemical Characteristics and Genesis of the Quartz-Feldspathic Rocks in the Archean Crust of Greenland. Contrib. Mineral. Petrol. 107(2), 163-179.

Weidner, J. R., 1968. Phase equilibria in a portion of the system Fe-C-O from 250. to 10000 bars and 400 °C to 1200 °C and its petrologic significance, Pennsylvania State University.

Weidner, J.R., 1968. Phase equilibria in a portion of the system Fe-C-O from 250. to 10000 bars and 400 °C to 1200 °C and its petrologic significance, Pennsylvania State University, 162 p

Weidner, J.R., 1972. Equilibria in the system Fe-C-O part I: siderite-magnetite-carbon-vapor equilibrium from 500 to 10,000 bars. American Journal of Science, 272: 735-751.

Weisset, H. J., Lini, A., Follmi, K. B., and Kuhn, O., 1998. Correlation of Early Cretaceous carbon isotope stratigraphy and platform drowning events: a possible link? Palaeogeogr. Palaeoclimatol. Palaeoecol. 137, 189-203.

Werne, J. and Hollander, D. J., 2004. Balancing supply and demand: controls on carbon isotope fractionation in the Cariaco Basin (Venezuela) Younger Dryas to present. Mar. Chem. 92, 275-293.

Westall, F., de Wit, M. J., Dann, J., van der Gaast, S., de Ronde, C. E. J., and Gerneke, D., 2001. Early Archean fossil bacteria and biofilms in hydrothermally-influenced sediments from Barberton greenstone belt, South Africa. Precamb. Res. 106, 93-116.

Wheat, C. G. and Mottl, M. J., 1994. Hydrothermal circulation, Juan de Fuca Ridge eastern flank: Factors controlling basement water composition. Journal of Geophysical Research 100, 12527-12555.

Wheat, C. G. and Mottl, M. J., 2000. Composition of pore and spring waters from Baby Bare: Global implications of geochemical fluxes from a ridge flank hydrothermal system. Geochim. Cosmochim. Acta 64, 629-642.

Whitehouse, M. J., Kamber, B. S., and Moorbath, S., 1999. Age significance of U-Th-Pb zircon data from early Archaean rocks of west Greenland -a reassessment based on combined ion-microprobe and imaging studies. Chem. Geol. 160, 201-224.

Whiticar, M. J., Faber, E., and Schoell, M., 1986. Biogenic Methane Formation in Marine and Fresh-Water Environments - Co2 Reduction Vs Acetate Fermentation Isotope Evidence. Geochim. Cosmochim. Acta 50, 693-709.

Whitman, W. B., Coleman, D. C., and Wiebe, W. J., 1998. Prokaryotes: The unseen majority. Proc. Natl. Acad. Sci. U. S. A. 95, 6578-6583.

Whittle, G. L. and Alsharhan, A. S., 1994. Dolomitization and Chertification of the Early Eocene Rus Formation in Abu-Dhabi, United-Arab-Emirates. Sediment Geol 92, 273-285.

Widdel, F., Schnell, S., Heising, S., Ehrenreich, A., Assmus, B., and Schink, B., 1993. Ferrous iron oxidation by anoxygenic phototrophic bacteria. Nature 362, 834-835.

Wilde, S. A., Valley, J. W., Peck, W. H., and Graham, C. M., 2001. Evidence from detrital zircons for the existance of continental crust and oceans on the Earth 4.4 Gyr ago. Nature 409, 175-178.

Wildeman, T. R. and Haskin, L. A., 1973. Rare-Earths in Precambrian Sediments. Geochim. Cosmochim. Acta 37, 419-438.

Wildeman, T. R., Condie, K. C., 1973. Rare-Earths in Archean Graywackes from Wyoming and from Fig Tree Group, South-Africa. Geochim. Cosmochim. Acta 37(3), 439-453.

Wilks, M. E. and Nisbet, E. G., 1985. Archean Stromatolites from the Steep Rock Group, Northwestern Ontario, Canada. Can. J. Earth Sci. 22, 792-799.

Wilks, M. E. and Nisbet, E. G., 1988. Stratigraphy of the Steep Rock Group, Northwest Ontario - a Major Archean Unconformity and Archean Stromatolites. Can. J. Earth Sci. 25, 370-391.

Williams, L. A. and Crerar, D. A., 1985. Silica Diagenesis .2. General Mechanisms. Journal of Sedimentary Petrology 55, 312-321.

Williams, L. A., Parks, G. A., and Crerar, D. A., 1985. Silica Diagenesis .1. Solubility Controls. J Sediment Petrol 55, 301-311.

Williams, M. and Druffel, E. R. M., 1987. Radiocarbon in Dissolved Organic-Matter in the Central North Pacific-Ocean. Nature 330, 246-248.

Wilson, J.F., Nesbitt, R.W., Fanning, C.M., 1995. Zircon geochronology of Archaean felsic sequences in the Zimbabwe craton: a revision of greenstone stratigraphy and a model for crustal growth, In: Coward, M., Ries, A.C. (eds.), ‘Early Precambrian Processes’, Geological Society, London, Special Publications, 95, p 109-126.

Winefield, R., 2000. Development of Late Paleoproterozoic aragonitic seafloor cements in the McArthur Group, northern Australia, Carbonate sedimentation and diagenesis in an evolving Precambrian world.

Wingate, M. T. D., 1999. Ion microprobe dabbeleyite and zircon ages for late Archaean mafic dykes of the Pilbara Craton, Western Australia. Aus. J. of Earth Sci. 46, 493-500.

Winterer, E. L., Riedel, W. R., Bronnima.P, Gealy, E. L., Heath, R., Kroenke, L., Martini, E., Moberly, R., Resig, J., and Worsley, T., 1970. Main Geological and Geophysical Results of Dsdp-Leg-7 (Guam to Honolulu). Geophysics 35, 1172.

Winterwerp, J. C. and Kranenburg, C., 2002. Fine sediment dynamics in the marine environment. Elsevier, Amsterdam, Netherlands ; New York.

Wise, S. W. and Kelts, K. R., 1972. Inferred Diagenetic History of Weakly Silicified Deep-Sea Chalk. American Association of Petroleum Geologists Bulletin 56, 1906.

Wittgenstein, L., 1969. Über Gewißheit (On Certainty). Basil Blackwell, Oxford.

Woo, K. S., Choi, D. W., and Lee, K. C., 2008. Silicification of cave corals from some lava tube caves in the Jeju Island, Korea: Implications for speleogenesis and a proxy for paleoenvironmental change during the Late Quaternary. Quaternary International 176-177, 82-95.

Wright, D. T., 1999. The role of sulphate-reducing bacteria and cyanobacteria in dolomite formation in distal ephemeral lakes of the Coorong region, South Australia. Sediment Geol 126, 147-157.

Wright, D. T. and Wacey, D., 2004. Sedimentary dolomite: a reality check. In: Braithwaite, C. J. R., Rizzi, G., and Darke, G. Eds.), The geometry and petrogenesis of dolomite hydrocarbon reservoirs. Geological Society of London, London.

Wright, V., 1990. Lacustrine carbonates. In: Tucker, J. and Wright, V. Eds.), Carbonate sedimentology. Blackwell Scientific, Oxford.

Wronkiewicz, D.J., Condie, K.C., 1987. Geochemistry of Archean Shales from the Witwatersrand Supergroup, South Africa - Source-Area Weathering and Provenance. Geochim. Cosmochim. Acta 51(9), 2401-2416.

Wronkiewicz, D.J., Condie, K.C., 1989. Geochemistry and Provenance of Sediments from the Pongola Supergroup, South Africa - Evidence for a 3.0-Ga-Old Continental Craton. Geochim. Cosmochim. Acta 53(7), 1537-1549.

Wyche, S., Nelson, D.R., Riganti, A., 2004. 4350-3130 Ma detrital zircons in the Southern Cross Granite-Greenstone Terrane, Western Australia: Implications for the early evolution of the Yilgarn Craton. Australian Journal of Earth Sciences 51(1), 31-45.

Xu, H., Ai, L., Tan, L. C., and An, Z. S., 2006. Stable isotopes in bulk carbonates and organic matter in recent sediments of Lake Qinghai and their climatic implications. Chem. Geol. 235, 262-275.

Yakushev, E. V., Chasovnikov, V. K., Debolskaya, E. I., Egorov, A. V., Makkaveev, N., Pakhomova, S. V., Podymov, O. I., and Yakubenko, V. G., 2006. The northeastern Black Sea redox zone: Hydrochemical structure and its temporal variability. Deep-Sea Res Pt Ii 53, 1769-1786.

Yamamoto, K., Itoh, N., Matsumoto, T., Tanaka, T., and Adachi, M., 2004. Geochemistry of Precambrian carbonate intercalated in pillows and its host basalt: implications for the REE composition of circa 3.4 Ga seawater. Precamb. Res. 135, 331-344.

Yates, K. K. and Robbins, L. L., 1998. Production of carbonate sediments by a unicellular green alga. Am. Mineral. 83, 1503-1509.

Yee, N., Phoenix, V. R., Konhauser, K. O., Benning, L. G., and Ferris, F. G., 2003. The effect of cyanobacteria on silica precipitation at neutral pH: implications for bacterial silicification in geothermal hot springs. Chemical Geology 199, 83-90.

Yuen, G. U., Pecore, J. A., Kerridge, J. F., Pinnavaia, T. J., Rightor, E. G., Flores, J., Wedeking, K. W., Mariner, R., Des Marais, D. J., and Chang, S., 1990. Carbon isotopic fractionation in Fischer-Tropsch type reactionsLPSC XXI.

Yui, S., 1966. Decomposition of siderite to magnetite at lower oxygen fugacities: a thermodynamical interpretation and geological implications. Economic Geology 61, 768-776.

Yakushev, E. V., Chasovnikov, V. K., Debolskaya, E. I., Egorov, A. V., Makkaveev, N., Pakhomova, S. V., Podymov, O. I., and Yakubenko, V. G., 2006. The northeastern Black Sea redox zone: Hydrochemical structure and its temporal variability. Deep-Sea Res Pt Ii 53, 1769-1786.

Zegers, T. E., de Keijzer, M., Passchier, C. W., and White, S. H., 1998. The Mulgandinnah Shear Zone: an Archean crustal scale strike-slip zone, eastern Pilbara, Western Australia. Precamb. Res. 88, 233-247.

Zegers, T. E., White, S. H., de Keijzer, M., and Dirks, , 1996. Extensional structures during deposition of the 3460 Ma Warrawoona Group in the eastern Pilbara Craton, Western Australia. Precamb. Res. 80, 89-105.

Zerkle, A. L., House, C. H., and Brantley, S. L., 2005. Biogeochemical signatures through time as inferred from whole microbial genomes. Am. J. Sci. 305, 467-502.

Zhang, C. L., Horita, J., Cole, D. R., Zhou, J. Z., Lovley, D. R., and Phelps, T. J., 2001. Temperature-dependent oxygen and carbon isotope fractionations of biogenic siderite. Geochim. Cosmochim. Acta 65, 2257-2271.

Zhang, Y., 2002. The age and accretion of the Earth. Earth Science Review 59, 235-263.

Zolotov, M. and Shock, E., 1999. Abiotic synthesis of polycyclic aromatic hydrocarbons on Mars. Journal of Geophysical Research-Planets 104, 14033-14049.

Zolotov, M. Y. and Shock, E. L., 2000. A thermodynamic assessment of the potential synthesis of condensed hydrocarbons during cooling and dilution of volcanic gases. Journal of Geophysical Research-Solid Earth 105, 539-559.

Zolotov, M. Y. and Shock, E. L., 2001. Stability of condensed hydrocarbons in the solar nebula. Icarus 150, 323-337.